Characterization of footwall lithologies to the Greens Creek volcanic-hosted massive sulfide (VHMS) deposit, Alaska, USA

Patrick Sack
BSc. Hons. (University of Victoria, Canada)

Submitted in fulfilment of the requirements
for the degree of Doctor of Philosophy

UNIVERSITY
OF TASMANIA

Hobart, Australia
November, 2009

Declaration

This thesis contains no material which has been accepted for the award of any other degree or diploma in any tertiary institution and, to the best of my knowledge and belief, contains no copy or paraphrase of material previously published or written by another person, except where due reference is made in the text of this thesis.

Patrick J. Sack

Date: October 20, 2009

This thesis may be made available for loan. Copying any part of this thesis is prohibited for 18 months from the date this statement was signed; after that time limited copying is permitted in accordance with the Copyright Act 1969

Patrick J. Sack

Date: October 20, 2009

Abstract

The Greens Creek volcanic-hosted massive sulfide (VHMS) deposit is located on northern Admiralty Island, southeastern Alaska, which is part of the Admiralty sub-terrane of the Alexander Terrane, a Late Proterozoic to Paleozoic island arc. The Alexander and Wrangellia Terranes are thought to have joined to become the Wrangellia Superterrane in the Late Carboniferous. The collision between the Wrangellia Superterrane and the North American craton probably occurred between the Early Jurassic and the Early Tertiary. The Late Triassic rifting of the eastern margin of the Alexander Terrane resulted in the most important metallogenic episode in southeast Alaska. Significant VHMS deposits, such as Windy Craggy and Greens Creek, are hosted in a Late Triassic rift sequence. The global resource of Greens Creek is approximately 24 million tonnes at an average grade of 14% Zn, 5% Pb, 600 g/t Ag and 5 g/t Au with insignificant Cu. There are three main ore bodies at Greens Creek: East, West (Northwest, 5250) and Southwest (200 South).

There are three basic divisions in the mine sequence at Greens Creek: hanging wall argillite with minor volcanic rocks (Tr3 and Tr4), mineralized horizon (Tr2), and the altered mafic footwall with minor sedimentary rocks (C1 to Tr1). Footwall rocks (C1 and C2) are dominantly subalkaline basaltic rocks of Early Carboniferous age, Tr1 is a Late Triassic polymict breccia. The Late Triassic hanging wall argillite is made up of organic rich pelagic muds and distal turbidites. The upper portion of the hanging wall sequence contains a minor igneous component consisting of gabbroic sills (I3), basalt, dacite and rhyolite. The regionally extensive Hyd basalts (Tr4) form the youngest Late Triassic stratigraphic element.

The structure of the Alexander Terrane is complex, reflecting its complex Cenozoic and Mesozoic history. There is a strong northwest-southeast structural fabric to the region which is formed by regional recumbent folds and thrusts. Metamorphic and plutonic belts are common. At Greens Creek, there have been at least four folding events, one major thrust event and one brittle strike-slip fault event.

The chemistry of Silurian to Devonian siliceous sedimentary rocks and Early Carboniferous mafic volcanic rocks indicates an island arc environment for the footwall and basement. The Late Triassic hanging wall basalts are slightly alkaline and are interpreted to have formed in a rift of the existing island arc. Late Triassic serpentinite rocks have both mafic and ultramafic chemical composition. The intensely altered refractory compositions are interpreted to have been peridotite. Ti versus Zr ratios for the Early Carboniferous fine-grained layered volcaniclastic footwall lithologies (C2) indicate at least two potential end member sources: (1) recycled footwall greenstones and (2) background marine sedimentation.

A new geochronology protocol, using small zircon grains, was developed in this project. Reliable U-Pb zircon dates on small in-situ zircon grains are possible if careful attention is paid to the quality of the analyses. Small zircon grains tend to have high U (and Th) content which can lead to Pb loss due to radiation damage. However, a precision of 1-2% relative error of the weighted mean age of the rock was achieved by analyzing small zircons where an adequate number of grains were present.

The oldest known rocks in the vicinity of Greens Creek are Late Proterozoic gneissic tonalitic to dioritic rocks from False Point Retreat (Karl et al., 2006). Schistose basement rocks at Greens Creek have a depositional age of Early Silurian to Middle Devonian and contain metamorphic zircon grains with a Late Permian age. The footwall is composed of massive coherent mafic volcanic rocks with a crystallisation age of 342

± 4 Ma (Early Carboniferous) and layered mafic volcaniclastic rocks with a possible crystallization age of 333 ± 6 Ma (Early Carboniferous). Permian metamorphic zircon grains from an amphibolite sample in Cliff Creek formed during the D1 metamorphic and deformational event that affects all Early Carboniferous footwall lithologies (units C1 and C2). The hanging wall argillite was deposited during the Carnian to Norian (Late Triassic). Volumetrically significant serpentinite bodies (I2 - undated) within the footwall show features associated with minor intrusion into the argillite and have anhydrous compositions that overlap with the Late Triassic microgabbros suggesting a Late Triassic emplacement age. Hanging wall microgabbro was emplaced at 221 ± 6 Ma and the overlying rhyolite crystallized at 226.9 ± 0.2 Ma. The Seymour Canal Formation is Late Jurassic to Early Cretaceous. An unfoliated set of mafic dikes offset by a northwest trending brittle fault were emplaced at 85 Ma, constraining the ductile deformation to older than 85 ± 4 Ma and brittle deformation to younger than 85 Ma.

Four alteration zones were recognized within the footwall to the Greens Creek deposit. From distal to proximal these are the chlorite alteration zone, the sericite alteration zone, the quartz-sericite alteration zone and the quartz-pyrite alteration zone. Infrared spectral data indicates a systematic change in white mica composition from phengite to muscovite with increasing proximity to mineralization. The wavelength position of the AlOH feature for background white micas is variable with values between 2190 and 2230 nm and is heavily dependent on bulk rock composition. Near mineralization the white mica composition is dominated by the hydrothermal fluid effects and the AlOH values are restricted to the 2200–2215 nm range. White mica alteration index (WMAI) values show an increase in the abundance of sericite, relative to chlorite, when near mineralization. Chlorite shows limited compositional variation and no recognizable systematic zoning. The wavelength position of the FeOH feature of chlorite is typically between 2246 and 2257 nm indicating Mg-chlorite to intermediate chlorite compositions.

Whole rock geochemical analyses show systematic trends in major oxides, trace elements and alteration indices as the ore position is approached. SiO_2 shows the greatest increase towards mineralization and Na_2O shows the greatest decrease. Trace elements Ba and Tl are elevated above background levels of 50 ppm and 0.1 ppm respectively, up to 500 feet (150 m) from mineralization. The Ishikawa alteration index is an effective monitor of the alteration intensity. The S/Na_2O ratio shows four orders of magnitude increase from background levels of <0.1 to approximately 20 at an unmineralized hanging wall – footwall contact with further increase up to >200 close to a mineralized contact.

Metal zoning within the footwall was investigated by concentrating on samples immediately below the ore position. The footwall to the Northwest West (NWW) ore body is Cu-rich throughout with Zn, Pb and Ag enrichment on the margins of the ore body. The footwall to the East ore body is Cu-poor throughout with moderate Zn and Pb contents, the entire footwall is enriched in Ag. High Cu ratios (>30) with coincident moderate Zn ratios (<83) within the footwall to the NWW ore body outline a feeder zone that is elongated north – south, along the restored western margin of the Maki Fault Zone. Moderate to high Cu ratios (>20) with coincident low Zn ratios (<70) in the footwall to the East ore body outline a feeder zone that is also elongate north – south. In the footwall to both ore bodies, Cu is largely associated with quartz-pyrite alteration and Zn, Pb and Ag with sericite alteration. Morphology and zone refining of the NWW ore body combined with alteration zonation and the Zn ratio and Cu ratio within the footwall feeder zones are all consistent with the NWW ore body forming at temperatures close to 200°C from a relatively prolonged and focused vent source. Zone refining of the East ore body, morphology of the East ore body and alteration zonation and the Zn ratio and Cu ratio within the footwall feeder zones are all consistent with the East ore body forming at temperatures <200°C from a diffuse vent source with a relatively short duration.

Two stages are envisaged for the formation of the Greens Creek deposit: Stage 1 is initiation and ground preparation. Rifting of the existing arc resulted in numerous sub-parallel, steeply dipping faults that initially provided sites for high crustal level intrusions. The heat from these mafic to ultramafic intrusions created an early stage hydrothermal system that locally altered the Early Carboniferous mafic footwall. The end of this stage is marked by the deposition of a polymict breccia with variably hydrothermally altered clasts. Stage 2 is ore deposition, burial and waning. Intense hydrothermal alteration along fluid conduits and proximal to fluid discharge sites signifies increased hydrothermal activity. Ore deposition occurred after the deposition of the polymict breccia and mineralization was immediately buried by fine-grained sediments. This hanging wall sequence is weakly altered which indicates that burial began while the hydrothermal system was still operating. No alteration of the basalts in the Hyd Formation was recognized.

In conclusion, the majority of the footwall to the Greens Creek deposit formed in the Early Carboniferous and was metamorphosed in the Permian. Therefore the deposit sits close to the base of the Late Triassic stratigraphy, above an approximately 100 Ma unconformity and the footwall was metamorphosed prior to ore formation. The apparently unusual base- and precious-metal endowment of the Greens Creek VHMS deposit can be partially explained by its stratigraphic position. The metal source must have included the underlying basement, not just the immediate mafic footwall. Furthermore, preciou- metal enrichment can be explained by low temperature boiling of the hydrothermal fluids, possibly as a result of shallow water depths.

Contents

Figures

Chapter 1: Introduction

Chapter 2: Regional setting

Chapter 3: Local geology

Chapter 4: U-Pb dating methodology

Chapter 5: Chronostratigraphy

Chapter 6: Alteration

Chapter 7: Metal zoning

Chapter 8: Geologic evolution

Tables

Chapter 3: Local geology

Chapter 4: U-Pb dating methodology

Chapter 5: Chronostratigraphy

Chapter 6: Alteration

Chapter 7: Metal zoning

Chapter 8: Geologic evolution

Chapter 9: Conclusions

Appendices

Acknowledgments

This thesis is the result of support and encouragement from Bruce Gemmell and Ron Berry. Individually they both have been crucial to the completion of this project and together they are a superb supervisory team. I am grateful for the opportunity to have been part of the ARC Centre of Excellence in Ore Deposit (CODES) at the University of Tasmania. Sincere thanks are owed to the Greens Creek Mining Company for the funding and support for this project. Andy West knows the geology of the Greens Creek area better than anyone and has always gone beyond the call of duty to assist in this project. A hearty "thank you" to the other Greens Creek geologists (Brian Erickson, Ben Gage, Mike Satre, Mike Steinhoek, Elizabeth Hollingsworth and Bob Scoggins) who have assisted with the fieldwork for this thesis. Thank you to John Proffett for the field mentoring and thought provoking conversations.

The geochronology section of this thesis would not have been possible with out the SEM-MLA and LA-ICP-MS crews. I am indebted to Karsten Goemann, Maya Kamenetsky, Sebastien Meffre, Sarah Gilbert, Chris Hollitt and Leonid Danyushevsky for their expertise in finding and dating zircons. Also thanks to Ron Berry who first proposed the new method for finding in-situ zircons. Invaluable technical and organizational assistance was provided by June Pongratz, Chris Higgins, Peter Cornish, Nilar Hilang, Di Steffens, Helen Scott, Annette Young, Katie McGoldrick, Phil Robinson and Simon Stevens. Numerous post doctoral fellows and PhD students have made the time at CODES pass all that much quicker - thank you to all my co-conspirators. The Canadian Club has made homesickness obsolete. In particular Jacqueline Blackwell and Tim Stubley are gratefully thanked for their friendship and willingness to sit on a baby at any time.

Thank you to my parents who instilled in me a love of learning. My Dad deserves a medal for being the only non-geologist in history to edit 400 pages of geo-speak. Krig on ya Ol' Zircon! Finally, the real reason this thesis was such a blast is that my wife, Nikki, was always at my side with encouragement, love and laughter. The additions of Elliott and Lucas during the last two years has been the icing on the cake. Thanks everyone.

Terminology, nomenclature and frequently used abbreviations

Terminology

Several terms used throughout this thesis need to be defined in order to avoid confusion.

1) Volcanic-hosted massive sulfide (VHMS): Franklin et al. (2005) defined these deposits as volcanogenic massive sulfide (VMS) deposits as they are related spatially, temporally or genetically to volcanism. However, in this thesis, the term volcanic-hosted is used because the deposit is hosted in a submarine, volcano-sedimentary sequence.
2) Deposit, ore zone and ore body: In this thesis, these terms are scale dependent. Deposit refers to all of the mineralization at Greens Creek, ore zone to the rocks in the vicinity of the specific ore body and ore body is the body of ore outlined as a resource by the mine geologists.
3) Mine contact: Is defined as the contact between the stratigraphic hanging wall and footwall. This is also known as the ore equivalent horizon or hanging wall – footwall contact. The hanging wall lithology is always argillite, but the footwall lithology varies.
4) Argillite: Argillite is the term given to the fine-grained distal turbiditic and pelagic sedimentary rocks found in the hanging wall (lithology Tr3). Though the argillite unit contains sand and rarely pebble beds and therefore does not match the strict definition of an argillite, the vast majority of the unit is clay to silt sized. The argillite was not studied and therefore the nomenclature of these hanging wall rocks was not addressed. The term ‘argillite’ was inherited from the mine geologists and been used in this thesis.
5) Units - U.S. standard units are the primary distance units used in this thesis because they are the units used at the mine. The exceptions to this are distances less than one centimeter, where metric units are used. All U.S. standard

measurements are followed by their metric equivalent in brackets.

6) Footwall and hanging wall - These terms are used in the stratigraphic sense. The footwall is the sequence of rocks that was below the deposit when it formed and the hanging wall is the sequence above. This distinction is necessary because complex deformation has overturned many parts of the deposit.

Nomenclature and abbreviations

Units of measurement

nm - nanometer
µm - micrometer
mm - millimeter
cm - centimeter
m - meter
km - kilometer
" - inch (2.54 cm)
' - foot (30 cm)
Mi - mile (1.6 km)
opt - troy ounces per dry short ton
(troy ounce = 31.1035 g)
(dry short ton = 907 kg)

Miscellaneous

~ - approximately
PPL - plane-polarized light
XPL - cross-polarized light
RL - reflected light
Ls - long section
Xs - cross section
° - degree
ASL - above sea level
BSL - below sea level
FOV - field of view
CODES - ARC Centre of Excellence in Ore Deposit located at the University of Tasmania in Hobart

Chapter 1: Introduction

Preamble

The classification of deposits into discrete deposit types inevitably results in exclusion or misclassification of some deposits because of their complexity or apparent contradictions, i.e. they do not fit the mould. The Greens Creek deposit is one of these contradictory deposits and as a result has been classified as a Besshi volcanic-hosted massive sulfide (VHMS) deposit (Dressler and Dunbire, 1981), a VHMS-sedimentary exhalative (SEDEX) hybrid deposit (Taylor et al., 1999) and a Kuroko VHMS deposit (Nokleberg et al., 2005). Study of this deposit provides an ideal opportunity to add to the overall understanding of VHMS deposits as well as to re-evaluate the deposit classification scheme.

When this project was initiated, the Greens Creek polymetallic VHMS deposit was understood to be unusual in several fundamental ways:

1. The age of the footwall was unknown with estimates ranging from Late Triassic to Devonian (Taylor et al., 2008; Duke et al., in press).
2. The metal endowment of the deposit was contrary to the accepted VHMS models of Franklin et al. (1981).
3. Several aspects of the deposit were thought to be related to a SEDEX deposit model and a hybrid VHMS-SEDEX deposit model was proposed (Taylor et al., 1999).

This project was designed to investigate these unique aspects of the deposit by detailed study of the footwall lithologies. As the Greens Creek deposit is unusual in several fundamental ways and is found in an under-explored belt of rocks with an extensive

strike length of over 600 km, study of this deposit provides a perfect opportunity to add to the global understanding of VHMS deposits while outlining important criteria for local mineral exploration.

Location and setting

The Greens Creek VHMS deposit is located in the northern portion of the Admiralty Island National Monument on Admiralty Island, southeast Alaska, USA (Figure 1). Access to the mine site is via a 30 minute boat ride from Auke Bay, outside of Juneau, to Young Bay on the east side of Admiralty Island. From the Young Bay pier there is a 13 mile gravel road to the mine site (Figure 2). Mine accommodation is at Hawk Inlet (Figure 3), eight road miles (13 km) from the mine site. The mine portal and milling facilities are located near the headwaters of Greens Creek at an elevation of 900 feet (272 m) (Figure 4 and Figure 5). Elevation on the property ranges from sea level to 3900 feet (1180 m) in the Cliff Creek area on the southeast corner of the property.

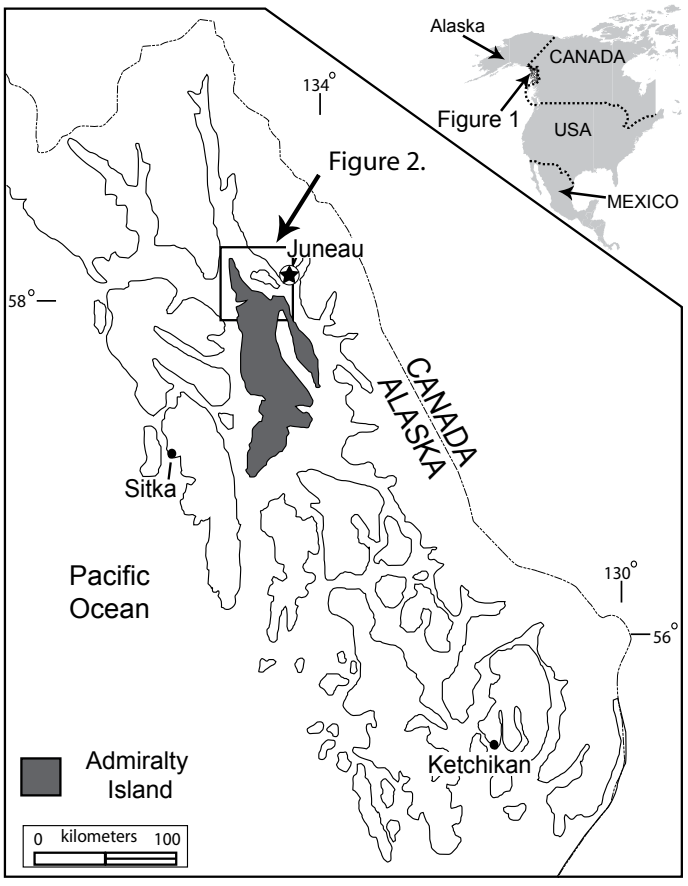

Figure 1 Location of Admiralty Island, southeast Alaska, USA. Note the location of Figure 2.

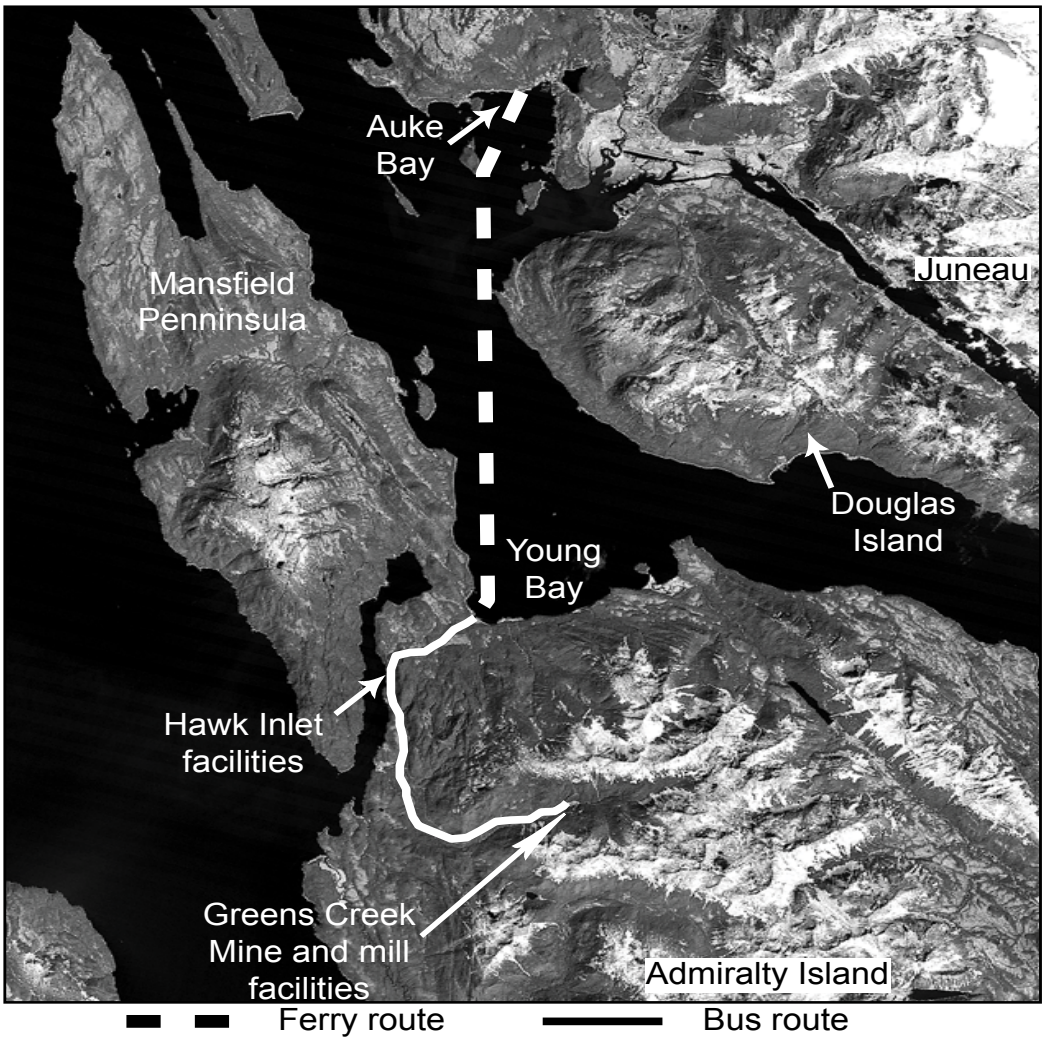

Figure 2 Satellite photograph of Northern Admiralty Island with key locations and facilities. (photo credit: A. West, KGCMC)

Figure 3 The Hawk Inlet facilities with an ore ship in the foreground. (photo credit: A. West, KGCMC)

Figure 4 The Greens Creek Mine and mill site. (photo credit: A. West, KGCMC)

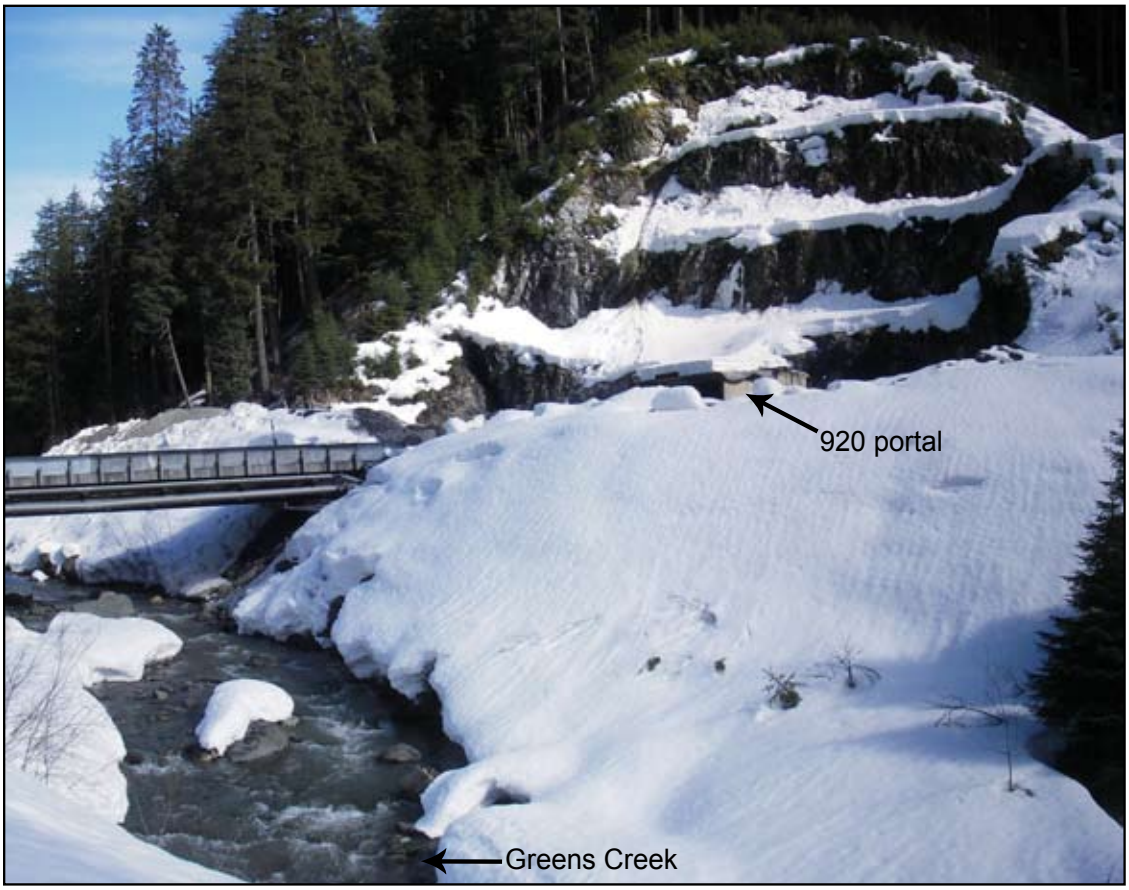

Figure 5 The 920 portal with Greens Creek in the foreground.

The Zn + Pb + Ag ± Au ore bodies at Greens Creek occur at the contact between a hanging wall primarily made up of argillite and a footwall of hydrothermally altered volcanic and sedimentary rocks. From east to west, the four ore bodies are: East ore, West and Northwest West ore, 5250 ore and Southwest and Lower Southwest ore (Figure 6).

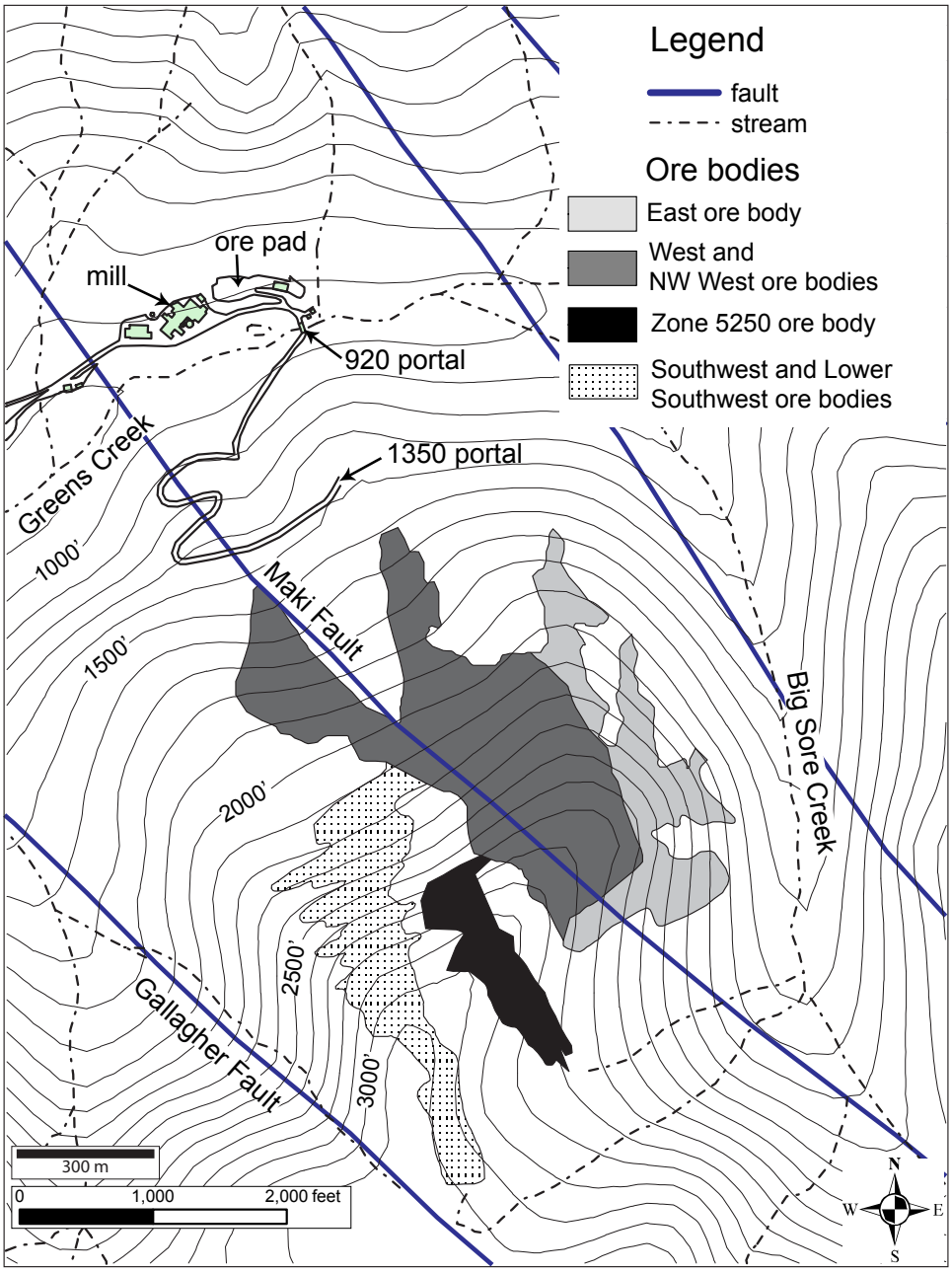

Figure 6 Greens Creek ore bodies projected to surface. Note the location of the active 920 portal. The 1350 portal was used between 1979 and 1989. The surface trace of major NW trending faults are shown, the Maki Fault has 1800 foot dextral offset and dips steeply to the SW at the surface but flattens with depth (Lindberg, 1996).

Project aims

The aims of this PhD project are to examine the surface geology, underground workings, drill core and computer database at Greens Creek in order to:

1) Characterize the geologic and structural setting of the footwall lithologies by:
    i) Mapping volcanic and sedimentary facies within the footwall;
    ii) Detailed examination of relationships between footwall lithologies and the ore horizon;
    iii) Recognition of the deformation history (brittle and ductile) and the contribution of this deformation to the present location of footwall lithologies.
2) Determine the depositional environment and architecture of the footwall lithologies and their relationships to massive sulfide formation by:
    i) Mapping footwall lithologies below mineralized and unmineralized zones;
    ii) Examination of primary rock textures;
    iii) Creating a detailed chronostratigraphy of the footwall lithologies.
3) Describe the alteration mineralogy, assemblages, and textures of the footwall by:
    i) Petrographic examination of footwall lithologies;
    ii) Identification of relic mineralogy and textures;
    iii) Identification of chemical variation and zonation in individual alteration mineral phases;
    iv) Short wave infrared (SWIR) spectral study of footwall rocks.
4) Determine the geochemical (major and trace element) characteristics and signature of the footwall lithologies by:
    i) Examination of major and trace element variation;
    ii) Rare earth element analysis;
    iii) Comparing chemical zonation in the footwall below mineralized zones and unmineralized zones;
    iv) Using alteration lithogeochemistry and alteration indices to characterize alteration.

5) Locate the hydrothermal fluid upflow (i.e. stringer) zones within the footwall by:
    i) Examination of primary metal dispersion within the footwall;
    ii) Examination of mine-scale variations in whole-rock major and trace element signatures.
6) Develop a genetic model for the formation of the deposit, based on data from the stratigraphic footwall.
7) Develop useful criteria, based on characteristics of the footwall, for exploration in the Greens Creek district.

Work plan

Field work

The fieldwork for this project was carried out over three field seasons equating to seven months on-site between August 2005 and August 2008. The fieldwork consisted of underground mapping in the West ore and Northwest West ore zones; logging of surface and underground diamond drill core; limited surface mapping in the Cliff Creek, Upper Gallagher Creek, Lil' Sore areas and along the Greens Creek road; examination of exploration and mine databases; and collection of data from mine sections.

The variation in the footwall lithologies across the property and facies associations within the footwall were mapped by logging 36 diamond drill holes. A full list of drill hole details and examples of drill logs can be found in Appendix I. Detailed (1" = 20') underground mapping was carried out in the West ore and Northwest West ore zones (see Appendix I for examples of underground mapping). The areas mapped are shown in Figure 7 and include drifts 4211 and 2148; West Wall ore accesses 675, 705, 720 and 765; West ore access 480; Northwest West ore accesses 878, 818, 758, 743, 728, 668, 638, 579 and 578.

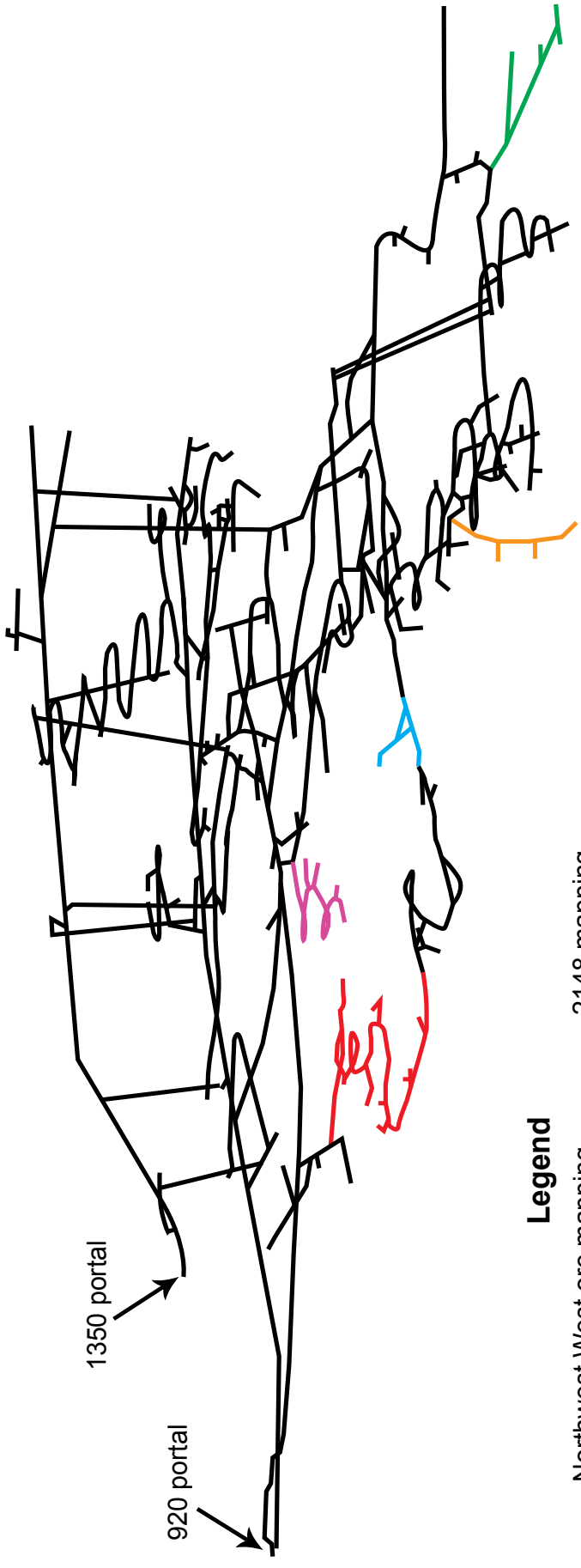

Figure 7 Greens Creek underground workings. Colored areas indicate the locations of mapping as part of the present study. View looking northeast at a slight decline.

Laboratory work

Laboratory work included slabbing of core samples and rock samples for polishing; polished thin sections and polished laser mounts; petrologic study of thin sections; rock crushing for whole rock major and trace element analysis with XRF and ICP-MS; rock crushing and gravity separation of zircon grains; SEM analysis of polished laser mounts; U-Pb isotope analysis of zircon grains using LA-ICP-MS; imaging of zircon grains using cathodoluminescence; and measurement of SWIR spectrum of footwall rocks.

Previous work

Documentation of geology

The first geological investigation on Admiralty Island was made in 1895 and was a report on coal prospects of the area (Dall, 1896). Spencer and Wright (1906) created the first reconnaissance map of the island based primarily on coastal outcrops. The first regional survey was completed between 1921 and 1925, and correlated Spencer's and Wright's geology with the rest of southeast Alaska (Buddington and Chapin, 1929). Barker (1957) mapped the geology on the northern tip of Admiralty Island as part of his 1:63,360 map of the Juneau (B-3) quadrangle. The first detailed study of the geology on Admiralty Island, conducted between 1957 and 1959, was a detailed (1:15,840 scale) geologic map of the Pybus and Gambier Bay areas (Loney, 1964). The first mapping in the Greens Creek area was done during the summers of 1957 and 1959 by Lathram et al. (1965). They created a reconnaissance-scale (1:63,360) geologic map of Admiralty Island. Loney (1964) and Lathram et al. (1965) named most of the geologic units on Admiralty Island and produced the first stratigraphic column for the area.

A second wave of study began in the mid to late 1990s and was focused on the Greens Creek area. A PhD project was carried out on the geology and structure of the Lower Southwest ore body by Freitag (2000). U.S. Geological Survey (USGS) geologist C.D. Taylor worked in the region from 1994 to 2001. Between 1996 and 1999 he

conducted several short field studies of the Greens Creek geology. In 2001 a PhD study on the hanging wall to the deposit was initiated by R. Fulton at CODES, University of Tasmania. This study is still in progress.

Company geologists and consultants have established the mine sequence which was described in field guides and company reports (e.g. Marten, 1987; Proffett, 1987). Structural nomenclature used at the mine was developed by Proffett (1987), who also calculated the displacement along the Maki and Gallagher Faults (Proffett, 2004, in press). Detailed structural analysis and reconstruction of the Maki Fault was done by Lindberg (1996). Duke et al. (in press) described the geology of the Greens Creek mining district and Taylor et al. (1999) proposed the currently accepted model for Greens Creek of a VHMS-SEDEX hybrid deposit with a Devonian footwall.

Exploration history

The Juneau area saw increased prospecting around 1900 with Ni-Cu-Au deposits on the Mansfield peninsula of Admiralty Island receiving the bulk of the exploration interest in the first half of the 1900s (Lathram et al., 1965). A small adit on the Mammoth claims, approximately 2 miles northwest of the mine site, was built to follow a massive galena-sphalerite vein (West, in press).

The Greens Creek deposit was discovered as a result of a regional exploration program by the Pan Sound Joint Venture ((Noranda Exploration (29.73%), Marietta Resources (29.73%), Exhalas Resources (29.73%), and Texas Gas Exploration (10.81%)) (West, in press). In 1974, follow-up prospecting of stream sediment anomalies from the previous year resulted in the discovery of the ‘Big Sore’, the only surface expression of the Greens Creek ore bodies (West, in press). The following year, the first drill hole intersected 89 feet (30 m) of massive sulfide mineralization in what was to become the East ore zone. Definition drilling of this initial resource was done between 1976 and 1980, a period that overlapped the largest conservation movement of the 20th century in the United States of America (West, in press).

The Greens Creek Mine was twice affected by this conservation movement. In 1978, President Carter declared 56 million acres of federal land as national monuments, including the Greens Creek property on Admiralty Island. The second effect was the passage of the Alaska National Interest Lands Conservation Act (ANILCA) in 1980. These two acts gave the Greens Creek Mining Company eight years to prove ore reserves and legitimize their claims (West, in press). This was completed successfully and production started in 1989 but shut down in 1993 due to depressed metal prices. The 1991 discovery of the high-grade Southwest ore zone ensured that the mine reopened in 1996 when metal prices rebounded (West, in press). The mine has been in constant production since with ten years of mine life left.

The global resource of Greens Creek is approximately 24 million tons (21.7 million tonnes) at an average grade of approximately 14% Zn, 5% Pb, 21 opt Ag (665 g/t) and 0.17 opt Au (5.3 g/t) with insignificant Cu. Historical production from 1989 to mid-2006 was 166 million ounces of silver, 927,000 tons of zinc, 1.3 million ounces of gold and 375,000 tons of lead from 8 million tons of ore (Satre, 2006). Current reserves are 8.5 million tons (7.7 million tonnes) at 13.72 opt silver (426.7 g/t), 10.2% zinc, 0.11 opt gold (3.4 g/t) and 3.8% lead (Smuts and Walker, 2008).

Organization of the thesis

The regional setting and local geology of Greens Creek are discussed in Chapters 2 and 3. A methodology of the new in-situ U-Pb dating of small zircon grains is given in Chapter 4. A detailed chronostratigraphy was constructed for the property and is presented in Chapter 5. Chapter 6 describes the alteration of the footwall rocks and the resulting alteration patterns. Chapter 7 focuses on the primary dispersion of metals in the footwall and highlights potential feeder zones. Chapter 8 uses information presented in the previous chapters to present a geologic evolution of the footwall and to create a deposit model. Chapter 9 highlights the potential exploration vectors within the footwall and presents the conclusions of the thesis.

Chapter 2: Regional setting

Introduction

Admiralty Island is situated along the west coast of North America within the 'panhandle' of southeast Alaska (Figure 8). The basement rocks of Admiralty Island belong to the Alexander Terrane which is a Precambrian to Paleozoic island arc system (Gehrels and Berg, 1994). The Greens Creek VHMS deposit is hosted by a Late Triassic volcano-sedimentary package which is thought to represent rifting of this island arc system (Gehrels and Berg, 1994).

This chapter gives an overview of the tectonic setting, regional stratigraphy, metamorphism and regional structure of southeast Alaska. The metallogeny of the Insular Belt and a summary of other Insular Belt VHMS deposits are also included.

Regional geology

Tectonic setting

Admiralty Island is part of the Insular Belt of the North American Cordillera. This belt is one of five northwest-trending belts that together make up the North American Cordillera (Gabrielse et al., 1991) (Figure 9). These belts are identified by their distinct lithologies, internal structure and physiography. The Insular Belt is the western-most belt and is an amalgam of several geologic terranes, the largest of which are the Wrangellia and Alexander (Gabrielse et al., 1991). This belt extends south from Alaska, along the west coast of Canada. The formation of these belts is the result of prolonged accretion of exotic crustal fragments (allochthonous terranes) against the ancient continental margin of North America (Gabrielse et al., 1991).

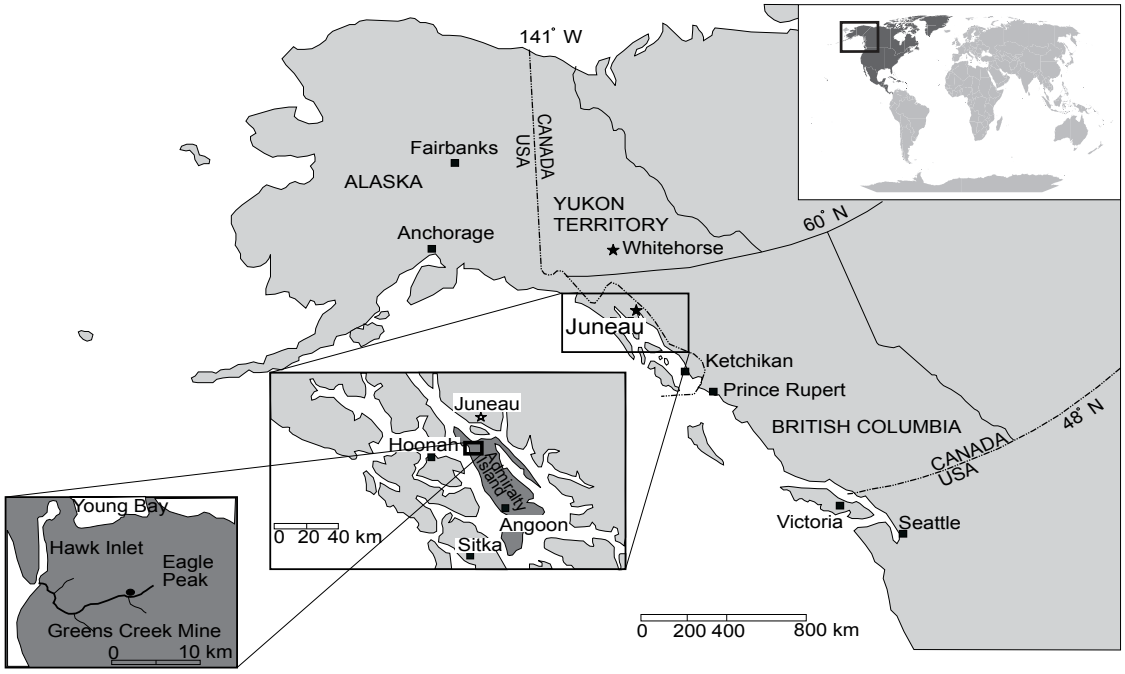

Figure 8 Location map of the Greens Creek Mine, southeastern Alaska. (modified from Freitag, 2000)

The Alexander Terrane is an allochthonous terrane with the most recent paleomagnetic, paleontological and detrital zircon studies indicating, in the Early Devonian, the terrane was located at low latitudes (~15° N) near to Baltica, offshore of the Siberian craton (Bazard et al., 1995; Gehrels et al., 1996; Soja and Antoshkina, 1997). Throughout the Late Paleozoic, the Alexander Terrane evolved in an intra-oceanic setting within the paleo-Pacific basin (Gehrels and Berg, 1994). Since the Late Triassic, the Alexander Terrane has migrated northwards along the eastern margin of the Pacific Ocean and reached its present position, relative to the North American craton, prior to the Late Tertiary (Haeussler et al., 1992).

The Alexander and Wrangellia terranes make up the larger Wrangellia Superterrane (Figure 9) although the exact timing of amalgamation of this superterrane is somewhat controversial. Gabrielse et al. (1991) interpreted the Early Cretaceous to Late Jurassic Gambier overlap assemblage as indicating amalgamation just prior to the deposition of these sediments (i.e. Jurassic amalgamation) while Gardner et al. (1988) reported a Carboniferous pluton stitching the two terranes together. Paleomagnetic data from the

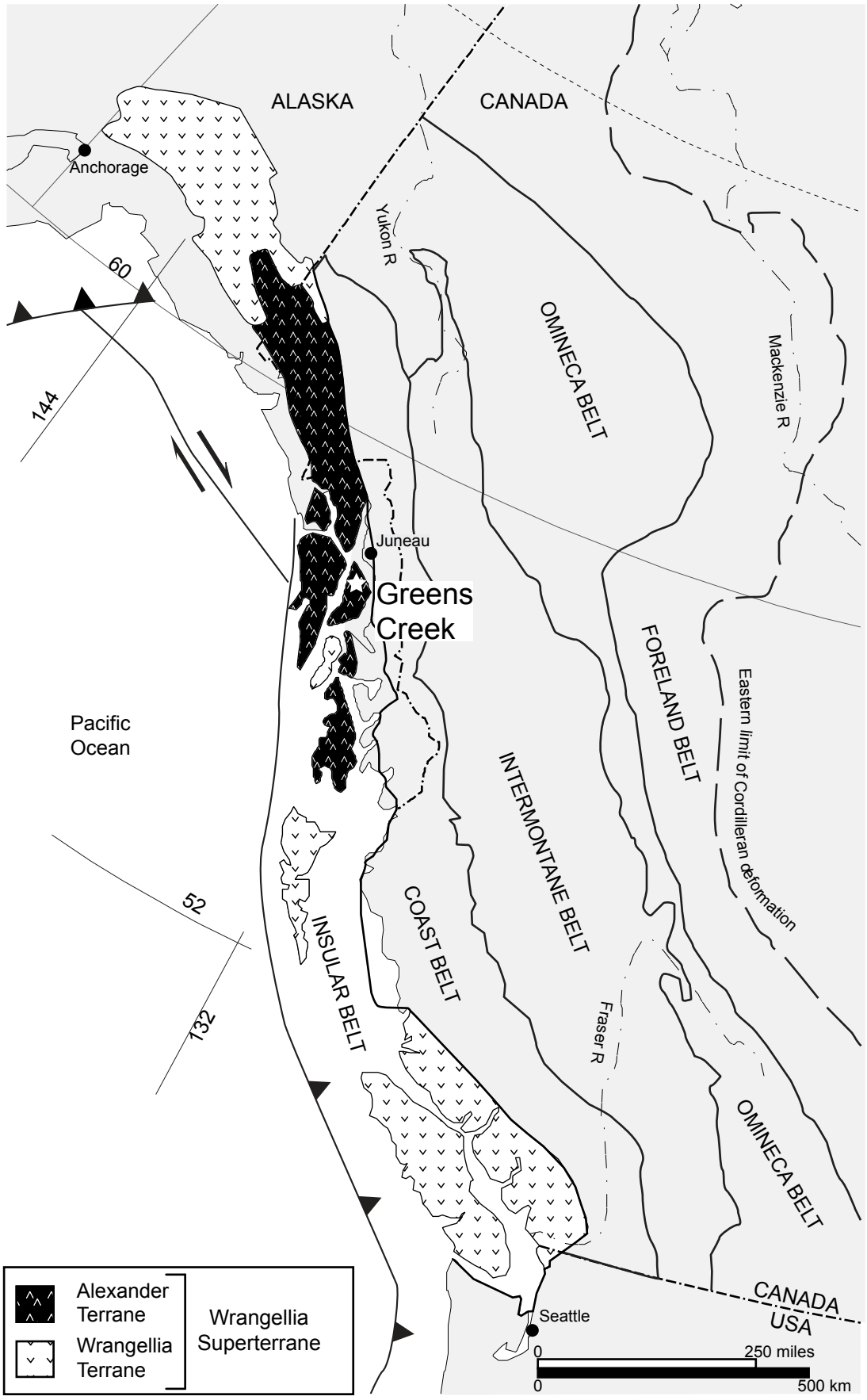

Figure 9 Physiographic belts of the North American Cordillera. Modified from Gabrielse et al. (1991). Alexander and Wrangellia terranes from Nokelberg et al. (2005).

Hound Island Volcanics support a pre-Mesozoic amalgamation (Haeussler and Coe, 1992). The most recent interpretation is that the Alexander and Wrangellia terranes have been in proximity at least since Late Carboniferous time (Gehrels and Berg, 1994).

The Alexander Terrane began accreting to the margin of the North American craton in the Mesozoic. The first indication of tectonic interaction is an Early to Middle Jurassic shear zone along the eastern edge of the terrane (McClelland and Gehrels, 1990). Paleomagnetic data from the Hound Island Volcanics record an overprinting event that indicates the Alexander Terrane was still being emplaced in the Late Cretaceous (Haeussler and Coe, 1992). Panuska (1985) uses paleomagnetic evidence from the Wrangellia terrane to indicate the terrane had not reached its present position, in relation to the North American craton, until after the end of the Cretaceous. The age of the protracted accretion of the Wrangellia Superterrane against the western margin of North America is thus interpreted as Early to Middle Jurassic through to Early Tertiary (Gehrels and Berg, 1994).

The collision of the Alexander Terrane with the margin of North America is responsible for much of the physiographic and structural character of Admiralty Island. Throughout most of southeast Alaska, the physiographic features are largely northwest-southeast trending and reflect the dominant foliation or bedding in the rocks (Lathram et al., 1965). The most conspicuous structural features of Admiralty Island are the northwest-southeast trending regional strike-slip fault zones that are a result of accretion (Gehrels and Berg, 1994) and the Admiralty anticlinorium (Lathram et al., 1965) (Figure 10).

Admiralty Island was glaciated to an elevation of 3000 feet (900 m) during the Pleistocene (Lathram et al., 1965). Quaternary glacial features such as eskers, glacial outwash, glacial erratics and moraines are common below this elevation.

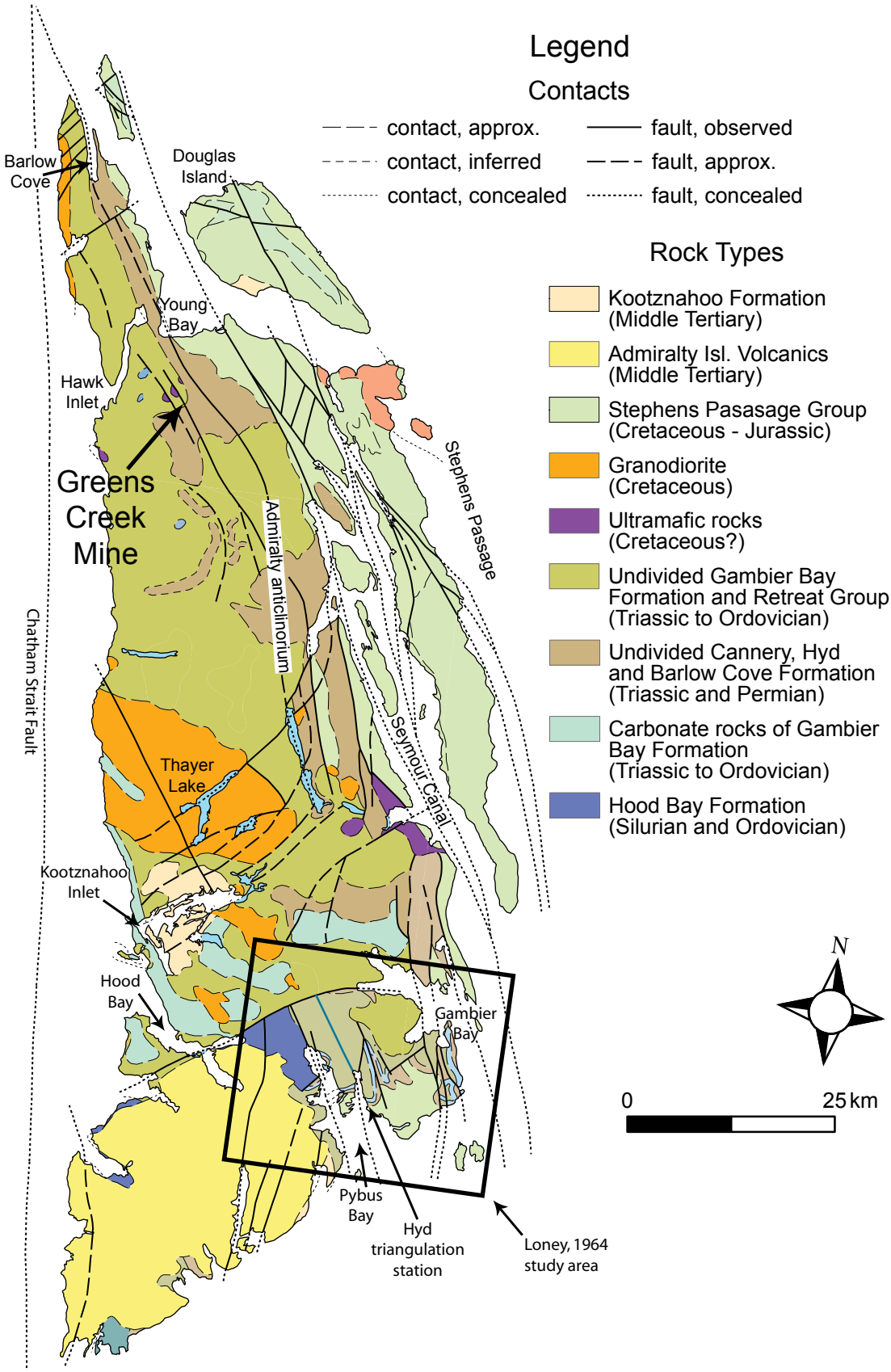

Figure 10 Simplified geology of Admiralty Island. Geology after Lathram et al. (1965) and Gehrels and Berg (1992).

Stratigraphy of Admiralty Island

The Alexander Terrane consists of the Craig and Admiralty sub-terranes (Gehrels and Saleeby, 1987). The Admiralty sub-terrane is restricted to the central portion of the Alexander Terrane, mainly outcropping on Admiralty Island. The Craig sub-terrane is found throughout the Alexander Terrane on Prince of Wales Island, Chicagof Island and on the mainland in the St Elias Mountains of Canada and the Wrangell Mountains of Alaska. The Craig and Admiralty sub-terranes are distinguished by differences in their Carboniferous and older strata (Gehrels and Saleeby, 1987). The majority of data for this regional stratigraphy is from Lathram et al. (1965) and Loney (1964) with the more recent interpretations from Gehrels and Berg (1994). Gehrels and Berg (1994) conducted the majority of their work on the Craig sub-terrane, south of Admiralty Island.

The basement to Admiralty Island is the Admiralty sub-terrane. The layered rocks of Admiralty Island record six depositional cycles; five marine and one non-marine (Lathram et al., 1965). These depositional cycles are all separated by unconformities. A simplified stratigraphic column (Figure 11), illustrates the main geologic units that make up Admiralty Island. The Greens Creek VHMS deposit is hosted by the Upper Triassic Hyd Formation that is found along the eastern margin of the Alexander Terrane.

The oldest rocks on Admiralty Island are Ediacaran (~545 Ma) tonalite to meta-diorite rocks found on the northwest tip of the island (Karl et al., 2006). The second oldest are Ordovician mudstones with minor impure limestone of the Hood Bay Formation (Churkin and Eberlein, 1977). Stratigraphically above these rocks is a spatially restricted Silurian (?) greywacke, slate and limestone unit which is unconformably overlain by Devonian (?) schist and marble of the Retreat Group and Gambier Bay Formation (Loney, 1964). The Permian is represented by fine to coarse-grained siliciclastic rocks of the Cannery Formation, capped by the Pybus Dolomite (Loney, 1964). The next youngest rocks of the Admiralty sub-terrane are the Late Triassic

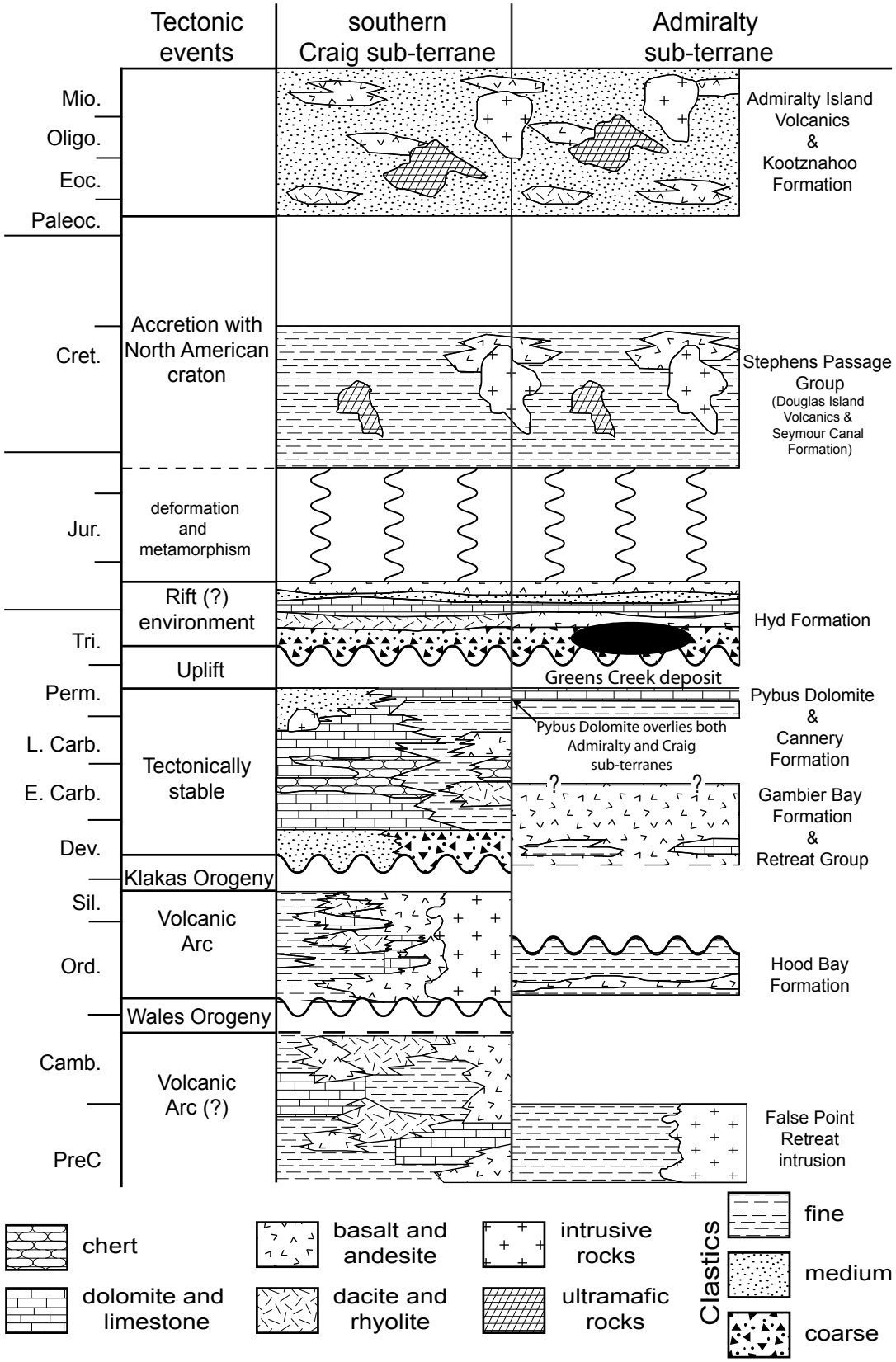

Figure 11 Simplified stratigraphy for the Alexander Terrane. Late Carboniferous and older tectonic events apply only to the Craig sub-terrane. Craig sub-terrane and tectonic event data from Gehrels and Saleeby (1987). Admiralty sub-terrane data from Loney (1964), Lathram et al. (1965), Churkin and Eberlein (1977) and Karl et al. (2006).

marine sediments and mafic volcanic rocks, of the Hyd Formation which host the Greens Creek deposit and are interpreted as a rift–fill sequence (Loney, 1964). The Jurassic-Cretaceous rocks of the Seymour Canal Flysch depositionally overlie the Admiralty sub-terrane and tie it to the inboard terranes (Lathram et al., 1965). The youngest rocks on Admiralty Island are non-marine, Tertiary to Quaternary, siliciclastic rocks of the Kootznahoo Formation and the Admiralty Island Volcanics (Lathram et al., 1965).

Ediacaran rocks

Intrusive rocks on the west side of the northern tip of Admiralty Island were first recognized by Barker (1957). They were interpreted as being the same age (Cretaceous) as the Thayer Lake batholith and its related satellite bodies. However, Karl et al. (2006) reported zircon grains yielding U-Pb ages of ~545 Ma from two sites in this area and has reinterpreted the age of the intrusive as Ediacaran. The main rock type is plagioclase-biotite-quartz diorite that is lineated and foliated.

Ordovician rocks

Hood Bay Formation

The Hood Bay Formation was defined by Loney in 1964 during a detailed examination of the Pybus-Gambier area of southern Admiralty Island (Figure 10). The unit consists of a thick section of black argillite, lesser thin-bedded black chert and minor inter-beds of black impure limestone. This unit is differentiated from the Retreat Group and Gambier Bay Formation mainly by its lower level of metamorphism. The thickness of the unit is unknown. The Hood Bay Formation is overlain with angular unconformity by the Admiralty Island volcanics. Loney (1964) interpreted the age of these rocks to be Devonian but earlier workers assigned them to the Permian or Triassic. In the most recent interpretation, based on a *Climacograptus bicornis* fauna, the Hood Bay Formation is assigned to the Middle Ordovician (Churkin and Eberlein, 1977).

Silurian (?) rocks

The next oldest rocks on Admiralty Island are only found on the southern tip of the island. The rocks at this location are schistose greywacke, slate, chert and minor greywacke conglomerate. These are capped by a thin-bedded limestone. The sequence is folded and the thickness is unknown. The upper contact with younger units is covered but is interpreted as unconformable. The age of these rocks is based on a fossil collection made on Carroll Island. The fossil *Tryplasma* is indicative of Early Devonian, or more likely, Silurian age (Lathram et al., 1965).

Devonian rocks and Devonian (?) rocks

Retreat Group and Gambier Bay Formation

The western side of the island is predominantly Devonian metasedimentary and metavolcanic rocks with the Cretaceous Thayer Lake batholith cutting the belt of rocks roughly in half. The northern portion of the belt is mapped as the Retreat Group and the southern portion of the belt is mapped as the Gambier Bay Formation. These two units are similar in lithology, metamorphism, structure and stratigraphic position and are interpreted as correlates (Lathram et al., 1965).

The dominant rock types in these units are schists with lesser phyllite. The schists are typically chlorite-albite-epidote schist, calc-silicate schist, sericite-chlorite-albite schist, graphitic quartz-muscovite schist, sericite schist, amphibole schist and garnet-muscovite-quartz-feldspar schist. The graphitic schist is typically pyritiferous. Thin- to thick-bedded marble is common, as are thin beds of fine-grained quartzite (Loney, 1964).

The thickness of these units is not known and the base of the units has not been recognized. The conspicuous layering in the rocks is typically a cleavage with bedding only recognized as bands across the cleavage. The units are strongly folded and the layering is discontinuous. Based on poorly preserved *Thamnipora?*sp. and

*Amphipora?*sp. fossils from the Gambier Bay Formation, the age of the unit is probably Middle Devonian (Loney, 1964).

Permian rocks

Cannery Formation

The Cannery Formation was named by Loney in 1964 after the type section from Cannery Cove in Pybus Bay on the southeastern end of Admiralty Island. This rock unit is discontinuously exposed along the eastern portion of the island. As originally described by Loney (1964), this unit consists largely of black argillite, grey to green greywacke, dark grey to green chert and grey phyllite. The amount of argillite and the grain size of the greywacke decreases from the north to south. The amount of chert increases from north to south and the amount of phyllite decreases.

The thickness of the Cannery Formation is not known due to structural complexity but may be as much as several thousand feet (up to1000 m). The formation overlies the Devonian schist unconformably. The Pybus dolomite apparently overlies the Cannery Formation but is commonly missing or the contact is covered and the nature of the contact is uncertain (Loney, 1964).

The northern-most Cannery Formation rocks are in the vicinity of the Greens Creek Mine and the deposit is found at the contact, as mapped by Lathram et al. (1965), between the Cannery Formation and Retreat Group. Locally, the Cannery Formation has been remapped and interpreted as being part of the Hyd Formation, Late Triassic in age, based on conodont fossils (Duke et al., in press). Lathram (1965) assigned the Cannery Formation an age of Early Permian, based on several fossil collections including one from approximately 3 miles east of the Greens Creek Mine. It is not known if both units are present on the property or if one of the age determinations is incorrect.

Pybus Dolomite

The Pybus Dolomite was originally described by Loney (1964). It is named for the type locality and only area where it has been recognized, Pybus Bay, on the southern end of Admiralty Island (Figure 10). The dominant rock type is light colored fossiliferous dolomite with minor chert. The amount of chert increases up-section to a maximum of 90% of the rock.

The thickness of the unit is highly variable, ranging from negligible to a maximum of 1000 feet (300 m). The Pybus Dolomite is unconformably overlain by the Late Triassic Hyd Formation with fragments of the dolomite common in the basal breccia unit of the Hyd Formation (Loney, 1964).

Undifferentiated Permian and Triassic rocks

Undifferentiated Permian and Triassic rocks on Admiralty Island mainly consist of the Barlow Cove Formation and related rocks on Mansfield Peninsula located on the northern tip of the island. The rock types are greenschist and fine to coarse-grained metasediments. The Barlow Cove Formation is named for the type locality in Barlow Cove (Barker, 1957).

Barlow Cove Formation has the same deformation history as the overlying Jurassic-Cretaceous Seymour Canal Flysch. The location and nature of the contact with the Retreat Group is uncertain. The formation was originally interpreted as Jurassic-Cretaceous, but was later reinterpreted as Permo-Triassic (Lathram et al., 1965). Local remapping by Greens Creek geologists has assigned these rocks to the Hyd Formation (Duke et al., in press).

Late Triassic rocks

Hyd Formation

The Hyd Formation is named for the type locality of the argillite member at the Hyd triangulation station on the northeast shore of Pybus Bay at the southern end of

Admiralty Island (Loney, 1964). The Hyd Formation is typically found along the eastern side of Admiralty Island. The formation is composed of a lower siliciclastic section and an upper volcanic section (Loney, 1964).

The sedimentary section consists of a basal breccia, a middle and upper limestone, slate and chert unit. This sedimentary section is best seen in the Pybus Bay and Gambier Bay area on southern Admiralty Island. Outside of this area the sedimentary section is often incomplete (Loney, 1964).

The upper volcanic section forms the majority of the Hyd Formation north of Gambier Bay and thickens rapidly northwards. The volcanic section typically consists of massive or thick-bedded, jasper-bearing red and green amygdaloidal altered basic flows. Pillow structures are common although none have been identified on the Greens Creek property. In the northern half of Admiralty Island, layers of fine-grained greenschist are common and are interpreted as volcaniclastic beds. These are rare on the southern half of the island (Loney, 1964).

The basal breccia of the sedimentary unit has a maximum thickness of 300 to 400 feet (~100 m) and is highly variable. The middle limestone unit has a maximum thickness of several hundred feet (up to 100 m) but is typically thinner. The upper unit of the sedimentary section is consistently 200 to 300 feet (60-90 m) thick. The thickness of the volcanic unit is highly variable but reaches maximum thickness of several thousand feet (up to 1000m) in the northern portion of the island (Loney, 1964).

The base of the Hyd Formation rests unconformably on the Permian rocks. The top of the Hyd Formation appears to be concordant with the overlying Jurassic-Cretaceous rocks. The middle limestone in the lower sedimentary unit of the Hyd Formation is commonly fossiliferous and contains Late Triassic fauna of Carnian age (Crafford, 1989; Taylor et al., 1999).

Late Jurassic and Early Cretaceous rocks

Stephens Passage Group:

The Stephens Passage Group is named for the type locality, Stephens Passage, the waterway between Admiralty Island and the mainland. The group consists of the Seymour Canal Formation and the Douglas Island Volcanics. Regionally, the Stephens Passage Group is part of the Gravina overlap assemblage, a late Mesozoic marine-flysch-dominated sequence that depositionally overlies the Alexander Terrane and the Taku Terrane to the east (Berg et al., 1972).

The Seymour Canal Formation is mainly fine-grained sediments with lesser lenses of greywacke conglomerate. The Douglas Island Volcanics are volcanic flow breccias with minor volcaniclastic and fine-grained siliciclastic rocks. The Douglas Island Volcanics are the dominant unit in the Stephens Passage Group (Lathram et al., 1965).

The Douglas Island Volcanics conformably overlie the Seymour Canal Formation with some inter-fingering in the central portion of Admiralty Island. Fossils from the Seymour Canal Formation indicate a Late Jurassic to Early Cretaceous age. The Stephens Passage Group ties the Alexander Terrane to the inboard Taku Terrane in the Late Jurassic (Berg et al., 1972).

Thayer Lake Batholith:

The Thayer Lake Batholith is the dominant rock unit in the central west portion of Admiralty Island. The unit consists of a large intrusive body (~150 square miles) and several smaller satellite bodies. The intrusive rocks are intermediate in composition and Early Cretaceous in age (Lathram et al., 1965). They have been deformed (Lathram et al., 1965).

Tertiary rocks

Kootznahoo Formation

The Kootznahoo Formation was defined by Lathram et al. (1965) and is named for its type location in Kootznahoo Inlet (Figure 10). The formation consists of non-marine clastic rocks ranging from fine-grained sandstones to pebble and cobble conglomerates. Clasts with a composition and texture similar to the Thayer Lake Batholith are common. The unit appears to thin northwards from a maximum of approximately 5000 feet (1500 m). The base of the unit rests unconformably on the Stephens Passage Group and the top of the unit is erosional in the type area. Fossil floras indicate a Paleocene to Miocene age (Lathram et al., 1965).

Admiralty Island Volcanics:

The Admiralty Island Volcanics cover an area of approximately 350 square miles (900 square km) on the southwestern corner of Admiralty Island. This unit occupies a broad, elongate basin with an approximately northeast-trending axis. The rocks are dominantly basic flows with no significant compositional or textural variation (Loney, 1964).

The current thickness of the Admiralty Island Volcanics is 10,000 feet (3000m) but the top surface is erosional and the original thickness is not known. In places this unit conformably overlies the Kootznahoo Formation and, in other locations, it rests with angular unconformity on pre-Tertiary rocks. Plant fossils and stratigraphic relationships indicate an Eocene to Oligocene age (Loney, 1964).

Regional metamorphism

Admiralty Island is located within the western metamorphic belt in the Coast Plutonic-Metamorphic Complex of southeast Alaska (Figure 12) (Brew et al., 1992). This belt is characterized by widespread low to moderate pressure/temperature dynamothermal metamorphism. Admiralty Island metamorphism is divided into the western metamorphic sub-belt M1 and the Admiralty metamorphic belt. Sub-belt M1

contains the Late Jurassic and younger sediments on the eastern edge of island while the Admiralty Island metamorphic belt contains the Late Triassic and older strata to the west.

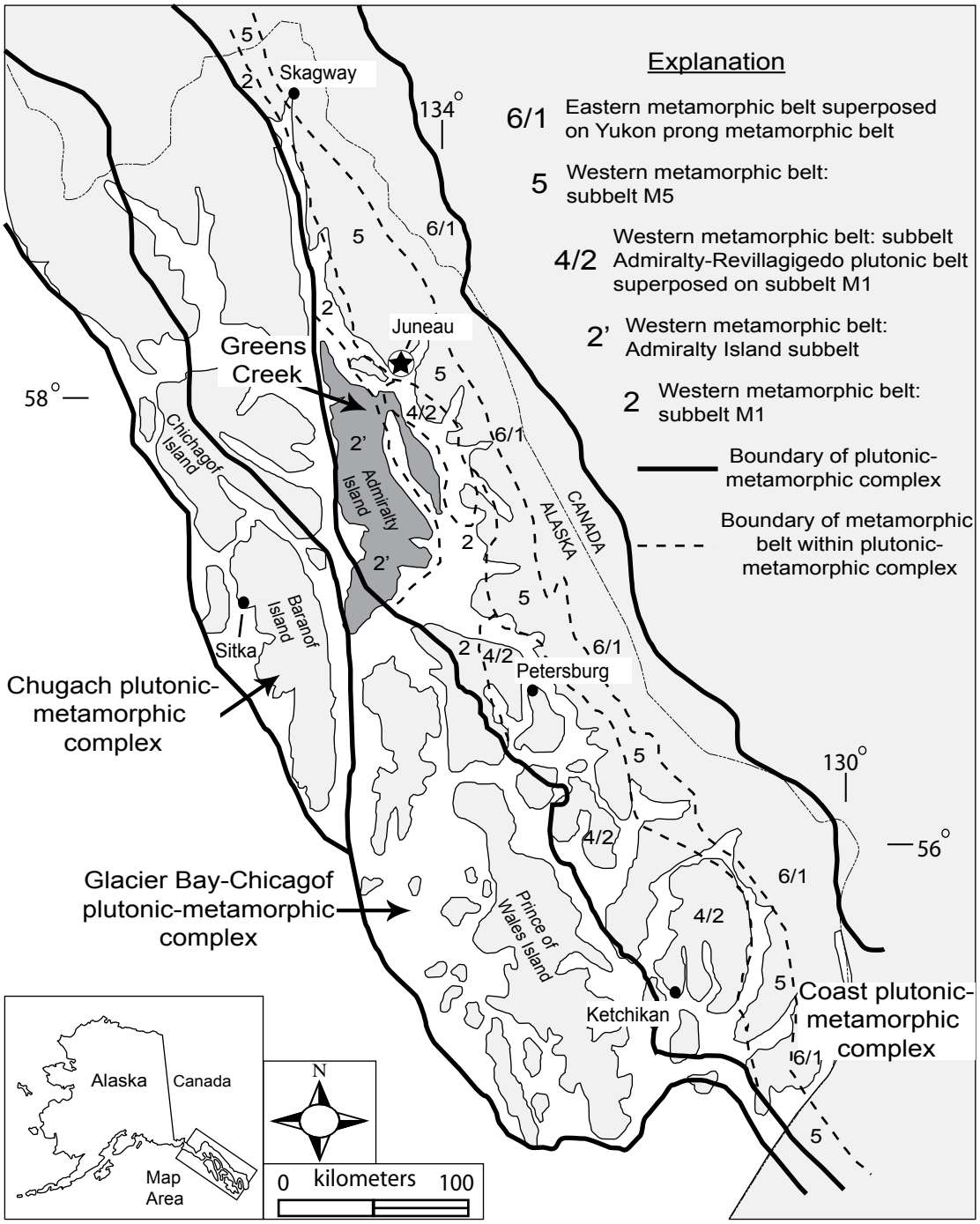

Figure 12 Metamorphic belts of southeast Alaska. From Brew et al. (1992).

The earliest metamorphic event to affect the rocks of the Coast plutonic-metamorphic belt is the M1 event of Brew et al (1992). This event is related to the contractional collapse of the Gravina-Nutzotin basin during accretion of the Alexander Terrane and resulted in an eastward increasing metamorphic gradient (Himmelberg et al., 1991). In the Juneau area, the metamorphic grade increases from prehnite-pumpellyite in the west to greenschist in the east. On Admiralty Island, this metamorphic event is only recognized on the eastern edge in the Stephens Passage Group. The age of the M1 metamorphic event is interpreted to be Middle Cretaceous (Dusel-Bacon et al., 1996).

The Admiralty Island metamorphic belt (Figure 12) is a poorly understood zone which covers most of Admiralty Island and consists of all the pre-Jurassic rocks (Hyd Formation, Cannery Formation, Pybus Dolomite, Retreat Group, Gambier Bay Formation and Hood Bay Formation). This belt is spatially close to the M1 sub-belt and the metamorphism appears similar in age but the protoliths are older. There has not been any mapping of metamorphic trends on Admiralty Island but Loney (1964) suggested an eastward increase in metamorphic grade, similar to that in sub-belt M1. Earlier metamorphic events have been noted, for rocks of the Craig sub-terrane, in the Middle Cambrian to Early Ordovician (Wales Orogeny) and in the Middle Silurian to Early Devonian (Klakas Orogeny) (Gehrels and Berg, 1994). These events have not been documented in the Admiralty sub-terrane and the relationship between the two sub-terranes during these periods of time is not clear.

Structure

The structure of Admiralty Island is complex. There is a strong northwest-southeast oriented structural trend to the region. This trend includes regional fold axes, normal faults, reverse faults, strike-slip faults and the elongation of many discrete structural blocks (Lathram et al., 1965).

The majority of the published data on the structural history of the Alexander Terrane is from work done on the southern portion of the Craig sub-terrane (Gehrels and Saleeby,

1987; McClelland and Gehrels, 1990; Saleeby, 2000). The most recently published works on the structure of the Admiralty sub-terrane are by Loney (1964), who studied the southwest portion of Admiralty Island in detail and Lathram et al. (1965) which was a reconnaissance survey (Figure 10). These two bodies of work are the main sources of data for this summary of Admiralty Island structure.

Gehrels and Saleeby (1987) interpreted the Admiralty sub-terrane as having a partially distinct metamorphic and deformational record from that of the Craig sub-terrane. The two sub-terranes appear to have evolved independently from the Precambrian through to the Permian. Gehrels and Berg (1994) suggested that the pre-Carboniferous Admiralty sub-terrane was either a volcanic basin (rift?) proximal to the stable Craig sub-terrane or a distinct tectonic fragment. The two sub-terranes are convincingly linked in the Permian by clasts of Admiralty chert deposited on the Craig sub-terrane and by the Pybus Dolomite, which was deposited on both sub-terranes. Subsequent to the deposition of this dolomite, the Admiralty and Craig sub-terranes have similar stratigraphy.

In the Late Triassic, the Alexander Terrane rifted along its eastern flank (Gehrels and Berg, 1994). The Late Triassic strata in the southern portion of the terrane are typically coarse-grained sedimentary rocks with felsic volcanic rocks and limestone. The central and northern portions of the terrane typically have fine-grained sedimentary rocks and mafic volcanic rocks. The limestone unit pinches out on southern Admiralty Island. Based on these changes in the stratigraphy, it is interpreted that the rift propagated southwards.

Deformation of the Admiralty sub-terrane prior to accretion with North American craton occurred between the Ordovician and the Late Triassic. There are three documented pre-accretion events but they are poorly understood because they are heavily over-printed by the younger deformation. The earliest deformation described in Admiralty rocks is

Devonian or older, broad, open folds that occur in the Retreat Group, Gambier Bay and Hood Bay Formations. The second deformational event, as seen in the Permian Cannery Formation and Pybus Dolomite, resulted in gentle folds. The final pre-accretion event was the uplift of the Late Triassic Hyd Formation without any noticeable deformation (Loney, 1964).

The dominant structural features on Admiralty Island are related to the accretion of the Alexander Terrane to the North American craton. Loney (1964) identified three phases of intense folding related to accretion. Overall, the three generations of folds have northwest-striking, steeply dipping axial planes. The first episode of intense folds resulted in isoclinal folds with gentle to moderate plunges to the north-northeast or south-southwest and sub-vertical axial planes. The second folds range from minute crenulations to large-scale antiforms and synforms that plunge moderately to the southeast. The third episode of folding resulted in small-scale chevron folds plunging to the south and do not appear to have any large-scale folding effects.

There is a series of northwest-striking thrust faults that displace all of the Mesozoic and older folds but do not displace Tertiary rocks. These faults generally dip eastwards and appear to have an east-over-west sense of motion. A slightly younger set of northeast-striking, east-side-down, normal faults are seen in the Gambier Bay area (Loney, 1964). The margins of the Alexander Terrane and Admiralty Island are defined by large-scale, strike-slip faults, i.e. the Chatham Strait Fault, which strikes north to northwest and have offsets of tens to hundreds of kilometres (Gehrels and Berg, 1994). These large-scale faults are related to the northwestward migration of the Insular Belt. Many of these faults are still active today.

Tertiary rocks of Admiralty Island are slightly deformed. The Admiralty Island Volcanics are found in a north-trending syncline (Loney, 1964).

Regional metallogenic setting

Metallogenic episodes

The metallogenic evolution of the Insular Belt changes significantly at the Cretaceous-Jurassic boundary (Dawson et al. 1992; Goldfarb, 1997). Ore formation from the Jurassic period or older occurred primarily in oceanic environments adjacent to continental North America (Goldfarb, 1997). Ore formation from the Cretaceous period and younger is primarily related to terrane accretion (Goldfarb, 1997). As the Greens Creek deposit formed during the Late Triassic in an oceanic environment, this review will focus on the pre-Cretaceous metallogenic episodes.

There were four main metallogenic episodes in Insular Belt rocks before the Cretaceous period. The first was Late Proterozoic to Early Paleozoic and consisted mainly of formation of precious-metal bearing copper (Cu) and Zn VHMS deposits, such as Niblak, that are now located in the southwestern portion of the Alexander Terrane (Figure 13). These deposits are the result of two separate periods of submarine arc volcanism and are the oldest deposits recognized in Alaska (Goldfarb, 1997). Though these deposits have undergone recent mineral exploration, they have only produced minor amounts of metals.

The second metallogenic episode occurs during the Devonian period and is best observed in the southern Wrangellia Terrane. Southern Wrangellia is dominated by three volcanic sequences, the oldest of which is the Devonian Sicker Group (Dawson et al., 1992). On Vancouver Island, felsic volcanic rocks of the Sicker Group host significant VHMS mineralization in the Myra Falls district, the Mount Sicker Mine and the Lara deposit (Dawson et al., 1992).

Geologic evidence indicates that the Alexander Terrane rifted during the early Mesozoic (Gehrels and Berg, 1994). This rifting resulted in the most economically significant period of massive sulfide formation of the superterrane. The present day strike length

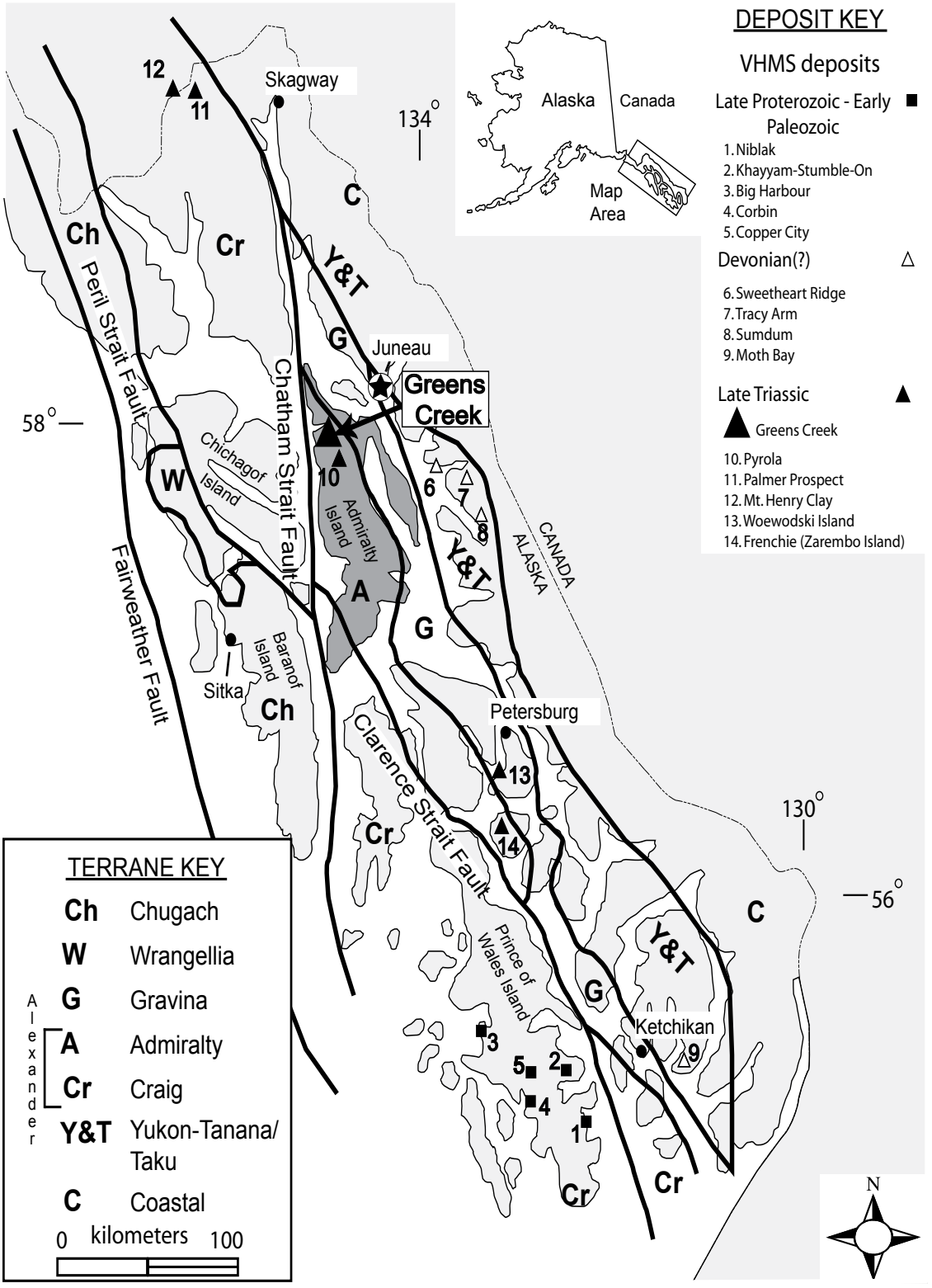

Figure 13 Southeast Alaska VHMS deposits. From Newberry et al. (1997).

of the prospective belt of bimodal volcanic rocks is 750 km, from the Windy Craggy deposit in the north to several small unnamed deposits to the south in the Petersburg region (Nokleberg et al., 2005) (Figure 13). The Greens Creek deposit is located in the middle of the belt. Windy Craggy, a 190 Mt Cu-Co-Au VHMS deposit (Peter, 1989) is the largest deposit in the terrane, with Greens Creek at 24 Mt as second largest. The Late Triassic Quill Creek Complex in the northern portion of Wrangellia located in southwest Yukon has several Ni, Cu, Co, platinum-group-element occurrences associated with it (Dawson et al., 1992).The early Mesozoic was the most economically significant metallogenic era in the Insular Belt.

The final period of the pre-Cretaceous metallogenic episodes is the Jurassic. Deposits of this period developed in arc-trench environments distal to the continental margin of North America (Goldfarb, 1997). In the Alexander Terrane, ultramafic-associated PGE and iron deposits are the two most important deposit types of this period. The PGE deposits are small and have not produced economically significant amounts of metal (Goldfarb, 1997). The iron deposits are large and low grade, and have not produced metal. In southern Wrangellia, skarn and porphyry copper mineralization is associated with the Island Intrusive Suite with several significant deposits such as Argonaut and the Island Copper mine (Dawson et al., 1992).

Insular Belt VHMS deposits

There are three main VHMS regions within the Insular Belt. The eastern margin of the Alexander Terrane hosts Late Triassic mineralization while the south central to southwestern corner of the terrane hosts pre-Devonian mineralization (Newberry et al., 1997); southern Wrangellia hosts Devonian mineralization (Dawson et al., 1992). Though there are sizeable deposits in all three regions, only the Greens Creek deposit in southeast Alaska and Myra Falls deposits on Vancouver Island have produced significant amounts of metal. Greens Creek is the most productive VHMS deposit in the Alexander Terrane but not the largest.

VHMS deposits in the Alexander Terrane vary in age, from Late Proterozoic to Cretaceous, and geographic location with a strike length of over 750 km (Newberry et al., 1997) (Figure 13). The Late Triassic rocks along the eastern margin of the Alexander Terrane host the largest and most productive VHMS deposits in the terrane (Figure 13) (Newberry et al., 1997). Generally, the deposits in the Alexander Terrane are less than 1 Mt with grades below 1.4% Cu with the notable exceptions of the Greens Creek deposit and Windy Craggy deposit (Newberry et al., 1997). Deposits such as Niblak and Stumble On are hosted by the basal portion of the Alexander terrane in the Proterozoic to Early Paleozoic Wales Group (Newberry et al., 1997). Felsic volcanic rocks of the Devonian Sicker Group host the Myra Falls deposits and the majority of VHMS mineralization in the Wrangellia Terrane (Dawson et al., 1992).

Sulphur (S) isotope values for Alaskan VHMS deposits conform to trends found in VHMS deposits worldwide with values approximately 17‰ less than seawater at the time of formation (Newberry et al., 1997). As expected, lead isotope values from Alaskan VHMS deposits largely reflect two characteristics: age and degree of contribution from various reservoirs (Newberry et al., 1997). Au and tin (Sn) concentrations in Alaskan VHMS deposits are indicative of the oxidation state of the mineralizing fluids (Newberry et al., 1997). In some cases, such as at Greens Creek and Windy Craggy, redox conditions have been used to explain apparently odd metal endowments (Newberry et al., 1997). Overall, Alaskan VHMS deposits conform well to world models and classifications. However, there is a shortage of geochemical data for the deposits and their associated rock types (Newberry et al., 1997).

Summary

- Admiralty Island is part of the Admiralty sub-terrane of the Alexander Terrane. The Alexander Terrane and Wrangellia Terrane are thought to have joined to become the Wrangellia Superterrane in the Late Carboniferous. The Wrangellia Superterrane is the largest part of the Insular Belt which is the outermost belt of the North American Cordillera.

- The time of collision between the Wrangellia Superterrane and the North American craton is Early Jurassic through to Early Tertiary.

- The Alexander Terrane is a Late Proterozoic to Paleozoic island-arc system. The Late Triassic Hyd Formation represents the rifting of this arc system and hosts the Greens Creek VHMS deposit.

- Admiralty Island is part of the western metamorphic belt of the Coast plutonic-metamorphic complex. This belt is characterized by an eastward-increasing metamorphic gradient from prehnite-pumpellyite to greenschist. Metamorphism is associated with the accretion of the terrane.

- The structure of the Alexander Terrane is complex, reflecting its protracted Cenozoic and Mesozoic accretionary history. There is a strong northwest-southeast structural fabric to the southeast Alaska region. This fabric is formed by large folds, faults and metamorphic and plutonic belts.

- The Late Triassic rifting of the eastern margin of the Alexander Terrane resulted in one of the most important metallogenic episodes in southeast Alaska. Significant VHMS deposits such as Windy Craggy and Greens Creek were formed during this event.

Chapter 3: Local geology

Introduction

Where Chapter 2 gave an overview of the geology on the entire property and of Admiralty Island, this chapter focuses on a more detailed description of the local geology of the Greens Creek Mine. The Greens Creek VHMS deposit is found at the contact between a stratigraphic footwall of altered and deformed volcanic rocks (phyllites) and a stratigraphic hanging wall of less altered and deformed sedimentary rocks (argillites). These rocks are known as the 'mine sequence'. The host rocks and the deposit have been metamorphosed to lowest greenschist facies (Himmelberg et al., 1995).

The approximate chronological order of lithological units in the Greens Creek mine area, based on work by Freitag (2000), West and Proffett (2003) and reorganized by the geochronology portion of this study, is outlined in Table 1. The age of the siliciclastic hanging wall rocks and ore types is fairly well constrained by their geometry and the various fossil assemblages found within them. The dominant conodont species found within carbonate beds in the slatey argillite unit is *Metapolygnathus nodosus* indicating deposition in the Late Carnian to Earliest Norian (Late Triassic) (Taylor et al., 1999). This age for the lower hanging wall is supported by a poorly preserved *Halobia* macrofossil found in an argillite clast within the ore (Crafford, 1989).

Table 1 Summary of Greens Creek lithologies and their characteristics. (Modified after Freitag, 2000; West and Proffett, 2003). The chronologic order is from the present study.

Lithology	GC terminology	General hand sample characteristics	Descriptive stratigraphy
Post Triassic lithologies	diabase dikes	massive, unaltered with fine to coarse grained plagioclase phenocrysts, common chilled margins, unfoliated	basalt (J2) and siltstone (J1) and diabase dikes (I4)
Stratigraphic hanging wall - "Argillites"	Hyd basalt	metabasalt flows, less altered than greenstone, often amygdaloidal; contains minor limestone beds, pods and fragments	Tr4 - coherent volcanic rocks
	rhyolite and dacite	fine-grained to weakly porphyritic, siliceous , massive coherent to monomictic breccia	
	Hyd gabbro	medium to dark green, fine to medium grained, massive, crystalline texture	I3 - microgabbro
	serpentinite	soapy texture, dark green	I2 - serpentinite
	slatey argillite	very fine-grained, finely laminated, usually intercalated between massive argillite beds, can form thick (>3 m) units	Tr3 - siliciclastic rocks
	massive argillite	fine-grained, forms up to 0.3 m thick beds, which are characterized by quartz-carbonate ladder veins	
Mineralized rocks	massive base-metal sulfide	contains fine- to very fine-grained sphalerite and galena ± chalcopyrite	Tr2 - ore
	massive pyrite	brassy color, primary textures (colloform pyrite) common	
	white carbonate ore	massive dolomite, typically veined, often contains high grade silver minerals	
	white baritic ore	coarse, sugary textured massive barite ± dolomite, sericite, mariposite, commonly barren of sulfides, however locally enriched in silver	
	white siliceous ore	abundant to massive quartz ± dolomite, sericite, mariposite, barite	
Stratigraphic footwall	breccia	granule to pebble, moderately to poorly sorted, monomictic and polymict	Tr1 - polymict breccias
	quartz-carbonate-mariposite	light grey to light purple, massive, can be heavily quartz-carbonate veined	I1 - quartz-carbonate-mariposite rock
	siliceous rock	white to grey, fine-grained, massive, dense, quartz-rich	C2b - siliceous rocks and monomict breccias
	carbonate phyllite	layered to nearly massive, granular texture, dominantly dolomitic, light grey to tan	C2a - layered rocks
	siliceous phyllite	light grey, up to 70% quartz, varying amounts of sericite	
	maripositic phyllite	mariposite gives the phyllite a distinct green tint	
	sericitic phyllite	light grey, very fine-grained sericite, varying amounts of pyrite, quartz	
	chloritic phyllite	light to dark green, laminated to layered, chlorite-rich rock	
	graphitic phyllite	light grey to black, laminated to layered, graphitic partings	
	greenstone	light to dark green, massive, chlorite-rich rock	C1 - massive rocks
Basement	schists	light grey to black to green layers, schistose	S-D2 - schistose rocks
	marble	coarsely recrystallized, massive dark grey marble	S-D1 - recrystallized marble
	NA	light grey with mafic phenocrysts	E1 - gneissic intrusive? basement

The existing classification of footwall lithologies is based on the macroscopic qualities of the various types of phyllite and is largely based on alteration mineralogy (i.e. chloritic phyllite, sericitic phyllite, siliceous phyllite etc.). As a result of detailed core logging, mapping and petrography, this study has grouped some of the phyllites into one protolith with various alteration mineral assemblages (Table 1). In this chapter, the footwall lithology discussion is based on interpreted primary features. Alteration features will be discussed in Chapter 6. Also, as a result of the this study, the chronology has changed considerably. The new chronology is used to organize the discussion on the footwall lithologies (Table 1); the dates that resulted in this change are discussed in Chapter 5.

There are three basic subdivisions within the mine sequence:

- Tr3 and Tr4: hanging wall sedimentary and volcanic rocks (‘argillites’)
- Tr2: mineralized horizon
- C1-Tr1: altered footwall volcanic and minor sedimentary rocks (‘phyllites’)

Four intrusive lithologies, I1-4, are recognized at Greens Creek. Each of these basic units can be further subdivided into the divisions described in Table 1. The only known and easily recognized stratigraphic marker within the mine sequence is the mineralized horizon (Tr2), or the contact between the argillites (Tr3) and the altered footwall (C1 or C2); this contact is known at the mine as the ‘mine contact’.

Pre-Triassic volcanic and sedimentary lithologies (E1 to C2)

E1 and S-D1&2 - schistose rocks

The oldest known unit on northern Admiralty Island is a foliated tonalitic to dioritic gneiss (E1) from near False Point Retreat which has an Ediacaran emplacement age (Karl et al., 2006). This unit is found with metasedimentary rocks of similar metamorphic grade, but the contact relationship is not known. There are several outcrops of marble (S-D1) near Hawk Inlet, the largest of which is ‘Limestone Bluff’

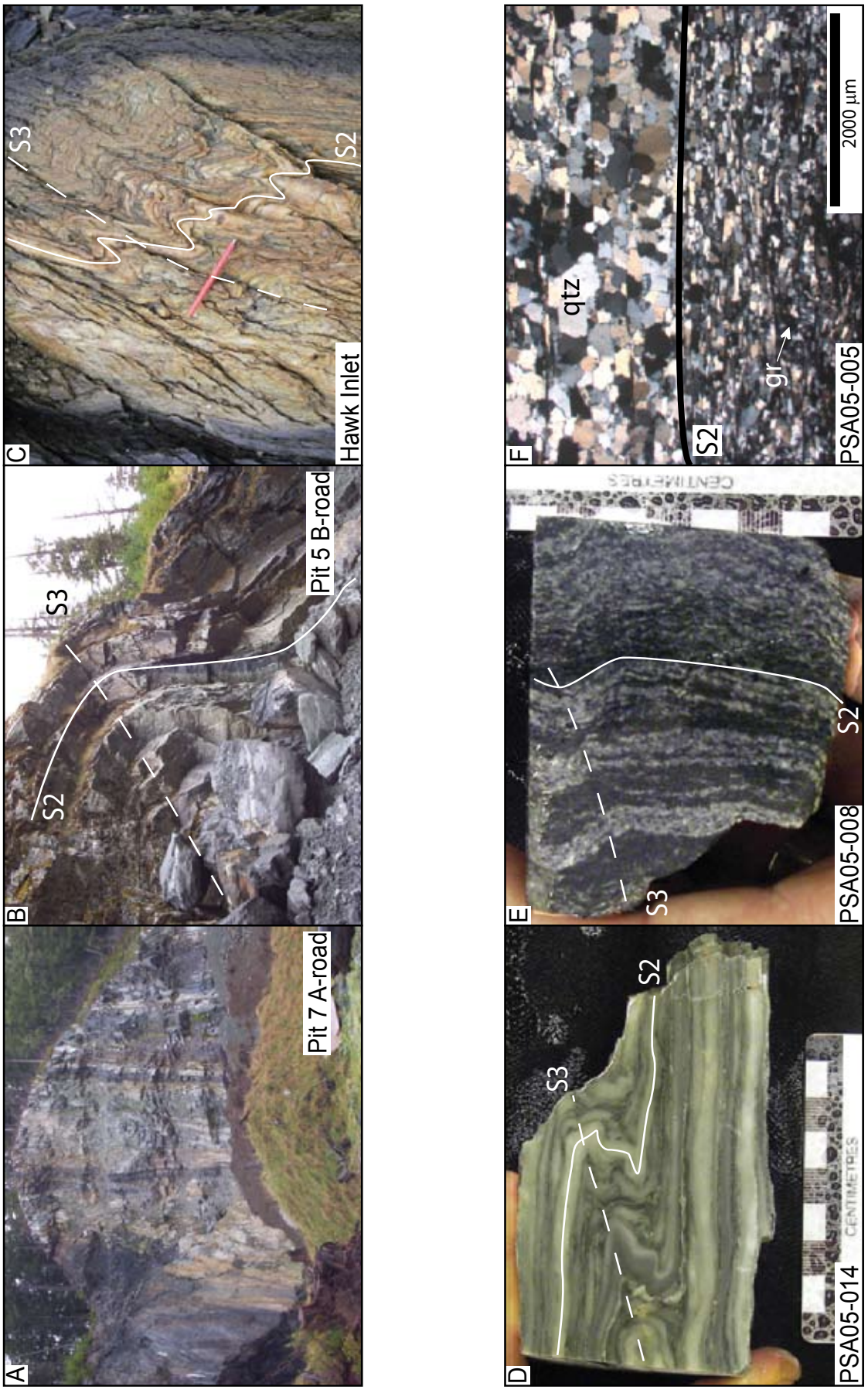
A
Pit 7 A-road
B
S3
S2
Pit 5 B-road
C
S3
S2
Hawk Inlet
D
S3
S2
PSA05-014
CENTIMETRES
E
S3
S2
PSA05-008
F
qtz
S2
gr
2000 µm
PSA05-005

Figure 14 Representative photographs of the coarse-grained schistose unit (S-D2).
(A) Interlayered, steeply dipping quartz mica schist (light grey layers), chlorite quartz mica schist (light green layers) and graphitic quartz mica schist (black layers). Layer types vary in thickness from several feet (~1 m) thick to sections several tens of feet thick (up to 10 m). Photograph taken looking northwest in Pit 7. Outcrop is approximately 250 feet (75 m) (across (2475120E, 2309741N, mile 1.9 (km 3.0) on the A-road).

(B) Chlorite quartz mica schist and graphitic quartz mica schist layers showing S2 sub-parallel to compositional banding and open S3 folds. Photograph taken looking northwest in Pit 5. Outcrop is approximately 20 feet across (6 m) (2476645E, 2298440N, approximately mile 0.9 (km 1.4) on the B-road).

(C) Quartz mica schist with graphitic quartz mica schist on either side. S2 is sub-parallel to compositional layering and is crenulated by S3. Photograph taken looking southeast in on the eastern shore of Hawk Inlet. Magnet is 12cm long (2474370E, 2313900N, eastern shore of Hawk Inlet north of Pit 7)

(D) Thickly laminated to very thinly layered chlorite quartz mica schist with a well developed F3 fold. Scale bar is in cm (2481828E, 2313311N, approximately mile 3.6 (km 5.8)on the A-road).

(E) Coarse-grained graphitic quartz mica schist. Scale bar is in cm (2475670E, 2300728N, Hawk Inlet fuel bay).

(F) Photomicrograph (XPL) of quartz mica schist showing grain size variation in layering and compositional variation between fine and coarse sand sized layers. Fine grained layers have more graphite (gr) while coarse grained layers are cleaner and composed almost entirely of quartz. (2475670E, 2300728N, Hawk Inlet fuel bay)

approximately 3 km east of the Hawk Inlet camp facilities. A sample from this lithology provides the Silurian-Devonian depositional age for these rocks (Oliver and Berg, 1981). Quartz-mica schists (S-D2) are found along the shores of Hawk Inlet and are visually different from any of the fine-grained layered phyllitic footwall units. They can be highly siliceous, with up to 95% quartz, typically have broadly spaced foliation, are thinly to thickly-layered and the micas are coarser than the Carboniferous footwall rocks (Figure 14A-E). The mineralogy is dominantly quartz with layers defined by grain size variation between coarse sand and fine sand and by the presence of chlorite, muscovite or graphite (Figure 14F). There can be minor carbonate. S2 is defined by oriented mica and is typically at a low angle to the grain size and compositional layering (S1). S0 has not been recognized in these rocks (Proffett, in press). This unit cannot be distinguished from the apparently younger rocks (C1 or C2) based on the number of foliations or fold generations. It was probably metamorphosed at higher grade.

C1 - massive rocks

The greenstone is primarily fine-grained, light to dark green with a massive texture (Figure 15A-C). The unit can be evenly fine-grained to porphyritic (Figure 15B). The porphyritic texture is a result of even distribution of the relict plagioclase phenocrysts up to 1 mm within a groundmass of chlorite, carbonate, quartz, feldspar and minor sericite (Figure 15D-F). The unit can be weakly to highly foliated with very faint chlorite-rich zones defining the foliation (Figure 15C); the chlorite-rich zones may be poorly preserved examples of flow banding. Typically the foliation increases with alteration intensity as a result of the increase in the amount of mica (primarily chlorite and sericite) in the rock. Based on the porphyritic, massive uniform texture and homogenous character, this unit is interpreted as being coherent volcanic in origin with field relationships indicating either flows or shallow level intrusions ranging from a few feet (~1 m) to 100 feet (30 m) in thickness (Scherkenbach, 1983; this study). However, due to the intense deformation and the lack of clear textural evidence, the possibility of either some or all of this unit being another type of massive, fine-grained volcanic or volcaniclastic rock cannot be entirely discounted. The total stratigraphic thickness of

this unit is not known. This lithology may occur in a number of stratigraphic elements interlayered with C2 lithologies.

C2a and C2b - layered rocks

C2a - graphitic phyllite

The graphitic phyllite is fine-grained and black with carbonaceous partings in a dominantly quartz-rich rock (West and Proffett, 2003; this study) (Figure 16A). The unit is finely laminated with layers between 0.5 and 5 mm in thickness (Figure 16B). The light grey layers are primarily made up of medium to very fine-grained sand size quartz grains with minor amounts of fine grained white mica and rarely chlorite (Figure 16C-F). The dark grey to black layers are composed of graphite, sericite and lesser silt-size quartz grains. These alternating layers of metasandstone and metasiltstone are interpreted as primary features of the rock but it is not possible to determine if they represent sedimentary beds or severely attenuated clasts that now resemble beds. The low angle between the compositional layering (S1) and the S2 foliation is discernible in the graphitic phyllites and this is the unit that best illustrates the presence of a pre-mineralization foliation which is absent in the Triassic host sequence and hanging wall lithologies (Figure 16C). This unit is often intimately interlayered with either the greenstone or the other phyllites and is interpreted as representing background sedimentation (Duke et al., in press; this study). This lithology forms units that range from inches thick to consistent sections several hundred feet (~100 m) thick.

C2a - chloritic, sericitic, carbonate, mariposite and siliceous phyllite

The five lithologies: chloritic phyllite, sericitic phyllite, carbonate phyllite, mariposite phyllite and siliceous phyllite are all thinly to thickly laminated with compositional and grain size variation between layers (Figure 17A-D). There are generally two layer types: (1) finer grained, typically silt size, mica dominated with lesser quartz, plagioclase and carbonates; (2) coarser grained, typically medium to very fine-sand size, quartz and plagioclase dominated with lesser carbonates and minor chlorite or sericite. The

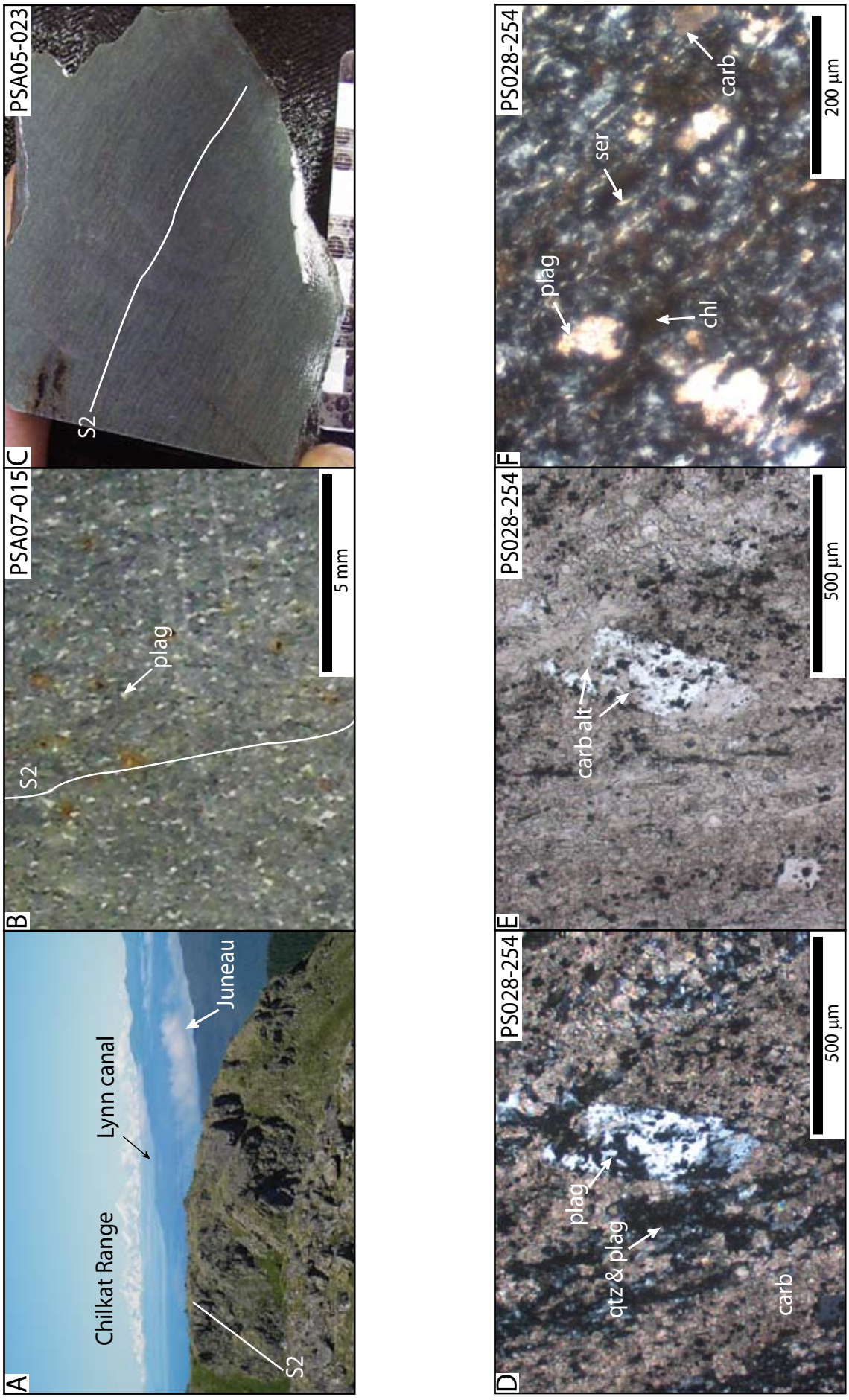
A
Chilkat Range
Lynn canal
Juneau
S2
B
PSA07-015
S2
plag
5 mm
C
PSA05-023
S2
D
PS028-254
plag
qtz & plag
carb
500 µm
E
PS028-254
carb alt
500 µm
F
PS028-254
plag
ser
chl
carb
200 µm

Figure 15 Representative photographs of the greenstone unit (C1).
(A) Photograph looking north, down the Lynn Canal, towards the Chilkat Range near Haines, Alaska from a greenstone outcrop on Mammoth Ridge, directly north of the mine site. As is the norm, Juneau is below the clouds in the middle of the photograph on the right side. The outcrop is massive and shows weak S2 foliation. FOV in the foreground is approximately 25 feet (8 m).

(B) Evenly porphyritic, massive greenstone. Phenocrysts are moderately sericite altered subhedral plagioclase (plag), ground mass is fine-grained chlorite (chl), sericite (ser), carbonate (carb) and plagioclase with minor quartz (qtz). Weak S2 foliation visible. Scale bar is in cm (2477831E, 2292613N, approximately mile 2.0 (km 3.2) on the B-road).

(C) Massive, fine-grained greenstone with very faint chlorite-rich zones aligned parallel to S2. The groundmass is fine-grained chlorite, sericite, carbonate and plagioclase and there are rare, plagioclase phenocrysts <200 µm. Scale bar is in cm (2481594E, 2281161N, approximately mile 4.6 (km 7.4) on the B-road).

(D&E) Photomicrographs (E – XPL and F- PPL) of a pseudomorph of a 500 µm plagioclase phenocryst in a groundmass of carbonate and minor feldspar and quartz. The plagioclase is completely recrystallized by the carbonate. (2501875E, 22801867N, East ore zone, drill hole PS028 at 254 feet (80.0 m))

(F) Photomicrographs (XPL) of typical fine-grained altered groundmass of chlorite, sericite, plagioclase and carbonate. (2501875E, 22801867N, East ore zone, drill hole PS028 at 254 feet (80.0 m)).

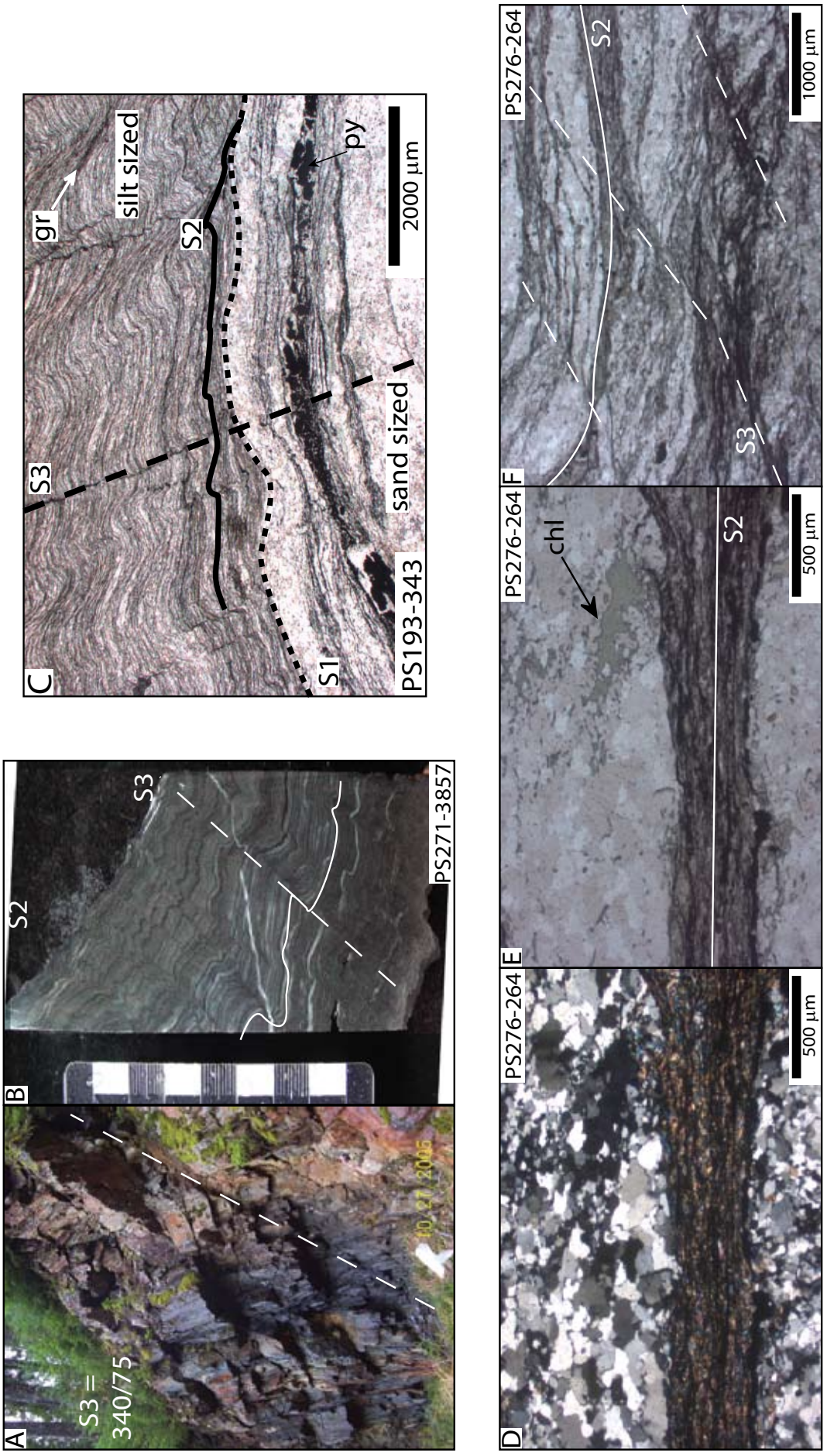
A
S3 = 340/75
B
S2
S3
PS271-3857
C
gr
silt sized
S2
py
2000 µm
S3
sand sized
S1
PS193-343
D
PS276-264
500 µm
E
PS276-264
chl
S2
500 µm
F
PS276-264
S2
S3
1000 µm

Figure 16 Representative photographs of the graphitic phyllite unit (C2a).
(A) Outcrop of the graphitic phyllite, sample PSA05-020. S3 is shown; S2 is not recognized at this location. Photograph taken looking northeast in Pit 174 (2479990E, 2287328N, mile 3.3 (km 5.3) on the B-road).

(B) Thinly laminated, alternating sand sized and silt sized layers. Both S2 and S3 are visible; generally S1 is only visible with a hand lens or in thin section. S2 is defined by spaced cleavage or compositional layers; S3 crenulates S2. A late stage, undeformed quartz vein can also be seen. Scale bar is in cm (2498116E, 22764457N, Upper Gallagher prospect, drill hole PS271 at 3857 feet (1168.8 m)).

(C) Photomicrograph (PPL) of foliation. S2 is at a very low angle to S1 and in hand sample the two often cannot be differentiated. S3 is at a high angle and deforms both S1 and S2. The sandy layer has coarse-grained recrystallized pyrite. (2495334E, 2286907N, West Bruin prospect, drill hole PS193 at 343 feet (103.9 m)).

(D&E) Photomicrographs (E – XPL and F- PPL) of layering. The metasiltstone layer is composed of graphite, sericite and quartz; metasandstone layers consists of quartz and minor chlorite. Only S2 is visible in this sample. (Ls6118, Xs4234, East ore zone, drill hole PS276 at 264 feet (80.0 m)).

(F) Photomicrographs (PPL) of S2 at 10° to compositional layering. S2 is heavily cross-cut by S3 with S3 dragging graphite and sericite into the foliation plane. Note the refraction of S3 as it passes though the sand sized layers. In quartz-poor material S3 is only visible as a differentiation cleavage. (Ls6118, Xs4234, East ore zone, drill hole PS276 at 264 feet (80.0 m)).

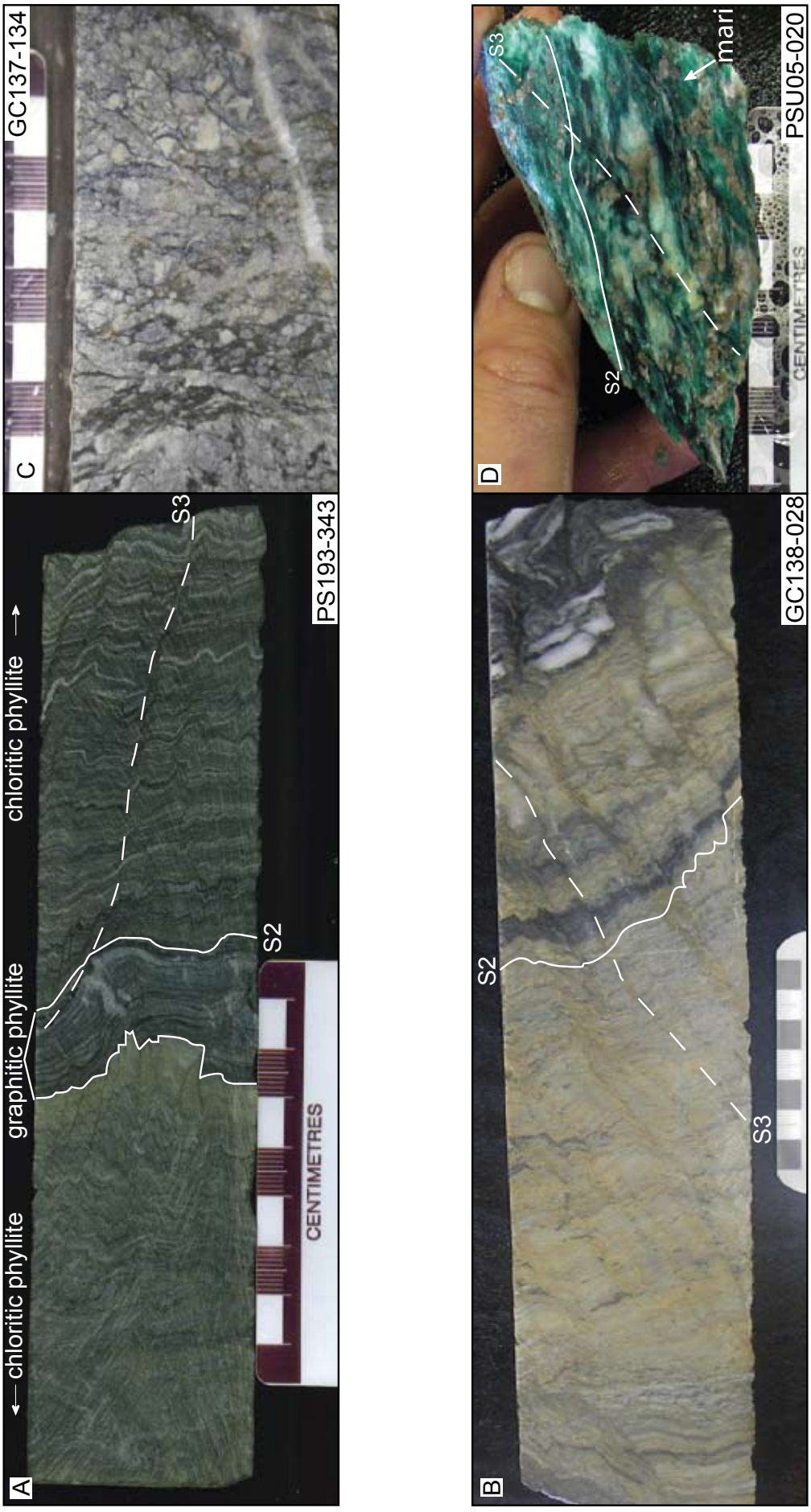
A
← chloritic phyllite
graphitic phyllite
chloritic phyllite →
S3
S2
PS193-343
CENTIMETRES
B
S2
S3
GC138-028
C
GC137-134
D
S3
S2
mari
PSU05-020
CENTIMETRES

Figure 17 Representative photographs of the fine-grained layered volcaniclastic unit (C2a).
(A) Example of fine-grained, thinly laminated rock with the darker layers primarily composed of chlorite and quartz with minor plagioclase and the lighter layers dominantly quartz with lesser sericite, quartz and carbonate. This is a type example of the chloritic phyllite unit. Note the approximately 2cm section of thinly laminated graphitic phyllite near the centre of the core. (2495334E, 2286907N, West Bruin prospect, drill hole PS193 at 343 feet (103.9 m)).

(B) Thinly laminated sericitic phyllite. This is a representative example of the most common lithology in the mine workings, sericitic phyllite. Note the graphitic layers towards the right side of the core. The individual layers are not as easily seen as in the above example. The sericitic phyllite probably represents altered feldspathic rocks. The tight crenulations of S2 by S3 are visible in the graphitic layers. Scale bar is in cm (Ls 6573, Xs1973, East ore zone, drill hole GC138 at 28 feet (8.5 m)).

(C) Granular, carbonate dominated rock. Typically, the rock retains a crude layering but it is not visible at the scale of this photograph. The scale bar is in cm (Ls 6582, Xs1981, East ore zone, drill hole GC137 at 134 feet (40.6 m)).

(D) Crudely layered, mariposite-rich (mari) rock with quartz and coarse-grained recrystallized pyrite. S2 and S3 are weak. This sample has an anomalously high abundance of mariposite (>5). (Gallagher cross-cut, drift 4211).

abundance, size and character of the secondary minerals – chlorite, sericite, carbonate, quartz and pyrite vary primarily with distance from the mine contact and are related to alteration. This is discussed in Chapter 6.

Where large plagioclase crystals (>100 μm) have visible twinning, the margins of the crystals are embayed and altered by either sericite or carbonate. Due to the compositional and grain size variation between the layers, the laminated texture, the small grain size and the presence of rare chlorite altered pumice fragments, this unit is interpreted to be volcaniclastic in origin. However, due to extreme deformation and alteration the dominant layering could be a result of almost any volcano-sedimentary process.

C2b - siliceous rock

The siliceous rock lithology is composed of over 80% quartz and has a massive to pseudo-breccia texture (Figure 18A-C). The lithology is light to medium grey and can have broadly spaced foliations (Figure 18C). The monomict pseudo-breccias (C2b) are poorly sorted, sand to boulder sized, can have jigsaw fit textures, are generally of the same lithology as the surrounding rocks and, in places, grade into undisturbed units of the same lithology (Figure 18A&B). Where the pseudo-breccia texture is present, the margins of the pseudo-fragments are defined by a mineral assemblage of pyrite + sericite + quartz (Figure 18D&E). The pseudo-fragments themselves are primarily very fine-grained quartz with minor sericite and some contain small, euhedral barite laths.

Previous studies have grouped the monomict and polymict breccia (Tr1) lithologies (Scherkenbach, 1983; Freitag, 2000). The present study separates the two and interprets the monomict breccia as extremely altered C2. This lithology is generally found near the mine contact and can reach over 100 feet (30 m) in thickness (Scherkenbach, 1983). This lithology is interpreted as an alteration facies and is discussed further in Chapter 6.

Triassic volcanic and sedimentary lithologies (Tr1-4)

Tr1 - polymict breccias

There are two types of breccia recognized at Greens Creek: monomict and polymict (Scherkenbach, 1983; West and Proffett, 2003). The monomict breccia lithology is interpreted as footwall lithology C2b and was discussed with those rocks. The polymict breccias (Tr1) are poorly sorted, silt to pebble sized and have several different clast types (Figure 19A-D). Clast types, in order of decreasing abundance, are: (1) light grey clasts with sand sized quartz grains, (2) dark grey to black silt sized quartz grains with graphite and sericite, (3) light to dark green chlorite -rich clasts and rarely (4) bright green, clasts with visible mariposite. All of these clast types appear to be locally derived as they match pre-mineralization lithologies and are sub-angular to angular in less deformed samples. These breccia units are found in elongate exposures or lenses and are thought to represent clastic wedges that have developed along a fault scarp (Scherkenbach, 1983; Duke et al., in press;). Regionally, the polymict breccia is interpreted as the base of the Late Triassic Hyd Formation (Taylor et al., 2008).

Tr2 - mineralized lithologies

The ore at Greens Creek can be broadly separated into black (sulfide) ores and white ores. The black ores are characterized by greater than 50% fine to very fine-grained base-metal sulfides and/or pyrite content and include massive base-metal ore and massive pyrite ore (Frietag, 2000). The white ores have less than 50% semi-massive to disseminated sulfides (pyrite, sphalerite, galena, chalcopyrite, arsenopyrite), are often enriched in precious-metal-rich minerals (pyrargyrite, acanthite, other Pb-Sb-As-(Hg-Tl) sulfosalts, electrum, gold) and include carbonate ore, baritic ore and siliceous ore (Petersen, 1991; Frietag, 2000).

Massive base-metal ore

This ore type contains at least 50% sulfides with base-metal sulfides greater than total pyrite (Figure 20A). The ore is further subdivided by grain size into fine-grained (MFB)

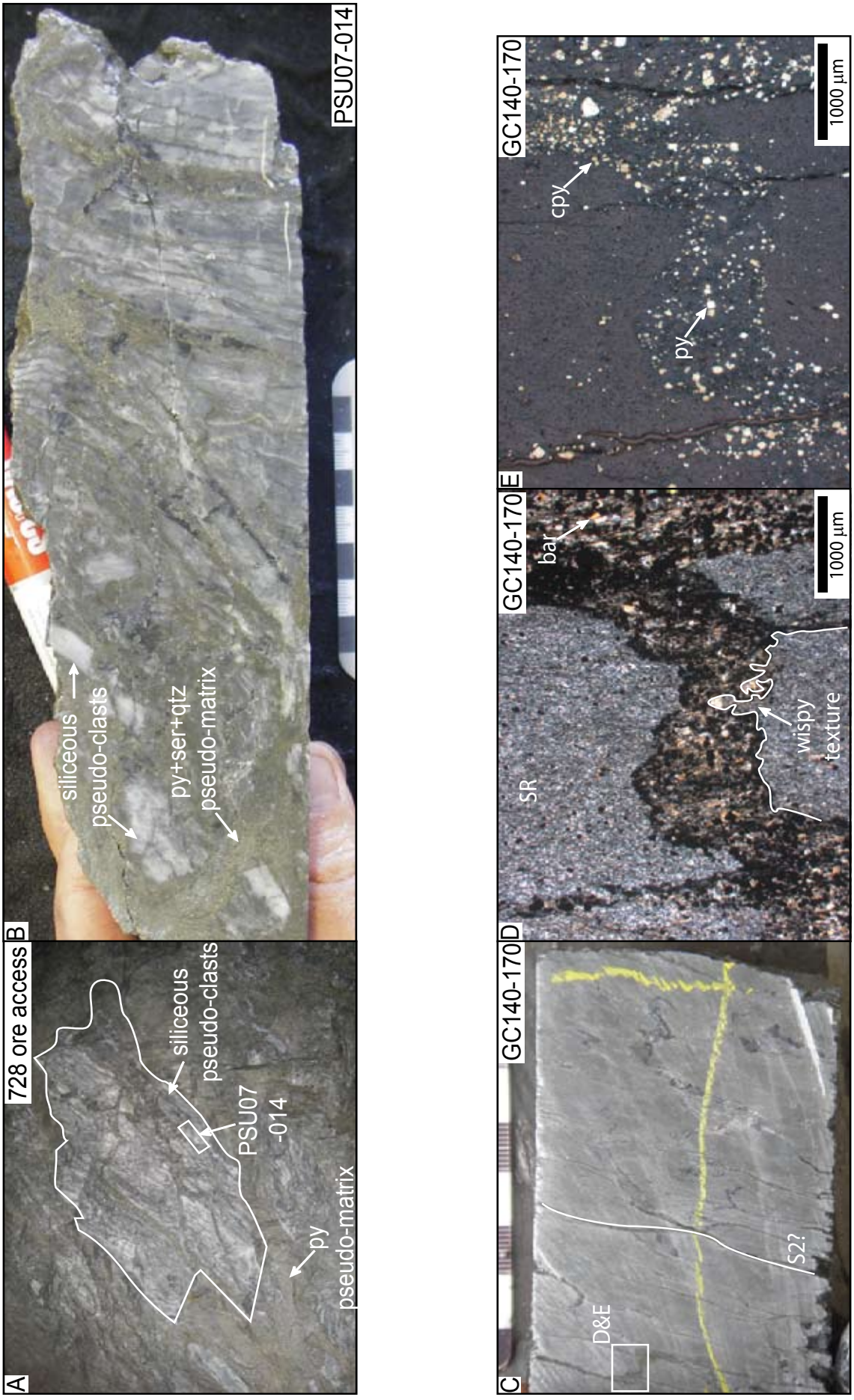
A
728 ore access
siliceous
pseudo-clasts
PSU07
-014
py
pseudo-matrix
B
PSU07-014
siliceous
pseudo-clasts
py+ser+qtz
pseudo-matrix
C
GC140-170
D&E
S2?
D
GC140-170
SR
bar
wispy
texture
1000 µm
E
GC140-170
cpy
py
1000 µm

Figure 18 Representative photographs of the siliceous rock unit (C2b).
(A) Monomict, jigsaw fit, poorly sorted, pebble to boulder pseudo-breccia. Pseudo-clasts are light grey to white, weakly layered, highly siliceous and surrounded by a pyrite (py) dominated matrix. This pseudo-clastic texture is similar to that seen in the siliceous rock unit but the pyrite and quartz alteration is much more intense. Due to the inherent variability of S2 in the layered volcanic rocks, it is not possible to determine if the slight difference in orientation of the layering between the pseudo-clasts is caused by D2 or D3 deformation or if these are true clasts that have been rotated with respect to each other. Field of view is approximately 5 feet (~2 m) (Ls4685, Xs5035, Northwest West ore zone, 728 ore access).

(B) Monomict, jigsaw fit, clast supported, poorly sorted, pebble pseudo-breccia. Pseudo-clasts are light grey to white as well as dark grey and are quartz dominated. The pseudo-matrix is dominantly fine-grained pyrite with sericite (ser) and quartz (qtz). Scale bar is in cm (Ls4685, Xs5035, Northwest West ore zone, 728 ore access).

(C) Massive, siliceous rock with weak pseudo-breccia texture. The mineralogy is dominantly quartz with minor sericite, barite. The pseudo-breccia fragments are defined by an increase in sulfide minerals and barite along fractures. The sulfide minerals are dominantly sphalerite with lesser pyrite. The white box marks the location of photomicrographs C&D. (Ls6600, Xs1985, East ore zone, drill hole GC140 at 170 feet (51.5 m)).

(D&E) Photomicrographs (D – XPL and E- RL) of typical pseudo-breccia texture. The very fine-grained siliceous rock (SR) makes up the pseudo-fragments while the pseudo-matrix is composed of barite (bar) and sulfide minerals. The delicate wispy textures are interpreted as the result of alteration along fractures as opposed to alteration of matrix between fragments. (Ls6600, Xs1985, East ore zone, drill hole GC140 at 170 feet (51.5 m))

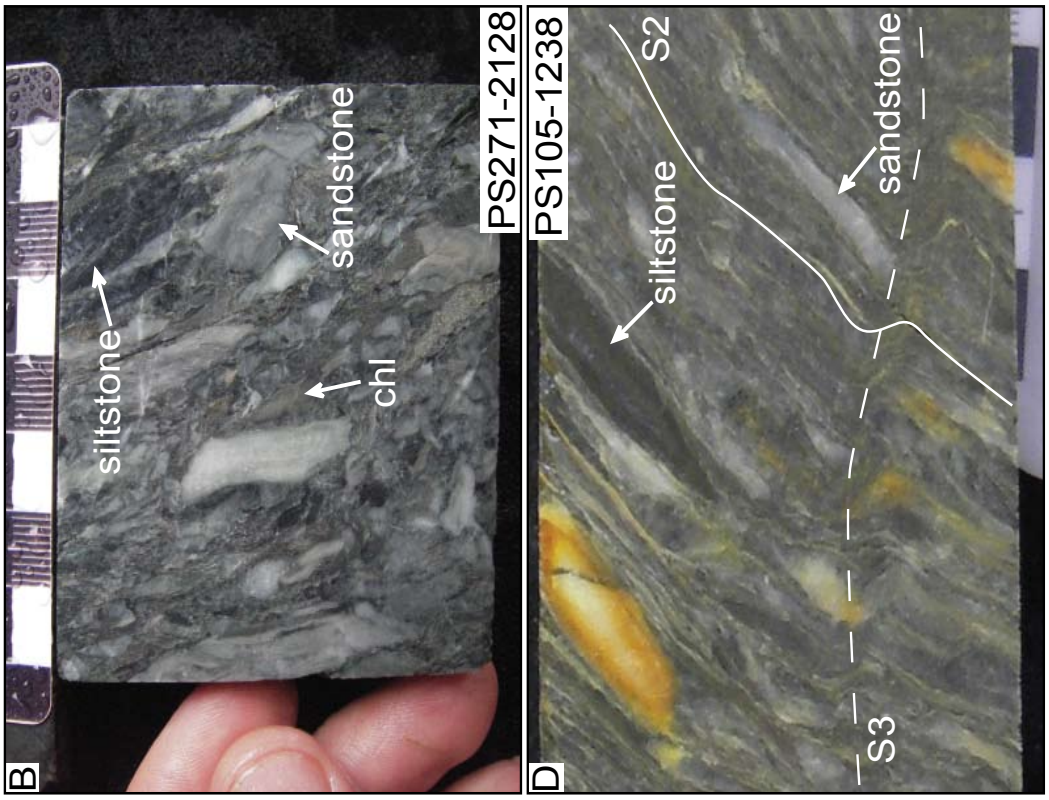
B
siltstone
sandstone
chl
PS271-2128
D
PS105-1238
S2
siltstone
sandstone
S3

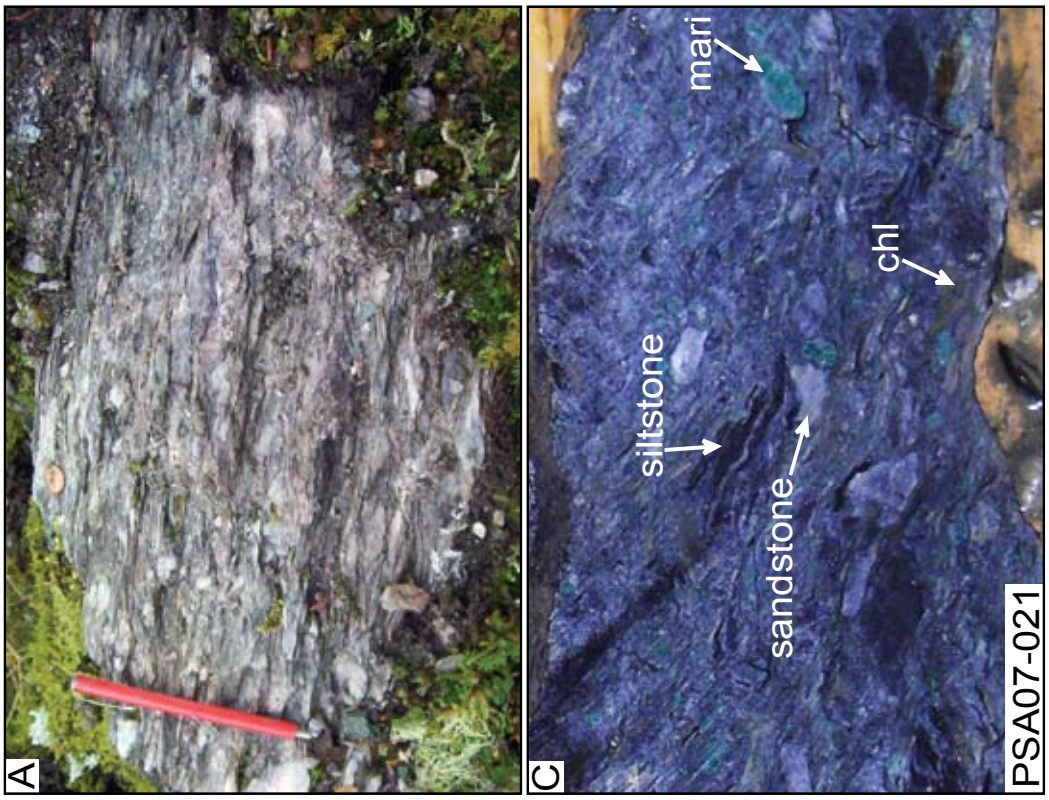
A
C
mari
chl
siltstone
sandstone
PSA07-021

Figure 19 Representative photographs of the breccia units (Tr1).
(A) Outcrop of foliated, polymict, pebble breccia. Magnet is 12 cm long (Young Bay)

(B) Polymict, matrix supported pebble breccia. Chl = chlorite-rich (chloritic phyllite or greenstone). Scale bar is in cm (2498116E, 2276445N, Upper Gallagher prospect, drill hole PS271 at 2128 feet (644.8 m)).

(C) Polymict, matrix supported pebble breccia. Clast types include graphitic phyllite, chlorite-rich and mariposite-rich (mari - mariposite phyllite or possibly ultramafic clast). Scale bar is in cm (2481038E, 2289312N, Lower Zinc Creek prospect).

(D) Polymict, matrix supported pebble breccia. Clasts are elongate and flattened in S2. S3 is weakly developed. Only two clast types are visible in this sample, siltstone and sandstone clasts which could both be clasts of graphitic phyllite. Scale bar is in cm (Ls4584, Xs4732, Northwest West ore zone, drill hole PS105 at 1238 feet (375.2 m)).

and very fine-grained (MVB). Very fine-grained base-metal ores typically have sulfide grains smaller than can be distinguished with the naked eye (Taylor et al., in press-a). These ore types are medium to dark grey to blue-grey (Taylor et al., in press-a). The gangue minerals of this ore type are quartz, carbonate, sericite, fuchsite and barite (Taylor et al., in press-a).

Massive pyrite ore

Massive pyritic ore is at least 50% sulfides with pyrite being the dominant sulfide (Figure 20B). This ore type is also subdivided into massive fine-grained (MFP) and very fine-grained (MVP) divisions. The color of these ores is typically bronze to metallic brown (Frietag, 2000; Taylor et al., in press-a). Gangue minerals include pyrite, quartz, carbonate, fuchsite and barite (Taylor et al., in press-a).

White carbonate ore

The white carbonate ore is made up of less than 50% sulfides (Figure 20C). This ore type has abundant silver sulfosalt minerals and gold. It has medium- to coarse-grained sulfides and the silver sulfosalt minerals commonly occur in veins or vugs (Frietag, 2000). The dominant gangue mineral is Fe-rich to Fe-poor dolomite (Frietag, 2000) with minor amounts of the same gangue mineralogy as seen in the black ores (Taylor et al., in press-a).

White baritic ore

Baritic ore contains less than 50% sulfides and typically has medium- to coarse-grained sulfides that partly occur in veins. In rare cases there are abundant silver sulfosalt minerals and gold (Frietag, 2000). The dominant gangue is coarse-grained barite (Figure 20D); often this ore type is low grade (Taylor et al., in press-a).

White Siliceous ore

Siliceous ore has less than 50% sulfides, typically has abundant silver sulfosalt minerals and gold. The sulfides are medium- to coarse-grained and can occur in veins (Frietag,

2000). The gangue is dominated by fine-grained quartz or chert and contains significant dolomite, sericite, fuchsite and barite (Taylor et al., in press-a).

Tr3 - siliciclastic rocks

Massive argillite

The massive argillite unit is made up of discrete 4 inch (10 cm) to 6 feet (2 m) thick beds of dark grey to black dolomicrite (Fulton et al., 2003) interbedded with lesser siliciclastic mudstone (Figure 20E). There are rare graded beds of siliciclastic material throughout the unit. Massive argillite mineralogy is dominantly dolomite and quartz with variable organic matter and minor pyrite, apatite, calcite, chlorite, cymrite and paragonite. Some beds of the massive argillite unit contain crinoid stems and several samples from the unit have yielded conodont fossils that indicate a Carnian (Late Triassic) depositional age (Taylor et al., 1999). Samples from the massive argillites have nodular carbonate that has been interpreted as having an evaporitic origin (Fulton et al., 2003). The massive argillite unit is more common towards the base of the stratigraphic hanging wall and often sits directly above the ‘mine contact’ (Fulton et al., 2003).

Slatey argillite

The slatey argillite unit is a black phyllitic rock that is typically strongly foliated, pyritic, organic-rich and dark grey to black in color (Fulton et al., 2003) (Figure 20F). The mineralogy is dominantly quartz, calcite, dolomite and muscovite with lesser pyrite and organic matter and minor apatite, chlorite, albite, paragonite, cymrite and rutile (Fulton et al., 2003). Slatey argillite is typically interbedded with the massive argillite unit in the lower portion of the stratigraphic hanging wall and is the dominant unit higher in the hanging wall stratigraphy (Fulton et al., 2003).

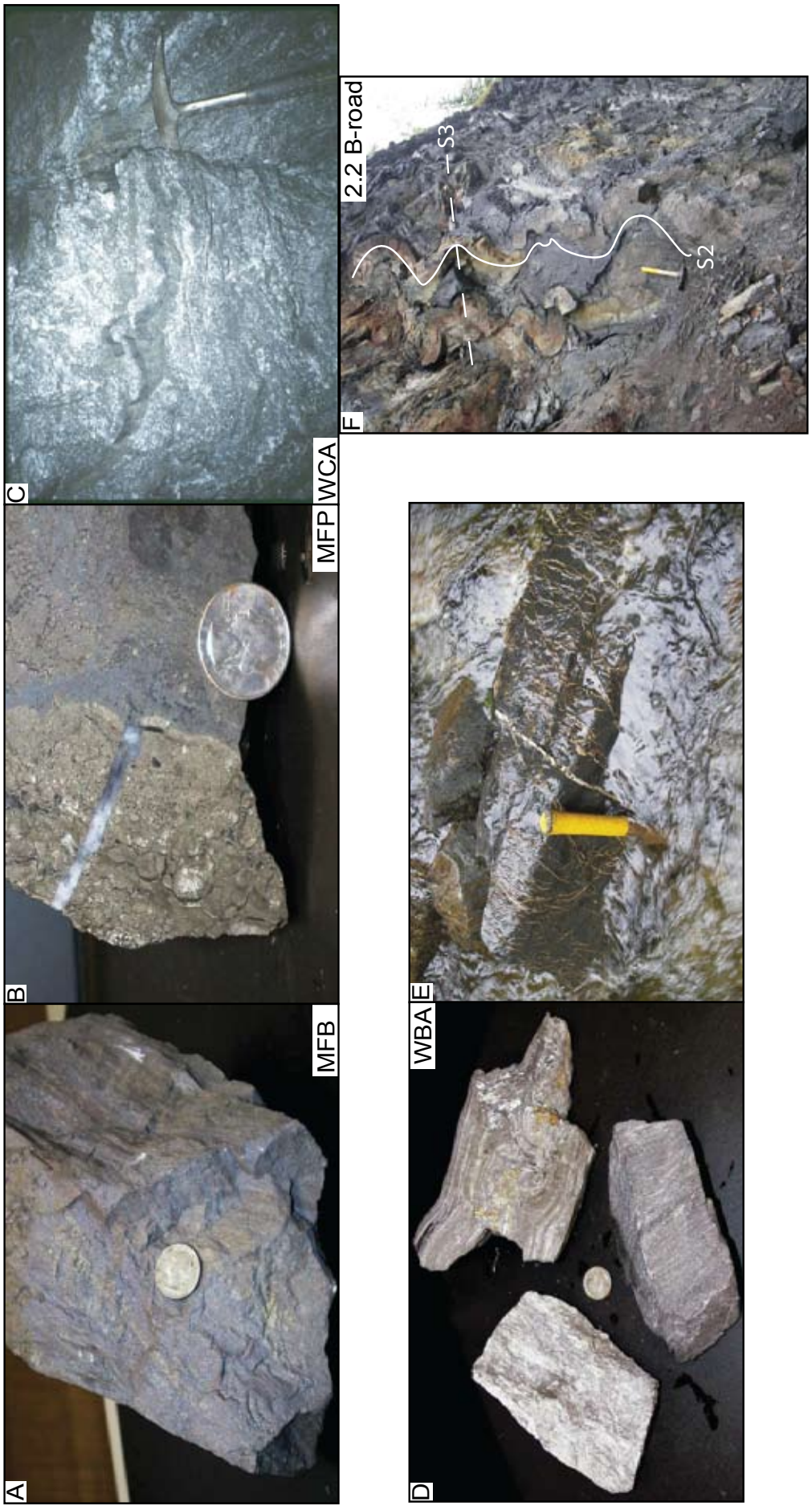
A
MFB
B
MFP
C
WCA
D
WBA
E
F
2.2 B-road
S3
S2

Figure 20 Representative photographs of the ore and argillite units (Tr2&3).
(A) Massive fine-grained base metal ore (MFB) dominant ore minerals are galena and sphalerite. Coin is approximately 1.8 cm. Photograph courtesy of A. West Greens Creek Mining Co.

(B) Massive fine-grained pyritic ore (MFP) dominant sulfide mineral is pyrite. Coin is approximately 1.8 cm. Photograph courtesy of A. West Greens Creek Mining Co.

(C) Underground exposure of white carbonate ore (WCA) dominant gangue mineral is carbonate. Hammer is 30 cm long. Photograph courtesy of A. West Greens Creek Mining Co.

(D) White baritic ore (WBA) dominant gangue mineral is barite. Photograph courtesy of A. West Greens Creek Mining Co. Coin is approximately 1.8 cm.

(E) Creek bed outcrop of massive argillite. Note the characteristic quartz + carbonate ladder/lightning veins cross cutting massive black argillite. Yellow handle is 18 cm long (Lower Zinc Creek prospect).

(F) Type example of near vertical cascading F2 folds with open F3 folds in argillite. Hammer is 45 cm long (mile 2.5 (km 4.0) on the B-road).

Tr4 - coherent volcanic rocks

Gallagher rhyolite

The following description for the Gallagher rhyolite is summarized from Proffett (2005; 2007). This lithology has only been identified on Gallagher Ridge, south of the mine and has not been recognized in any drill holes (Figure 21A&B). The rhyolite is typically hard and siliceous and has a weak S2 foliation. The rhyolite is dominantly fine-grained and contains several percent rounded to rectangular-shaped feldspar phenocrysts up to several millimeters in size. The groundmass contains fine-grained quartz and minor sericite with small amounts of fine-grained biotite occurring in both the groundmass and replacing mafic phenocryst sites (Figure 21C&D). In thin section, the rock contains moderately abundant plagioclase, rare quartz phenocrysts and altered mafic phenocrysts in a very fine-grained felsic groundmass. Plagioclase phenocrysts have been partially altered to sericite (Figure 21E) and/or altered to secondary K-feldspar. Quartz phenocrysts are partially resorbed and mafic phenocrysts are altered to a mixture of sericite, carbonate, minor chlorite and leucoxene. Dense clusters of leucoxene commonly pseudomorph subhedral magnetite. Small zircon crystals are present and many of these are euhedral short prisms with square cross sections that are clean and unaltered with no evidence of older, inherited cores.

The main part of the rhyolite unit is massive and several tens of feet (~10 m) thick. Below the main unit, rhyolitic rocks occur in thin layers consisting of rhyolite fragments in a rhyolitic matrix which are interlayered with brecciated basalt. The main unit of rhyolite is interpreted to be a coherent flow or dome and the breccias to be autoclastic or volcaniclastic in nature.

Hyd basalt

The basalt member of the Hyd Formation is a metabasalt that is flow dominated and commonly amygdaloidal (Taylor et al., 2008). It is typically less altered than the footwall greenstone. In many locations, volcanic textures such as pillows and autoclastic

breccia are recognizable (Figure 22A). The phenocryst mineralogy is dominantly plagioclase with lesser chlorite and biotite pseudomorphs of mafic phenocrysts for which the mineralogy cannot be determined. The ground mass is typically fine-grained plagioclase with chlorite and biotite. Interlayered within the metabasalt are minor beds, pods and fragments of limestone. In the field, this lithology can resemble the footwall greenstone (C1) but in thin sections, these hanging wall basalts have fine to coarse-grained biotite which is not seen in the footwall greenstones. This unit is the uppermost member of the Hyd Formation and is found regionally throughout the Alexander Terrane though locally it is only found south of the mine property.

Lil' Sore dacite

This lithology has only been identified in the Lil' Sore area and is exposed at surface at Lil' Sore pad #3. The present study investigated this unit on the ground as well as in diamond drill hole PS232. The dacite is typically siliceous with weak S2 foliation. It is dominantly fine-grained and with rare to common millimeter-sized feldspar phenocrysts. The groundmass is very fine-grained with sericite, plagioclase and quartz and is light grey to light brown. The plagioclase phenocrysts have been weakly to moderately sericite altered. The rock varies from coherent, massive sections with between 10 feet (3 m) and 100 feet (30 m) of drilled thickness, to dacitic breccia fragments in a dacite matrix with volcanic textures such as perlite and jigsaw fit breccias with drilled thicknesses of up to 150 feet (45 m) (Figure 22B-D). It is interpreted that this lithology is found in several coherent dacitic domes with autoclastic carapaces.

Triassic intrusive lithologies (I1-3)

I1 - quartz-carbonate-mariposite

The quartz-carbonate-mariposite (QCM) lithology is hard, massive, has extensive networks of synkinematic fibrous quartz-carbonate veining and is generally medium-grey with a slight purple or green tinge (Figure 23A&B). This unit is composed primarily of quartz, ankerite and mariposite with minor plagioclase and rarely contains

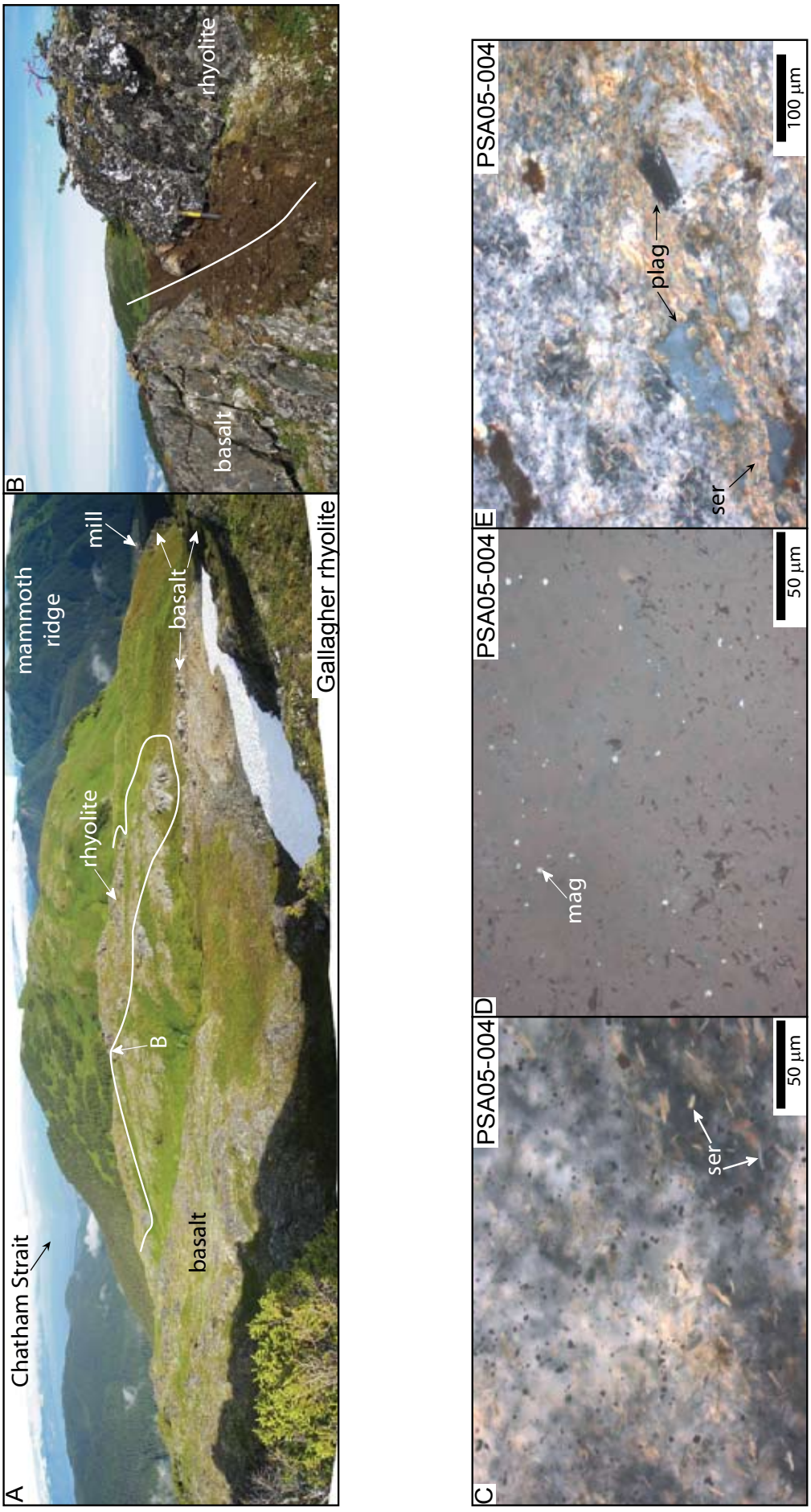
A
Chatham Strait
basalt
rhyolite
B
mammoth ridge
mill
basalt
Gallagher rhyolite
B
basalt
rhyolite
C
PSA05-004
ser
50 µm
D
PSA05-004
mag
50 µm
E
PSA05-004
plag
ser
100 µm

Figure 21 Representative photographs of the rhyolite unit (Tr4).
(A) Western most outcrop of rhyolite on Gallagher ridge. Photograph is taken looking northwest along the length of Gallagher Ridge. Note the location of photograph B. (2495807E, 2275532N, Gallagher Ridge).

(B) Close up of the rhyolite – basalt contact. Rhyolite is more siliceous and appears to conformably overlie the basalt. Hammer is 30 cm long (2495807E, 2275532N, Gallagher ridge).

(C&D) Photomicrograph (C-XPL and D-RL) of very fine-grained felsic groundmass with sericite (ser) and magnetite (mag) throughout. (2495807E, 2275532N, Gallagher Ridge)

(E) Photomicrograph (XPL) of a plagioclase phenocrysts (plag) moderately sericite altered. Groundmass is very fine-grained felsic material with disseminated magnetite. (2495807E, 2275532N, Gallagher Ridge)

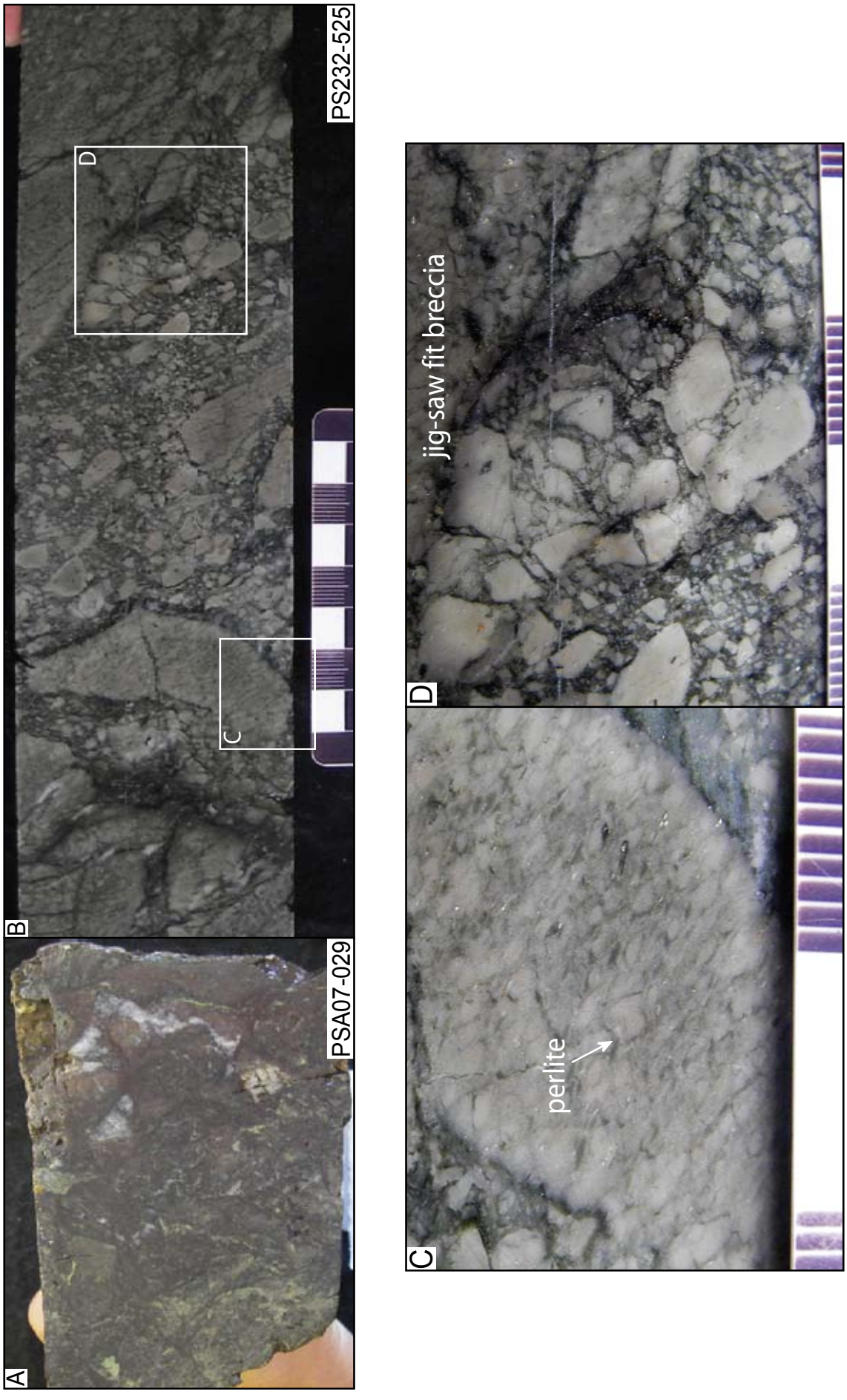
A
PSA07-029
B
PS232-525
C
D
C
perlite
D
jig-saw fit breccia

Figure 22 Representative photographs of the dacite and basalt units (Tr4).
(A) Monomictic pebble breccia of basaltic fragments in a basaltic matrix. This sample is interpreted as an autoclastic breccia, possibly a flow breccia. Note two basaltic clasts highlighted. Sample is 15 cm across (2499050E, 2275100N, south Gallagher Ridge).

(B) Light grey, siliceous monomictic breccia with dacitic fragments in dacitic matrix. Note the location of photographs F & G. Scale bar is in cm (2486321E, 2298855N, Lil' Sore prospect, drill hole PS232 at 525 feet (159.1 m)).

(C) Close up of breccia fragment with perlitic textures. Scale bar is in cm (2486321E, 2298855N, Lil' Sore prospect, drill hole PS232 at 525 feet (159.1 m)).

(D) Close up of breccia fragment with jigsaw fit textures. Scale bar is in cm (2486321E, 2298855N, Lil' Sore prospect, drill hole PS232 at 525 feet (159.1 m)).

kammererite (West and Proffett, 2003). The grain size of the carbonates is between 100 μm and 500 μm, while the quartz grains are typically ≤100 μm (Figure 23C). The plagioclase grains are typically carbonate altered (Figure 23D). The vein networks are fibrous quartz-carbonate that cross-cut the groundmass (Figure 23E). Late-stage quartz veins cross-cut all features including the fibrous quartz-carbonate veins. In diamond drill core and exposures in the underground workings, this lithology is typically less than 20 feet (7 m) thick with elongate map patterns (Figure 24) and is found discontinuously throughout the footwall. It has not been recognized in the hanging wall sequence. The QCM lithology is folded by F2 and F3 and its relationship to F1 is not known. Based on its geometry, irregular distribution and presence of plagioclase phenocrysts, this lithology is interpreted as sub-volcanic sills or dikes (Freitag, 2000; this study). As these rocks are highly altered and have not been recognized within the hanging wall sequence, they are interpreted to be pre-mineralization in age and are the oldest intrusive rock type recognized at Greens Creek.

I2 - serpentinite

The serpentinite lithology, referred to as serpentinite at the mine, is a soft rock that is dark green (Figure 25A&B). The mineralogy is dominantly serpentine with less chlorite, mariposite, carbonate, talc and quartz (Figure 25C-F); remnant magnetite grains with talc halos are common throughout (Figure 25D&E). This unit is generally massive with the edges of the serpentinite bodies often highly foliated. The thickness and spatial location of the serpentinite rocks varies considerably but generally this rock type is more abundant in the lower portions of the footwall (Scherkenbach, 1983; Frietag, 2000) and near major structures. Due to the presence of magmatic minerals such as magnetite, the presence and distribution of several large bodies (km^2) that in a few locations have chilled margins, it is interpreted that the serpentinite unit was, at least partially, magmatically emplaced. However, the serpentinite unit in the mine workings is generally associated with major structures (i.e. Klaus Shear, Upper Shear Zone and the Maki Fault) and, locally, the present texture and geometry reflects deformation, not emplacement.

I3 - microgabbro

The gabbroic rocks found at Greens Creek are weakly layered to massive, have a granular texture and subhedral plagioclase grains visible to the naked eye (Figure 26A&B). The phenocryst assemblage is plagioclase, clinopyroxene and hematite within a groundmass of plagioclase, chlorite, biotite and minor quartz. Both the phenocrysts and the groundmass are moderately to completely chlorite or biotite altered (Figure 26C-E). The grain size of the phenocrysts ranges from 1 mm to 5 mm, and are therefore microgabbros. The microgabbros commonly have chilled margin contacts and typically have elongate map patterns. In hand sample, the finest grained examples of the microgabbro appear very similar to the greenstone unit (C1). However, in thin section the microgabbros have fine-grained biotite which is not seen in the greenstone. Based on the geometries of the microgabbro bodies and the chilled margin contacts, the microgabbros are interpreted as sills and dikes (Taylor et al., 2008; this study). The sills vary in thickness.

Post-Triassic lithologies (J1&2, I4)

J1&2 - Seymour Canal Formation

J1 - siltstone

Post-Triassic siltstones are only recognized in Young Bay, approximately 300 feet (100 m) west of the basalt described below, near the west end of the parking lot. The sericitic siltstones are phyllitic beds up to 1 m thick. The mineralogy is primarily quartz and sericite with minor chlorite. Only one cleavage is visible. This cleavage is strong, parallel to bedding and dips steeply to the east. Regionally, these siltstones are mapped as part of the Seymour Canal Formation (Lathram et al., 1965). Abundant small zircons were identified in this sample and the results of the U-Pb dating of these zircons are discussed in Chapter 5.

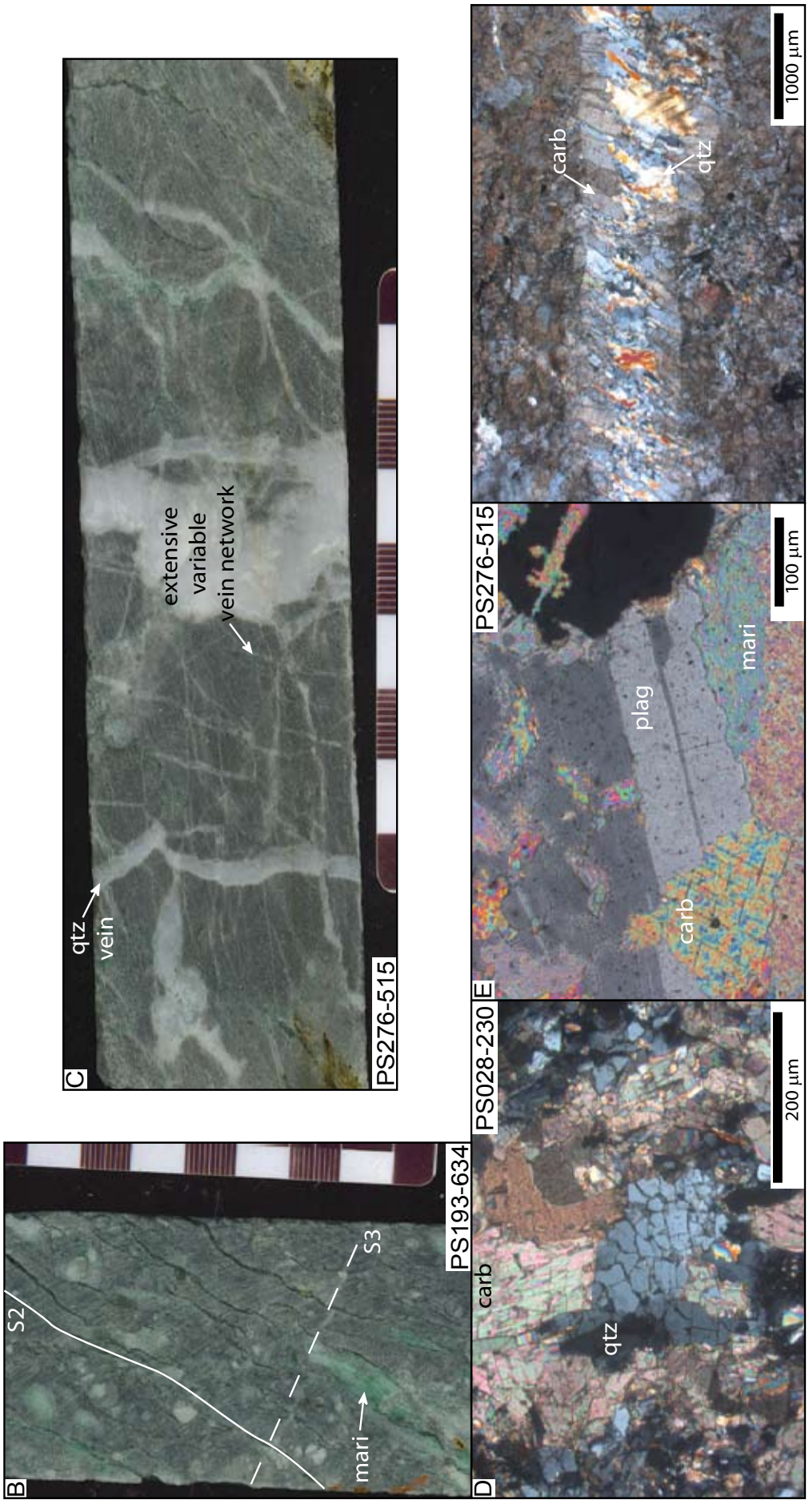
B
S2
S3
mari
PS193-634
C
qtz
vein
extensive
variable
vein network
PS276-515
D
carb
qtz
PS028-230
200 µm
E
PS276-515
plag
carb
mari
100 µm
carb
qtz
1000 µm

Figure 23 Representative photographs of the quartz + carbonate + mariposite (QCM) unit (I1).
(A) Crudely foliated, massive quartz + carbonate + mariposite sample with granular texture. Weak S2 foliation mineral is dominantly mariposite. Scale bar is in cm (2495334E, 2286907N, West Bruin prospect, drill hole PS193 at 634 feet (192.1 m)).

(B) Extensive variable vein network of quartz + carbonate + mariposite. QCM is slightly granular, massive and cross-cut by distinctive quartz + carbonate ladder/ lightning veins. Also present are several later stage quartz veins that cross-cut the smaller ladder/lightning quartz + carbonate veins. Mariposite is throughout the rock as well as along quartz + carbonate veins. Scale bar is in cm (Ls6118, Xs4234, East ore zone, drill hole PS276 at 515 feet (156.1 m)).

(C) Photomicrograph (XPL) of medium-grained quartz (qtz) and carbonate (carb) with jigsaw fit breccia textures. Sample is located within the lower portion of the Upper Shear Zone and this shearing may be responsible for the brecciated texture of the grains. (Ls6823, Xs2008, East ore zone, drill hole PS028 at 230 feet (69.7 m))

(D) Photomicrograph (XPL) of plagioclase grain (plag) with multiple twins, altered by carbonate (carb) and mariposite (mari). (Ls6118, Xs4234, East ore zone, drill hole PS276 at 515 feet (156.1 m)).

(E) Photomicrograph (XPL) of a fibrous quartz + carbonate vein. The carbonate is along the margin while the quartz makes up the core of the vein. The rock being cut by the vein is fine-grained carbonate with minor quartz. (Ls6823, Xs2008, East ore zone, drill hole PS028 at 230 feet (69.7 m))

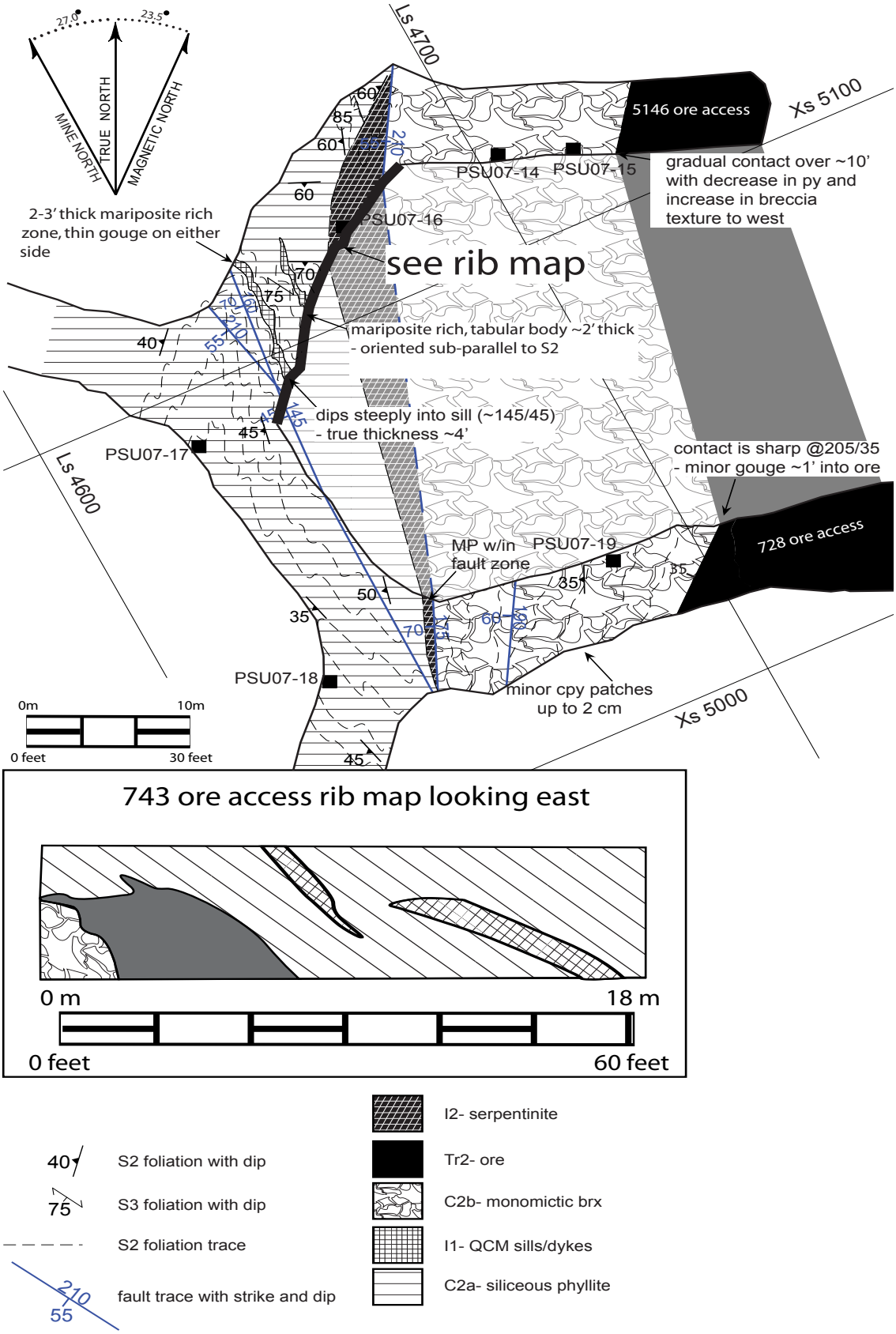

Figure 24 Underground mapping of 743 and 728 ore accesses in the Northwest West ore zone. Mapping is chest height plan projection. The monomictic breccia consists of cobble- to boulder-sized fragments that are light grey to white and are very siliceous, weakly layered clasts within a pyrite and chalcopyrite matrix. Quartz + carbonate + mariposite (QCM) unit is intruded into quartz + pyrite + sericite altered layered volcaniclastic rocks, sub-parallel to S2.

J2 - basalt

These basalts are light green, fine- to medium-grained, massive volcanic flows that are visually distinct from the Retreat greenstone and Hyd basalt. They are interlayered with limestone beds up to 1 m thick, dip steeply to the east and are not as complexly folded as the Triassic and older strata (Figure 27A). Young Bay is the only location these rocks were observed and only one sample was collected. Regionally these rocks are thought to be part of the Seymour Canal Formation that is found along the eastern margin of Admiralty Island (Lathram et al., 1965). In thin section the sample is made up of plagioclase crystals and chloritic masses up to 1 mm in size within a ground mass of plagioclase, prehnite and chlorite (Figure 27B). The plagioclase crystals are anhedral to subhedral and in places are cross-cut by radiating prehnite crystals. The chloritic masses are anhedral with irregular grain boundaries. The limestone interbeds indicate a submarine depositional setting for these basalts.

I4 - diabase dikes

These dikes are massive and unaltered with fine- to coarse-grained plagioclase phenocrysts and fine-grained disseminated magnetite and hematite (Figure 27C). The dikes are up to ten feet (3 m) thick and have chilled margins. They have only been recognized in the underground workings in the 4211 drift and on the surface in the Gallagher bowl (Xs2500, Ls2100). They cross-cut all foliations and appear to be offset by the youngest strike-slip faulting. As the dikes post-date the ductile deformation of the Greens Creek deposit and are offset by the youngest brittle deformation they have been used to estimate a dextral displacement of 2750 feet (830 m) on the Gallagher Fault (Proffett, 2004a).

Geometry and distribution of lithologies

Property-scale geometry and distribution of lithologies

Figure 28 is a map of the surface geology on the Greens Creek property and surrounding area with key locations labeled. The mine property lies at the northern end of Admiralty

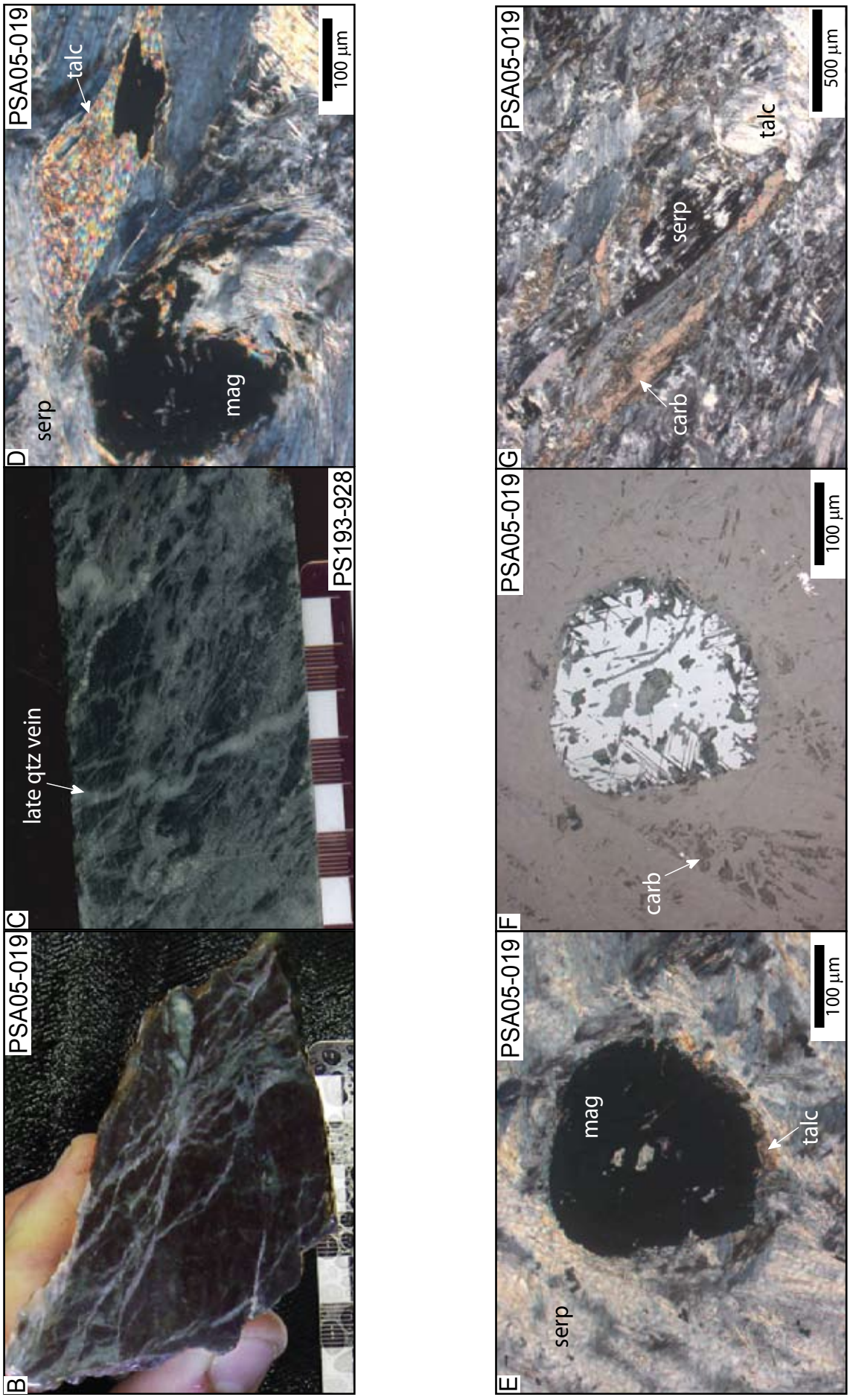
B
PSA05-019
C
late qtz vein
PS193-928
D
PSA05-019
talc
serp
mag
100 µm
E
PSA05-019
mag
talc
serp
100 µm
F
PSA05-019
carb
100 µm
G
PSA05-019
serp
talc
carb
500 µm

Figure 25 Representative photographs of the serpentinite lithology (I2).
(A) Massive dark-green to black serpentine + chlorite rock with thin talc shears throughout. Scale bar is in cm (2478282E, 2294570N, approximately mile 1.9 on the B-road).

(B) Altered serpentine + chlorite rock with carbonate and talc throughout. A late-stage quartz vein can be seen cutting across the middle of the core. (2495334E, 2286907N, West Bruin prospect, drill hole PS193 at 924 feet)

(C) Photomicrograph (XPL) of typical serpentine and talc mineralogy with remnant magnetite (mag) grains with talc strain shadows. (2478282E, 2294570N, approximately mile 1.9 on the B-road)

(D&E) Photomicrographs (D – XPL and E- RL) of 300 μm chromite grain surrounded by a very thin talc halo within serpentine groundmass. Small carbonate grains are visible in the RL image. (2478282E, 2294570N, approximately mile 1.9 on the B-road)

(F) Photomicrographs (XPL) of typical serpentine, carbonate and talc mineralogy and textures. (2478282E, 2294570N, approximately mile 1.9 on the B-road)

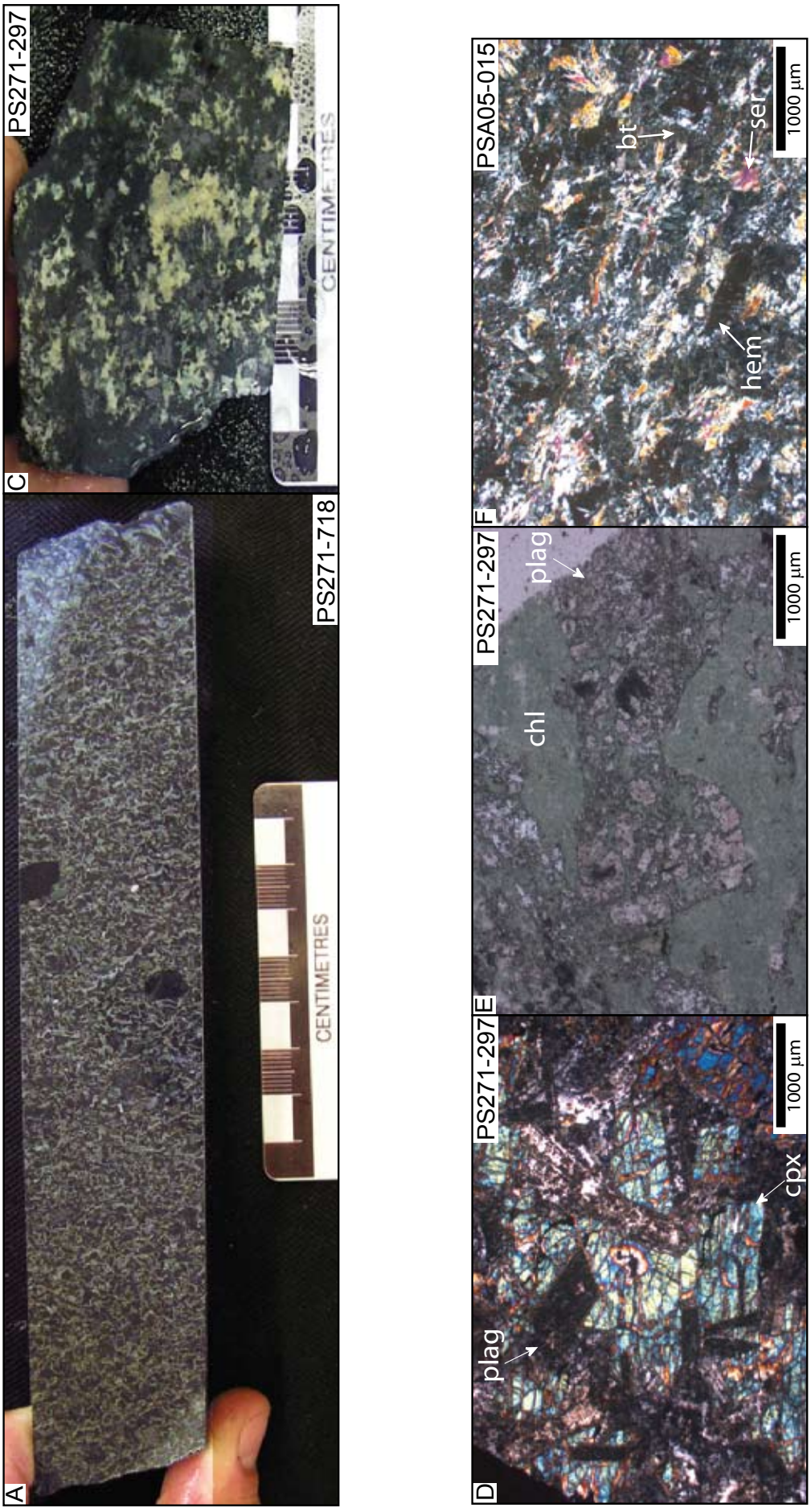
A
PS271-718
CENTIMETRES
C
PS271-297
CENTIMETRES
D
PS271-297
plag
cpx
1000 µm
E
PS271-297
plag
chl
1000 µm
F
PSA05-015
bt
ser
hem
1000 µm

Figure 26 Representative photographs of the microgabbro lithology (I3).
(A) Crudely foliated fine-grained microgabbro. Scale bar is in cm (2498116E, 2276445N, Upper Gallagher prospect, drill hole PS271 at 718 feet).

(B) Fine to medium-grained microgabbro. Mineralogy is 1-5 mm plagioclase laths, intergrown with coarse-grained clinopyroxene (cpx) and hematite in a fine-grained groundmass of plagioclase, chlorite and hematite. This is the coarsest grained sample of microgabbro on the Greens Creek property. Scale bar is in cm (2498116E, 2276445N, Upper Gallagher prospect, drill hole PS271 at 297 feet).

(C) Photomicrograph (XPL) of medium-grained, intergrown plagioclase and clinopyroxene crystals. (2498116E, 2276445N, Upper Gallagher prospect, drill hole PS271 at 297 feet).

(D) Photomicrograph (PPL) of a plagioclase phenocryst heavily embayed and altered by chlorite. (2498116E, 2276445N, Upper Gallagher prospect, drill hole PS271 at 297 feet).

(E) Photomicrograph (XPL) of typical fine-grained microgabbro with plagioclase, biotite, muscovite and hematite throughout the groundmass. (2481132E, 2311103N, 3.2 mile on the A-road).

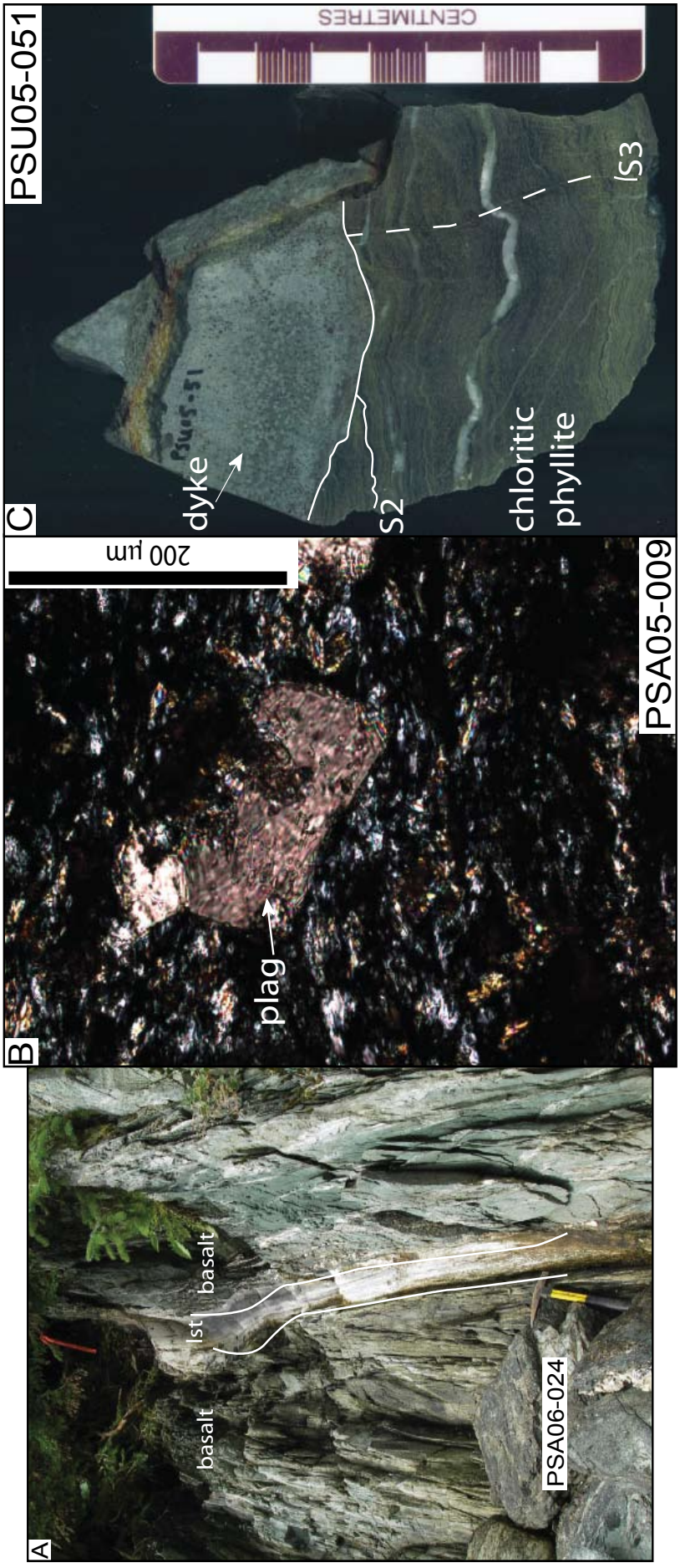
A
basalt
lst
basalt
PSA06-024
B
plag
200 µm
PSA05-009
C
PSU05-051
CENTIMETRES
dyke
S2
S3
chloritic
phyllite

Figure 27 Representative photographs of the post-Triassic lithologies (J2 and I4).
(A) Green, fine- to medium-grained, massive basalt with limestone (lst) interbed. Both the basalt and limestone are strongly cleaved and dip steeply to the northeast. Photograph is taken looking northwest. Hammer is 30cm long (2486720E, 2317305 N, Young Bay).

(B) Photomicrograph (XPL) of altered plagioclase phenocryst within a groundmass of fine-grained chlorite, carbonate and minor sericite. (2486770 E, 2317307 N, Young Bay)

(C) Chilled margin of massive, fine-grained plagioclase phyric diabase dike cross-cutting both S2 and S3 in chloritic phyllite. Scale bar is in cm (Ls5300, Xs0820, 4211 drift)

Island. Stratigraphy generally youngs to the east with the schistose sediments (S-D1&2) along the western margins of Admiralty Island being the basement upon which the Carboniferous volcano-sedimentary footwall (C1-4) was built, the subsequent Triassic volcano-sedimentary sequence (Tr3-4) was then built upon these rocks. To the east of the property the Late Mesozoic marine-flysch dominated assemblage of the Stephens Passage Group (Berg et al., 1972) overlaps the Triassic package. Major northwest-trending faults are also shown.

The basement on which the footwall rocks are built is the Devonian Retreat Group, sedimentary and volcanic rocks which are found along the western half of Admiralty Island (Lathram et al., 1965). The only recognized exposures of these rocks near the Greens Creek property are the schistose sediments and the marble along the eastern shore of Hawk Inlet.

The massive fine-grained greenstones (C1) and layered fine-grained rocks (C2) are grouped together at a property scale and are found across the mine property in a crude circular pattern roughly centered on the serpentinite unit (I2). The medium-grained massive rocks with mafic to ultramafic mineralogy (I1) are predominantly found on the Mammoth ridge system to the northwest of the mine site in the centre of the property. Smaller bodies of these rocks are found further to the north and locally along shears near the mine workings. On surface the polymict breccia unit (Tr1) is best exposed in an elongate pattern from Lower Zinc Creek through the Lil' Sore prospect and down to Young Bay. The monomict breccia unit is restricted to near the mine and is not large enough to be displayed on a property scale map.

The ore deposit only outcrops at the 'Big Sore' on the southwest side of Big Sore Creek. The hanging wall units (Tr3) are dominantly found on the eastern portion of the property and are typically in contact with the fine-grained footwall rocks (C1 and C2). The exceptions to this are local shear zones where hanging wall siliciclastic rocks are in contact with serpentinite (I1) and along Lower Zinc Creek through to Young Bay where

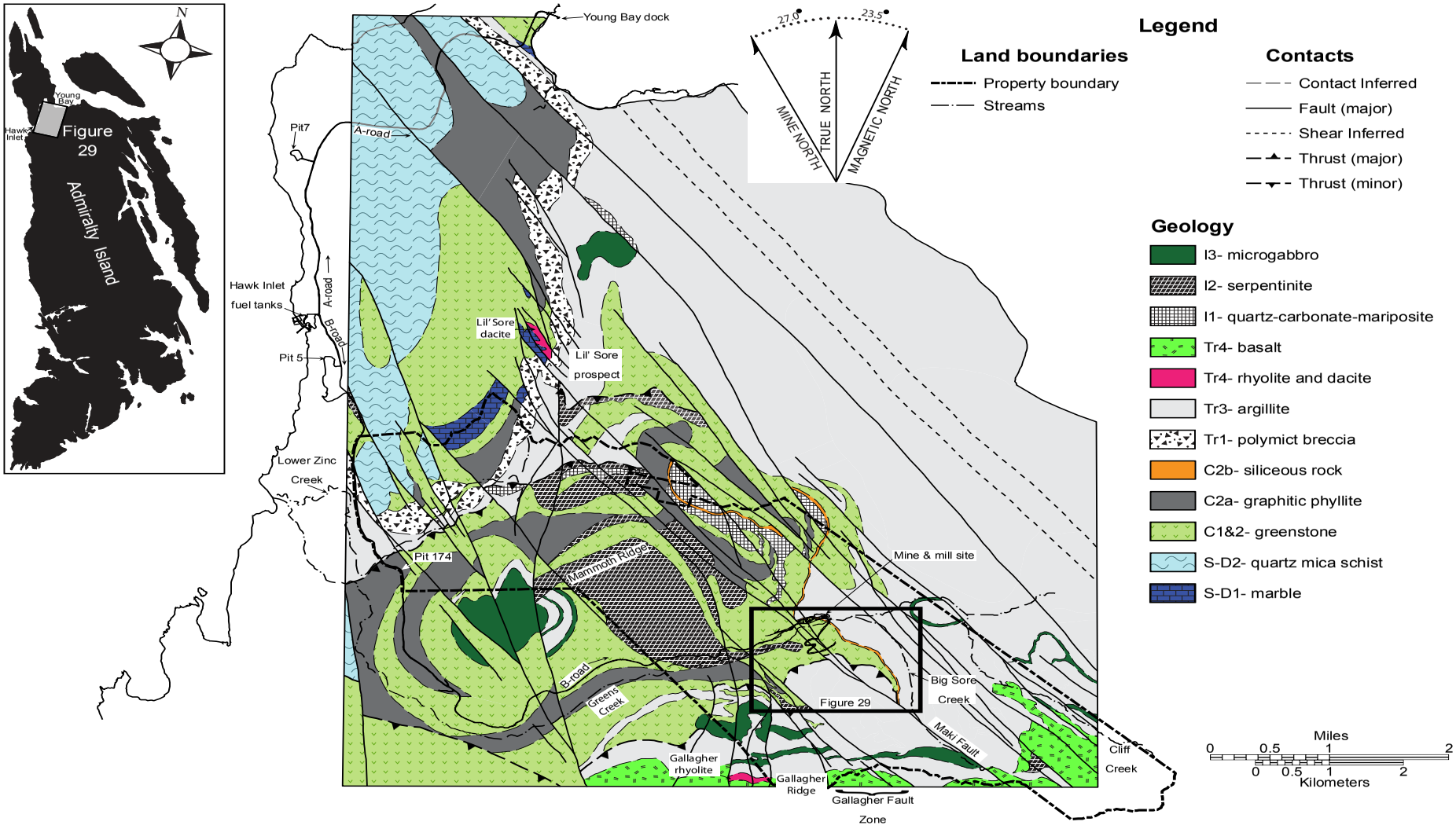

Figure 28 Map of the Greens Creek property and surrounding area. Key locations are labeled. Property geology from Duke (2007). Note the slight clockwise rotation of the Admiralty Island inset map.

they are in contact with the polymict breccia unit (Tr1). The fine- to medium-grained microgabbros (I3) are generally found in small, elongate or circular bodies within the hanging wall siliciclastics. A large circular body is found in the middle of the property surrounded by fine-grained footwall rocks (C1 and C2), proximal to the large body of serpentinite (I2).

The remaining units are restricted in their locations with most of the units being found in a few outcrops or drill intersections. The hanging wall dacite (Tr4) is only found in the Lil' Sore prospect near Lil' Sore drill pad #3 where it occurs in a lens with several diamond drill hole intersections up to 500 feet (150 m) thick. The rhyolite unit (Tr4) has only been recognized on Gallagher Ridge to the southwest of the mine workings and outcrops as an elongate body approximately 25 feet (8 m) thick. It has not been intersected in any diamond drill hole. The fine-grained metabasalt unit (Tr4) is more extensive but has still only been recognized on the Gallagher Ridge – Cliff Creek ridge system south of the mine; it has not been intersected in any diamond drill hole. The post-Triassic fine- to medium-grained, undeformed diabase dikes (I4) have only been recognized in the 4211 drift underground and in the Gallagher bowl to the southwest of the mine workings. On Admiralty Island, the Seymour Canal Formation (J1&2) is only found along the eastern portion of the island (Lathram et al., 1965). Near the Greens Creek property these units have only been recognized in Young Bay near the ferry dock and to the north.

Mine-scale geometry and distribution of lithologies

The geology in the immediate mine area is an overturned limb of an F2 fold that dips steeply to the southwest, shallowing at depth. Argillite is found on both limbs of the fold. To the northeast, the footwall – hanging wall contact is conformable but the southwest contact is the Upper Shear Zone (Figure 29). This shear zone has a top-to-the-west displacement (Proffett, in press). The steeply dipping Maki Fault cross-cuts the mine with a northwest strike and has 1800 feet (550 m) right lateral displacement (Lindberg, 1994, 1996b; Proffett, in press). The dominant units found on the surface

in the immediate mine area are C2a – fine-grained layered rocks and Tr3 – siliciclastic rocks (‘argillite’). There are minor amounts of C1 and C2b – fine-grained massive rocks. The only exposure of the ore body on the surface is the ‘Big Sore’ to the west of Big Sore Creek.

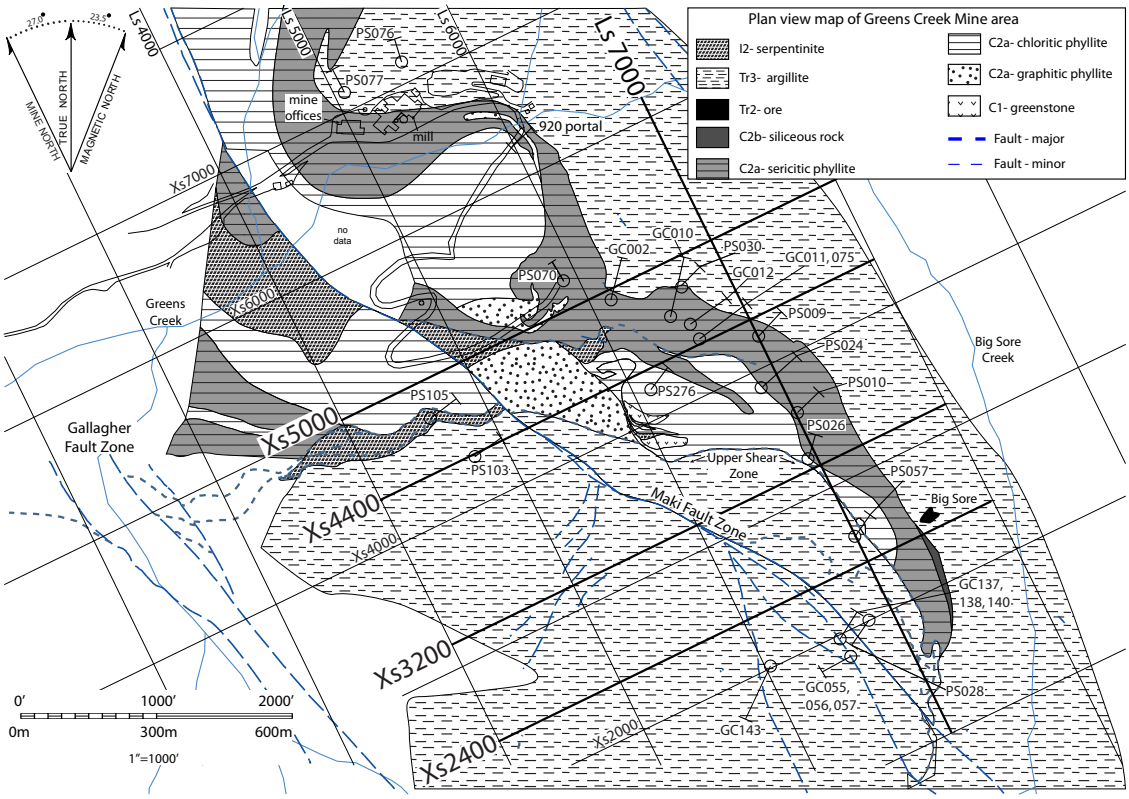

Figure 29 Detailed surface geology map of the Greens Creek mine. See Figure 28 for location. Geology from Proffett (2007). The mine grid is shown with the key sections highlighted.

The geology of the Greens Creek deposit was evaluated by examining a fence diagram located on long-section 7000, down the eastern flank of the deposit and cross-sections 2400, 3200, 4400 and 5000 which bisect the deposit. These sections were specifically chosen according to availability of diamond drill core for study and because, when 1800 feet (550 m) to 2000 feet (600 m) of dextral displacement is restored on the Maki Fault, cross-sections 5000 and 3200 (50-32) and 4400 and 2400 (44-24) are approximately aligned (Figure 30) (Lindberg, 1996b). Restored cross-sections 50-32 and 44-24 are approximately 600 feet (180 m) to 800 feet (240 m) apart and bisect the thickest portions of the West ore body and Northwest West ore body. Based on

alteration patterns and increased Cu-Au grades, this thicker portion of the ore body has been interpreted as the vent proximal ore facies (i.e. Taylor et al., 1999; Taylor et al., in press-b). A fence diagram illustrates the variation in the footwall along the distal, eastern margin of the deposit (Figure 31). Cross-section 5000 and 4400, east of the Maki Fault and the restored cross-sections 50-32 and 44-24, allow study of both the distal and proximal facies across the deposit (Figure 32 to Figure 37).

Cross-sections were created with a 200 feet (60 m) data window (100 feet (30 m) either side of the section) with holes from this study projected up to 250 feet (75 m) onto the sections. Cross-section geology is largely from (Lindberg, 1996b) and is correlated with the logging from this study. When restoring the cross-sections the sections created by Lindberg (1996b) were used as templates. These sections have the motion restored on the Maki but do not correct for the ductile deformation in either the Upper Shear Zone or the Klaus Shear. These sections are used because the brittle deformation is well characterized (Lindberg, 1994; Proffett, in press) where as the ductile deformation is not well understood (per. comm. A. West, KGCMC).

The fence diagram, located approximately along long-section 7000 (Figure 31), is composed of 12 diamond drill holes with lengths between approximately 30 feet (10 m) and 900 feet (270 m). Only one hole intersects mineralization but all holes cross the mine contact and finish in hanging wall argillite (Tr3). The dominant footwall lithology is fine-grained layered rocks (C2a) with sericite the principal alteration mineral. There are a few thin bodies of fine-grained massive rock (C1) intersected and PS057 has an approximately 100 feet (30 m) intersection of serpentinite that is in the Upper Shear Zone. PS028 intersects a few thin quartz + carbonate + mariposite dikes near the top of the hole, possibly from within the Upper Shear Zone.

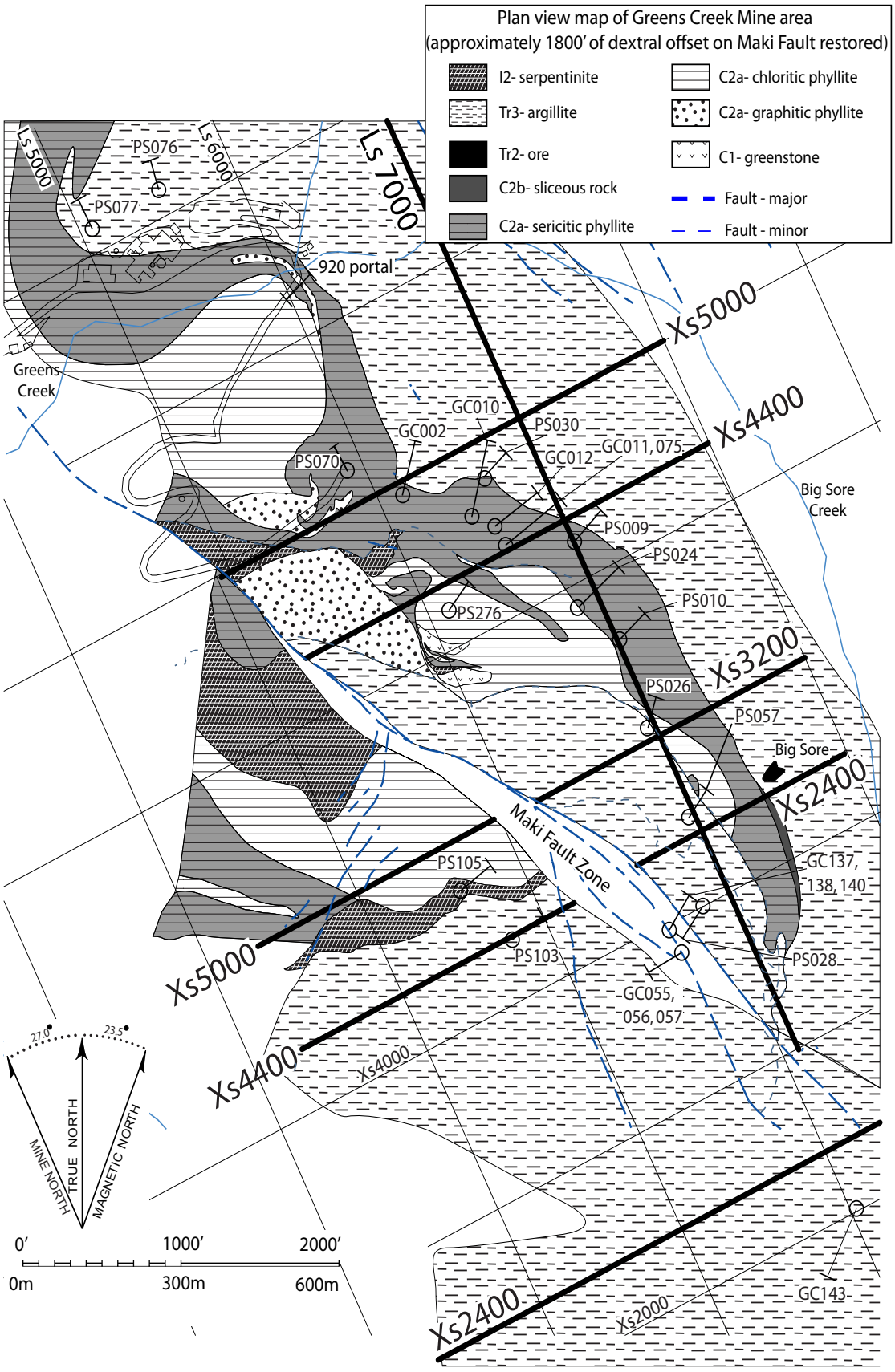

Figure 30 Surface map of the Greens Creek mine area with Maki Fault restored. Approximately 1800 feet (550 m) to 2000 feet (600 m) of dextral motion restored on the Maki Fault (Lindberg, 1996b; Proffett, in press). Surface geology is from Proffett (2007).

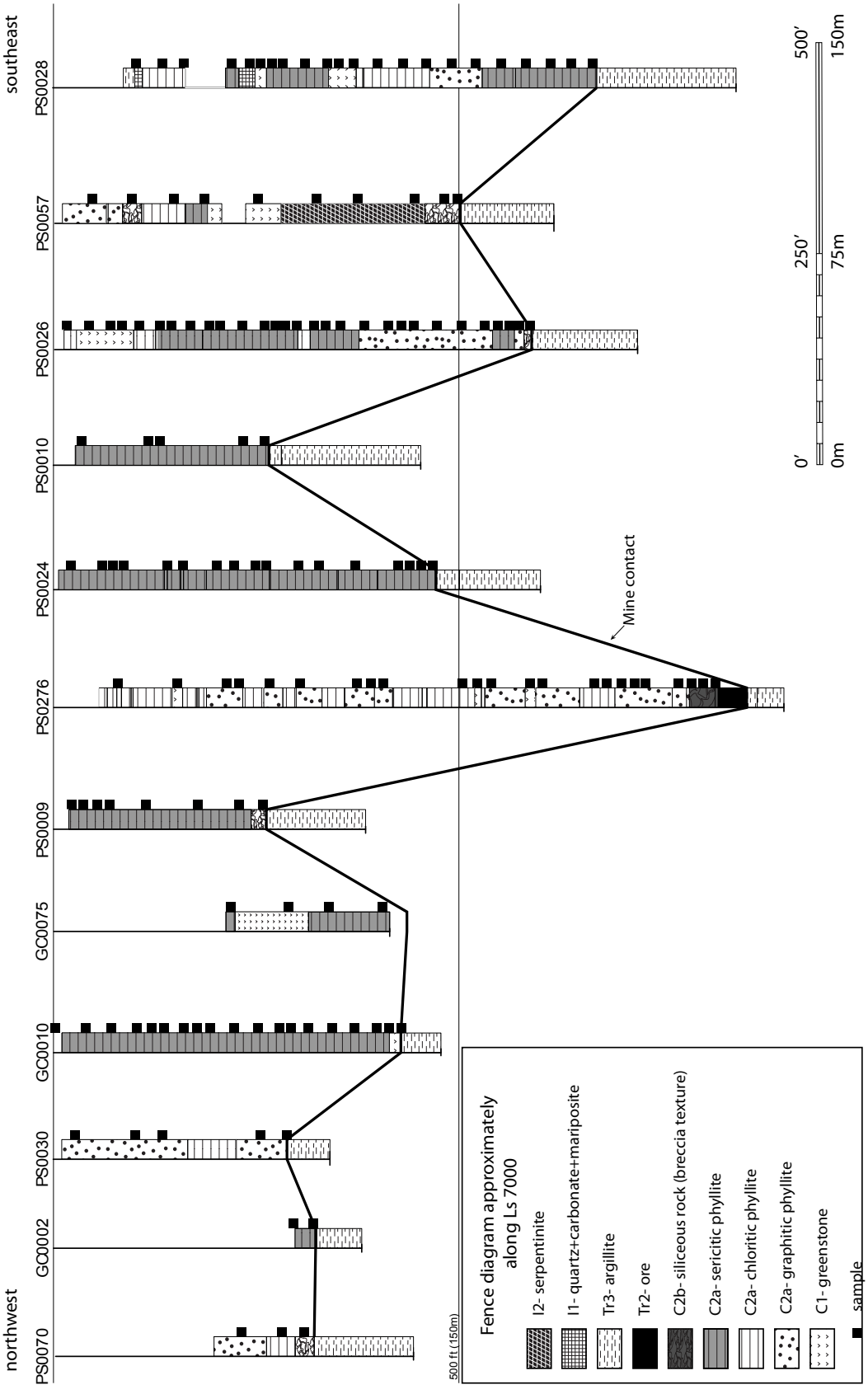

Figure 31 Fence diagram of surface and underground diamond drill holes located approximately along long-section 7000. Horizontal distance of diagram is approximately 3500 feet (1100 m); vertical exaggeration is X 4. Note footwall lithologies are above the mine contact as this is the inverted limb of a F2 fold.

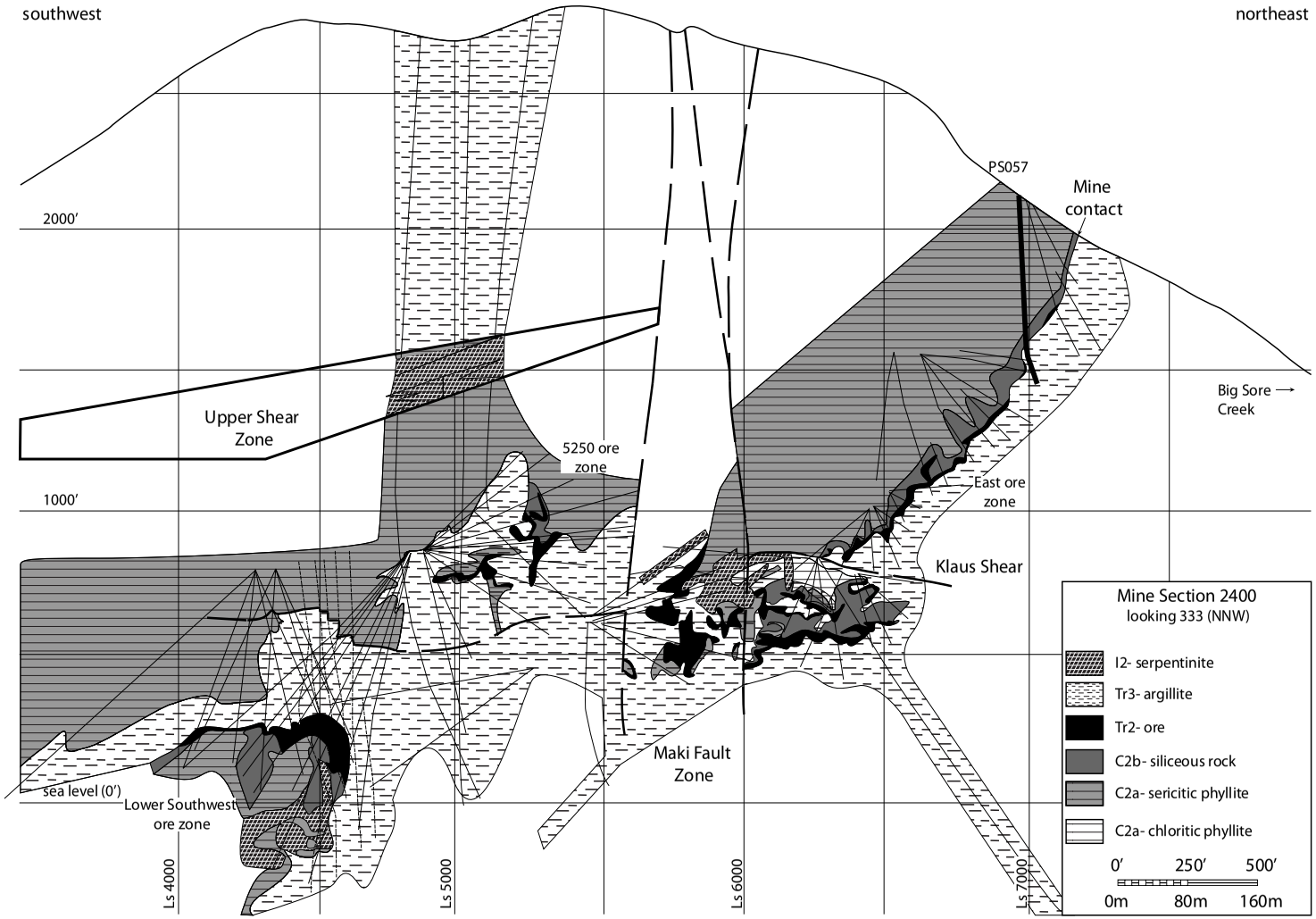

Figure 32 Southwest-northeast cross-section 2400. Section is located at the southern end of the Greens Creek deposit and created with a 200 foot data window. The mine contact dips steeply on the eastern side and shallows with depth where it is cut by the Klaus Shear and the Maki Fault. The 5250 and Lower Southwest ore bodies are to the west of the Maki Fault.

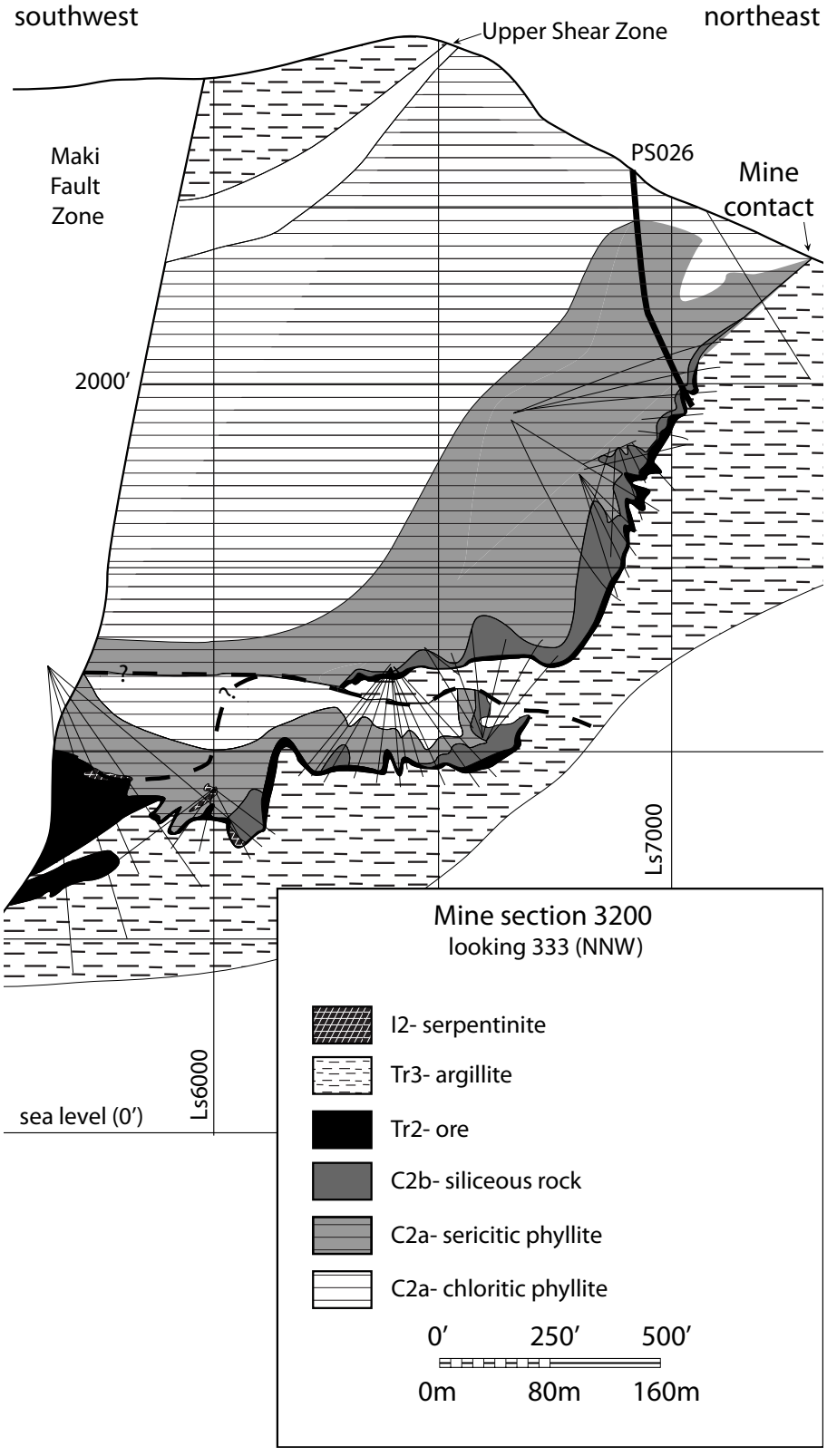

Figure 33 Southwest-northeast cross-section 3200. Section is located at the southern end of the Greens Creek deposit and east of the Maki Fault. Section created with a 200 foot (60 m) data window. The mine contact dips steeply to the southwest at the surface and shallows with depth where it is cut by the Klaus Shear. Below the Klaus Shear, the mine contact is sub-horizontal with several open to tight F3 folds before the mineralization thickens into the eastern portion of the West ore body.

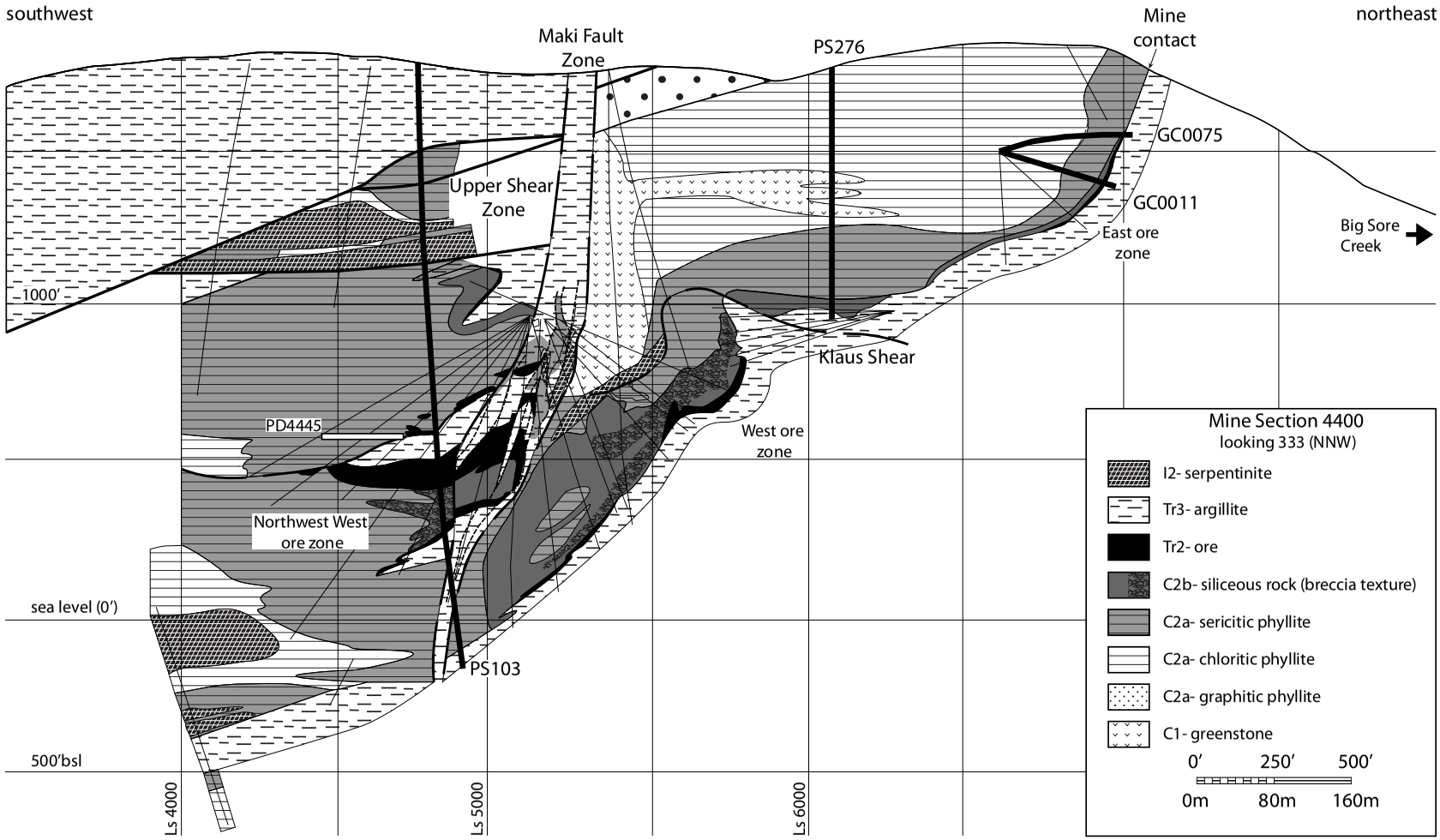

Figure 34 Southwest-northeast cross-section 4400. Section located at the northern end of the Greens Creek deposit and created with a 200 foot data window. The mine contact has a shallower dip to the southwest than on sections to the south and the East and West ore bodies are very thin. On the western side of the Maki Fault, the Northwest West ore body outlines a recumbent isoclinal fold with minor shearing on the upper ore-argillite contact. Directly beneath the Northwest West and West ore bodies is the thick, silicified monomictic breccia lithology.

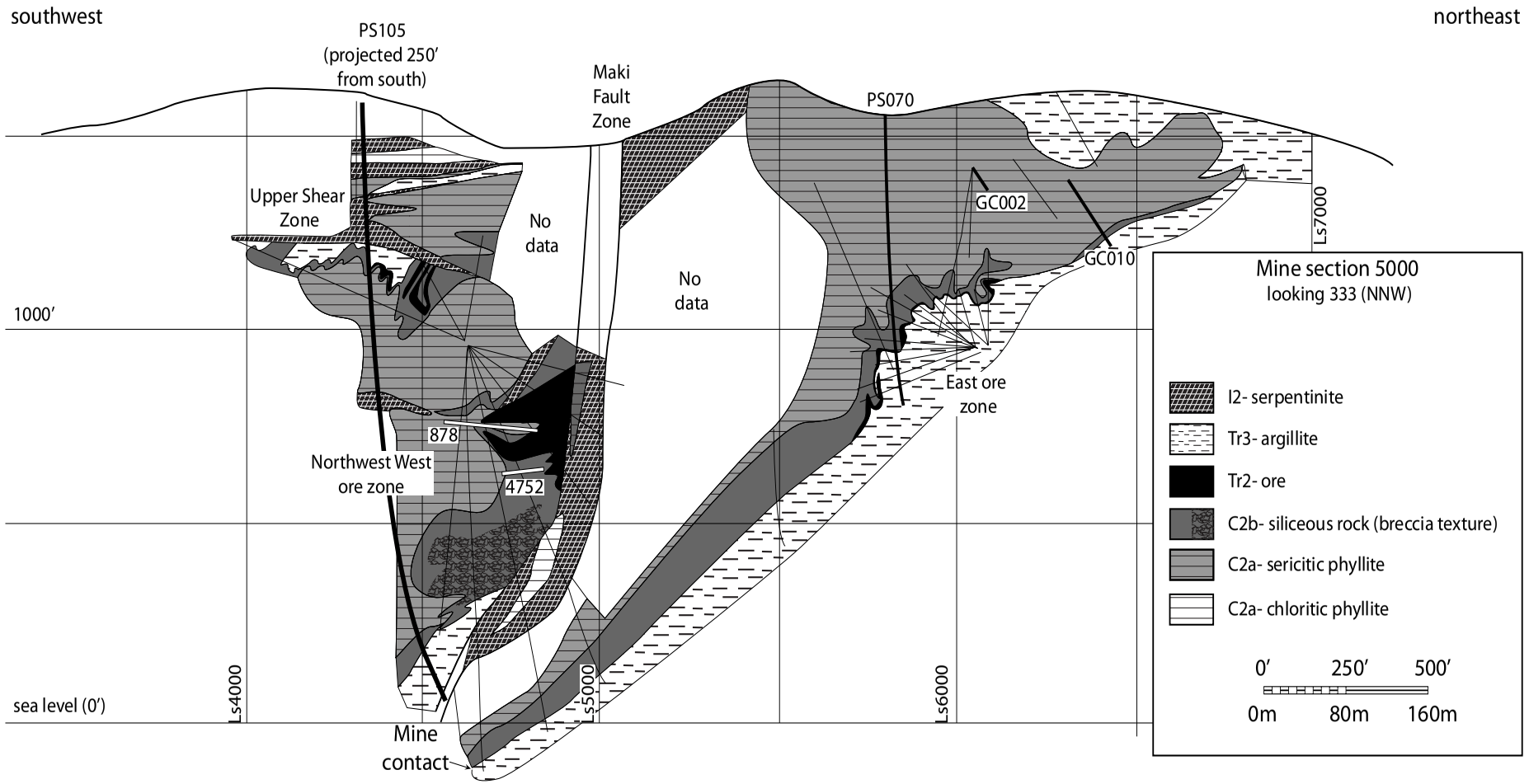

Figure 35 Southwest-northeast cross-section 5000. Section located at the northern end of the Greens Creek deposit and created with a 200 foot data window. The mine contact to the east of the Maki Fault has a moderate dip to the southwest and the East West ore bodies are thin. The Maki Fault is contains serpentinite. To the west of the Maki Fault, the Northwest West ore body outlines two recumbent isoclinal F2 folds and an open F3 fold. The same silicified monomictic breccia as on cross-section 4400 is found beneath the Northwest West ore body.

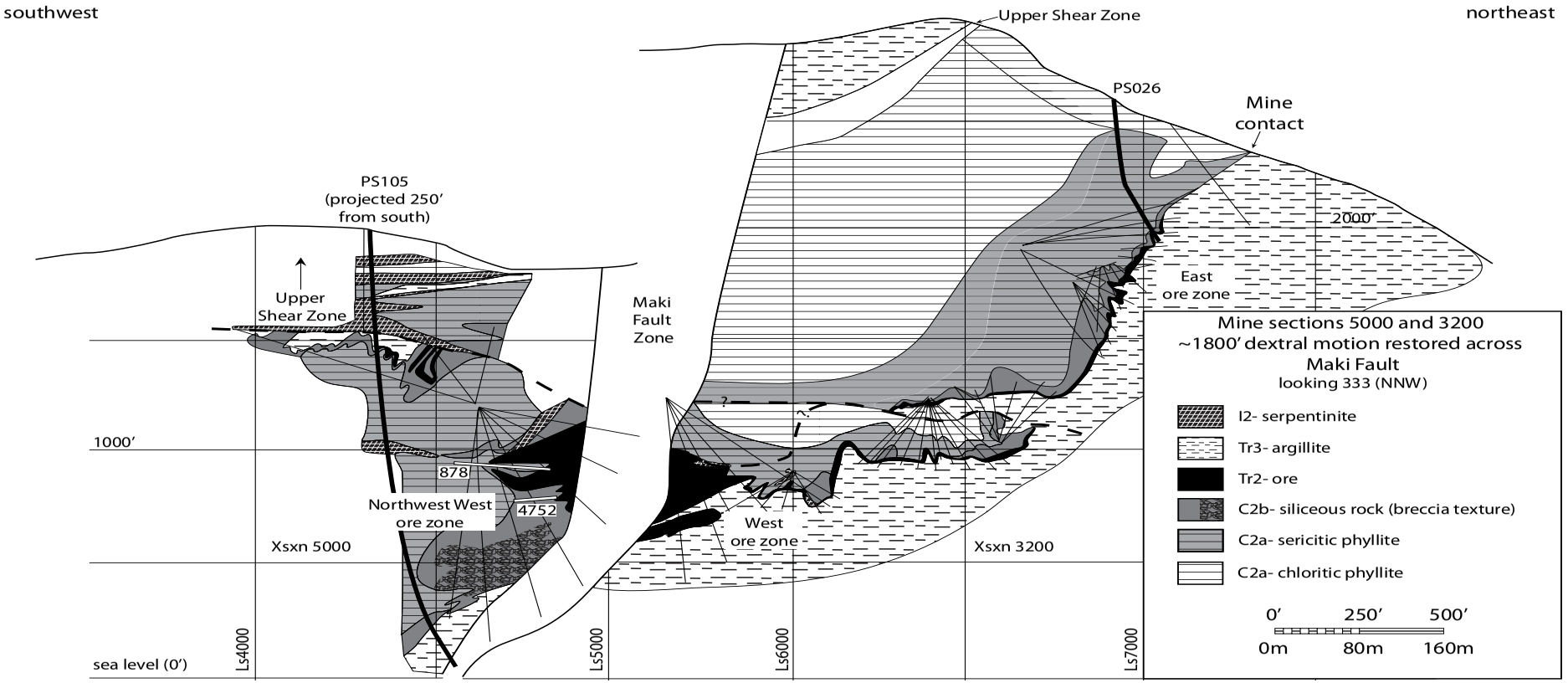

Figure 36 Restored cross-sections 5000 and 3200. 1800 feet (550 m) right lateral displacement along the Maki Fault has been restored to join cross section 5000 (W of Maki) and 3200 (E of Maki). Geology from Lindberg (1994: plate 2).

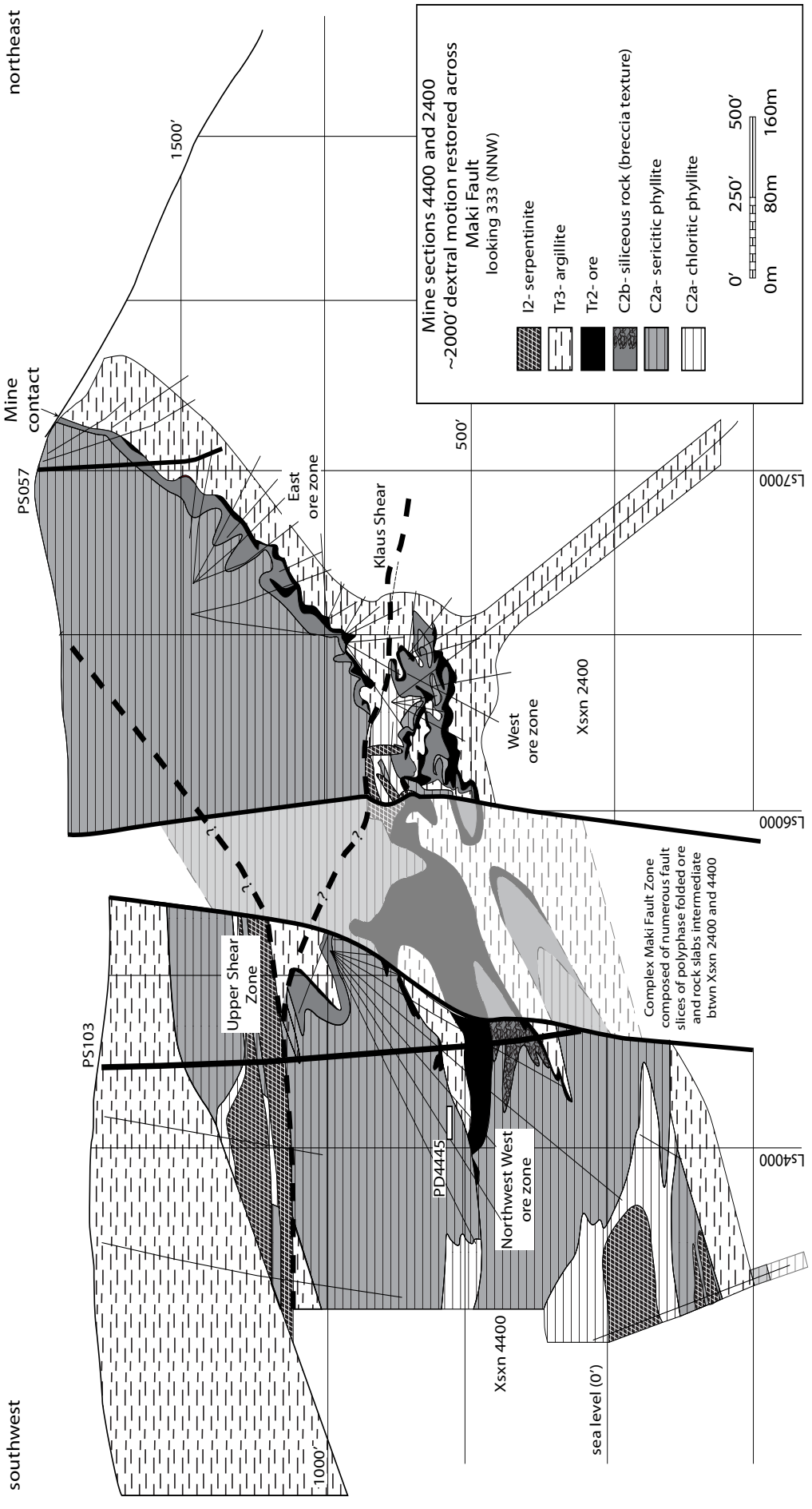

Figure 37 Restored cross-sections 4400 and 2400. 2000 feet (600 m) right lateral displacement along the Maki Fault has been restored to join cross section 4400 (W of Maki) and 2400 (E of Maki). No adjustment was made along the Klaus Shear or Upper Shear Zone. Geology from Lindberg (1996a).

Cross-section 2400 shows the typical thin East ore lens dipping to the southwest. At 800 feet (240 m) ASL, the ore body is cut by the Klaus Shear. At this elevation, the Maki Fault is vertical, 400 feet (120 m) thick with the eastern edge located near cross-section 6000. Between the elevations of approximately 500 feet (150 m) ASL and 750 feet (225 m) ASL, the East ore is highly sheared, folded and faulted. On the western side of the Maki Fault are the 5250 and Lower Southwest ore bodies. PS057 is projected south onto the 2400 cross-section and is the only hole from this section examined during this study. The dominant footwall lithology is the fine-grained layered rocks (C2).

Cross-section 3200 was examined on the eastern side of the Maki Fault. The mine contact dips steeply southwest and shallows to sub-horizontal before being cut by the Klaus Shear. Below the Klaus Shear, the mine contact has a sub-horizontal enveloping surface across several open to tight S3 folds before the main thickened portion of the West ore zone is encountered. The footwall lithologies are dominantly fine-grained layered rocks (C2) with minor serpentinite near the Klaus Shear. There are no recognized fine-grained massive rocks (C1) on this section. PS026 on the eastern flank of the East ore zone is the only hole examined from this section.

In cross-section 4400, the East ore lens has largely pinched out and is only seen near long-section 7000 where underground diamond drill holes GC0011 and GC0075 intersect a thin band of ore. At the surface, the footwall rocks dip steeply to the southwest. Layering shallows at depth to sub-horizontal before dipping steeply to the southwest below the Klaus Shear. This lower portion of steeply dipping footwall is heavily silicified and in places is composed of monomictic breccia (Tr1) particularly where it is near the southern flank of the West ore body. The footwall is still composed mainly of the fine-grained layered lithologies (C2) but there is a fine-grained massive body (C1) near the centre of the section. Again, the serpentinite lithology (I2) is only found near major structures. Four holes were examined from this section: PS103, PS276, GC0011, and GC0075.

The East ore body is very thin on cross-section 5000 and only found near long-section 6000. The overall dip of the mine contact is shallower than farther southeast with the thickness of the silicified footwall increasing with depth. The majority of the footwall consists of layered fine-grained rocks with a significant amount of massive fine-grained silicified rocks proximal to the mine contact. The Klaus Shear is not recognized on this section. On the western side of the Maki Fault, the top portion of the section is defined by the Upper Shear Zone. This shear has unknown displacement. The Maki Fault cuts the Northwest West ore body which shows a recumbent isoclinal F2 fold refolded by an open F3 fold. Below the Northwest West ore zone there is a thick section of intensely silicified footwall which is a monomictic breccia (C2) in places. The remaining footwall is fine-grained layered rocks (C2) with serpentinite (I2) along major structures. The geology within the Maki Fault zone is a complex arrangement of fault blocks of ore, footwall and hanging wall lithologies and serpentinite. Four holes were examined from this section: PS070, PS105, GC002 and GC010.

Restored cross-sections 5000 and 3200 (50-32) and 4400 and 2400 (44-24) are constructed with 1800 feet (550 m) to 2000 feet (600 m) right-lateral motion restored (Lindberg, 1996b). Cross-section 50-32 (Figure 36) shows a steeply dipping East ore zone that flattens with depth before being cut by the Klaus Shear. Below the Klaus Shear the ore horizon is nearly horizontal before thickening into the main West ore body which is cut on the western side by the Maki Fault. On the eastern side of the Maki Fault, the Northwest West ore body is of approximately the same thickness as the West ore body. The Northwest West ore body defines two recumbent isoclinal F2 folds that are refolded by an open F3 fold. Cross-section 44-24 (Figure 37) shows a similar pattern to Cross-section 50-32 on the eastern side of the Maki Fault with the exception that the West ore body is not as thick. The other main difference with this reconstructed section is that a larger portion of what is interpreted to be the thickest part of the main ore body is found within the Maki Fault zone and the reconstruction of this ore body is not well constrained.

The cross-section and fence diagram (Figures 31–37) illustrate several useful generalizations about the geology of the footwall. First, the dominant footwall protolith on the mine cross-sections is the fine-grained layered lithology (C2a) and the fine-grained massive lithology (C1) forms only a minor component. Serpentinite (I2) is found within or near major structures and the quartz + carbonate + mariposite sills or dikes (I1) are rare. The brecciated units (C2b and Tr1) are found only near the mine contact. Secondly, the mine contact is steeply southwest-dipping at the surface and shallows with depth. This shallowly dipping portion is overprinted by several tight to open F3 folds on the east side of the Maki Fault. The Maki Fault strikes northwest through the thickest portion of the original ore body. To the west of the Maki, two recumbent isoclinal F2 folds are refolded by an open F3 fold. The Klaus Shear intersects the East ore body before being offset by the Maki Fault. The Upper Shear Zone is located approximately 750 feet (225 m) to 1000 feet (300 m) above mineralization on both sides of the Maki Fault. As the sense of motion is poorly constrained on the Upper Shear Zone, it precludes investigation at greater depths into the footwall. Thirdly, the alteration mineralogy of the fine-grained layered unit changes systematically with proximity to the mine contact. Distally it is chlorite dominated, grading through to sericite dominated and finally becoming quartz + pyrite dominated directly at the mine contact. The alteration mineralogy, zonation and chemistry is discussed in Chapter 6.

Ore body morphology, mineralogy, and metal zoning

The Greens Creek deposit is made up of three ore bodies (East, West and Southwest) with three extensions (Northwest, 5250 (or Fred), and 200 South) (Figure 38) that lie nearly continuously along the mine contact (Taylor et al., in press-b). The ore bodies are dominated by a pyrite-base-metal sulfide assemblage where metal abundance decreases from Fe, Zn, Pb to Cu. High Ag and Au grades are common (Frietag, 2000). Tetrahedrite is the major silver-bearing mineral, with other silver minerals including pyrargyrite, acanthite, and other Pb-Sb-As-(Hg-Tl) sulfosalts (Taylor et al., 1999). Au is variable in its occurrence and is found within pyrite and as native gold (mainly electrum

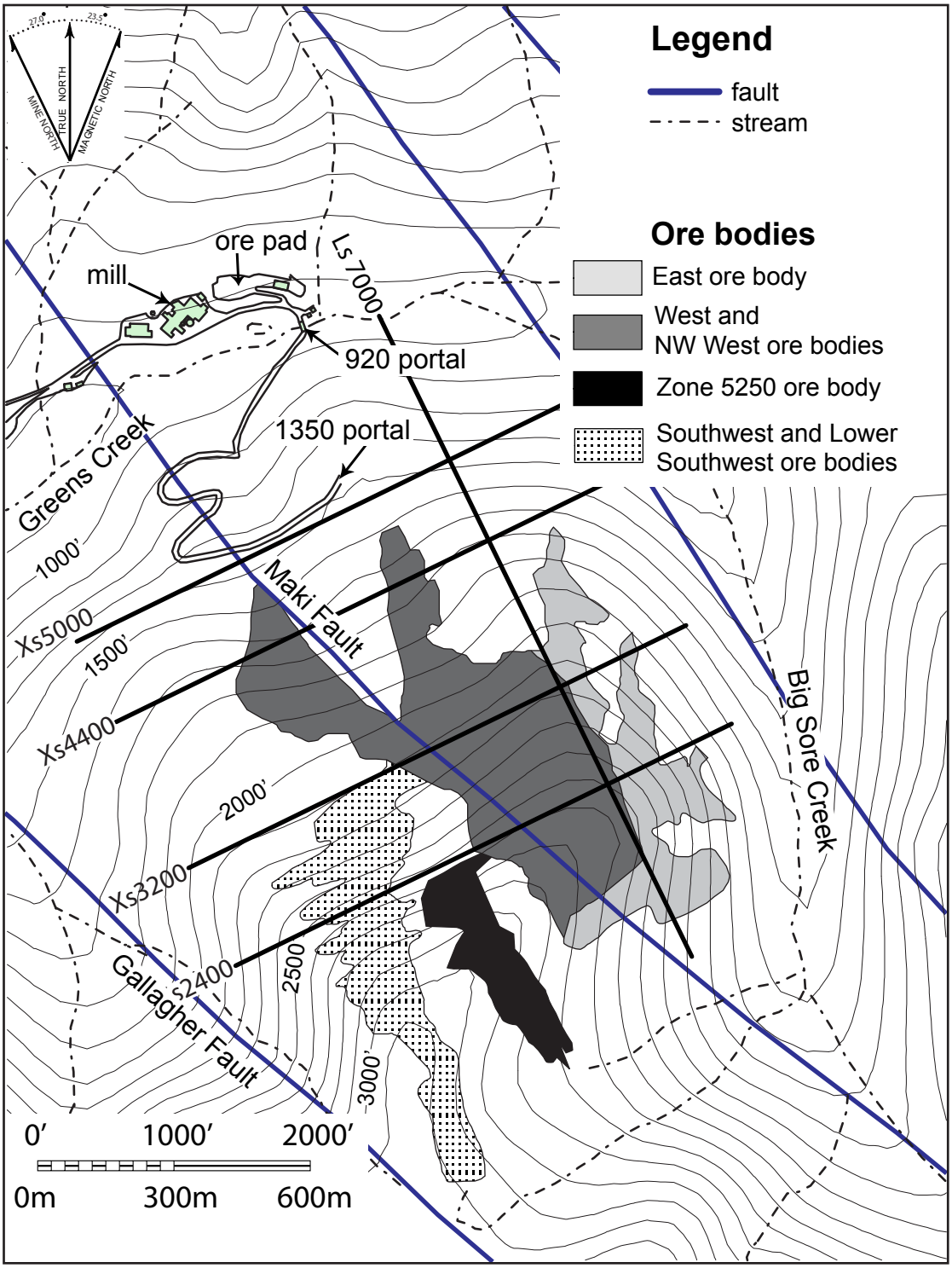

Figure 38. Plan view showing surface projection of ore bodies of the Greens Creek deposit (modified after Taylor et al., 1999). Sections investigated as part of the present study are shown.

with 10–40% Ag) associated with quartz veinlets (Petersen, 1991). Table 2 summarizes the tonnage and average grade of the ore bodies.

Table 2 Grade and tonnage data for Greens Creek deposit. Reserves, resources and average grades of the main ore bodies and their extensions as of 31 December, 2007 (courtesy of Greens Creek Mining Company). Reserves and resources are in dry short tons (DST), grade is in percent (%) or ounces per ton (opt).

Ore body	Reserves and average grades
East ore body	188,547 tons @ 8.37% Zn, 3.26% Pb, 0.079 opt Au, 15.57 opt Ag
West ore body	1,292,394 tons @ 12.52% Zn, 3.88% Pb, 0.146 opt Au, 10.07 opt Ag
5250 extension (Fred)	484,961 tons @ 7.93% Zn, 2.85% Pb, 0.044 opt Au, 17.04 opt Ag
Northwest extension	3,395,272 tons @ 11.14% Zn, 3.70% Pb, 0.120 opt Au, 11.98 opt Ag
Southwest ore body	202,560 tons @ 8.73% Zn, 4.07% Pb, 0.152 opt Au, 24.64 opt Ag
200 South extension	387,452 tons @ 10.42% Zn, 4.45% Pb, 0.173 opt Au, 19.22 opt Ag
Totals	8,450,433 tons, 10.18% Zn, 3.79% Pb, 0.107 opt Au, 13.72 opt, Ag

The East ore body crops out at the discovery site, the Big Sore (Figure 29). From there, the ore body extends 3000 feet (900 m) along a strike of 010-020°, dipping steeply to the west and plunging 20° to the southwest (Taylor et al., in press-b). It gradually flattens out into the West ore body. Folding has produced three lobes of the East ore body known as the North, Central and South zones (Frietag, 2000).

The West ore body thickens to a true thickness of 35 feet (10 m), which is about 1000 feet (300 m) wide (mine E-W) and 3500 feet (1050 m) long (mine N-S) (Taylor et al., in press-b). To the south, the 5250 ore body forms an extension of the West ore body (Figure 38), and is hosted entirely within the hanging wall argillite. The Northwest extension, a large but lower-grade ore body, is interpreted to represent the western portion of the West ore body which is offset to the north along the Maki Fault (Lindberg, 1996a).

The Southwest ore body, which contains high precious-metal grades, is located south of the West/Northwest ore body (Figure 38). It is divided into an upper part (Upper Southwest ore body), which has thinner massive sulfide bands and a lower part (Lower Southwest ore body) which is characterized by up to 75 feet (25 m) thick, abundant white carbonate ore and massive sulfide sections (Frietag, 2000). The ore thins toward the periphery of the Lower Southwest ore body (Frietag, 2000). The 200 South ore body is the southward extension of the Southwest ore body.

Metal zoning within the ore bodies, on a deposit scale, has not been studied in detail. However, Taylor et al. (1999) suggested that on an ore body scale, ores that are proximal and distal to vent areas can be distinguished by ore lithologies and their metal contents. Proximal ores, such as found in the Northwest ore body, comprise massive fine-grained pyritic ore with the highest Cu and Au grades. This ore is located above a thick footwall sequence of highly siliceous rocks. A lateral progression outward from this proximal setting is white siliceous ore followed by white carbonate ore and then white barite ore. The white ores are overlain by massive fine-grained pyritic ore which contains lower Cu-Au grades. Towards the argillite hanging wall contact and at the margins of the ore body, the Zn-Pb-Ag-(Au) content of massive sulfide increases. Chapter 7 discusses the metal zonation within the footwall lithologies beneath the Northwest West and the East ore bodies.

Local structure

Deformation at the Greens Creek deposit is complex with at least four folding events, one semi-ductile shearing event and one brittle faulting event (Proffett, in press) (Table 3). The focus of structural studies in the Green Creek area has been on the post-mineralization deformation (Figure 39) and, though two pre-mineralization deformational events are recognized, they have not been well studied. The first detailed structural studies at the Greens Creek Mine were done by Proffett (1987) and Marten (1987). These two authors provided the framework and nomenclature that future workers built upon. In the mid-1990s, consulting structural geologist P.A. Lindberg

mapped the location and offset of the Maki Fault and Klaus Shear (Lindberg, 1994, 1996a, b). Recent detailed structural geology investigations discovered the Upper and Lower Shear Zones, mapped the location and offset along the Gallagher Fault and produced detailed interpretations of various ore bodies (Proffett, 1997, 2000, 2001, 2002, 2003, 2004a, b, 2005, 2006). Proffett (in press) is the most recent and most detailed summary of the structure found at the Greens Creek mine. The following section is largely summarized from that paper.

Table 3 Summary of the deformation events in the Greens Creek area (modified from Proffett, in press and Freitag, 2000)

Deformation Event	Symbol	Folds	Cleavage	Lineation	Description
First	D1	F1	S1	L1?	relict foliation
Second	D1.5				metamorphic layering
Third	D2	F2	S2	L2	tight to isoclinal folds with axial planar cleavage
Fourth	D2.5				Klaus Shear, Upper and Lower Shear Zones
Fifth	D3	F3	S3	L3	open to tight, upright folds with axial planar cleavage
Sixth	D4	F4	S4	L4	open folds with axial planar cleavage
Seventh	D5				brittle, high-angle strike-slip faults; “Maki and Gallagher faults”

Pre-mineralization structure

There are two foliations recognized prior to mineralization. These foliations are found in metamorphic clasts within the conglomerate (breccia) units and in the graphitic quartz-mica schists of the Paleozoic Retreat or Cannery Groups (Proffett, in press). Metamorphic foliations of varying orientations, found within clasts and truncated by the matrix of the conglomerate are defined as S1.5 (Proffett, in press). S1 is defined as the segregation layering found within outcrops of the graphitic quartz-mica schists of Paleozoic age. These two pre-mineralization foliations are attributed to a Permian metamorphic event which was documented by Haeussler et al. (1999) (Proffett, in press). Haeussler et al. (1999) described the Early Permian metamorphic event as being related to intra-arc deformation.

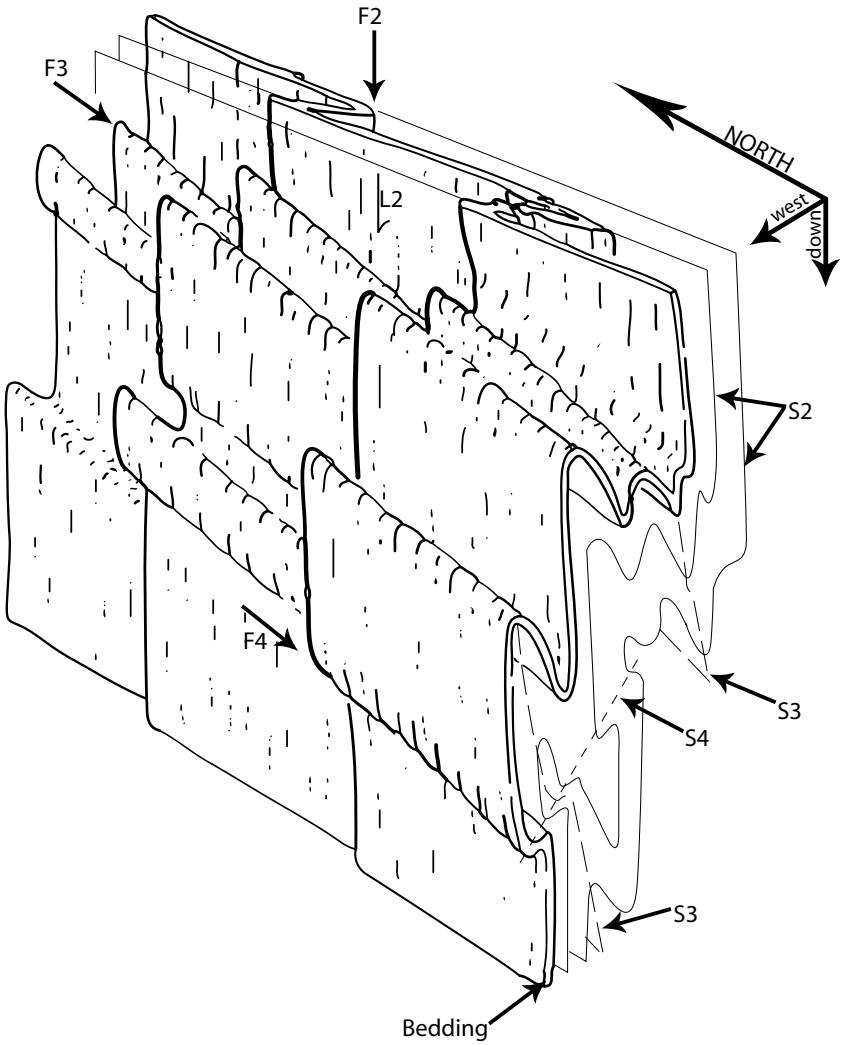

Figure 39 Diagrammatic three-dimensional drawing showing the style of D2, D3 and D4 structural features (from Proffett, 1987)

Post-mineralization structure

F2 folding and S2 foliation

The earliest deformation known to affect all of the mine lithologies is F2 folding and associated axial planar S2 cleavage (Proffett, 1987). S2 cleavage is generally strong and pervasive (Proffett, in press). F2 folds are tight to isoclinal, have amplitudes up to 300 feet (90 m) and wavelengths as short as 30 feet (10 m) (Taylor et al., in press-b). Though F2 fold axes generally trend west to southwest, refolding by later deformational events caused the axes to vary considerably with trends to the northwest, south and locally even southeast (Taylor et al., in press-b). S2 generally strikes north to northwest,

dips steeply on the east limbs of F3 synforms, has a gentle dip in F3 hinge zones and dips gently to moderately to the east on west limbs of F3 synforms (Proffett, in press). When the effects of F3 folding are removed, the average orientation of S2 is striking southeast and dipping moderately to the southwest (Proffett, in press). F2 folds and the related S2 foliation are attributed to the middle Cretaceous deformation that occurred along the eastern margin of the Alexander Terrane as documented by Hauessler (1999) (Proffett, in press).

Shear zones (S2.5)

Several low angle ductile shear zones are identified throughout the mine workings and in diamond drill core. The two key shear zones are the Klaus Shear and the Upper Shear Zone (USZ). The Klaus Shear was identified by and named after a company geologist during the early 1990s (Lindberg, 1994). The Klaus Shear appears to have a top-to-the-northwest sense of motion with a few hundred feet (60 m) of offset (Lindberg, 1994). The USZ is a major ductile shear zone exposed above the uppermost mine workings and separates geology of the mine (mine plate) from the geology found on the surface above the mine (upper plate) (Lindberg, 1994; Proffett, in press). The USZ is between 10 feet (3 m) and several hundred feet (60 m) thick. Rocks within this zone are overprinted by a strong mylonitic foliation (S2.5) that is defined by slightly undulating and anastomosing, thin, discrete layers-rich in sheet silicates separated by thin lenses of quartz and/or carbonate (Proffett, in press). Sense of motion and displacement are not well understood. It is thought that the USZ has a top-to-the-west sense of motion and the displacement is not known. The shear foliation in the USZ displaces S2 and is folded by F3 indicating that it is between D2 and D3 in age. The Klaus Shear also appears to be between D2 and D3 in age but is less well constrained (Proffett, in press).

F3 folding and S3 foliation

F3 folds and S3 cleavage are the most distinct structural features seen in the mine workings (Proffett, in press). These folds are tight to open, upright folds that fold bedding, S2, S2.5, and are subsequently refolded by F4 folds (Proffett, in press) (Figure

39). F3 fold axes generally plunge gently between the south-southeast and south-southwest and the axial planes (S3) dip steeply to the east or very steeply to the west except where they are strongly affected by F4 folds where they dip gently to the east (Taylor et al., in press-b). F3 synforms typically have steeply dipping east limbs and moderately east dipping west limbs (Proffett, in press). F3 folds have wavelengths up to several hundred feet (60 m) (Proffett, in press). The S3 cleavage is usually spaced or zonal crenulation cleavage. In lithologies with abundant sheet silicates (i.e. sericitic phyllite, chloritic phyllite), S3 cleavage in F3 hinge zones can obliterate S2 (Proffett, in press).

F4 folding and S4 foliation

The youngest folds recognized at the Greens Creek mine are the F4 folds. These folds are only locally developed and are best recognized when they refolded small-scale F3 folds. F4 folds are open with fold axes plunging gently to the south-southeast, similar to F3 fold axes. However, the axial planes dip gently between west and south at high angle to S3 (Proffett, in press). S4 cleavage is only locally developed and is either a spaced cleavage or a crenulation cleavage (Proffett, in press).

Brittle faulting

The most important brittle faults in the mine area are the northwest striking, steeply dipping, right lateral Maki and Gallagher Faults (Proffett, in press). The Maki Fault separates the east and west parts of the mine whereas the Gallagher Fault is found to the west of the mine. The west side of the Gallagher Fault is one of the current focuses for exploration. The Maki Fault is steeply dipping near the surface, shallowing at depth and is 600 feet (180 m) thick in the southern portion of the mine, narrowing to 30 feet (10 m) thick in the north portion of the mine (Proffett, in press). Proffett (in press) calculated a right lateral displacement of 1775 feet (538 m) with 110 feet (33 m) west side up slip. This agrees well with Lindberg's (1996b) estimation of 1800 feet (550 m) of right lateral displacement. Proffett (2004a) used diabase dikes that post-date the

folding of the Greens Creek deposit to estimate a net dextral displacement of 2750 feet (830 m) along the Gallagher Fault.

Primary geochemical features of the footwall lithologies

Introduction

This section describes the lithogeochemistry of the stratigraphic footwall and hanging wall volcanic lithologies to the Greens Creek VHMS deposit. The footwall rocks at Greens Creek are heavily deformed and/or altered and, therefore, pre-alteration textural features are largely absent or, if present, are difficult to interpret. As a result, the geochemical properties of each lithology are an important source of data regarding the protoliths of the footwall.

Aims

Immobile trace- and major-element geochemistry are used to recognize the original geochemical characteristics of the footwall lithologies at Greens Creek, particularly in view of their widespread, intense alteration and deformation. Major-element geochemistry is used to broadly identify the lithologies with an ultramafic composition and the immobile element geochemistry at Greens Creek is used to assesses compositional variation of the various volcanic footwall and hanging wall lithologies. The geochemical characteristics are then used to interpret tectonic settings for each rock suite.

Previous geochemical investigations

The lithogeochemistry of the footwall lithologies at Greens Creek has been investigated by Newberry et al. (1989, 1990), Newberry and Brew (1997) and Taylor et al. (1995, 1999, 2008). Geochemical studies by Newberry et al. investigated the protolith and alteration geochemistry of the footwall rocks near the deposit. Their geochemical model for Greens Creek is a geochemically homogenous mafic volcanic footwall with minor sediments throughout, the variation within the footwall being largely a result of alteration (Newberry and Brew, 1997). Taylor et al.'s studies have focused on the

regional metallogenic setting and the tectonic implications of the immobile and rare earth element geochemistry of the footwall rocks (Taylor et al., 2008). Taylor et al. (2008) characterized the footwall volcanic rocks as transitional between alkaline and tholeiitic basalt and interpret the environment of formation to be a back arc rift setting. These studies have been done on smaller sample sets (i.e. Newberry and Brew, 1997 – n = 71; Taylor et al., 2008 – n = 11) than the present study and were done prior to the chronostratigraphic work of the present study.

Sample details

The samples available to the present study come from three sample sets, each with a different collection and analysis history. The oldest sample set consists of 95 samples collected by Greens Creek exploration geologists from across the property. This sample set has been added to annually. Samples were analyzed by ICP-MS at the Acme Analytical laboratory in Vancouver, Canada. A second set of 239 samples was collected for the present study from across the property. One hundred and nineteen of these samples were analyzed using XRF at the University of Tasmania and 120 were analyzed by ICP-MS at the Acme Analytical laboratory in Vancouver.

This sample set contains representative samples of the lithological variation found within the footwall both at the property scale (covering an area approximately 100 km^2) and at the mine scale (up to approximately 1000 feet (300 m) into the footwall). The complex structural nature of the geology and the location of drill holes precluded investigation of the entire stratigraphy along a single section. The breakdown of geochemical samples used in this thesis is given in Table 4.

Analytical techniques

Major and trace-element whole-rock analyses determined with Inductively Coupled Plasma techniques (ICP) were done using the Group 4A-4B methods described below. Total abundances of SiO_2, Al_2O_3, Fe_2O_3, MgO, CaO, Na_2O, K_2O, TiO_2, P_2O_5, MnO, Cr_2O_3, C and S (Group 4A) were determined using 0.1 g of sample analyzed by ICP-

emission spectrometry (ICP-ES) following a lithium metaborate/tetraborate fusion and dilute nitric digestion. Loss on ignition (LOI) is by weight difference after ignition at 1000°C. As, Ba, Be, Co, Cs, Ga, Hf, Nb, Rb, Sc, Sn, Sr, Ta, Th, Tl, U, V, W, Y, Zn, Zr, La, Ce, Pr, Nd, Sm, Eu, Gd, Tb, Dy, Ho, Er, Tm, Yb and Lu (Group 4B) were determined by ICP mass spectrometry (ICP-MS) following a lithium metaborate/ tetraborate fusion and nitric acid digestion of a 0.1 g sample. In addition a separate 0.5 g split was digested in Aqua Regia and analyzed by ICP-MS to report Au, Ag, Bi, Cd, Cu, Hg, Mo, Ni, Pb, Sb and Se (Group 4B). See Appendix II for complete results with upper and lower detection limits for each element using each method.

Table 4: List of geochemical samples analyzed at Greens Creek.

Lithology	GC sample set (ICP-MS)	CODES sample set (ICP-MS)	CODES sample set (XRF)	Total
S-D2- qtz mica schist	0	0	2	**2**
S-D2- gr+qtz mica schist	0	0	1	**1**
S-D2- qtz+chl mica schist	0	0	2	**2**
C1- greenstone	24	11	10	**45**
C2a- graphitic phyllite	6	10	15	**31**
C2a- chloritic phyllite	9	20	17	**46**
C2a- sericitic phyllite	27	37	21	**85**
C2a- siliceous phyllite	2	15	11	**28**
C2a- carbonate phyllite	0	3	0	**3**
C2a- mariposite phyllite	10	0	5	**15**
C2b- siliceous rock	2	2	6	**10**
I1- qtz+carb+mari	0	5	2	**7**
Tr1- polymict breccia	1	11	7	**19**
I2- serpentinite	12	0	5	**17**
I3- microgabbro	2	4	6	**12**
Tr4- rhyolite	0	2	2	**4**
Tr4- dacite	0	0	2	**2**
Tr4- basalt	0	0	2	**2**
J2- basalt	0	0	1	**1**
J1- silt stone	0	0	1	**1**
I4- diabase dikes	0	0	1	**1**
Total	**95**	**120**	**119**	**334**

Major and trace-element whole-rock analyses carried out using the X-Ray Fluorescence (XRF) technique were done at the School of Earth Sciences, University of Tasmania. Rock samples were initially crushed using a hydraulic press to produce fragments less than 1 cm. These fragments were then hand picked and ground in either a chrome-steel or tungsten-carbide ring mill for two minutes to produce a rock powder (<200 μm). Approximately 1 g of each sample was ignited initially at 500° C for four hours (to oxidize the high sulfur content), and again at 1000° C overnight. Volatile loss on ignition (LOI) was calculated by weighing the samples before and after ignition. Major-elements were determined as oxides SiO_2, Al_2O_3, Fe_2O_3, MgO, CaO, Na_2O, K_2O, TiO_2, P_2O_5, MnO, Cr_2O_3 and S, using fused disks. Trace-elements Sb, Sn, Cd, Ag, Nb, Zr, Sr, Cr, Ba, Sc, V, La, Ce, Nd, Y, U, Rb, Th, Pb, As, Bi, Zn, Cu, Ni, Se and Ga were determined using pressed powder pills. Both major and trace-element determinations were carried out on a Phillips 1410 automated XRF under the guidance of Phil Robinson (analyst) using the standard procedures outlined by Norrish and Chappell (1977).

Comparison of analytical techniques

Seven samples have been analyzed using both the ICP techniques at Acme Analytical and the XRF techniques at the University of Tasmania. Samples TasBas, Dior4 and Dol7 are well characterized in-house standards at the University of Tasmania that have been analyzed multiple times with several techniques. The values reported are the values from the best technique for that element. The other four samples, PSA05-01, -04, -12 and PSA06-15, are samples collected during this study and analyzed with both methods. These samples have only been analyzed once with each method and are less well characterized.

This section will focus on elements considered immobile (MacLean and Barrett, 1993), with the exception of some major-elements that are used to calculate the original mineralogy of the serpentinite lithology. Mobile elements are fully discussed in Chapter 6 and the quality control of these can be found there. Incompatible and immobile

elements Zr, Nb, Y, Ta, Th and P are discussed as well as compatible and immobile elements TiO_2, Al_2O_3, Cr, V, Sc, La, Yb, and Hf. These are the elements that were investigated for immobility, some of which were then used for volcanic and tectonic discrimination diagrams. Maclean and Barrett (1993) recommended only using data for Zr, Y and Nb obtained by XRF methods. However, in comparing our data from the seven standards, the ICP and XRF data were typically within 5% for these elements and we have included both the XRF and ICP data in our immobility plots. Thorium by ICP was within 3.5% of the XRF value but Ta and P varied by 19% and 11% respectively and only XRF data was used for these elements. TiO_2, Al_20_3, Yb, and Hf ICP data varied 2.5%, 2.0%, 2.4% and 5.0% respectively and both ICP and XRF data were used in the immobility study. Cr, V, Sc and La ICP data were different from the expected XRF results by greater than 10% and only the XRF data was used in this study. See Table 5, Figure 40 and Figure 41 for comparisons of ICP and XRF data.

Table 5: Summary statistics comparing ICP and XRF data. Elements in bold are the ones we used both the ICP and the XRF data for. UTas standards are samples TasBas, Dior4 and Dol7; Greens Creek duplicates are samples PSA05-01, -04, -12 and PSA06-15.

	Utas standards		Greens Creek duplicates		Combined	
Element	Mean difference (%)	std dev	Mean difference (%)	std dev	Mean difference (%)	std dev
Al2O3	**3.72**	**0.31**	**0.35**	**0.15**	**2.04**	**0.11**
TiO2	**-2.79**	**0.09**	**-2.22**	**0.01**	**-2.50**	**0.06**
P2O5	4.93	0.03	17.39	0.01	11.16	0.02
Sc	11.51	1.00	14.79	0.58	13.15	0.30
Hf	**-5.06**	**0.38**	**NA**	**NA**	**NA**	**NA**
Nb	**-10.47**	**3.97**	**1.07**	**0.86**	**-4.70**	**2.20**
Ta	18.93	1.29	NA	NA	NA	NA
Th	**-3.54**	**0.05**	**NA**	**NA**	**NA**	**NA**
V	-7.33	3.30	10.83	6.18	1.75	2.04
Zr	**7.00**	**13.61**	**1.93**	**9.32**	**4.46**	**3.03**
Y	**-3.03**	**1.68**	**-7.15**	**2.06**	**-5.09**	**0.27**
La	0.67	2.07	-45.71	3.35	-22.52	0.91
Yb	**2.41**	**0.08**	**NA**	**NA**	**NA**	**NA**
Cr	14.80	41.86	-85.19	1038.37	-35.19	704.64

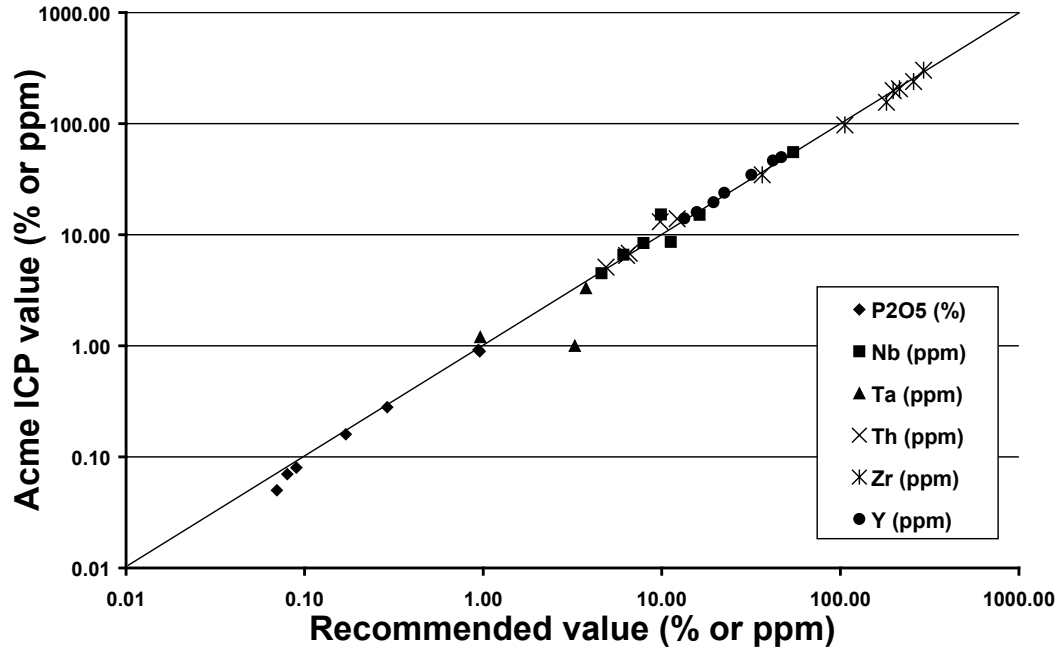

Figure 40 Immobile and incompatible elements for 7 samples analyzed by both XRF at UTas and ICP at Acme.

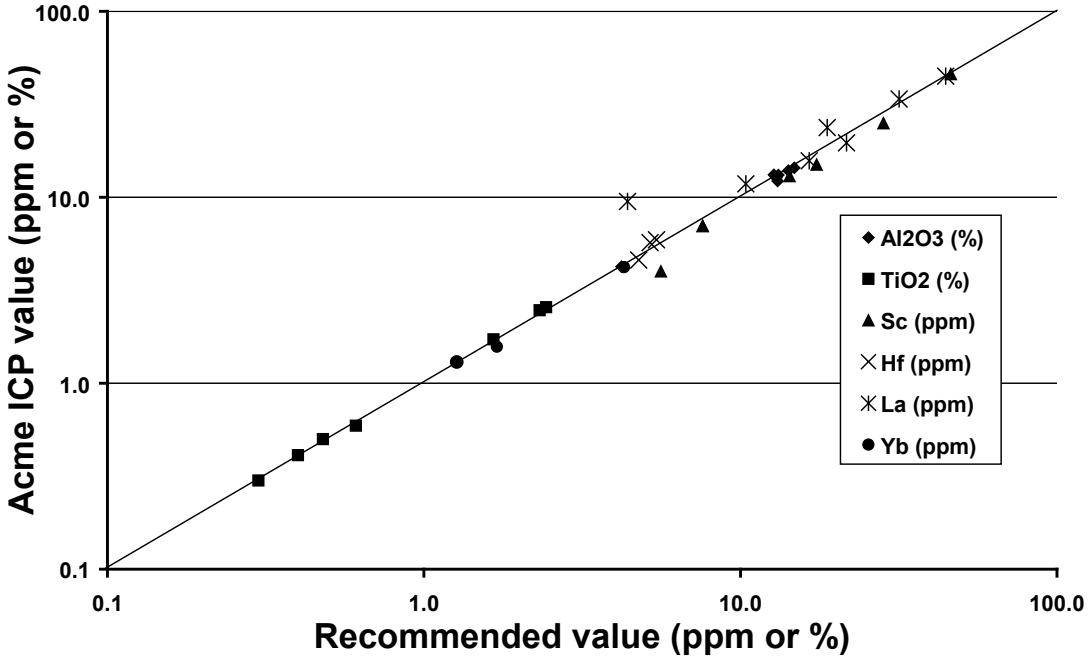

Figure 41 Immobile and compatible elements for 7 samples analyzed by both XRF at UTas and ICP at Acme.

Immobile element characterization

In rocks with intense alteration or deformation resulting in loss of obvious igneous textures that allow reliable interpretation of protolith, Pearce (1996) recommended using a geochemical diagram such as Ni versus Zr/TiO_2 from Winchester et al. (1980) to filter samples of sedimentary origin. This diagram works on the premise that sedimentary processes result in high Zr/TiO_2 ratios similar to felsic volcanic rocks while still having high Ni content of mafic volcanic rocks allowing them to be separated from igneous rocks. The obvious exception to this is sedimentary rocks with a proximal volcanic source which may be classified as igneous because the sedimentary processes may have been too short to significantly modify the chemistry of the sediments. The coherent volcanic rocks from Greens Creek all plot well into the igneous field (Figure 42). To screen out cumulate rocks, samples with ≥20% Al_2O_3, ≥50 ppm Sc and ≥200 ppm Ni should not be plotted on basalt discrimination diagrams (Pearce, 1996). The Greens Creek coherent volcanic rocks all have <20% Al_2O_3 and <50ppm Sc, but several footwall greenstone samples and half of the hanging wall microgabbros have ≥200 ppm Ni; these samples were not classified on the basalt discrimination diagrams.

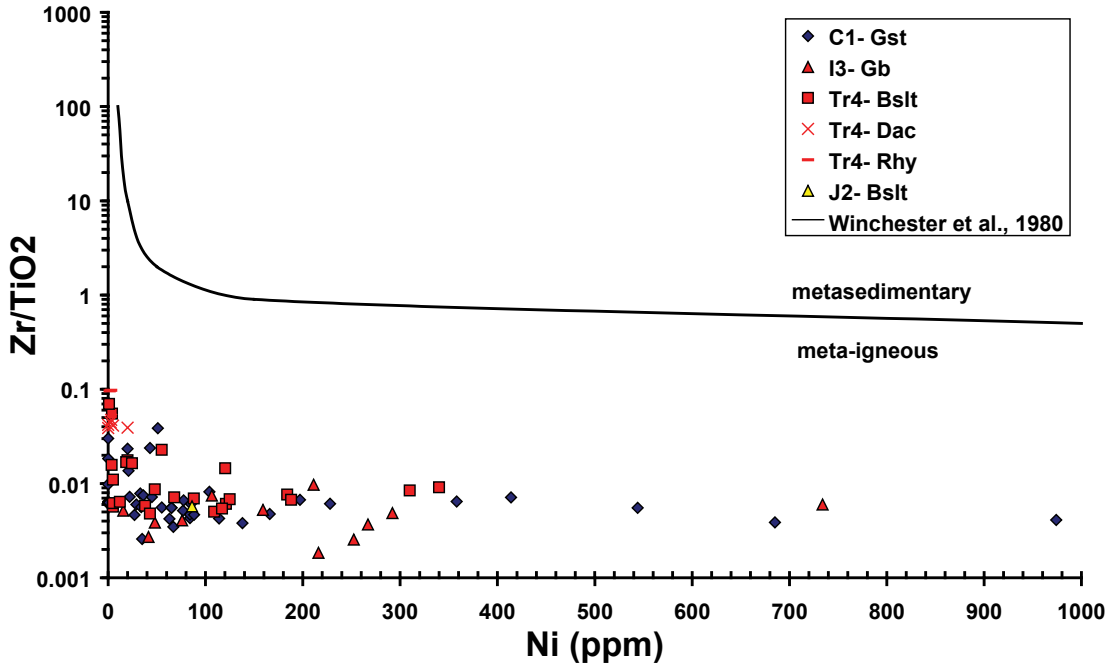

Figure 42 Ni vs. Zr/TiO_2 after Winchester et al. (1980) showing the coherent volcanic rocks from Greens Creek plotting well into the igneous field with no sedimentary affinity.

Immobile elements were used to determine the primary composition of the footwall lithologies at Greens Creek. Only lithologies interpreted as coherent are used to demonstrate immobility. In general, the suite of elements demonstrated to remain immobile under greenschist facies metamorphism and hydrothermal alteration are: Ti, Zr, Y, Nb, Ga, P, REE, V, Cr, Sc, Hf, Ta, Th (Winchester and Floyd, 1977). Table 6 shows the ranges of these immobile elements in various coherent lithologies.

Table 6 Ranges in immobile elements of the interpreted coherent volcanic rocks from the Greens Creek deposit. Note n = number of analyses.

	FW1- Gst	HW3- Gb	HW4- Bslt	HW4- Dac	HW4- Rhy	Post-Tr-Bslt
n	29	6	25	6	2	1
Al_2O_3 (wt%)	0.84-20.64	114.5-117.0	4.21-18.01	11.60-17.57	11.94-13.19	17.06
TiO_2 (wt%)	0.03-2.35	1.22-2.18	0.40-3.31	0.40-0.57	0.23-0.30	1.82
Zr (ppm)	9-130	40.1-90.9	35-406	158-218	221-303	104
Y (ppm)	4.6-53.1	14.5-31.1	13.0-70.0	24.0-39.0	26.0-46.5	20.7
Ga (ppm)	1.7-25.3	15.8-18.3	5.4-27.0	11.7-18.3	NA	NA
Nb (ppm)	0-20	4.5-28.0	0-30	7.7-20.3	11.0-15.1	9.5
Yb (ppm)	0.43-5.00	NA	1.19-7.17	2.58-3.37	6	NA

The linear correlation of high field strength elements (HFSE) reflects the preservation of primary element ratios due to their immobility (i.e. MacLean and Barrett, 1993). At Greens Creek, Zr, Y, Ga, Nb, Yb are immobile as demonstrated in Figure 43 by constant Ti/Zr, Nb/Zr and Y/Zr ratios that project through the origin.

The wide variation of Ti/Zr and Nb/Zr ratios in the hanging wall volcanic lithologies suggests either inherent heterogeneity that is not recognized or the possibility that this lithology is composed of two (or more?) separate volcanic series. In thin section, the hanging wall lithologies appear to be less altered than the footwall greenstones. Therefore it is thought the variation in the immobile elements is an original feature of these rocks.

Al and Ti are typically considered immobile (i.e. Whitford et al., 1989) except in zones of extreme hydrothermal alteration where these elements are slightly mobile

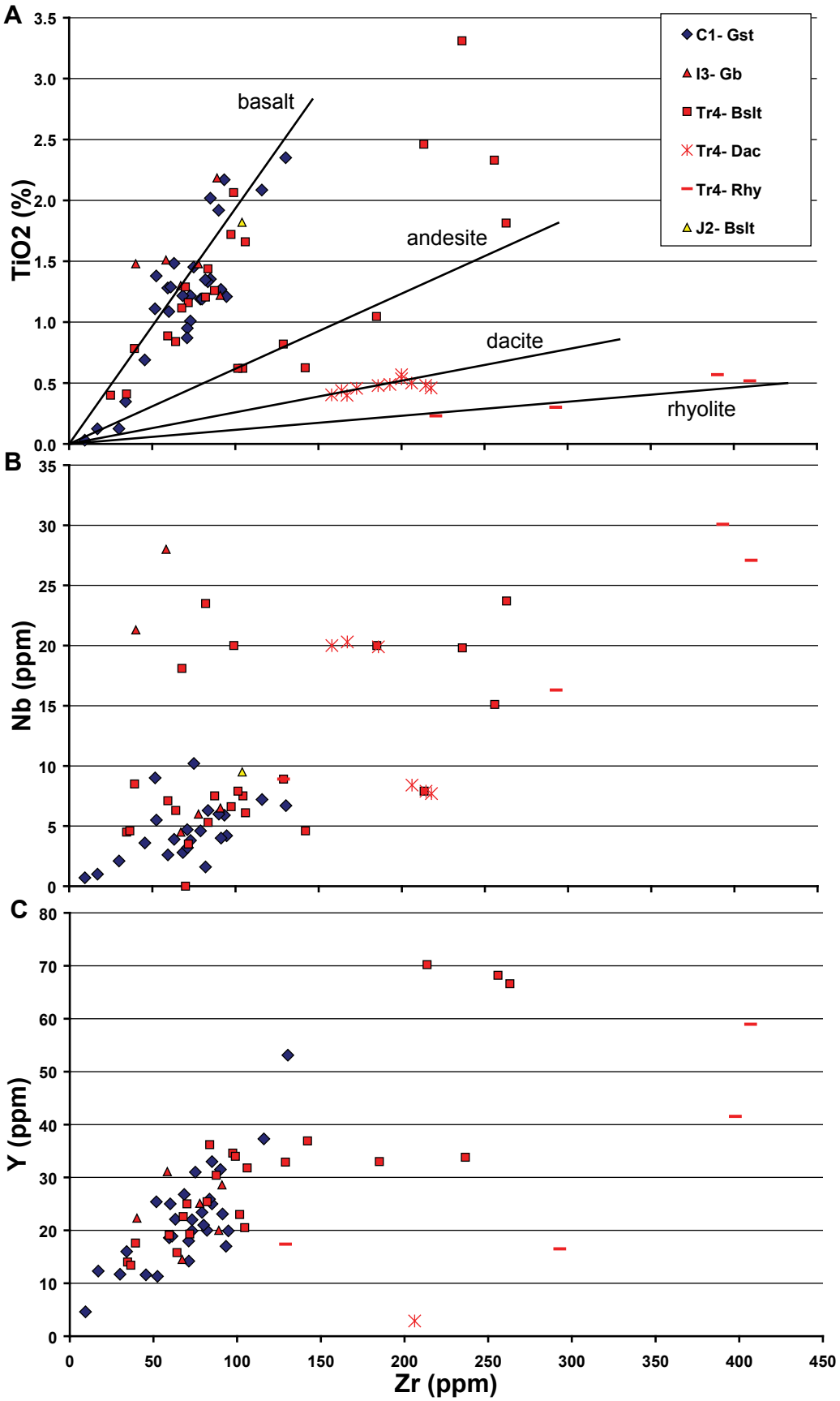

Figure 43 Immobile element plots. (A) TiO_2 vs. Zr, (B) Nb vs. Zr and (C) Y vs. Zr. The positive linear correlation in (A), (B) and (C) indicates that primary Ti/Zr, Nb/Zr and Y/Zr ratios have been preserved.

(i.e. Larson, 1984; Wynne and Strong, 1984). At Greens Creek, TiO_2-Zr has a positive correlation for the footwall greenstones and is much more scattered for the hanging wall basalts (Figure 43A). Nb and Y are similar (Figure 43B&C). The variation in the Ti/Zr ratio in the hanging wall basalts is also thought to represent primary variations in this ratio as these units are less altered than the footwall units. One explanation for this variation may be the presence of multiple hanging wall volcanic series which have not been identified in the mapping. The footwall greenstone samples that are intensely altered plot along a linear trend in TiO_2–Al_2O_3 space (Figure 44). The variation from the linear trend is seen in the less altered samples that have TiO_2 contents of approximately 1.5%; these samples vary up to 10% from the main Al_2O_3 trend but are typically within 5% (Figure 44). It is interpreted that this variation is a cumulate trend with the Al_2O_3 enrichment indicating plagioclase cumulates.

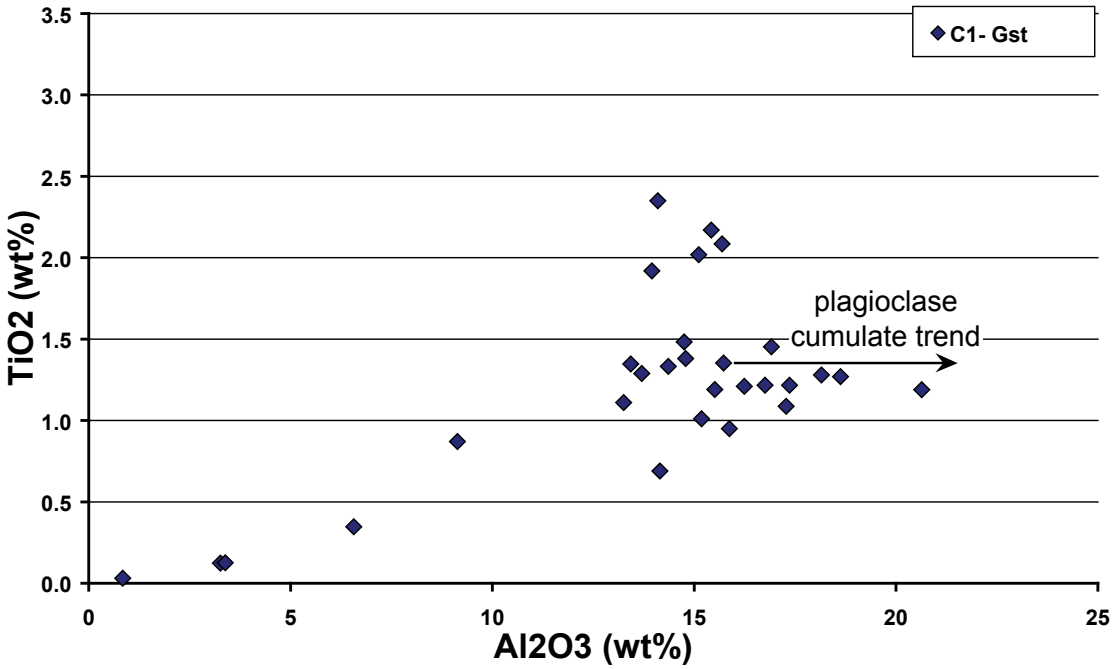

Figure 44 TiO_2 vs. Al_2O_3 illustrating a weak positive correlation for the footwall greenstones (C1) that indicates possible mobility of these elements. The lack of a linear trend in the hanging wall basalts is interpreted as indicating igneous fractionation trends.

Pearce (1996) revised the Winchester and Floyd (1977) volcanic discrimination diagram based on Zr/Ti versus Nb/Y. This diagram characterizes different rock types and their magmatic affinity based on the assumption that the relative abundance of immobile trace-elements is a function of magmatic differentiation. The Zr/Ti ratio is used as a proxy for magmatic differentiation and the Nb/Y ratio as an alkalinity index. The footwall greenstones at Greens Creek lie mostly in the andesite or sub-alkaline basalt fields. The hanging wall igneous rocks span a large range in composition from basalt to rhyolite (Figure 45). The footwall greenstones have relatively restricted compositions with Zr/Ti ratio, between 0.007 and 0.01, and Nb/Y ratios between 0.06 and 0.7. The Late Triassic volcanic rocks (I2–4) plot along a tholeiitic fractionation curve (MacLean and Barrett, 1993) (Figure 46) and have similar REE patterns (Figure 47) supporting the view these rocks are related by fractionation.

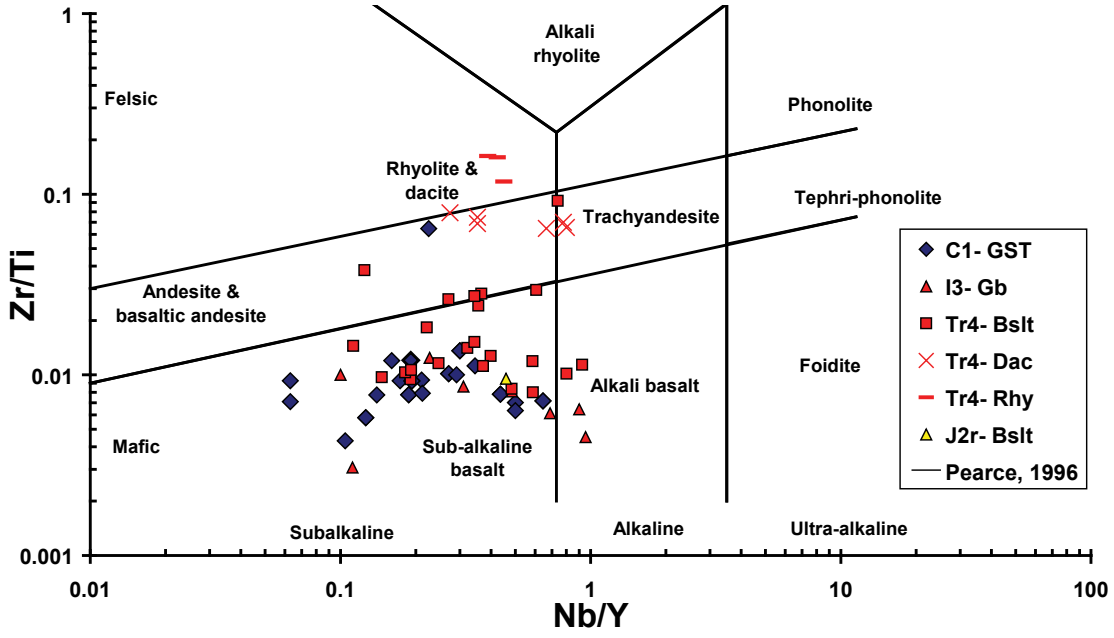

Figure 45 Zr/Ti vs. Nb/Y discrimination diagram after Pearce (1996), illustrating the composition of the coherent volcanic facies at Greens Creek.

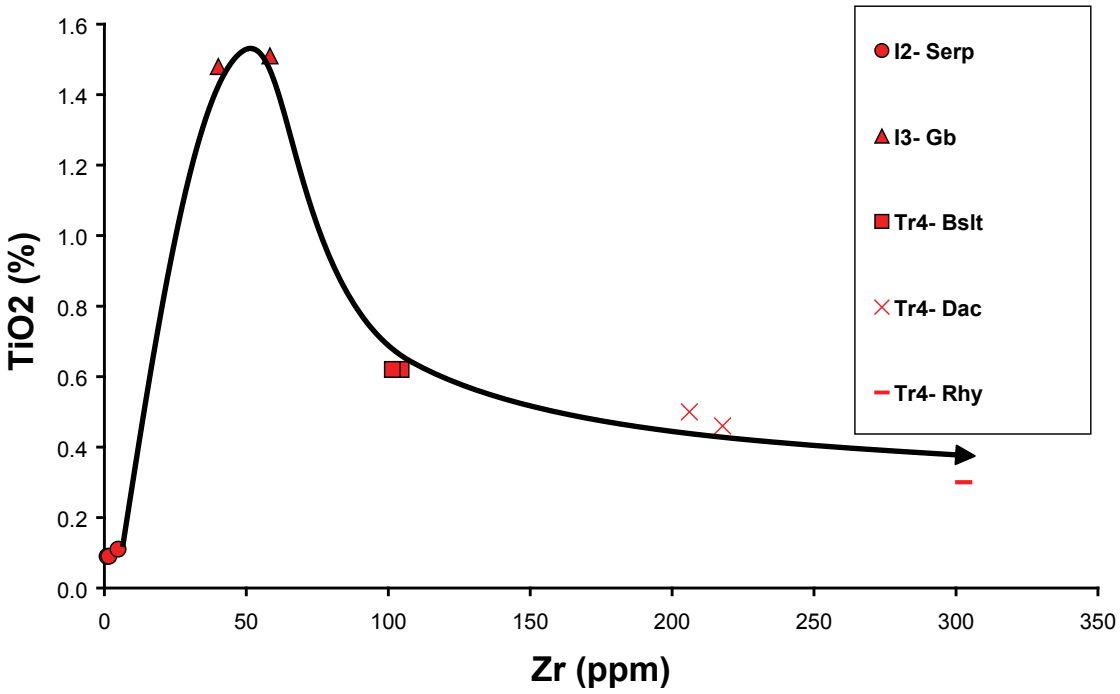

Figure 46 TiO_2 vs. Zr showing a tholeiitic fractionation curve from serpentinite through to rhyolite in Late Triassic volcanic rocks at Greens Creek.

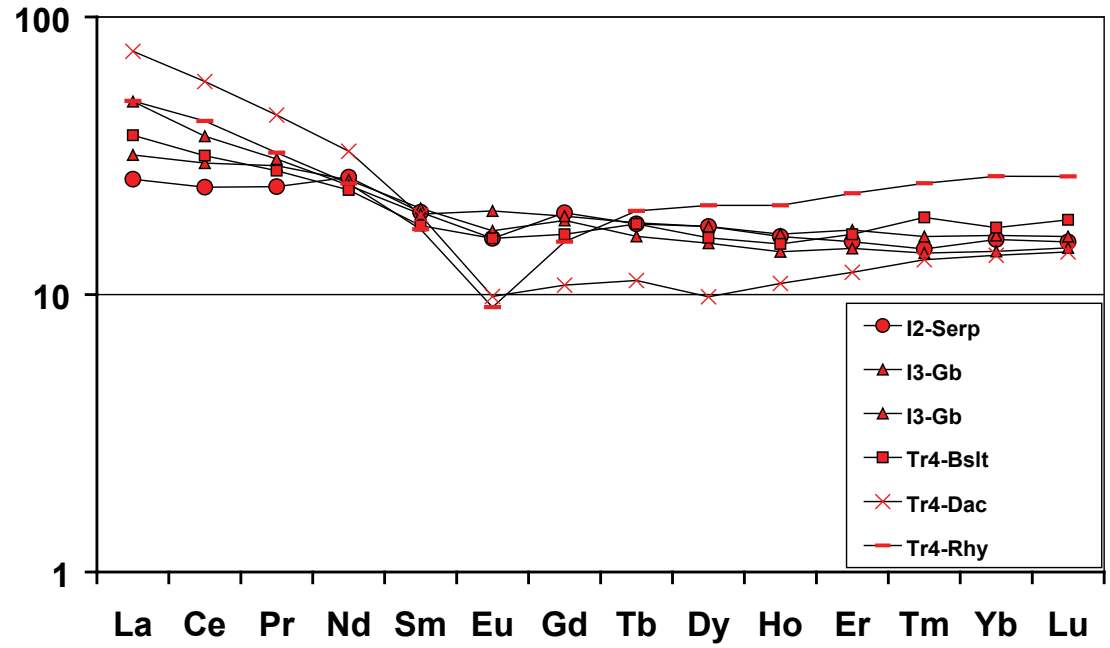

Figure 47 Rare earth element (REE) plot for Late Triassic volcanic rocks. Analyses are chondrite normalized using Taylor and Gorton, 1977.

Mafic volcanic rocks at Greens Creek occur in footwall greenstones, the hanging wall basalts and microgabbros and the post-Triassic basalt. MacLean and Barrett (1993) use Y versus Zr to determine magmatic affinity of mafic volcanic rocks. The HFSE ratios, particularly Zr/Y, change with rock affinity and, as they are also immobile, can be used to discriminate between geochemical suites of various tectonic affinities. The coherent mafic volcanic rocks at Greens Creek mostly cluster in the tholeiitic field with a few hanging wall samples scattering into the transitional and calc-alkaline fields (Figure 48).

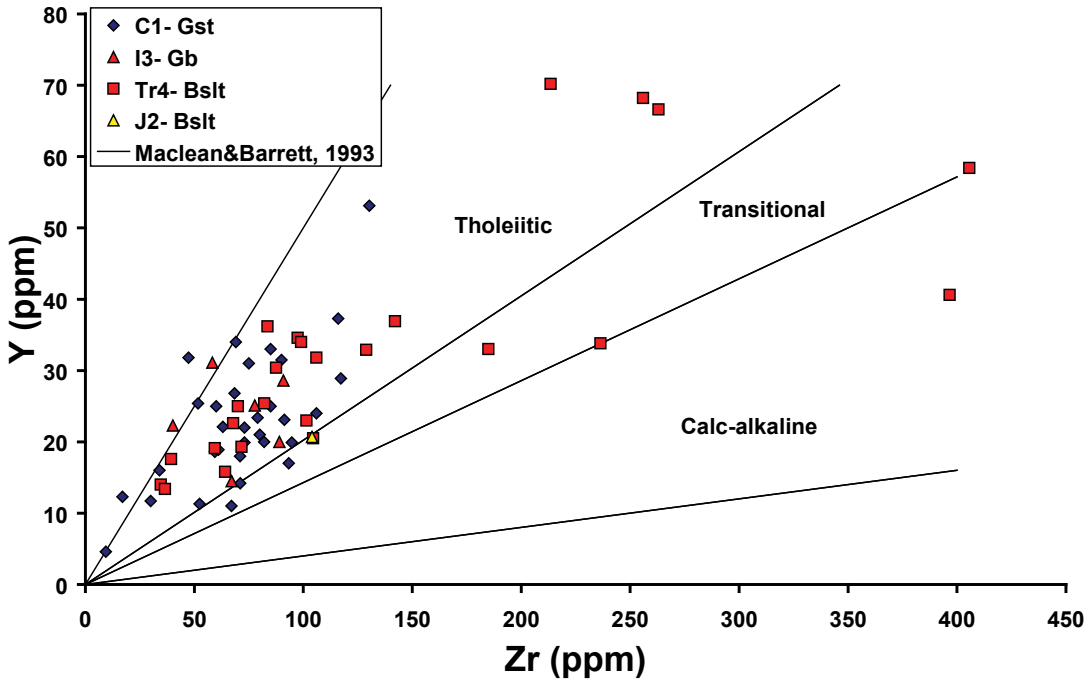

Figure 48 Y vs. Zr plot of coherent volcanic rocks at Greens Creek. Most samples, regardless of stratigraphic position, plot in the tholeiitic field with a few Triassic samples plotting in the transitional and calc-alkaline fields.

Applications of discriminant analysis of the coherent mafic volcanic rocks from the Greens Creek area provide additional information regarding the tectonic settings of the lithologies. Three ternary diagrams based on immobile elements Ti, Zr, Th, Nb and Y (Figure 49) illustrate the difference between the various lithologies. The Ti-Zr-Y plot of Pearce and Cann (1973) is most effective for separating within-plate basalts (WPB) from basalts showing arc (volcanic arc-basalts – VAB; calc-alkaline basalts – CAB; or island arc tholeiites –IAT) or mid-ocean ridge basalt (MORB) chemistry. All Greens

Creek coherent mafic volcanic rocks broadly cluster in and around the MORB, IAT and CAB field indicating a tectonic environment transitional between within plate and plate margin. The Zr-Th-Nb diagram of Wood (1980) is most efficient at separating VAB from MORB-WPB compositions and at separating calc-alkaline and tholeiitic trends. The footwall greenstones from Greens Creek mainly plot in the VAB field while the hanging wall volcanics scatter between the VAB and WPB fields. The Zr-Nb-Y plot of Meschede (1986) is similar to the first plot with the additional advantage of discriminating between normal MORB (N-MORB) and enriched (E-MORB). The footwall greenstones broadly plot within the VAB field while the hanging wall volcanics have more scatter and plot into the E-MORB and WPB-tholeiite fields.

Overall, the footwall greenstones tend to plot in slightly more juvenile fields such as VAB or MORB while the hanging wall volcanics are much more scattered and tend to plot in slightly more enriched or transitional fields such as E-MORB or WPB-tholeiites (Figure 49). Taylor et al. (2008) found that the capping basalts of the Triassic sequence for the Alexander Terrane (similar lithologies to our Tr4- Bslt) were also transitional in chemistry and interpreted this as indicating they were the product of an incipient rift in an existing island arc system. This is consistent with the footwall greenstones being a more typical island arc and the hanging wall basalts being the slightly enriched rift-related products.

The footwall serpentinite lithology has been classified as ultramafic (Taylor et al., 1995; Newberry and Brew, 1997). As the original mineralogy has been destroyed by serpentinization, alteration and deformation, recalculating the mineralogy of these rocks using whole-rock major-element analyses and plotting them on the mafic and ultramafic International Union of Geosciences (IUGS) classification diagrams is the most reliable way to classify them. The whole-rock analyses were recalculated as anhydrous compositions and original mineral proportions were calculated using MINSQ (Herrmann and Berry, 2002). MINSQ is a least-squares spreadsheet method for calculating mineral proportions from whole-rock major-element analyses given

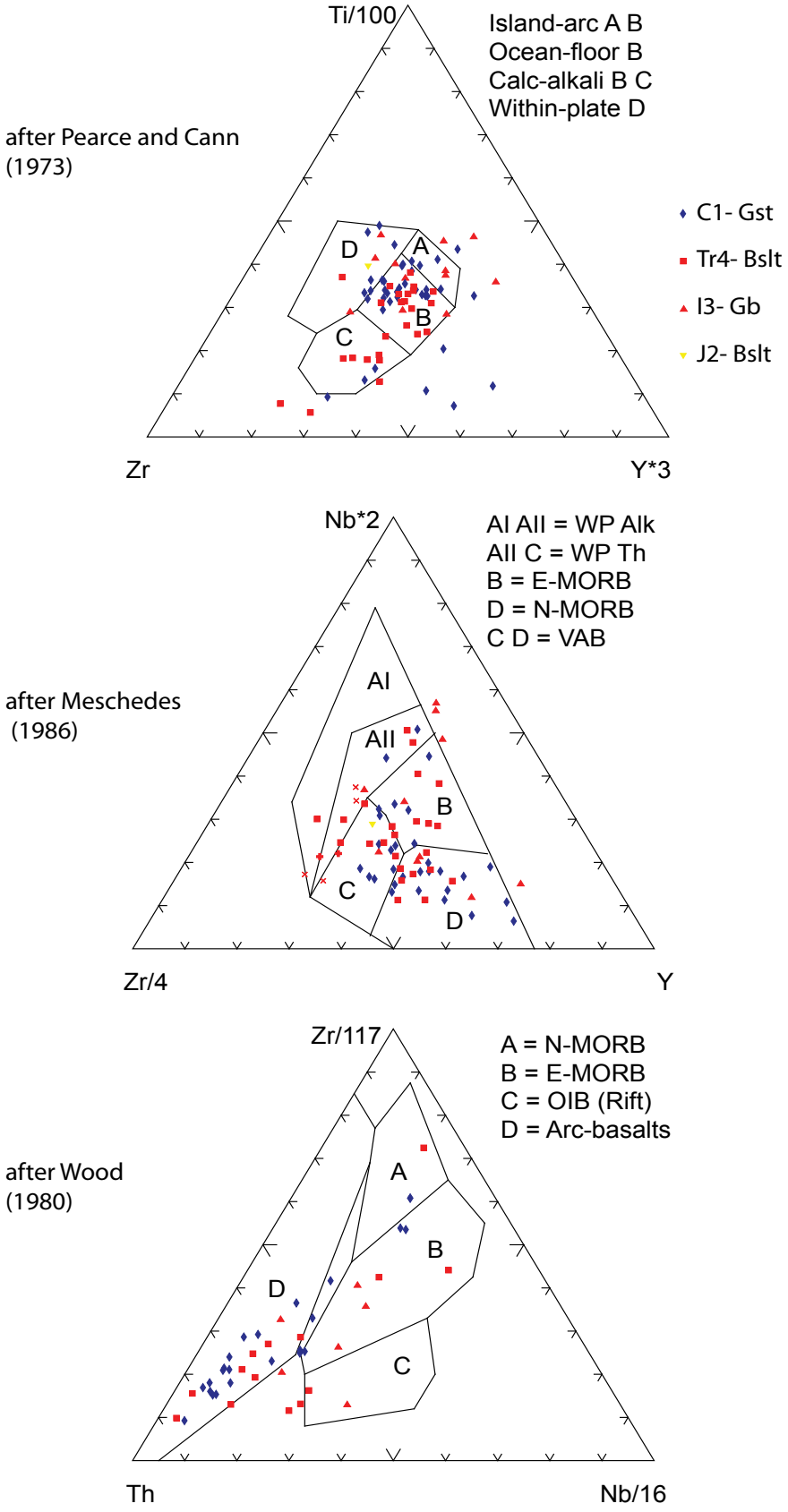

Figure 49 Tectonic discrimination diagrams after Pearce and Cann (1973), Wood (1980) and Meschede (1986). Greens Creek footwall greenstones plot primarily in fields of ocean floor or arc settings while the hanging wall volcanic lithologies are more scattered and plot into the transitional fields (E-MORB, WPB-tholeiites).

a user-defined composition for each of the minerals inferred to have been in the protolith (Table 7). The composition of anorthite was taken from an olivine norite from Deer et al. (1992: Table 38, analysis 7), the compositions of olivine, orthopyroxene, clinopyroxene, Cr-spinel and magnetite-spinel were taken from analyses of crystals in Alaskan-type ultramafic xenoliths from the Aleutian arc reported in Conrad and Kay (1984). These two sources are from Alaskan-type ultramafic bodies which appear to have the correct mineral chemistry as demonstrated by a sum of the residuals squared (Residual SSQ) of ≤3.

Table 7 Mineral compositions used in recalculating the original mineralogy of lithologies I1&2. References for each mineral are quoted in the text. Opx = orthopyroxene, cpx = clinopyroxene, - = 0% of that element.

Element	wt%	Quartz	Anorthite	Labradorite	Olivine	Opx	Cpx	Cr-spinel	Mag-spinel	Amphibole
SiO2	%	100.0	44.2	52.4	39.9	55.0	53.1	0.1	0.1	42.6
TiO2	%	-	-	0.1	-	0.1	0.2	0.6	7.5	1.0
Al2O3	%	-	36.2	29.7	0.0	1.1	1.7	10.1	2.5	12.2
Fe2O3	%	-	0.1	0.5	8.7	14.9	5.0	22.3	86.2	11.0
MnO	%	-	-	-	0.2	0.4	0.2	0.3	0.5	0.2
MgO	%	-	19.4	0.1	50.5	29.2	17.2	11.2	3.4	15.8
CaO	%	-	0.2	12.7	0.1	0.7	22.5	-	-	11.5
Na2O	%	-	-	4.0	-	0.1	0.3	-	0.5	2.5
K2O	%	-	0.3	0.2	-	-	-	-	-	0.8
P2O5	%	-	-	-	-	-	-	-	-	-
Cr2O3	%	-	-	-	-	-	0.7	48.2	2.2	0.5
NiO	%	-	-	-	0.2	-	-	-	-	-
Total	%	100.0	100.0	100.0	100.6	100.6	99.6	99.6	99.6	99.6

The re-calculation of mineralogy relies upon major-elements, most of which are at least partially mobile under extreme alteration. For the following three reasons, the altered serpentinite unit was tested by this approach: (1) locally, the serpentinite unit retains possible primary magmatic textures, indicating it may be less altered, (2)most of the samples are from the major body on Mammoth ridge which is over 1 km across and, though some of the major-elements are mobile, it is doubtful they would be removed from the entire body and (3) for the serpentinite lithology, the method produced realistic residual SSQ values generally <3. Four of ten samples of footwall serpentinite have

calculated mafic mineralogy that plots in the olivine gabbronite to olivine norite fields of the IUGS mafic classification diagram (Figure 50A). The remaining six samples plot in the plagioclase-bearing ultramafic field and, as such, are examined on the IUGS ultramafic classification diagram where they plot in the peridotite portion of the diagram, in the lherzolite to wehrlite fields (Figure 50B). The same calculations were attempted on the quartz + carbonate + mariposite dikes in the footwall but the results were far from typical values for igneous rocks. This lithology is highly altered and the individual dikes are typically quite thin. The dikes were not classified because the proportional mineralogy was high in quartz and the residual SSQ values were generally >80. Figure 50A and B suggests that half of the serpentinites that were previously classified as ultramafic are mafic in composition and the rocks that are truly ultramafic are peridotitic in nature. These compositions are similar to those from Alaskan-type mafic-ultramafic bodies (Conrad and Kay, 1984).

The layered footwall lithology (C2) is likely clastic in origin and examination of immobile-element ratios may indicate clastic components of this lithology. Ti and Zr are apparently immobile in the footwall greenstones and may also be immobile in the footwall graphitic phyllites (Figure 51). The Ti/Zr ratio, for the footwall greenstone, is 105 and the graphitic phyllite ratio is 30 (Figure 51). When Ti versus Zr is plotted for the layered footwall volcaniclastic lithologies (C2) the data are highly scattered. Many samples plot along Ti/Zr=100 or cluster along Ti/Zr=30 (Figure 52).

The Ti/Zr ratios in the footwall volcaniclastic lithologies probably reflect the respective input from two sources the footwall greenstones and the footwall graphitic phyllites. The footwall chloritic phyllites, tan phyllites and siliceous phyllites appear to be primarily composed of material with a similar composition to that of the footwall greenstones. The siliceous rock lithology appears to have a similar composition to the graphitic phyllites. The footwall sericitic phyllites appear to have compositions varying

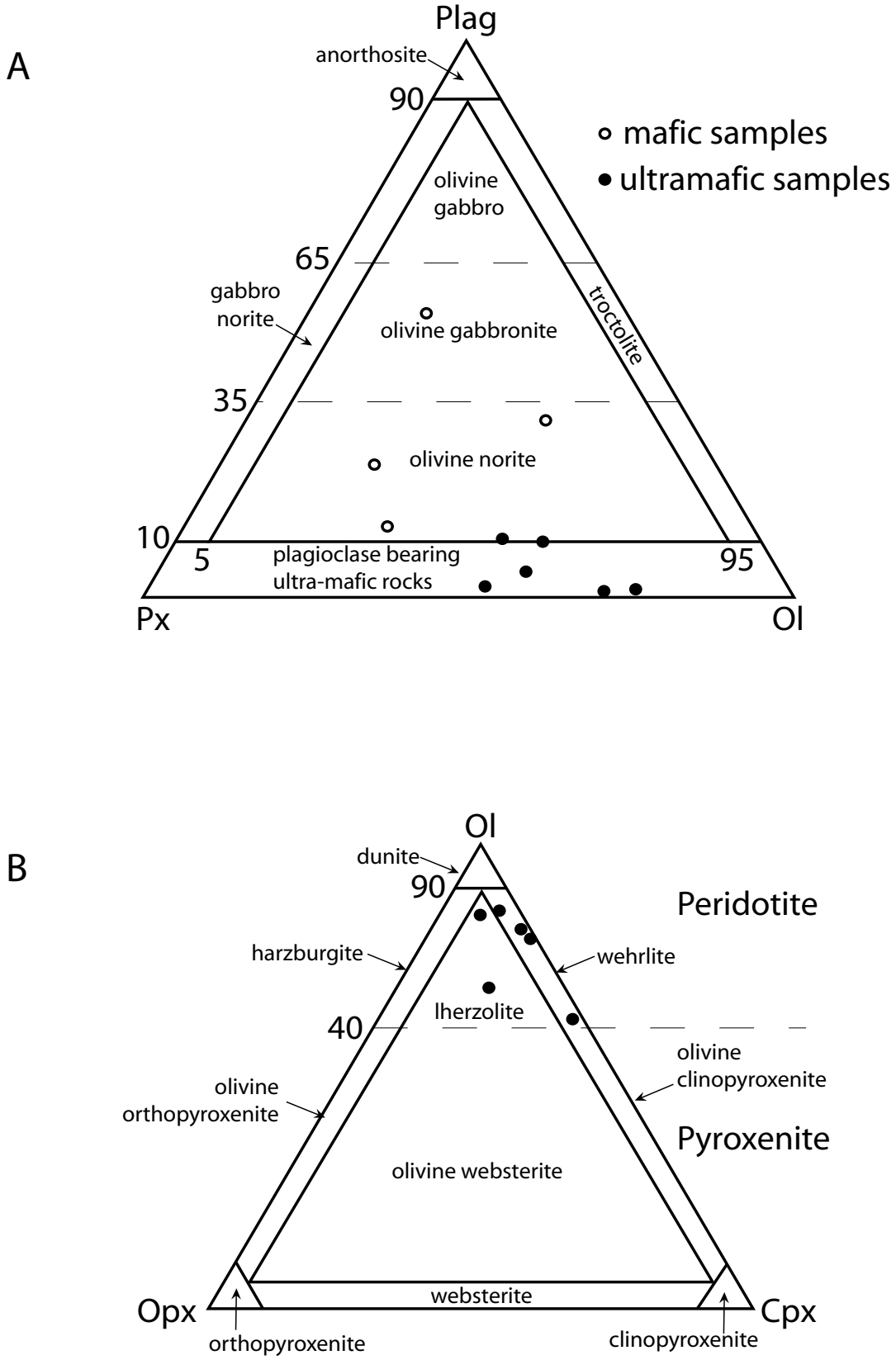

Figure 50 IUGS mafic and ultra-mafic classification diagrams. (A) IUGS mafic classification diagram illustrating 4 of 10 serpentinite samples are mafic, not ultramafic. (B) IUGS ultra-mafic classification diagram illustrating 6 of 10 serpentinite samples are ultramafic. Mineral proportions were calculated from whole-rock major-element analyses using MINSQ (Herrmann and Berry, 2002).

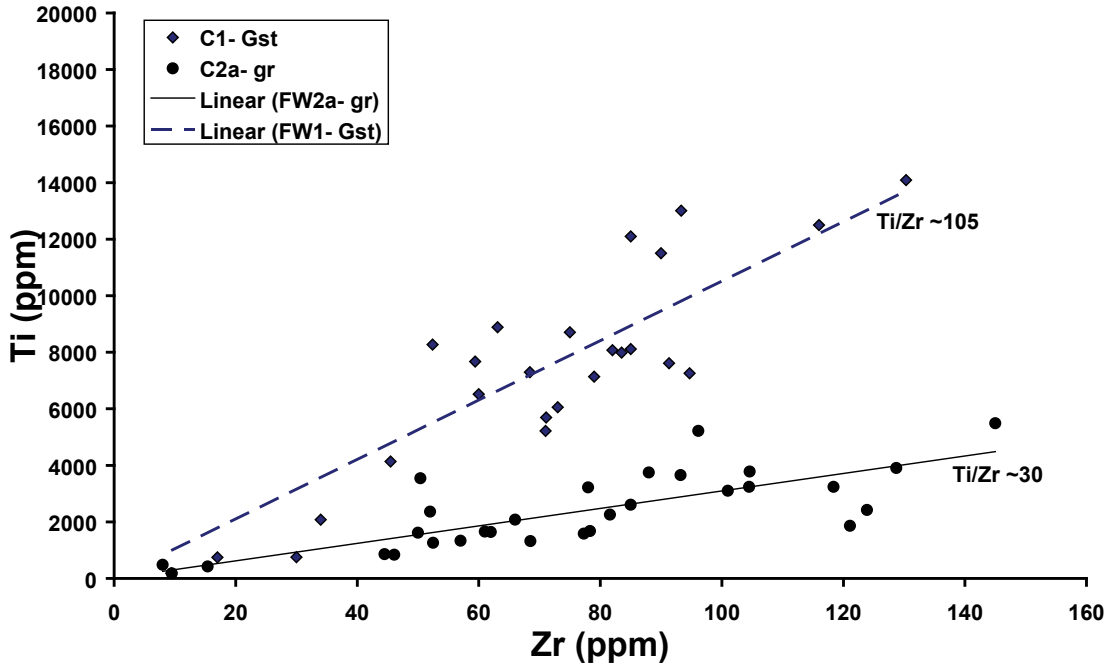

Figure 51 Ti vs. Zr for footwall greenstones and graphitic phyllites. Note the Ti/Zr ratios of approximately 105 and 31 respectively. Regression lines forced through the origin.

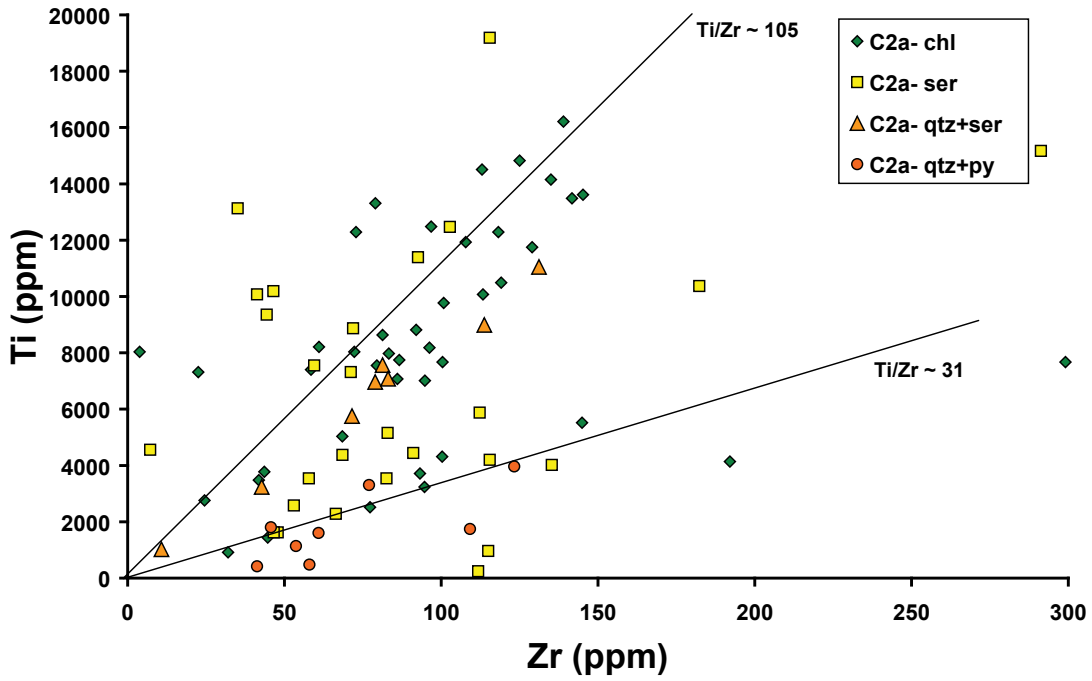

Figure 52 Ti vs. Zr for footwall volcaniclastic lithologies (C2). Note the two weak positive correlations along approximately 105 and 31.

from similar to the graphitic phyllite through to compositions with a slightly higher Ti/Zr ratio than the footwall greenstones.

Summary

- From stratigraphic top to bottom, there are three units within the mine sequence:
    1. Hanging wall argillites with minor volcanics (Tr3 to Tr4)
    2. Mineralized horizon (Tr2)
    3. Altered footwall of metabasalt and minor sediments (C1 to Tr1).
- Footwall phyllites are predominantly mafic volcanic and volcaniclastic rocks. The majority of the mineralogical variation seen in the upper portion of the footwall is the result of hydrothermal alteration.
- Two major ore types are black ore and white ore. The black ore can be subdivided based on the dominant sulfides (galena and sphalerite vs. pyrite). The white ores are subdivided on the dominant gangue mineral (carbonate, barite or silica). The white ores can be greatly enriched in precious metals (Au and Ag). There are three main ore bodies at Greens Creek with three extensions: East ore, West ore (Northwest, 5250) and Southwest ore (200 South).
- Hanging wall argillites are carbonate-rich pelagic muds and distal turbidites. There is weak hydrothermal alteration in the bottom part of the hanging wall sequence. There is a minor volcanic component consisting of microgabbro, basalt, dacite and rhyolite within the hanging wall; the capping basalts at the top of the Hyd Formation are regionally extensive.
- The Greens Creek deposit and its host rocks have been poly-deformed. There are at least four generations of folding and two faulting events.
- All of volcanic rocks in both the footwall and hanging wall are classified as igneous on the Ni versus Zr/TiO_2 diagram of Winchester et al. (1980) and Zr, Y, Ga, Nb and Yb are generally immobile in the coherent volcanic rocks at Greens Creek.

- The coherent volcanic rocks at Greens Creek are dominantly tholeiitic. The footwall greenstones are basaltic. The hanging wall volcanic suite ranges from basaltic through to rhyolitic in composition.
- The tectonic discrimination diagrams of the mafic volcanic rocks indicate the footwall greenstones are volcanic arc basalts (VAB). The hanging wall basalts have a more complex chemistry that suggests a source such as a rift of an existing island arc. Serpentinites have both mafic and ultramafic mineralogy with the ultramafic rocks having a peridotitic nature. The mafic compositions are similar to the hanging wall microgabbros.
- Ti/Zr ratios of the fine-grained layered volcaniclastic footwall lithologies indicate at least two potential end members: footwall greenstones and background sedimentation.

Chapter 4: U-Pb dating methodology

Introduction

This chapter describes a new method which was developed to date small, in-situ zircons. In this study, small zircons are defined as having a surface area of between 25 μm^2 (i.e. 5 μm by 5 μm) and 1000 μm^2 (i.e. 20 μm by 50 μm). Ultimately, the minimum size of the zircon needed for a reliable analysis is determined by the volume of the zircon and its U-Pb content (Kosler and Sylvester, 2003; Tiepolo, 2003). Studies such as Tiepolo (2003) have found the limiting factor for U-Pb dating to be radiogenic Pb content and not spot size. Using this as a starting point, we attempt to push the LA-ICP-MS technique by reducing the volume of zircon analyzed by an order of magnitude and comparing this '10 μm spot size' data with data generated at 35 μm spot sizes. Conventional U-Pb zircon dating studies (TIMS, SHRIMP and LA-ICP-MS) are done on 'large zircons' that typically have surface areas of 5,000 μm^2 (i.e. 50 μm by 100 μm) or greater. These large zircons are very rare in the study area while small zircons are much more abundant.

The stratigraphic footwall rocks of the Greens Creek deposit are ideal candidates to attempt the dating of small zircons because the age constraints are poor and even low-accuracy results are likely to be significant. Currently the minimum age of the footwall is well constrained by several samples in the immediate mine hanging wall that have a low diversity assemblage of latest Carnian – earliest Norian (Late Triassic) conodonts (*Metapolygnathus nodosus* (Taylor et al., 1999)). The maximum age of the mine footwall is interpreted from regional mapping as Devonian (Duke et al., in press). The mine footwall is likely to have formed between 415 Ma and 225 Ma, a time span of 190

m.y. A well constrained minimum age is important because it allows the identification of zircons with anomalously young ages that are metamict with lead loss. The potential age range of 190 m.y. is important because the LA-ICP-MS typically achieves a 2σ precision of between 1–10% (Kosler and Sylvester, 2003). At Greens Creek this would still give geologically meaningful dates (i.e. at worst precision, Late Triassic rocks could have dates such as 225 ± 22 Ma). It is important is that one rock unit within the Greens Creek footwall has both large and small zircons that can be dated with normal U-Pb zircon methods acting as an internal standard against which to compare our method and results.

The use of laser ablation-inductively coupled plasma-mass spectrometry (LA-ICP-MS) is well established as a method of measuring U-Pb isotopic data in zircon and deriving geologically meaningful dates from these data (i.e. Feng et al., 1993; Fryer et al., 1993; Hirata and Nesbitt, 1995; Kosler and Sylvester, 2003; Tiepolo, 2003; Jackson et al., 2004; Gehrels et al., 2008). The LA-ICP-MS method has slightly less spatial resolution and precision than the sensitive high mass resolution ion microprobe (SHRIMP) but is a fraction of the cost and is much more widely available. The LA-ICP-MS method has an order of magnitude less precision than the isotopic dilution thermal ionization mass spectrometry (ID-TIMS) method but has better spatial resolution and is also much less expensive. The strengths of the LA-ICP-MS method lie in its low cost (~$250AUD/ sample), good spatial resolution and ability to give moderately precise ages.

In the past 30 years there have been two overall trends in zircon geochronology. The well-established ID-TIMS method has focused on achieving smaller errors so that, now, dates with ± 0.1% (2σ) are common (Ireland and Williams, 2003). The SHRIMP method has focused on increasing spatial resolution to the point that spot sizes as small as 10 μm with a depth of 2 μm (volumes of approximately 150 μm^3) can be used to date portions of individual zircon grains (Kosler and Sylvester, 2003). Research in terms of the LA-ICP-MS method for U-Pb of zircons in the past 15 years has largely been

focused on improving the technique so that it is comparable in precision and spatial resolution to the SHRIMP method (i.e. Feng et al., 1993; Fryer et al., 1993; Hirata and Nesbitt, 1995; Jackson et al., 2004). Now that the LA-ICP-MS method is established, a logical step is to use its strengths to date smaller, harder-to-find zircons: those zircons that are too small to date with the ID-TIMS method and too time intensive to attempt with the SHRIMP method.

In order to test the use of small zircons as geochronometers, a simple experiment was devised. One rock unit from the mine footwall that had large and small zircons was used as the test sample. This sample was dated using the conventional ID-TIMS method at the University of British Columbia using methods described in Scoates and Friedman (2008). This sample was also dated at the CODES geochronology laboratory at the University of Tasmania using conventional LA-ICP-MS methods described in Meffre et al. (2007). Finally, this sample was dated using the new in-situ LA-ICP-MS method. The small in-situ zircons in the rock mount were divided into four size ranges: <100 μm^2; 100 μm^2 to 150 μm^2; 150 μm^2 to 1000 μm^2; and >1000 μm^2. Approximately 12 grains from each of these ranges were analyzed using the small spot technique and the results used to indicate the viability of each range as a geochronometer. The best quality analyses, as defined by the integration interval criteria outlined in the data processing section, from across all of the size ranges were selected in order to give a more realistic example of what may be achieved in a rock that has fewer zircon grains from which to choose.

Locating zircon grains, sample preparation and textural analysis

The first step of any zircon-dating study is to find zircon grains. Conventionally, this is done by crushing the sample, separating the heavy minerals, hand picking the zircons and mounting them in epoxy. The practical minimum size of a zircon crystal easily separated this way is 50 μm by 50 μm. Smaller crystal sizes require more complex

equipment such as centrifuges (Lodewijk, 1973). Small grains are best analyzed in-situ eliminating the potential for contamination, preserving the original crystal shapes and providing a geological context for the growth of the crystal. Both SHRIMP and LA-ICP-MS methods can analyze in-situ rock mounts. However, finding and marking small grains under the reflected light microscope is difficult. With the development of commercial Scanning Electron Microscope-based Mineral Liberation Analysis (SEM-MLA) software pioneered for applied mineralogy and metallurgical processing, it has become feasible to map small mineral grains within a rock mount in an automated fashion on a large number of samples (Gu, 2003; Fandrich et al., 2007).

Even with the automated SEM-based technique, locating of the zircons is time consuming. For every 12 unknown zircons analyzed in this project, approximately two hours were spent locating grains and one hour analyzing them.

Sample preparation

To compare small zircon and large zircon analytical techniques, the grains had to be prepared in three different ways. For the TIMS and the conventional LA-ICP-MS method the zircons were prepared by crushing approximately 300 g of rock, milling in a Cr-steel ring mill and sieving to a grain size <425 μm. The heavy minerals were separated using a gold pan and the magnetic fraction was removed using a Fe-B-Nd hand magnet. Zircons were hand-picked from the concentrate. The zircons for conventional LA-ICP-MS analysis were mounted in a 2.5 cm diameter epoxy mount which was polished using clean sandpaper and a clean polishing lap. Prior to analysis, the sample was washed with distilled water in an ultrasonic bath. For the TIMS method, the zircons were left free and analyzed individually. For the in-situ LA-ICP-MS method, a 2.5 cm piece of rock was encased in epoxy, polished and carbon-coated prior to mapping using the automated MLA software. Cathodoluminescence images of the zircons were then obtained using the SEM prior to removal of the carbon coating and washing in an ultrasonic bath in distilled water.

Mineral liberation analysis (MLA)

The MLA analyses were undertaken on a FEI Quanta 600 SEM instrument controlled by the MLA software package developed at JKTech, University of Queensland. The specific method of MLA analysis used in this study was the Sparse Phase Liberation-Lite (SPL-LT) with the specific operating conditions outlined in Table 8. This method searches a high resolution Back Scatter Electron (BSE) image of the sample for grains with a defined BSE grey scale range. It then collects an Energy Dispersive Spectrum (EDS) for each particle that meets this criterion (Fandrich et al., 2007). The BSE image of the entire mount is stitched together from approximately 500 to 600 individual frames, each with a resolution of 1024 X 800 pixels. This BSE-based search method will be referred to in this chapter as the SPL-LT search method.

Table 8 Specific conditions used during the SPL-LT search method of locating zircons within rock mounts.

Method	SPL-LT and EDS
Accelerating voltage	25 kV
Magnification	250X
Beam size ("spot size")	6 to 7
Resolution	1024 X 800
BSE contrast/ brightness standard	Au
BSE zircon grey value standard	Zircon 91500
Minimum size of zircon identified	5 μm

Offline classification of the resulting spectra was done with the commercial MLA software package from JKTech. For classification, reliability (closeness of fit between the spectra of the standard and the unknown) of 10^{-30} was used and the zircon 91500 spectrum was used as the standard for identifying zircons. The map of zircon grains was then overlaid on the BSE image and the location of the grains highlighted in order to digitally record their location within the laser ablation cell. Figure 53 shows examples of images collected during the present study.

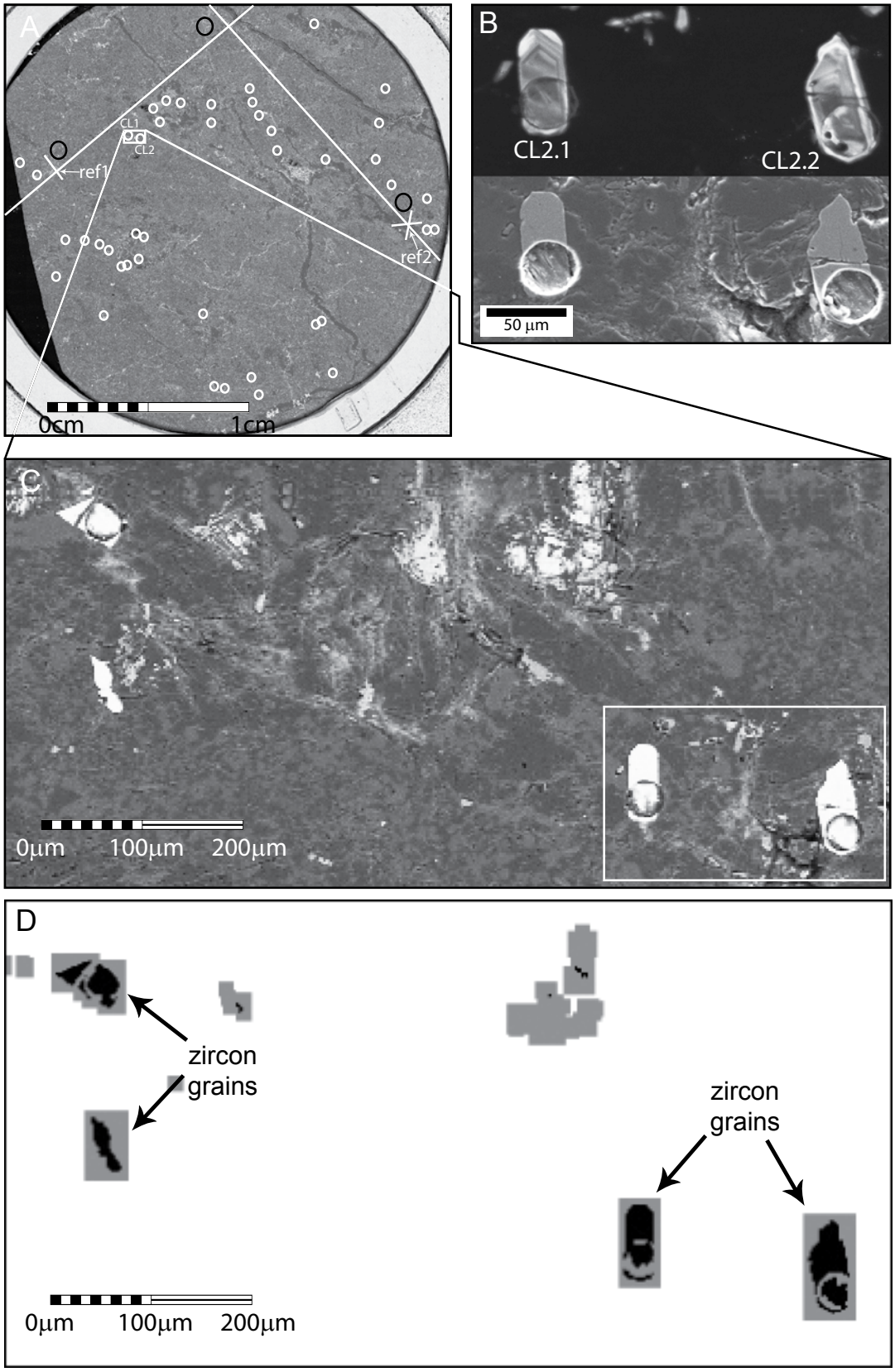

Figure 53 Example of a zircon map generated using the SPL-LT search method of MLA analysis. (A) High Resolution composite BSE image with location of zircons analyzed in this study marked by white circles, black circles indicate location of matrix analysis. (B) CL image (top) and SE image (bottom) of zircons CL2.1 and CL2.2; these are two of the larger zircons found in-situ. (C) Enlarged portion of BSE image. (D) Enlarged portion of classified zircon map.

Cathodoluminescence (CL) imaging and optical photomicrographs

Once zircon grains have been selected for analyses, it is critical to characterize the textures found within each crystal to determine its history. Cathodoluminescence (CL) imaging is a routine method of investigating the internal structure of zircon grains (Nasdala et al., 2003). The CL imaging for this study was panchromatic imaging using a Gatan PanaCLF detector with a blue filter. The detector was attached to the same SEM as was used for the MLA work. Secondary electron (SE) images were also acquired for all the grains analyzed. An accelerating voltage of 20 kV was used for obtaining both the CL and SE images. Optical photomicrographs of the crystal mounts were taken with a Color View soft imaging system attached to an Olympus BX60 optical microscope with a 5X objective. Zircons free of inclusions and fractures were selected for analysis. The rock mounts are approximately 1 cm thick and it is not possible to view the in-situ zircons with transmitted light microscopy. Reflected light microscopy does not reveal inclusions and therefore zircons analyzed in-situ were selected solely on the basis of the CL images.

Mass spectrometry instrumentation and operating conditions

Laser

The CODES geochronology laboratory uses a New Wave 193 nm (quintupled) solid state Nd:YAG Q-switched laser ablation system. All laser parameters such as spot size, laser energy, pulse rate and the firing of the laser are controlled by the MEOLaser 193 software. The laser beam is fixed and the sample is moved underneath by a motorized x-y-z stage. A digital video camera mounted above the optical system allows both real time and still imagery of the sample. The original New Wave ablation chamber was modified to provide greater sensitivity, faster washout and more controlled gas flow over the ablation site. A small (30 mm) chamber containing the He outlet was suspended inside the original New Wave ablation chamber using a set of small magnets.

Table 9 LA-ICP-MS operating conditions and data acquisition parameters.

ICP-MS	**Analysis and Tuning**	
Model	Agilent 7500cs	
Forward Power	1200 W	
Gas flows:		
Plasma (Ar)	15 l/min	
Auxillary (Ar)	1.0 l/min	
He	0.8 l/min	
Ar	0.95 l/min	
LA	**Grain mounts**	**In situ**
Wavelength	193 nm	193 nm
Repetition rate	5 Hz	5 Hz
Pre-ablation laser warm up	30 s	30 s
Pulse duration (FWHM)		
Focusing objective	8X	8X
Degree of defoccusing	0	0
Spot size	35and 10 µm	10 µm
Incident pulse energy	55%	55%
Energy density on sample	ca. 3 mJ/cm^2	ca. 1.8 mJ/cm^2
Data acquisition parameters		
data acquisition protocol	time resolved	
Scanning mode	Peak hopping, 1 point per peak	
Detector mode	Pulse mode, dead time correction applied	
Isotopes determined	^{49}Ti, ^{96}Zr, ^{178}Hf, ^{202}Hg, ^{204}Pb, ^{206}Pb, ^{207}Pb, ^{208}Pb, ^{232}Th, ^{238}U	
Dwell time per isotope	^{49}Ti-10ms, ^{96}Zr-5ms, ^{178}Hf-5ms, ^{202}Hg-10ms, ^{204}Pb-10ms, ^{206}Pb-30ms, ^{207}Pb-30ms, ^{208}Pb-15ms, ^{232}Th-5ms, ^{238}U-10ms	
Quadrupole settling time	ca. 4ms	
Time/scan	0.1512 s	
Data acquisition (s)	60 s (30 s gas blank plus 30 s ablation)	
Samples and standards	**Grain mounts**	**In situ**
mounts	25mm diameter polished grain mounts	25mm diameter polished whole rock mounts
standards	TEMORA1 (417Ma); zircon 91500 (1065Ma)	

For this study, two sets of laser conditions were used. The standard method of Meffre et al. (2007) used a spot size of 35 μm, a frequency of 5 Hz and an energy density of approximately 3 mJ/cm^2 (Table 9). This method was used on the crystal mount. The laser conditions used on the in-situ zircons were a spot size of 10 μm, a frequency of 5 Hz and an energy density of approximately 1.8 mJ/cm^2 (Table 9).

Previous studies (i.e. Eggins et al., 1998; Jackson et al., 2004) found that ablation in a He atmosphere significantly increased the strength of the signals and reduced the short-term noise in the signals of both U and Pb isotopes, thereby increasing the precision in the measurement of the U-Th-Pb isotopes. All ablations in our study were done in a He atmosphere and blended with Ar immediately outside the sample chamber.

ICP-MS

The laser ablation system described above is the sampling tool for the Agilent 7500cs quadrupole ICP-MS. The ICP-MS is tuned daily to optimize counts for the masses 45, 139 and 238, typically in the range 40–50 × 10^4 count per second for ^{238}U, and to minimize the production of oxides and doubly charged ions within the plasma. For tuning, the international standard glass NIST612 is ablated with a 100 μm wide line rastering at 3 μms^{-1} and 10 Hz at ~4 Jcm^{-2}. Oxides are tuned to <0.2% ThO/Th and doubly charged ions to <0.5% Ce^{2+}/Ce.

Data processing

The data reduction described here is a summary of the method outlined in Appendix 1 of Meffre et al. (2007) which was modified from the methods used at the Australian National University (Harris et al., 2004) to suit the ICP-MS and laser at the University of Tasmania. Data was reduced for each ‘run’. A run consists of four primary standards, two secondary standards, 12 unknowns, four primary standards, two secondary standards analyzed over the course of approximately one hour. The primary standard used to correct for mass bias, machine drift and downhole fractionation on the Pb/U and Pb/Th ratios was TEMORA1 (Black et al., 2003) and the secondary standard used was

zircon 91500 (Wiedenbeck et al., 1995). International standard NIST612 was ablated at the beginning of the analytical day for tuning purposes as well as at the end of the analytical day to correct for mass bias on the $^{207}Pb/^{206}Pb$ ratio. The $^{207}Pb/^{206}Pb$ mass bias is not determined using the Temora zircons because the counting statistics on ^{207}Pb are very poor and these grains sometimes have a detectable amount of common Pb (either in apatite inclusions or due to surface contamination). Individual analyses consisted of a 30 second gas blank followed by 30 seconds of ablation giving approximately 200 mass scans over a penetration depth of approximately 15 μm (Table 10). All data reduction calculations were done with Microsoft Excel using macros designed at the University of Tasmania.

Table 10 Ablation rates in zircon for various spot sizes and ablation durations. All ablations were done at a frequency of 5 Hz with an energy density of between 2 and 3 mJ/cm^2 depending on spot size. All spot sizes were at 55% energy. N/A indicates that the depth of the pit was too small to be determined reliably.

Duration (s)	100 μm spot (μm)	35 μm spot (μm)	10 μm spot (μm)	Average (μm)	Average rate (μm/s)
1	N/A	N/A	N/A	N/A	N/A
2	2	N/A	N/A	2	1
5	1.5	2.5	1	1.7	0.34
10	5	7	8	6.7	0.67
20	10	6.5	8	8.2	0.41

After triggering the laser, the mass spectrometer took approximately 2 seconds (s) (~15 mass scans) to achieve a steady signal. The average of the background count rates (first 30 s of analysis) was subtracted from each isotope. Pb and U isotopic ratios were then calculated for each 0.15 s of measurement. These ratios were filtered to exclude the top and bottom 1%, eliminating spikes and spurious data. The resulting filtered ratios were corrected for machine drift, downhole fractionation and mass bias.

Machine drift was calculated by fitting a line to the primary and secondary standard data that were collected before and after every 12 unknowns. The maximum time between analyses of standards (both primary and secondary) was one hour. The downhole

fractionation and mass bias correction factors (e.g. Hirata and Nesbitt, 1995; Horn et al., 2000) were calculated by averaging the drift corrected ratios on each quadrupole sweep (0.15 s) on the primary standard measurements (relative to the start of the analysis), fitting a curve to the data then dividing each the Pb, U and Th ratio for each sweep by the recommended value for TEMORA1. A set of correction factors was thus generated for each sweep and for each isotopic ratio. The corrected age data for each quadrupole sweep for each analysis was plotted against the analysis time to examine the reliability of the calculated ages. The standard errors quoted are based on the standard error of the measurements within the integration intervals and includes the measurement errors of the standards.

The integration interval was chosen based on the following criteria. First, the analyses are examined for evidence of inclusions, signified by notable increase in ^{49}Ti, indicating the presence of phases such as titanite that could have both radiogenic and common Pb. Portions of the analyses interpreted as being inclusion-free and having at least 20 mass scans (>3 s) were then selected for intensive data interpretation and were evaluated on three further criteria: 1) the most stable, horizontal portion of the analysis was used (preferably in the first 15 s of ablation), avoiding or treating separately portions with either elemental or age zonation; 2) grains or zones with >2500 ppm U were interpreted as being metamict and were rejected; 3) analyses which were significantly different to the rest of the analyses (typically > two standard deviations from the mean) were rejected as having either inherited (xenocrystic) components or having suffered partial loss of Pb. Generally, these criteria reduced the population MSWD to <2.0.

Pb corrections

U-Pb geochronology relies on two decay systems to determine a single age. A third decay system of ^{232}Th was also measured during these analyses. This gives four estimates of the age including the three daughter/parent systems ($^{206}Pb/^{238}U$, $^{207}Pb/^{235}U$ and $^{208}Pb/^{232}Th$) and the $^{207}Pb/^{206}Pb$ system which relies on the differences in the rates of decay of the two U isotopes. In a perfect zircon which has not been affected by Pb

loss or common Pb contamination and does not show mixing between zones of different ages, these decay systems give ages that are within error of each other. When this is the case, the $^{206}Pb/^{238}U$ system gives the most precise ages for examples in this study. However, old and/or high U zircons (>2500 ppm U; this study) tend to accumulate radiation damage in their crystal lattice allowing Pb to leak out. In these metamict zircon grains, the Pb/U ages tend to be much younger than the $^{207}Pb/^{206}Pb$ ages and the analyses plot off concordia (Geisler et al., 2002).

Most of the zircons reported in this study plot slightly above concordia on the reverse concordia diagram with the $^{207}Pb/^{206}Pb$ and $^{208}Pb/^{232}Th$ age being slightly older than the $^{206}Pb/^{238}U$ age indicating that they have a small amount of common Pb. Some of this common Pb probably resides in inclusions and cracks in the zircons and makes the apparent $^{206}Pb/^{238}U$ very slightly older than the preferred age of the zircon. A small correction was made in this study for common Pb using the ^{207}Pb correction method (see Compston, 1999 for details). The correction can be visualized by projecting a line from global crustal common Pb through the zircons and onto concordia. In this study the $^{207}Pb/^{206}Pb$ value of 0.85±0.15 was estimated using the model of Stacey and Kramer (1975) for the age of the rocks (~240Ma). The alternative ^{204}Pb method of correcting for common Pb which is widely used in thermal ionization mass spectrometry cannot be used for the LA-ICP-MS because of a significant isobaric interference from ^{204}Hg present in the gas stream (i.e. Compston, 1999; Jackson et al., 2004).

When analyzing zircon grains with a surface area smaller than that of the laser spot size (i.e. grains with a diameter of less than 10 μm), a portion of the matrix was ablated and incorporated into the analyzed volume. To assess this potential source for Pb contamination (both common and radiogenic) three analyses of matrix from the sample were analyzed (100 μm, 10 Hz & 1.4 J cm^{-2}) (Figure 53). In all cases, minor Pb and U (1–2.5 ppm and 3–6 ppm respectively) with variable Th (7–68 ppm) were detected. The total Pb in the matrix is much lower than in an individual zircon grains (10–60 ppm)

and accordingly should not greatly affect results. However, as matrix is the most likely source of Pb contamination in these zircon grains, the analyses which incorporate minor matrix material will plot slightly off concordia.

A few of the zircons analyses in this study show evidence of mixing between two age domains. Most of this mixing take place during a single analysis as the laser drills from one age zone to the next. In these cases, the time resolved ICP-MS data plot on a discordia line on the concordia diagrams with the intercepts (as calculated using the Isoplot software of Ludwig 2003) corresponding to the age of the zones being analyzed.

General correction procedures for 35 µm and 10 µm spot sizes

In conventional LA-ICP-MS isotopic analysis of grain mounts, the grains are all placed close together and analysis of standards and unknowns are done in approximately the same location within the chamber. As a result pseudo-age zonation within the sample chamber is not significant. Pseudo-age zonation is the result of chamber design. The chamber design affects gas flow across the sample surface. Subtle variations in gas flow result in heterogeneous delivery of material to the ICP-MS which in turn can give inconsistent ages across the chamber. With the in-situ method, the zircons are located anywhere on the 2.5 cm diameter mount. To test for age zonation artefacts within our chamber several pieces of zircon 91500 were placed in a cross configuration on a 2.5 cm diameter epoxy mount and analyzed with an east-west and a north-south traverse. The furthest east analysis was slightly young (~5%), but the extreme ends of the north-south traverse were much younger (~13%). To avoid this chamber zonation, in-situ samples were oriented east-west, and if possible, analyses were avoided in the extreme north, south or east portion of the mounts. No specific correction for chamber zonation was applied.

In order to minimize the duration of each run (4xTEMORA1, 2x91500, 12xUnknowns, 4xTEMORA1, 2x91500) and to minimize machine drift, locations of the zircons were pre-recorded relative to a set of reference points. These reference points were

permanently scribed on the sample (Figure 53). When the sample was inserted into the chamber for analysis it was reoriented so the maximum spread in the distribution of the zircons was oriented east-west, avoiding errors associated with north-south position in the chamber. The accuracy of this location system was ±50 μm, accurate enough to quickly locate the zircons during analysis.

Spatial resolution

One measure of spatial resolution using the LA-ICP-MS is the volume (or weight) of sample analyzed (Kosler and Sylvester, 2003). The spatial resolution is the result of both spot size and ablation depth. The ablation rate in zircon was determined by ablating a piece of Mud Tank zircon (Black and Gulson, 1978) with various combinations of spot size and ablation duration (Table 10). The depth of the ablation pits were measured under an optical microscope by focusing on the surface of the mount and the bottom of the pit, the difference being the depth. Our findings for ablation rates in zircon (Table 10) are similar to those reported by Jackson et al. (2004). The present study found that the longer ablation times allowed for a more accurate estimate of pit depth, probably because the difference between pit depth and the residual topography on the floor of the pit is quite large. An estimated drilling rate of 0.5 μm s^{-1} was used in our calculations. A sudden decrease in counts of ^{96}Zr and ^{178}Hf during the analysis was used to indicate zircon was no longer being ablated. In this study, zircons larger than 10 μm across have an ablation area equal to the area of the spot size used (10 μm spot gives 80 μm^2). In order to quantify the volume of material analyzed for the in-situ zircons, it was assumed that pit area was constant with a maximum usable ablation of 15 μm depth.

Assuming that 2 s ablation time at a frequency of 5 Hz is approximately equal to 1 μm ablation depth (Jackson et al., 2004; this study) and the zircons are continuous to the depth ablated, the volume of zircon analyzed was calculated by multiplying the surface area by the depth of zircon ablated. The spatial data for each zircon analyzed is only reported for the in-situ method. For the conventional LA-ICP-MS method, the zircon surface areas are much larger than the spot size and, therefore, all of the volumes are

identical at the maximum values of 14,000 μm^3 and 1200 μm^3 respectively for 35 μm and 10 μm spot sizes.

As spot size decreases, analysis sensitivity decreases and U/Pb downhole fractionation increases (Horn et al., 2000; Tiepolo, 2003). In order to achieve the highest quality data and, therefore, the most precise dates, studies typically use spot sizes >35 μm (as large as possible depending on the zircons being analyzed) (Feng et al., 1993; Fryer et al., 1993; Horn et al., 2000; Jackson et al., 2004; Meffre et al., 2007). The smallest spatial resolution using the LA-ICP-MS technique found in the literature is a 20 μm spot size ablated for 60 s (Tiepolo, 2003). The maximum volume of zircon ablated under these conditions (using assumptions stated above) is 20,000 μm^3 or approximately 15 times our maximum volume of 1200 μm^3 using the in-situ method. LA-ICP-MS systems using multi-collectors reported similar spatial resolutions to the values reported here (i.e. Gehrels et al., 2008).

Results of TIMS and LA-ICP-MS methods

Short-term precision

The short-term precision (~1 hr) of the in-situ LA-ICP-MS zircon dating method has been evaluated by repeated analyses of two zircon standards (TEMORA1, 91500). Typically the short-term precision of 12 analyses at 35 μm spot size on separated grains of either standard using the ^{206}Pb/ ^{238}U age is between 0.5% and 0.9%. The analyses are much less precise (^{206}Pb/^{238}U = 1.6%) when analyzing 12 spots with the smaller 10 μm laser spot size (Figure 54).

The less precise ratios with the 10 μm spot size are the result of less material being analyzed and increased elemental fractionation with depth (Horn et al., 2000; Tiepolo, 2003). The analysis of less material results in weaker signal strength and an increase in the relative noise in the signal. The ratio of laser pit diameter/depth is much greater with 35 μm spot size than the 10 μm spot size which results in increased downhole

fractionation with the 10 µm spot size (Figure 55). To minimize any problems with elemental fractionation with depth using the in-situ method, analyses were selected from the first 15 s of ablation when possible. The decrease in precision with the in-situ method is unavoidable and as a result the in-situ method is best applied to geologic problems where this lower precision is acceptable.

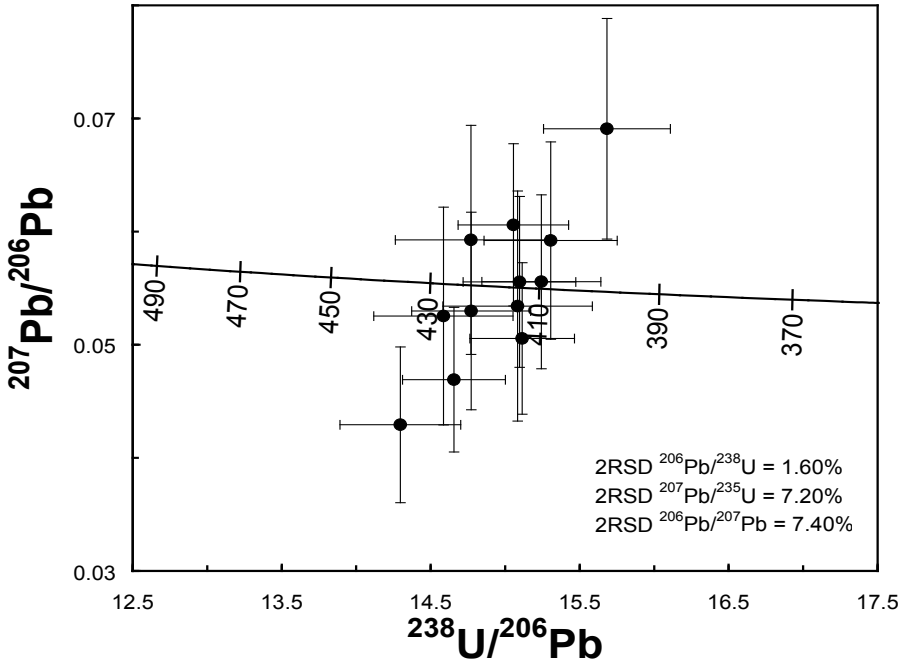

Figure 54 Reverse concordia plot of 12 consecutive analyses of TEMORA1. This zircon standard was analyzed with the in-situ LA-ICP-MS method (10 µm spot size) demonstrating reproducibility of $^{206}Pb/^{238}U$ (2σ 1.6%), $^{207}Pb/^{235}U$ (2σ 7.2%), and $^{207}Pb/^{206}Pb$ (2σ 7.4%) . Data-point error crosses are 1σ.

Long-term precision and accuracy

The long-term precision and accuracy of the technique have been established by repeated analyses of three zircons; TEMORA1 (Black et al., 2003; Table 11 and Figure 56), 91500 (Wiedenbeck et al., 1995; Table 12 and Figure 57) and Mud Tank (Black and Gulson, 1978; Table 13 and Figure 58). These are analyzed as unknowns for quality control purposes in every analytical run in the CODES geochronology laboratory. The current LA-ICP-MS system (Agilent 7500cs quadrupole ICP-MS with a New Wave193 nm solid state Nd:YAG Q-switched Laser) was installed in 2006 and a new sample chamber, designed in-house, was installed in May 2007. All analyses discussed below

were from the 7500cs ICP-MS between May 2007 and May 2008 using the same sample chamber. The following summary of the laboratory's long-term precision and accuracy only includes data obtained using the conventional LA-ICP-MS parameters (i.e. 30 s ablation time and 35 µm spot size).

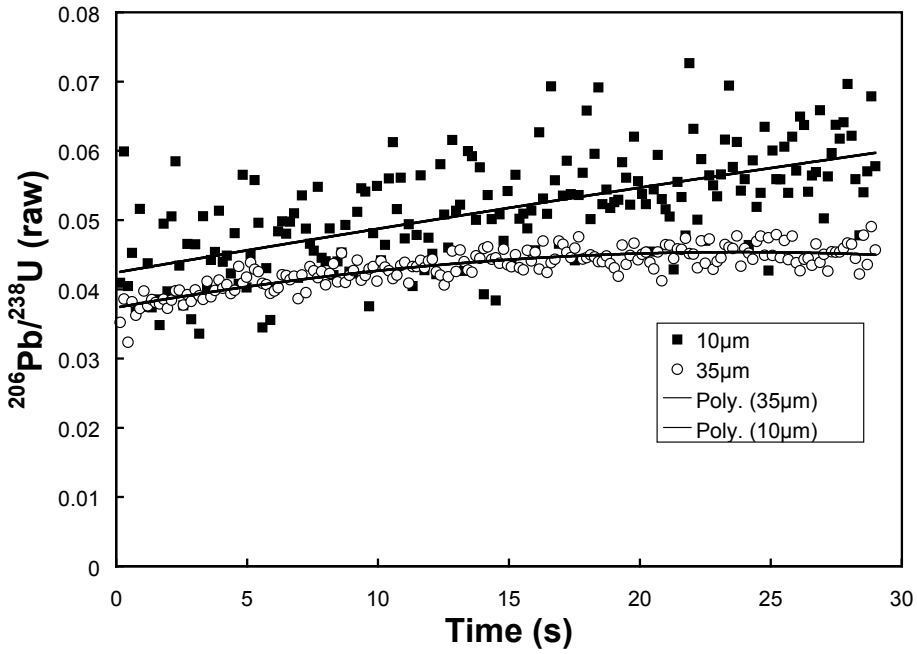

Figure 55 Increased downhole fractionation with 10 µm spot size. Data are uncorrected averages of eight analyses of TEMORA1 each for 30 s of analyses; the gas blank portion of the analyses is not shown.

The long-term average of the ^{207}Pb corrected $^{206}Pb/^{238}U$ on the primary standard Temora is slightly low (0.14%) due to a minor problem with the data reduction. This problem arises from a minor amount of contamination by common Pb (50–60 ppb) which resides either in the gasses, on the surface of the sample, in the ablation cell or in the laser–ICP-MS interface. This Pb is not taken into account when calculating the mass bias correction factors for $^{206}Pb/^{238}Pb$, but is taken into account when calculating the ^{207}Pb corrected $^{206}Pb/^{238}Pb$ age. This small inaccuracy is insignificant when calculating weighted average ages using fewer than 100 zircons (such as in this study) but must be taken into account for very precise work involving hundreds of analyses.

A few of the zircons (~5%) were rejected by the weighted average algorithm in the Isoplot 3.0 software of Ludwig (2003) and the MSWD statistics are slightly higher

than expected (1.3–2.1 instead of 1). These problems arise because all of the zircons analyzed in the past year were used with no rejection of analyses or adjustment of the integration intervals. Most of the rejected analyses can be traced back to problems with ablation (occasional grains ablate poorly due to cracks and inclusions) and transient problems with the chamber due to operator errors such as gas flow problems due to leaks or empty gas bottles.

Table 11 Summary of LA-ICP-MS and TIMS U-Pb isotopic ages for the TEMORA1 zircon (n=946). TIMS data from Black et al. (2003).

Isotopic ratios determined by LA-ICP-MS			Weighted mean age (Ma) +/- errors (at 95% confidence)			TIMS age (Ma)	
	Mean	st. dev. of indiv. anal.		weighted mean	2 std. error	Mean	2σ error
$^{207}Pb/^{206}Pb$	0.056	6.3	^{207}Pb corr.				
$^{207}Pb/^{235}U$	0.510	6.9	$^{206}Pb/^{238}U$ age	416.16	0.34	416.75	0.2
$^{206}Pb/^{238}U$	0.067	1.7					
$^{208}Pb/^{232}Th$	0.021	7.8					

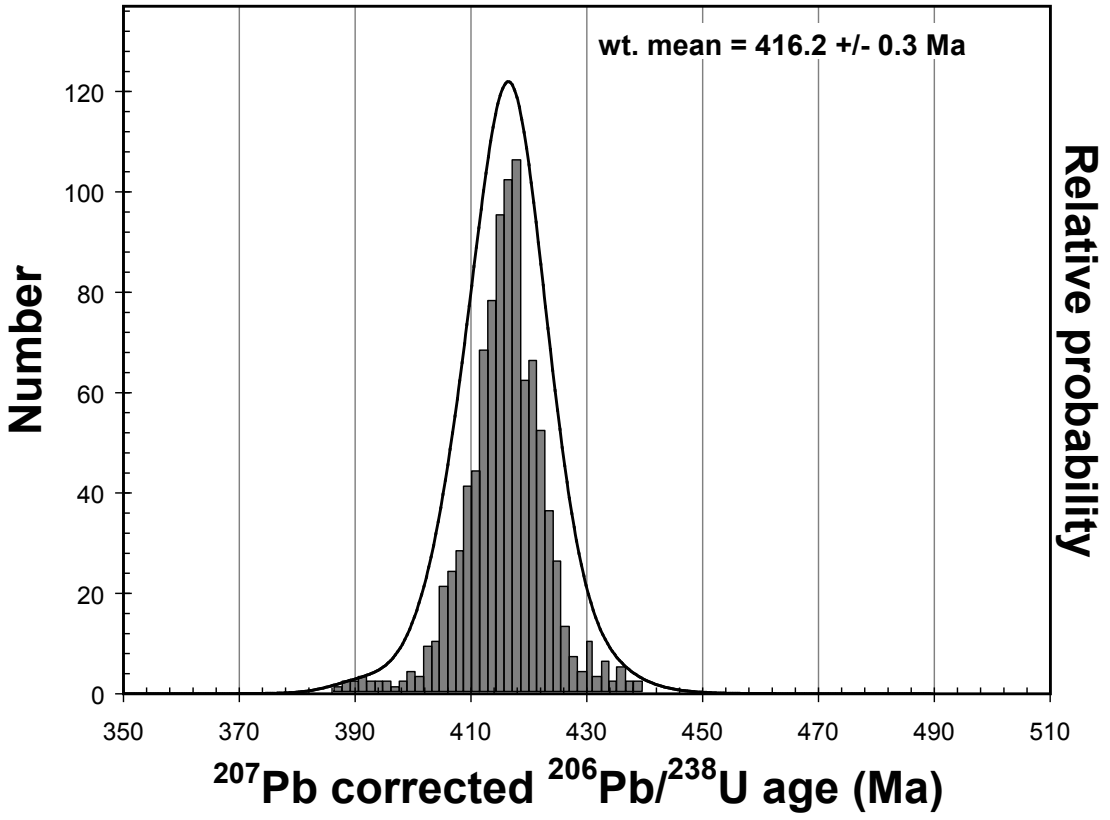

Figure 56 Frequency distribution diagram for $^{206}Pb/^{238}U$ age (207 corrected) determinations (n=946) of the TEMORA1 zircon. Mean age quoted is $^{206}Pb/^{238}U$ ages (207 corrected). The age is close to the accepted value of Black (2003). The small discrepancy is discussed in the text.

Table 12 Summary of LA-ICP-MS and TIMS U-Pb isotopic ages for the 91500 zircon (n=469). TIMS data from Wiedenbeck (1995).

Isotopic ratios determined by LA-ICP-MS			Weighted mean age (Ma) +/- errors (at 95% confidence)			TIMS age (Ma)	
	mean	st. dev. of indiv. anal.		weighted mean	2 std. error	mean	2σ
$^{207}Pb/^{206}Pb$	0.078	3.0%	^{207}Pb cor				
$^{207}Pb/^{235}U$	1.868	3.7%	$^{206}Pb/^{238}U$ age	1064.6	1.3	1065.0	0.4
$^{206}Pb/^{238}U$	0.180	1.7%					
$^{208}Pb/^{232}Th$	0.058	5.2%					

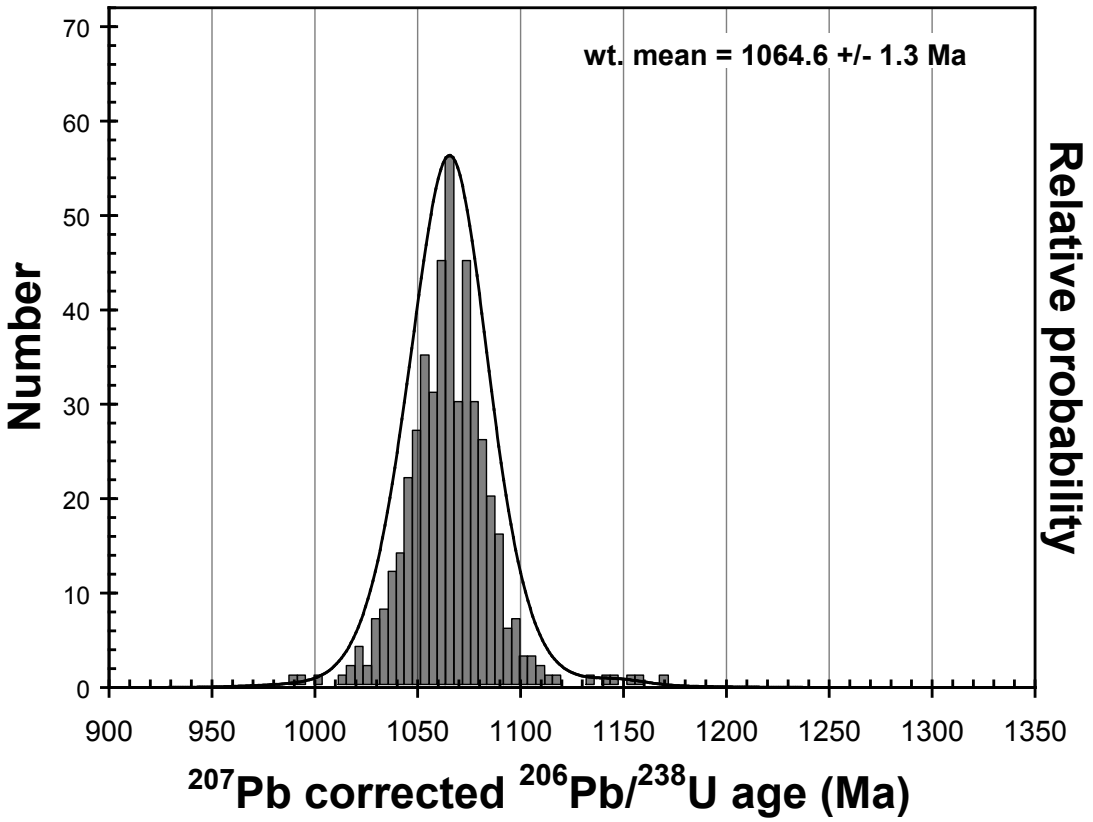

Figure 57 Frequency distribution diagram for $^{206}Pb/^{238}U$ age (207 corrected) determinations (n=469) of the 91500 zircon. Weighted mean ages quoted are $^{206}Pb/^{238}U$ ages (207 corrected). Both averages are within error of the accepted value of Wiedenbeck (1995).

Table 13 Summary of LA-ICP-MS and TIMS U-Pb isotopic ages for the Mud Tank zircon (n=53). TIMS data from Black and Gulson (1978).

Isotopic ratios determined by LA-ICP-MS			Weighted mean age (Ma) +/- errors (at 95% confidence)			TIMS age (Ma)	
	Mean	st. dev. of indiv. anal.		weighted mean	2 std. error	Mean	2σ
$^{207}Pb/^{206}Pb$	0.067	13.8%	^{207}Pb corr.				
$^{207}Pb/^{235}U$	1.058	12.7%	$^{206}Pb/^{238}U$ age	729.8	4.4	732	5
$^{206}Pb/^{238}U$	0.122	5.1%					
$^{208}Pb/^{232}Th$	0.037	18.3%					

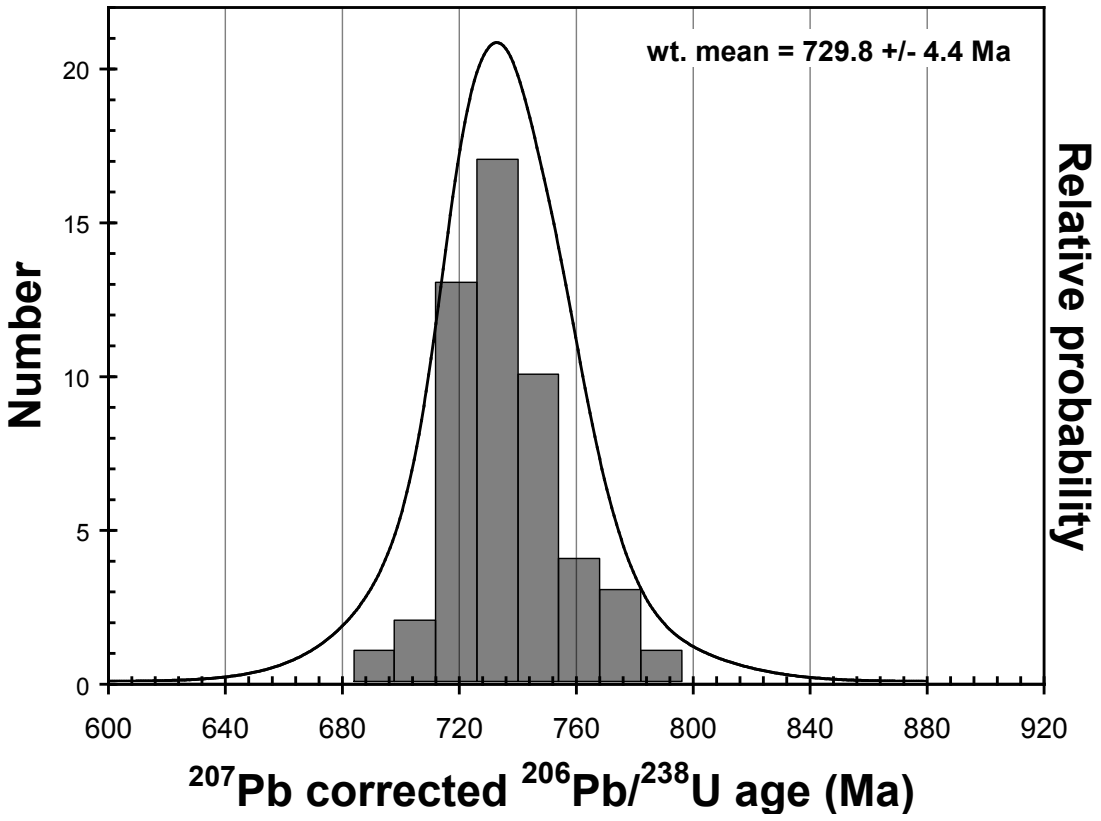

Figure 58 Frequency distribution diagram for $^{206}Pb/^{238}U$ age (207 corrected) determinations (n=53) of the Mud Tank zircon. Weighted mean ages quoted are $^{206}Pb/^{238}U$ ages (207 corrected). Both averages are within error of the accepted value of Black and Gulson (1978).

The long-term (over approximately one year) precision and accuracy of the CODES geochronology laboratory is very good. The weighted mean of the ^{207}Pb corrected ^{206}Pb/^{238}U ages from repeated analyses of our primary standard (n=946; TEMORA1) is 416.16±0.34 Ma, (2σ, 0.08%, MSWD of 1.3). Though this age is slightly young (as discussed above) it is still very close to the TIMS age (Black et al. 2004). The weighted mean of the ^{207}Pb corrected ^{206}Pb/^{238}U ages from repeated analyses of our secondary standard (n=469; 91500) is 1065.0±1.5 Ma, (2σ, 0.14%, MSWD 2.1). These results indicate that the CODES geochronology laboratory is producing high-quality, reliable data.

Gallagher rhyolite

The following description for the Gallagher rhyolite is summarized from Proffett (2005; 2007) which used the field classification dacite. However Ti/Zr ratios determined by both XRF and ICP-MS whole-rock analyses in our study are <10, indicating the rock has a rhyolitic chemistry. The whole-rock Zr content of our sample, determined by XRF, is 303 ppm. A complete discussion of the immobile-element geochemistry of the unit is found in Chapter 3 and the location of the sample is shown in Figure 59.

The rhyolite is typically hard and siliceous and has a weak S2 foliation. The rhyolite is fine-grained and contains several percent rounded to rectangular-shaped feldspar phenocrysts up to several millimeters in size. The matrix contains fine-grained quartz and minor sericite with small amounts of fine-grained biotite occurring in both the groundmass and replacing mafic phenocryst sites. In thin section, the rock contains moderately abundant plagioclase, rare quartz phenocrysts and altered mafic phenocrysts in a very fine-grained felsic matrix. Many plagioclase phenocrysts have been partially altered to secondary K-feldspar, quartz grains are partially resorbed. Mafic phenocrysts are altered to a mixture of sericite, carbonate, minor chlorite and leucoxene. Their original mineralogy generally cannot be determined. Dense clusters of leucoxene commonly have equant shapes typical of euhedral to rounded subhedral magnetite. Small zircon grains are present and many of these are euhedral short prisms with square

cross sections. Many of these are clean and unaltered with no petrographic evidence of older inherited cores. Detailed examination by cathodoluminescence revealed two zones of growth in a minority of zircon grains, see discussion below in the results section.

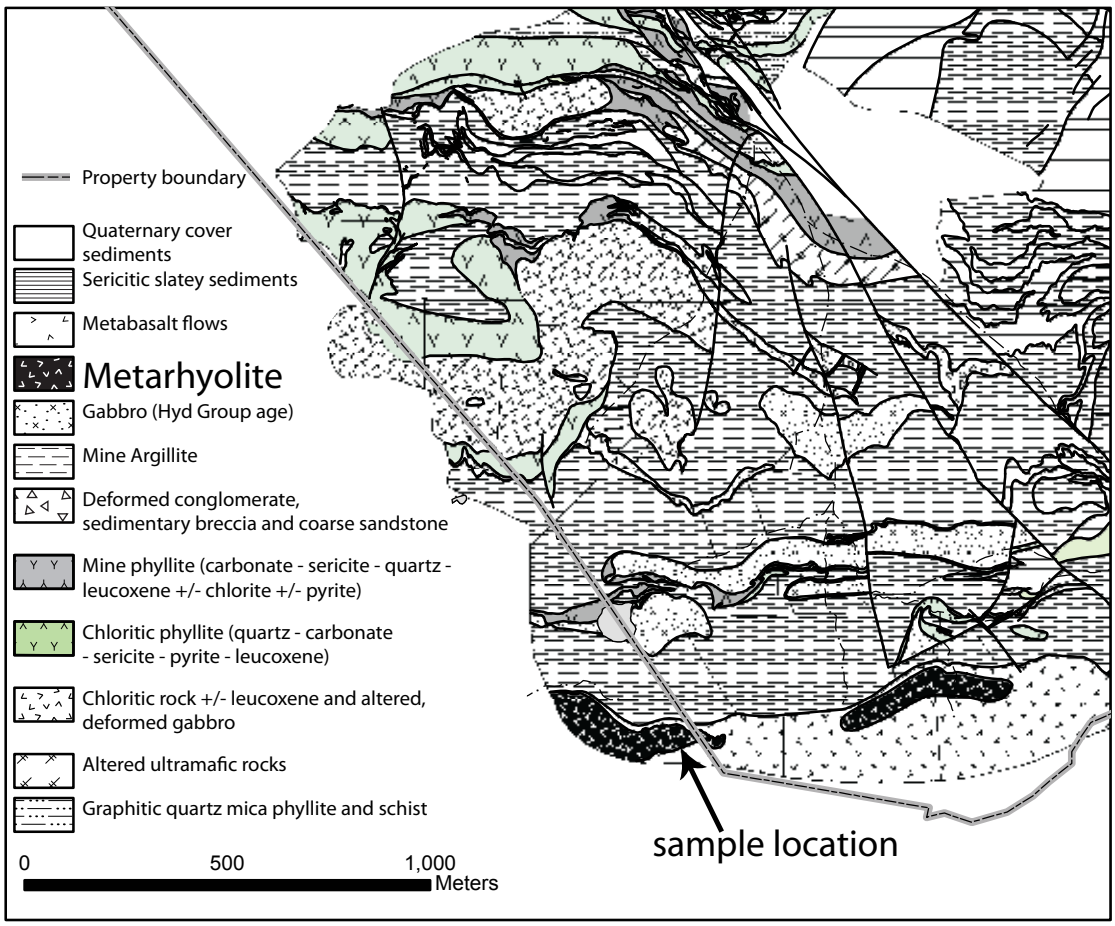

Figure 59 Interpreted geologic map of the Upper Gallagher area on the Greens Creek Mine property (Proffett, 2007). The Gallagher rhyolite (Proffett's Gallagher dacite) is in black with white symbols.

The main part of the rhyolite unit is massive and is several tens of feet (up to 10 m) thick. Structurally below the massive rhyolite, rhyolitic rocks occur in thin layers consisting of rhyolite fragments in a rhyolitic matrix. They are interlayered with brecciated basalt. The main unit of rhyolite is interpreted to be a coherent flow or dome and the breccias are considered to be autoclastic or volcaniclastic in nature. The sample used here comes from the massive rhyolite.

Results

TIMS method

The TIMS dating was done at the University of British Columbia (UBC) under the supervision of R. Friedman using the U-Pb zircon chemical abrasion ID-TIMS technique described in Scoates and Friedman (2008). Fifty zircon grains were hand-picked at the University of Tasmania and sent to the UBC geochronology laboratory where five grains were analyzed. The grains were chemically abraded before analysis. Results from the five grains are shown in Figure 60 and Table 14. The ^{204}Pb corrected ^{206}Pb/^{238}U ages for all five grains are overlapping and within 5% of concordia. The weighted mean of the ^{204}Pb corrected ^{206}Pb/^{238}U ages for all five grains is 226.86 ± 0.24 Ma. This is the best estimate for the emplacement age of the rhyolite. This age of 226.86 ± 0.24 Ma is the age against which the results of the LA-ICP-MS methods will be compared.

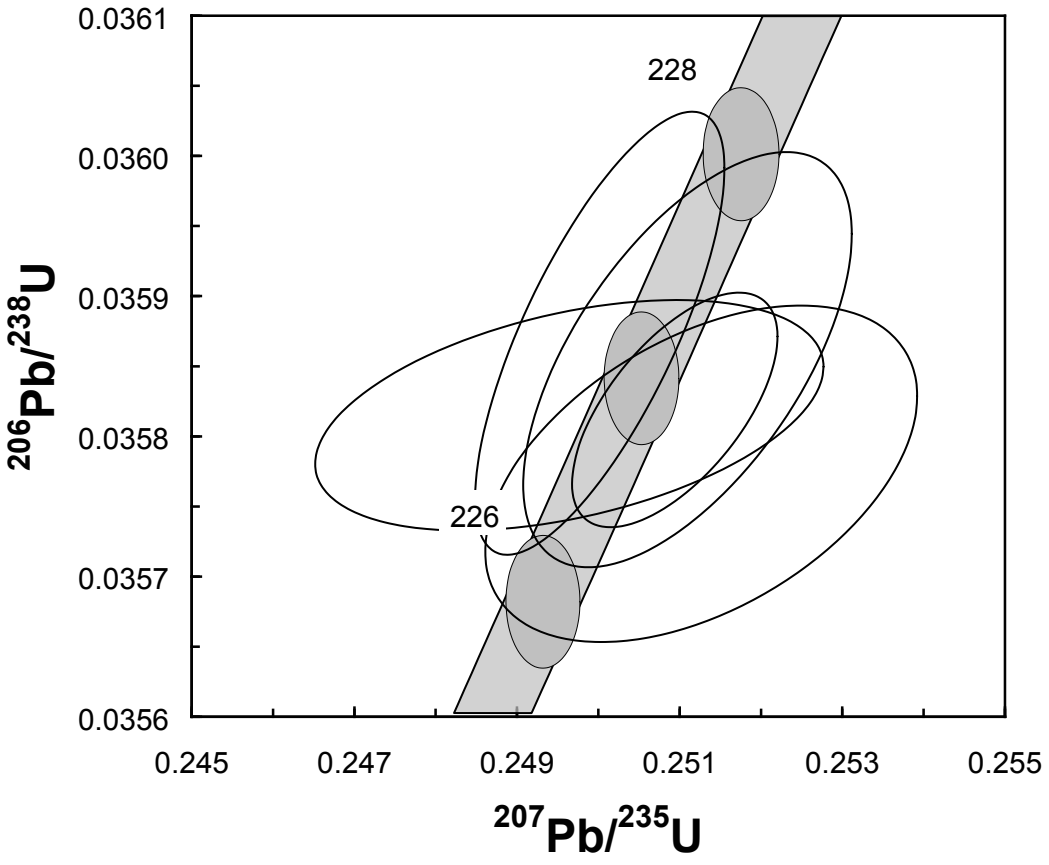

Figure 60 Concordia plot for five zircon grains analyzed with the conventional TIMS method of Scoates and Friedman (2008).

Table 14 Conventional ID-TIMS technique ages of five zircon grains.

Analysis no.	207Pb/ 206Pb	rse	206Pb/ 238U	rse	207Pb/ 235U	rse	U (ppm)	% discord	206Pb/ 238U age (204corr.)	+/-1s
CA1	0.051	0.481	0.036	0.094	0.250	0.516	576	-3.0	226.83	0.42
CA2	0.051	0.165	0.036	0.096	0.251	0.208	479	2.3	226.86	0.43
CA3	0.051	0.391	0.036	0.138	0.251	0.435	502	5.0	226.57	0.62
CA4	0.051	0.169	0.036	0.181	0.250	0.253	424	-3.3	227.20	0.81
CA5	0.051	0.267	0.036	0.170	0.251	0.332	287	1.9	227.09	0.76

35 µm and 10 µm spot sizes with large, separated zircons

Forty-five zircon grains were isolated from one sample of the rhyolite unit and prepared in the conventional method of hand-picking and mounting on 2.5cm diameter epoxy mounts as described above. The zircon grains selected for analysis were chosen based on their optical and luminescent properties. Twenty-four zircon grains, from the Gallagher rhyolite, were analyzed using the conventional LA-ICP-MS technique (spot size of 35 µm). These grains had U contents between 300 ppm and 1000 ppm and the radiogenic Pb contents were between 10 ppm and 60 ppm (Table 16). The CL images of the zircons indicate two growth stages: (1) a magmatically zoned core with a weakly resorbed margin and (2) a magmatically zoned outer rim with CL banding offset from that in the core (Figure 61). The second growth stage is not always seen. The results of 24 analyses from 24 zircon grains using a 35 µm spot size (Table 15) and 30 analyses from the same 24 zircon grains using a 10 µm spot size (Table 16) are reported in this section.

From the two populations of zircons identified by CL imaging, six grains had two growth zones (core and rim) and 18 grains had one growth zone (see Figure 61 for representative CL and SE images). When analyzed with a 35 µm spot size, all but three $^{206}Pb/^{238}U$ and $^{207}Pb/^{235}U$ determinations lie on or close to concordia (Figure 62). Two zircon grains (marked with asterisks on Table 15) were rejected from all calculations based on the criteria discussed previously in the data processing section. The weighted average of the ^{207}Pb corrected $^{206}Pb/^{238}U$ ages is 224.7 ± 1.3 Ma, and represents the best

estimate of the age of this sample using 35 µm spots. This estimate is within 0.5% of the TIMS estimate of 226.86 ± 0.24 Ma. The 19 most coincident analyses by this method lie within approximately 1% of concordia (Figure 62). A limit of ≤1% common Pb was used to determine if analyses were "close to or on concordia" for the other LA-ICP-MS method included in this study.

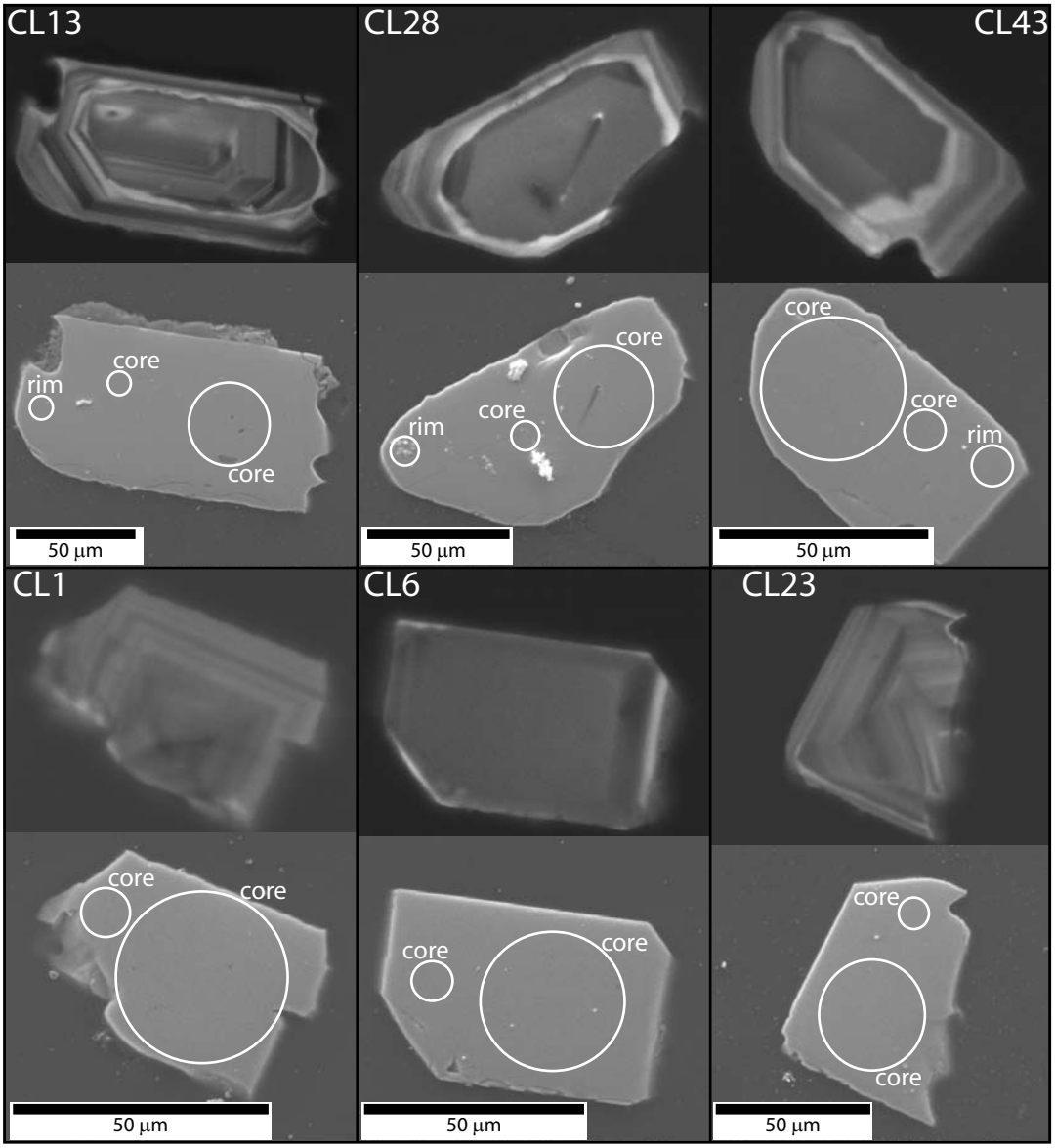

Figure 61 Selection of representative zircons analyzed by conventional LA-ICP-MS technique. CL images on top and corresponding SE images on the bottom of each picture pair. Top three zircons (CL13, 28 and 43) show evidence of two stages of growth. Bottom three zircons (CL1, 6 and 23 show only one stage of growth). Large circles show approximate location of 35 µm spots (cores) and small circles show 10 µm spots (cores and rims).

Table 15 Conventional LA-ICP-MS method ages (193 nm laser with 35 µm spots) of 24 zircons from the Gallagher rhyolite. TIMS age 226.86 ± 0.24 Ma. Analyses with an asterisk are rejected from the weighted means on the basis of criteria stated in main text above.

Zircon no.	Analysis no.	207Pb/206Pb	rse	206Pb/238U	rse	207Pb/235U	rse	208Pb/232Th	rse	U	+/-1σ	206Pb/238U age (207corr.)	+/-1σ
CL8	fe27d5	0.075	5.66%	0.036	1.84%	0.373	5.54%	0.017	5.53%	235	11	222.1	4.2
CL30	fe28a8	0.051	3.79%	0.036	1.11%	0.247	3.68%	0.013	3.84%	401	8	225.2	2.5
CL12	fe27d9	0.054	3.35%	0.035	1.53%	0.256	3.23%	0.012	2.94%	422	18	219.3	3.3
CL4	fe27d3	0.126	6.62%	0.039	2.30%	0.717	7.89%	0.034	8.64%	452	19	225.8	5.8
CL24	fe28a5	0.053	3.43%	0.036	1.20%	0.261	3.53%	0.013	3.43%	452	9	227.5	2.7
CL23	fe28a4	0.052	3.58%	0.035	1.08%	0.251	3.41%	0.013	3.53%	455	9	223.8	2.4
CL20	fe28a2	0.052	3.12%	0.036	1.17%	0.263	3.26%	0.012	3.21%	467	10	226.9	2.7
CL15	fe27d11	0.049	3.08%	0.035	1.15%	0.245	3.02%	0.011	3.03%	472	19	224.7	2.6
CL10	fe27d7	0.050	2.89%	0.035	1.05%	0.240	2.81%	0.011	2.74%	496	20	221.3	2.3
CL13core	fe27d10	0.049	3.24%	0.035	1.42%	0.235	3.03%	0.011	3.04%	515	21	221.3	3.1
CL2	fe27d2	0.050	3.84%	0.035	1.41%	0.245	3.77%	0.011	3.44%	548	23	222.1	3.1
CL40	fe28a11	0.052	3.06%	0.035	1.07%	0.249	3.07%	0.013	3.12%	555	12	224.2	2.4
CL6	fe27d4	0.052	2.96%	0.035	1.03%	0.251	2.71%	0.012	2.64%	571	24	223.1	2.3
CL43core	fe28a12	0.054	4.02%	0.035	1.42%	0.255	4.14%	0.014	3.60%	574	11	223.3	3.2
CL17	fe27d12	0.049	2.58%	0.036	1.00%	0.245	2.57%	0.011	2.57%	574	24	227.7	2.3
CL1	fe27d1	0.051	2.75%	0.036	1.11%	0.256	2.72%	0.011	2.64%	611	25	225.5	2.5
CL18core	fe28a1	0.049	2.68%	0.036	1.11%	0.250	2.68%	0.012	2.89%	614	12	228.5	2.5
CL28core	fe28a7	0.121	2.97%	0.040	1.07%	0.664	3.19%	0.035	3.06%	624	14	230.1	2.7
CL33	fe28a10	0.055	3.68%	0.036	1.59%	0.269	3.66%	0.014	3.25%	682	15	226.0	3.6
CL22	fe28a3	0.052	2.94%	0.036	0.98%	0.257	3.04%	0.012	2.88%	706	13	224.7	2.2
CL27core	fe28a6	0.051	2.41%	0.036	0.94%	0.250	2.51%	0.013	2.44%	983	21	225.8	2.1
CL32core	fe28a9	0.051	2.74%	0.035	1.09%	0.245	2.81%	0.012	2.32%	1574	31	221.5	2.4
CL9	fe27d6*	0.053	2.80%	0.033	0.95%	0.244	2.74%	0.010	2.50%	520	21	203.7	2.7
CL11	fe27d8*	0.054	2.86%	0.032	1.33%	0.243	2.77%	0.010	2.39%	1060	45	209.1	2.0
									Weighted mean			**224.7**	**1.3**

Table 16 New LA-ICP-MS method ages (193nm laser with 10 µm spots) from 30 analyses of 24 zircons from the Gallagher rhyolite. TIMS age 226.86 ± 0.24 Ma.

Zircon no.	Analysis no.	207Pb/206Pb	rse	206Pb/238U	rse	207Pb/235U	rse	208Pb/232Th	rse	U	+/-1σ	206Pb/238U age (207corr.)	+/-1σ
CL1	fe27b1	0.060	16.5%	0.035	2.5%	0.305	16.8%	0.009	17.0%	364	12	227.8	5.2
CL13rim	fe27b10	0.051	14.2%	0.035	2.1%	0.295	13.1%	0.012	13.5%	682	20	227.9	11.2
CL13core	fe27b11	0.046	15.6%	0.035	2.1%	0.291	14.6%	0.012	13.1%	663	20	229.2	7.9
CL15	fe27b12	0.054	17.3%	0.036	2.3%	0.329	15.8%	0.012	15.2%	454	14	232.0	5.0
CL17	fe27b13	0.051	22.8%	0.036	3.2%	0.308	20.3%	0.011	18.6%	571	19	227.4	5.8
CL2	fe27b2	0.055	17.0%	0.036	2.6%	0.279	17.9%	0.010	17.1%	314	13	224.9	6.0
CL4	fe27b3	0.056	16.5%	0.036	2.3%	0.292	16.1%	0.011	14.6%	416	13	229.0	6.0
CL6	fe27b4	0.048	16.5%	0.035	2.4%	0.266	16.9%	0.013	15.2%	523	19	228.2	5.0
CL8	fe27b5	0.072	18.9%	0.035	3.5%	0.376	17.8%	0.013	19.3%	389	14	226.2	6.1
CL9	fe27b6	0.062	16.0%	0.036	2.5%	0.325	15.8%	0.011	17.4%	328	11	225.6	6.3
CL10	fe27b7	0.055	20.2%	0.035	3.3%	0.311	19.7%	0.011	20.7%	400	14	223.2	6.9
CL11	fe27b8	0.044	15.9%	0.036	2.0%	0.276	15.1%	0.012	13.7%	704	23	223.6	6.1
CL12	fe27b9	0.054	15.5%	0.035	2.2%	0.307	14.7%	0.010	13.2%	1011	30	225.1	5.7
CL18rim	fe28c1	0.057	12.4%	0.035	2.6%	0.309	11.6%	0.012	12.8%	496	32	225.1	5.8
CL28core	fe28c10	0.043	13.3%	0.035	2.3%	0.214	12.8%	0.011	11.1%	603	41	222.9	6.0
CL28rim	fe28c11	0.052	13.6%	0.035	2.8%	0.267	13.3%	0.010	13.7%	639	42	220.8	5.3
CL30	fe28c12	0.059	16.9%	0.035	2.9%	0.279	16.8%	0.010	14.3%	535	35	221.3	6.4
CL32rim	fe28c13	0.052	11.7%	0.036	2.1%	0.272	11.3%	0.011	10.9%	615	40	224.7	5.0
CL33	fe28c14	0.058	15.7%	0.036	2.9%	0.313	14.7%	0.010	13.9%	968	63	221.2	7.8
CL40	fe28c15	0.051	10.5%	0.036	2.2%	0.258	10.2%	0.010	9.7%	901	60	224.9	5.3
CL43core	fe28c16	0.055	13.0%	0.036	2.5%	0.289	12.1%	0.012	11.2%	595	41	218.4	8.5
CL43rim	fe28c17	0.055	13.2%	0.036	2.4%	0.273	12.7%	0.011	12.5%	541	36	221.3	5.0
CL18core	fe28c2	0.056	13.7%	0.036	2.5%	0.293	13.1%	0.011	13.0%	496	32	218.0	5.0
CL18rim	fe28c3	0.057	13.3%	0.036	2.5%	0.312	12.3%	0.009	13.9%	553	36	224.2	5.8
CL24	fe28c7	0.072	22.1%	0.037	4.5%	0.435	20.6%	0.017	24.3%	417	30	216.5	6.0
CL27core	fe28c8	0.062	10.6%	0.035	2.2%	0.316	10.7%	0.011	10.5%	866	58	221.7	5.0
CL27rim	fe28c9	0.051	10.3%	0.035	2.2%	0.254	9.8%	0.011	9.3%	842	55	217.6	6.9
CL20	fe28c4	0.038	18.6%	0.033	2.8%	0.179	18.0%	0.011	16.0%	418	28	208.5	4.9
CL22	fe28c5	0.071	11.1%	0.034	2.2%	0.342	10.8%	0.010	13.3%	567	38	211.4	5.6
CL23	fe28c6	0.050	14.0%	0.033	2.5%	0.232	12.9%	0.011	12.5%	507	33	211.8	6.2
									Weighted mean			**225.1**	**2.3**

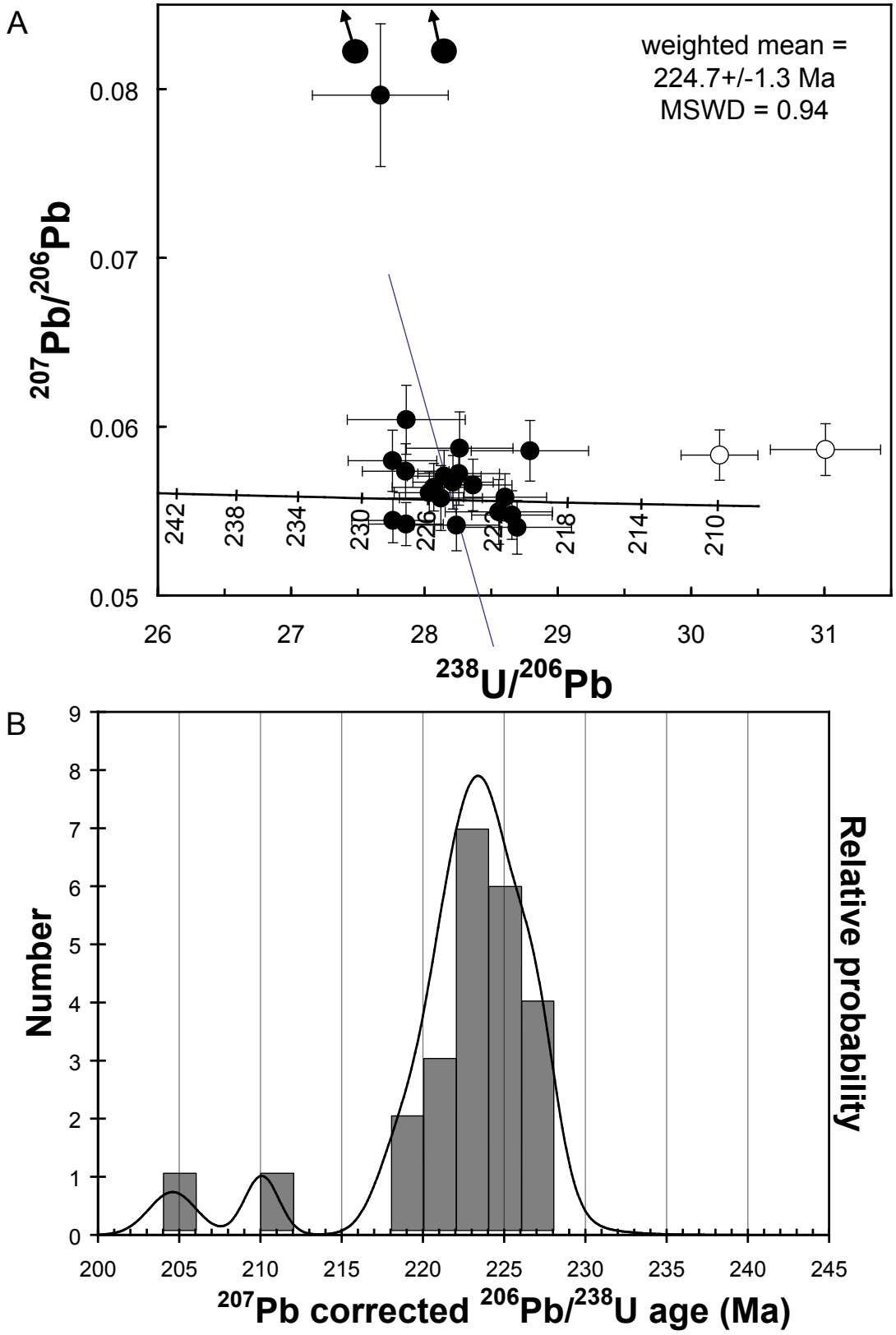

Figure 62 Reverse concordia and frequency distribution for 35 µm analyses. (A) Reverse concordia plot for 24 zircons analyzed with the conventional method of Meffre (2007) using a 35 µm spot size. Data-point error crosses are 1σ. (B) Frequency distribution for 24 $^{206}Pb/^{238}U$ age determinations (207 corrected).

The same 24 grains were re-analyzed by LA-ICP-MS using a 10 μm spot size; thirty analyses were made on cores and rims (Table 17). The weighted means for the core, rim and single growth zone zircons are all within error of each other and can not be sub-divided by age. Therefore, these data are treated as a single population of 30 dates.

Table 17 Summary table of weighted mean $^{206}Pb/^{238}U$ ages (corrected for ^{207}Pb) generated with a 10 μm spot size on the same 24 zircons as analyzed with the conventional LA-ICP-MS method using a 35 μm spot size. [a] Number of spots analyzed; [b] Number of individual grains analyzed; [c] Mean weighted average and errors

Location	No. of analyses[a]	No. of crystals[b]	Age (Ma)[c]	2σ (Ma)[c]	MSWD[c]
core	5	5	221.4	5.4	0.4
rim	7	6	222.7	4.4	0.2
single growth	18	18	224.0	2.8	1.0

The weighted mean ^{207}Pb corrected $^{206}Pb/^{238}U$ age of the 25 most concordant analyses is 225.1±2.3 Ma (Figure 63). This estimate is statistically identical to the LA-ICP-MS results using a 35 μm spot size. Although the analyses carried out with the 10 μm spot size are less precise, the dates show no systematic errors.

Application to dating of small, in-situ zircons

In one 2.5 cm diameter mount of Gallagher rhyolite, over 200 zircons ranging in surface area from 25 μm^2 to >10,000 μm^2 were located using the SPL-LT search method on the SEM based MLA. The zircons were subdivided into four groups based on surface area (<100; 100–150; 150–1000; and >1000 μm^2). At least 12 grains from each of these ranges were analyzed for total of 49 analyses from 48 grains (Table 18). The location of the individual zircons in the 2.5 cm diameter mount can be seen in Figure 53 and representative CL images are in Figure 64. The CL images of the in-situ zircons show the same simple and complex zoning as the large separated zircons in the grain mounts. However, there is a higher proportion of single growth zircons in-situ compared to that in the grain mounts, probably due to the smaller cross sectional area of the zircons.

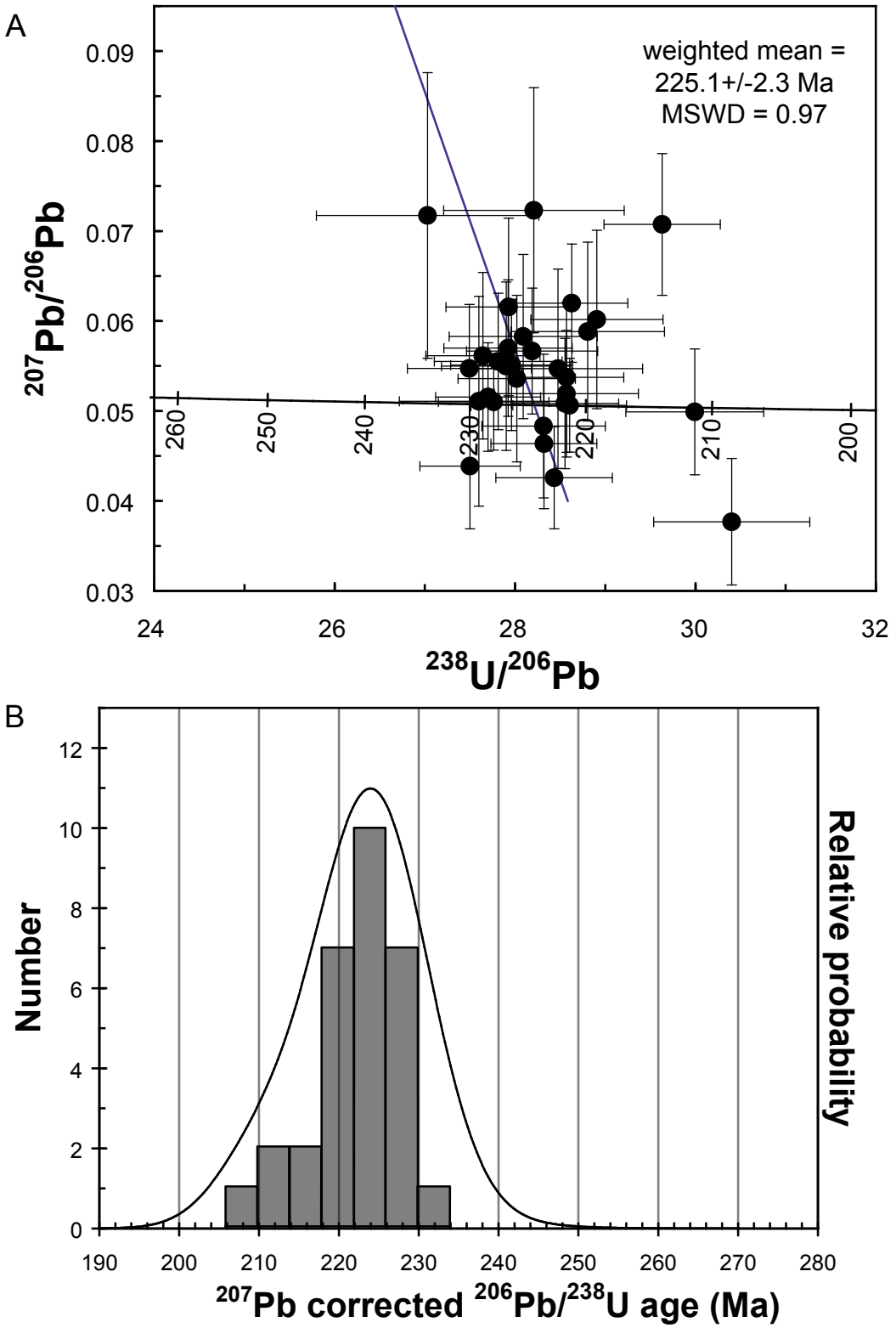

Figure 63 Reverse concordia and frequency distribution for 10 µm analyses. (A) Reverse concordia plot for 30 zircons analyzed with all parameters the same as the conventional LA-ICP-MS method of Meffre (2007) except a 10 µm spot size was used. Data-point error crosses are 1σ. (B) Frequency distribution for 30 $^{206}Pb/^{238}U$ age determinations (207 corrected).

When analyzed in-situ, using a 10 µm spot size, 13 of 49 analyses lie on or close to concordia (Figure 65), the seven that are discordant due to minor common Pb are included in the age calculations. Twenty-nine zircon analyses were rejected (marked with an asterisk on Table 18) primarily because of their high U contents (>2500 ppm). The weighted mean ^{207}Pb corrected ^{206}Pb/^{238}U ages of the 20 most concordant points when plotted on a concordia diagram (Figure 65) is 223.5 ± 2.6 Ma. This estimate is statistically identical to the conventional LA-ICP-MS estimate for the sample, however, the number of zircons that were rejected is much higher.

The results for the in-situ method show that the smallest zircons were much more prone to having high U and Pb loss than the larger grains (Table 19). Zircons with a U content <2500 ppm were always reliable and the greater the U content (>2500 ppm) in the zircons, the younger the apparent ^{206}Pb/^{238}U age (white circles on Figure 65 reverse concordia plot). Though the spread of ages from approximately 80 Ma to 200 Ma could be related to regional metamorphic or hydrothermal events such as those documented by Karl et al. (1998) and Taylor et al. (1995) there are not any distinct age-populations in data from the present study. The preferred interpretation is that these effects are related to the presence of a high-U rim on the outside of the larger grains and throughout the smaller grains which is strongly metamict and prone to Pb loss.

The age estimates from the two techniques and the various LA-ICP-MS methods that were used in this study are in good agreement (Table 20). The TIMS age is taken as the most accurate and precise and is the standard against which the various LA-ICP-MS methods are compared. Not surprisingly, the large spots on large grains have a more accurate and precise age with a lower MSWD value than the 10 µm spots. The 10 µm spots on large grains have a precision decreased two. Using the new in-situ method, the age is still within error, but precision is low and a large number of grains had to be rejected, particularly when analyzing small zircons. In this method, the data needs to be scanned carefully to detect inferior analyses.

Table 18 New in-situ LA-ICP-MS method ages (193 nm laser with 10 µm spots) from 49 analyses of 48 zircons from the Gallagher rhyolite. TIMS age is 226.86 ± 0.24 Ma. Analyses marked with an asterisk are rejected on the basis of criteria stated in the text.

Zircon no.	Analysis no.	Approx. ablation volume (µm³)	207Pb/206Pb	+/-1σ	206Pb/238U	+/-1σ	207Pb/235U	+/-1σ	208Pb/232Th	+/-1σ	U	+/-1σ	Th	+/-1σ	206Pb/ 238U age (207Pb corr.)	+/-1σ
CL2.2	fe28d4	785	0.056	14.2%	0.035	3.3%	0.276	13.4%	0.013	12%	479	32	179	11	219	7.4
CL1.2	fe28d2	785	0.048	19.3%	0.036	3.7%	0.234	20.2%	0.014	14%	564	37	217	13	226	8.6
CL26	ma11a3	900	0.057	12.0%	0.036	2.6%	0.285	12.1%	0.011	10%	860	44	472	25	225	6.0
CL17	ma11b5	636	0.048	18.9%	0.035	3.2%	0.255	18.1%	0.014	15%	2531	172	1234	84	222	7.4
CL27	ma11a4	1178	0.078	14.8%	0.038	3.7%	0.413	13.9%	0.023	12%	387	19	151	8	230	9.1
CL11	ma11a12	1178	0.046	19.1%	0.036	3.6%	0.217	18.9%	0.010	17%	432	21	152	8	232	8.5
CL22	ma11b12	1178	0.054	19.1%	0.037	4.9%	0.310	19.3%	0.013	18%	441	30	160	12	236	11.9
CL4.1	fe28d9	1178	0.045	14.2%	0.036	2.6%	0.229	13.8%	0.012	12%	499	31	182	10	229	6.1
CL1.1	fe28d1	1178	0.060	13.0%	0.035	2.1%	0.282	12.5%	0.010	12%	522	33	214	12	220	5.0
CL8.1	fe28e6	1178	0.053	10.8%	0.035	2.1%	0.259	11.2%	0.011	9%	627	23	240	11	223	4.8
CL36	ma11a10	1178	0.075	13.4%	0.037	2.9%	0.395	13.2%	0.018	10%	656	35	296	16	226	7.0
CL25	ma11a2	1178	0.057	9.0%	0.036	1.9%	0.296	8.9%	0.013	8%	721	36	333	17	226	4.5
CL2.1	fe28d3	1178	0.057	9.2%	0.034	2.0%	0.279	8.9%	0.013	8%	839	53	381	22	216	4.5
CL3.1	fe28d5	1178	0.054	18.9%	0.034	3.5%	0.249	17.2%	0.011	14%	853	56	419	26	214	7.9
CL8.2	fe28e7	1178	0.062	17.2%	0.034	3.0%	0.276	16.0%	0.014	13%	919	34	447	22	210	6.9
CL9.1	fe28e8	1178	0.044	10.2%	0.036	1.8%	0.215	10.6%	0.012	8%	1003	33	438	17	228	4.2
CL13	ma11b2	1178	0.052	7.1%	0.036	1.5%	0.265	6.8%	0.011	6%	1866	110	1077	61	230	3.6
CL12	ma11b1	1178	0.053	7.5%	0.035	1.7%	0.271	7.1%	0.011	7%	1914	117	1107	66	223	4.0
CL37	ma11a11	1178	0.060	9.2%	0.034	2.2%	0.304	8.7%	0.012	7%	2336	113	1670	81	216	5.0
CL42.1	fe28e2*	450	0.052	12.8%	0.030	2.5%	0.214	12.9%	0.008	10%	2985	118	2127	93	191	5.1
CL30	ma11a6*	715	0.062	11.3%	0.031	2.7%	0.272	11.8%	0.009	9%	3467	316	2795	134	195	5.4
CL5.3	fe28d12*	500	0.055	14.1%	0.029	2.7%	0.220	13.4%	0.009	12%	3730	308	1717	139	183	5.3
CL35	ma11a1*	110	0.068	14.1%	0.029	3.9%	0.256	13.2%	0.008	10%	3893	285	3398	229	178	7.1
CL46.1	fe28e11*	667	0.061	9.8%	0.027	2.8%	0.223	9.6%	0.009	8%	4201	145	3286	141	167	4.7

Zircon no.	Analysis no.	Approx. ablation volume (μm³)	207Pb/206Pb	+/-1σ	206Pb/238U	+/-1σ	207Pb/235U	+/-1σ	208Pb/232Th	+/-1σ	U	+/- 1σ	Th	+/-1σ	206Pb/ 238U age (207Pb corr.)	+/- 1σ
CL28	ma11a5*	460	0.057	9.4%	0.031	2.1%	0.249	9.1%	0.010	7.6%	4554	216	3281	156	195	4.2
CL31	ma11a7*	567	0.052	14.5%	0.028	4.3%	0.188	14.6%	0.007	14.4%	4659	241	3077	177	175	7.6
CL47.1	fe28e12*	1001	0.060	7.7%	0.025	2.8%	0.204	7.4%	0.007	6.3%	4826	234	4468	257	157	4.5
CL38.1	fe28d6*	785	0.060	6.4%	0.026	1.6%	0.230	6.5%	0.010	6.9%	6043	435	2011	163	163	2.7
CL32	ma11a8*	525	0.060	8.8%	0.022	2.3%	0.203	8.7%	0.008	7.0%	6069	281	5327	248	139	3.3
CL41.1	fe28e1*	48	0.058	25.8%	0.018	3.7%	0.159	25.9%	0.006	18.2%	6112	272	6880	361	114	4.7
CL33	ma11a9*	283	0.062	10.9%	0.023	2.5%	0.197	10.1%	0.006	9.2%	6435	307	8344	484	147	3.9
CL5.2	fe28d11*	785	0.066	11.4%	0.020	2.4%	0.200	11.6%	0.007	9.5%	6614	437	7774	474	126	3.3
CL44.1	fe28e9*	495	0.064	13.7%	0.019	4.2%	0.174	13.6%	0.007	11.3%	6639	269	5406	244	119	5.1
CL43.1	fe28e3*	1125	0.060	13.4%	0.016	2.7%	0.132	13.6%	0.006	10.6%	6714	255	6142	286	102	2.9
CL45.1	fe28e10*	900	0.072	6.6%	0.019	2.1%	0.190	7.2%	0.006	6.5%	6938	199	5936	276	118	2.5
CL18	ma11b6*	767	0.066	7.1%	0.021	1.9%	0.205	7.0%	0.009	7.5%	7667	490	3216	195	133	2.6
CL24	ma11b11*	267	0.101	9.0%	0.020	2.7%	0.267	9.7%	0.008	9.2%	7717	562	7257	519	122	3.6
CL19	ma11b7*	480	0.078	11.0%	0.018	2.7%	0.210	11.0%	0.006	8.6%	7976	493	8290	482	110	3.2
CL40.1	fe28d8*	589	0.061	8.5%	0.020	1.8%	0.176	8.4%	0.009	7.9%	8676	659	2467	170	126	2.3
CL16	ma11b4*	520	0.068	10.3%	0.014	2.7%	0.144	10.0%	0.005	7.4%	9564	577	11105	639	86	2.4
CL15	ma11b3*	334	0.066	11.4%	0.017	3.3%	0.152	10.9%	0.005	9.2%	9612	634	8949	581	107	3.6
CL5.1	fe28d10*	1178	0.053	15.0%	0.031	3.3%	0.245	15.3%	0.010	14.2%	3598	240	2171	131	195	6.6
CL6.1	fe28e4*	1178	0.069	8.7%	0.028	1.8%	0.255	8.2%	0.010	7.4%	5608	170	4355	158	171	3.3
CL10	ma11b8*	1178	0.074	9.4%	0.030	2.8%	0.304	8.6%	0.009	9.7%	6045	361	4950	328	182	5.3
CL39.1	fe28d7*	1178	0.065	6.3%	0.022	1.3%	0.203	6.3%	0.008	5.9%	7170	485	3532	207	135	1.9
CL48	ma11b9*	1178	0.059	10.3%	0.018	2.1%	0.155	9.7%	0.006	8.3%	7406	444	5008	296	115	2.6
CL51	ma11b10*	1178	0.064	5.5%	0.021	1.7%	0.197	5.3%	0.008	5.1%	8500	499	4835	308	130	2.2
CL7.1	fe28e5*	1178	0.059	6.8%	0.015	1.4%	0.126	7.0%	0.005	5.5%	10031	346	6596	266	97	1.4
												Weighted mean			223.5	2.6

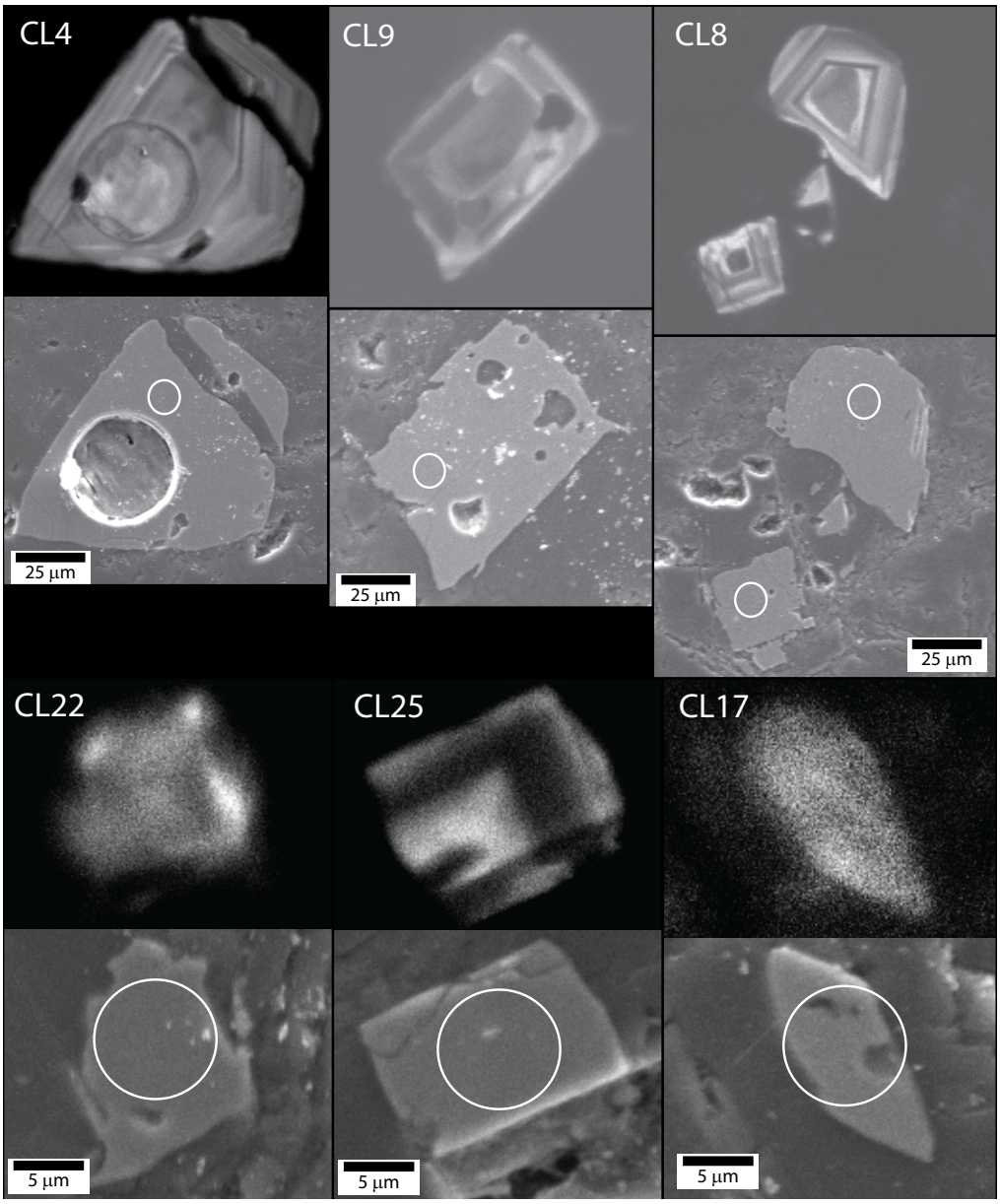

Figure 64 Selection of representative zircons analyzed with the new in-situ U-Pb dating technique. CL images on top and corresponding secondary electron (SE) images on the bottom of each picture pair. Zircons CL4 and 9 are examples of the largest size group; CL4 has the same two-stage growth zoning as some of the zircons analyzed with the conventional method. CL8 is an example of the 150 µm² to 1000 µm² size range; possible two stages of growth in this zircon. CL22 and 25 are from the 100 µm² to 150 µm² size range and show only one stage of growth. The smallest size range (<100 µm²) is shown in CL17 which has only one growth stage without CL banding. Note the scale is different on each photograph pair. The white circles on each crystal are all 10 µm in diameter and show the approximate location of the ablation sites.

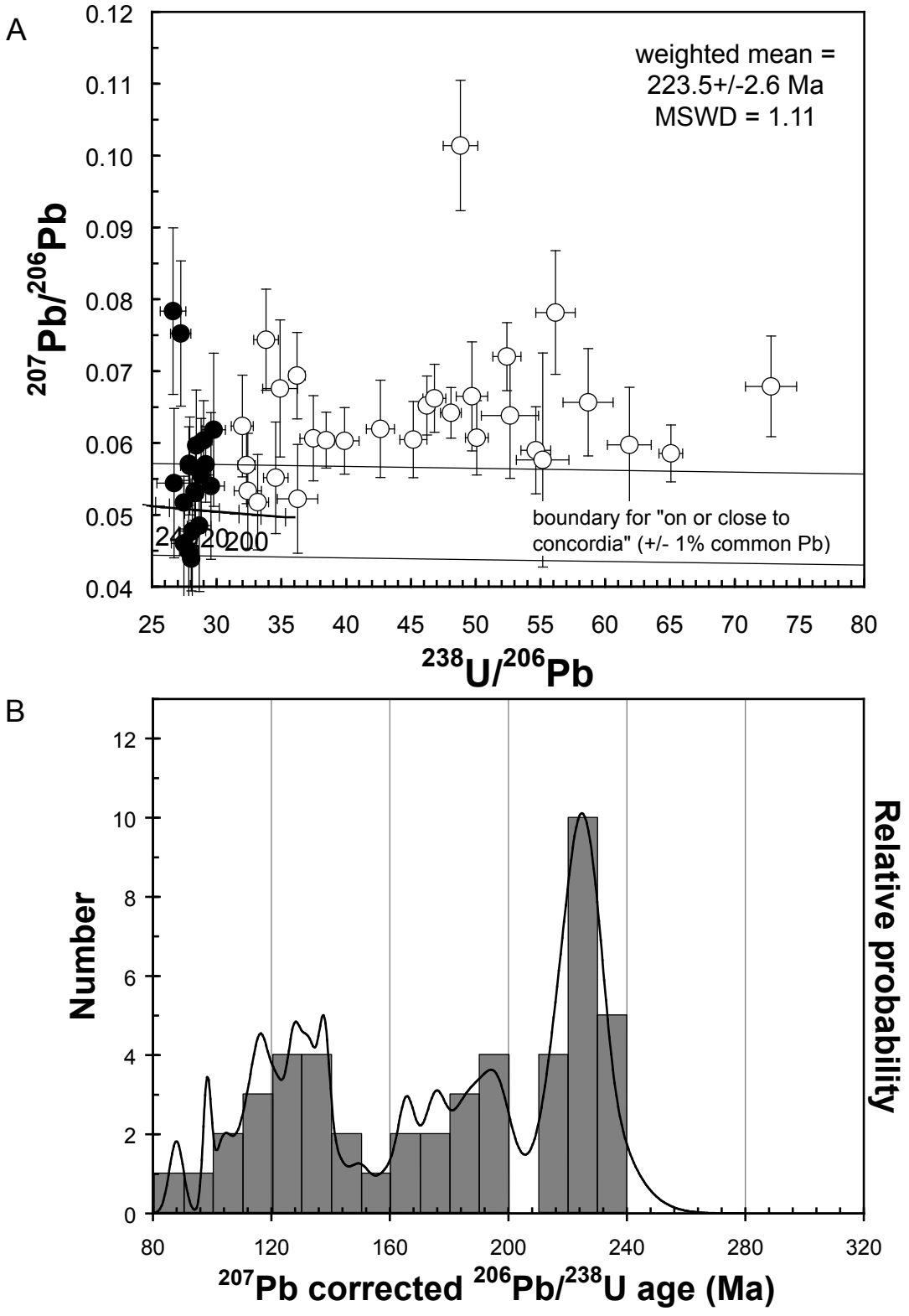

Figure 65 Reverse concordia and frequency distribution for 10 µm in-situ analyses. (A) Reverse concordia plot for 49 zircons analyzed with the new in-situ method using a 10 µm spot size. Data-point error crosses are 1σ. (B) Frequency distribution for 49 ^{207}Pb corrected $^{206}Pb/^{238}U$ age determinations.

Table 19 $^{206}Pb/^{238}U$ ages (^{207}Pb corrected) for each surface area fraction. [a] Number of spots analyzed; [b] Number of individual grains analyzed; [c] Analyses were rejected based on the criteria stated above in main text; [d] Number of analyses used in the estimation of the age of the sample; [e] Mean weighted average and errors calculated using the ^{207}Pb corrected $^{206}Pb/^{238}U$ data of the most coincident analyses.

Surface area (μm^2)	No. of analyses[a]	No. of crystals[b]	No. of rejected analyses[c]	No. of analyses used[d]	Age (Ma)[e]	2σ (Ma)[e]	2σ (%)[e]	MSWD[e]
>1000	13	12	4	9	221.7	5.5	2.5	1.5
150 to 1000	12	12	8	4	222.9	5.7	2.6	1.2
100 to 150	12	12	7	5	226.0	4.3	1.9	0.6
<100	12	12	11	1	222.0	7.4	3.3	N/A
Combined	49	48	30	19	223.5	2.6	1.2	1.11

Table 20 Summary of results from the present study. Subscripts same as Table 19.

Method	No. of analyses[a]	No. of crystals[b]	No. of rejected analyses[c]	No. of analyses used[d]	Age (Ma)[e]	2σ (Ma)[e]	2σ (%)[e]	MSWD[e]
TIMS	5	5	0	5	226.86	0.24	0.1	0.49
LA-ICP-MS conventional (35 µm spot)	24	24	2	22	224.7	1.3	0.5	0.94
LA-ICP-MS conventional (10 µm spot)	30	24	0	30	225.1	2.3	1.0	0.97
LA-ICP-MS new in situ (10 µm spot)	49	48	29	20	223.5	2.6	1.2	1.11

Discussion

Automatic SEM zircon identification

Locating zircons using the automated SEM (MLA) is a viable way to find zircons for U-Pb geochronology. The main advantages of the method are that it requires little sample preparation, it is very good at finding small zircon grains and it eliminates the potential for contamination of zircon from other samples in the laboratory. The method is not suitable for medium-grained to coarse-grained rocks with large zircons as the chance of finding large grains on only one 2.5 cm surface is low.

Zoning of zircons

Although zones of zircon growth (separated by a period of dissolution) are identified by CL imaging, the age of the cores and the rims were within statistical error of each other and permit two interpretations, (1) the cores are not inherited and the zircons underwent two stages of growth within the magma chamber before emplacement, or (2) the cores are inherited from a source of virtually the same age. As the age difference is too small for our technique to separate, the zircons can be treated as a single population for our purposes. This applies also to the zircon grains analyzed with the TIMS technique where the zircons were chemically abraded before analysis.

Volume analyzed

The volume of zircon included in each analysis using the in-situ method assessed as part of this study is an order of magnitude less than that of typical LA-ICP-MS studies (i.e. Tiepolo, 2003; Harris et al., 2004; Jackson et al., 2004). Studies have previously shown that halving the spot size reduces signal intensity by approximately 40% (Tiepolo, 2003), reducing the precision of the calculated ages. However, rocks such has the Green Creek footwall rocks cannot, at present, be dated using conventional spot sizes and the errors of 1.5% are acceptable for many regional studies including Greens Creek.

Pb loss

Pb loss is a problem which is more prevalent at a 10 μm spot size. This is apparently due to the generally higher U content found in the small grains (Figure 66, Figure 67). The higher U content of the small zircon grains versus the large zircons grains could be caused by small-scale differences in the U content of the melt as it cools. However, this study has not addressed the systematic variation in the U content. All zircon grains in this study with more than 2700 ppm U content had Pb loss. These zircon grains can easily be identified. Not only are they are high in U, but for most rocks there is a negative correlation in the time-resolved LA-ICP-MS data between the apparent $^{206}Pb/^{238}U$ and the U contents, with an increasing $^{207}Pb/^{206}Pb$ incompatible with a real lower age (Figure 67, Figure 68).

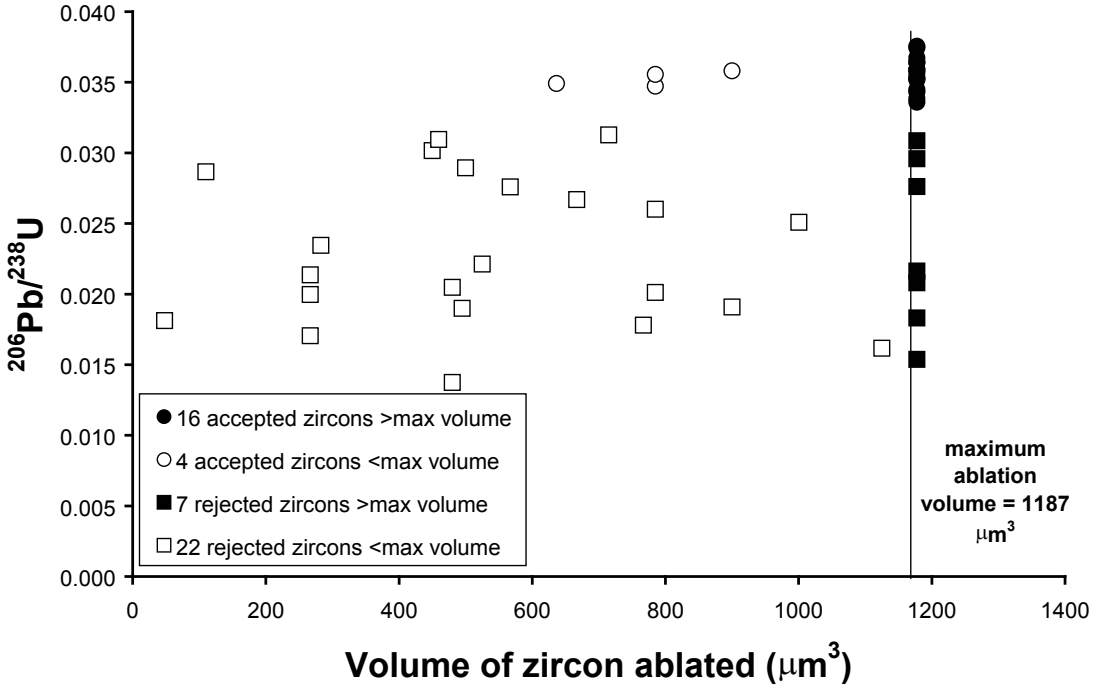

Figure 66 $^{206}Pb/^{238}U$ (uncorrected, 10 µm spot size) against volume of zircon ablated for 48 grains from the Greens Creek in-situ sample. The anomalously low $^{206}Pb/^{238}U$ ratios, indicating Pb loss, are more prevalent in zircon analyses where less material was ablated.

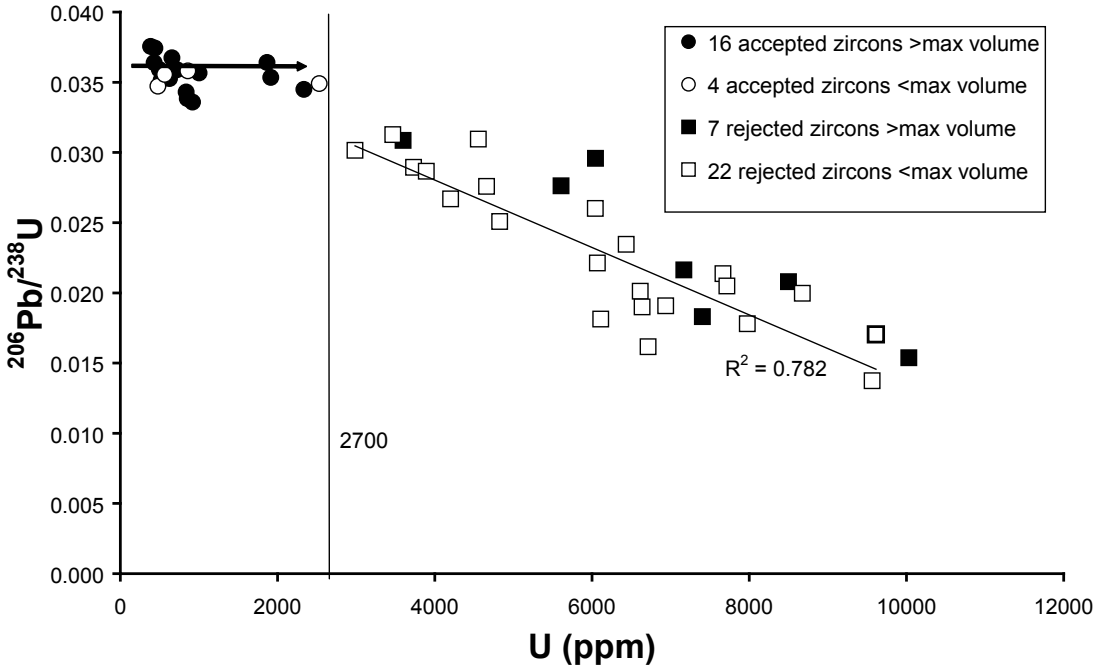

Figure 67 $^{206}Pb/^{238}U$ (uncorrected, 10 µm spot size) against U content for 48 grains from the Greens Creek in-situ sample. This is interpreted as indicating chronic Pb loss in the zircons with greater than 2700 ppm U. Note the R^2 value of 0.75 indicating the correlation between increasing U content and decreasing $^{206}Pb/^{238}U$ (uncorrected).

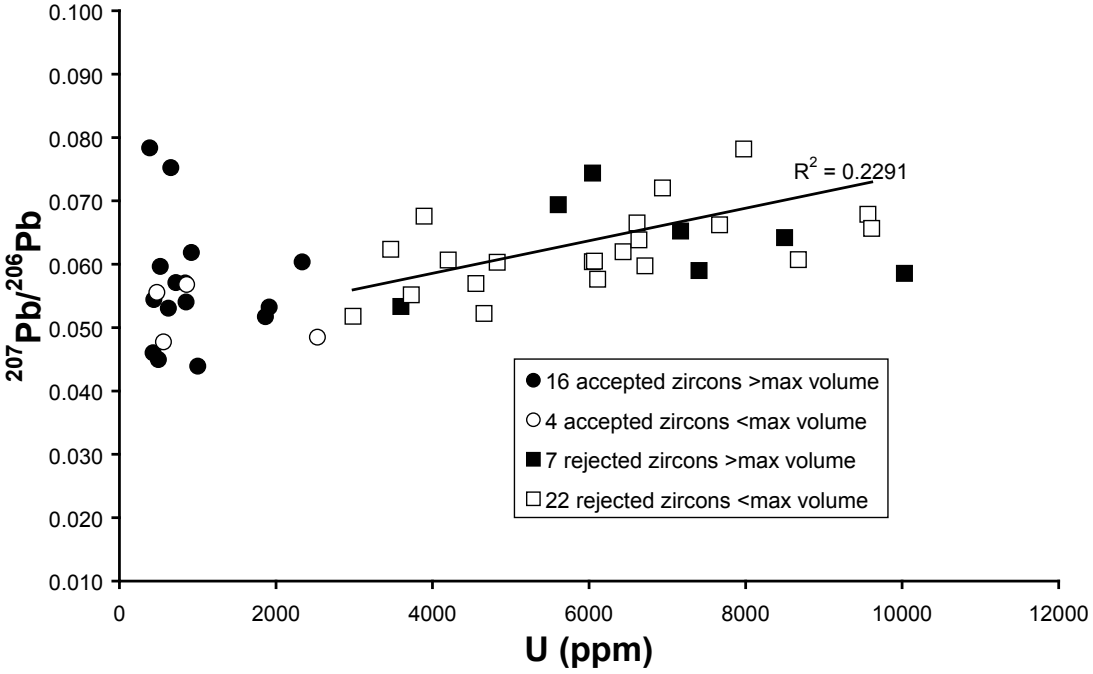

Figure 68 $^{207}Pb/^{206}Pb$ (uncorrected, 10 µm laser spot size) against U content for 48 grains from the Greens Creek in-situ sample. This is interpreted as indicating common Pb gain in radiation-damaged zircons with greater than ~2500 ppm U. The weak correlation suggests that the greater the zircon damage, the more common Pb is taken in.

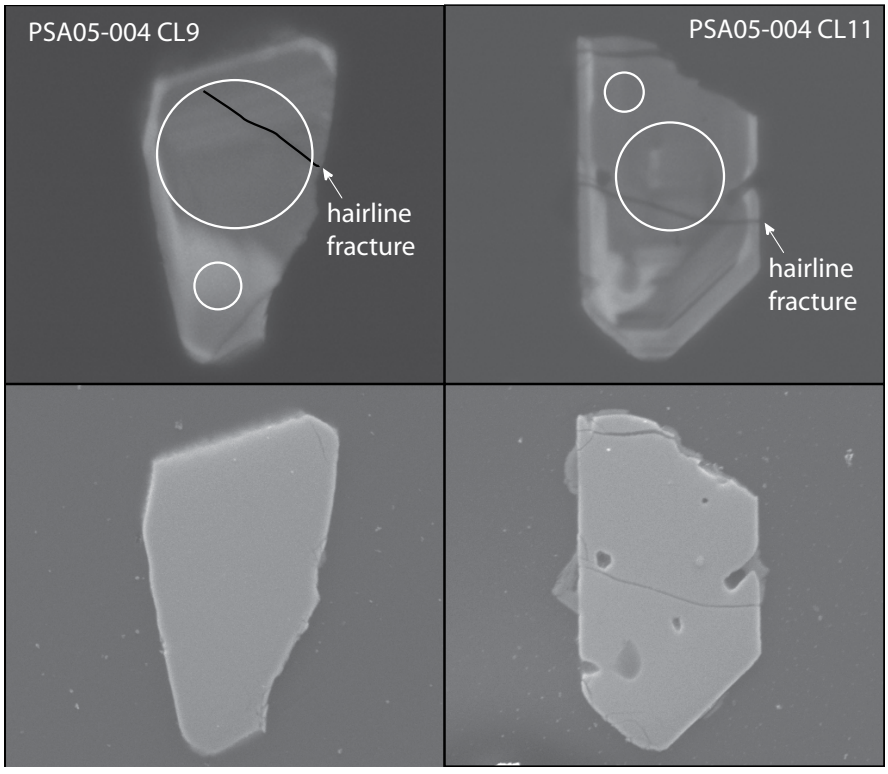

Figure 69 Zircons CL9 and CL11 each showing a hair line fracture at the location of the 35 µm spot analysis and no fractures in the vicinity of the 10 µm spot analysis. CL images on top and corresponding SE images on the bottom of each picture. Note the scale is different on each photograph pair. The large white circles on each grain are 35 µm in diameter and the small white circles are 10 µm in diameter; these circles show the approximate location of the ablation sites.

Only two low U grains, CL9 and 11 (U contents of 520 and 1060 ppm), showed evidence of Pb loss. These were analyzed with a 35 μm spot size. These grains are interesting because the 10 μm spot analyses on these same grains have accurate ages (226 and 224 Ma, respectively). Detailed examination of the CL images of these grains shows a small hairline fracture in the area where each 35 μm spot was ablated, but none where the 10 μm spots were ablated (Figure 69). It is possible that these fractures may have facilitated the escape of radiogenic Pb or somehow allowed mobile radiogenic Pb from the high U zone on the outside of the crystal to contaminate the analyses. In these two cases the fractures can explain the slightly young ages for each zircon when analyzed with a 35 μm spot size and their reliable age when analyzed with a 10 μm spot size.

The results of this study illustrate three points regarding Pb loss in zircons: (1) small zircon grains in this sample have higher U contents and therefore Pb loss is more common in these grains; (2) independent of size, all zircon grains with >2700 ppm U have undergone Pb loss; and (3) zircon grains with <2700 ppm U which have undergone Pb loss can be explained through careful examination of CL images. To pick the integration interval and to assess the validity of zircon ages, analyses with U content of >2500 ppm should be rejected. This critical U content may be a function of the geological history at Greens Creek and cannot be given as a definite cut-off value for all zircon grains.

Precision and accuracy

The results outlined above indicate that the small in-situ technique is a viable method for obtaining ages on rocks where only small zircon grains are present. The best estimate for the age of the Gallagher rhyolite comes from the TIMS data and is 226.86 ± 0.24 Ma, similar to that obtained using the conventional LA-ICP-MS method (224.7 ± 1.3 Ma). The slight difference in these ages (<0.3%) may indicate the rims of the zircon grains are slightly younger than the cores and the chemical abrasion preparation

in the TIMS method has removed this portion of the grain. The slightly young age of the rims could be magmatic in origin or could be the product of minute Pb loss. However the difference in age between the rims and the cores is below the level of precision of our LA-ICP-MS technique. The best estimate for the age of the zircon grains by the conventional LA-ICP-MS method using a 35 μm spot size is essentially the same as the TIMS estimate and accuracy of the LA-ICP-MS method is confirmed by this result.

Reducing the spot size from 35 μm to 10 μm with the conventional LA-ICP-MS method and analyzing the same 24 zircons, the age determinations become less precise with uncertainties increasing from ±1.1 Ma to ±2.3 Ma. Finally, when using the 10 μm spot size and analyzing zircons in-situ, the precision decreases to ±2.6 Ma and many zircon analyses had to be rejected due to Pb loss. Zircons can be analyzed in-situ using the LA-ICP-MS with a 10 μm spot size, but additional care is required in assessing the results. More zircon analyses are required to get around Pb loss problems, larger zircons give better results and the analytical error is doubled compared to the same zircon grains analyzed at 35 μm.

Suitability of the technique

For the new in-situ 10 μm spot technique four criteria must be met. (1) Zircons must be sufficiently old to allow for appreciable concentration of radiogenic material. The lower the concentration of radiogenic material, the larger the volume of material and therefore larger spot sizes needed for reliable data. (2) The sample must be fine-grained and have the highest Zr content possible. The finer grain size increases the probability of locating zircon using the MLA technique but may increase the chances of Pb loss. (3) U content of zircons must be reasonably low to decrease the chances of Pb loss. The actual U content at which Pb loss occurs will depend on the age and thermal history of the rocks. For Late Triassic zircons at Greens Creek the maximum U content appears to be 2500 ppm. (4) The geological problem must be solvable given the 1–5% error inherent in the in-situ method.

Summary

- It is possible to efficiently locate small zircon grains on surface of polished laser mounts using the SEM-based MLA software. Once located, CL images of these grains can be acquired and used to investigate internal zircon textures.

- The CODES geochronology laboratory has demonstrated long-term (~one year) and short-term (~one hour) success in U-Pb dating of zircon grains. Long-term precision on standard zircons Temora1, 91500 and Mud Tank is approximately 1.0 to 1.5%.

- The Gallagher rhyolite is located on Gallagher Ridge and has abundant large and small zircon grains. The best estimate for the age of this sample comes from TIMS analyses of five grains with a weighted mean of $^{206}Pb/^{238}U$ ages of 226.86±0.24 Ma.

- The LA-ICP-MS estimates of the weighted mean $^{206}Pb/^{238}U$ ages for 24 separated grains using a 35 μm and 10 μm spot respectively are 224.7±1.3 Ma and 225.1±2.3 Ma. These ages are very similar to the TIMS estimate indicating that reducing the spot size doubles the analytical error but does not produce any systematic errors.

- The in-situ LA-ICP-MS method had the lowest precision (1.2% 2σ error), but the weighted mean estimate of the $^{206}Pb/^{238}U$ age for the best 20 analyses was similar to the TIMS age estimate (223.5±2.6 Ma versus 226.9±0.2 Ma).

- Small zircon grains with high U (≥2500 ppm) invariably showed the effects of Pb loss. As the in-situ zircon grains had higher U contents than the separated grains, the rejection rate of in-situ grains was much higher. However, if a sufficient number of in-situ grains can be located, errors on the weighted mean of the $^{206}Pb/^{238}U$ ages can be ±1%.

Chapter 5: Chronostratigraphy

Introduction

Previous workers have characterized the Greens Creek massive sulfide deposit as stratiform with a stratigraphic footwall of altered volcanic and volcaniclastic rocks and a stratigraphic hanging wall of dominantly sedimentary rocks (i.e. Dressler and Dunbire, 1981; Crafford, 1989; Newberry et al., 1989; Newberry and Brew, 1997; Taylor et al., 2008). However, extending this simple stratigraphy beyond the immediate mine area is difficult because of structural complications and strong alteration. In order to resolve the property- to regional-scale chronostratigraphy, absolute age dating is required as many of the field relationships are ambiguous.

This chapter discusses results from the U-Pb dating of zircon grains from rocks collected on or near the Greens Creek property and then uses these results to construct a chronostratigraphy for the Greens Creek area. The results of this geochronological study are organized by the geochronological usefulness of each sample. Samples with abundant zircon grains, but having unreliable ages are briefly discussed. Samples with reliable ages are discussed in detail, using the format: geologic setting and interpretation of both the unit and the sample, interpretation of the isotopic data and the origin of the zircon grains. The presentation of the results is followed by a synthesis of the age data into a new chronostratigraphy of the Greens Creek area.

Background

Previous workers in the vicinity of the Greens Creek Mine encountered many difficulties in resolving the stratigraphy (e.g. Table 21). These difficulties have stemmed largely from two issues: (1) the age control within the stratigraphy was largely based

on fossils which are primarily restricted to the hanging wall argillite, and (2) the deformation and alteration are intense, obscuring original stratigraphic relationships. The aim here is to provide a chronostratigraphic framework using radiometric ages that will allow consistent correlation between units surrounding the Greens Creek Mine.

Table 21 Summary of the historical development of ideas on the Greens Creek stratigraphy and intrusive rock relationships. Black squares indicate approximate ages of intrusive rocks.

Era	Lathram et al., 1965		Brew and Ford, 1985; Brew, 2007	
Post-Triassic	Stephens Passage Group (Jura-Cretaceous)	■ serpentinized peridotite	Gravina Overlap Assemblage (Jura-Cretaceous)	
Triassic	Hyd Formation (Triassic)		Hyd Formation (Late Triassic)	
			mineralization	■ serpentinized peridotite
Paleozoic	Cannery Formation (Permian)		Gambier Bay Group (Devonian)	
	Retreat Group (Devonian)		False Point Retreat Complex (Early Paleozoic)	

Aims

This chapter examines the regional stratigraphy near the Greens Creek Mine from the basement (S-D2) through to the post-Triassic lithologies (Table 21). The geochronological investigations reported here complement the stratigraphic studies of Taylor et al. (2008). Part of the present study required the development of a new method in U-Pb isotopic dating for small zircon grains (see Chapter 4). Investigations in this chapter are focused on the footwall (units C1, C2 and Tr1). However, due to uncertainty

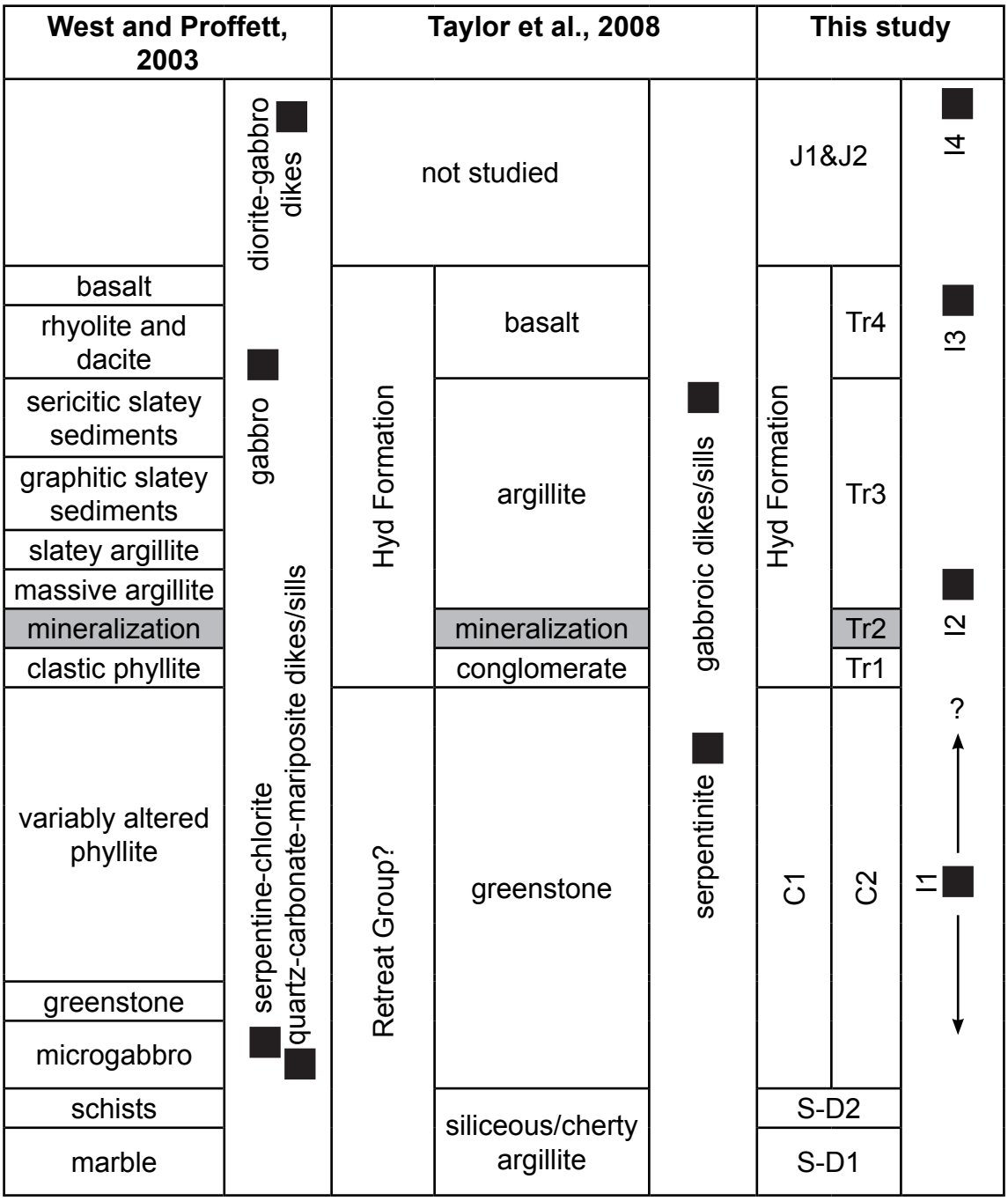

as to which rocks are from the footwall, a significant number of samples from the hanging wall and Triassic intrusive rocks (units Tr4, I2–4) and a few regional samples (units S-D2, J1 and J2) were also studied.

Data collection

Samples for geochronological investigation in the present study were selected based on 1) geologic significance and 2) suitability for U-Pb dating of zircons. Samples were selected based on the stratigraphy of Taylor et al. (2008) and, through discussions with A. West, senior exploration geologist at Greens Creek and J. Proffett, consulting structural geologist. The units given highest importance were volcanic rocks (potential for direct dating of igneous zircons) and rocks near the footwall–ore contact (units C1, 2, 3 and I2, 3, 4). Suitability for dating is discussed in detail in Chapter 4. Essentially, the in-situ zircon dating technique works best on fine-grained rocks with Zr contents ≥100 ppm. Some rocks with lower Zr contents or coarser grain sizes were included in the study but had low rates of success. For each sample an initial attempt was made to isolate zircon grains using traditional gravity separation of crushed rocks. This was only successful on one sample, PSA05-004. The remaining ages discussed in this chapter were obtained solely by in-situ dating of small zircons. The distribution of regional samples is shown in Figure 70 and the mine sample sites are shown in Figure 71.

Previous geochronology

Age constraints on the rocks at Greens Creek are poor. Reconnaissance geologic mapping in the 1960s (Lathram et al., 1965) identified the lithologic units in the vicinity of Greens Creek as Devonian Retreat Group and those at the mine portal as Permian Cannery Group. Thus the deposit was originally thought to be located at the contact between Devonian metavolcanics and Permian sediments. The unaltered ultramafic bodies on Mariposite Ridge northwest of the mine were originally mapped as Middle(?) Cretaceous in age and the quartz-carbonate-fuchsite-altered serpentinite body north of the mine was identified as a Middle(?) Devonian serpentinized dolomite. The next round of mapping by the United States Geological Survey (USGS) (Brew and Ford, 1985)

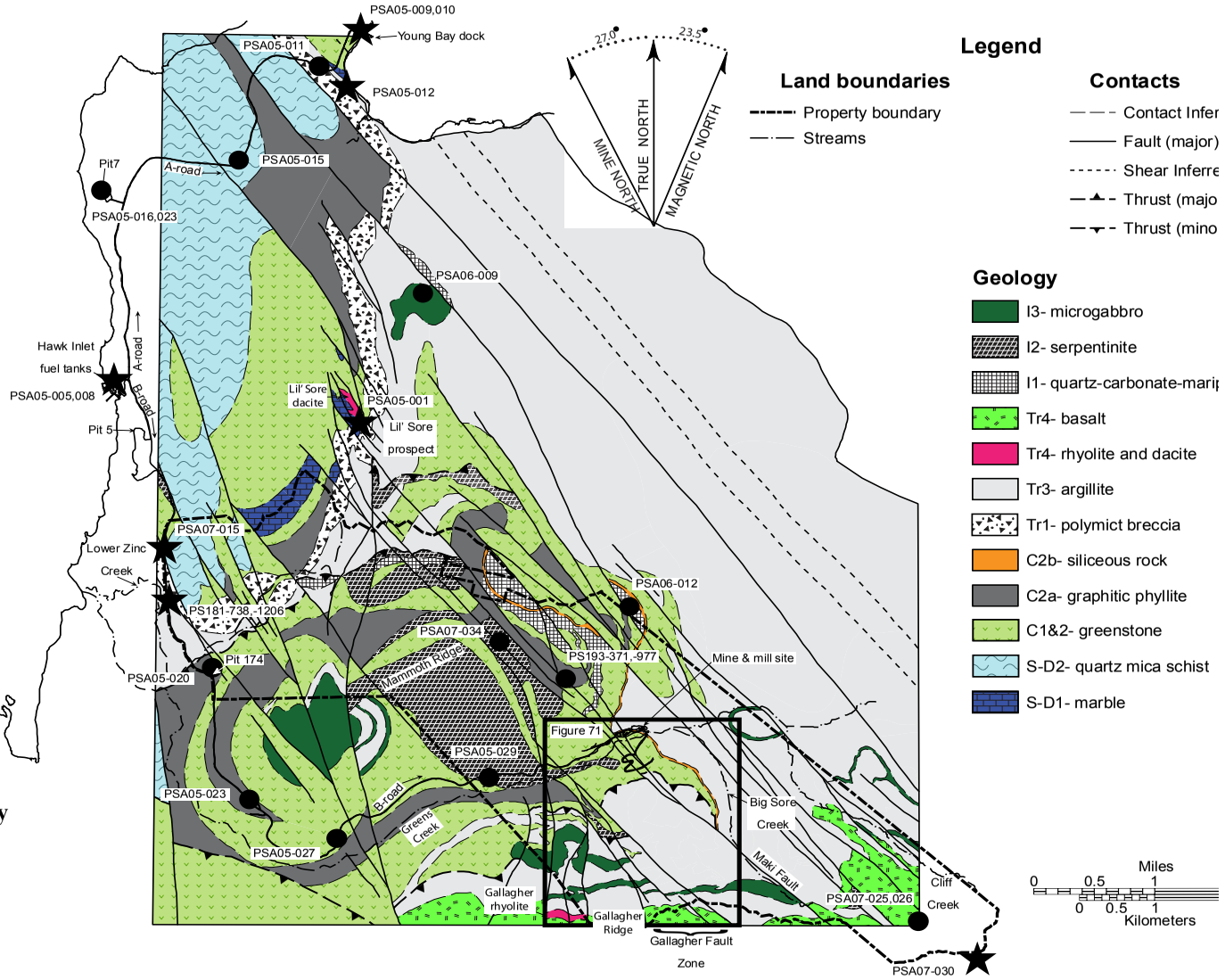

Figure 70 Map of the Greens Creek property and surrounding area. Key locations are labelled and the location of geochronology samples with an insufficient number of zircon grains (circles) and abundant zircons grains (stars) are shown. Geology from Duke (2007). Note the location of Figure 71.

showed the mine hosted in the Cannery Group and revised the age of the Retreat Group from Devonian to Silurian. They also noted that the ultramafic bodies on Mariposite Ridge to the north of the mine are variably altered dunites and peridotites and revised their age to Mesozoic.

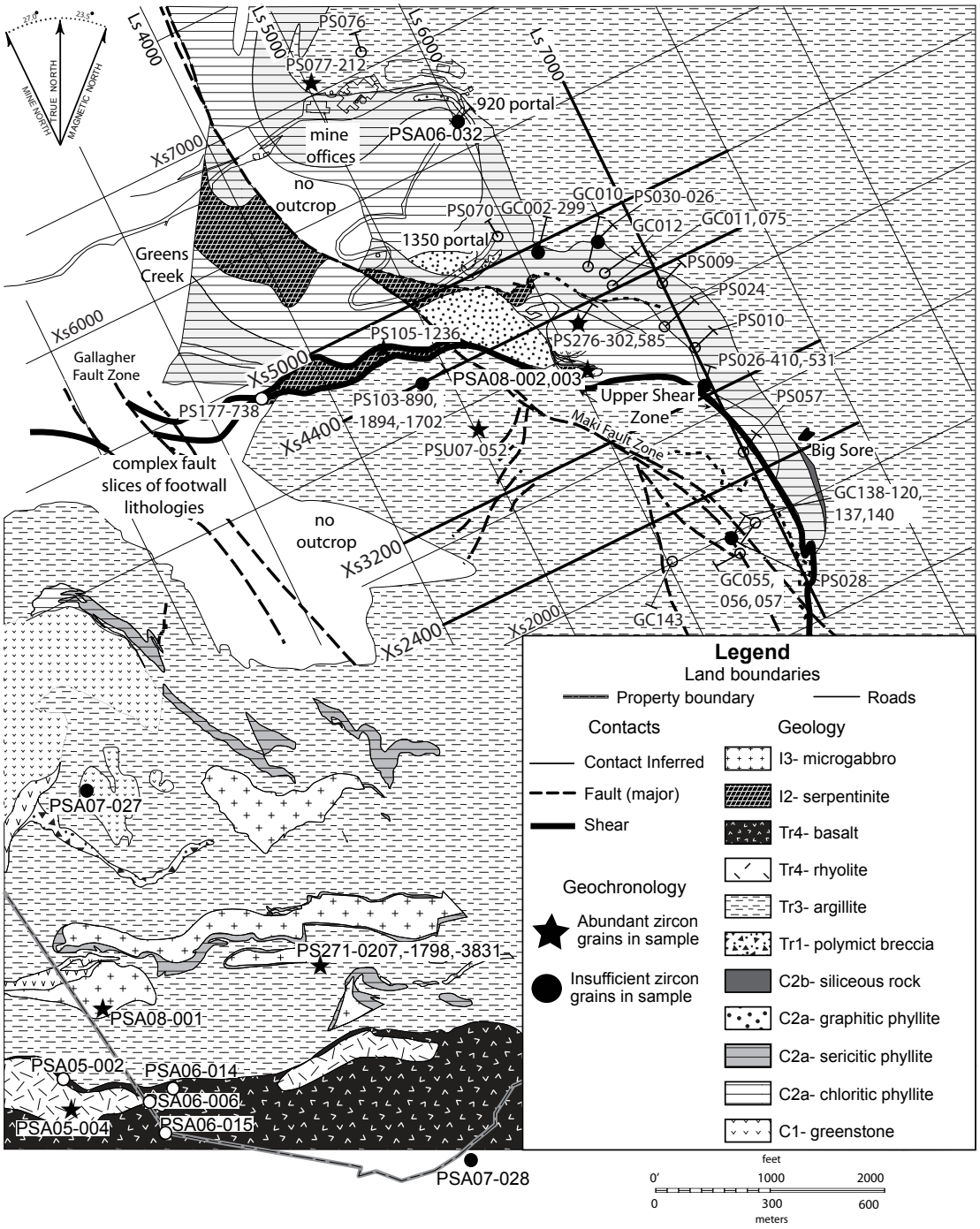

Figure 71 Detailed surface geology map of the Greens Creek Mine. See Figure 70 for location. Geology from Proffett (2007). Locations of geochronology samples with an insufficient number of zircon grains (circles) and abundant zircons grains (stars) are shown. The mine grid is shown with the key sections highlighted.

The first important age constraint, based upon data collected at the mine was the discovery of macrofossils, *Halobia*, found in clasts of siliceous argillite that were interpreted to have been tectonically milled into massive sulfide ore (Crafford, 1989). Prior to the USGS study (Taylor and Lear, 2001), the *Halobia* were the only direct evidence for the age of the mine host rocks and the mineralization. Based on this evidence, the age of the deposit was considered to be Late Triassic (Crafford, 1989; Newberry et al., 1990; Newberry and Brew, 1997). The Triassic age was supported by the similarity of the mineralization, basalt geochemistry and stratigraphy to other Late Triassic massive sulfide occurrences in southeastern Alaska and British Columbia (MacIntyre, 1986; Taylor et al., 1995; Newberry and Brew, 1997; Taylor, 1997; Taylor et al., 1999).

The USGS study of the deposit in the late-1990s paid special attention to geochronology of the Greens Creek host rocks (Premo et al., in press). The dating methods employed by the USGS include conodont collections from the hanging wall argillite, $^{40}Ar/^{39}Ar$ analyses of sericite and fuchsite alteration from ore and altered footwall phyllites, and construction of U/Pb and Sm/Nd mineral and whole-rock isochrons on specific footwall lithologies (Premo et al., in press).

Seven samples from the mine host rocks and from carbonate-bearing units in and around the mine area yielded conodonts that provide usable age constraints (Premo et al., in press). The samples contained *Polygnathus*, *Metapolygnathus*, *Epigondolella* and *Neogondolella* morphotypes that restrict the hanging wall argillite in the mine area and Hyd Formation argillite within several kilometers of the mine to the late Carnian through middle Norian (middle Late Triassic) (Premo et al., in press). Three of these samples were collected from the underground workings in the hanging wall within ~ 50 m of the ore–hanging wall contact (samples 620-2955, 37 ramp and 480S). Two additional samples, one collected from the cirque at the head of Cliff Creek (sample Upper Cliff Ck 2) and a second collected from drill core from Big Sore

Ridge immediately above the mine workings (sample PS112-1347) provided even tighter age constraints (Proffett, in press). These collections defined a low diversity assemblage consisting essentially of *Metapolygnathus nodosus* A.Z. and *Epigondolella pseudodibelli-Metapolygnathus communisti* A.Z. (Harris, 2000). Thus a reliable age assignment for the hanging wall argillite unit and for the Hyd Formation argillite in the mine vicinity is latest Carnian to earliest Norian (Late Triassic) (Premo et al., in press). This age agrees well with the latest Carnian-earliest Norian age of the mineral belt in southeastern Alaska and British Columbia (Taylor et al., 1999).

$^{40}Ar/^{39}Ar$ geochronological studies of sericite and fuchsite alteration in the mine and of fuchsitic alteration of ultramafic bodies in the mine area were conducted in an attempt to constrain the timing of ore formation (Taylor et al., 1999). Seven samples yielded reliable data, all of which indicate Cretaceous metamorphic(?) resetting of micas occurred prior to 95 Ma. However, a regional sample reported in Taylor et al. (1995) provides a possible age constraint on the Greens Creek hydrothermal system. On the southeastern side of Admiralty Island, on the north shore of Gambier Bay, there are several mineral occurrences hosted in Late Triassic rocks that bear a strong resemblance to Greens Creek (Taylor et al., 1992). These occurrences are associated with bodies of altered ultramafic rocks similar to the ones at Greens Creek (Taylor et al., 1992). Geochronological data from a fuchsite separate from the thickest of these alteration zones yielded a two-step $^{40}Ar/^{39}Ar$ plateau age of 210.7 ± .3 Ma and a total gas age of 204.6 ± 0.4 Ma (Taylor et al., 1995).

U/Pb and Sm/Nd isochrons were constructed using whole-rock and mineral separates from the least-altered basalt and gabbroic intrusive equivalents from outcrops surrounding the mine (Taylor et al., 1999). Whole-rock U/Pb data from Hyd Formation basalt samples collected from Gallagher Ridge, south of the mine, define an isochron age of 215.3 ± 6.4 Ma and have an initial $^{206}Pb/^{204}Pb$ value of 18.55 (Premo et al., in press). Samples of massive unaltered microgabbro immediately underlying the Hyd

Formation basalts of Gallagher Ridge form an imprecise whole-rock isochron with an age of ~205 Ma and an initial $^{206}Pb/^{204}Pb$ value of 18.46 (Premo et al., in press). In a plot of the same rocks in the Sm/Nd system, two of the Hyd basalts from Gallagher Ridge form a line corresponding to an age of ~219 Ma with an initial epsilon Nd value of +7.3 (Premo et al., in press). This age agrees well with the ~215 Ma age determined for the same suite of rocks by the U/Pb system (Premo et al., in press). The most precise Sm/Nd isochron, using five whole-rock and mineral data points from the microgabbros on Gallagher Ridge, defines an age of 212 ± 36 Ma with an initial epsilon Nd value of +5.6 (Premo et al., in press). Although the error is large, the age is geologically reasonable and is consistent with the stratigraphic and cross-cutting relationships which place the Hyd Formation basalts over the Hyd Formation argillite, with both units intruded by the Gallagher Ridge microgabbros.

The USGS study did not obtain age constraints on the protolith age of the serpentinites in and around the mine area due to their low trace- and rare-earth-element abundances and their high susceptibility to isotopic resetting. Two serpentinite samples from Mariposite Ridge, north of the mine, yielded results which suggest resetting of the U/Pb system at approximately 40 Ma (Premo et al., in press). Geological data on the probable age of the serpentinites is sparse but the available data are consistent with a Late Triassic age. Regionally, serpentinite bodies on the north shore of Gambier Bay have hornfelsed the Hyd Formation argillite, implying that they were intruded into these sediments while still hot (Taylor et al., 1995). One of the serpentinite bodies on Mariposite Ridge is in contact with, but does not cross-cut, the overlying Hyd Formation basalt (Proffett, in press).

Taylor et al. (in press) interpreted the above data as suggesting that the microgabbros, serpentinites and Hyd Formation basalts in the mine area are co-magmatic and of Late Triassic age. They further asserted, that if these relationships are correct, then the available age constraints suggest that intrusion of mafic and ultramafic rocks at

Greens Creek occurred at ~212 Ma and were then altered and cooled below the closure temperature (with respect to argon in fuchsite) by ~211 Ma.

The stratigraphy for the Greens Creek area as described in the late-1990s by Taylor et al. (2008) (Figure 72) shows the following key features: (1) Permian basement, (2) footwall of uncertain Late Triassic, Permian or older age unconformable on the basement, (3) serpentinite sills and dikes cross-cutting the basement and footwall but not cutting the breccia or younger lithologies, (4) polymict breccia and/or minor limestone immediately below the ore position, (5) ore immediately overlain by argillite which is in turn capped by another limestone and (6) thick sequence of massive to pillowed basalts capping the entire section and fed by gabbroic dikes and sills.

Regional geology programs have been successful in dating several Permian metamorphic events throughout the northern portion of the Admiralty Terrane (Karl et al., 1998; Karl et al., 1999). Samples of volcanic rocks from Gallagher Ridge have Late Triassic ages (Karl pers. comm.). These two studies by the USGS provide most of the age constraints on the rocks in the Greens Creek area and they are the starting point for the geochronological investigation of the present study.

Methods

Zircon dating was done using the in-situ method described in Chapter 4. Once zircon grains were located, cathodoluminescence (CL) imaging was done on all grains over 5 μm. Sixty-three samples (Table 22) from ten stratigraphic units were processed. Twenty-one samples had ≥ 15 zircon grains with areas ≥ 50 μm^2 and two samples had other U-Pb bearing mineral phases. Of the samples with abundant zircon grains, 15 provided reliable results. No further dating was attempted on samples with other U-Pb-bearing phases. All 21 samples with abundant zircon grains and the two samples with other U-Pb-bearing phases are discussed in this chapter, however, only zircons grains with reliable results are discussed in detail. For most reliable samples a reverse concordia

diagram and a cumulative probability distribution plots with a histogram of the data are presented. The raw data files, interpreted data files, CL and SE images can be found in Appendix 3.

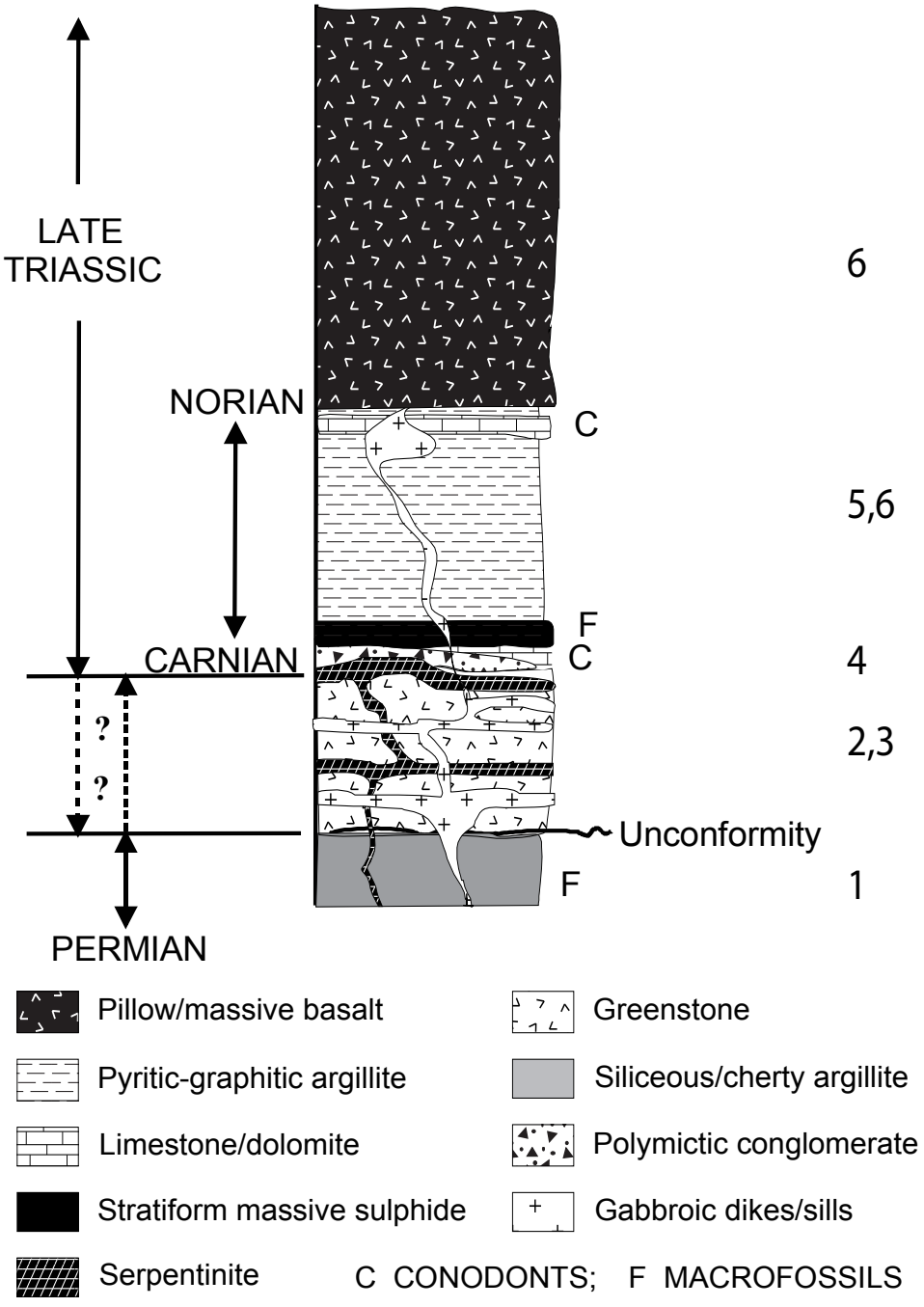

Figure 72 Composite stratigraphic column of the Late Triassic section at Greens Creek (Taylor et al., 2008). Numbers along right side indicate key features noted in above paragraph.

Table 22 List of samples used in the geochronological investigation of the present study. Samples with an 'X' in the Zr column had reliable age data; samples with an 'O*' in the Zr column had U-Pb-bearing minerals other than zircon and were not dated; samples with an 'O' in the Zr column were rejected from age calculations for reasons discussed in the text; and samples with nothing in the Zr column had an insufficient number of zircon grains on which to attempt dating. Coordinates for surface samples (i.e. PSA05-*) are State Plane (SP) using the NAD27 datum; coordinates for diamond drill hole samples (i.e. PS103-***) are collar coordinates in State Plane with the NAD27 datum, the digits after the dash indicate down-hole depth (in feet); coordinates for underground samples (i.e. PSU05-***) are in cross-section (in SP=E) and long-section (in SP=N). The lithology (CODES) column is based on the stratigraphy outlined in the right hand column of Table 21; the lithology (mine) column is based on West and Proffett (2003).**

Field Number	SP East (ft)	SP North (ft)	Prospect	Zr	Lithology (CODES)	Lithology (mine)
PSA05-005	2475574	2300807	Hawk Inlet	X	S-D2	QMS
PSA05-008	2475670	2300728	Hawk Inlet	X	S-D2	GQMS
PSA07-015	2477831	2292613	B-road	X	C1	GST
PSA08-003	2499978	2281910	1350 Creek (E. Ore)	X	C1	GST
PSA07-030	2512575	2273900	Cliff Creek	X	S-D2/C1?	amphibolite
PS276-585.5	2500268	2281883	East Ore	X	C2	SPc
PS077-212	2498031	2284043	East Ore	X	C2	SP
PS105-1236	2498670	2281656	NWW Ore	X	C2	SR
PSU07-052	4390	4485	PD4445	X	C2	SPt
PS271-207	2498116	2276445	Upper Gallagher	X	I3	HGB
PSA08-001	2495883	2276373	Gallagher Ridge	X	I3	HGB
PSA05-004	2495807	2275532	Gallagher Ridge	X	Tr4	SR
PSA05-010	2486428	2317140	S of Y. Bay pier	X	J1	siltstone
PS181-738	2478610	2290640	Lower Zinc	X	C2	SPs
PSA08-002	2500094	2281852	East Ore	X	I4	DG
PSA05-001	2486377	2298709	Little Sore	O*	Tr4	SR
PSA07-028	2498957	2275120	S. Gallagher Ridge	O*	Tr4	HGS
PSU05-045	910	3500	4211	O	C2	SPc
PSA07-026	2510100	2275550	Cliff Creek	O	Tr4	GST
PSA05-027	2485410	2279256	5.6 mile B road	O	C1	GST
PSA05-023	2481594	2281161	4.63 mile B road	O	C1	GST
PSA05-020	2479990	2287328	NW corner of Pit 174	O	C2	SPgr
PSA05-012	2485720	2315438	Y. Bay beach	O	C1?	GST
GC002-299	2499997	2282525	East Ore		C2	SPs
GC138-120	2501667	2280049	East Ore		C2	SP
PS103-0890	2498992	2281379	NWW Ore		C2	SP
PS103-1894	2498992	2281379	NWW Ore		C2	SP
PS105-1702	2498670	2281656	NWW Ore		C2	SPc
PS177-738	2497651	2281767	Lower Gallagher		C2	SPs
PS181-1206	2478610	2290640	Lower Zinc		C2	SPc
PS193-371	2495334	2286907	West Bruin		C2	SPc
PS193-977	2495334	2286907	West Bruin		C1	GST
PS26-410	2501428	2281362	East Ore		C2	SPgr
PS26-531	2501428	2281362	East Ore		C2	SPgr
PS271-1798	2498116	2276445	Upper Gallagher		Tr4	HGS

Field Number	SP East (ft)	SP North (ft)	Prospect	Zr	Lithology (CODES)	Lithology (mine)
PS271-3831	2498116	2276445	Upper Gallagher		C2	SPgr
PS276-302	2500268	2281883	East Ore		C2	SPgr
PS30-026	2500505	2282615	East Ore		C2	SP
PSA05-002	2495658	2275724	Gallagher Ridge		Tr4	HGS
PSA05-006	2477858	2293200	1.9 mile on B road		S-D2	QMS
PSA05-009	2486770	2317307	N of Y. Bay pier		J2	basalt
PSA05-011	2484675	2315555	4.55 mile on A road		Tr1	SPcx
PSA05-015	2481132	2311103	3.2 mile A road		I4	DG
PSA05-016	2475120	2309741	Pit 7 A road		S-D2	QMS
PSA05-029	2493456	2282373	7.4 mile B road		I2	SC
PSA06-009	2489095	2304550	Lil' Sore		I3	GST
PSA06-012	2498040	2290430	Mammoth Ridge		C1	HGB
PSA06-015	2496465	2275420	Gallagher Ridge		Tr4	GST
PSA06-032	2498995	2284053	mine portal		C2	SPc
PSA07-025	2510950	2275400	Cliff Creek		Tr4	GST
PSA07-027	2495750	2278300	W Gallagher Ridge		I3	HGB
PSA07-034			Serpentine Gulch		I3	HGB
PSU05-026	1010	4030	4211		C2	MSPs
PSU05-041	960	3675	4211		C2	SPc
PSU05-051	815	3300	4211		I4	DG
PSU05-054	770	3170	4211		C2	SPc
PSU07-007	4697	4650	878		C2	MSPs
PSU07-008	4565	4753	878		C2	SR
PSU07-012	4438	4970	5044		I1	QCM
PSU07-019	4685	5035	4750		C2	SR
PSU07-023	4733	4775	4747		C2	SPgr
PSU07-041	4235	4812	PD4247		I1	QCM
PSU07-051	4440	4415	PD4445		C2	SPgr

Interpretation of the quality of the isotopic data collected from a zircon grain is important in the overall reliability of the calculated U-Pb ages. For an analysis interval to be deemed suitable in the present study, it had to be longer than ~ 3 s (approximately 15 mass scans), be free of inclusions, have a stable horizontal signal, have <2000 ppm U content and be within two standard deviation of the mean of other grains in that sample. Grains were rejected outright from further data reduction and interpretation if no suitable integration interval could be found in the analyses. Six samples (PSU05-045, PSA07-026, PSA05-012, PSA05-020, PSA05-023 and PSA05-027 (marked with an 'O' in Table 22)) had abundant zircon grains identified during the SEM-MLA search.

Between six and 24 zircon grains were in analyzed in each sample but there were no acceptable integration intervals identified and the samples were rejected.

Two samples (PSA05-001 and PSA07-028) had zircon grains identified during the SEM-MLA search (marked with an 'O*' in Table 22), but the grains turned out to be other mineral phases as identified by their Energy Dispersive Spectra (EDS) on the SEM. In PSA05-001, the grains are composed of a mixture of xenotime and zircon. The zircon grains in PSA05-001 were too small to analyze separately from the intimately intergrown xenotime and were rejected. However, several composite grains of the two phases were analyzed and the age was inferred to be Mesozoic (S. Meffre pers. comm.), with no further age refinement possible. PSA07-028 had approximately 20 small baddeleyite grains identified by MLA and EDS. These grains were not rigorously analyzed because of the lack of a baddeleyite standard at the CODES geochronology laboratory. Again, a few grains were analyzed against zircon standards and a Mesozoic age was inferred (S. Meffre pers. comm.).

Results

Basement

The basement rocks analyzed are generally siliceous, micaceous, schistose rocks with minor marble and found along the eastern edge of Hawk Inlet, approximately 7–10 km northwest of the mine. The basement is composed of quartz mica schists, quartz chlorite schist and graphitic quartz mica schists; each found as layers from several centimeters to tens of meters thick. The depositional age of these basement rocks is thought to be Silurian or Devonian based on the presence of tabulate coral in a marble sample, within 3 km of Hawk Inlet, associated with these schists (Oliver and Berg, 1981).

Sample PSA05-005 is from the quartz mica schist and PSA05-008 is a sample of the graphitic quartz mica schist. Both samples were collected from the fuel bay at the Hawk Inlet facilities. Due to the proximity of the samples and the similarities of the

results, the results have been combined and are discussed together. Twelve zircon grains were analyzed from PSA05-005 and 17 from PSA05-008. Twenty grains were rejected outright because they had U contents >2000 ppm. A small group of six grains is interpreted as detrital in origin with a Proterozoic ^{207}Pb corrected $^{206}Pb/^{238}U$ age (Figure 73). Most of these grains show some evidence of Pb loss. One anomalous zircon in PSA05-008 had a moderate U content and a $^{206}Pb/^{238}U$ - 207 corrected age of 179 ± 6 Ma. Four zircon grains have a weighted mean ^{207}Pb corrected $^{206}Pb/^{238}U$ age of 264 ± 23 Ma with an MSWD of 2.90 which is considered the metamorphic age for these rocks.

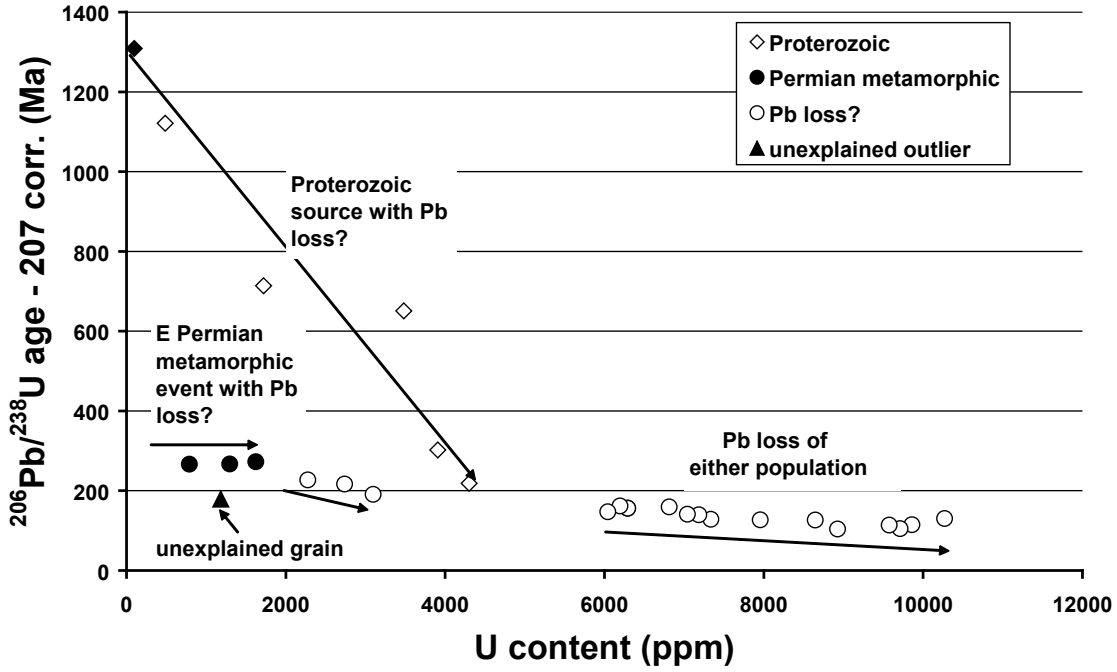

Figure 73 $^{206}Pb/^{238}U$ - 207 corrected ages versus U content for analyses of 29 zircon grains from samples PSA05-005 and PSA05-008. Solid symbols represent analyses that yielded acceptable ages and hollow symbols represent analyses that were rejected based on criteria discussed in the text.

C1 – massive mafic volcanic rocks

The massive mafic volcanic footwall lithology is more common lower in the footwall, but examples of this lithology can be found close to the ore position. At a property scale of observation, the massive (C1) and layered (C2) volcanic rock types are combined and, volumetrically, make up the majority of the footwall. The massive volcanic rocks are identified by their massive texture and slightly coarser grain size (up to 1 mm) than the layered rocks. The best examples of the massive rocks have fine-grained feldspar

'phenocrysts' evenly distributed throughout the rock. This lithology is interpreted to be igneous in origin but it is not known if it is extrusive or intrusive. Prior to the present study, the only age constraint on these rocks came from Permian metamorphic ages of micaceous minerals which form a pre-mineralization foliation (Karl et al., 1998). The entire footwall package (units C1-3) is thought to sit unconformably upon the basement (Taylor et al., 2008).

Sample PSA07-015 is from a boulder located at the bottom of a cliff on the B-road, 200 feet (60 m) north of mile marker 2.0 (km 3.2) (Figure 70). This sample is from the same rock type that makes up the cliffs and was safer to sample (i.e. is treated as an outcrop sample, not float). PSA07-15 is fine-grained, light green to grey with a moderate number of light colored, fine-grained feldspar phenocrysts throughout. On outcrop scale, the rock is massive, poorly to moderately foliated and is interpreted as a massive coherent basalt. PSA07-15 is from 2000 feet (600 m) north of the mine contact and no major structural breaks have been recognized between the sample and the mine contact. This sample is thought to be a proximal footwall sample located on the northern thrust block (i.e. not the same block as the mine) and therefore its original lateral distance from the centre of mineralization is unknown.

Twenty-four grains of zircon larger than 10 μm were analyzed. Analyses from four zircon grains were rejected outright because of U contents >2000 ppm. The 12 most concordant zircons have a weighted average ^{207}Pb corrected $^{206}Pb/^{238}U$ age of 340 ± 5 Ma (Figure 74). This is interpreted as the crystallization age of the basalt. There is a scatter of results to younger ages but the weighted mean of all 20 grains is 339 ± 6 Ma with a MSWD = 1.09, very similar to the weighted mean age for the 12 most concordant grains.

PSA08-003 is from an outcrop located in the 1350 creek, approximately 2000 feet (600 m) southeast of the mine portal (Figure 71). The sample is medium-grained with

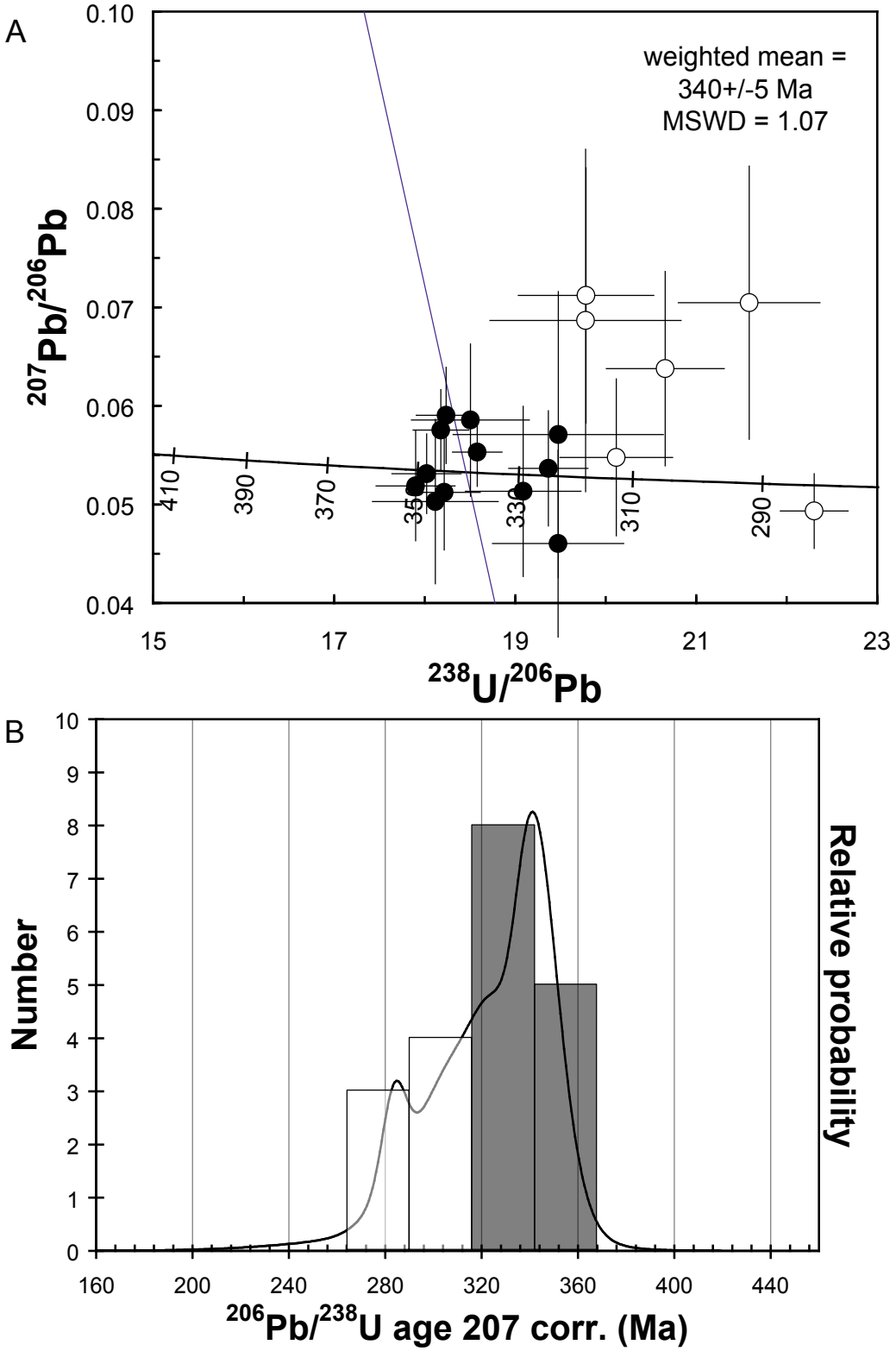

Figure 74 Reverse concordia and probability density plots of analyses from PSA07-015. (A)Reverse concordia plot and (B) probability density plot of analyses from 20 zircon grains in sample PSA07-015. Not shown are four rejected analyses. Black symbols represent analyses used in final weighted mean and white symbols represent analyses rejected from the final age calculations. The weighted average of the ^{207} Pb corrected $^{206}Pb/^{238}U$ age for the 12 best analyses is 340 ± 5 Ma. Data-point error crosses are 1σ.

abundant 1 mm white carbonate patches in a dark green matrix. Abundant fine-grained leucoxene is found throughout. Late-stage quartz-carbonate veins are common. At outcrop scale, the rock is massive, medium-grained and moderately foliated. This sample is interpreted to be from a coherent igneous rock, which, based on grain size may be hypabyssal (i.e. a diabase). The sample is located approximately 1000 feet (300 m) from the mine contact, from the same thrust block as the deposit and represents the best example in the study of a coherent igneous rock from the immediate footwall of the deposit.

Twenty-four zircon grains were analyzed with analyses of nine zircon grains from PSA08-003 rejected because they had U contents >2000 ppm. The weighted average ^{207}Pb corrected ^{206}Pb/^{238}U age based on the seven most concordant grains is 337 ± 5 Ma with a MSWD of 0.98 (Figure 75). This is interpreted as the age of crystallization of this diabase. As in sample PSA07-015, there is a scatter to younger ages. However, these younger zircon grains are interpreted to have lost radiogenic Pb.

Sample PSA07-030 is an amphibolite collected from the headwaters of Cliff Creek, approximately 5 miles (8 km) to the southeast of the mine portal (Figure 70). This is the only location near Greens Creek at which an amphibolite unit has been identified. The rapid change in grade from lower greenschist to amphibolite in the Cliff Creek area occurs at a thrust fault and the original relationship of greenschist facies rocks to the amphibolite is unknown (Duke et al., in press). One hypothesis is that the amphibolites are higher metamorphic grade equivalents of the massive volcanic footwall unit (C1).

Twenty-four zircon grains were analyzed from sample PSA07-030, all grains had at least portions of the analyses with U contents <2000 ppm and none were rejected. Two grains had Silurian ^{207}Pb corrected ^{206}Pb/^{238}U ages, and 22 grains had Permian ages (Figure 76). The two Silurian zircon grains had low to moderate U contents and correspondingly weak to moderate CL response (Figure 76), with no banding visible

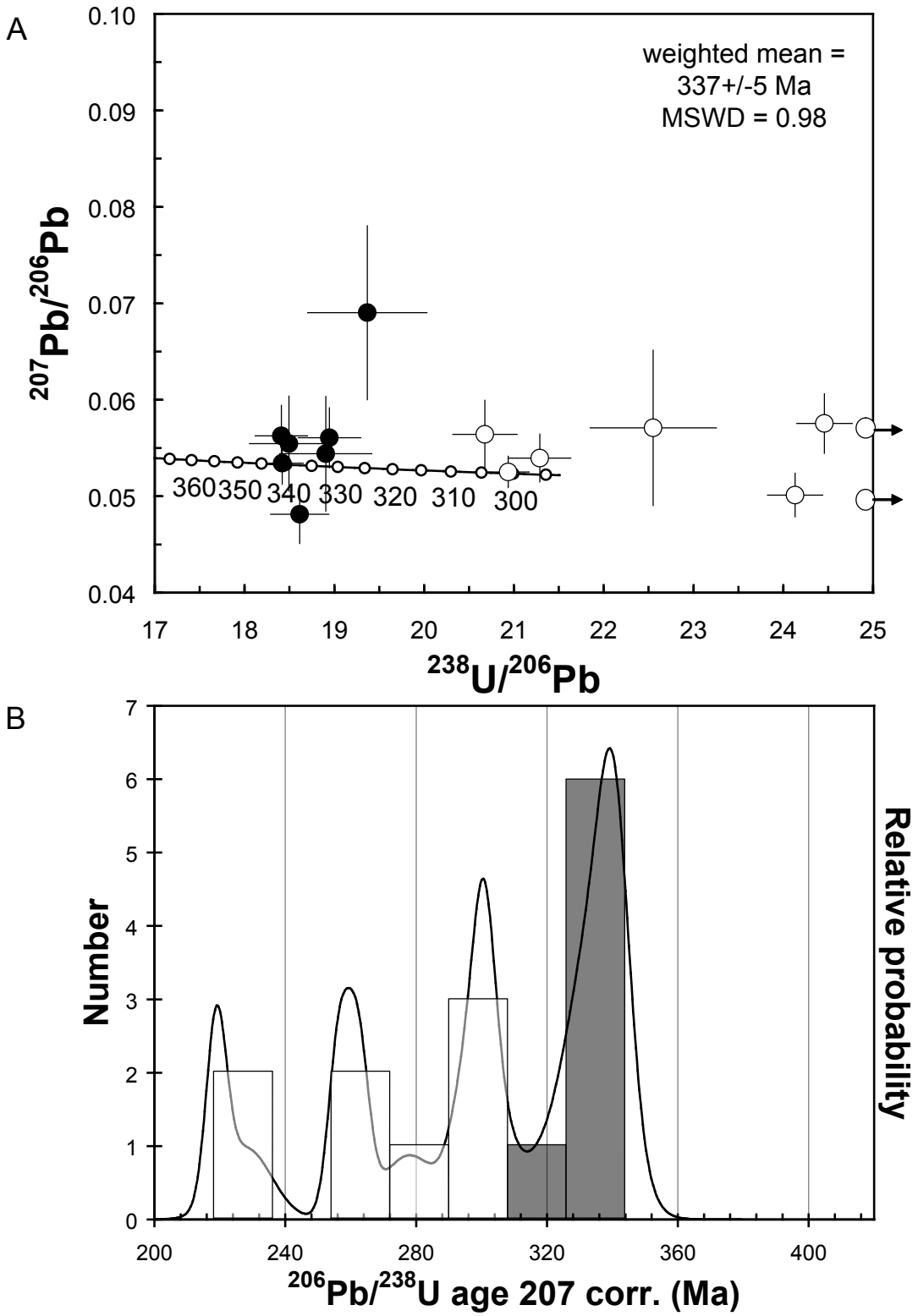

Figure 75 Reverse concordia and probability density plots of analyses from PSA08-003. (A) Reverse concordia plot and (B) probability density plot of analyses from 15 zircon grains in sample PSA08-003. Black symbols represent analyses used in final weighted mean and white symbols represent analyses rejected from the final age calculations. Data-point error crosses are 1σ. The weighted average ^{207}Pb corrected $^{206}Pb/^{238}U$ age of the seven best analyses is 337 ± 5 Ma.

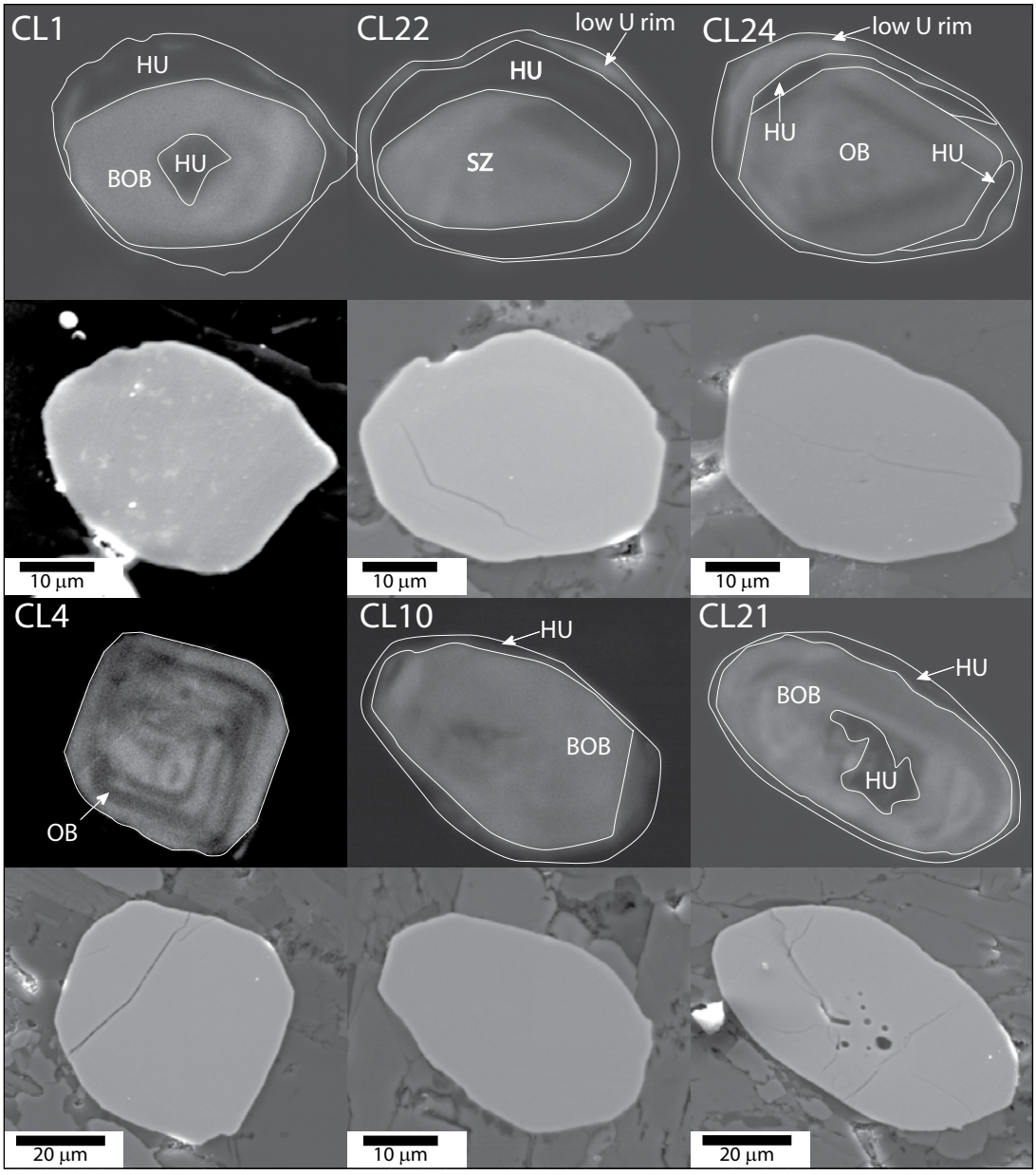

Figure 76 CL (top) and SE (bottom) images of representative zircon grains from sample PSA07-030 CL1 has a Silurian core. CL1, 22 and 24 show the spectrum of textures: OB = oscillatory banding; BOB = blurred oscillatory banding, SZ = sector zoning; HU = high U content. CL4, 10 and 21 are three of the five grains most likely to have had their U-Pb isotopic system reset according to the criteria of Hoskin and Black (2000).

and one dark zone surrounding a lighter zone. Zircon grain CL1 had a Th/U ratio of 0.006 while CL3 had a ratio of 0.61. Analyses reported for these grains are both from the brighter, higher U content cores with a weighted mean ^{207}Pb corrected $^{206}Pb/^{238}U$ age of 434 ± 38 Ma. Seven of the Permian grains have rims with ages younger than the cores. These core/rim relationships were generally, but not always, visible in the CL images with a brighter core (higher U content) and darker rim (lower U content). Zircon grain CL14 had a core and rim but with the opposite relationship, a higher U rim and lower U core. The remaining 15 Permian zircon grains have single low to moderate U zones in the analyses which sampled the cores of the grains. The CL images of these grains generally show the same core and rim patterns as the grains with mixed ages but the laser did not sample the rims (Figure 76). All of the Permian zircon grains have Th/U ratios between 0.074 and 0.001 with CL images generally showing weak sector zoning or blurred oscillatory banding. Two grains had oscillatory banding (Figure 76).

Two age-populations of grains are separable (Figure 77), the rationale for this and interpretations will be discussed below. All 27 accepted analyses have a weighted mean of the ^{207}Pb corrected $^{206}Pb/^{238}U$ ages of 291.7 ± 7.4 Ma with a MSWD of 3.0. The oldest population, consisting of 21 analyses, has a weighted mean of 297.4 ± 5.5 Ma with a MSWD of 1.4. The youngest six analyses are mostly discordant and have a weighted mean of 255.3 ± 8.8 Ma with a MSWD of 0.15.

C2 – layered volcanic and volcaniclastic rocks

The layered volcanic and volcaniclastic rocks of C2 are typically found in the upper portions of the footwall. The dominant visual feature of these rocks is their highly foliated and/or layered texture. Various alteration styles are differentiated based on the dominant mineralogy (Table 21; West and Proffett column). With increasing proximity to the mine contact, the typical progression is chloritic phyllite, sericitic phyllite, siliceous phyllite and siliceous rock. The one layered lithology that is not related to alteration is the graphitic phyllite which is found throughout the footwall and is interpreted as the background sedimentation (Duke et al., in press; this study). There is

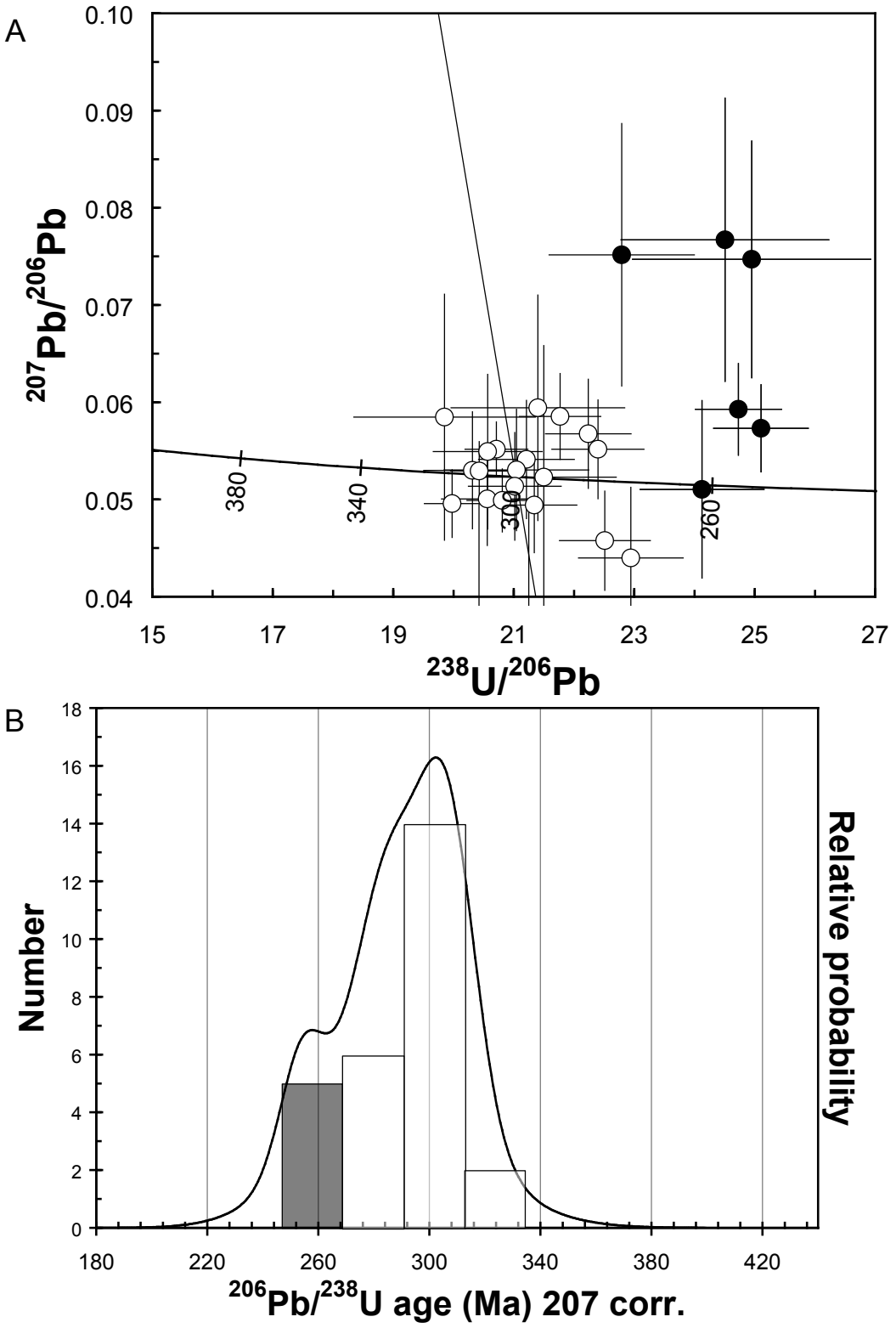

Figure 77 Reverse concordia and probability density plots of analyses from PSA07-030. (A)Reverse concordia diagram and (B) probability density plot of 27 analyses from 22 Permian zircon grains (the two inherited Silurian zircon grains are not included). The black (younger) and white (older) symbols indicate the two populations that are separable. Data-point error crosses are 1σ.

very little direct textural evidence to aid in the interpretation of the origin of the layered volcanic and volcaniclastic footwall unit. The contact relationships with other units are highly ambiguous due to intense deformation and/or alteration. These rocks are very fine-grained and no unambiguous volcanic textures have been documented in them. The immobile-element geochemistry is highly variable, indicating that they are not a coherent volcanic facies. For the purpose of interpreting the zircon geochronology, these rocks are interpreted as clastic.

Diamond drill hole PS276 is located above the northern end of the East Ore zone 2000 feet (600 m) southeast of the mine portal (Figure 71). A fine-grained, thinly layered (5–20 mm) chloritic phyllite was sampled at a depth of 585 feet (177.3 m) (Figure 78). The chloritic phyllite unit has a 15 foot (5 m) drill intersection and is bounded by medium grey to black, thinly laminated graphitic phyllites for approximately 50 feet (15 m) on either side. The mine contact is located 225 feet (68 m) further down hole with no major structural breaks recognized in this interval.

Seventeen zircon grains were analyzed in sample PS276-585. Seven analyses were rejected. Two of the remaining ten grains (CL1 & CL3) have a core and a rim identifiable on the CL images (Figure 79) as well as in the analyses. The two rims have a weighted mean of the $^{206}Pb/^{238}U$ 207 corrected ages of 254 ± 13 Ma. In the remaining ten grains, four have common Pb contamination and are rejected from final age estimates. The best ten analyses, including the two cores mentioned above, have a weighted mean of the ^{207}Pb corrected $^{206}Pb/^{238}U$ age of 331 ± 8 Ma (Figure 80). This Early Carboniferous age is interpreted as the maximum depositional age of the sample. The rims on zircons CL1 and CL3 may be coincidental products of Pb loss but the preferred interpretation is that they are thin metamorphic rims with a latest Permian age. The preferred interpretation here is that the depositional age of this sample is Early Carboniferous.

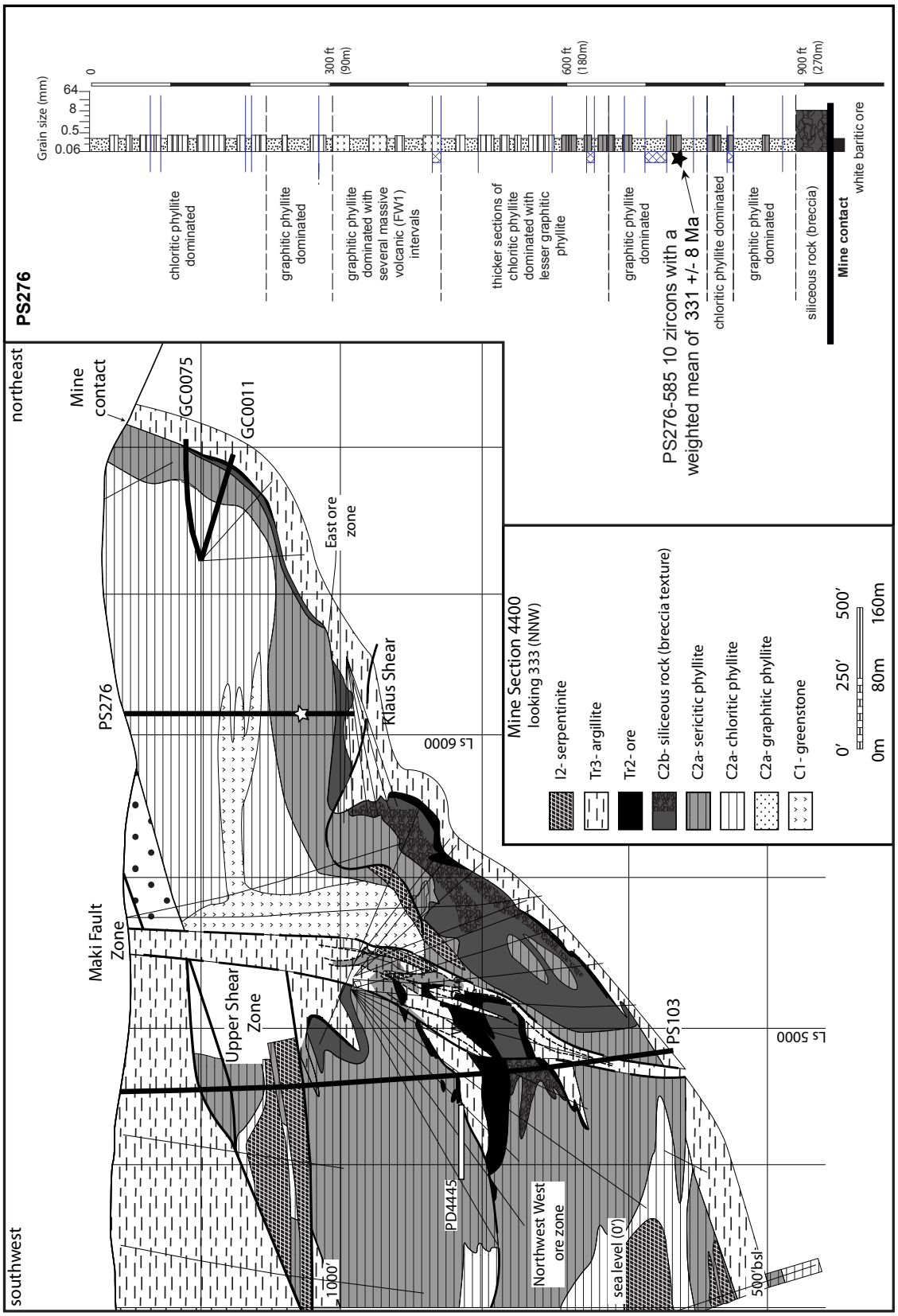

Figure 78 Southwest–northeast cross-section 4400 showing the geological context of diamond drill hole PS276, inset on the right side of the page is the graphic log of PS276. Legend in the cross-section applies to the graphic log as well; cross hatch pattern on the log indicates an interval of highly broken core and solid line indicates a fault or gouge zone.

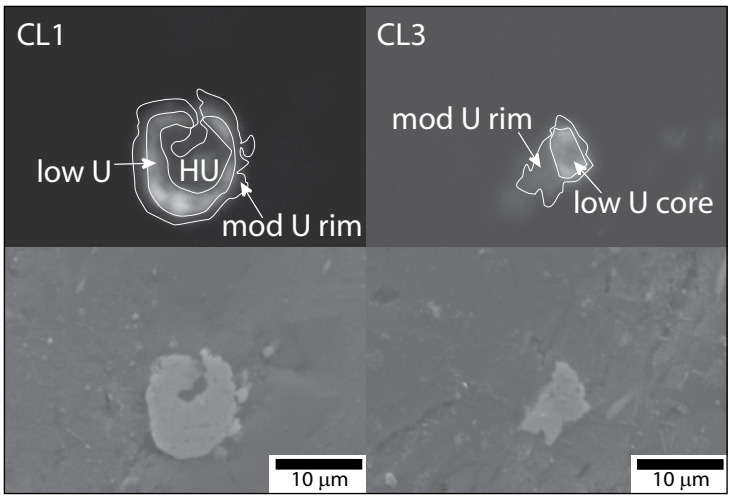

Figure 79 CL (top) and SE (bottom) images of zircon grain CL1 and CL3 from sample PS276-585. The low U zones have ^{207}Pb corrected $^{206}Pb/^{238}U$ ages respectively of 322 ± 11 Ma and 332 ±17 Ma; the moderate U zones have ^{207}Pb corrected $^{206}Pb/^{238}U$ ages respectively of 248 ± 10 Ma and 260 ± 9 Ma. HU = high U content zone. See Figure 80 for the reverse concordia plot of these ages.

Sample PS077-212 is from diamond drill hole PS077 at a depth of 212 feet (64.2 m). Drill hole PS077 is located approximately 1000 feet (300 m) northwest of the mine portal, directly behind the mill (Figure 71). Sample PS077-212 is from a 3-foot (1 m) thick, medium to dark grey, massive sericitic rock within a 340-foot (100 m) interval dominated by chloritic phyllite. The mine contact is located 200 feet (60 m) further down-hole with no major structural breaks recognized in this interval. Twelve zircon grains from PS077-212 were analyzed, seven analyses were rejected. The weighted mean of the ^{207}Pb corrected $^{206}Pb/^{238}U$ ages of the remaining five grains is 342 ± 7 Ma (Figure 81). This Early Carboniferous age is interpreted as the maximum age of deposition of PS077-212.

Diamond drill hole PS105 is collared 2000 feet (600 m) south of the mine portal, above the Upper Shear Zone (USZ) (Figure 71). The hole intersects the USZ from 354 feet (107.3 m) to 510 feet (154.5 m) and the sample was taken from below the USZ, on the same fault block as the deposit. Sample PS105-1236 is from a 30 feet (10 m)-thick interval of light grey, massive, siliceous, very fine-grained rock interpreted as an extremely silica altered member of the layered volcaniclastic lithology (C2). It is located approximately 215 feet (65 m) drilled thickness above the downward-facing

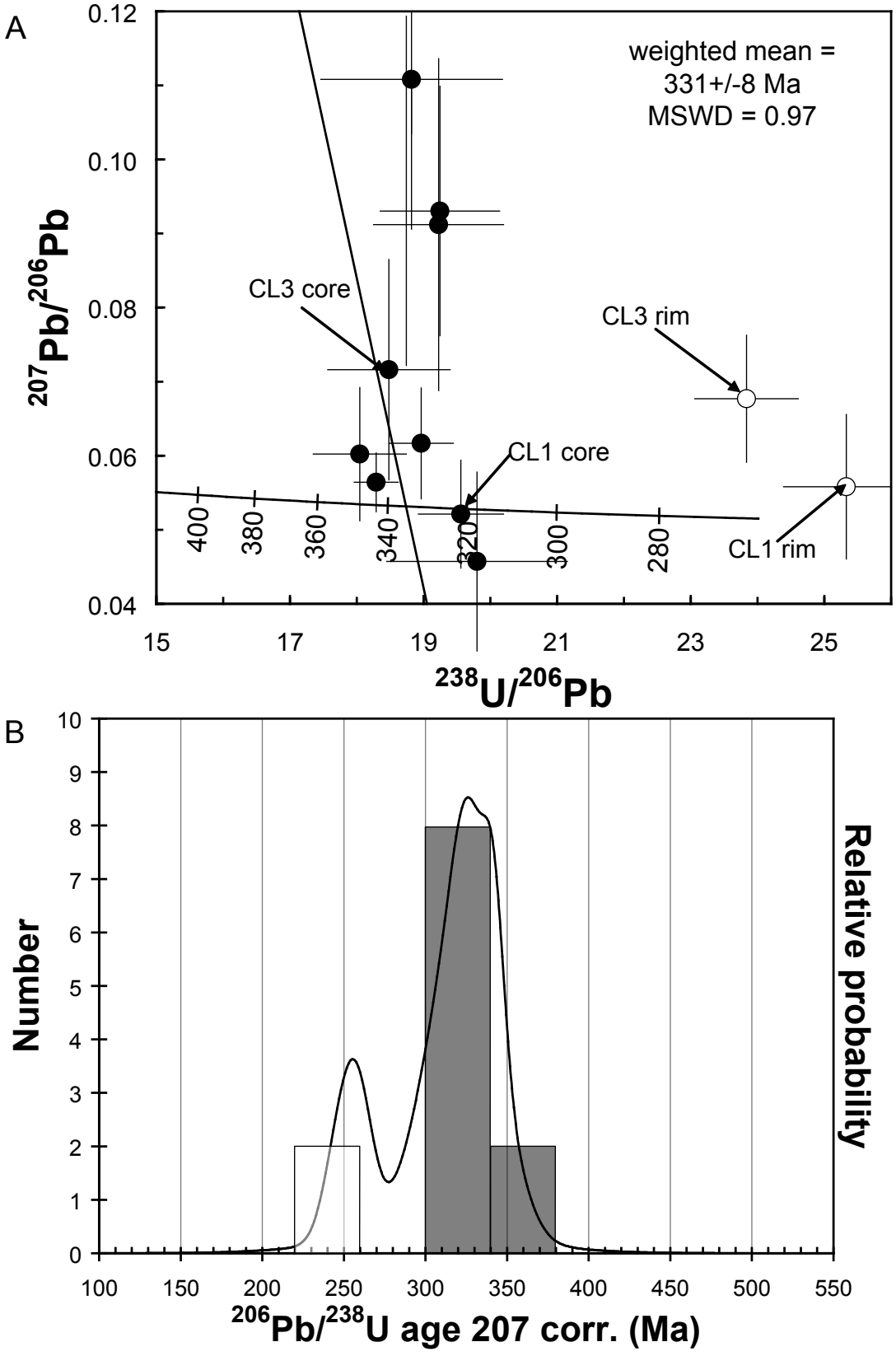

Figure 80 Reverse concordia and probability density plots of analyses from PS276-585. (A) Reverse concordia plot and (B) probability density plot of analyses from ten zircon grains in sample PS276-585. Black symbols represent analyses used in final weighted mean and white symbols represent analyses rejected from the final age calculations. The weighted average $^{206}Pb/^{238}U$ 207 corrected ages of the ten best analyses is 331 ± 8 Ma. This age is interpreted as the maximum depositional age of the layered volcanic unit (C2). Data-point error crosses are 1σ.

mine contact (Figure 82). No major structural breaks have been recognized between the sample and the mine contact.

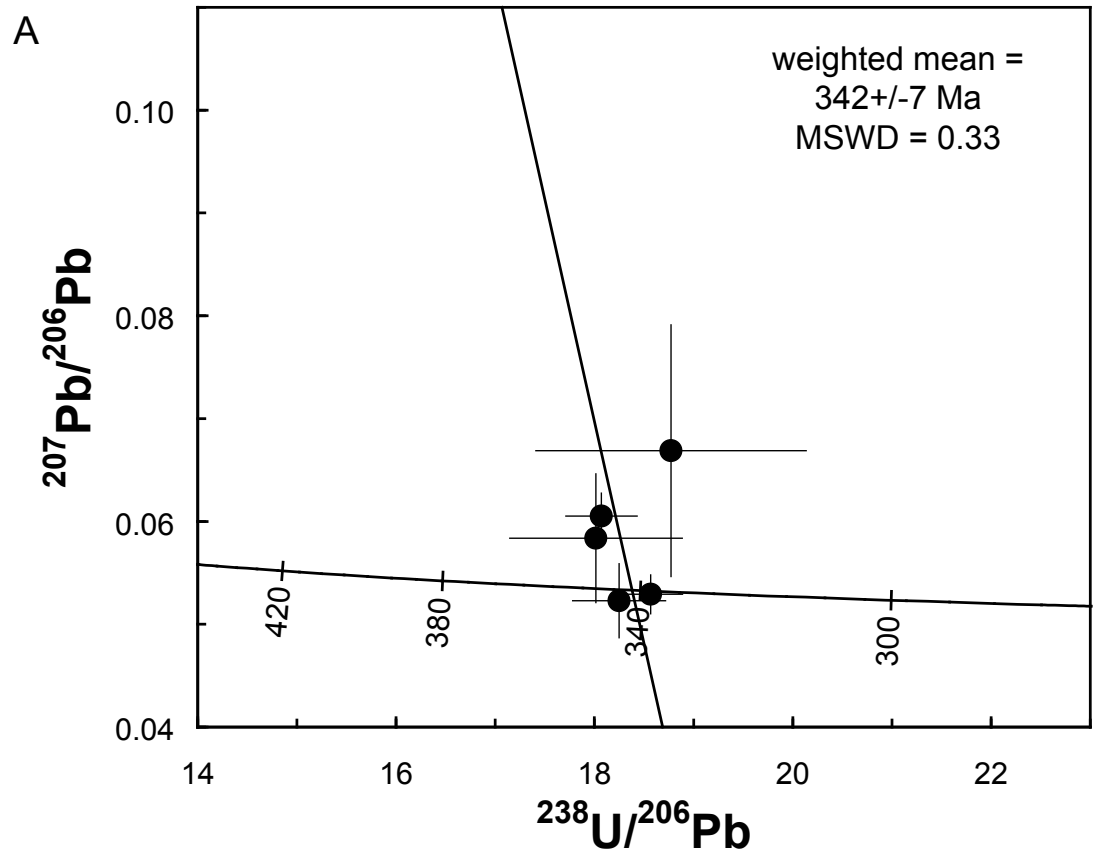

Figure 81 Reverse concordia plot analyses from five zircon grains in sample PS077-212, not shown are seven analyses rejected outright. The weighted average $^{206}Pb/^{238}U$ 207 corrected ages of the five best analyses is 342 ± 7 Ma. Data-point error crosses are 1σ.

Twelve analyses of 11 zircon grains were carried out on sample PS105-1236. Nine analyses were rejected. Grain CL1 has a bright, low U core with a dark, moderate U rim (Figure 83). The core has a ^{207}Pb corrected $^{206}Pb/^{238}U$ age of 1124 ± 47 Ma (two analyses), the CL1 rim and CL7 grain have a weighted mean age of 323 ± 21 Ma. Zircon CL1 may be evidence for inheritance of Proterozoic zircons. The Early Carboniferous CL7 grain and the thin overgrowth on zircon CL1 are similar in age to other zircon grains from this unit. Unfortunately, this sample only had two zircon grains with low U and the result is not conclusive.

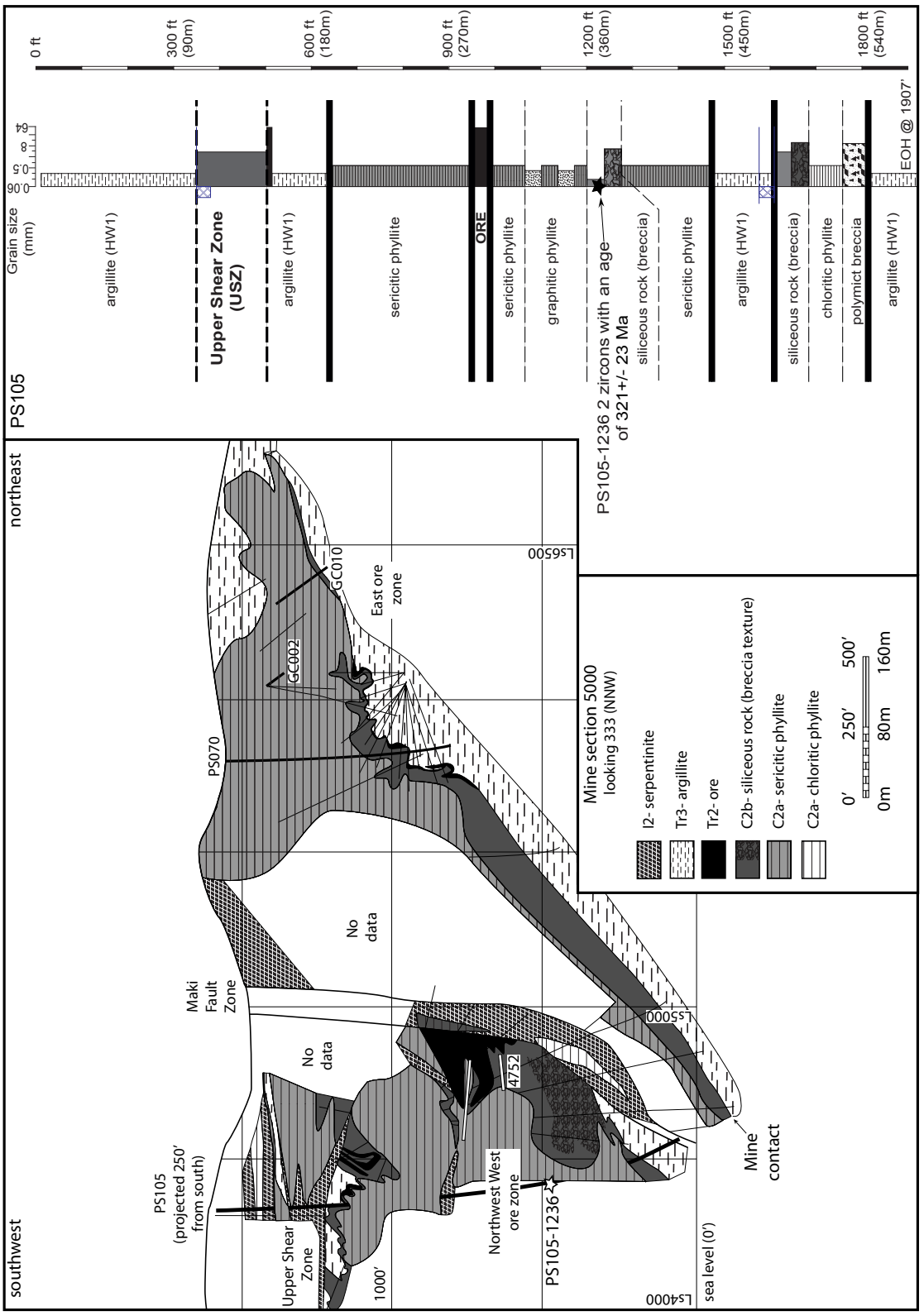

Figure 82 Southwest –northeast cross-section 5000 through the northern end of the Greens Creek deposit showing the geologic context of PS105; inset on the right side of the page is the graphic log of PS105. PS105 intersects the Upper Shear Zone (USZ) from depths of 354 feet (107.3 m) to 510 feet (154.5 m). The sample at depth 1236 feet (374.5 m) is below the USZ. The Northwest West ore body shows two recumbent isoclinal F2 folds and an open F3 fold. Legend for graphic log as in the cross-section. Cross hatch pattern on the log indicates an interval of highly broken core and solid line indicates a fault or gouge zone.

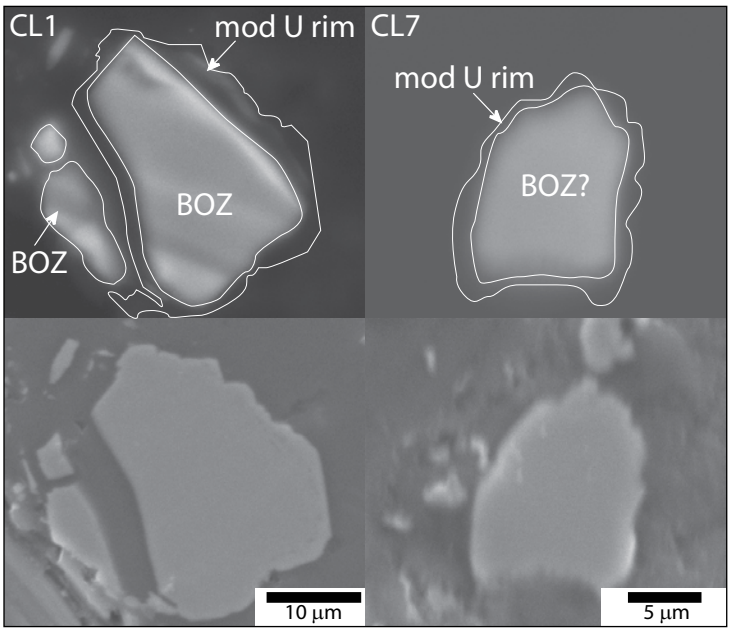

Figure 83 CL (top) and SE (bottom) images of zircon grains CL1 and CL7 from PS105-1236. Two analyses from the bright, low U core of this grain have a Proterozoic age; one analysis of grain CL1 intersected the dark, moderate U rim which has a Carboniferous age. BOZ = banded oscillatory zoning.

The final zircon-bearing sample of the layered footwall volcanic and volcaniclastic unit (C2) is sample PSU07-052 from the 2853 ramp accessing the Northwest West ore body. The sample is located approximately 50 feet (15 m) west of the collar to the 579 ore access (Figure 84). PSU07-052 is a sample of sericitic phyllite from C2 (Table 21). This sample is from within a foot (30 cm) of a distinct sericitic phyllite – graphitic phyllite contact (inset photograph in Figure 84).

Sixteen zircon grains were analyzed from PSU07-052. Analyses of eight grains were rejected. Two populations of zircon grains in PSU07-052 are identified: a Triassic population with six grains and a Carboniferous population with four grains (Figure 85). Two grains have Carboniferous cores and Triassic rims identifiable in single analyses. The four Carboniferous zircon grains have a weighted mean ^{207}Pb corrected ^{206}Pb/^{238}U age of 320 ± 20 Ma which is the maximum age of deposition of the rock. The six Triassic zircon grains have low U content (<2500 ppm) and may be hydrothermal in origin based on their lower Th/U ratios and irregular morphology. These six grains have

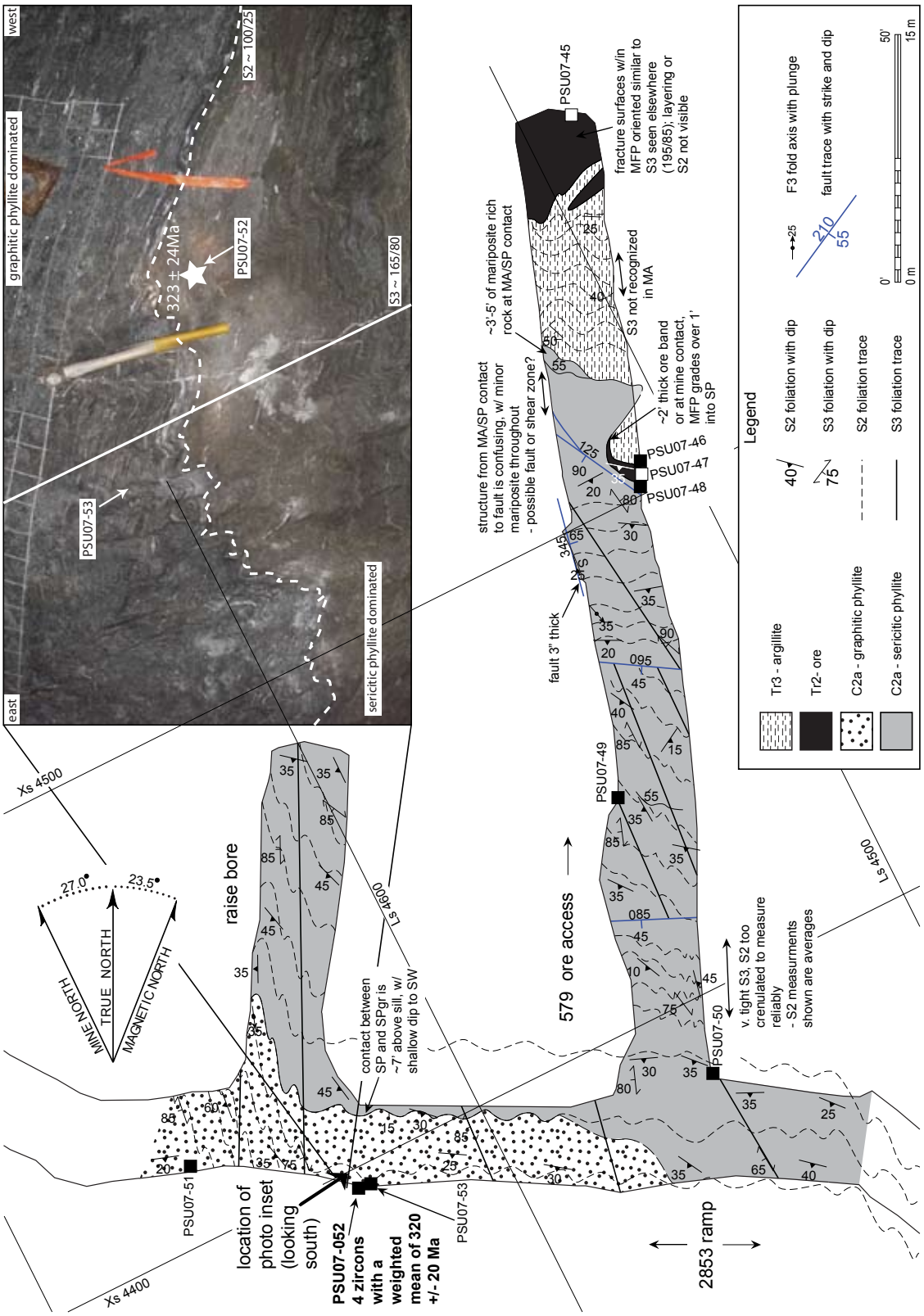

Figure 84 Underground mapping of 579 ore access in the Northwest West ore zone. Mapping is chest height plan projection. Inset photograph is of the sample location on the south rib of the 2853 ramp.

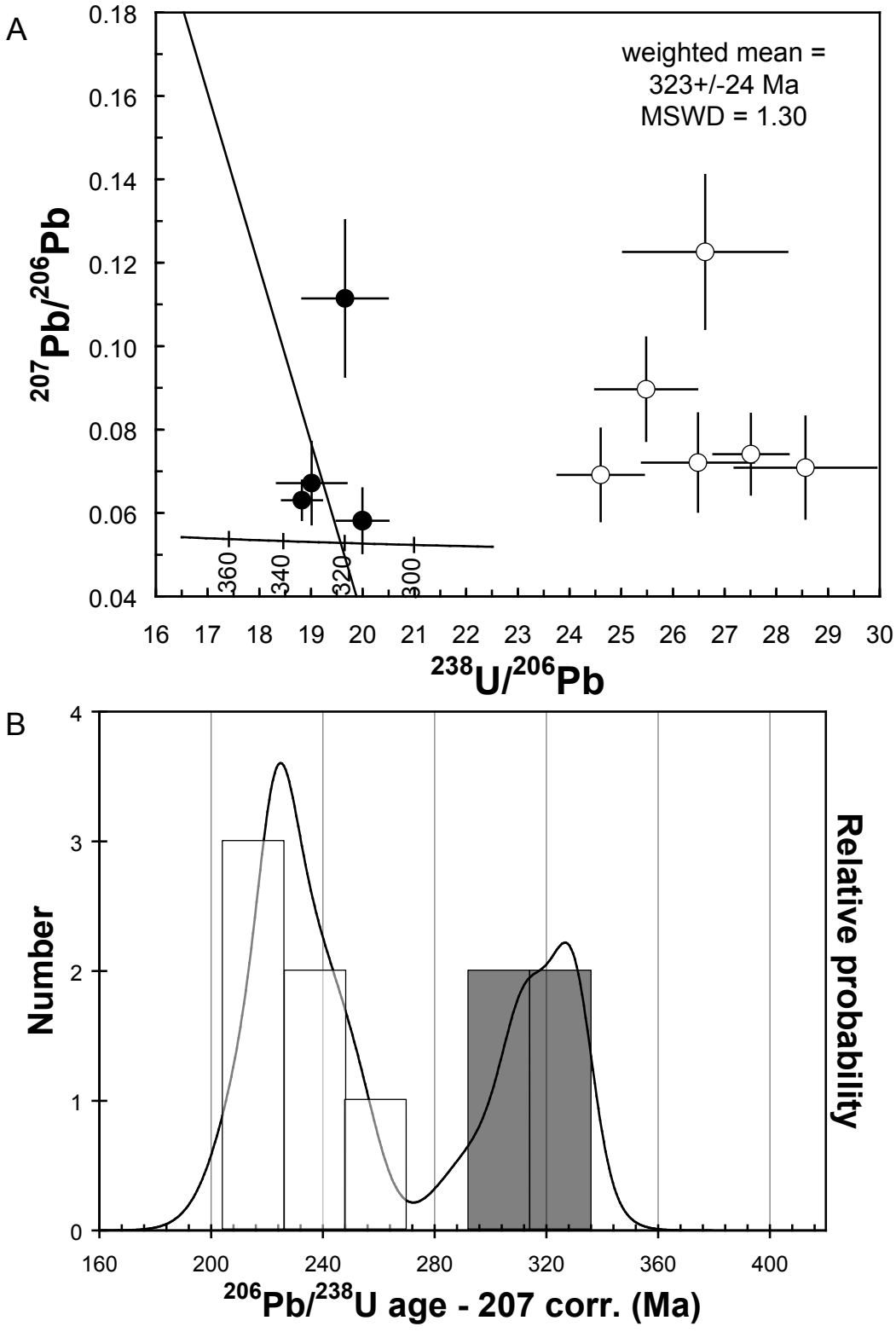

Figure 85 Reverse concordia and probability density plots of analyses from PSU07-052. (A) Reverse concordia plot and (B) probability density plot of analyses from ten zircon grains in sample PSU07-052. Black symbols represent analyses used in final weighted mean and white represents analyses considered to be hydrothermal in origin. Data-point error crosses are 1σ.

a weighted mean ^{207}Pb corrected age of 230 ± 13 Ma and may indicate the age of the mineralizing event.

I3 – mafic intrusive rocks

The fine to medium-grained mafic intrusive rocks (I3) are typically found within the hanging wall assemblage and there are only a few unambiguous locations where I3 microgabbros are in contact with footwall rocks (units C1 and C2). Within the hanging wall, the microgabbro typically has elongate map patterns and can have chilled margins against argillite (unit Tr3). Where the microgabbro is mapped within footwall lithologies chilled margins have not been observed. The two samples analyzed in this study are from the Upper Gallagher area approximately 1800 feet (550 m) apart in the same microgabbro dike. Taylor et al. (in press) have U/Pb and Sm/Nd whole-rock and mineral isochrons from this rock type with a preferred age of 219 Ma. An unpublished zircon age of 227 Ma and a hornblende age of 236 Ma are also available (S. Karl pers. comm.).

Sample PS271-207 is from a medium-grained microgabbro located in diamond drill hole PS271 in Upper Gallagher bowl (Figure 71). This sample is located at a depth of 207 feet (62.7 m) (Figure 86). The Upper Shear Zone is found further down this hole between depths 2140 feet (650 m) and 2660 feet (800 m); therefore the sample is from the fault block above the Greens Creek Mine.

Thirteen zircon grains were analyzed from PS271-207. Five analyses were rejected. Two analyses with U contents of 2300 and 2500 were accepted as their ^{207}Pb corrected ^{206}Pb/^{238}U ages are within one standard deviation of the mean of six analyses with U content <2000 ppm. The weighted mean of the ^{207}Pb corrected ^{206}Pb/^{238}U ages from the eight best analyses is 223 ± 9 Ma with a MSWD of 0.62. This age is statistically identical to both the whole-rock isochron ages of Taylor et al. (in press) and S. Karl (pers. comm.). The eight Late Triassic zircon grains in this sample are less than 15 μm, have Th/U ratios of approximately 1 and simple CL images with weak zoning (Figure 87); they are interpreted as igneous in origin.

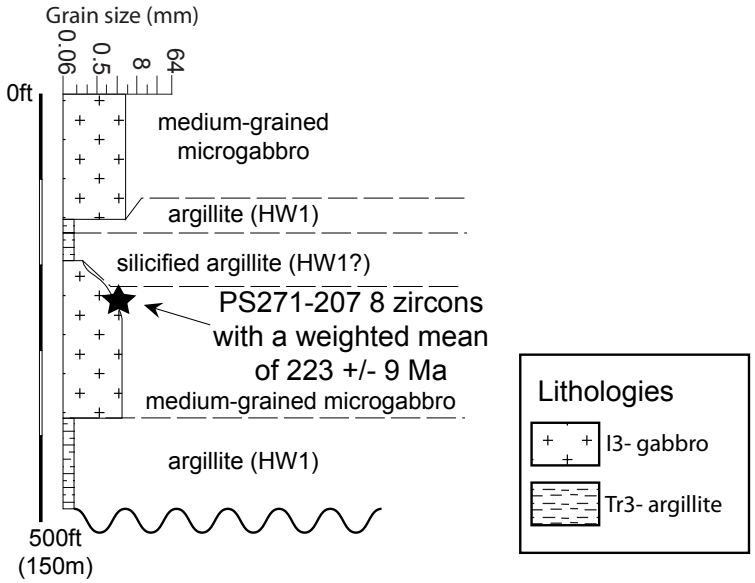

Figure 86 Graphic log of PS271. The microgabbro bodies have chilled margins indicating they were intruded into the argillite.

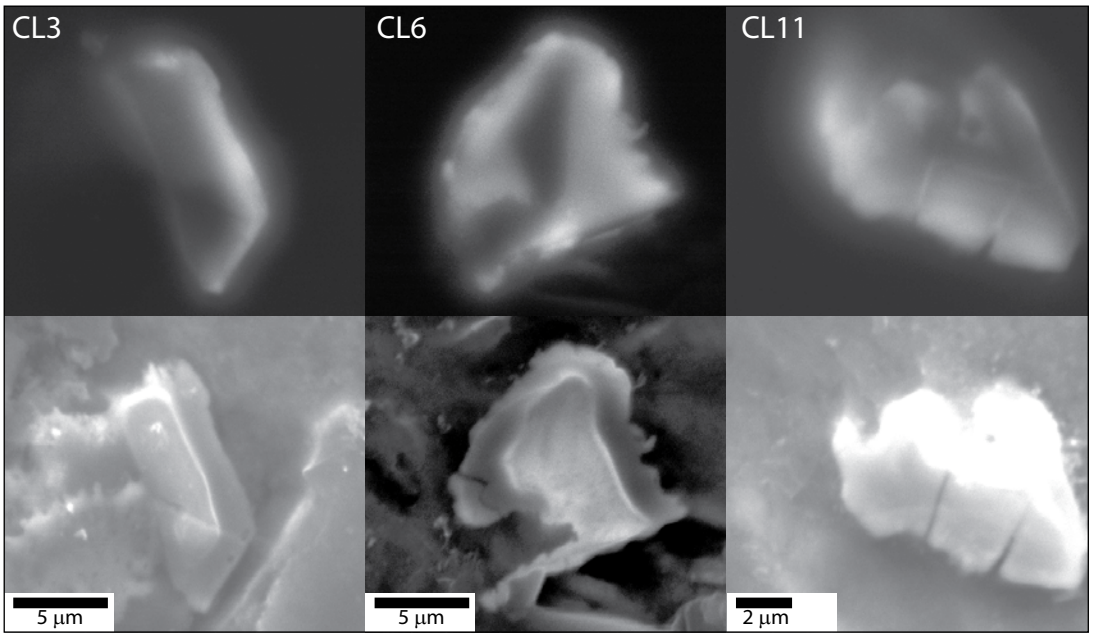

Figure 87 Photograph of the fine to medium-grained PS271-207 sample and CL (top) and SE (bottom) images of zircon grains CL3, CL6 and CL11. These grains are representative of the eight Late Triassic zircons in sample PS271-207. Note the simple zoning patterns in the CL images grains CL3 and CL6; CL11 has blurred oscillatory banding.

Sample PSA08-001 is a medium to coarse-grained microgabbro. The sample was taken from the microgabbro body approximately 250 feet (75 m) east of the small lake in the saddle on the northwest end of Gallagher Ridge (Figure 71). This sample is also in the fault block above the USZ. Twenty-five zircon grains were analyzed from PSA08-001.

Twenty-two analyses were rejected. The three best analyses have a weighted mean ^{207}Pb corrected $^{206}Pb/^{238}U$ age of 222 ± 8 Ma with a MSWD of 0.57. No CL images were collected for this sample, but the Th/U ratios are consistent and the best estimate for the age of this sample agrees, to within error, with the estimate from sample PS271-207. Combining the best data from both PS271-207 and PSA08-001, the best estimate for the age of intrusion for this microgabbro is 223 ± 6 Ma (Figure 88).

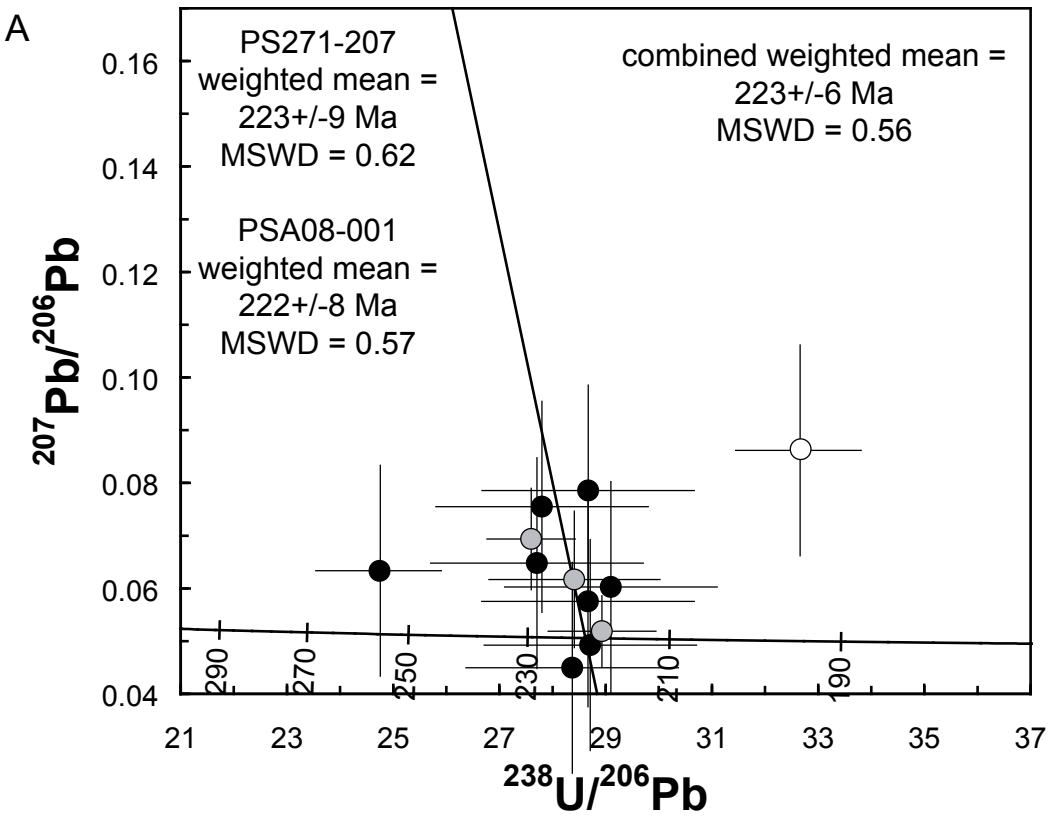

Figure 88 Reverse concordia plot of analyses from 11 zircon grains in samples PS271-207 and PSA08-001. Black symbols represent analyses from PS271-207 used in final weighted mean and grey represents analyses from PSA08-001. White circles are rejected analyses, most of which plot off the right side of the diagram. Data-point error crosses are 1σ.

Tr4 – coherent volcanic rocks

The basalt in the Hyd Formation is the youngest unit in the Late Triassic stratigraphy in the Greens Creek area (Taylor et al., 2008). Several small rhyolite bodies have recently been mapped along Gallagher Ridge (Proffett, 2005, 2007) and are interpreted to be coherent volcanic rocks which are minor constituents of this sequence. Sample PSA05-004 is from the western-most of these bodies (Figure 71). Taylor et al. (in press) plotted

whole-rock U/Pb isochrons for basalt samples from Gallagher Ridge as well as regional samples from Gambier Bay on southern Admiralty Island; reported ages are 215 ± 6 Ma and 216 ± 16 Ma respectively. The associated minor rhyolite bodies were not recognized during Taylor's studies of the 1990s and, as a result, no direct age constraints are known but they are thought to be Late Triassic in age.

Sample PSA05-004 has been exhaustively studied as part of the method development portion of this thesis which is reported in detail in Chapter 4. PSA05-004 has abundant large and small zircon grains. These grains were prepared in three ways for three separate dating methods. The zircon grains have euhedral morphologies, oscillatory banded cores with some grains having resorption zones which offset further oscillatory zoning in rims, and Th/U ratios between 0.31 and 0.77. Both cores and rims were analyzed where possible and the ages were statistically identical. These zircon grains are interpreted as igneous in origin. The best estimate for the age of the zircon grains in PSA05-004 is from the ID-TIMS method which has a weighted mean ^{204}Pb corrected ^{206}Pb/^{238}U age of ages of 226.9 ± 0.2 Ma. This age is interpreted as the emplacement age for the rhyolite bodies and is older that the preferred age of the basalt in the Hyd Formation but is close to the age of the Gallagher Ridge microgabbro.

Post-Triassic

The post-Triassic lithologies investigated in the present study include the Seymour Canal Formation and a post-deformational mafic dike set. The Seymour Canal Formation is composed of slate, greywacke and conglomerate (Lathram et al., 1965). Fossils collected from Gambier Bay and Pybus Bay in the slate and greywacke members of this unit are characterized by the pelecypod *Buchia* which has an age range of Late Jurassic to Early Cretaceous (Loney, 1964).

Sample PSA05-010 was collected from the south side of the Young Bay bus parking lot (Figure 71). The sample is a soft, strongly cleaved sericitic phyllite from a greywacke in the Seymour Canal Formation. The 12 zircon grains analyzed from PSA05-010 form

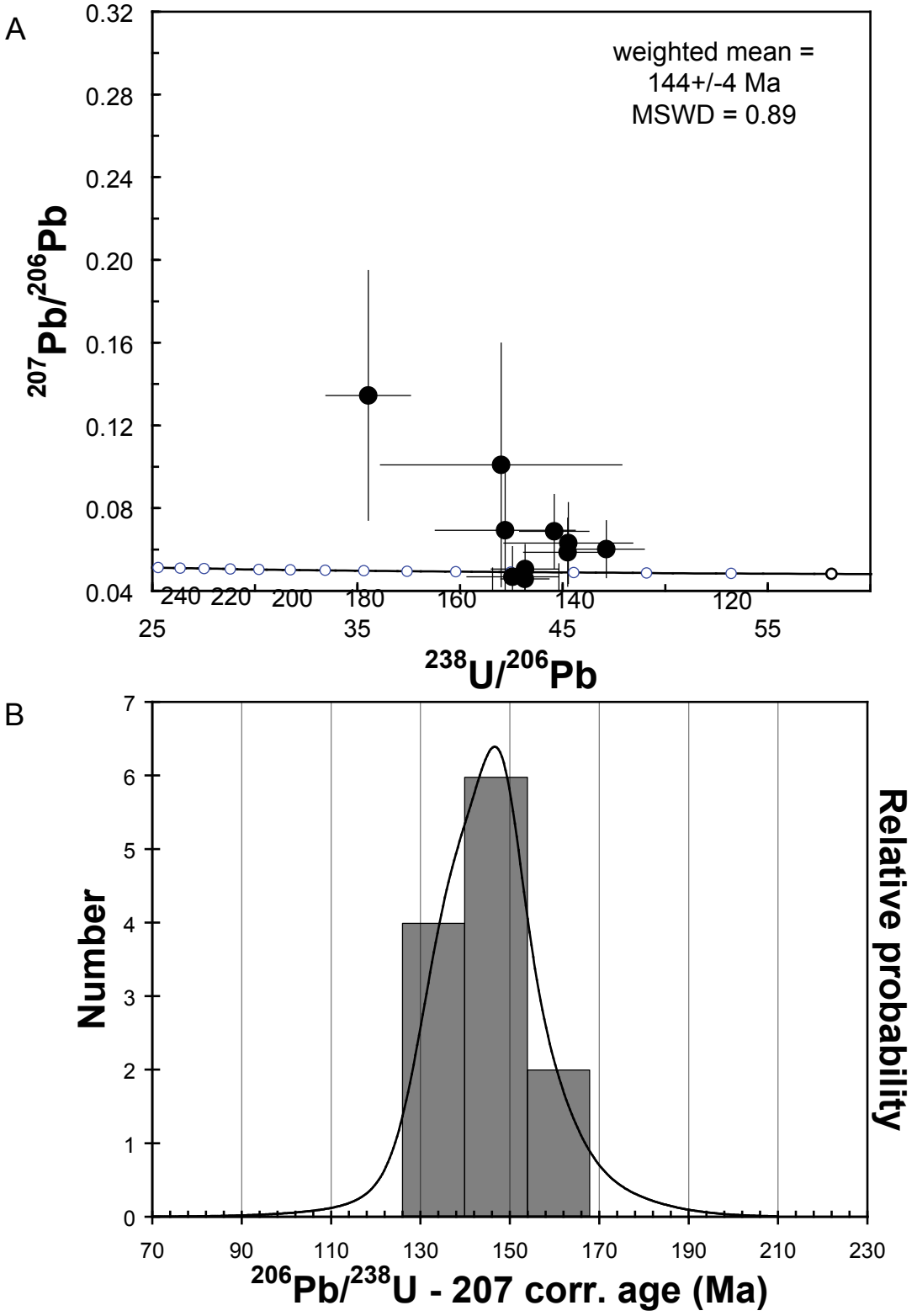

Figure 89 Reverse concordia and probability density plots of analyses from PSA05-010. (A) Reverse concordia plot and (B) probability density plot of all analyses from 12 zircon grains in samples PSA05-010. Data-point error crosses are 1σ.

one well-constrained population based on their ^{207}Pb corrected $^{206}Pb/^{238}U$ ages (Figure 89), Th/U ratios and CL images. These 12 grains have a weighted mean of the^{207}Pb corrected $^{206}Pb/^{238}U$ age of 144 ± 4 Ma, which is interpreted as the maximum age of deposition of this sample.

Sample PS181-738 is from a depth of 738 feet (223.6 m) in diamond drill hole PS181 which is collared approximately 600 feet (180 m) east of mile 2.4 (km 3.8) on the B-road (Figure 70). This drill hole is located north of the Zinc Creek Thrust and is not on the same fault block as the Greens Creek Mine. PS181-738 is a sedimentary sample with thinly laminated dark grey to black and light grey layers with two foliations visible that was originally thought to be graphitic quartz mica schist from the basement unit (S-D2). Twelve zircon grains were analyzed from PS181-738, six analyses were rejected. The remaining six zircon grains can be grouped into three populations based on their ^{207}Pb corrected $^{206}Pb/^{238}U$ ages (Figure 90). The weighted average of ^{207}Pb corrected $^{206}Pb/^{238}U$ age of the three Early Cretaceous analyses is 128 ± 7 Ma. This age is interpreted as the maximum depositional age of the rock and the rock is now interpreted to be a fault slice of the Seymour Canal Formation and not a sample of the basement unit.

The youngest known unit in the Greens Creek vicinity is set of diorite to diabase dikes found underground in the 4211 crosscut and on the surface on the east side of Gallagher bowl. These dikes cross-cut all foliations and are themselves offset by the Gallagher Fault (Proffett, 2004). Sample PSA08-002 was identified in the field as an unfoliated, massive diorite-microgabbro, but, due to poor exposure, the relationship between the sample and local foliation surfaces could not be determined. It is interpreted to be an intrusive rock that may cross-cut all foliations. PSA08-002 was collected from the 1350 Creek, 2000 feet (600 m) southeast of the mine portal (Figure 71) which is 4000 feet (1200 m) north of the known surface location of a post-Triassic dike. Therefore, PSA08-002 is thought to be from the late-stage mafic dikes, but is not from the type locality.

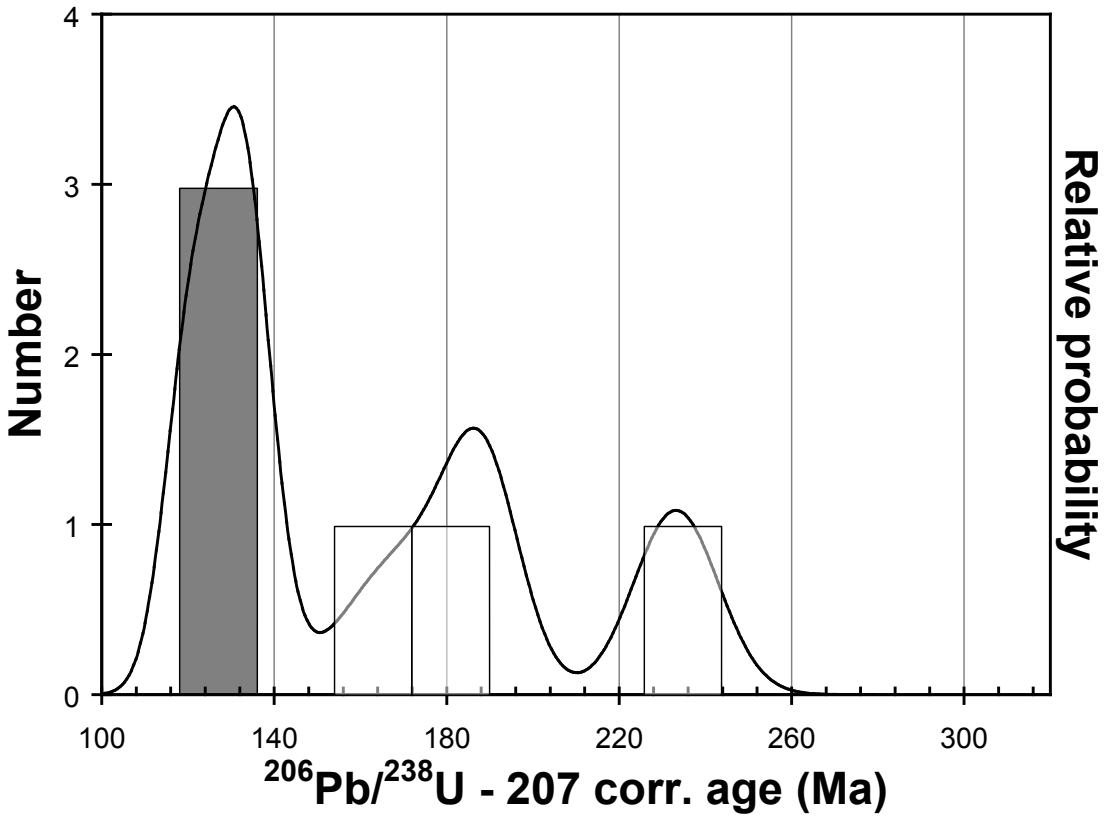

Figure 90 Probability density plot of six analyses from sample PS181-738. The weighted average of ^{207}Pb corrected ^{206}Pb/^{238}U 207 corrected ages of the three Early Cretaceous analyses is 128 ± 7 Ma.

Twenty-three zircon grains were analyzed in PSA08-002, but 13 were rejected (Figure 91). Of the ten analyses that were acceptable, one had a ^{207}Pb corrected ^{206}Pb/^{238}U Carboniferous age of 323 ± 63 Ma. This age is statistically identical to ages for both the layered and massive footwall units (C1 and C2) and is interpreted as an inherited grain. The weighted average of the ^{207}Pb corrected ^{206}Pb/^{238}U ages of the remaining nine analyses is 85 ± 4 Ma, which is the best estimate for the emplacement ages of the post-Triassic diabase dikes.

Discussion

Fifteen samples from seven lithologies were successfully dated during the present study (Table 23). For units with more than one successful geochronology sample (S-D2, C1, C2, I3 and J1) the preferred ages are consistent. The interpretations concerning the geological significance of the detrital and igneous zircon grains in the present study are straightforward; however, interpretations of the metamorphic zircons are less so. Also,

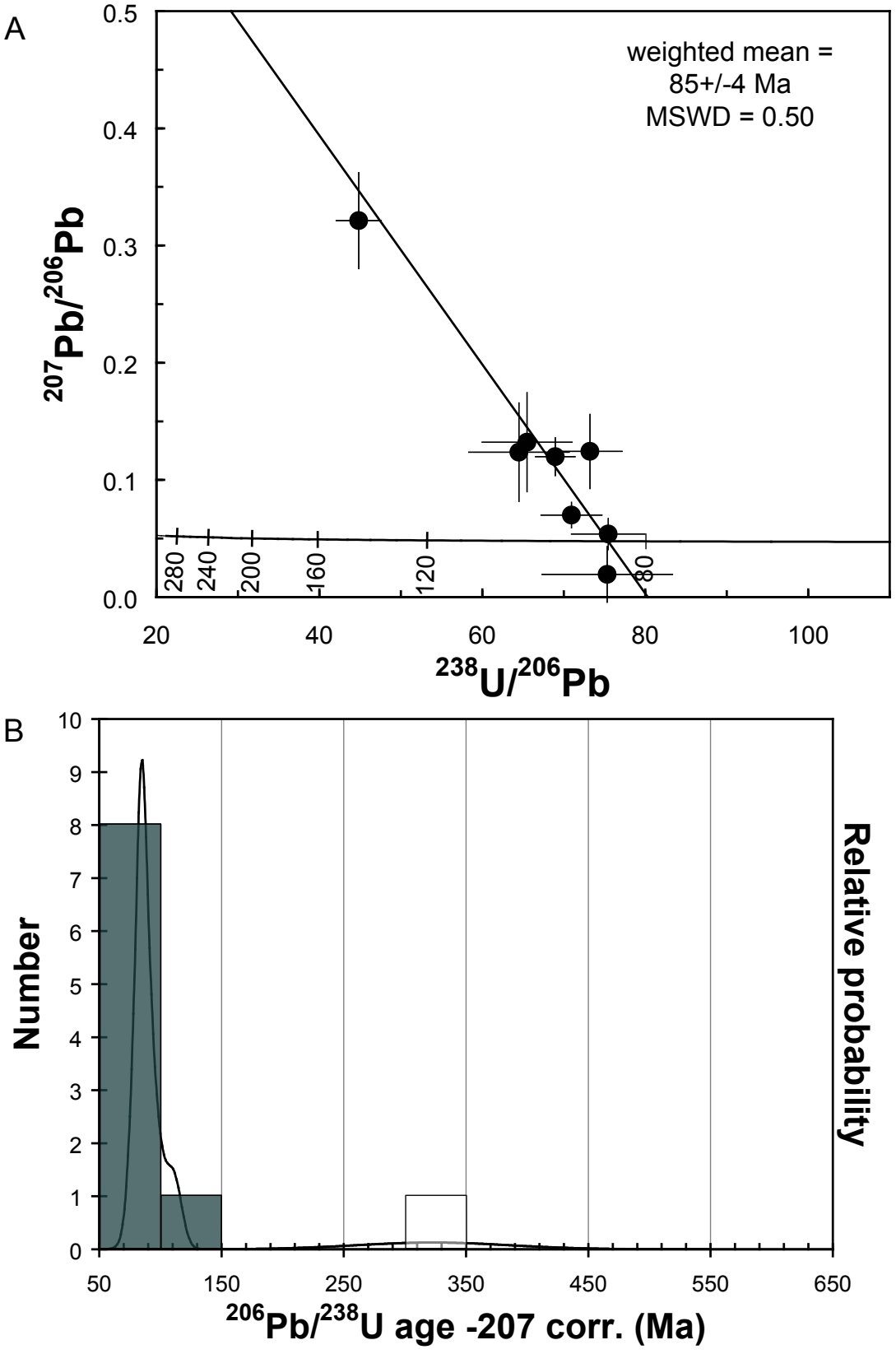

Figure 91 Reverse concordia and probability density plots of analyses from PSA08-002. (A) Reverse concordia plot and (B) probability density plot of analyses from 10 zircon grains in samples PSA08-002. The weighted average of the $^{206}Pb/^{238}U$ 207 corrected ages of the 9 best analyses (black) is 85 ± 4 Ma. One xenocrystic zircon grain (white) is shown in B. Data-point error crosses are 1σ.

there is currently debate within the literature on the radiometric age of the Carnian-Norian boundary which impacts on the interpretation of the Late Triassic ages. For these reasons, the discussion will focus on the interpretation of the metamorphic zircon grains and the radiometric age of the Carnian-Norian boundary.

Table 23 Summary of geochronological results for samples analyzed in the present study. Results are organized by stratigraphic unit defined in Table 21; coordinates of samples are in Table 22. [a] Number of spots analyzed; [b] Number of analyses rejected for reasons stated in main text and described in detail in Chapter 4; [c] interpreted origin of the zircon grains used in the estimation of the age; [d] Number of analyses used in the estimation of the age of the sample; [e] Mean weighted average and errors calculated using the ^{207}Pb corrected $^{206}Pb/^{238}U$ data of the best analyses.

Stratigraphic Unit	Sample	No. of analyses[a]	No. of outright rejected analyses[b]	Zircon origin[c]	No. analyses used to calculate age[d]	Sample age (Ma)[e]	2σ (+/-)	MSWD
S-D2	PSA05-005&008	29	24	metamorphic?	4	264	23	2.90
S-D2/C1?	PSA07-030	30	0	metamorphic	27	250-300	N/A	N/A
C1	PSA07-015	24	4	igneous	12	340	5	1.07
C1	PSA08-003	24	9	igneous	7	337	5	0.98
C2	PS276-585	17	7	detrital?	10	331	8	0.97
C2	PS077-212	12	7	detrital?	5	342	7	0.33
C2	PS105-1236	12	11	detrital?	2	323	21	0.26
C2	PSU07-052	16	8	detrital?	3	323	24	1.30
I3	PS271-207	13	5	igneous	8	223	9	0.62
I3	PSA08-001	25	22	igneous	3	220	9	0.15
Tr4	PSA05-004*	24	0	igneous	22	225	1	0.85
J1	PSA05-010	12	0	detrital	12	144	4	0.89
J1?	PS181-738	12	6	detrital	3	128	18	1.30
I4	PSA08-002	23	8	igneous	9	85	4	0.50

Basement lithologies

Metamorphic zircon grains generally have Th/U ratios ≤0.1 (Rubatto and Gebauer, 2000), have rounded anhedral morphologies (Schaltegger et al., 1999) and, depending on the proposed mechanisms for zircon growth, show patterns in CL images varying from sector zonation to oscillatory banding to highly irregular, convolute banding (i.e. Hoskin and Black, 2000 and references therein). The 22 Permian zircon grains in PSA07-030 have Th/U ratios <0.1, are all sub-round to round, show weak sector zonation with a few examples of weak oscillatory banding (see Figure 76) and are, therefore, interpreted as metamorphic zircon grains.

There are two basic methods for interpreting the metamorphic age of zircon grains. The primary difference between the methods is the estimation of the degree to which the radiogenic isotopic systems have been reset by metamorphism. Populations that are normally distributed as one population are generally interpreted to be completely reset and the best estimate for the age of the zircon forming event is the weighted mean of the entire population (i.e. Schaltegger et al., 1999; Geisler et al., 2002). However, when probability density plots of ^{207}Pb corrected $^{206}Pb/^{238}U$ ages show a skewed distribution, Hoskin and Black (2000) used age probability plots to separate populations of grains. The youngest statistically coherent group of analyses is interpreted as having the best chance of having been completely reset and can then be used to calculate the age of zircon re-crystallization with the weighted mean of this population giving the best estimate of age.

The degree of isotopic resetting in the zircon grains of PSA07-030 is unclear. The slightly skewed distribution of ages and moderate to high MSWD indicates partial resetting (Figure 77). However, the consistent Th/U ratios and lack of correlation between age and Th/U content (Figure 92) suggests the grains have been completely reset. The age probability plot in Figure 93 shows two potentially separable populations within the 27 analyses from PSA07-030. The younger statistically coherent population of zircon grains, illustrated by the break in slope of ages on the probability plot, has a weighted mean age of 255 ± 9 Ma with a MSWD of 0.15. If one assumes that the isotopic systems have been completely reset the weighted mean of all 27 analyses is 292 ± 7 Ma with an MSWD of 3.0. Regardless of the degree of resetting, these zircon grains appear to record a metamorphic event between approximately 250 Ma and 300 Ma. This age range correlates with the Permian metamorphic ages reported by Karl et al. (1998) which are from $^{40}Ar/^{39}Ar$ analyses of biotite and muscovite in greenschist facies rocks of the Pile Driver greenstone (S. Karl pers. comm.). It also correlates with the Permian metamorphic ages recorded here in the amphibolite-grade basement or possibly footwall rocks (Table 23).

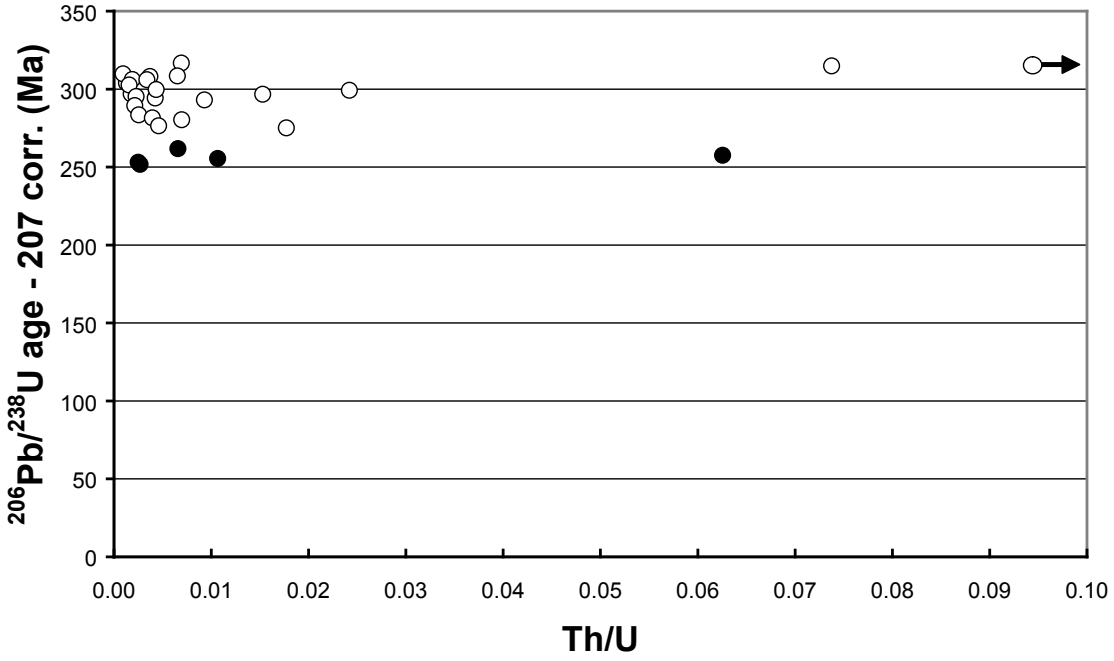

Figure 92 Age vs. Th/U for 30 analyses of zircon grains from sample PSA07-030. Note the lack of correlation between ^{207}Pb corrected $^{206}Pb/^{238}U$ ages and Th/U indicating complete resetting of the isotopic system. Black symbols represent the younger statistically coherent population and white the older.

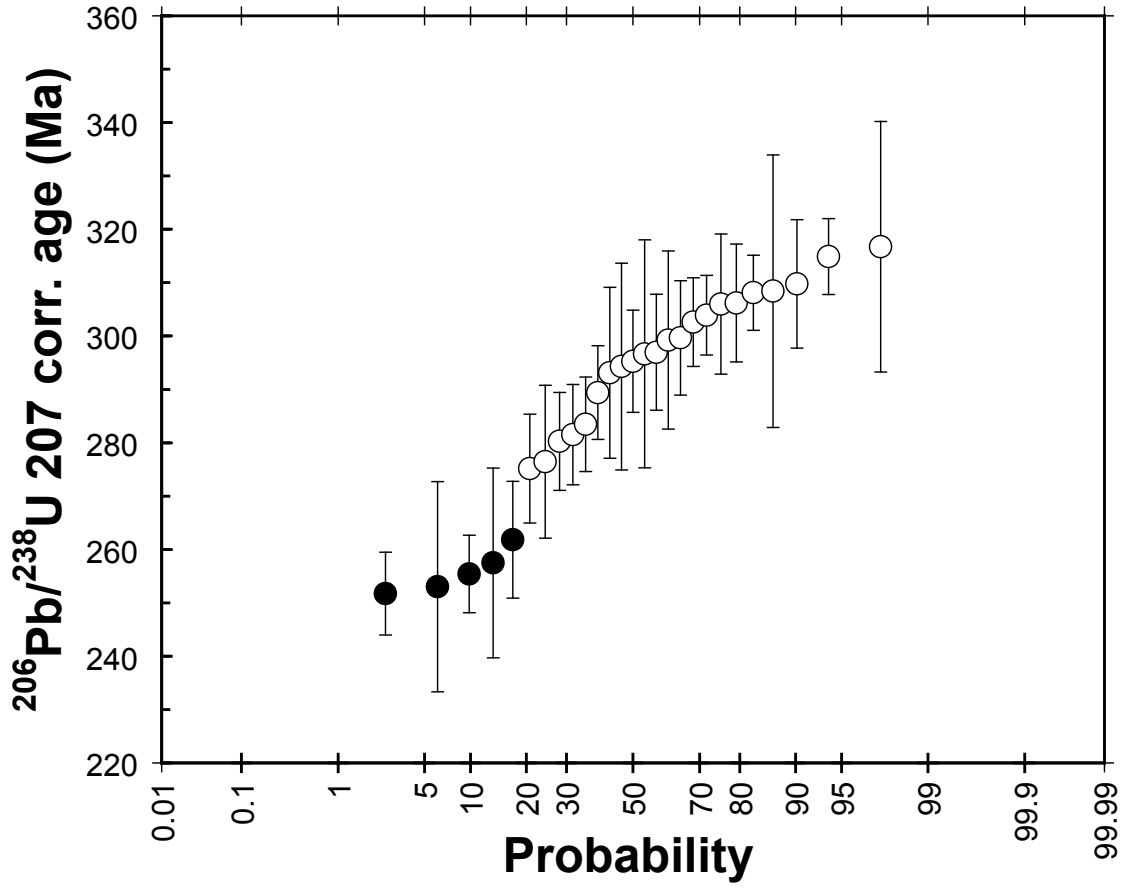

Figure 93 Age probability plot of 27 analyses from PSA07-030. Black symbols represent the younger statistically coherent population and white the older population.

One inherited population and one possible metamorphic population are identifiable from the analyses of the 29 zircon grains in PSA05-005 and PSA05-008. The precursor to these basement samples is sedimentary. Therefore, the Paleozoic to Proterozoic zircon grains are interpreted as inherited detrital grains. There are two interpretations of the three best Permian, moderate U zircon grains which have a preferred age of 265 Ma. These may be detrital zircon grains, indicating that these rocks are Permian or younger or the grains may be metamorphic in origin indicating the rocks were metamorphosed in the Permian. The Th/U ratios of these analyses is between 0.10 and 0.50, with the exception of one grain with a Th/U ratio of 1.5, and do not clearly indicate a magmatic or metamorphic origin (Rubatto and Gebauer, 2000). The grains are typically anhedral to subhedral with CL images that have weak sector zoning in a dark indistinct core surrounded by a very thin, brighter rim. The preferred interpretation here is that these zircon grains are metamorphic and were formed during a Permian metamorphic event.

The footwall lithologies (C1 and C2) are Carboniferous and the metamorphism of footwall and basement (C1, C2, S-D1 and S-D2) must be post-Carboniferous. There is no local evidence for an unconformity between these 'basement' lithologies and the footwall lithologies (C1 and C2). The most likely interpretation is that the 'basement' lithologies are other footwall lithologies of higher metamorphic grade. The best age estimate for the deposition of the basement schists is still from Oliver and Berg (1981) who suggested a probable age of deposition of Wenlockian to Givetian (428 to 385 Ma; Gradstein et al., 2004). Whether any rocks of this age are exposed in the Greens Creek area is not known.

Early Carboniferous lithologies (C1 and C2)

The footwall has always been characterized as being made up of mafic volcanic and volcaniclastic rocks (i.e. Dressler and Dunbire, 1981; Crafford, 1989; Newberry et al., 1990; Newberry et al., 1997; Taylor et al., 2008), but due to the high degree of deformation and often alteration, volcanic textures, which would normally be used to

interpret the volcanic origins of the footwall, are not present. C1 and C2 are fine-grained and typically green to light grey. Unambiguous evidence for volcanic and volcaniclastic origins for the footwall rocks has not been documented. Therefore the interpretation of the origins of the zircon grains within these footwall lithologies is ambiguous. A graphic representation of the Carboniferous chronostratigraphy is shown in Figure 94.

C1 – massive mafic volcanic rocks

The massive volcanic footwall unit (C1) is interpreted as a coherent basalt because of the relatively consistent nature of immobile elements Zr, Ti, Nb and Y (Chapter 3) and the rare examples within the unit of samples with evenly distributed feldspar crystals throughout. The preferred age of the two samples from this lithology overlap to within error and the Early Carboniferous age for this volcanic event is estimated as ~340 Ma. In both samples there was a separate population of analyses with Permian ages. It is possible that these grains have been partially reset during the Permian metamorphism (i.e. Hoskin and Black, 2000). However, there is no statistically coherent group of grains and no specific geologic significance can be inferred to the ages calculated from these analyses. Sample PSA07-030 is an amphibolite that may be a higher grade metamorphic equivalent of C1. The best estimate for the age of metamorphism for this sample is between 250 Ma and 300 Ma. This age range overlaps with the metamorphic age inferred from the basement samples and previously documented $^{40}Ar/^{39}Ar$ cooling ages of biotite and muscovite (Karl et al., 1998).

C2 – layered volcanic and volcaniclastic rocks

The layered footwall unit (C2) has more ambiguous origins than the C1 massive unit. The centimeter-scale layering appears to be compositional and is probably evidence for a clastic origin. However, the depositional environment is impossible to say and interpretations vary from highly deformed conglomerates or breccias (J. Proffett, pers. comm.) to finely interlaminated volcaniclastic sandstones (i.e. Dressler and Dunbire, 1981).

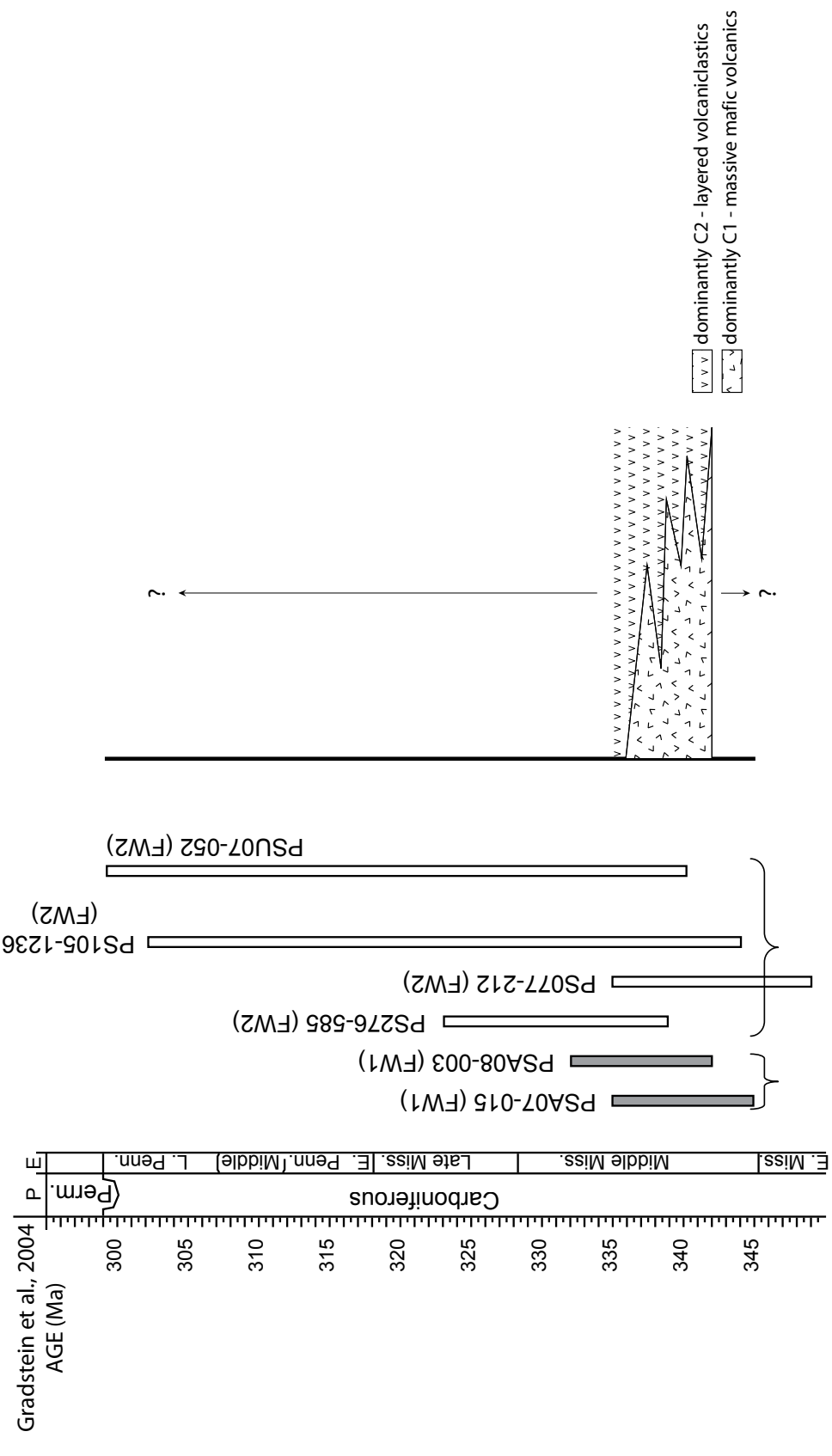

Figure 94 Chronostratigraphic diagram for the Carboniferous portion of the footwall (units C1-2) using time scale of Gradstein et al. (2004). P = Period; E = Epoch. Coherent volcanic samples (unit C1) are in dark grey, volcaniclastic(?) units (C2) are unfilled. Note the overlapping errors on all samples indicating a coeval origin for the zircon grains. Interlayered relationship of C1 and C2 lithologies is interpreted.

Four samples from the footwall layered volcanic and volcaniclastic unit (C2) have consistent results from U-Pb analyses of zircon grains. The zircon grains in these four samples appear to have three populations. The oldest population consists of one zircon grain, analyzed twice with a Mesoproterozoic age. The main zircon population is Carboniferous and is well constrained with the best estimate for the age ~335 Ma. This probably represents the maximum depositional age for these rocks. Based on the ages of zircon grains in the layered volcanic and volcaniclastic unit (C2), the maximum age of deposition is interpreted to be Early Carboniferous. One Proterozoic zircon grain indicates proximity to a source for old zircons. These samples all have the appearance of low maturity sandstones or epiclastic rocks. The preferred interpretation is the depositional age is Carboniferous and very similar to the age of the associated basalts. This result supports the view that the source of volcanic material in C2 is C1 or its associated volcaniclastic material (see Chapter 3). On this basis C1 and C2 are probably part of an arc basalt terrane with C1 representing facies proximal to volcanic centres and C2 distal facies. In this scenario the coherent zircon population in C2 can be considered a close estimate of the depositional age.

There are two obvious interpretations of the fairly homogenous Carboniferous population of zircon grains from the layered footwall unit (C2): (1) the clastic rocks are sedimentary in origin and the source for the zircon grains could be the massive coherent footwall unit (C1) or (2) the clastic rocks are volcaniclastic and are part of the same volcanic succession that formed the massive coherent unit (i.e. essentially contemporaneous). The main difference between the two interpretations has to do with the minimum depositional age for this unit. In option 1 the zircon age constrains the maximum age of the rocks (i.e. Carboniferous or younger) while option 2 indicates the zircons are part of the juvenile volcanic material. Option 2, a volcaniclastic origin, is preferred here because of the homogenous zircon population and the relatively consistent nature of immobile elements Ti, Zr, Nb, and Y within the layered unit (Chapter 3). The best estimate for the depositional age of C2 is ~335 Ma.

The remaining analyses of zircon grains in the C1 and C1 lithologies scatter from Permian to Triassic in age. Sample PS276-585 has two Carboniferous grains with thin rims which have a weighted mean of the ^{207}Pb corrected $^{206}Pb/^{238}U$ ages of 254 ± 13 Ma and PSU07-052 has a Triassic group of analyses including two rims and four grains which have a combined age of 230 ± 13 Ma. These Permian to Triassic analyses do not correlate well between samples. Broadly, the grains are likely to be either metamorphic or hydrothermal in origin. They are consistently smaller or form as rims on Carboniferous cores, have irregular CL images, and the rims typically have Th/U ratios lower than the associated cores. There are several fluid-flow events regionally documented that could theoretically be responsible for the growth of these zircon grains (Taylor et al., 1995; Karl et al., 1998). The zircon population is compatible with the history of Permian metamorphism and Triassic hydrothermal alteration defined from other samples.

Late Triassic lithologies (Tr1 to Tr4 and I1 to I3)

I1 – medium-grained massive rocks

No zircon grains were located in samples of the quartz-carbonate-mariposite medium-grained massive rock unit (I1). The stratigraphic location of this lithology comes from underground mapping and diamond drill core logging. This lithology is difficult to place in the stratigraphy because it is volumetrically minor and can be confused with examples of the altered serpentinite unit (I2). When observed as part of the present study, it was always found as uniform, massive elongate bodies sub-parallel to S2 within the layered footwall unit (C2) and is, therefore, interpreted as dikes or sills within the footwall. The chemistry supports an association with the I2 lithology and therefore the quartz-carbonate-mariposite lithology probably intruded in the Triassic.

Tr1 – polymict breccias

A key stratigraphic marker at the Greens Creek Mine is the breccia unit (Tr1). When present, the breccia unit along with mineralization always marks the footwall – hanging wall boundary. Unfortunately, zircon grains were not located in samples of the breccia unit. The breccia is inferred to be Late Triassic in age, based on regional correlations (Taylor et al., 2008).

Tr2- mineralized rocks and Tr3 – argillite

The age of mineralization is constrained directly by geology and indirectly by Late Triassic fossils (see below) and age dating of hydrothermal micas. At the Greens Creek Mine, mineralization is found at the contact between Tr1 and Tr3. The footwall lithology immediately beneath mineralization can be the breccia unit (Tr1) or the layered volcaniclastic unit (C2). If the mineralization is syngenetic (the preferred model) it must be after Permian metamorphism and before 227 Ma (in the range of 265 to 227 Ma).

Taylor et al. (1995) reported a mariposite two-step $^{40}Ar/^{39}Ar$ plateau date of 210.7±0.3 Ma (1σ) for an ultramafic body from Gambier Bay in southern Admiralty Island. This body is interpreted as a possible correlate of the serpentinite unit (I2) near Greens Creek and may be a potential heat source for the mineralizing event and, therefore, the age of the ultramafic body is a proxy for the age of mineralization. However, the mariposite age is too young to match the stratigraphic constraints on the age of mineralization. The depositional age of the hanging wall argillite is latest Carnian to earliest Norian (Taylor et al., 1999). A mineralization age of 210 Ma requires the mineralization to be epigenetic and this is unlikely given other geological constraints (see Chapter 6 and 7).

I2 – medium-grained intrusive rocks

The age of the hanging wall massive serpentinite unit (I2) is difficult to constrain as these rocks are generally exposed in areas of complex structure. Their original

emplacement mechanism is ambiguous. In a few diamond drill holes on the Greens Creek property (i.e. PS292), the serpentinite and massive argillite form intricate breccias that are possibly peperitic in nature suggesting the intrusion of the serpentinite into unlithified hanging wall argillite. A similar timing relationship has been documented on southern Admiralty Island where an ultramafic body has a chilled margin against argillite (Taylor, in press). These relationships indicate that the serpentinite (I2) was intruded into the argillite, possibly in the Late Triassic. Rare-earth-element patterns (Chapter 3) and initial $^{206}Pb/^{204}Pb$ ratios similar to the Late Triassic microgabbro (I3) support a Late Triassic age of emplacement.

I3 – fine to medium-grained intrusive rocks

In two samples (PS271-207 and PSA08-001) collected from the intrusive hanging wall microgabbro unit (I3). The preferred age based on combining two samples from the same microgabbro body is 221 ± 6 Ma. This results confirms previous evidence for a Late Triassic age (S. Karl pers. comm.; Taylor et al., in press). The medium-grained intrusive microgabbros (I3) are found throughout the argillite unit and chilled margins have been recognized. The primary mineralogy of the microgabbros is often altered suggesting that they were either already emplaced when the mineralizing hydrothermal system was still active or that a subsequent event altered the mineralogy.

Tr4 – coherent volcanic rocks

The youngest hanging wall lithology (Tr4) is dominantly made up of basalt flows with several rhyolite bodies identified within the basalts. Taylor et al. (in press) reported U/Pb whole-rock ages for the basalts as 215 ± 6 Ma. The present study shows the emplacement age for the rhyolite bodies is 226.9 ± 0.2 Ma, slightly older than the estimate of the basalt, but more reliable. This body is interpreted as a coherent volcanic with the zircon grains in the sample interpreted as igneous in origin. The preferred interpretation of the present study is that the U/Pb whole-rock age is slightly too young and that the entire volcanic package on Gallagher Ridge is ~227 Ma.

The fossil assemblage for the argillite samples highlights the difficulties of comparing paleontological age data with absolute dating methods. The Geologic Time Scale released by the International Commission on Stratigraphy (ICS) in 2004 (Gradstein et al., 2004) defines the Norian epoch as 203.6 Ma to 216.5 Ma and the Carnian from 216.5 Ma to 228 Ma. This interpretation of the time scale would make the Late Triassic volcanism dated in the present study Carnian and likely older than the argillite (Figure 95). Two recent papers (Muttoni et al., 2004; Furin et al., 2006) suggested that the Norian-Rhaetian boundary should be shifted downwards by approximately 6.5 Ma from 203.6 Ma (Gradstein et al., 2004) to approximately 210 Ma and the Norian-Carnian boundary should be shifted downwards by approximately 10 Ma from 217.4 Ma (Gradstein et al., 2004) to approximately 227 Ma. These changes to the boundaries would make the Norian epoch from approximately 210 Ma to 227 Ma and the Carnian from approximately 227 Ma to 235 Ma. This interpretation of the time scale allows the Late Triassic volcanism (unit Tr4) to be coeval to possibly slightly younger than at least some of the argillite (Figure 95). This interpretation of the time scale better reflects the current interpretations of the geology in the Greens Creek vicinity and is the preferred interpretation for the present study. For these reasons, the Late Triassic boundaries of Muttoni et al. (2004) and Furin et al. (2006) are preferred and the chronostratigraphy presented in Figure 96 is a graphic representation of the stratigraphic and intrusive relationships for the Late Triassic rocks at Greens Creek. In combination, these data indicate the entire Late Triassic stratigraphy and intrusive history was compressed into a short time, probably from 230 Ma to 224 Ma.

Post-Triassic lithologies

Sample PSA05-010 is located in an area mapped as the Seymour Canal Formation (Gehrels and Berg, 1992) while PS181-738 is from a diamond drill hole which was previously interpreted as having intersected only Retreat Group lithologies. The similarity of the zircon age between the youngest grains in PS181-738 and the grains in PSA05-010 suggests that sample PS181-738 may be from a structurally emplaced section of the Seymour Canal Formation. The Early Cretaceous (143 Ma) maximum age

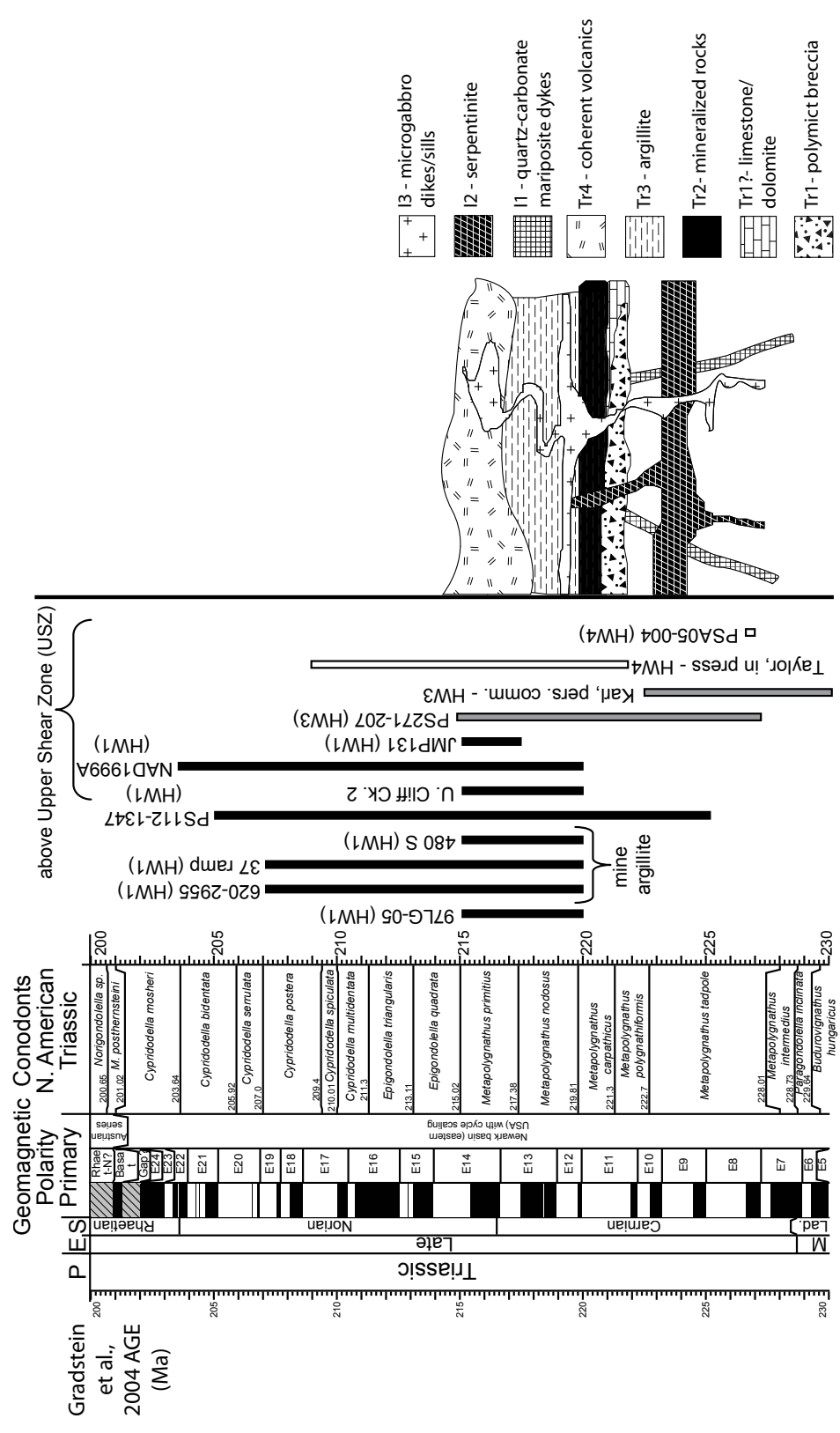

Figure 95 Chronostratigraphic diagram for the Late Triassic portion of the footwall (unit Tr1) and for the hanging wall (units Tr2-4) using Late Triassic boundaries of Gradstein et al. (2004). Time scale is from Gradstein et al. (2004). E = Epoch; S = Stage. Conodont-bearing argillite samples (unit Tr3) are in black, medium- to coarse-grained microgabbro samples (unit I3) are in medium grey and intrusive fine-grained coherent volcanic samples (unit Tr4) are in white.

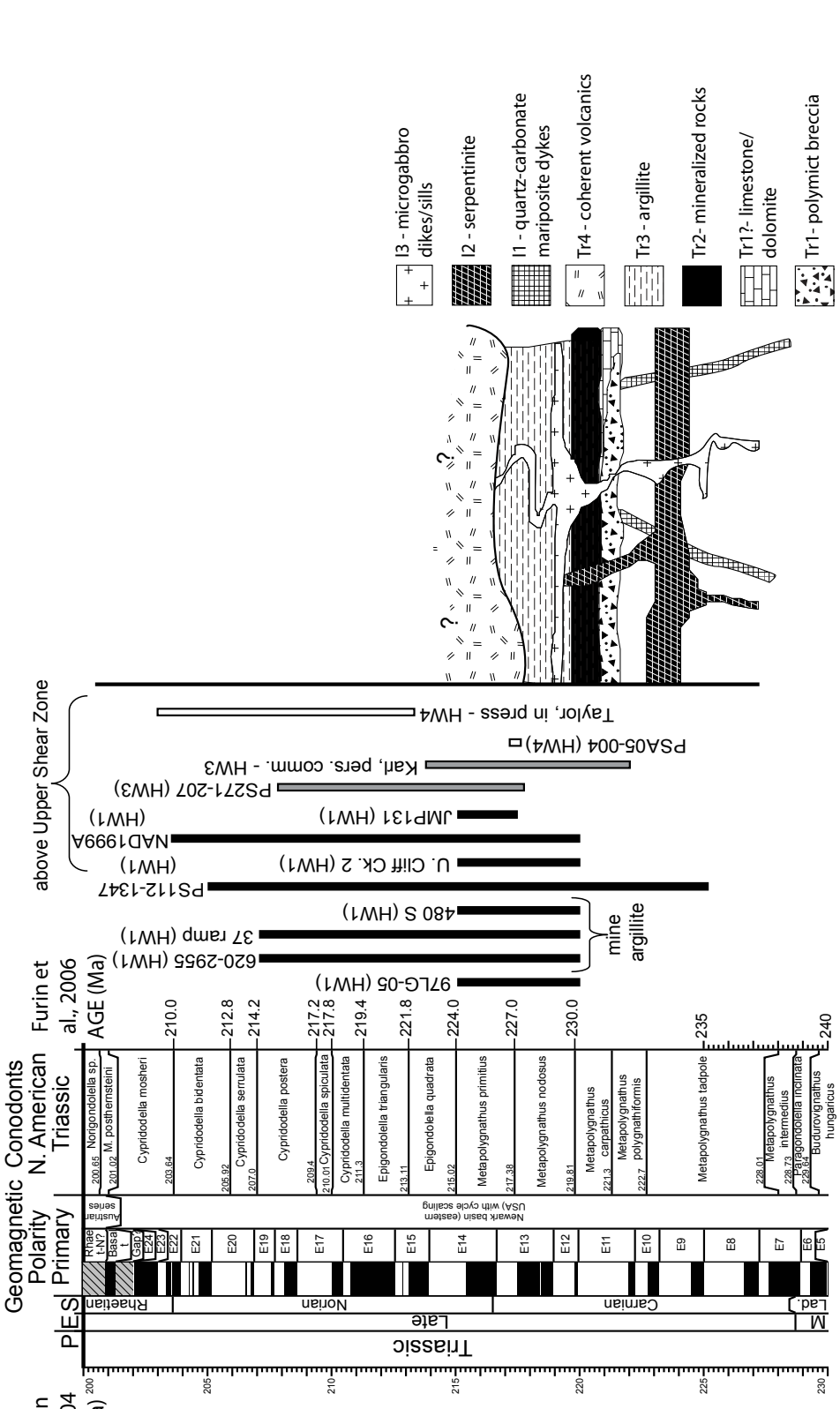

Figure 96 Chronostratigraphic diagram for the Late Triassic portion of the footwall (unit Tr1) and for the hanging wall (units Tr2-4) using Late Triassic boundaries of Furin et al. (2006) and Muttoni et al. (2004). Note that the I3 and Tr4 age ranges do not correspond with the present understanding of the geology. Time scale is from Gradstein et al. (2004). Conodont ranges are from Orchard and Tozer (1997). P = Period; E = Epoch; S = Stage. Conodont bearing argillite samples (unit Tr3) are in black, medium- to coarse-grained microgabbro samples (unit I3) are in medium grey and intrusive fine-grained coherent volcanic samples (unit Tr4) are in white.

of deposition is similar for each sample. Though the number of grains is much smaller than the typical number quoted in defining populations of zircon grains in sedimentary rocks, the results are consistent. The depositional age of the Seymour Canal Formation has been estimated from a fossil assemblage, characterized by the pelecypod *Buchia,* to be Late Jurassic to Early Cretaceous (Loney, 1964). The youngest population of detrital zircon grains from this unit have an age of 143 ± 5 Ma (Late Jurassic) and agree with the depositional age of Loney (1964). The post-deformational mafic dikes have an emplacement age of 85 ± 4 Ma and are the youngest rock unit included in the present study. These dikes post-date F4 and are offset by strike-slip faulting.

Table 24 Summary of geochronological results for lithologic units defined in Table 21.

Lithologic unit	Depositional age (Ma)	Crystallization age (Ma)	Metamorphic age (Ma)
S-D2			265
C1	342 ± 4		250–300
C2	<340		
I3		223 ± 6	
Tr4		226.9 ± 0.2	
J1	<143		
I4		85 ± 4	

Summary

- Sixty-three samples searched for zircon grains, 21 samples with enough zircon grains identified to attempt dating, 15 samples with reportable dates.

- The U-Pb dating of small in-situ zircon grains from samples collected in the vicinity of the Greens Creek Mine have identified a Carboniferous volcanic sequence, a Permian metamorphic event, a Late Triassic volcanic sequence and a Late Cretaceous igneous event (Table 24).

- Figure 97 illustrates the chronologic sequence of deformational and metamorphic events in the Greens Creek area.

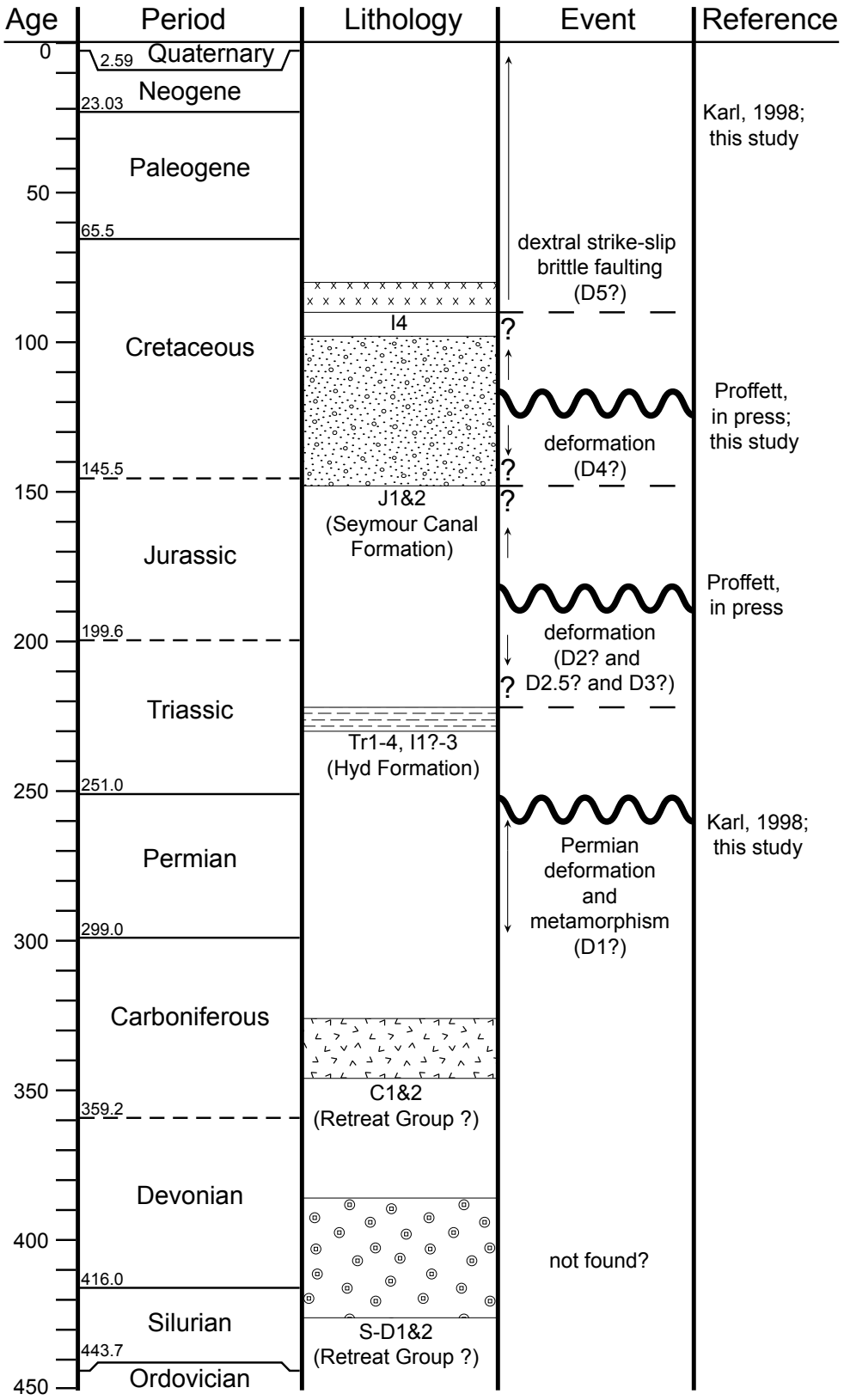

Figure 97 Chronologic diagram for the sequence of deformational and metamorphic events as they relate to the stratigraphy in the vicinity of the Greens Creek Mine. Stratigraphy is from the present study and the structural nomenclature is from Proffett (in press). Timing of D2, D2.5, D3 and D4 is relative and only broadly constrained by the fact that all four foliations (S2, S2.5, S3 and S4) are found in the Late Triassic rocks, but only one foliation (S4?) is found in Seymour Canal Formation rocks. Time scale is from Gradstein et al. (2004).

- Schistose basement rocks have a depositional age of Early Silurian to Middle Devonian and several possibly metamorphic zircon grains with a Late Permian age.

- Metamorphic zircon grains with a Permian age from an amphibolite sample in Cliff Creek possibly date the D1 footwall metamorphic and deformational event.

- Footwall breccia unit and/or mineralization mark the footwall–hanging wall contact position. The breccia is composed of clasts with a S1 foliation but is unaffected by D1.

- Argillite deposition is constrained from Carnian to Norian in age.

- The age of mineralization is constrained by the deposition of the overlying fossiliferous Carnian-Norian argillite. The best estimate for the age of mineralization is Carnian – using the Carnian boundary estimates of Muttoni et al. (2004) and Furin et al. (2006).

- Undated, volumetrically significant serpentinite bodies show possible features associated with intrusion into the argillite and are weakly chemically similar to the microgabbros suggesting a Late Triassic emplacement age for these rocks.

- Hanging wall microgabbros were emplaced at 223 ± 6 Ma and the overlying rhyolites were emplaced at 226.9 ± 0.2 Ma. These ages are coeval with previous reported ages for the hanging wall microgabbro, basalt and limestone.

- The overlapping Seymour Canal Formation is Late Jurassic to Early Cretaceous in age.

- An unfoliated set of mafic dikes was emplaced at 85 ± 4 Ma constraining the ductile deformation to older than 85 ± 4 Ma

Chapter 6: Alteration

Introduction

The alteration mineral assemblage at Greens Creek is relatively simple consisting of chlorite, white mica, quartz, pyrite and carbonate. This mineral assemblage reflects the lower greenschist metamorphism and local hydrothermal alteration associated with massive sulfide mineralization. Alteration mineral chemistry and zonation have been briefly described by Newberry et al. (1989) and Anderson and Taylor (2000, in press). The present study provides a description of the alteration mineralogy and distribution with a brief summary of previous work but emphasizes the downhole variation in infrared spectra and geochemical alteration characteristics of the footwall rocks.

The simplicity of the alteration suite, the fine-grained nature of the rocks and the dominance of white mica within the mine workings has made alteration mapping at Greens Creek difficult. Mineral isograds are only broadly recognized and are generally gradational. However, short-wavelength infrared (SWIR) spectral analysis can be used to measure subtle compositional variations within individual hydrous minerals such as chlorite and white mica. Recent studies, based on SWIR analyses in volcanic-hosted massive sulfide (VHMS) districts and deposits, show that the composition of these minerals can vary systematically with proximity to mineralization (e.g. Herrmann et al., 2001; Yang et al., 2004; Jones et al., 2005; van Ruitenbeek et al., 2005). Downhole plots showing spectral shifts can be constructed, allowing recognition of domains in otherwise apparently homogeneous fine-grained rocks.

Whole-rock geochemical analysis is a standard technique for studying alteration associated with VHMS deposits (e.g. MacLean, 1990; Gemmell and Large, 1992; Large et al., 2001; Mireku and Stanley, 2006). Commonly, alteration indices are formulated from two or more components of major-element analyses in order to increase the contrast between variably altered samples (Gifkins et al., 2005). These whole-rock alteration indices typically combine elements that are either added or removed from the rock during hydrothermal alteration thereby emphasizing the change with proximity to mineralization. Even with sparse data these plots can be useful in defining potential vectors to mineralization (Gifkins et al., 2005). Downhole plots of alteration indices at Greens Creek show systematic changes with proximity to mineralization and support the findings of the SWIR spectral study.

The present study examines downhole plots of various spectral and geochemical alteration vectors. The spectral vectors are based on subtle compositional shifts in white mica and chlorite based on SWIR analyses and the geochemical vectors are based on major- and trace-element data from whole-rock analyses. Smaller scale maps showing alteration patterns across large areas were not constructed because the spatial density of the data points is too low. The main aims of the present study are to:

1. Determine SWIR spectral characteristics and variations of white mica and chlorite in regional and proximal areas in order to identify the controls on the white mica and chlorite compositions.
2. Determine major- and trace-element geochemical characteristics and variations in regional and proximal samples and to identify the controls on whole-rock compositions.
3. Identify any systematic trends in the SWIR spectral or geochemical response and, if present, establish whether they can be used as vectors to mineralization.

Alteration mineralogy and zonation

The complete stratigraphy for the Greens Creek property is outlined in Table 1 (Chapter 3). The footwall has four protolith units: C1–massive volcanic, C2–layered clastic

or volcaniclastic, I1–massive, veined dikes and Tr1–breccia or conglomerate (Table 25). The most common lithology in the mine workings is C2. Tr1 is also common but is typically only found within 60 feet (20 m) of the footwall–hanging wall contact (Newberry et al., 1989). The footwall has four distinct alteration zones associated with proximity to mineralization. From proximal to distal, these are: quartz–pyrite zone, quartz–sericite zone, sericite zone and chlorite zone. The two layered footwall lithologies, carbonate phyllite and maripositic phyllite, are not systematically spatially associated with mineralization (see Chapter 3). Therefore, these lithologies will not be discussed in this chapter.

Table 25 Summary of Greens Creek footwall lithologies and their characteristics (modified after Freitag, 2000; West and Proffett, 2003). The stratigraphic order is from the present study.

Lithology	Mine nomenclature	General hand sample characteristics	Descriptive stratigraphy used in this study
Stratigraphic footwall– "hydrothermally altered volcanic and volcaniclastic rocks"	breccia	granule to pebble, moderately to poorly sorted, polymict	Tr1 - polymict breccias
	quartz-carbonate-mariposite	light grey to light purple, massive, can be heavily quartz-carbonate veined	I1 - quartz-carbonate-mariposite
	siliceous rock	white to grey, fine-grained, massive, dense, quartz-rich	C2b - siliceous rocks and monomict breccias
	siliceous phyllite	light grey, up to 70% quartz, varying amounts of sericite	
	sericitic phyllite	light grey, very fine-grained sericite, varying amounts of pyrite, quartz	
	chloritic phyllite	light to dark green, laminated to layered, chlorite-rich rock	
	graphitic phyllite	light grey to black, laminated to layered, graphitic partings	C2a - layered rocks
	maripositic phyllite	mariposite gives the phyllite a distinct green tint	
	carbonate phyllite	layered to nearly massive, granular texture, dominantly dolomitic, light grey to tan	
	greenstone	light to dark green, massive, chlorite-rich rock	C1 - massive rocks

The four hydrothermal alteration zones associated with proximity to mineralization are outlined in Table 26 and will be described in this chapter. These alteration zones have been partially identified by previous workers (Newberry et al., 1989; Anderson and

Taylor, 2000). The present study provides a brief review of these two studies before describing the alteration zones.

Table 26 Mineral assemblages of alteration zones associated with proximity to mineralization. Mine lithology is from West and Proffett (2003), typical thickness is from Newberry et al. (1989) and as observed in the present study. *Mineral assemblage of Tr1 is from minerals observed between breccia fragments and does not include minerals within fragments. Mineral abbreviations are: qtz = quartz, ser = sericite, chl = chlorite, carb = carbonate (typically dolomite), py = pyrite, bar = barite, fspr = feldspar (typically too altered to identify specific phase).

Footwall unit	Mine lithology	Alteration zones	Mineral assemblage	Typical thickness
Tr1	SPcx	quartz - pyrite	*qtz>py>ser>bar +/- carb	0-60 feet (0-18 m)
C2	SR		qtz>py>ser>bar +/- carb	0-75 feet (0-23 m)
	SPs	quartz - sericite	qtz=ser>py +/- carb	0-200 feet (0-60 m)
	SP	sericite	ser>chl>qtz>carb +/- py	0-500 feet (0-150 m)
	SPc	chlorite	chl>carb>ser>qtz +/- fspr	>300 feet (90 m)
C1	GST		chl>carb>ser>qtz> fspr	>300 feet (90 m)

Previous work

Newberry and Brew (1989) described an interpreted stratigraphy for the Greens Creek deposit, from footwall to hanging wall, with >100 m of chloritic phyllite, 0–70 m of sericitic phyllite, 0–20 m of breccia, 0–10 m of massive sulfide and >50 m of graphitic calcareous argillite and limestone. This study also showed a decrease in the Mg# (100*Mg/Mg+Fe) of chlorite with increasing proximity to mineralization. They demonstrated that the chloritic phyllites are geochemically similar to unaltered greenstones. The sericitic phyllite, chloritic phyllites and greenstone rocks have the same immobile-element characteristics indicating that the variation in the footwall is the result of alteration, not protolith changes.

Newberry and Brew (1989) and Anderson and Taylor (2000) reported similar mineralogical, mineral chemistry and whole-rock geochemical trends within the footwall rocks. They described metasomatic changes with proximity to mineralization such as increasing SiO_2 and S, document an increasing Mg# and BaO content in sericite towards mineralization and demonstrated compositional zoning of carbonate minerals with distance to ore. The carbonate zonation grades from dolomite in the ore to ferroan

dolomite, magnesite, ankerite out to pure calcite in unaltered footwall rocks. These studies pointed out that the Mg# in individual mineral phases is independent of the bulk-rock Mg# indicating that the alteration halo within the footwall was not reset during metamorphism and should still be a useful exploration tool.

Chlorite alteration zone

The chlorite alteration zone is the least-altered zone and the mineral assemblage of chlorite > carbonate > sericite > quartz ± plagioclase reflects the lower greenschist metamorphic grade of the footwall rocks (Dusel-Bacon et al., 1996). There are two protoliths identifiable within the chlorite alteration zone. The massive volcanic C1 unit has plagioclase phenocrysts up to several millimeters within a groundmass with a grain size ≤300 μm. The layered clastic unit, C2, has fewer feldspar phenocrysts that are typically smaller (≥200 μm) within a groundmass with ≤100 μm grain size. In hand specimen, the C1 unit is slightly coarser grained than the C2 unit and the best examples have an evenly porphyritic texture with millimeter size pale feldspar phenocrysts in a very fine-grained green groundmass. The chlorite altered C2 unit is very fine- to fine-grained and thinly to thickly laminated with laminae defined by grain size and color variation. In some samples, the laminae can alternate between green and dark grey to black (Figure 98A). Phenocrysts are generally not distinguishable in hand specimens from the chlorite alteration zone of C2.

In both protoliths, chlorite is the dominant mineral. It typically has irregular grain boundaries and rarely embays and alters mafic phenocrysts (Figure 98B). Carbonate occurs as either coarse-grained (<500 μm) euhedral rhombs or fine-grained nodules of calcite and appears to alter other alteration phases in the rock (Figure 98C&D). Sericite is fine- to very fine-grained and is typically found on the margins of either chlorite grains or as thin halos on feldspar phenocrysts (Figure 98E). Quartz is very fine-grained and found only in the groundmass. Quartz phenocrysts were not observed in any samples. The feldspar phenocrysts are typically too altered to determine their original mineralogy but in rare cases plagioclase twins are visible. The margins of the feldspar

phenocrysts are irregular and commonly have very fine-grained sericite around them. They can also be heavily embayed by calcite. The laminae in the chlorite alteration zone of the C2 unit are defined by grain-size variation between sand size (63–250 μm) and silt size (15–63 μm). The same minerals are present in each laminae type.

The chlorite alteration zone is the background alteration zone and the dominant mineral assemblage observed in the rocks on a property scale. The chlorite alteration zone is rare in the underground workings as the majority of mine development is either within the hanging wall or the proximal footwall. The chlorite alteration zone is best observed in surface diamond drill holes in the vicinity of the East ore zone. In these holes, the chlorite alteration zone generally begins between 100 feet (30 m) and 300 feet (90 m) from mineralization. Unfortunately, the Upper Shear Zone (USZ) and erosion truncate the footwall so that a maximum of 1000 feet (300 m) of intact footwall remains to be studied (Figure 99). In diamond drill holes into the thicker ore bodies such as the Northwest West and Central West zones, the chlorite alteration zone is either not observed or is located more than 500 feet (150 m) from mineralization (Figure 99).

Sericite alteration zone

The sericite alteration zone has the mineral assemblage of sericite > chlorite > quartz > carbonate > pyrite and is the most common alteration style observed in the mine workings and in diamond drill holes in the immediate mine area. In hand specimen, the rock is fine- to very fine-grained, thinly to thickly laminated, tan to grey and typically fairly soft. In some samples, the laminae are strikingly defined by alternating tan-grey sericitic layers and black graphitic layers (Figure 100A).

Sericite is the dominant mineral observed in thin section and varies in grain size from <25 μm to >300 μm (Figure 100B). The grain boundaries are typically irregular and subhedral to euhedral. Chlorite is similar in size and appearance to sericite but is less abundant. Quartz grains are typically <50 μm with irregular, subhedral to anhedral grain boundaries. Quartz phenocrysts have not been recognized. Two morphologies of

carbonate are recognized: a coarse-grained, rhombohedral calcite and a fine-grained nodular calcite. Pyrite content is highly variable but, when present, is either fine-grained (<50 μm) or coarse-grained (≥200 μm). The coarse-grained variety can have well-developed strain shadows infilled with quartz and sericite or chlorite (Figure 100C).

Feldspar phenocrysts are rare and, if observed, they are often too altered to distinguish the specific phase. However, a few examples of feldspar phenocrysts with plagioclase twinning have been observed (Figure 100D). Individual laminae are typically defined by grain size and mineralogical variation between relatively quartz-rich sand (63–250 μm) and micaceous silt (15–63 μm) (Figure 100E). These features impart a subtle color variation to the laminae.

The sericite alteration zone is the most common of the alteration zones observed in the mine area. In the vicinity of the East ore zone, the sericite alteration zone can be found from the mine contact out to 300 feet (90 m) in the footwall. In the Northwest West and West ore zones, the thickness of the sericite alteration zone approximately doubles and it can be found up to 600 feet (180 m) into the footwall (Figure 101).

Quartz - sericite alteration zone

The quartz–sericite alteration zone is transitional between the less-altered sericite zone and the more altered quartz–pyrite zone. In hand specimen, these rocks are typically light to dark grey, hard and the laminations are less distinct than those in the sericite alteration zone (Figure 102A). Rare plagioclase phenocrysts are still visible but are heavily altered along their margins. The abundance of quartz and sericite varies considerably within this assemblage, but the abundance of quartz is always greater than or equal to the abundance of sericite. In thin section, the quartz grains are typically irregular, coarse- to very fine-grained and have anhedral to subhedral grain boundaries (Figure 102C). The sericite grains are typically fine to very fine-grained with irregular, subhedral to euhedral grain boundaries. Pyrite is coarse- to fine-grained and euhedral. Quartz-filled strain shadows surround larger pyrite grains (Figure 102D).

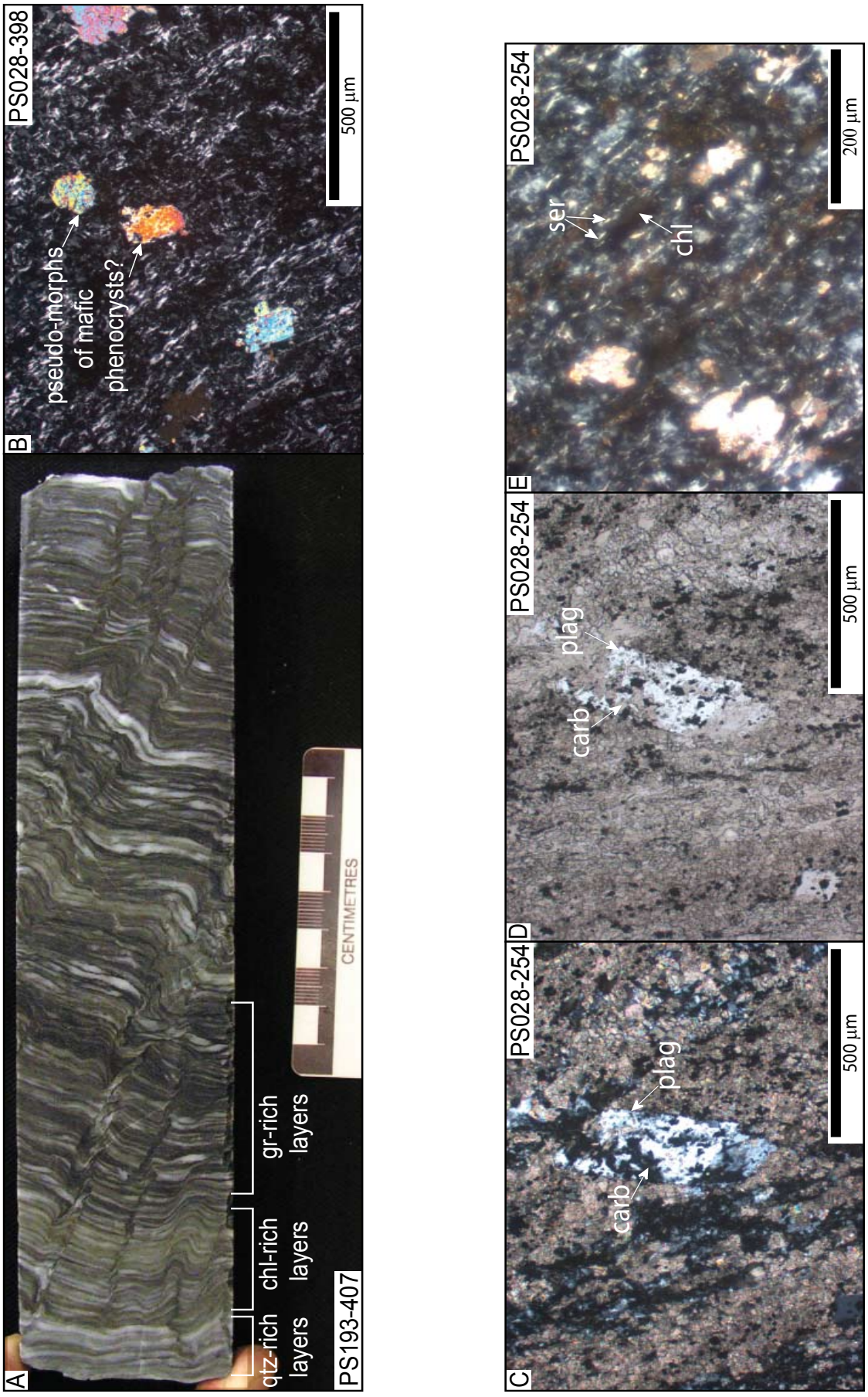
A
PS193-407
qtz-rich layers
chl-rich layers
gr-rich layers
CENTIMETRES
B
PS028-398
pseudo-morphs of mafic phenocrysts?
500 µm
C
PS028-254
carb
plag
500 µm
D
PS028-254
plag
carb
500 µm
E
PS028-254
ser
chl
200 µm

Figure 98 Representative photographs of samples from the chlorite alteration zone, protolith units C1 and C2.
(A) Distinctly layered, see labels. Three layer types are recognized: quartz rich, chlorite rich and graphite rich. Mineral abbreviations are: qtz–quartz, chl–chlorite, gr–graphite. (2495334E, 2286907N, West Bruin prospect, drill hole PS193 at 407 feet (123.3 m))

(B) Photographmicrograph (XPL) of chlorite spots (altered mafic phenocrysts?) within a feldspar and chlorite groundmass. Original mineralogy could not be determined. (2501875E, 2280186N, East ore zone, drill hole PS028 at 254 feet (80.0 m))

(C&D) Photographmicrographs (D–XPL and E– PPL) of carbonate altered feldspar phenocryst (plagioclase?) within a dominantly calcareous groundmass (carb). (2501875E, 2280186N, East ore zone, drill hole PS028 at 254 feet (80.0 m))

(E) Photographmicrograph (XPL) of very fine-grained sericite (ser) and larger chlorite grains (chl). This is typical of the mineralogy and grain size for the chlorite alteration zone. (2501875E, 2280186N, East ore zone, drill hole PS028 at 254 feet (80.0 m))

Figure 99 Southwest–northeast cross-section 4400 (200 foot (60 m) data window) through the northern end of the Greens Creek deposit. On the east side of the Maki Fault, the chlorite alteration zone is locally within 100 feet (30 m) of the mine contact while, in the vicinity of the Northwest West ore zone, the chlorite alteration zone is >500 feet (150 m) from the mine contact. In this section, erosion and the Upper Shear Zone (USZ) truncate the footwall 750 feet (225 m) from the mine contact. Holes in heavy black lines and labeled were examined as part of the present study.

Carbonate abundance is highly variable but when present, carbonate is either coarse- to fine-grained euhedral rhombs of dolomite or fine-grained nodular masses of anhedral dolomite (Figure 102E). Along the East ore zone, the quartz–sericite alteration zone extends a maximum of 200 feet (60 m) into the footwall but, in the Northwest West and West ore zones, it can extend up to 400 feet (120 m) into the footwall.

Quartz–pyrite alteration zone

The quartz–pyrite alteration zone is the most altered zone within the footwall rocks. There are two protolith units within the quartz–pyrite alteration zone but the intensity of the alteration can make identification of the protolith difficult. The stratigraphic positions of the quartz–pyrite alteration zone and the breccia unit (Tr1) are the same and it is not always possible to determine if a sample is intensely quartz–pyrite altered breccia (Tr1) or layered clastic (C2). In underground exposures in the Northwest West ore zone, pseudo-breccias have fragments up to several feet (~1 m) across that are heavily silicified with weak compositional banding similar to examples of the other alteration zones (Figure 103A). The pseudo-fragments are jigsaw-fit, with similar orientation of their internal layering. The matrix is quartz and sulfide (predominantly pyrite) and the pseudo-fragment margins are irregular. It is interpreted that these rocks are not breccias but rather have pseudo-breccia textures related to the intense silicification of a layered protolith.

In the East ore zone, the rocks immediately below mineralization are weakly to strongly silicified polymict breccias with clasts typically composed of other footwall lithologies. The clast types dominantly reflect the local footwall geology indicating that they are not far travelled. In the footwall proximal to mineralization the quartz–pyrite alteration is completely destructive and original clastic textures and mineralogy are obliterated. In these cases, the differentiation of the protolith is impossible and all that can be stated confidently is that the rock lies within the quartz–pyrite alteration zone.

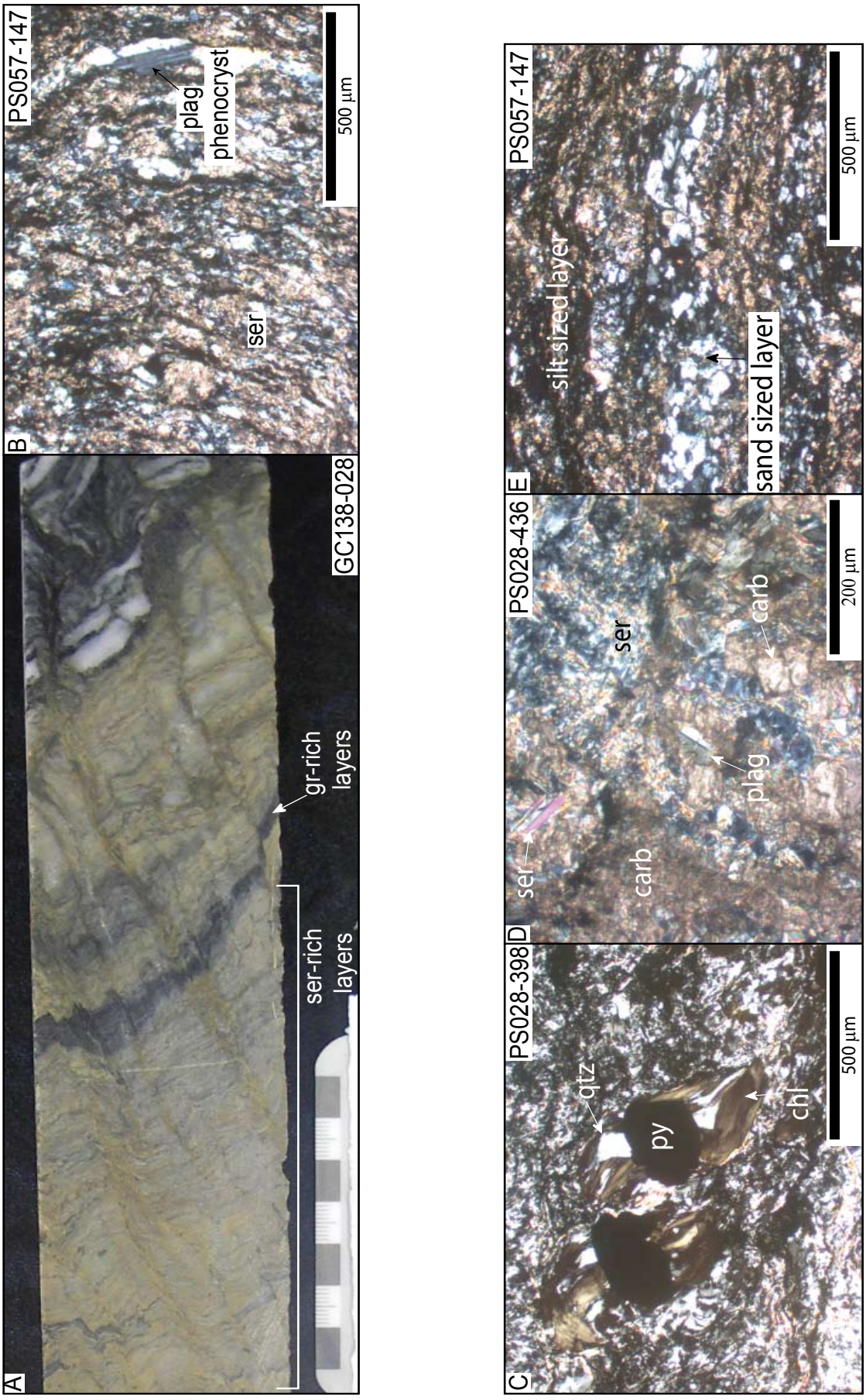
A
GC138-028
gr-rich layers
ser-rich layers
B
PS057-147
plag phenocryst
ser
500 µm
C
PS028-398
qtz
py
chl
500 µm
D
PS028-436
ser
carb
plag
carb
200 µm
E
PS057-147
silt-sized layer
sand sized layer
500 µm

Figure 100 Representative photographs of samples from the sericite alteration zone, protolith unit C2.
(A) Distinctly layered texture indicating a clastic protolith. Two layer types are recognized: sericite rich (ser) and graphite rich (gr). Scale bar is in cm. (2501667E, 2280049N, East ore zone, underground drill hole GC138 at 28 feet (8.5 m))

(B) Photographmicrograph (XPL) of altered plagioclase phenocryst (plag) within a dominantly quartz– sericite groundmass (ser). (2501763E, 2280798N, East ore zone, drill hole PS057 at 147 feet (44.5 m))

(C) Photographmicrograph (XPL) of a quartz (qtz) and chlorite (chl) filled strain shadow surrounding a pyrite grain (py). (2501875E, 2280186N, East ore zone, drill hole PS028 at 398 feet (120.6 m))

(D) Photographmicrographs (XPL) of a fine-grained plagioclase phenocryst within a sericite and carbonate (carb) groundmass. (2501875E, 2280186N, East ore zone, drill hole PS028 at 436 feet (132.1 m))

(E) Photographmicrograph (XPL) of alternating quartz-rich sand sized and micaceous silt sized layers. Layers are up to approximately 250 µm thick. (2501763E, 2280798N, East ore zone, drill hole PS057 at 147 feet (44.5 m))

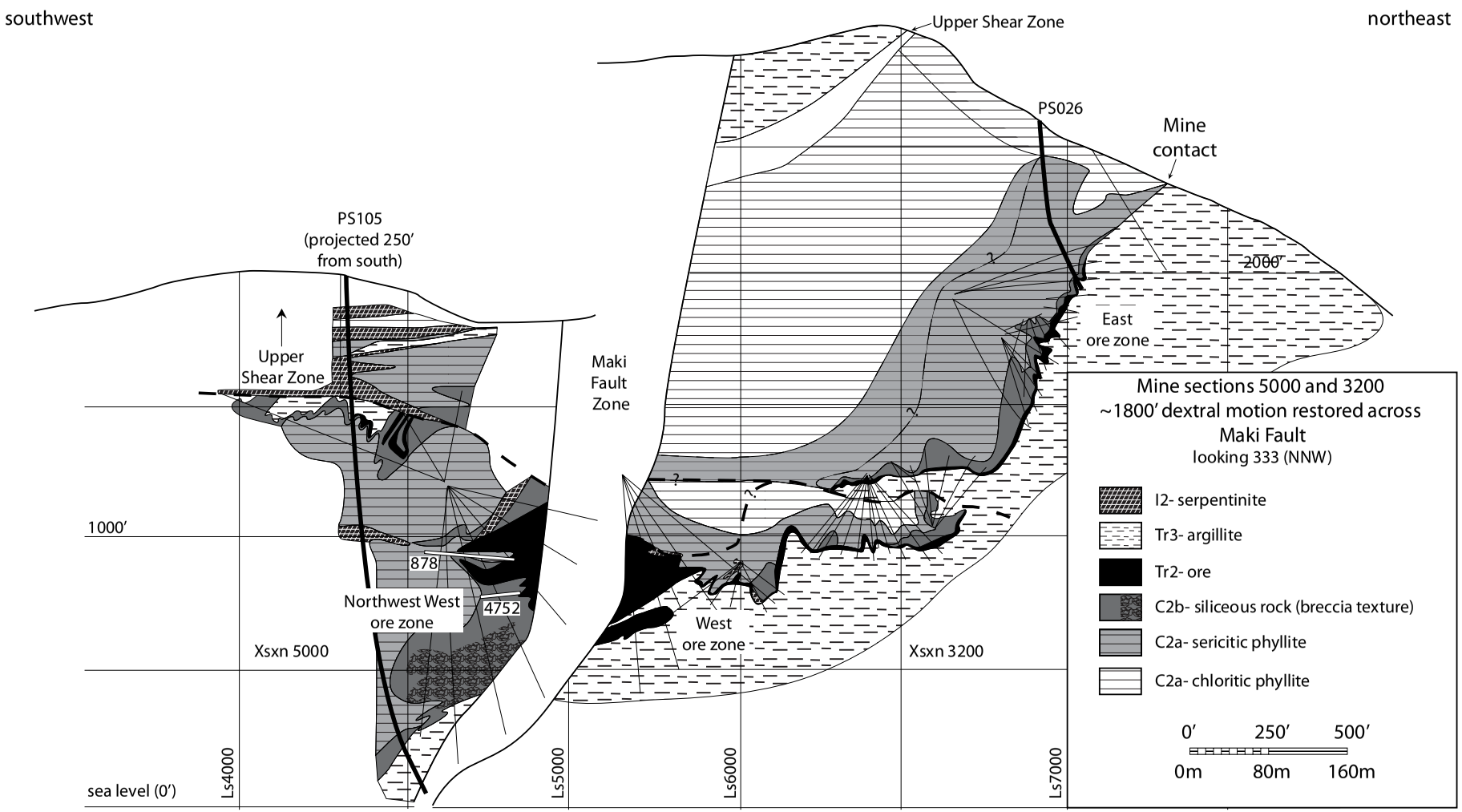

Figure 101 Restored cross-sections 5000 and 3200. Approximately 1800 feet (550 m) right lateral displacement along the Maki Fault zone has been restored to join cross sections 5000 (W of Maki) and 3200 (E of Maki). Geology from Lindberg (1994: plate 2). Holes PS026 aand PS105 were examined as part of the present study.

In hand specimen, the rocks are extremely hard, have a massive or pseudo-breccia texture and are light to dark grey. The alteration in this zone can be completely mineralogically and texturally destructive. No remnant feldspar phenocrysts have been observed, the laminations seen in the other alteration zones are either absent or faint and the mineral assemblage is apparently entirely hydrothermal in origin. A pseudo-breccia texture exists in some examples of this alteration zone but the pseudo-fragment margins are defined entirely by sulfide minerals (predominantly pyrite) and finer grained quartz ± barite. The pseudo-fragment margins are also extremely irregular in shape and somewhat gradational between the margins and interiors (Figure 103B&C).

Quartz is the most abundant mineral seen in thin section except near the margins of pseudo-fragments where pyrite is more abundant. Quartz grains are typically fine- to very fine-grained and anhedral with regular equant shapes (Figure 103D). Pyrite and other sulfide minerals such as galena and sphalerite are typically fine-grained and restricted to pseudo-fragment margins or are coarse grained and found in small cross-cutting veinlets with barite (Figure 103E). Barite occurs either as euhedral laths up to 200 μm in length or as large grains within small veinlets (Figure 103F). Carbonate is less abundant in this assemblage and when present, has either a coarse rhombohedral morphology or a fine-grained nodular morphology.

As the quartz–pyrite alteration zone is texturally destructive and has the same approximate stratigraphic position as the polymict breccia unit (Tr1), the depth of the quartz–pyrite alteration zone in the footwall is defined by either the presence of the polymict breccia or the presence of the quartz–pyrite alteration mineral assemblage. In the East ore zone, the quartz–pyrite alteration zone reaches a maximum of 150 feet (45 m) into the footwall but is typically <75 feet (22 m). In the Northwest West and West ore zones, the thickness of the quartz–pyrite alteration zone increases up to approximately 300 feet (90 m) into the footwall (Figure 104). The polymict breccia (Tr1) lithology is more commonly recognized in the vicinity of the East ore zone and

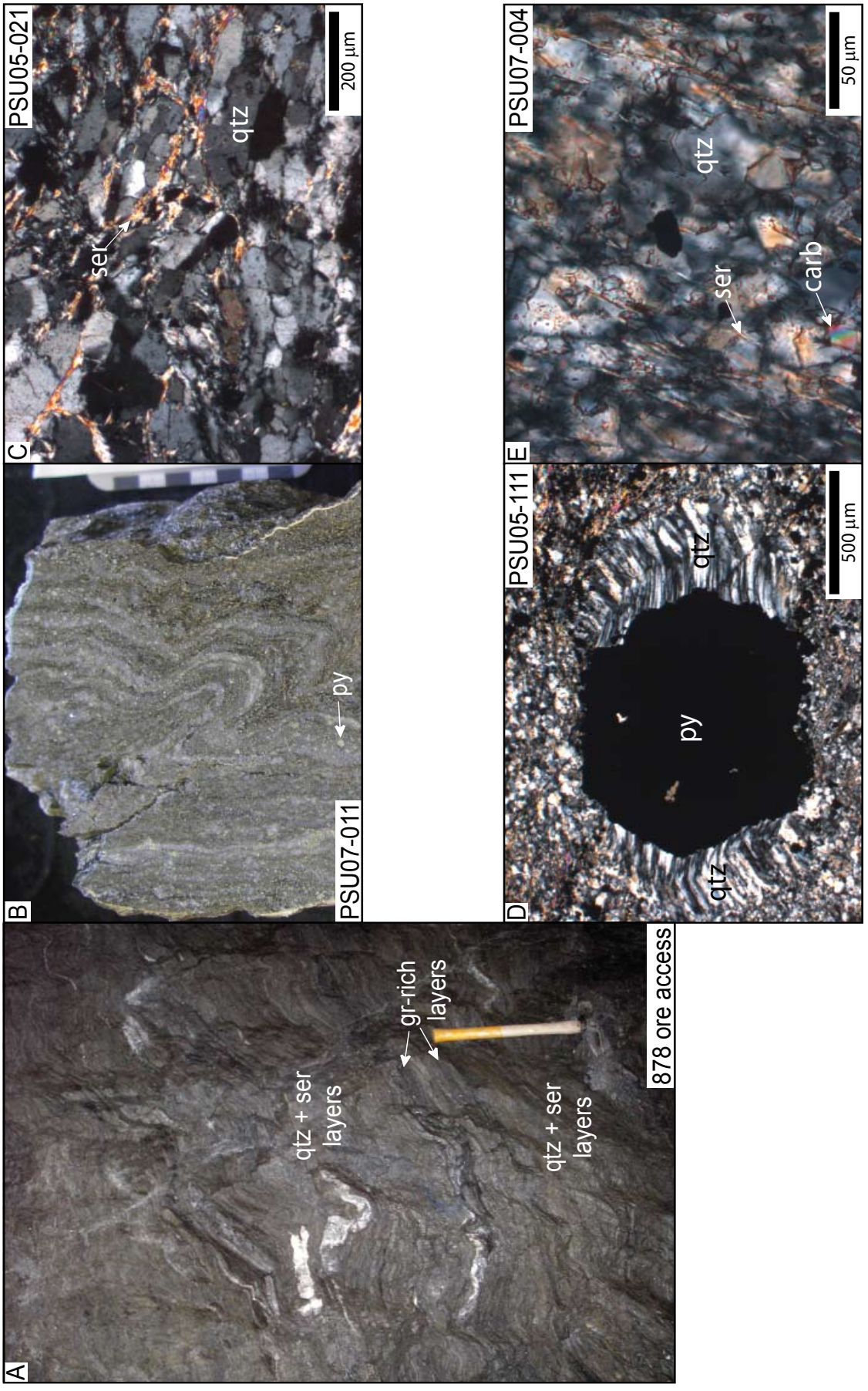
A
qtz + ser layers
gr-rich layers
qtz + ser layers
878 ore access
B
PSU07-011
py
C
PSU05-021
ser
qtz
200 µm
D
PSU05-111
qtz
py
qtz
500 µm
E
PSU07-004
qtz
ser
carb
50 µm

Figure 102 Representative photographs from the quartz–sericite alteration zone, protolith lithology C2.
(A) Layered texture slightly obscured but still visible indicating a clastic protolith. Two layer types are recognized: quartz–sericite rich (qtz+ser) and graphite rich (gr). Yellow portion of handle is approximately 18 cm long. (Approximately mine long section 4600 and cross section 4600, 758 ore access in the Northwest West ore zone).

(B) Layered texture still visible indicating a clastic protolith. This sample has significant pyrite (py) but, because the layering is visible, is not in the quartz–pyrite alteration zone. Scale bar is in cm. (Mine long section 4445 and cross section 4946, 668 ore access in the Northwest West ore zone).

(C) Photographmicrograph (XPL) of quartz grains (qtz) with sericite. (Mine long section 6060 and cross section 1105, 4211 cross-cut).

(D) Photographmicrograph (XPL) quartz filled (qtz) strain shadow surrounding a coarse-grained pyrite (py). (675 ore access in the Central West ore zone).

(E) Photographmicrograph (XPL) of fine-grained dolomite within a quartz–sericite groundmass. (Mine long section 4798 and cross section 4810, 878 ore access in the Northwest West ore zone).

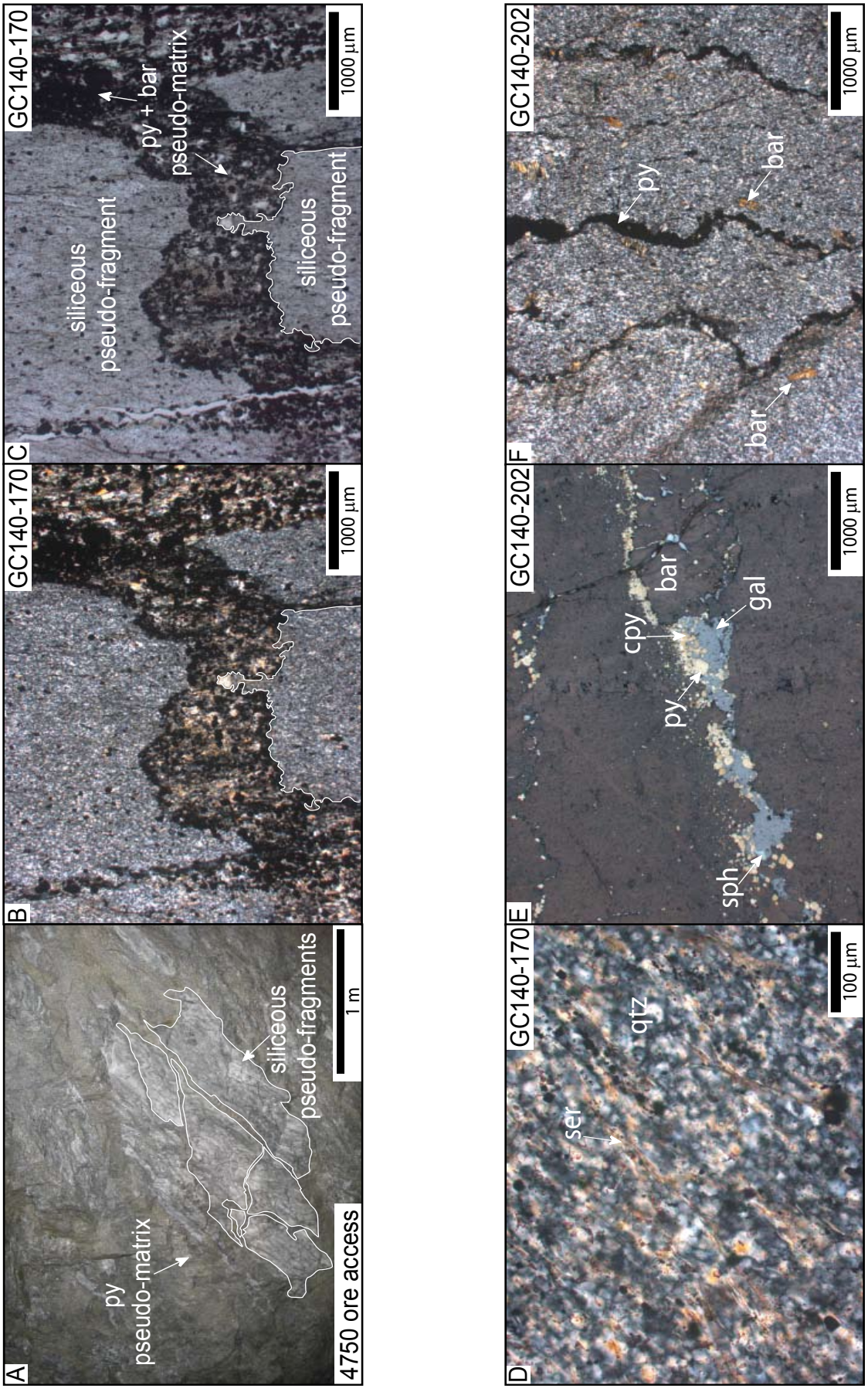
A
py
pseudo-matrix
siliceous
pseudo-fragments
1 m
4750 ore access
B
GC140-170
1000 µm
C
GC140-170
siliceous
pseudo-fragment
py + bar
pseudo-matrix
siliceous
pseudo-fragment
1000 µm
D
GC140-170
ser
qtz
100 µm
E
GC140-202
cpy
bar
py
gal
sph
1000 µm
F
GC140-202
py
bar
bar
1000 µm

Figure 103 Representative photographs from the quartz–pyrite alteration zone, protolith units C2 and Tr1.
(A) Pseudo-breccia texture with pseudo-fragments up to one metre across in a pyritic (py) pseudo-matrix. Note the jigsaw fit of the pseudo-fragments. (Approximately mine long section 4600 and cross section 5000, 4750 ore access in the Northwest West ore zone).

(B&C) Photographmicrographs (B–XPL and C–PPL) of pseudo-breccia texture. Note pseudo-fragment margins are intricately defined by pyrite (py) and barite (bar) mineralogy and may represent folded stringer veins. (2501685E, 2280072N, East ore zone, underground drill hole GC140 at 170 feet (51.5 m)).

(D) Photographmicrograph (XPL) of fine-grained quartz (qtz) with minor sericite (ser). (2501685E, 2280072N, East ore zone, underground drill hole GC140 at 170 feet (51.5 m))

(E) Photographmicrograph (RL) of a barite + galena (gal) + chalcopyrite (cpy) + pyrite ± sphalerite (sph) vein. The vein cuts across quartz–sericite-rich rock which is typical of the quartz–pyrite alteration zone. (2501685E, 2280072N, East ore zone, underground drill hole GC140 at 202 feet (61.2 m)).

(F) Photographmicrograph (XPL) of fine-grained quartz-rich rock with pyrite stringer veins throughout. Note 100–200 µm barite laths throughout photographmicrograph. (2501685E, 2280072N, East ore zone, underground drill hole GC140 at 202 feet (61.2 m)).

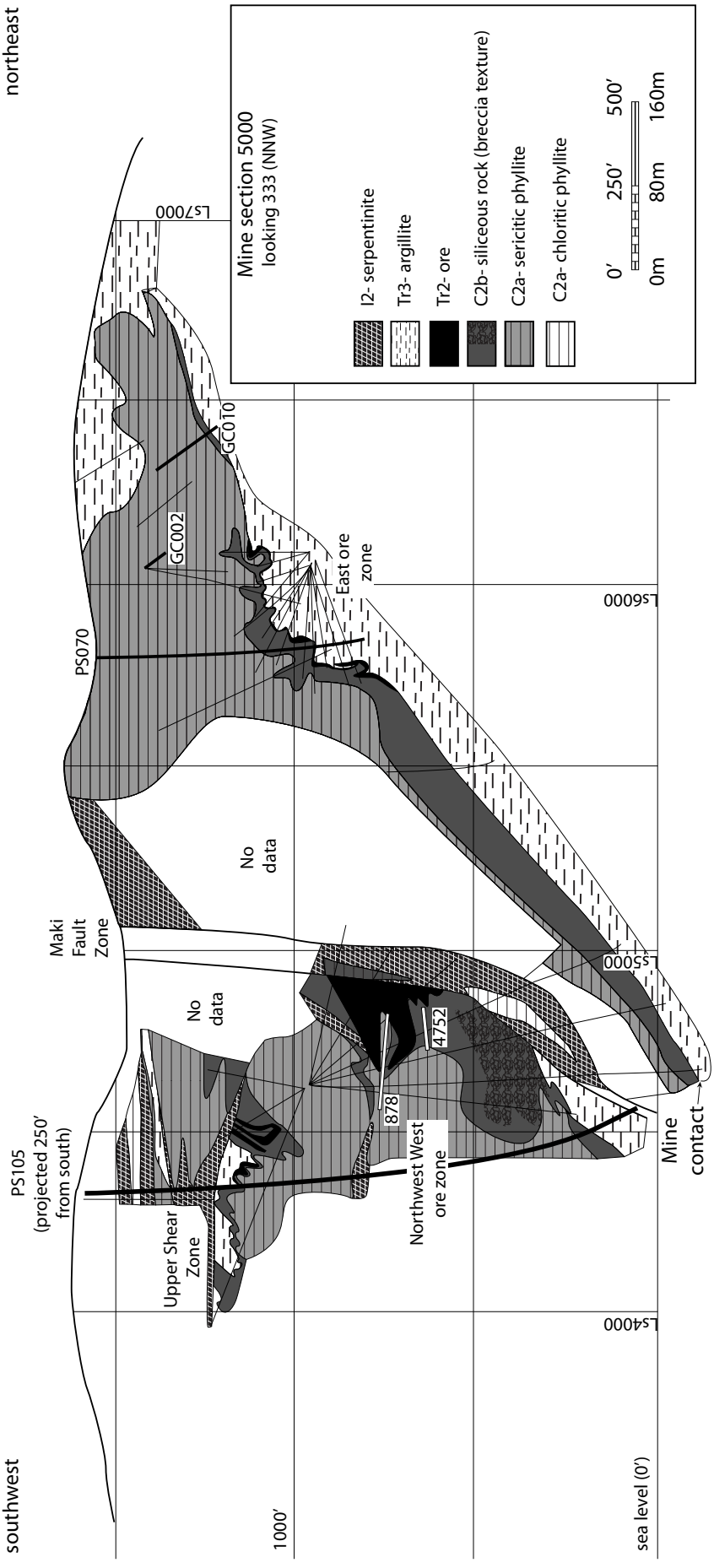

Figure 104 Southwest–northeast cross-section 5000 (200 feet (60 m) data window) through the northern end of the Greens Creek deposit. In the vicinity of the East Ore, the quartz–pyrite alteration zone is typically <75 feet (23 m) thick and remnant clastic textures are common. On the west side of the Maki Fault, the Northwest West and West ore zones have thicker quartz–pyrite alteration zones and pseudo-brecciated to massive textures are more common.

the monomict pseudo-breccia to massive quartz - pyrite alteration of the C2b lithology is more common in the Northwest West and West ore zone.

Spectral characteristics of the footwall lithologies

Methods

For the spectral study, the majority of samples were collected from the layered footwall lithology (C2) which is the most common footwall lithology found within the mine. A few samples of the footwall breccia unit (Tr1) and the massive volcanic unit (C1) were also analyzed. A set of property-wide samples, largely from the massive footwall unit (C1), was chosen to represent the least altered background facies and diamond drill hole PS193 from approximately 1 km northwest of the mine was found to best represent the downhole characteristics of a relatively unaltered section of the footwall. Rock samples were analyzed with a TerraSpec spectroradiometer using RS^3 version 4.0.23 software. Radiation in the visible to near-infrared wavelengths (300–1299 nm) and the mid-infrared wavelengths (1300-2500 nm) portions of the spectrum was measured. Hydrous minerals such as clays, white mica, chlorite and epidote have characteristic absorption features only within the mid-infrared range and therefore only wavelengths 1300–2500 nm were used in the interpretation of spectral features (Clark, 1999). The spectra of each analysis were compared against reference spectra using The Spectral Geologist (TSG) version 5.00.066 software. Spectral parameters such as wavelength, depth and reflectance of absorption features were automatically calculated from either the hull quotient-corrected spectra or reflectance spectra and all spectra were manually checked. The TSG software automatic identification of minerals was checked manually and generally agreed with that found by detailed petrographic study of a representative suite of samples. The main difference being in thin section only white mica (sericite) was identified and, with SWIR spectra, several species of K-white mica such as illite, muscovite and phengite, and paragonite were identified.

Sample preparation for the TerraSpec spectrometer was minimal. Generally, three readings were taken per sample, one on a flat (sawn) surface perpendicular to the dominant foliation, one on the dominant (usually S2) foliation surface and one on the outside of the core or hand sample. These three analyses were individually examined and, when all three were similar, the mean of the three analyses for each parameter calculated was used. The complete spectral data set is in Appendix 4. Where the spectra identified different minerals (typically a white mica and chlorite) two spectra were kept for that sample and two sets of parameters calculated. Rock samples were predominantly pale grey to green with few dark or opaque minerals such as graphite and leucoxene, to suppress spectral features. The main exception to this is samples with abundant pyrite which is typical within 30 feet (10 m) of mineralization. These proximal samples were often too dark to give reasonable spectra. The relatively simple mineralogy and absence of clay minerals, such as kaolinite or dickite, aided the identification of minerals and absorption features in the AlOH and FeOH bands were typically clean and clearly visible.

Definition of white mica and chlorite

White micas are very common in alteration mineral assemblages in VHMS systems and their complex chemical structure includes a wide range of compositions. Muscovite and paragonite can be expressed as:

$$(K,Na)^{it}_{2}(Al,Fe,Mg)^{vi}_{4}(Si, Al)^{iv}_{8}O_{20}(OH)_{4}$$

Where it, iv and vi represent the interlayer, tetrahedral and octahedral sites respectively (Yang, 1998). Na-rich white mica, paragonite, is the result of substitution of Na for K in the interlayer site (Deer et al., 1992; Guidotti and Sassi, 2002). For effective Na–K substitution, high temperatures (>600°C) are required and, as a result, paragonite has been reported proximal to mineralization (i.e. Herrmann et al., 2001). However, in HCL-H_2O-Al_2O_3-K_2O-$Na_2O(SiO_2)$ hydrothermal systems, paragonite also has a large stability field from 150°-300°C (Bowers et al., 1984). K-rich white micas are more common in acidic (pH 4 to 6), low- to moderate-temperature hydrothermal systems (<600°C) and compositional variation in these white micas is partly controlled by

Tschermak substitution of Mg and/or Fe for Al in the octahedral site and Si for Al in the tetrahedral site (Yang, 1998). These phengitic white micas range in composition from end-member muscovite, $K_2Al(Si_6Al_2)O_{20}(OH)_4$ to end-member celadonite, $K_2(Mg, Fe^{2+})_2(Al,Fe^{3+})_2Si_8O_{20}(OH)_4$ (Guidotti and Sassi, 2002). However, it is important to note that phengite, as defined in some of the literature as an intermediate composition - $K_2(Mg, Fe)_2Al_3(AlSi_7)O_{20}(OH)_4$, is not appropriate due to the miscibility gap in the muscovite - celadonite series (Yang, 1998). Another important variation in K-rich white micas is the formation of illite at temperatures <300°C by the substitution of $Si^{iv}X^{it}$ for $Al^{iv}K^{it}$, where X^{it} represents and interlayer vacancy (Yang, 1998). Four white mica species were identified in the Greens Creek rocks using the TSG software: paragonite, muscovite, phengite and illite. These mineral identifications have not been confirmed with other analytical techniques. In thin section and hand sample, the white mica species were all identified as sericite.

Chlorite is also a very common mineral in VHMS systems and in low- to moderate-grade metamorphic rocks, especially in rocks of mafic composition. In metamorphic environments, chlorite forms below temperatures of approximately 400°C and a several kilobars pressure (Deer et al., 1992). Chlorite can be expressed as:

$$(Mg,Fe^{2+},Fe^{3+},Mn,Al)_{12}[(Si,Al)_8O_{20}](OH)_{16}$$

The main compositional varieties of chlorite are clinochlore (Mg-rich chlorite), chamosite (Fe-rich chlorite) and pennanite (Mn-rich chlorite) (Deer et al., 1992). Mg↔Fe substitutions result in a wide range of compositions that can generally be expressed as varying combinations of end members clinochlore $(Mg_{10}Al_2)(Si_6Al_2O_{20})(OH)_{16}$, and chamosite $(Fe^{2+}_{10}Al_2)(Si_6Al_2O_{20})(OH)_{16}$. Three varieties of chlorite were identified at the Greens Creek Mine using TSG software: Fe chlorite, Mg chlorite and intermediate chlorite composed of an unspecified amount of the Fe and Mg members. In thin section and hand specimens, chlorite was not subdivided.

White mica and chlorite spectral characteristics

White micas have two easily observed absorption features, the most diagnostic of

which is the main AlOH absorption feature in the 2204 ± 24 nm range. There is also a secondary AlOH absorption feature in the 2392 ± 48 nm range. The main AlOH peak (2204 ± 24 nm) is commonly evident even in samples with a high noise to signal ratio and is very useful in mineral identification.

Shifts in the wavelength position of the AlOH peak in white micas have been shown to be related to Al content (Clark, 1999). For example, AlOH peak positions <2195 nm result from high proportions of Al (and corresponding low proportions of Mg-Fe) while AlOH peak positions >2216 nm reflect low proportions of Al (and correspondingly higher Mg-Fe contents). Generally, paragonite has an AlOH peak position between 2180 nm and 2195 nm, muscovite and illite have AlOH peak positions between 2200 nm and 2208 nm and phengite has an AlOH peak position between 2216 nm and 2228 nm (Herrmann et al., 2001). In analyses where more than one white mica phase is present or where white micas have intermediate compositions, the AlOH peak position will be intermediate between the above three ranges.

Chlorite has two main diagnostic absorption features, the first is located between 2235 nm and 2255 nm and associated with the FeOH absorption and the second is located between 2320 nm and 2360 nm and is associated with MgOH absorption. The peak position of the absorption features varies with chlorite composition. The shortest wavelength peak positions are associated with Mg-rich chlorite and the longest wavelength peak positions are associated with Fe-rich chlorites (Pontual et al., 1997).

Systematic shifts in the peak position of chlorites with respect to proximity to mineralization have been documented by several studies (Herrmann et al., 2001; Jones et al., 2005). In these cases, the chlorite became more Mg-rich towards mineralization and the subtle shift in the chlorite compositions results in shifts in the position of the FeOH and MgOH absorption peaks. These shifts in the absorption peaks can be used to

distinguish hydrothermal chlorite from metamorphic chlorite as regional metamorphic chlorite is typically more Fe-rich (Jones et al., 2005).

In samples without white mica, the MgOH and FeOH absorption peak wavelengths are easily recognizable but, in samples with white mica, the secondary 2340 nm absorption peak of the white mica obscures the exact position of the MgOH absorption peak. As a result, in the present study chlorite compositions were estimated only from the FeOH absorption peak.

Results of SWIR analysis

This study analyzed over 500 samples from across the property with an emphasis on samples from either within underground workings or from diamond drill holes into the deposit. The results of these analyses are used to characterize the alteration mineralogy associated with the hydrothermal alteration in the footwall of the Greens Creek deposit. First, the bulk-rock control on alteration mineralogy was examined. Then the background white mica and chlorite spectral features were compared and contrasted with the features seen in rocks proximal to mineralization. In general, SWIR spectra were of good quality with simple mineralogy dominated by white mica and chlorite which resulted in easily recognized absorption features.

White mica and chlorite spectral variation

Typical SWIR spectra collected for white mica and chlorite are shown in Figure 105 and Figure 106. Figure 105 illustrates the approximately 20 nm decrease in the wavelength position of the AlOH absorption peak with proximity to mineralization. Figure 106 illustrates a very weak increase to no change with proximity in the FeOH absorption peak. In general, there is a wide range of compositions within the white micas with shifts in the wavelength position of the AlOH peak from 2195 nm to 2228 nm while the range in compositions of chlorite appears to be fairly stable with shifts in the FeOH absorption peak position between 2259 nm and 2251 nm. The variation in the AlOH peak position in the white micas suggests a compositional variation from paragonite,

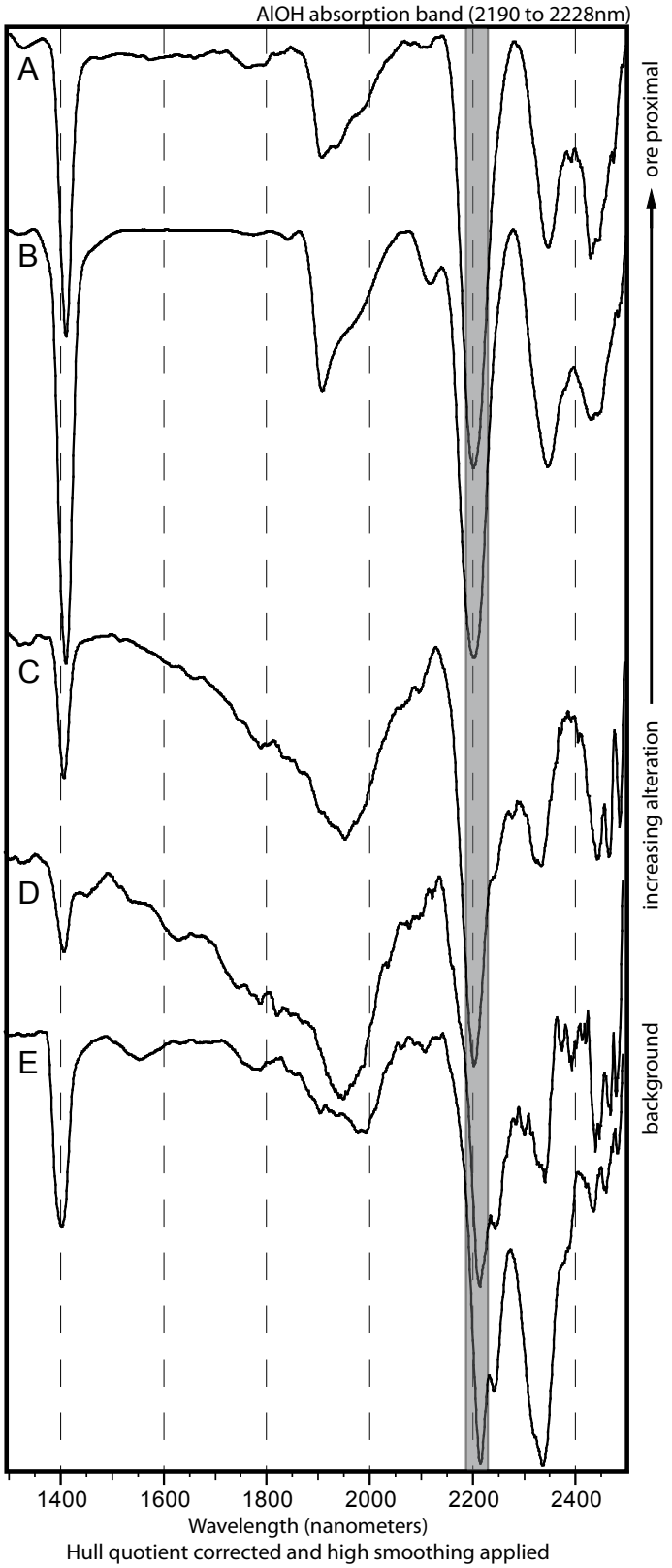

Figure 105 Typical SWIR spectra from the Greens Creek area illustrating the range of AlOH peak positions for white mica in regional samples through to samples proximal to mineralization. (A) white mica, sample PSU07-034, Northwest West ore zone; (B) white mica, sample GC010-191, East ore zone; (C) white mica + trace chlorite, sample PSU05-046, 4211 cross-cut; (D) white mica and chlorite, sample PS276-227, East ore zone; (E) white mica and chlorite, sample PSA05-022, 3.6 mile (km 5.8) B-road.

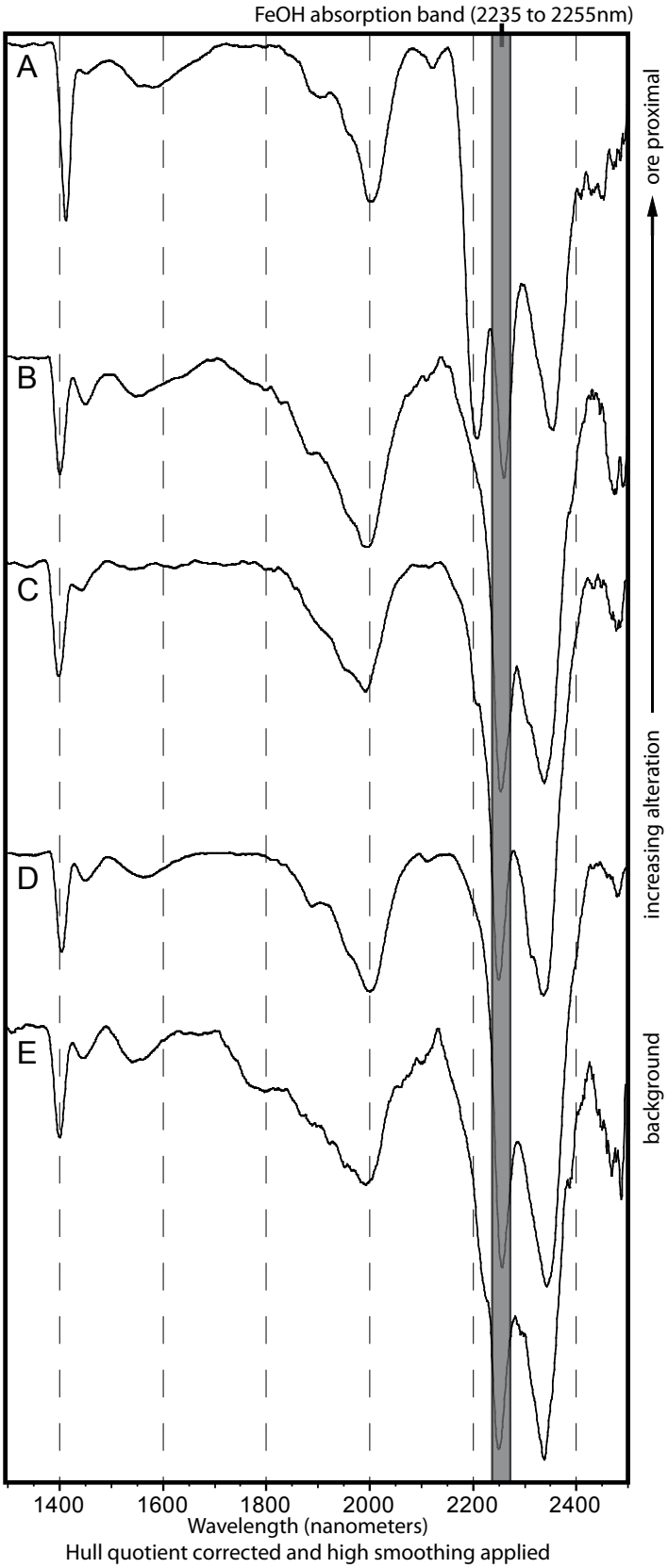

Figure 106 Typical SWIR spectra from the Greens Creek area illustrating the range of FeOH peak positions for chlorite in regional samples through to samples proximal to mineralization. (A) white mica and chlorite, sample GC056-000, East ore zone; (B) chlorite, sample PS276-585, East ore zone; (C) chlorite, sample PS276-372, East ore zone; (D) chlorite, sample PS276-084, East ore zone, East ore zone; (E) chlorite, sample PSU05-056, 4211 cross-cut.

to muscovite and phengitic micas. The restricted range of the FeOH absorption peak suggests the composition of the chlorites is dominantly Mg-rich to intermediate chlorite (Table 27).

Table 27 White mica and chlorite AlOH and FeOH wavelength variation in the footwall rocks to the Greens Creek deposit.

Unit	Alteration zone	White mica AlOH wavelengths	Chlorite FeOH wavelengths
C1	chlorite	2208 - 2229 nm average: 2221 nm	2253 - 2257 nm average: 2253 nm
C2	chlorite	2197 - 2229 nm average: 2216 nm	2246 - 2256 nm average: 2252 nm
	sericite	2193 - 2228 nm average:2207 nm	2248 - 2256 nm average: 2252 nm
	quartz - sericite	2189 - 2227 nm average: 2208 nm	2247 - 2251 nm average: 2248 nm
	quartz - pyrite	2201 - 2220 nm average: 2212 nm	2250 - 2253 nm average: 2252 nm
Tr1	quartz - pyrite	2191 - 2226 nm average: 2210 nm	2251 - 2253 nm average: 2252 nm

The histograms in Figure 107 and Figure 108 show the full range of AlOH and FeOH wavelengths measured and illustrate the differences in AlOH and FeOH wavelengths for white mica and chlorite in footwall lithologies C1, C2 and Tr1. Results from footwall lithology I1 are omitted because white micas and chlorite are not found in this lithology. The histograms indicate the difference in the wavelength position of the AlOH absorption peak between background samples and samples proximal to mineralization, as well as the consistent and fairly narrow range of FeOH absorption peak positions regardless of protolith or proximity to mineralization. For example, the AlOH absorption peak, in samples from the quartz–sericite alteration of C2, is located in a fairly restricted range with most samples between 2206 and 2212 nm. In comparison, samples from C2 in the least altered chlorite alteration zone have a wide range between 2205 and 2230 nm.

The histograms broadly suggest that both bulk-rock composition and proximity to alteration influence the composition of white micas while the composition of chlorite

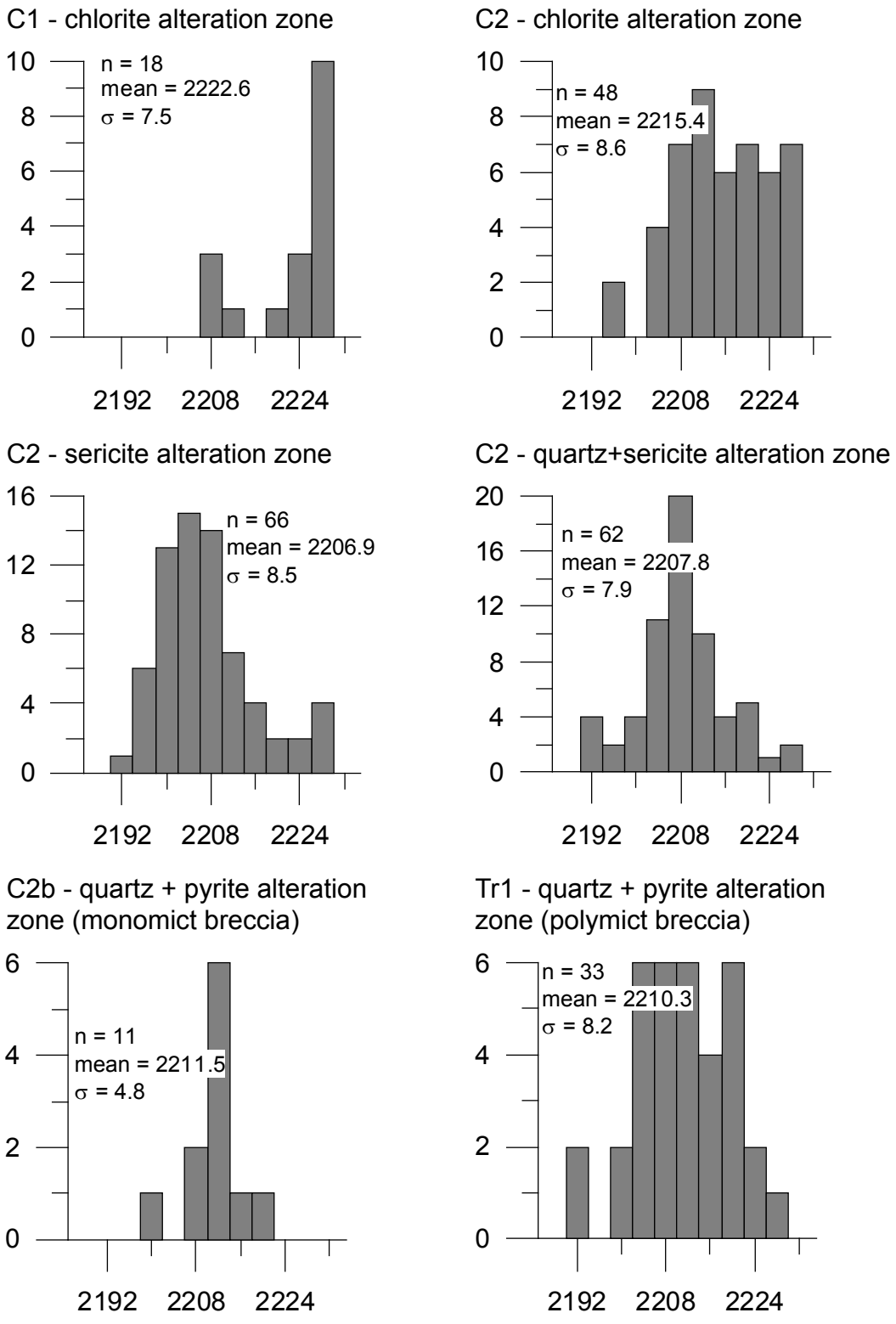

Figure 107 Histograms illustrating the variation in wavelength position of the AlOH absorption feature of white micas in proximal to distal samples from the footwall to the Greens Creek deposit. σ = standard deviation from the mean.

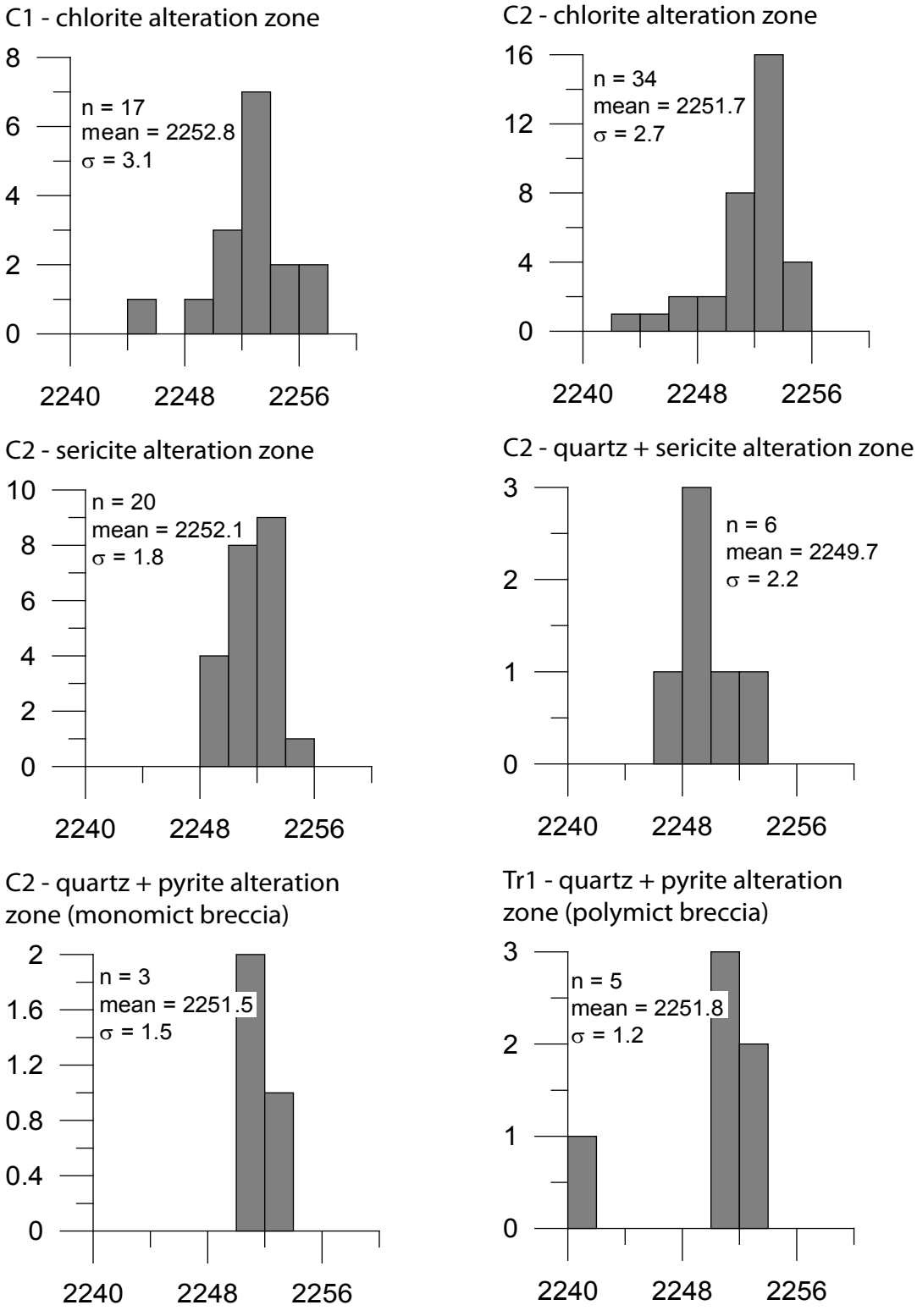

Figure 108 Histograms illustrating the variation in wavelength position of the FeOH absorption feature of chlorite in proximal to distal samples from the footwall to the Greens Creek deposit. σ = standard deviation from the mean.

is largely controlled by bulk-rock composition and is not effected by proximity to alteration. Changes in mineral compositions probably reflect varying water/rock ratios. Background samples are rock buffered with the bulk-rock composition controlling the composition of both the white mica and chlorite. In samples proximal to mineralization, the white mica composition is fluid buffered and chlorite is below the detection limit (less than 10% of samples have identifiable chlorite spectra in the quartz–sericite and quartz–pyrite alteration zones).

Bulk-rock control on white mica–chlorite spectral characteristics

The bulk-rock control on white mica spectral features appears to be greatest in distal or background samples. Figure 109 shows three graphic logs, the first (A) from a moderately to strongly altered sequence in the East ore zone, the second (B) from a weakly to moderately altered sequence in the East ore zone and the third (C) from a weakly altered sequence in the Bruin prospect located approximately 1 km northwest of the mine portal.

In the first log (GC010), the white mica AlOH wavelength position show little variation throughout the sequence despite significant variations in Ti/Zr ratio. In the sericite-altered layered clastic portion, the AlOH wavelength position is typically between 2200 and 2210 nm. In the chlorite-altered portion of the layered clastic rocks, the AlOH is markedly higher with values >2220 nm. In the second log (PS276), the AlOH wavelength position again shows little variation in relation to lithology changes but in this hole the absorption feature position is significantly higher with values between 2220 and 2230 nm. Within approximately 100 feet (30 m) of mineralization, the values decrease to between 2212 and 2220 nm. In the third log (PS193), the AlOH wavelength position changes markedly with lithology changes. The chlorite altered layered clastic rocks with significant graphitic layers have wavelength positions of 2195 to 2210 nm while the chlorite-altered massive volcanic rocks range from 2224 to 2228 nm. These plots suggest that bulk-rock composition is an important first order control on white

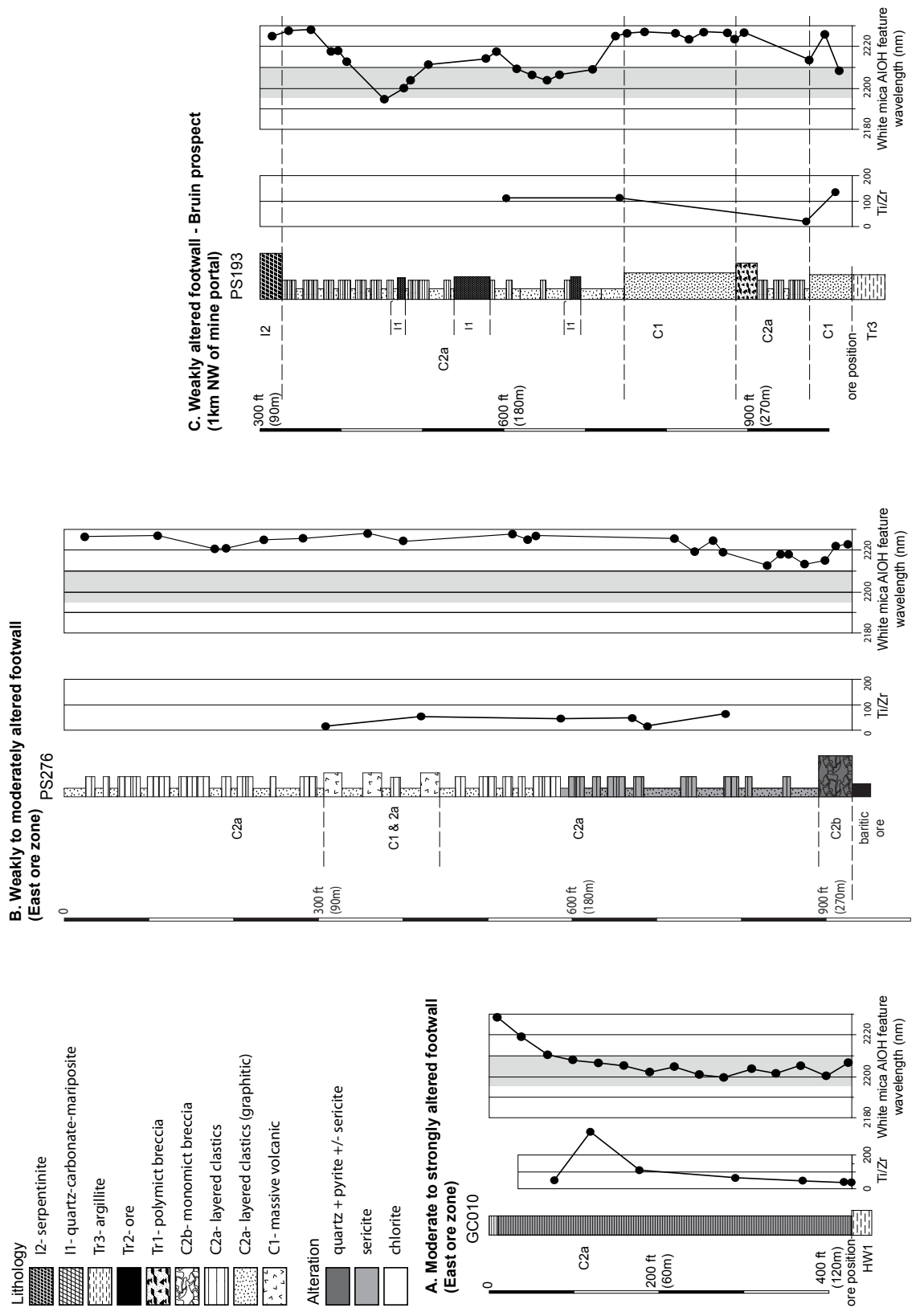
Lithology
I2- serpentinite
I1- quartz-carbonate-mariposite
Tr3- argillite
Tr2- ore
Tr1- polymict breccia
C2b- monomict breccia
C2a- layered clastics
C2a- layered clastics (graphitic)
C1- massive volcanic
Alteration
quartz + pyrite +/- sericite
sericite
chlorite
A. Moderate to strongly altered footwall (East ore zone)
GC010
C2a
200 ft (60m)
400 ft (120m)
ore position
HW1
Ti/Zr
White mica AlOH feature wavelength (nm)
B. Weakly to moderately altered footwall (East ore zone)
PS276
C2a
C1 & 2a
C2a
C2b
baritic ore
300 ft (90m)
600 ft (180m)
900 ft (270m)
C. Weakly altered footwall - Bruin prospect (1km NW of mine portal)
PS193
I2
I1
C2a
C1
C2a
C1
Tr3
ore position

Figure 109 Graphic logs and plots illustrating the relationship between lithology, intensity of alteration and the wavelength position of the AlOH absorption feature of white mica. Note the depth on the scale is distance in feet from the collar. (A) A sequence in a moderately to strongly altered portion of the East ore zone. (B) Drill hole PS276, shows a weakly to moderately altered zone. The wavelengths of the AlOH absorption feature of white mica are generally >2220 nm except within approximately 150 feet (45 m) of mineralization. (C) Drill hole PS193 is in an area of weak alteration. Lithological differences are shown by the Ti/Zr plot and shifts in the wavelength of the AlOH absorption feature of white mica appear to match the lithological changes.

mica compositions in weakly altered zones or regional areas, but is less important in zones of stronger hydrothermal alteration.

Within the footwall to the Greens Creek deposit, AlOH wavelengths typically decrease towards the hanging wall–footwall contact. Least-altered samples typically have AlOH wavelength positions between 2225 and 2230 nm indicating phengitic white mica compositions. Moderately altered samples have a wide range of AlOH feature positions ranging from 2206 to 2230 nm indicating compositions between phengite and muscovite. The highly altered samples have the lowest AlOH positions, between 2200 and 2215 nm indicating the white micas are dominantly muscovite.

Other studies show similar shifts in white mica compositions with lithology changes. For example, McLeod and Stanton (1984) showed that the Mg/(Mg+Fe+Mn) content of white micas changes with that of other coexisting phyllosilicates in several Paleozoic VHMS deposits including Captains Flat, Colo Creek, Que River, Rosebery and Woodlawn. In larger regional-scale studies, using spectroscopy, the octahedral aluminium content of white micas was also shown to vary with host lithology (Sabine, 1999). Clearly, in rocks not strongly altered by hydrothermal alteration, the bulk-rock composition is an important first order control on white mica composition and must be carefully considered when interpreting downhole spectral variation.

White mica spectral variation with increasing alteration

The Greens Creek deposit is structurally complex with at least five phases of deformation (Proffett, in press) and cross-sections of the deposit are typically the most useful for examining the geology. However, due to restricted sampling access in the present study, data density is too low to create realistic cross-sectional alteration maps based on SWIR characteristics within the footwall. For these reasons, the most instructive and applicable use of the SWIR spectra data, from the present study, is in plotting downhole variation.

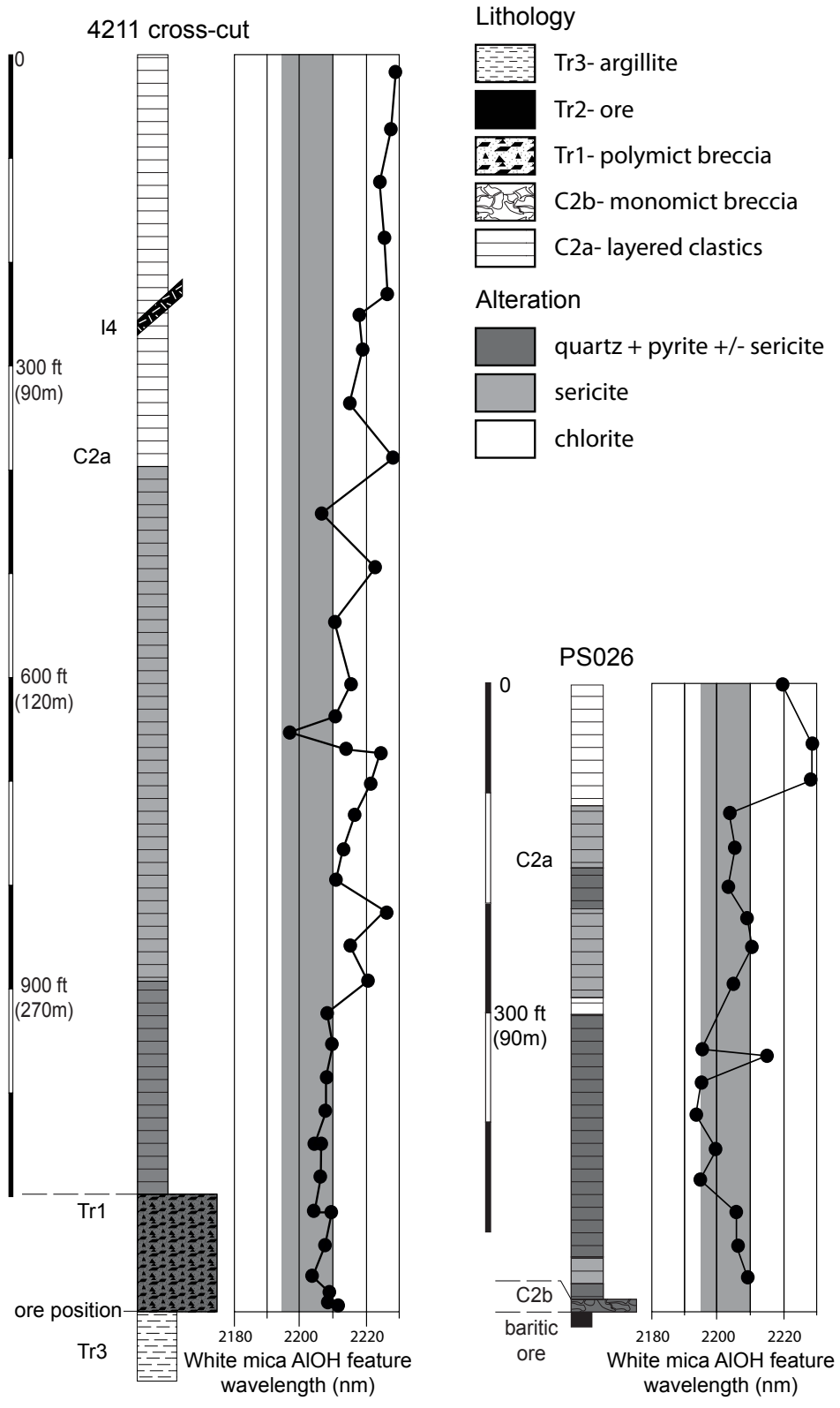

Figure 110 Graphic logs illustrating the decreasing wavelength position of the AlOH absorption feature for white mica in samples proximal to mineralization. Note the depth on the scale is distance in feet from the collar in the case of PS026 and distance along the drive for the 4211 cross-cut. In the 4211 cross-cut log, the wavelengths of the AlOH absorption feature decrease from background values of 2227–2215 down to 2210–2203 nm in samples proximal to ore. In diamond drill hole PS026, in the East ore zone, the AlOH position in the three most distal samples ranges from 2220 to 2228 nm. Near mineralization, these values decrease to between 2210 and 2195 nm.

Figure 110 illustrates the downhole shifts in white mica AlOH wavelength position with proximity to mineralization. White mica AlOH wavelength positions have values <2210 nm proximal to ore, but increase to values >2215 nm between 300 feet (90 m) and 450 feet (135 m) from the footwall–hanging wall contact. Systematic variation in white mica AlOH position provides a useful exploration vector in the footwall and can be used to define alteration zones approaching the footwall–hanging wall contact.

White mica alteration index (WMAI)

The White Mica Alteration Index (WMAI), as defined by van Ruitenbeek et al. (2005), is the ratio between abundance of white mica and abundance of chlorite. The WMAI is also a measure of Al content of white micas. The equation for the WMAI is:

(1) $WMAI = D_{AlOH}/(D_{AlOH} + D_{FeOH})$

The abundance of white mica is determined by the depth of the AlOH absorption feature (D_{AlOH}) and the abundance of chlorite is the depth of the FeOH feature (D_{FeOH}). Figure 111 illustrates the features described in equations 2–5. The van Ruitenbeek definitions of D_{AlOH} and D_{FeOH} are:

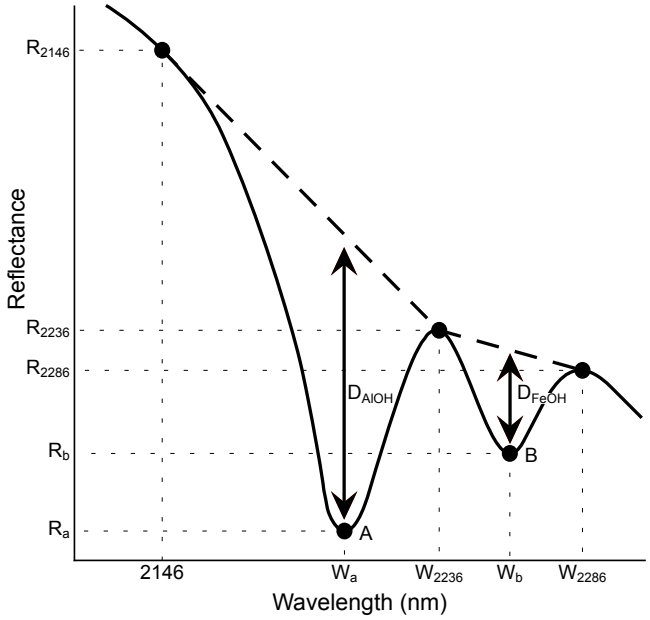

Figure 111 Reflectance spectrum showing spectral parameters that were determined from near-infrared reflectance spectra. D_{AlOH} is depth of the AlOH feature (Clark, 1999), D_{FeOH} is the depth of the FeOH feature (modified from van Ruitenbeek et al., 2005), A is reflectance minimum of the AlOH absorption feature, B is the reflectance minimum of the FeOH absorption feature, R_x is the reflectance at wavelength x and W_y is the wavelength position of feature y.

(2) $D_{AlOH} = R_{2146}–[(W_a\text{-}2146/90)*(R_{2146}–R_{2236})] - R_{Wa}$

(3) $D_{FeOH} = R_{2236}–[(W_b\text{-}2236/50)*(R_{2236}–R_{2286})] - R_{Wb}$

This equation has been modified to account for small variations in the position of the 2236 and 2286 nm peaks. In order more accurately measure the depth of the AlOH and FeOH features. The definition of the WMAI used in the present study is:

(4) $D_{AlOH} = R_{2146}–[((R_{2146}–R_{2236})/(W_{2236}–2146))*(W_b–2146)] - R_{Wa}$

(5) $D_{FeOH} = R_{2236}–[((R_{2236}–R_{2286})/(W_{2286}–W_{2236}))*(W_b–2236)] - R_{Wb}$

where: W_{2236} = wavelength of the peak position at 2236 ± 10 nm

W_{2286} = wavelength of the peak position at 2286 ± 10 nm

The WMAI can be used as a measure of hydrothermal alteration intensity and has been used to trace fossilized hydrothermal pathways (van Ruitenbeek et al., 2005). Values for the WMAI range from zero in samples without an AlOH feature, to one in samples without an FeOH feature (Table 28). Values >0.75 indicate that white micas dominate the spectrum whereas values <0.50 indicate that chlorite dominates, intermediate values indicate a mixture of chlorite and white mica.

Table 28 Range of WMAI and AlOH values grouped according to distance from footwall–hanging wall contact. Distance to the contact was calculated by measuring the angle between the drill hole or drift and the contact locally and making the appropriate geometric correction so that all samples are located at an approximately perpendicular distance.

interval	<100 feet (30 m)	100-300 feet (30-90 m)	300-500 feet (90-150 m)	>500 feet (150 m)	regional
n	163	146	42	18	9
std dev	0.18	0.24	0.26	0.27	0.25
mean WMAI	**0.93**	**0.88**	**0.80**	**0.59**	**0.17**
n	162	145	41	18	7
std dev	7.7	10.4	8.2	10.6	2.4
mean AlOH	**2207.2**	**2209.3**	**2214.2**	**2219.3**	**2227.5**

WMAI values for the Greens Creek footwall are lowest in the samples furthest from mineralization (ranging from 0 to 0.5) and are highest in samples proximal to

mineralization (ranging from 0 to 1.0). Table 28 shows the range of WMAI values and AlOH positions for samples in the footwall. The mean WMAI value increases with proximity to the footwall–hanging wall contact (Figure 112).

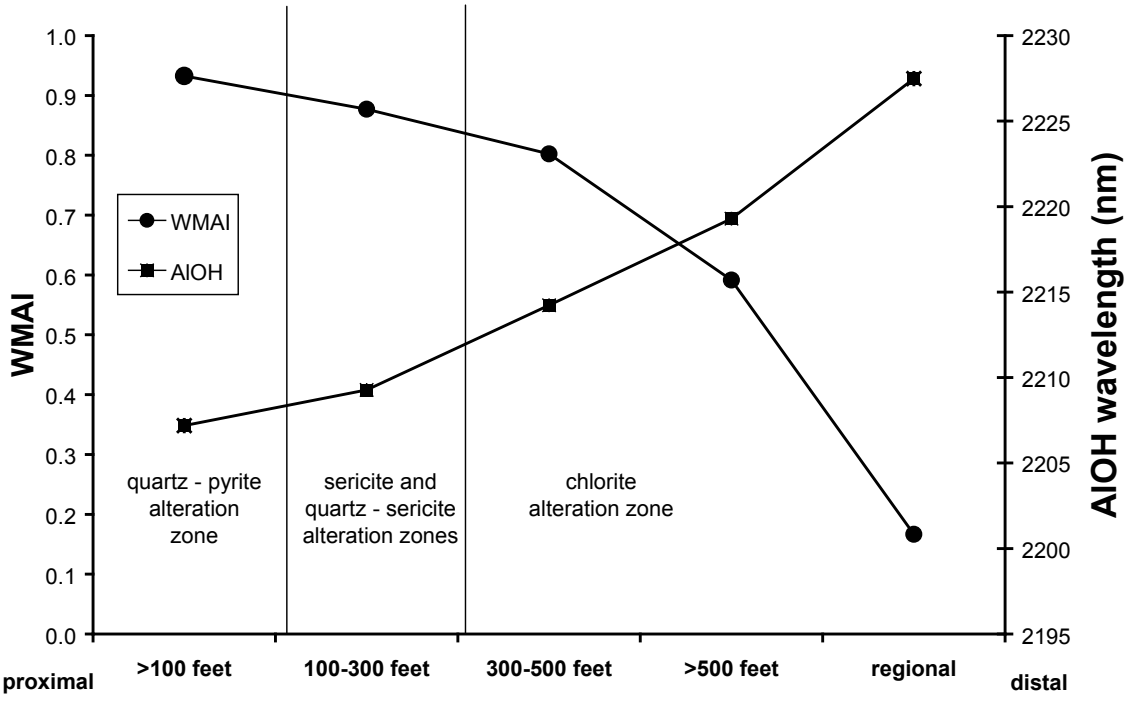

Figure 112 Increase of the mean WMAI values and decreasing AlOH position with proximity to the footwall–hanging wall contact. Error bars have been omitted for clarity but errors are in Table 28. The mean WMAI value of samples within 500 feet (150 m) of the contact is >0.75. This indicates white mica dominates over chlorite in the spectra and corresponds to a decrease in the AlOH position which indicates a shift from phengite composition to muscovite composition.

The increase in the WMAI value and decrease of AlOH value with respect to corrected distance to the footwall–hanging wall contact broadly corresponds to the alteration zones which were defined earlier in the chapter with the exception of the chlorite zone that has significant systematic variation of WMAI and AlOH values within it. The background and least-altered zone is the chlorite alteration zone which can be further subdivided into three distances from the ore position: regional samples, samples within the mine workings but >500 feet (>150 m) from the mine contact and samples 300 to 500 feet (90–150 m) from the mine contact. Regional samples from the chlorite alteration zone have a mean WMAI value of 0.17 and a mean AlOH position of 2227 nm, samples >500 feet (150 m) have a mean WMAI value of 0.59 with a mean AlOH

position of 2219 nm, and samples 300 to 500 feet (90–150 m) have a mean WMAI of 0.80 and an AlOH mean of 2214 nm. The sericite and quartz–sericite alteration zones correspond with samples located approximately 100 feet to 300 feet (30–90 m) from the contact that have a mean WMAI values of 0.88 and a mean AlOH value of 2209 nm. The most intensely altered zone is the quartz–pyrite zone, which has a mean WMAI value of 0.93 and a mean AlOH value of 2207 nm and roughly corresponds to a distance of <100 feet (30 m) from the footwall–hanging wall contact.

WMAI values in samples within the chlorite alteration zone, where bulk-rock composition significantly affects the AlOH position of white micas, are remarkably consistent with values of 0.63 ± 0.1 despite large shifts in the AlOH position with changes in lithology (Figure 113). These WMAI values indicate that both white mica and chlorite are present in the spectra and that the ratio of the two remains consistent even with lithology changes. This is consistent with the C1 and C2 lithologies being volcanogenic and basaltic. WMAI values in samples from alteration zones more proximal to mineralization show a similar consistency but, with higher values of 0.83 ± 0.29, reflect the dominance of white mica in the spectra (Figure 113).

Geochemical characteristics of the footwall lithologies

Methods

Two of the three sample sets used in the immobile-element characterization of Chapter 3 are used in this section to characterize the mobile elements in the footwall lithologies. The details of these sample sets are summarized here; for a full description see Chapter 3. Two-hundred and thirty nine samples were collected for the present study from across the property, with detailed sample collection from the footwall to the East ore and the Northwest West ore. One-hundred and nineteen of these samples were analyzed using XRF at the University of Tasmania and 120 were analyzed at the Acme Analytical laboratory in Vancouver. Major and trace-element whole-rock analyses were determined either with Inductively Coupled Plasma (ICP) techniques at

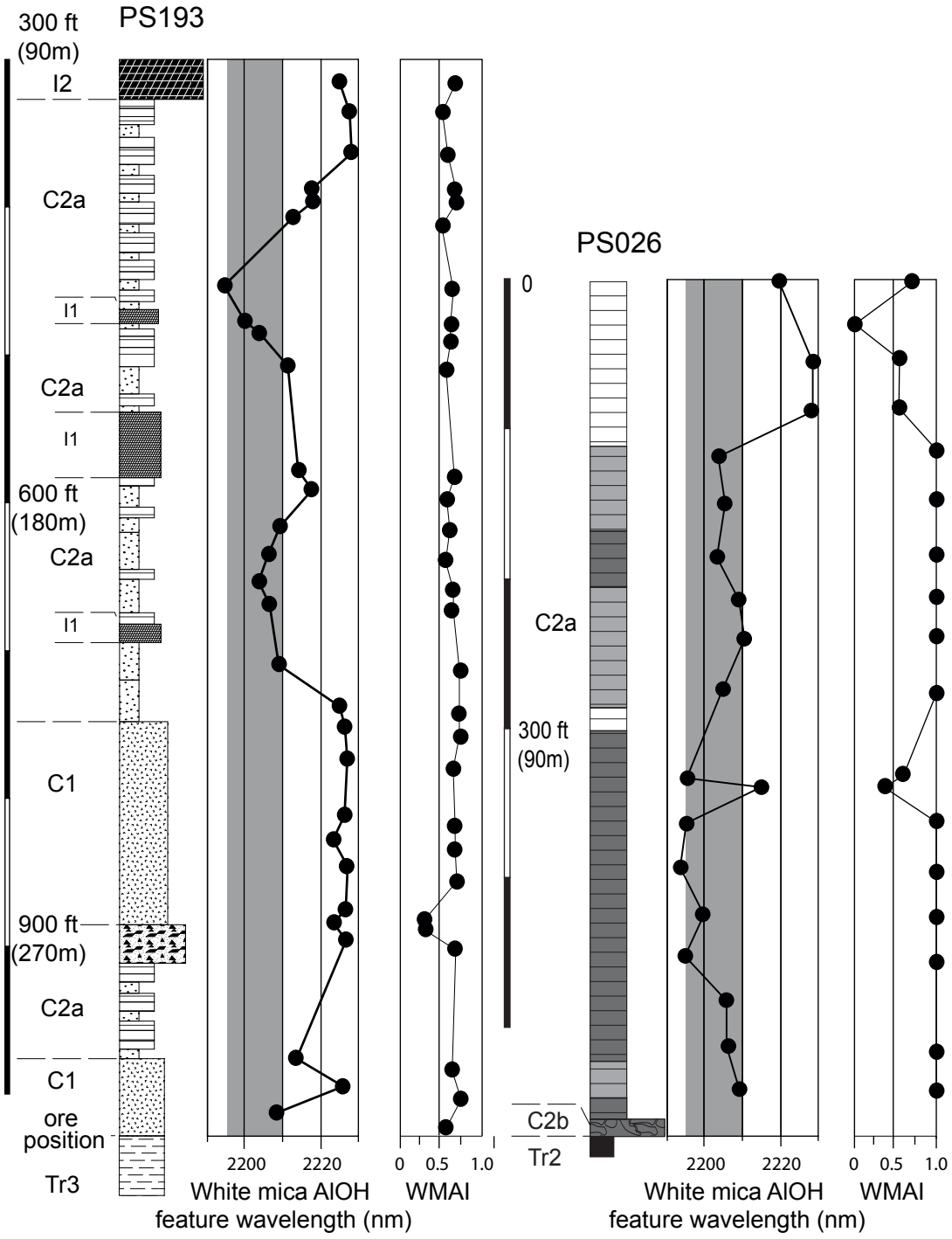

Figure 113 Graphic logs illustrating the consistency of WMAI values, despite the dependence on llithology of the AlOH absorption feature in white mica, in samples distal to mineralization (PS193). A similar consistency in WMAI value occurs in holes where bulk-rock composition has less effect on the AlOH wavelength position but the WMAI values are significantly higher (PS026). Note the scale is distance in feet from the collar. Lithology and alteration are the same as Figure 109.

Acme Analytical in Vancouver using the Group 4A-4B methods, or carried out using the X-Ray Fluorescence (XRF) technique. These techniques are described in detail in Chapter 3. The three geochemical data sets are tabled in Appendix 2.

This combined sample set is representative of the range of lithological and alteration types found within the footwall both at the property scale (an area approximately 100 km^2) and at the mine proximal scale (up to 1000 feet (300 m) into the footwall). The complex structural nature of the geology and the location of drill holes precluded investigation of the entire stratigraphy along a single section. The lithological breakdown of the geochemical samples is given in Table 4 of Chapter 3.

Comparison of analytical techniques

Seven samples have been analyzed using both the ICP and the XRF techniques. Samples TasBas, Dior4 and Dol7 are well characterized in-house standards at the University of Tasmania that have been analyzed multiple times with several techniques. The values reported are the values from the best technique for that element. The other four samples, PSA05-01, -04, -12 and PSA06-15, were collected during this study and analyzed with both methods. These samples have been analyzed only once with each method and are less well characterized.

This section will focus on major and trace-elements that are considered mobile during hydrothermal alteration (i.e. Pearce, 1996). The major-elements, reported in weight percent (wt%), discussed in this section are SiO_2, Fe_2O_3, MgO, CaO, Na_2O, K_2O, MnO and S. Total Fe is reported as Fe_2O_3 in this discussion and in all data tables. The trace-elements, in parts per million (ppm), include Ba, Sn, Cu, Pb, Zn, Tl and Sb. Comparing data from the same seven standards described in Chapter 3, the ICP and XRF data are typically within 5% for the major-elements. Major oxides MgO, CaO and MnO and trace-elements Sn, Cu, Pb, Zn, Tl and Sb show fairly large discrepancies between the accepted (or XRF) values and the ICP values when the analyses were near the limit of detection. However, when the analyses were above the detection limits, the quality was

much better. The lower quality analyses for major-elements were typically for values <0.1% and for values <1 ppm for trace-elements. See Table 29, Figure 114 and Figure 115 for comparisons of ICP and XRF data. Both the XRF and ICP data sets were used in the investigation of the footwall mobile element geochemistry, keeping in mind that the ICP data was of poorer quality near the detection limit. When investigating the mobile elements, the method outlined in Gifkins et al. (2005) was used, in particular the data set was not normalized prior to investigation.

Alteration geochemistry of the footwall

The geochemical character of the mobile elements within the footwall to the Greens Creek deposit is based on the variation within units C1 and C2. Footwall unit Tr1 is not included because it is a polymict breccia in which the clast composition is highly variable and therefore consistent compositions cannot be determined. Unit I1 is volumetrically minor with very few samples analyzed in the present study.

Table 29: Summary statistics comparing ICP and XRF data. UTas standards are samples TasBas, Dior4 and Dol7; Greens Creek duplicates are samples PSA05-01, -04, -12 and PSA06-15.

		Utas standards			GC standards			Combined standards		
Element		Mean difference	Mean difference (%)	std dev (%)	Mean difference	Mean difference (%)	std dev (%)	Mean difference	Mean difference (%)	std dev (%)
SiO2	%	-0.01	1.4%	1.2%	-0.33	-0.4%	1.1%	-0.17	0.5%	0.0%
Fe2O3	%	-0.02	0.3%	1.8%	0.00	1.6%	2.3%	-0.01	0.9%	0.4%
MgO	%	-0.81	1.4%	2.6%	0.10	24.0%	30.4%	-0.35	12.7%	19.7%
CaO	%	0.06	1.7%	1.8%	-0.06	-38.9%	46.4%	-0.00	-18.6%	31.6%
Na2O	%	0.08	2.7%	1.9%	0.04	9.0%	15.1%	0.06	5.8%	9.3%
K2O	%	0.05	2.4%	2.4%	0.10	-2.7%	12.1%	0.07	-0.2%	6.9%
MnO	%	0.00	2.7%	2.5%	0.01	17.5%	14.5%	0.00	10.1%	8.5%
S	%	0.00	8.6%	8.3%	0.00	0.0%	0.0%	0.00	4.3%	0.0%
Ba	ppm	0.64	-0.6%	4.9%	-45.16	-3.3%	3.7%	-22.26	-1.9%	0.8%
Sn	ppm	1.11	26.2%	15.0%	0.73	26.2%	25.1%	0.92	26.2%	7.1%
Cu	ppm	5.20	14.0%	9.8%	-4.63	7.4%	23.9%	0.29	10.7%	10.0%
Pb	ppm	4.30	30.9%	17.9%	-0.45	-8.1%	31.5%	1.92	11.4%	9.6%
Zn	ppm	21.48	17.9%	11.4%	27.38	40.1%	30.7%	24.43	29.0%	13.6%
Tl	ppm	0.26	51.6%	21.3%	N/A	N/A	N/A	0.26	51.6%	21.3%

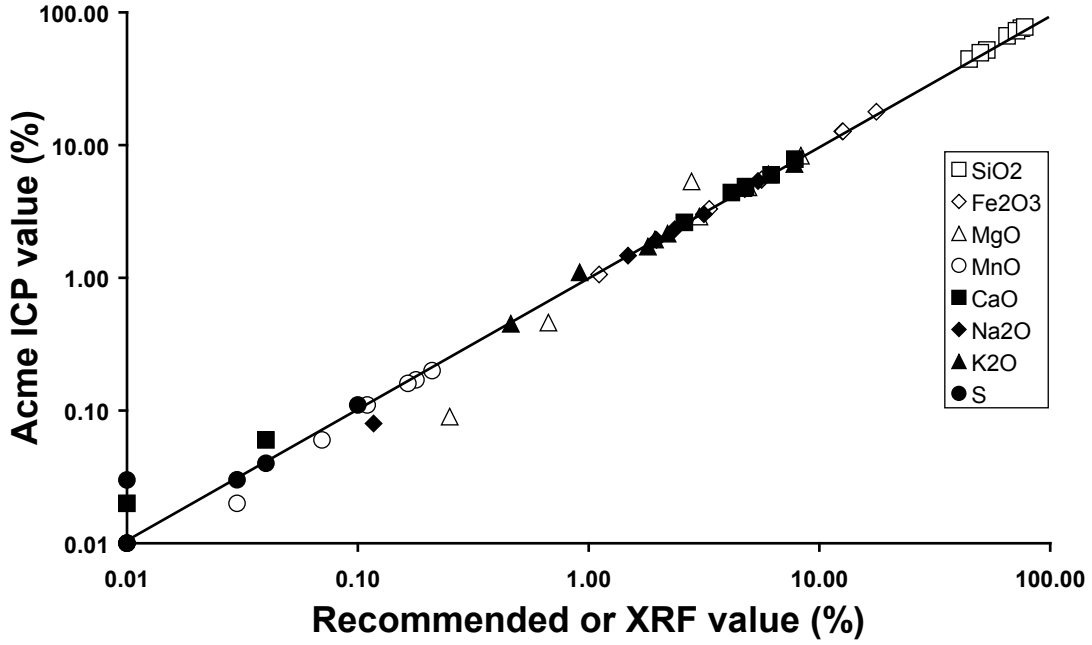

Figure 114 A plot of mobile major-elements for seven samples analyzed by both XRF and ICP.

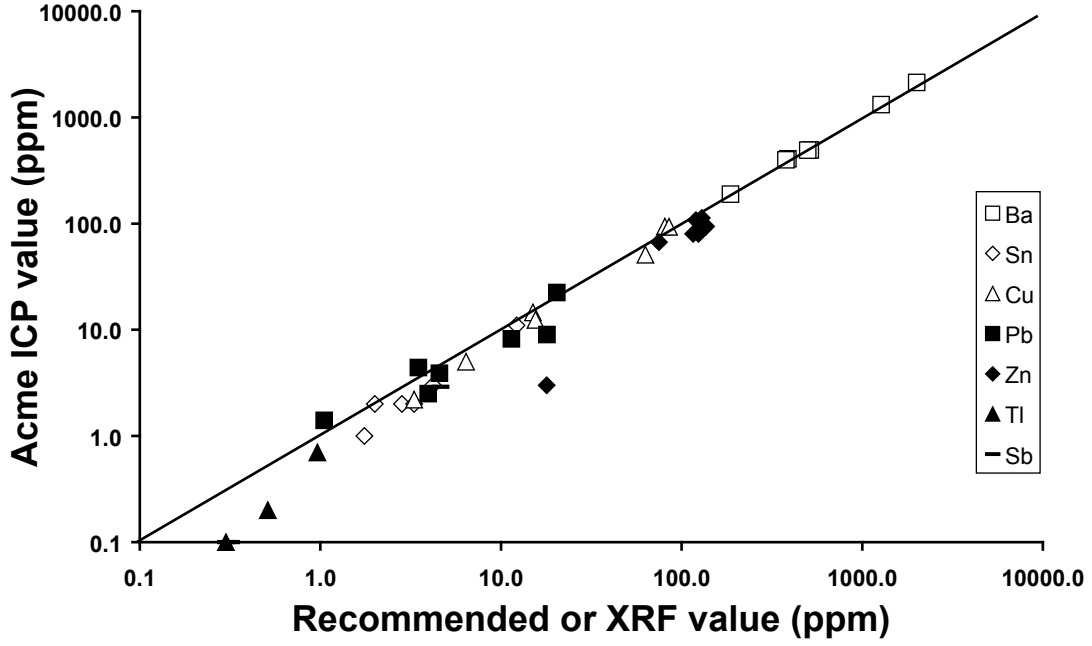

Figure 115 A plot of mobile trace-elements for seven samples analyzed by both XRF and ICP.

Major-element variations

Within hydrothermal alteration and greenschist facies metamorphism, the major oxides SiO_2, Fe_2O_3, MgO, CaO, Na_2O, K_2O, and MnO are typically mobile (Pearce, 1996). As described in the first half of this chapter, the footwall rocks have undergone

widespread sericite and silica alteration. In the quartz–pyrite alteration zone, the most intense alteration recognized, alteration minerals can comprise up to 100% of the rock. Although alteration is widespread throughout the footwall, the clastic nature of most of the footwall lithologies (C2? and Tr1) means that it is difficult to identify the initial composition.

The alteration within the footwall to the Greens Creek deposit is characterized by the changes in the relative abundance of quartz and sericite typically at the expense of chlorite and feldspar. This alteration is reflected by the increase in whole-rock SiO_2, the decrease in Na_2O, Fe_2O_3, MgO and MnO contents and the increase in K_2O of footwall unit C2 (Figure 116). CaO has a similar pattern to Na_2O when plotted against SiO_2, and MgO and MnO have similar patterns to Fe_2O_3 versus SiO_2. Only Na_2O, Fe_2O_3 and K_2O are plotted against SiO_2 to illustrate these patterns. The four alteration facies within the layered footwall unit have wide ranging compositions (Figure 116). The graphitic phyllite member of the C2a lithology is not included in these geochemical alteration plots as it is interpreted as sedimentary.

Analyses of samples from the quartz–pyrite alteration zone (Figure 116) are the most intensely altered with heavy silicification and variably K_2O enriched as demonstrated by their high SiO_2 contents of up to 86% and K_2O up to 3.5%. These quartz–pyrite altered rocks typically have the lowest Na_2O, CaO, Fe_2O_3, MgO and MnO with values respectively as low as 0.01%, 0.01%, 4.7%, 0.2% and 0.01%. These low values reflect the quartz-dominated alteration mineralogy with secondary sericite, no observable chlorite and rare feldspar phenocrysts and only minor carbonate. Samples from the quartz–sericite alteration zone (Figure 116) have less SiO_2 with values ranging from 50% to 77%, similar K_2O and have slightly elevated Na_2O, CaO, Fe_2O_3, MgO and MnO when compared with analyses from the quartz–pyrite alteration zone. These less extreme values reflect the lesser abundance of quartz and increased abundance of sericite and carbonate.

The analyses of samples from the sericite zone (Figure 116) are highly varied with respect to all major-elements, possibly indicating either variable alteration effects or variable protolith compositions. SiO_2 values range from 20 to 80% and K_2O ranges from 0.4 to 5.4%. Na_2O, CaO, Fe_2O_3, MgO and MnO respectively range from 0.01 to 4.1%, 0.1 to 16.9%, 2.1 to 25.0%, 0.3 to 15.2% and 0.02 to 1.0%. The highly variable compositions of these samples reflect the variability in the mineralogy. Samples from the least altered chlorite alteration zone typically have SiO_2 contents within the basalt field of approximately 40–52% and K_2O values are variable between 0.1 and 5.6%. Na_2O and CaO contents are <5 and 10% respectively. Fe_2O_3 and MgO have similar ranges between approximately 2 and 20% while MnO ranges from 0.04 to 0.8%.

Downhole variations

The geochemistry of the 4211 cross-cut and diamond drill hole PS026 were investigated to examine the alteration trends approaching the hanging wall–footwall contact. The 4211 cross-cut was selected to represent a distal portion of the footwall that does not intersect mineralization while PS026, from the East ore zone, was selected to represent the proximal portion. This drill hole intersects approximately 25 feet (8 m) of white baritic ore which is Zn and Pb-rich.

The 4211 cross-cut is located near the Gallagher Fault zone on the western margin of mine development at the Greens Creek deposit and is the least-altered section of footwall rock examined. The drift is sub-horizontal, approximately 1200 feet (360 m) long and intersects all four alteration zones. The lithology is dominantly C2 with approximately 100 feet (30 m) of possible Tr1 breccia immediately below the ore position. SiO_2 is fairly consistent, slightly below 50%, with the exception of one polymict breccia sample which has 77% SiO_2 (Figure 117). Fe_2O_3, MgO, CaO and MnO are fairly consistent until approximately 200 feet (60 m) from the ore position where they typically decrease in content (Figure 117). Na_2O decreases, from approximately 3% to below detection, towards the ore position while K_2O increases up to 3% (Figure 117).

A

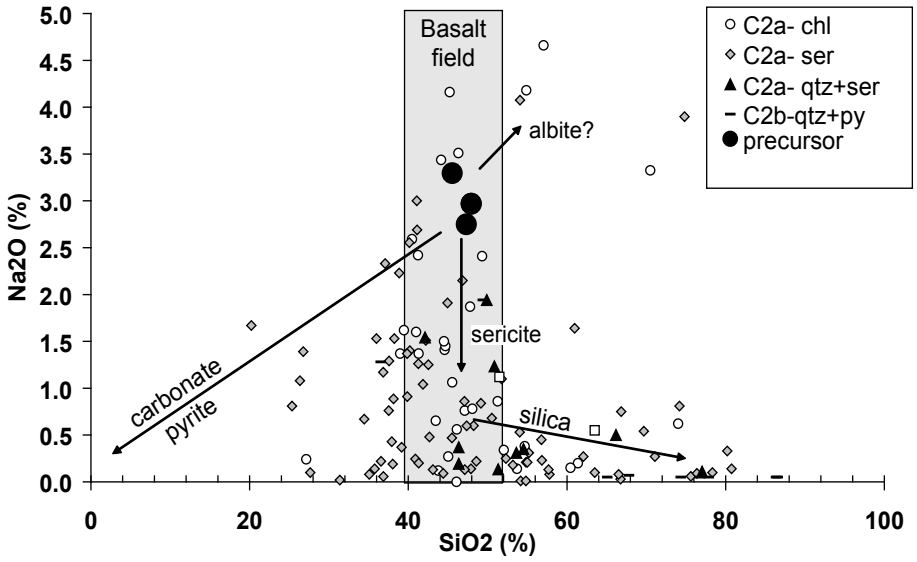
Basalt field
C2a- chl
C2a- ser
C2a- qtz+ser
C2b-qtz+py
precursor
albite?
sericite
silica
carbonate
pyrite
Na2O (%)
SiO2 (%)

B

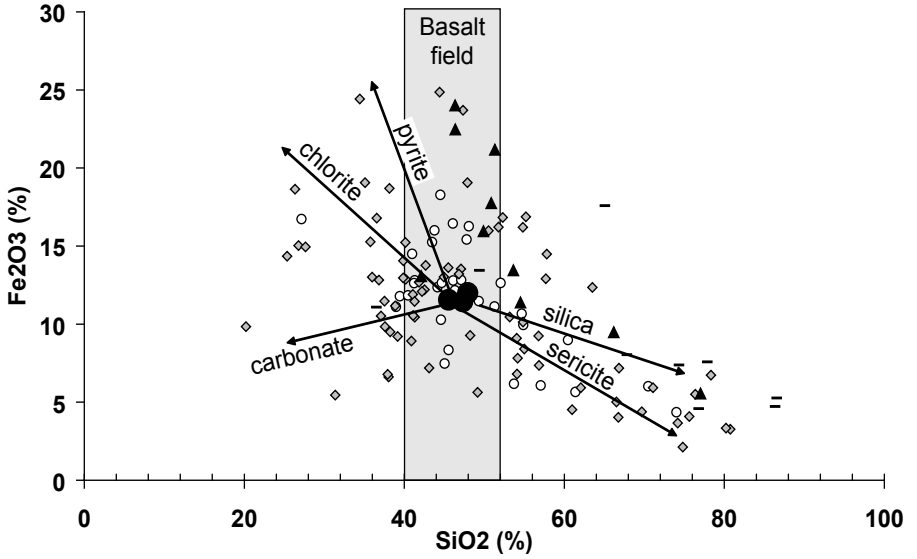
Basalt field
pyrite
chlorite
silica
sericite
carbonate
Fe2O3 (%)
SiO2 (%)

C

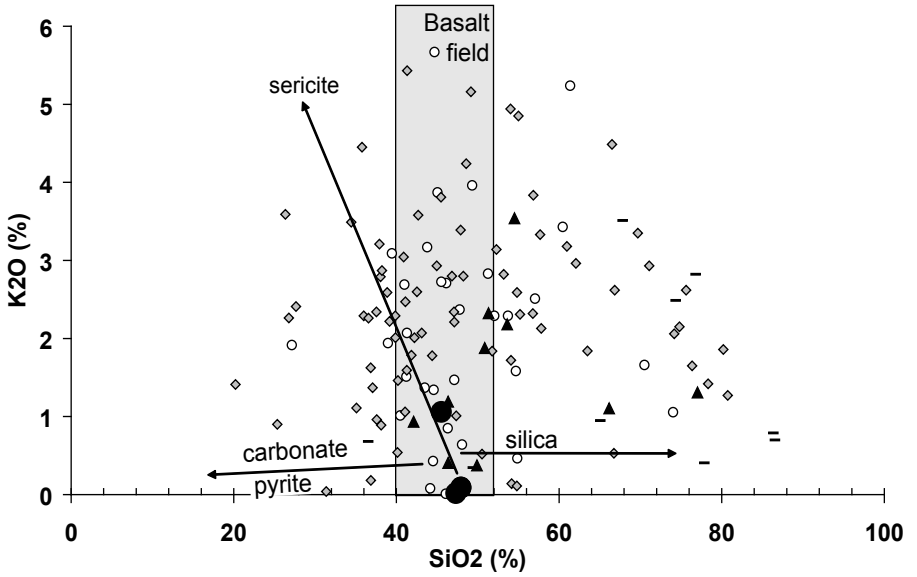
Basalt field
sericite
silica
carbonate
pyrite
K2O (%)
SiO2 (%)

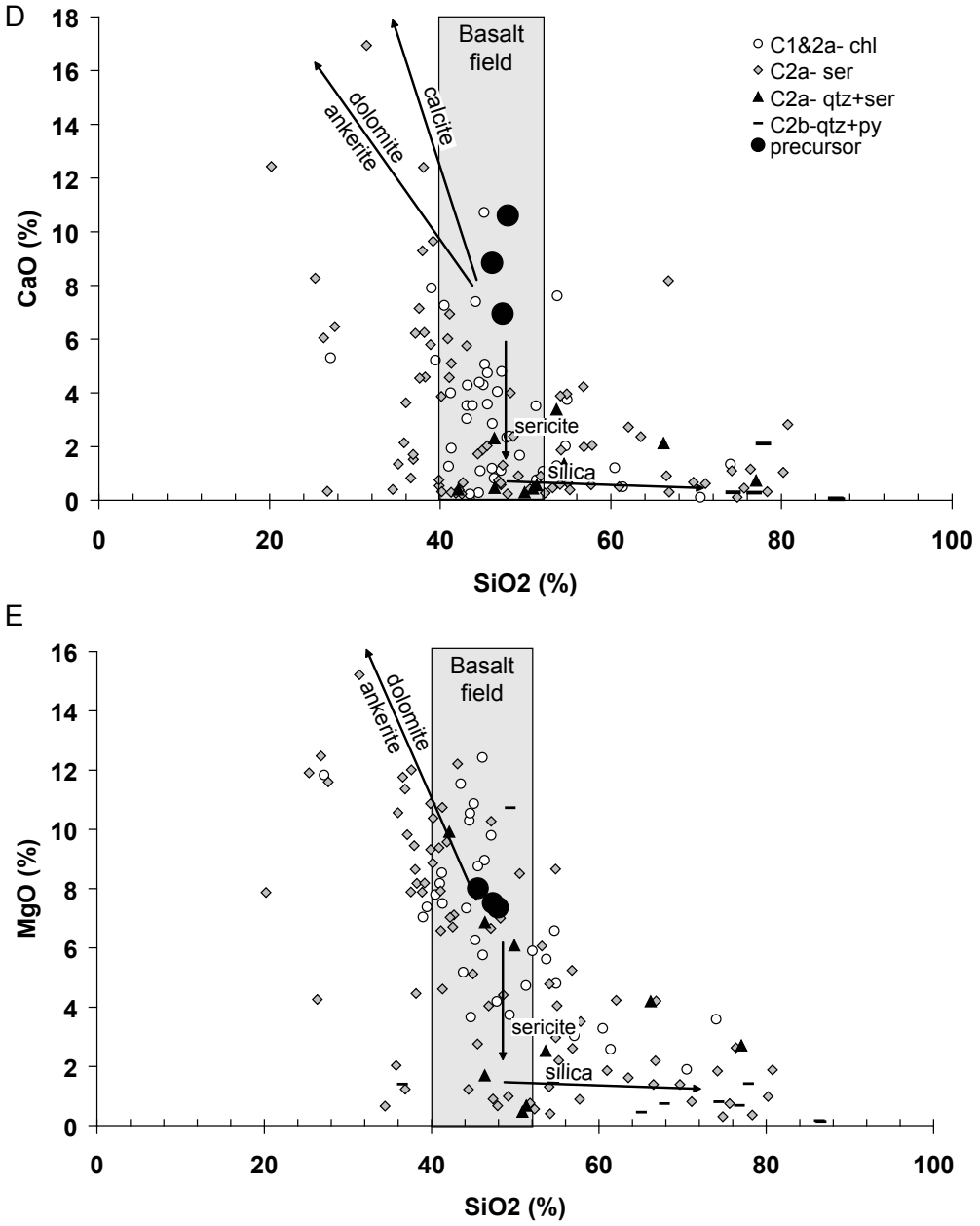

Figure 116 Whole-rock analyses of least-altered (heavy black circles) and altered samples from Greens Creek, illustrating the distribution of SiO_2, Na_2O, Fe_2O_3, K_2O, CaO and MgO. The distribution of these elements reflects the relative abundance of chlorite, sericite, carbonate and quartz in alteration. (A) Na_2O versus SiO_2 illustrating a decrease in Na_2O content with increasing alteration intensity, (B) negative correlation between Fe_2O_3 and SiO_2 illustrating both Fe_2O_3 enrichment and depletion relative to the least altered precursor samples, (C) K_2O versus SiO_2 illustrating an increase in K_2O content. (D) CaO versus SiO_2 illustrating a decrease in CaO content with increasing alteration intensity, (E) Negative correlation between MgO and SiO_2 illustrating both MgO enrichment and depletion relative to the least altered precursor samples. C2a- chl = lithology C2, chlorite alteration zone, C2a- ser = lithology C2, sericite alteration zone, C2a- qtz+ser = lithology C2, quartz–sericite alteration zone,C2a- qtz+py = lithology C2, quartz–pyrite alteration zone.

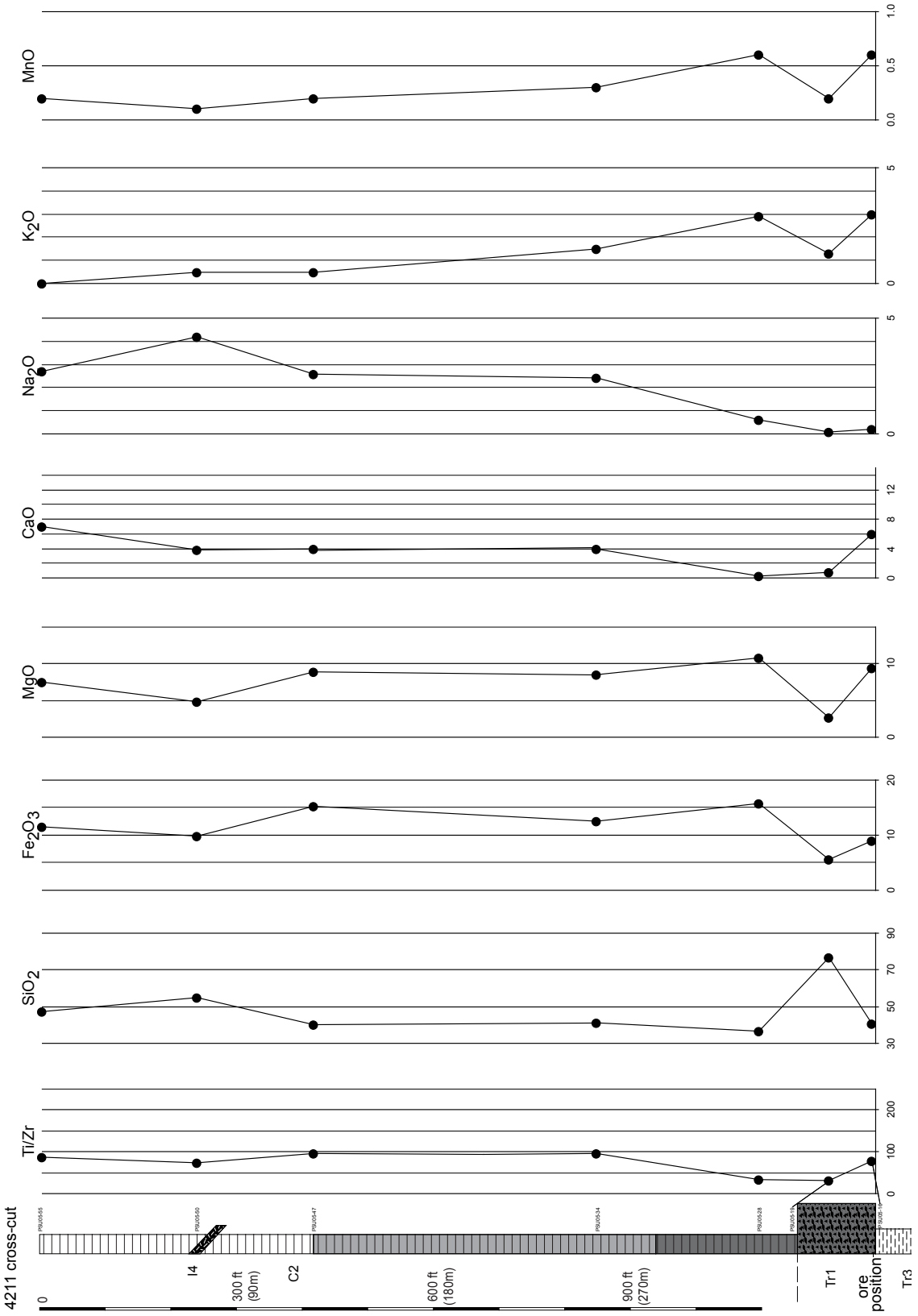

Figure 117 Downhole variation of major-element data along the 4211 cross-cut, distal to mineralization, on the western margin of the Greens Creek deposit. Lithology and alteration symbology same as Figure 109.

Diamond drill hole PS026 is located within the East ore zone on the eastern margin of the Greens Creek deposit and was selected to represent the footwall proximal to mineralization. This drill hole is oriented sub-vertical and intersects all four alteration zones within the footwall over an interval of approximately 600 feet (180 m). The stratigraphy in this portion of the deposit is overturned and the drill hole is collared in footwall rocks, intersects mineralization from approximately 605 feet to 625 feet (183.3 m to 189.4 m) and finishes in hanging wall rocks at a depth of 719 feet (217.9 m). Only the footwall portion of this hole was studied. Within approximately 300 feet (90 m) of the ore position, SiO_2 increases from 40 to 80%. Over the same interval, MgO and MnO decrease from approximately 10% and 0.5% respectively to near detection limits (Figure 118). Na_2O and CaO are depleted from approximately 4% and 8% respectively to <0.5% (Figure 118). Na_2O and CaO are affected further from the ore position, showing systematic depletion approximately 500 feet (150 m) away, indicating that they are more susceptible to alteration processes. Fe_2O_3 and K_2O are variable and change with Ti/Zr ratio indicating that the variation may be partly related to lithology changes (Figure 118).

Summary of major-element geochemistry

Major-element geochemical patterns within footwall units C1 and C2 reflect the distribution of alteration minerals quartz and sericite as well as chlorite, feldspar and carbonate. Changes in the relative proportion of these minerals and their composition affect the major-element geochemistry. The depletion of Na_2O, CaO, Fe_2O_3, MgO and MnO and variable enrichment of K_2O reflect the decreasing abundance of chlorite and feldspar and the increasing abundance of sericite with increasing alteration. Alteration proximal to mineralization is characterized by large increases in the SiO_2 content of the rocks which corresponds to intense silicification. Na_2O and CaO appear to be the most mobile of the major-elements as they become depleted at distances >500 feet (150 m) from mineralization while SiO_2 and MnO only appear to be mobile within 300 feet (90 m) of mineralization. The Fe_2O_3, MgO and K_2O contents may be partially controlled by

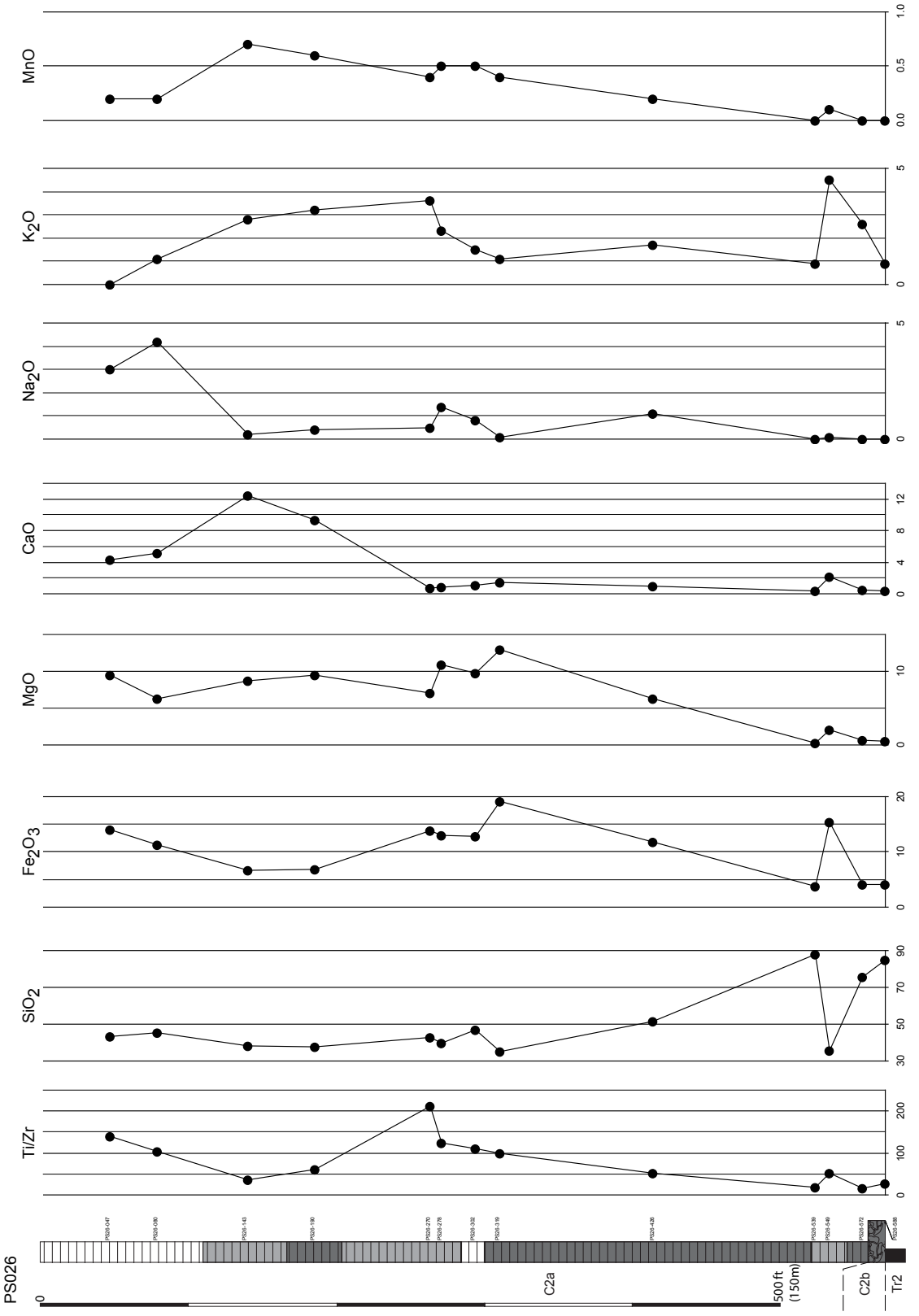

Figure 118 Downhole variation of major-element data along diamond drill hole PS026, proximal to mineralization, on the eastern margin of the Greens Creek deposit. Lithology and alteration symbology same as Figure 109.

lithology as they correlate with large Ti/Zr ratio shifts, indicating these elements may be only partially mobile.

Trace-element variations

For all samples, the trace-elements Rb, Sr, Ba, Cu, Pb, and Zn were analyzed either with XRF or ICP while Sn, Tl, and Sb were only analyzed with ICP. Figure 115 shows that the ICP and XRF analyses of trace-elements are typically within <5% of each other suggesting that the analyses are comparable except near the limits of detection.

Rb increases from background values of 1 ppm in less altered rocks to proximal values of 100 ppm near mineralization. Sr decreases with proximity to mineralization with background values of approximately 200 to 300 ppm and proximal values approximately 10 ppm (Figure 119). This increase in Rb and decrease in Sr mimics the pattern of variable K-enrichment and destruction of plagioclase as alteration intensity and proximity to mineralization increase.

Ba, Cu, Pb and Zn all increase with alteration intensity and proximity to mineralization. Ba has the greatest range with background samples typically <50 ppm and proximal samples up to 10,000 ppm. Cu content is highly variable with background samples having approximately 100 ppm and proximal samples having >1000 ppm. Samples from the sericite alteration zone have the greatest variability in Cu content ranging from four to 1200 ppm. A significant number of samples from the chlorite alteration zone and sericite alteration zone have Cu contents below that of the regional background sample suggesting that Cu could have been leached out of the footwall rocks in the vicinity of the mine workings. Pb and Zn have background values of approximately 2 ppm and 100 ppm respectively. The Pb and Zn content of the rocks increases with alteration intensity and proximity to mineralization (Figure 119). Pb and Zn values generally increase from background levels suggesting that the metals were not leached from the footwall rocks within the mine workings. Sn, Tl and Sb all increase with proximity to mineralization. Typical background levels for these three elements are below detection, using the ICP

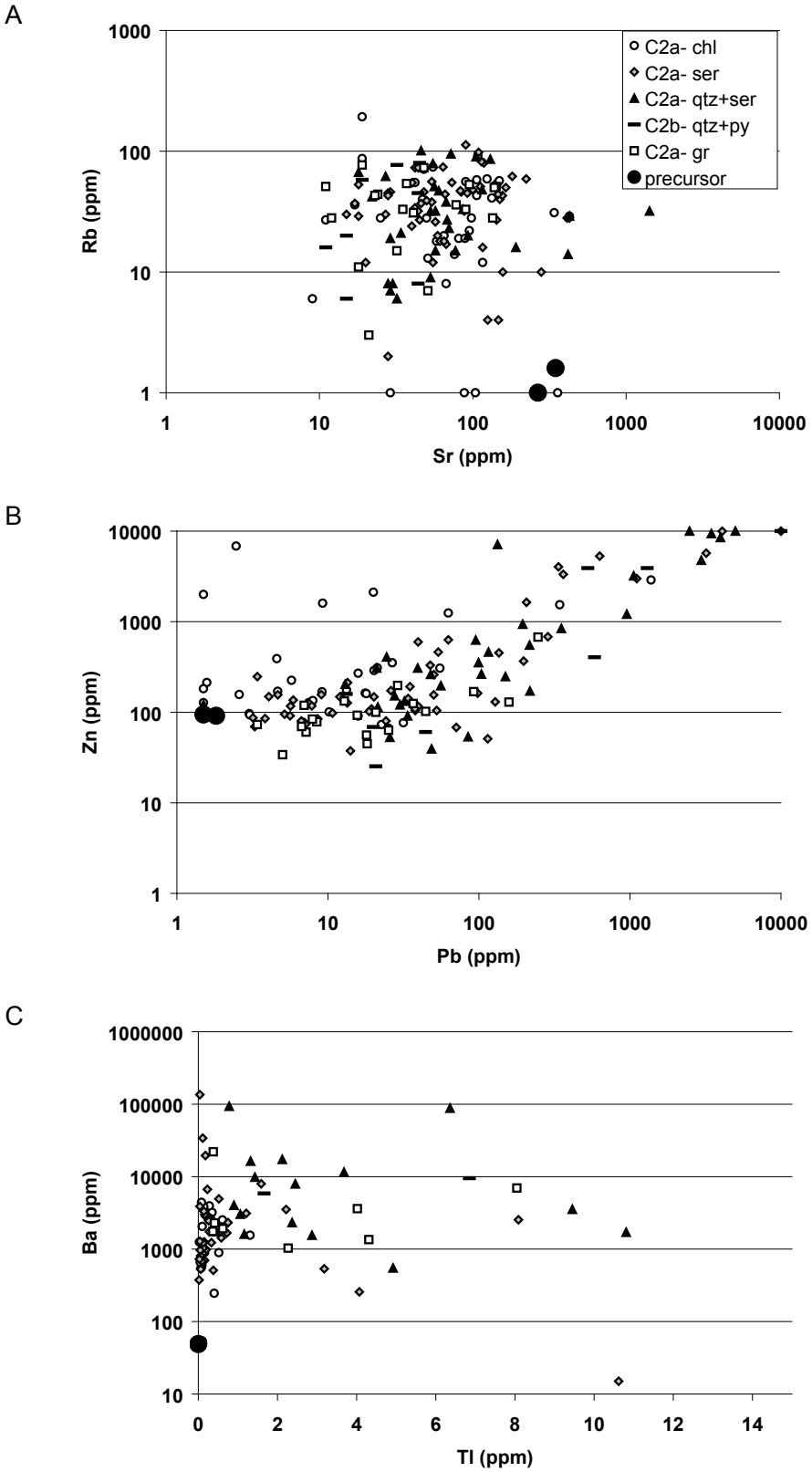

Figure 119 Whole-rock analyses of least altered (heavy black circle) and altered samples from Greens Creek, illustrating the distribution of Sr, Ba, Tl, Pb and Zn. The distribution of these elements reflects alteration intensity. (A) Rb versus Sr illustrating an increase in Rb and decrease in Sr content with increasing alteration intensity, (B) Zn versus Pb illustrating the positive correlation between the two metals and their increase with proximity to mineralization, (C) Ba versus Tl illustrating an increase in Tl content in sample from alteration zones proximal to mineralization. Symbols as for Figure 116.

technique, and increase to approximately 20 ppm for Sn and Tl and >100 ppm for Sb proximal to mineralization. Tl levels for samples from the chlorite alteration zone and sericite alteration zone are typically below 1 ppm, while samples from the quartz–sericite and quartz–pyrite alteration zones are typically between 1 and 15 ppm (Figure 119).

Downhole variations

In the 4211 cross-cut, trace-elements Sn, Pb and Zn show no increase towards the ore position and Cu shows a slight decrease (Figure 120). Tl was not included in the XRF analyses of these samples. Ba shows an increase of approximately half the magnitude of that in diamond drill hole PS026, approaching the ore position (Figure 120). In PS026, all of the metals discussed in this section increase towards mineralization (Figure 121). The metals Cu, Pb, Zn, and Sb begin to increase 50 to 75 feet (15 to 25 m) from the ore position while Sn begins to increase 300 feet (90 m) from mineralization and Tl begins to increase 500 feet (150 m) from mineralization (Figure 121).

Summary of trace-element geochemistry

Sr increases while Rb decreases with alteration intensity likely reflecting feldspar alteration. Ba is highly variable in the footwall and is elevated both distal and proximal to mineralization, suggesting that this element is highly mobile and the abundance is related to intensity of the hydrothermal alteration. The metals Sn, Cu, Pb, and Zn are significantly elevated only within 75 feet (25 m) of mineralization while Sb and Tl are elevated up to 500 feet (150 m) away.

Variation in alteration indices

Many alteration geochemical studies of VHMS deposits use alteration indices to characterise the intensity and style of alteration. Examples include the Ishikawa Index (AI) (Ishikawa et al., 1976) and the Chlorite–Carbonate–Pyrite Index (CCPI) (Large et al., 2001). Alteration indices typically use element ratios to highlight the relative enrichment and depletion of whole-rock oxides within hydrothermal alteration

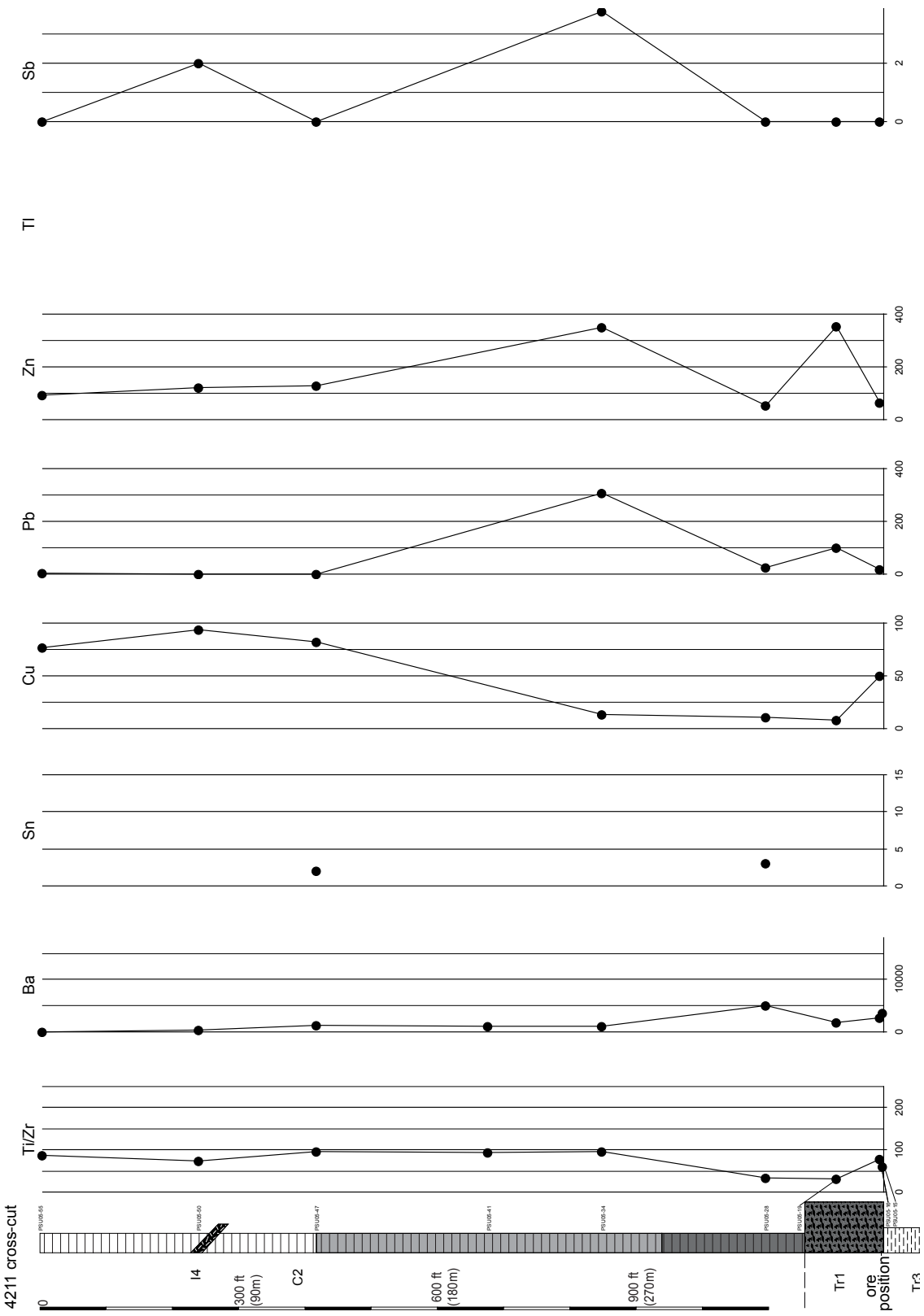

Figure 120 Downhole variation of trace-element data along the 4211 cross-cut distal to mineralization, on the western margin of the Greens Creek deposit. Note Tl was not analyzed for in these samples. Lithology and alteration symbology same as Figure 109.

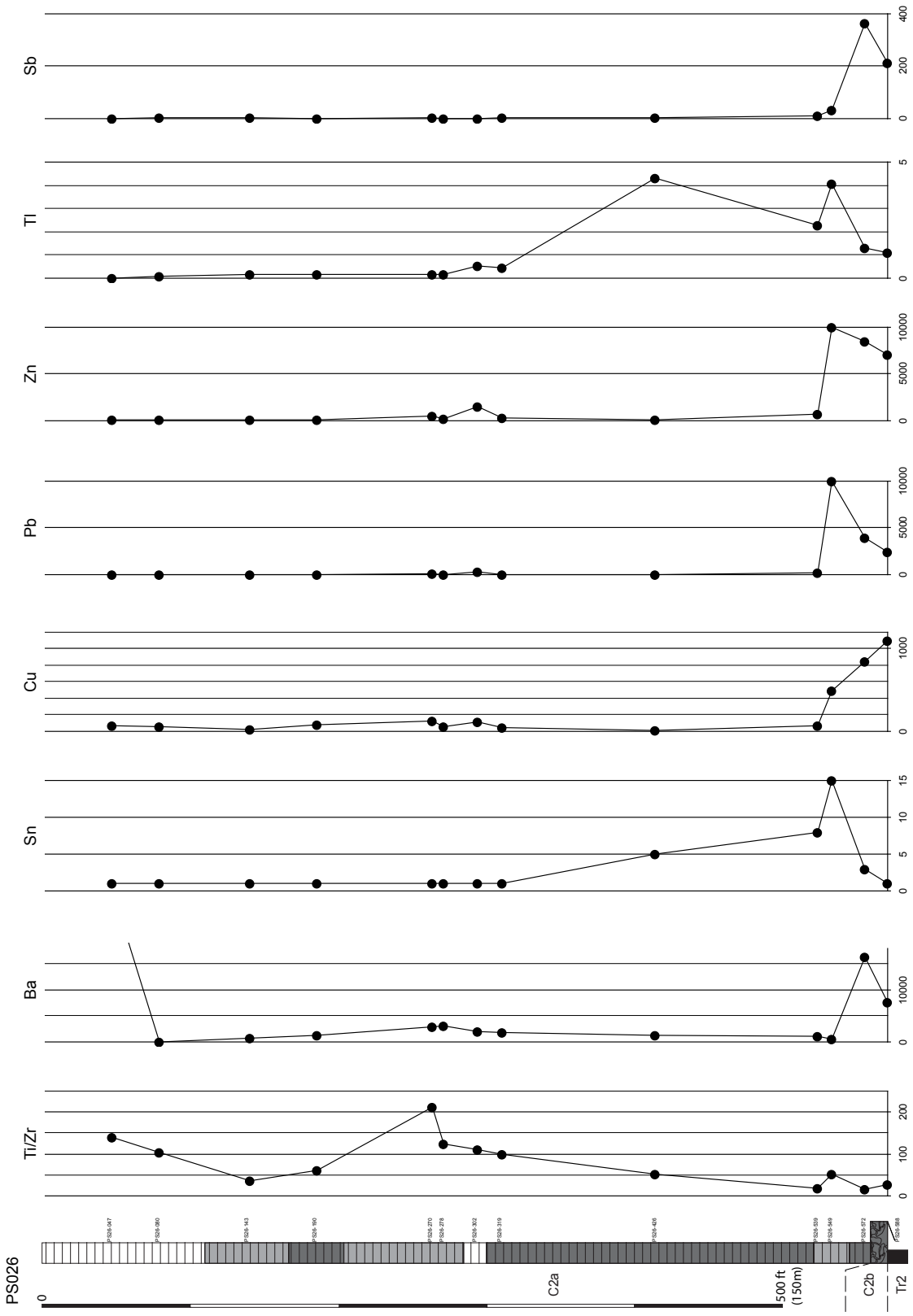

Figure 121 Downhole variation of trace-element data along diamond drill hole PS026 , proximal to mineralization, on the eastern margin of the Greens Creek deposit. Lithology and alteration symbology same as Figure 109.

surrounding VHMS deposits. The general formula for these indices is:

$$\text{General alteration index} = \frac{\text{elements added}}{\text{elements added + elements removed}}$$

The formula for the Ishikawa alteration index (AI) is:

$$AI = \frac{100*(K_2O + MgO)}{(K_2O + MgO + Na_2O + CaO)}$$

AI is a measure of feldspar destruction (Na_2O depletion) and muscovite and chlorite alteration (K_2O enrichment). Within the footwall rocks at Greens Creek, the chlorite, sericite and quartz–sericite alteration zones are characterized by decreasing feldspar abundance and increasing white mica abundance and AI is a good measure of alteration intensity. Samples from the chlorite alteration zone typically have AI values of <60, samples from the sericite alteration zone have AI values between 57 and 90 and samples from the quartz–sericite alteration zone typically have AI values of >80 (Figure 122). Samples from the quartz–pyrite alteration zone have AI values of 75 to 85, which are slightly lower than samples from the quartz–sericite zone but have SiO_2 contents of >75% which are significantly higher (Figure 122). The decrease in the AI value for the quartz–pyrite alteration zone proximal to mineralization is probably due to the intense silicification of the rocks and the lack of white mica development. Analyses from each alteration zone in a representative hole which intersects mineralization (PS026 on Figure 122) are tightly clustered and show the characteristic increase in AI from approximately 50 to approximately 85 with relatively flat SiO_2 contents of approximately 50% up to AI values of approximately 75 and SiO_2 contents of >75%. Analyses from the 4211 cross-cut (Figure 122) which intersects an unmineralized hanging wall–footwall contact are interpreted as distal to mineralization and follow a similar pattern. The AI and SiO_2 values within each alteration zone are more variable, likely reflecting primary compositional variation.

Downhole variations

Several other alteration indices were calculated for footwall rocks at Greens Creek. The formulae for these indices are:

Sericitization = $K_2O/(K_2O + Na_2O)$	(Large pers. comm.)
Sulfidation = S/TiO_2	(Mireku and Stanley, 2006)
Albite destruction = Na_2O/Al_2O_3	(Mireku and Stanley, 2006)
Sulfur–sodium = S/Na_2O	(Gifkins et al., 2005)

The sericitization index is another measure of sericite growth, typically at the expense of plagioclase. The sulfidation index is a measure of the abundance of sulphur (primarily in pyrite) and albite destruction is a measure of plagioclase break down. The sulphur–sodium ratio combines a pyritization measure with a plagioclase destruction measure to give a ratio which varies over four orders of magnitude from background-level rocks to ore proximal rocks.

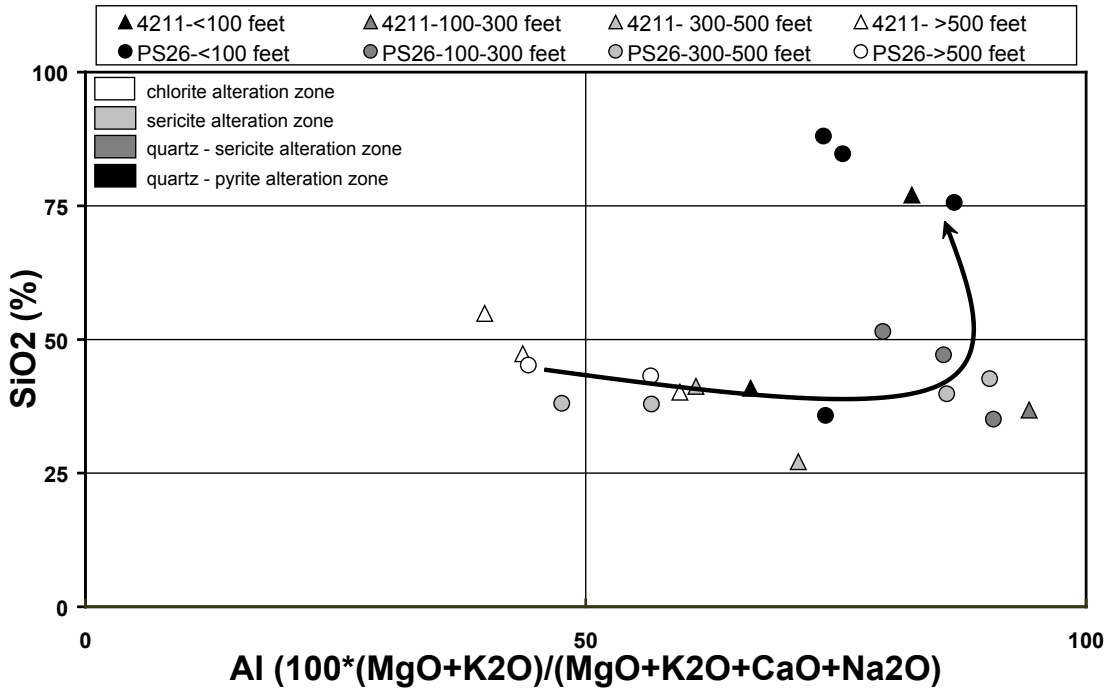

Figure 122 Distribution of the SiO_2 versus the Alteration Index (AI) for samples from the 4211 drift (distal to mineralization) and diamond drill hole PS026 (proximal to mineralization). The AI uses elements in the main alteration minerals from the chlorite through to the quartz–sericite alteration zones to indicate alteration trends within these zones and the high SiO_2 content differentiates the quartz–pyrite alteration zone. Arrow indicates increasing alteration and proximity to the ore position. Distance ranges refer to distance from the ore position.

Figure 123 and Figure 124 show the downhole variation of the various alteration indices calculated for the footwall rocks at Greens Creek. In both the 4211 cross-cut and diamond drill hole PS026, the AI and the sericitization index increase towards the ore position. The AI values are similar in both logs and range from approximately 50 furthest away to 90 near the ore position. The sericitization index ranges from 0 to 1.0. The albite-destruction indices decrease by similar amounts towards the ore position in both the 4211 cross-cut and PS026 with values ranging from approximately 0.3 distal to 0 near the ore position. In both the 4211 and PS026, the sulfidation and S/Na_2O indices increase towards the ore position with sulfidation values in each log ranging from 0 distally to 0.5 proximally. In the 4211 cross-cut, the S/Na_2O index systematically varies between 0.05 distally and 17 proximal to mineralization but in PS026, the index ranges from 0.03 at 900 feet (275 m) to over 300 near the ore position. The S/Na_2O index shows the greatest variation with respect to distance from the ore position and also differentiates between mineralized and non-mineralized footwall–hanging wall contacts.

Summary of variation in alteration indices

All indices calculated for the present study, with the exception of the albite-destruction index, increase towards the ore position. The S/Na_2O index varies over four orders of magnitude while the other indices vary over one order. The S/Na_2O best highlights variations in the footwall geochemistry. This index also appears to differentiate the mineralized PS026 from the unmineralized 4211 cross-cut with S/Na_2O values of >50 being anomalous for this index. To identify alteration patterns at greater distances from the ore position, the AI or sericitization index may be more appropriate.

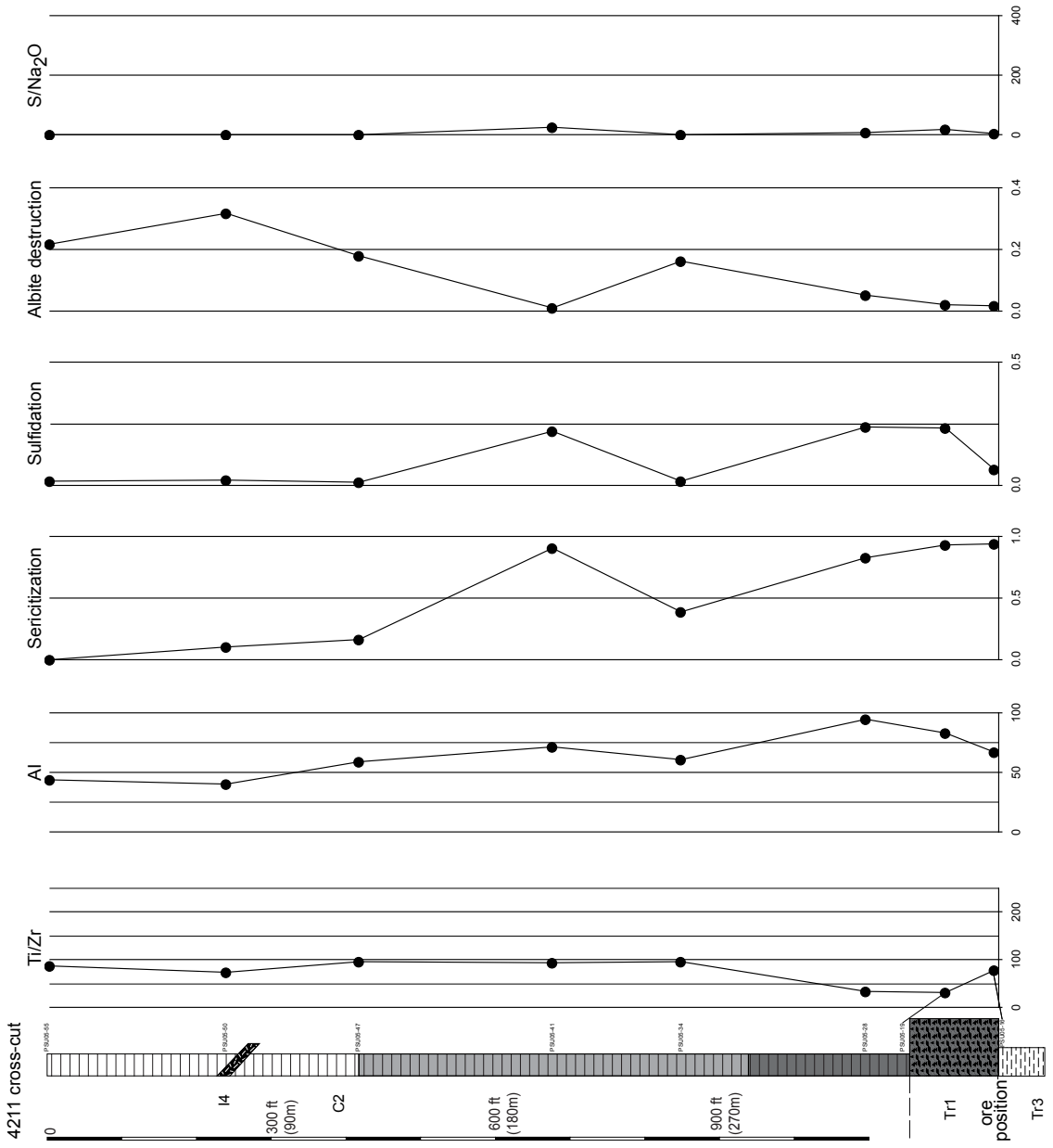

Figure 123 Downhole variation of alteration indices along the 4211 cross-cut , distal to mineralization, on the western margin of the Greens Creek deposit. Lithology and alteration symbology same as Figure 109.

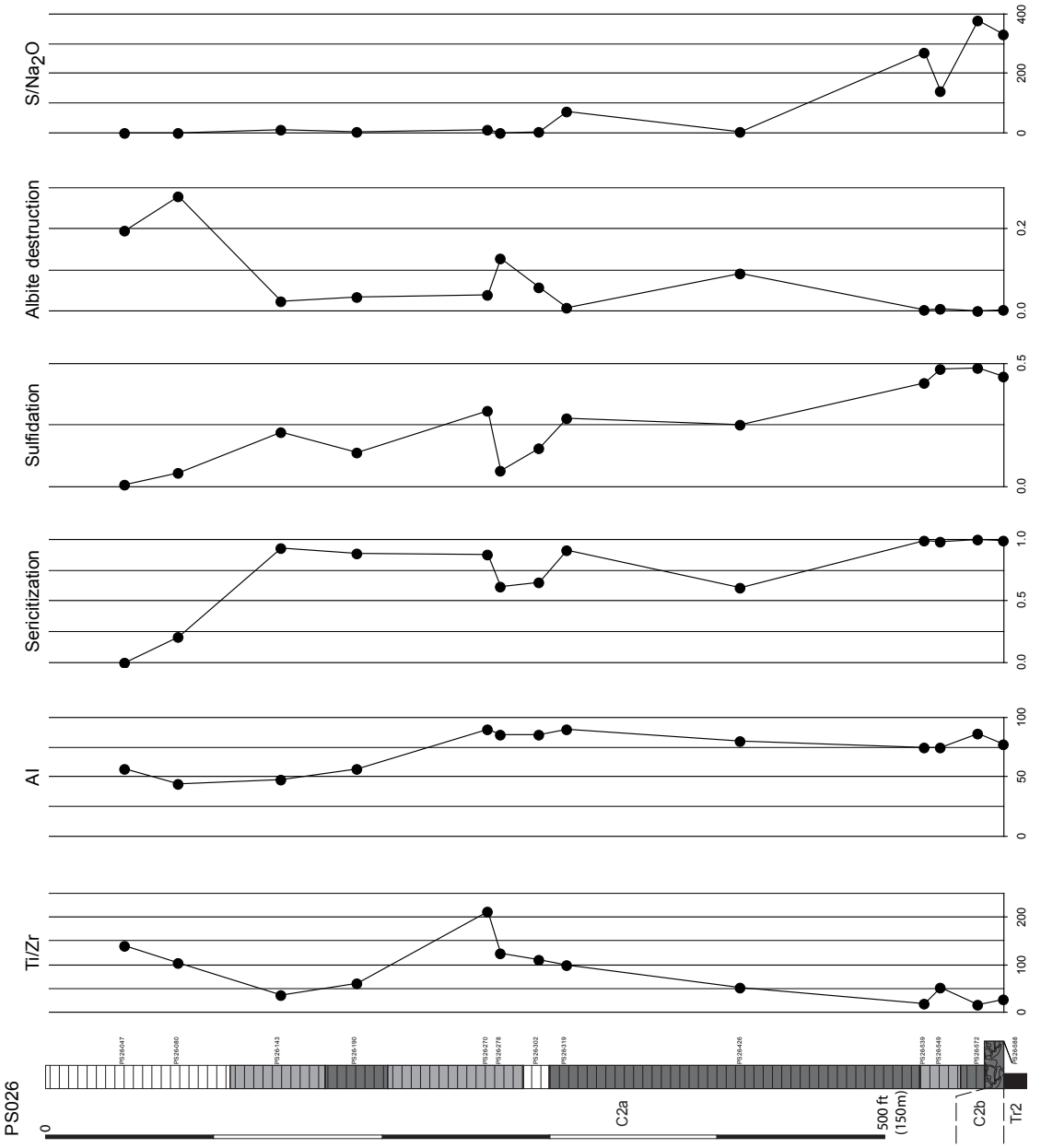

Figure 124 Downhole variation of alteration indices along diamond drill hole PS026 , proximal to mineralization, on the eastern margin of the Greens Creek deposit. Lithology and alteration symbology same as Figure 109.

Summary

- Previous studies have described systematic mineralogical, mineral chemistry and whole-rock geochemical trends related to proximity to the ore position. Examples of these vectors include carbonate composition variation and whole-rock and mineral Mg# variation.

- Four alteration zones are characterized for the footwall to the Greens Creek deposit. From distal to proximal these are: chlorite alteration zone, sericite alteration zone, quartz–sericite alteration zone and the quartz–pyrite alteration zone.

- Spectral data for >500 samples show a systematic change in white mica composition from phengite to muscovite with increasing proximity to mineralization. The wavelength position of the AlOH feature for background white micas is variable with values between 2190 and 2230 nm and is heavily dependent on bulk-rock composition. Proximal to mineralization the AlOH values are restricted to the 2200–2215 nm range and the white mica composition is dominated by the hydrothermal fluid effects. White mica alteration index (WMAI) values show an increase in the abundance of sericite, relative to chlorite, when approaching mineralization.

- Chlorite shows limited compositional variation without systematic zoning related to proximity to mineralization. The wavelength position of the FeOH feature of chlorite is typically between 2246 and 2257 nm indicating Mg-chlorite to intermediate chlorite compositions.

- Whole-rock geochemical analyses for 208 samples show systematic trends in major oxides, trace-elements and alteration indices related to proximity to the ore position. SiO_2 shows the greatest increase towards mineralization and Na_2O shows the greatest decrease.

- Trace-elements Ba (50 ppm) and Tl (0.1 ppm) are elevated above background levels up to 500 feet (150 m) from mineralization.

- The Ishikawa alteration index shows systematic variation with increasing alteration intensity but does not differentiate the quartz–pyrite alteration zone or mineralized from non-mineralized hanging wall–footwall contacts. The S/Na_2O ratio shows a four orders of magnitude increase (from background levels of <0.1 to approximately 20) when proximal to an unmineralized hanging wall–footwall contact, with further increase up to >200 when proximal to a mineralized contact.

- Figure 125 and Figure 126 illustrate the downhole variations of key ratios, spectral features, major oxides, trace-elements and alteration indices. The loss of Mg and Fe from the white mica structure and their corresponding compositional change may be too subtle to detect with whole-rock analyses, particularly proximal to mineralization when the quartz–pyrite alteration is intense. The shift in the peak position of the AlOH feature is typically seen several hundred feet (~60 m) from the ore position than changes in the whole-rock chemistry, high-lighting the importance of the spectral properties of the white micas as potential exploration vectors.

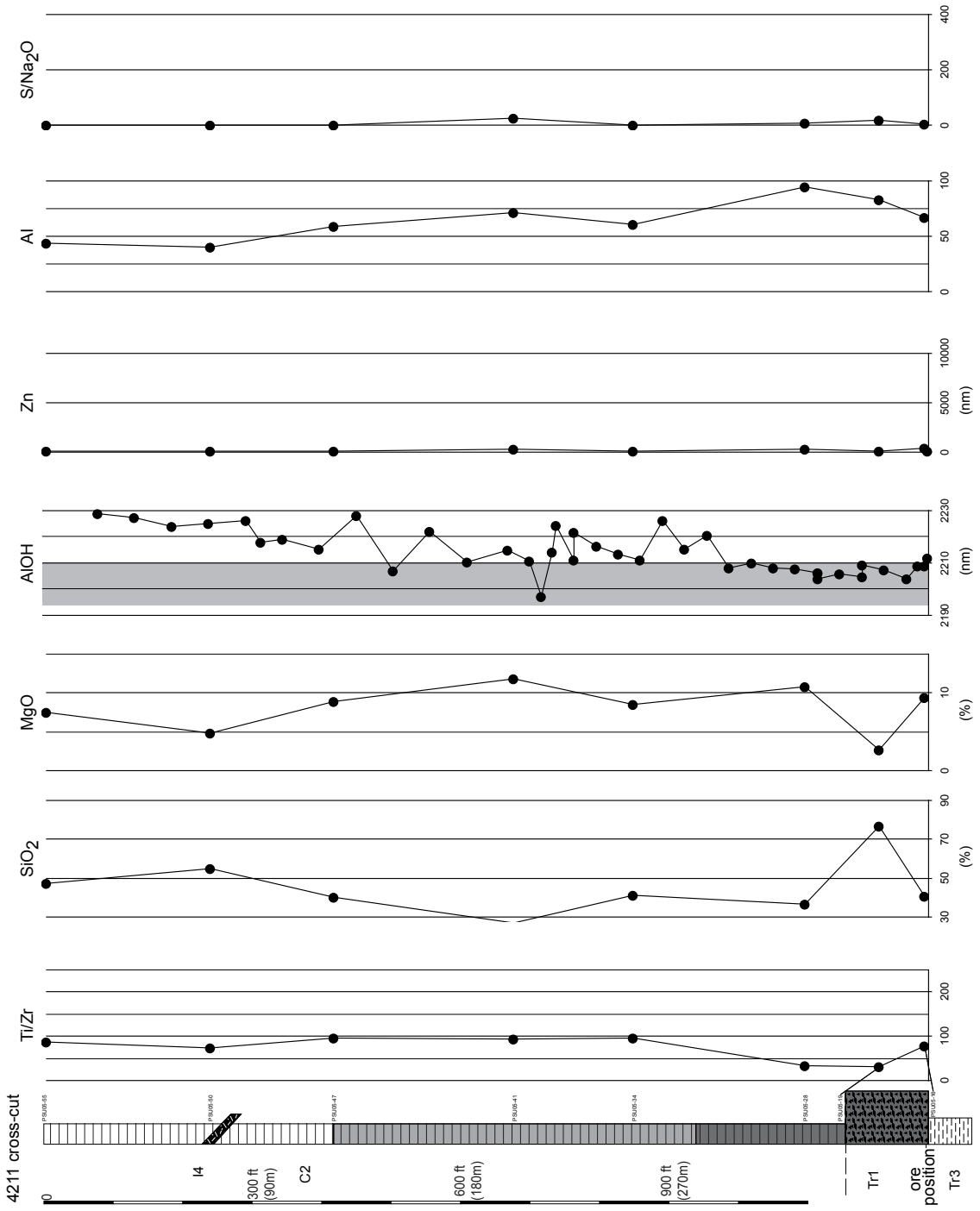

Figure 125 Downhole variation of select major oxides, trace-elements and alteration indices along the 4211 cross-cut , distal to mineralization, on the western margin of the Greens Creek deposit. Lithology and alteration symbology same as Figure 109.

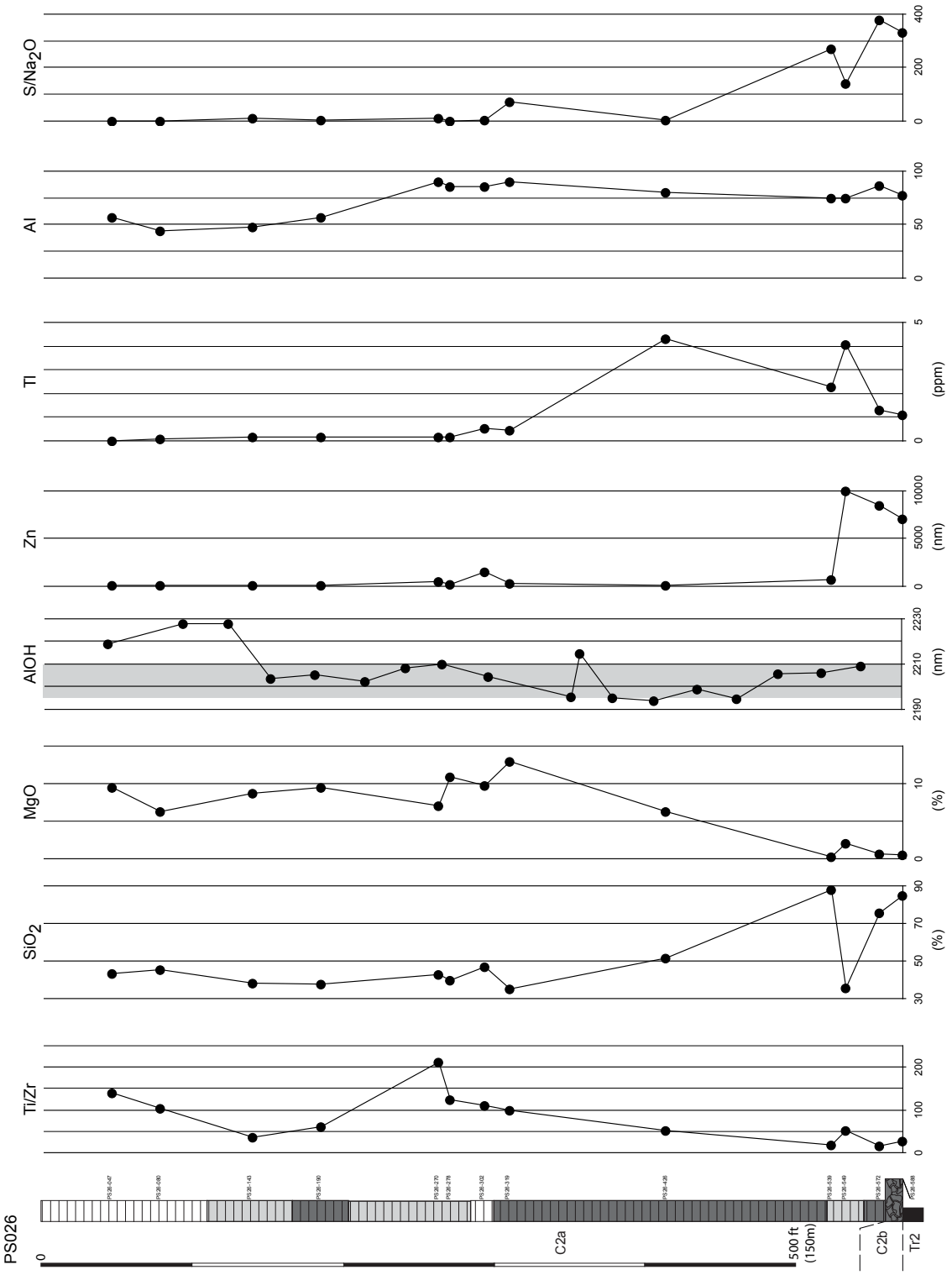

Figure 126 Downhole variation of select major oxides, trace-elements and alteration indices along diamond drill hole PS026 proximal to mineralization, on the eastern margin of the Greens Creek deposit. Lithology and alteration symbology same as Figure 109.

Chapter 7: Metal zoning

Introduction

The metal zonation of VHMS deposits has proven useful in understanding the genesis of this deposit type. It is widely recognized that VHMS deposits display a metal zonation that ranges from a central Fe- to Fe-Cu-rich core, passing upwards and outwards to zones of Cu-Pb-Zn metal enrichment and finally to zones of Pb-Zn-Ba metal enrichment (Large, 1977, 1992; Franklin et al., 1981). These metal-zonation patterns infer physiochemical conditions and temperatures of metal deposition, as well as metal transport mechanisms and the location of potential feeder sites to the deposits (Large, 1977; Solomon and Walshe, 1979; Knuckey et al., 1982; Huston and Large, 1987; Gemmell and Large, 1992). Despite well-constrained zonation models for mound deposits, the metal zonation of sheet- and blanket-type deposits are somewhat more complex (Large, 1992). This complexity arises from a less-focused feeder system and the probability of multiple feeder sites as proposed by Huston (1988).

Metal zonation studies of VHMS deposits typically use a combination of drill core, underground or open pit samples from the ore body. The studies are done on the ore bodies themselves and, where applicable, within the stringer system beneath the ore bodies (i.e. Knuckey et al., 1982; Eldridge et al., 1983; Huston and Large, 1987). Classic VHMS stringer-style mineralization has not been identified below the Greens Creek deposit (A. West pers. comm.). The present study was designed to investigate the footwall to mineralization in the Northwest West (NWW) ore zone and the East ore zone to identify metal zonation patterns and outline potential feeder systems within the footwall. For comparison, the footwall data are plotted against simplified metal zonation within the ore bodies. Identification of feeder systems within the footwall has proven

important in understanding the genesis of other deposits (i.e. Gemmell and Large, 1992) and, when compared with the metal zoning within the ore body itself, allows an interpretation of the relationship between the two. At Greens Creek, the coincident location of feeder systems within both the footwall and the ore body in the NWW and East ore zones, at least within the scale of observation of the present study, indicates that the ore bodies formed above their footwall feeder systems.

The Cu ratio [(100*Cu/(Cu+Zn)] and Zn ratio [(100*Zn/(Zn+Pb)] have proven useful in delineating zones that are interpreted as potential feeder systems below VHMS deposits (i.e. Knuckey et al., 1982; Huston and Large, 1987; Gemmell and Large, 1992). Ideally, the Zn ratio should have an antithetic relationship with the Cu ratio, and potential feeder zones should be defined by zones with an elevated Cu ratio and low-Zn ratio (Gemmell and Large, 1992). Furthermore, both the Cu and Zn ratios have been used to constrain physiochemical conditions of ore formation; the Zn ratio is the less variable and therefore more robust of the two (Knuckey et al., 1982; Huston and Large, 1987). This is particularly true when Cu contents are low, as is the case at Greens Creek.

The aims of the metal zonation study within the footwall to the Greens Creek deposit are to:

1. Identify gross zonation patterns within the footwall to the NWW ore body and the East ore body.

2. Examine the metal associations within the footwall of the NWW and East ore bodies and to compare them with the gross zonation patterns.

3. Use metal concentrations to define potential.

4. Compare the absolute and relative metal concentrations from the footwall to the NWW and East ore bodies in order to examine the genetic relationship between the two bodies.

Previous work

The most detailed metal zonation study conducted at the Greens Creek deposit was a PhD study undertaken at the Colorado School of Mines (Freitag, 2000). This study was done on a reconstructed portion of the Lower Southwest ore zone (LSW) which is located between cross-sections 2200 to 2800 and long-sections 4000 to 5000 on the west side of the Maki Fault (Figure 127). The reconstructed ore body consisted of a massive sulfide zone and a mineralized carbonate zone. Using assay data provided by the Greens Creek mine, Freitag (2000) examined the distribution of Fe, Zn, Pb, Cu, Au and Ag and concluded: (1) that for all metals, with the exception of Ag, the highest-grade-to-thickness ratios coincided with the thickest accumulations of mineralization; the highest grade to thickness ratios for Ag are found on the thinner accumulation; (2) that Fe, Zn, Pb, Cu and Au contents were higher in the lower portions of mineralization while Ag was higher in the upper portions and did not correlate with Pb; and (3) that the ore bodies are elongate north–south along a pre-mineralization fault. Freitag (2000) also concluded that for all metals studied, except Au, there was no correlation between increased grade and local F2 hinges, indicating that these elements were not significantly remobilized during the D2 deformation. Gold showed a weak correlation with F2 hinges, indicating minor remobilization.

Gemmell (2003) conducted a preliminary study on the element zonation within footwall lithologies primarily on the west side of the Maki Fault. The study was meant to focus on the LSW ore zone (cross-sections 500 to 3000) but also included the NWW ore zone (cross-sections 4000 to 6000). Gemmell (2003) examined Ag, Al, As, Au, Ba, Bi, Ca, Cd, Co, Cr, Cu, Fe, Hg, Mg, Mn, Mo, Ni, P, Pb, Sb, Sr, Tl, U, V, and Zn distributions within the footwall lithologies (SR, SP, CR, SC, MP, GST and GB) and delineated two hydrothermal feeder zones. The larger feeder zone was located between cross-sections 500 to 2000 and long-sections 3750 to 4500 from relative levels (RL) of 0 to –1000 feet (300 m). This feeder zone is located beneath the LSW ore zone and has anomalously high concentrations of Ag, As, Au, Cd, Co, Cr, Cu, Fe, Hg, Mg, Mo, Ni, Pb, Sb, Tl and Zn, coupled with anomalously low concentrations of Ba, Ca, Mg, Mn, Sr, U and V,

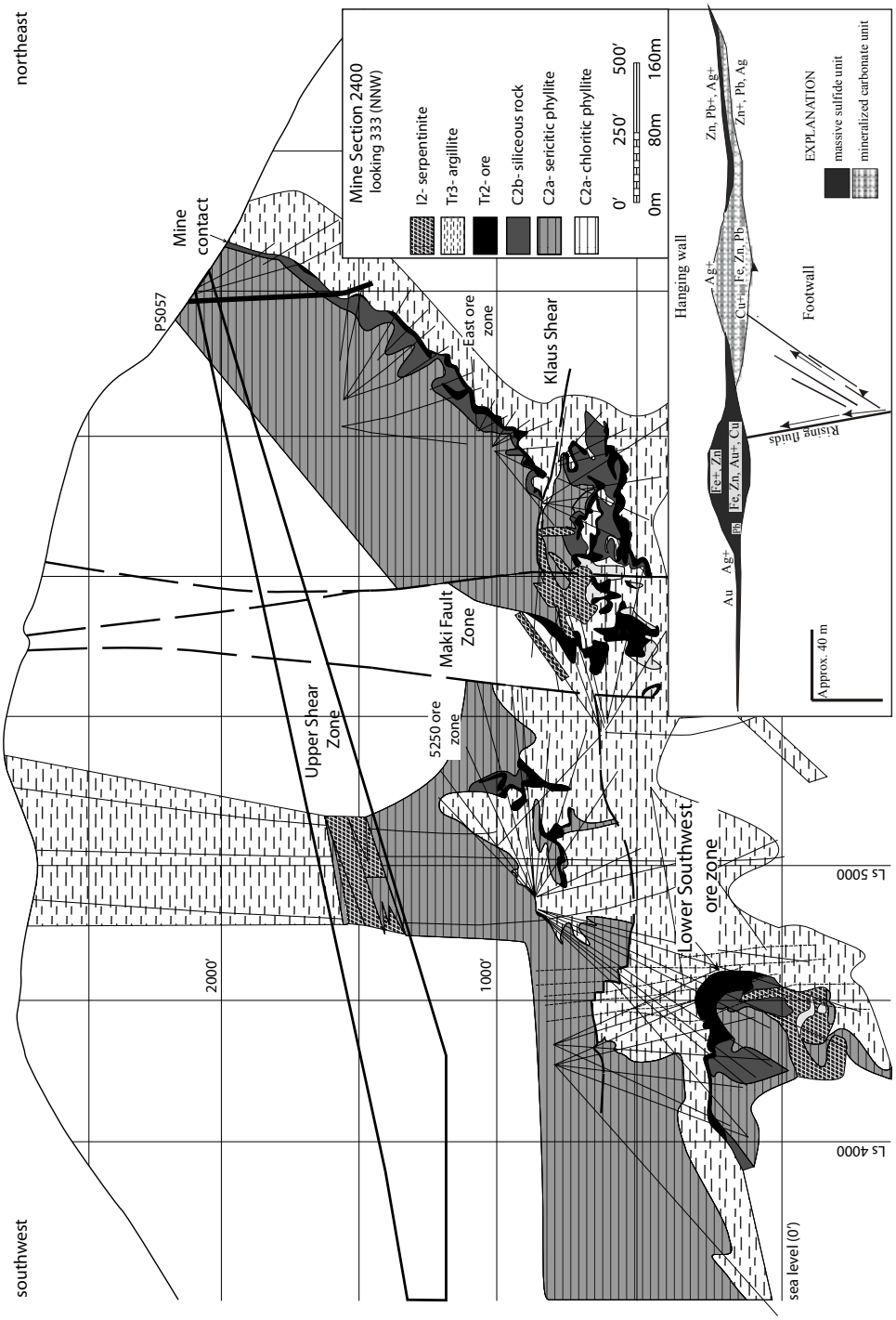

Figure 127 Southwest–northeast cross-section 2400 (200 feet (60 m) data window) through the southern end of the Greens Creek deposit. The Lower Southwest ore zone is located on the bottom left side of the figure. Inset of the schematic diagram of the Lower Southwest ore body showing the zoning of high metal values within the massive sulfide and mineralized carbonate units. Metals with "+" symbol indicate high concentrations (modified from Freitag, 2000).

and a low Zn ratio. A second feeder zone was delineated between cross-sections 4000 to 6000 and long-sections 4500 to 5000 from RL –1000 feet (300 m) to 500 feet (150 m). This feeder zone is located beneath the Northwest West ore zone (NWW) and is enriched in Ag, Au, Bi, Cd, Cu, Fe, Hg, Mo, P, Pb, Sb and Tl. It has high Zn and Cu ratios and is depleted in Ba, Ca, Cr, Mg, Mn, Sr, U and V.

Another brief study of the metal zonation, primarily on observations from the Central West ore zone and parts of the East ore zone, was conducted as part of the U.S. Geological Survey (USGS) study of the Greens Creek deposit undertaken in the late 1990s (Taylor, in press). The main finding of this study was the recognition of the classic Cu→Fe→Zn→Pb+Zn→Ag (polymetallic) zoning from the core upwards and outwards towards the margins of the ore bodies. The delineation of these zones was based on metal ratios such as Fe/Zn, Zn/Pb and metal contents. Taylor (in press) concluded that this simple zonation was appropriate only for each ore body and that a larger deposit-scale metal zonation pattern was not recognized. He attributed the lack of a simple ore body scale metal zonation to multiple feeder zones, each with their own zonation located along a paleo-Maki Fault.

These three previous metal zonation studies provide the background for the present study and indicate: (1) that metal zonation exists on a deposit scale, (2) that the metal zonation is accompanied by systematic variation in a larger suite of trace and major elements, (3) that the metals, possibly with the exception of Au, were not significantly remobilized during deformation, (4) that metal zonation within footwall lithologies is related to metal zonation within ore lithologies and (5) that the complexity of metal zonation on both a deposit- and ore-body-scale may be due to the existence of multiple feeder zones.

The average grade and tonnage data for the East, NWW and Southwest (SW) ore bodies highlight several important aspects of each ore body. The NWW ore body is more than

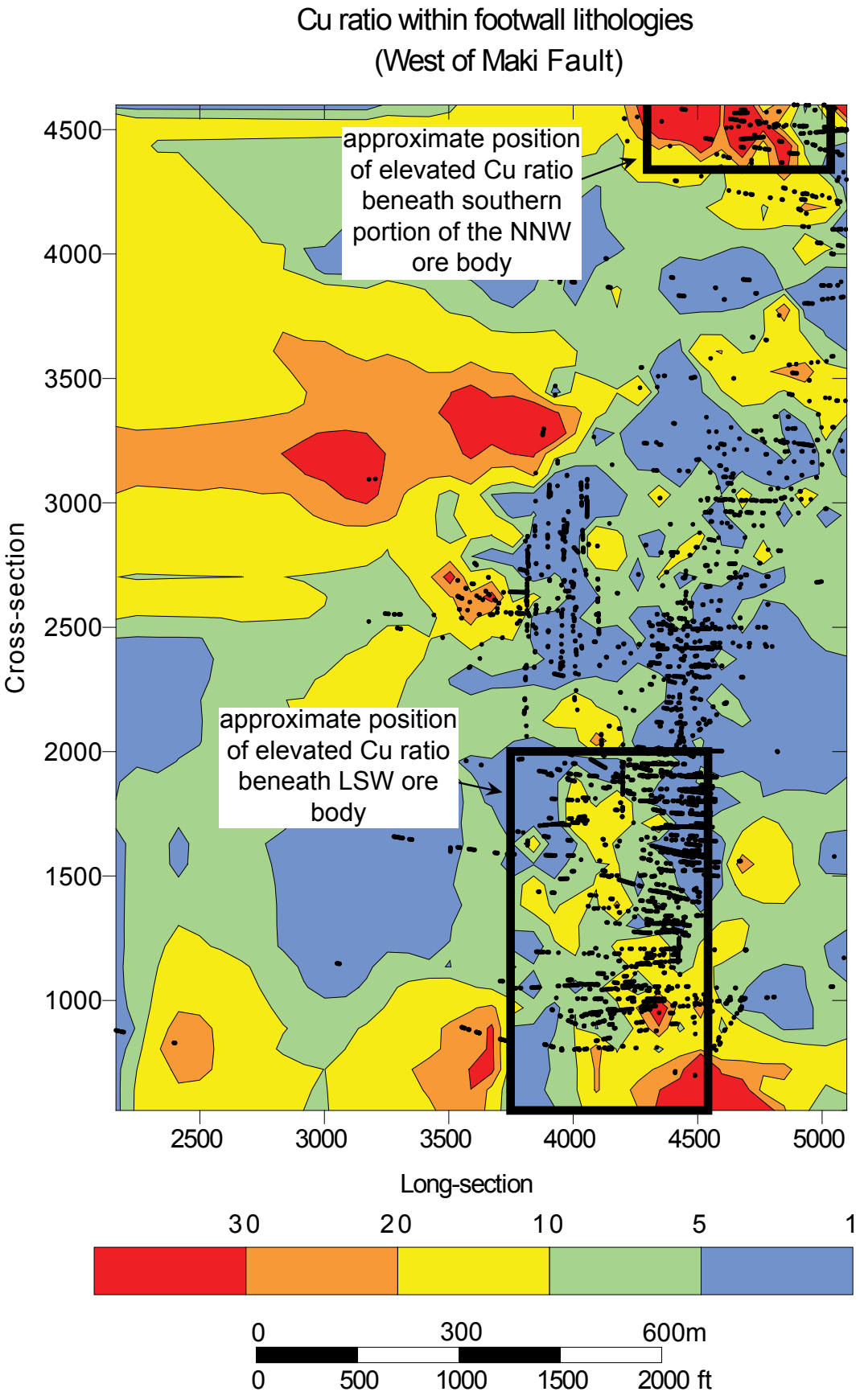

Figure 128 Plan view of Cu-ratio distribution through the footwall lithologies. Modified from an element zonation study located to the west of the Maki Fault (Gemmell, 2003).

three times larger than either the East or SW ore bodies with a slightly higher average Cu grade and has approximately half the Ag grade. The East and SW ore bodies are similar in size and grade, with the SW being slightly more precious metal rich. The Zn ratio is similar for all three ore bodies with values ranging from 69 to 77. The Cu ratio for the NWW and SW is also similar with values <3 in both cases. One qualification of the above grade and tonnage data is that it is for the entire deposit. This is particularly important in the case of the NWW ore body where the elevated Cu ratio and low Zn ratio feeder zones are obscured by the large tonnage of the lower temperature (low Cu ratio, high Zn ratio) mantling portion of the ore body.

Table 30 Grade, tonnage and Cu–Zn ratios for the East, Northwest West and Southwest ore bodies. Cu grade is not available for the East ore body. Data from Satre (pers. comm.).

Ore body	Tonnage (MT)	Cu (%)	Pb (%)	Zn (%)	Ag (ppm)	Au (ppm)	Zn ratio	Cu ratio
East	0.84	NA	4.56	11.41	610	4.2	71	NA
NWW	2.80	0.39	4.03	13.39	311	4.2	77	2.8
SW	0.73	0.29	5.47	12.09	762	7.7	69	2.3

Methods

The data used for the present footwall metal zonation study are a sub-set of the assay data collected by the Greens Creek Mining Company during diamond drilling exploration between 1983 and 2003. The Greens Creek sampling strategy dictates that two samples for assay are generally collected from the footwall immediately adjacent to the footwall–hanging wall (ore position) contact. The assay data represent analyses of split diamond drill core with a maximum length of 5 feet (1.5 m). Samples do not cross lithological or structural boundaries. The sub-set of data used for the present study consists of samples located approximately 5–10 feet (1.5–3.0 m) into the footwall (i.e. at least one sample between the sample selected and the footwall–hanging wall contact). For the NWW ore zone, 137 samples were selected from the Greens Creek assay database and 105 were selected from the East ore zone. A complete list of samples and assay data used in the present study can be found in Appendix V.

The original Greens Creek assay data (pre-1989 and pre-diamond drill hole GC0404) included analyses for Cu, Pb, Zn, Ag, Au, As and Sb which were carried out at the Silver Valley Laboratories in Kellog, Idaho. Subsequent analyses (i.e. post-diamond drill hole GC0404) include the same metals plus Fe, Bi, Cd, Co, Cr, Mo, Ni and Tl. These later analyses were carried out at Acme Analytical Laboratories in Vancouver, Canada. Both sets of analyses used an ICP technique with either a four-acid digest or a lithium-metaborate fusion. While the NWW ore body has assay data for the complete set of elements, only the southern half of the East ore zone does. Appendix V contains the ICP technique and digestion method listed for each sample. Samples are also routinely assayed for Ba but the digestion method has changed several times and the majority of samples were analyzed with an incomplete digestion, making the Ba values inaccurate. Au values are from the ICP method which has a detection limit of 2 ppm, however the fire assay results for these samples could not be located at the time of the present study and therefore only high-grade Au values (>2 ppm) are reported.

Approximate reconstructions of the footwall–hanging wall contact for both the NWW ore body and the East ore body were constructed in order to estimate the original sample positions. The complexity of deformation varies between the two ore zones. The NWW ore body is recumbently folded, with vergence to the northwest (Proffett, 1998) while the East ore zone is on a single moderately to steeply westward dipping limb that shallows with depth as it approaches the Klaus Shear (Lindberg, 1996b). The Maki Fault bounds the NWW ore body to the east and bounds the East ore body to the west.

In both the NWW and East ore zones, the locations of samples were estimated from cross-sections with data plotted using a 100 foot (30 m) data window. In the NWW ore zone, the reconstructed location of a given sample was estimated using the measured distance along linear segments approximating the large-scale geometry of the footwall–hanging wall contact (Figure 129). Minimum line segments of approximately 50 feet (15 m) were used and no adjustments were made for elongation or shortening. In the

East ore zone, with its simpler geometry, samples were divided into two sets: east and west of long-section 6400. Samples west of long-section 6400 were assumed to be in their reconstructed horizontal position and were projected vertically onto the reference plane at 1000 feet (300 m) elevation, while samples to the east were assumed to lie along a plane dipping 60° to the west. These samples were projected perpendicular to this plane onto the horizontal reference plane (Figure 130). Samples on this horizontal plane were then rotated 180° about long-section 6000 so that they were right-way-up. Table 31 shows the spatial boundaries, used to select data for each ore zone, and reference lines from which all distance measurements were made. Scans of the complete set of cross-sections used in these reconstructions can be found in Appendix V.

Table 31 Spatial limits of data used in the present study of the footwall metal zonation. Lsxn = long-section, RL = elevation in feet.

Ore body	Cross-section	Long-section	Elevation in feet (m)	Reference line
NWW	4300–5200	4400–5100	1000 to 300 (300–90)	Lsxn 5100
East	1800–3800	6000–7200	>800 (240) (above Klaus Shear zone)	RL 1000

In addition to reconstructing the position of the samples for the NWW and East ore zones, the approximate location of elevated Cu ratios (100*Cu/Cu+Zn ≥14) within the ore bodies were plotted. For the NWW ore body, the company provided the current mining block model (December 2008) which was overlain on the same cross-sections used to reconstruct the sample positions. The company does not have a block model for the East ore body so the ore assay data were statistically analyzed with a kriging method using a 10-foot interval and the resulting contour plot overlain on the same cross-sections used in the reconstructions. The approximate positions of the elevated Cu ratios were estimated from these overlays.

The reconstruction of the NWW and East ore zones is approximate. Samples are in the correct order across cross-sections and the geology does not change dramatically between cross-sections. Therefore, nearest-neighbor relationships should be relatively

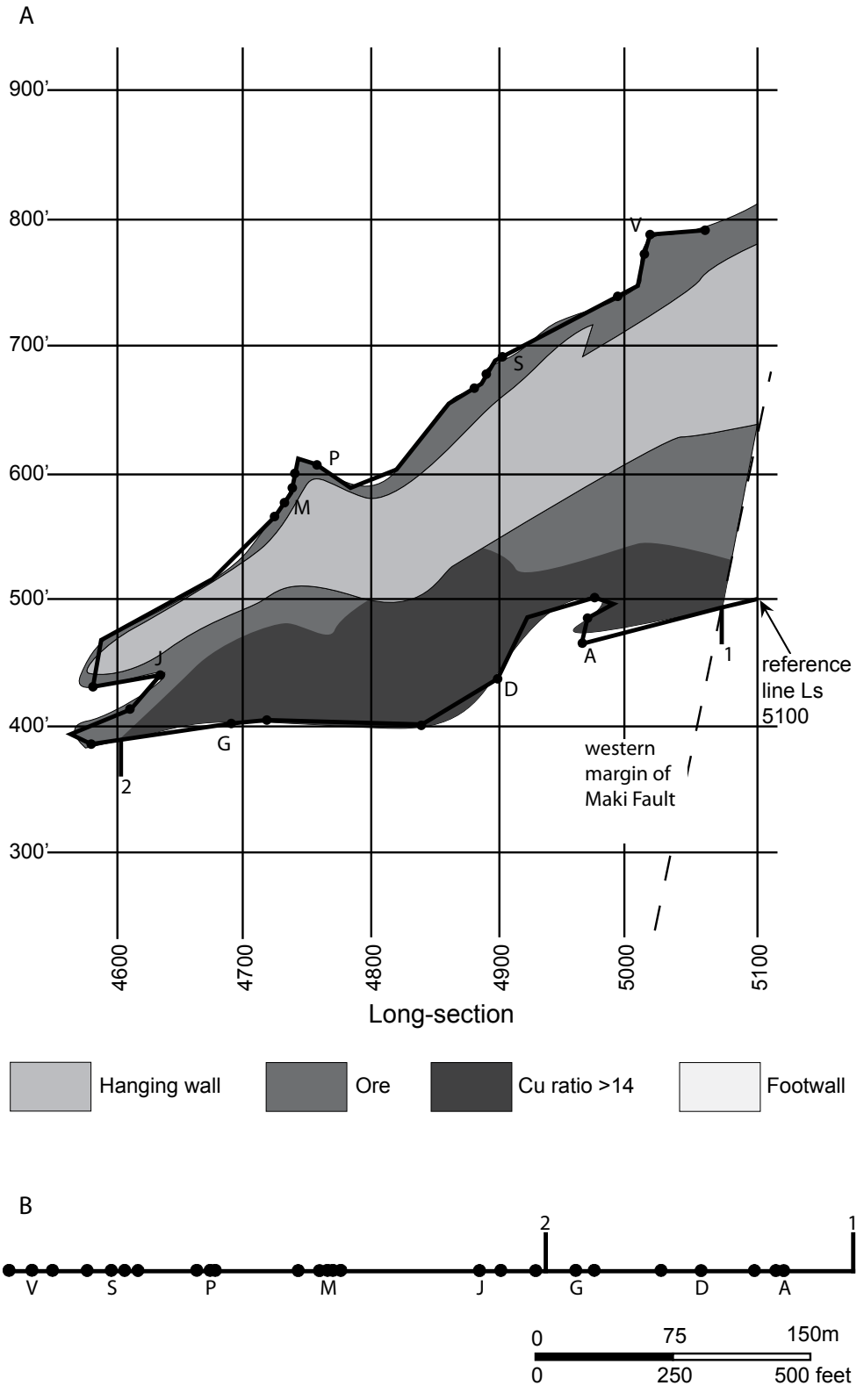

Figure 129 (A) East–west cross-section 4400 in the Northwest West ore zone illustrating the method of structural reconstruction used to estimate the original position of the samples. The Maki Fault represents the eastern limit of data used in the present study. All distances were measured away from long-section 5100 at the thick portion of the ore body. (B) Linear order of reconstructed sample positions, for samples 5–10 feet (1.5–3.0 m) into the footwall, along cross-section 4400. Letters label every fourth sample position and numbers label positions of elevated Cu ratios within ore.

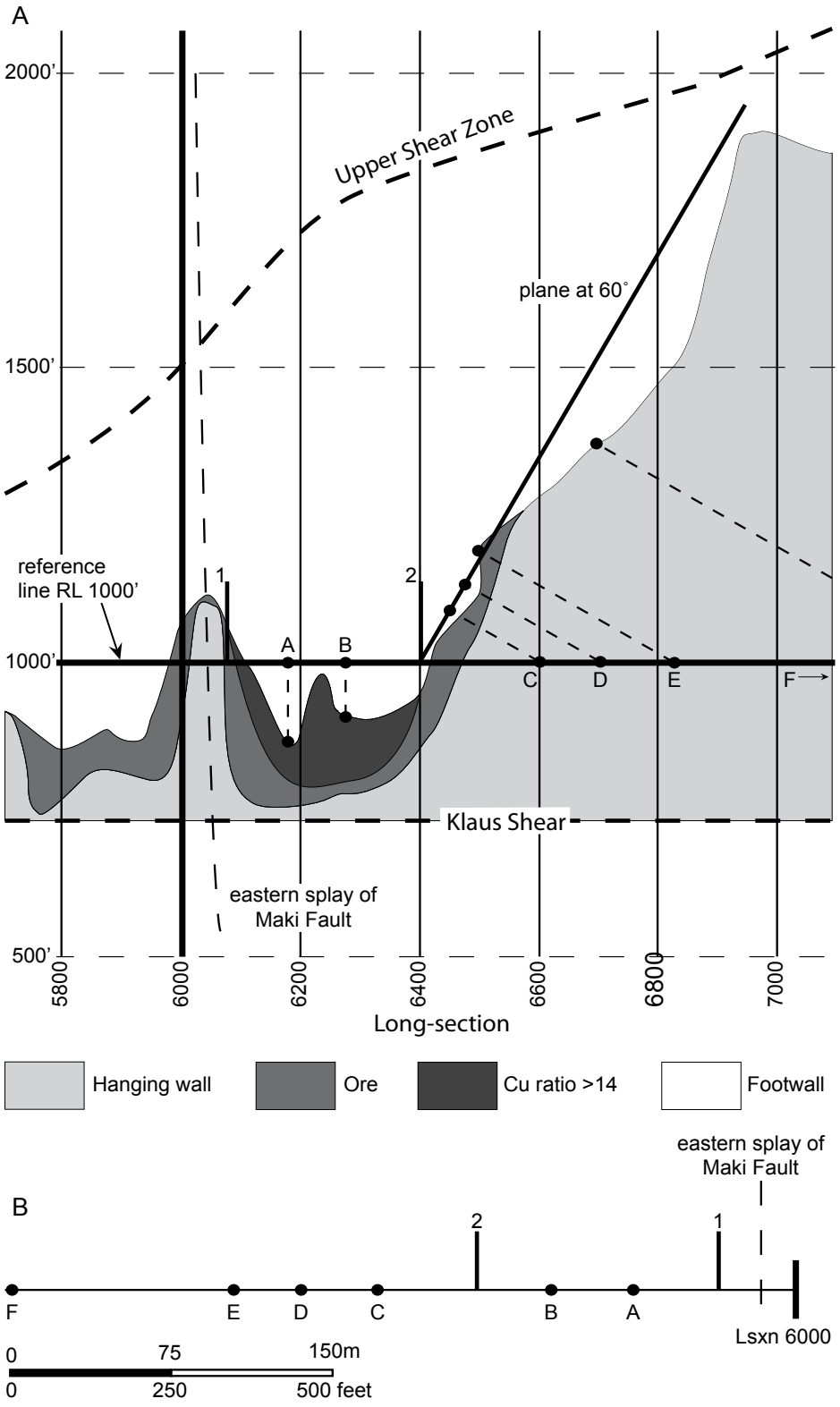

Figure 130 (A) Cross-section 2000 in the East ore zone illustrating the method of structural reconstruction used to estimate the original position of the samples. Note the locations of the Klaus Shear zone and Maki Fault used to constrain the data selected for analyses. Long-section 6400 was used to divide the samples into horizontal and inclined data sets. Samples were rotated 180° about long-section 6000 so that they were right-way-up. (B) Linear order of reconstructed sample positions, for samples 5–10 feet (1.5–3.0 m) into the footwall, along cross-section 2000. Letters label sample positions and numbers label positions of elevated Cu ratios within ore.

reliable. However, sample positions across many cross-sections may be quite inaccurate. This is particularly true the further a point is from the reference position in each section. In the case of the NWW ore zone, samples along the upper limb are the furthest from the reference position while in the East ore zone, samples at elevations >1500 feet (450 m) have a high likelihood of being inaccurately re-positioned.

As a result of the likely inaccuracies in the reconstructions, the trend and shape of features are considered to be approximate and are interpreted accordingly. For example, the trends in feeder zones, possibly related to synvolcanic structures identified in the present study, are broadly northwest–southeast. This is approximately 40° off the trend of synvolcanic structures identified by Freitag (2000) in the LSW ore zone. However, due to the low precision of the reconstruction method, the interpreted synvolcanic structures could be parallel to those identified by Freitag (2000). The clustering of samples in the present study is considered real and this is the basis upon which the interpretations are built. More sophisticated attempts at reconstructing the ore bodies were not attempted as they were much more time intensive and, due to the extreme deformation at Greens Creek, it is felt that they would only marginally improve the accuracy of the reconstructions.

Metal contours in this study were generated using the contouring program SURFER (v. 7.0). Due to the irregular spacing between samples, a contouring method of inverse distance squared was used. Contour thresholds were initially based on the first through third quartile values of the data (both NWW and East ore data combined) and adjustments were then made to these values in order to highlight subtle differences within the data.

Review of the geology

This section provides a brief overview of the geology and alteration in the NWW and East ore zones which are the areas reported on in this chapter. A complete description of the geology of these zones can be found in Chapter 3 and of the alteration in Chapter 6.

Figure 131 shows the approximate boundaries, in cross-sectional and plan views, of the present footwall metal zonation study. In this section, one representative cross-section from each ore zone is examined and the reconstructed plan view of sample locations with the alteration zonation of the footwall is presented. The method used to create the reconstructed plan views is discussed above and illustrated in Figure 129 and Figure 130.

The dominant structure in the NWW ore zone is a recumbently folded syncline verging to the east that is truncated, on the eastern side, by the Maki Fault at approximately long-section 5100 (Figure 132). The lower limb of the syncline has the thickest accumulation of massive sulfide (>50 feet (15 m) and the entire length of the ore along this limb has Cu ratios ≥ 14 between cross-sections 4300 and 4700. Below this is a thick section of intensely quartz–pyrite altered footwall rock that has variable textures ranging from pseudo-brecciated to massive. This quartz–pyrite alteration grades into the less altered sericite alteration zone. The chlorite alteration zone is not well developed here.

The upper limb has a thinner band of massive sulfide (<50 feet (15 m)) generally with lower Cu concentrations (<818 ppm) in the footwall. However, on this upper limb, there is one portion of the ore with an elevated Cu ratio centred on approximately long-section 4800 between cross-sections 4500 and 5000. The quartz–pyrite alteration zone along the upper limb is thin to non-existent and the alteration is dominantly sericite with lesser chlorite alteration. The NWW ore body gradually thins north of cross-section 4600 and rapidly thins south of cross-section 4300. The plan view of sample locations 5–10 feet (1.5–3.0 m) into the footwall illustrates that the most intense quartz–pyrite alteration is found beneath the zones in the ore body that have Cu ratios >14 and sericite alteration is dominant below the remainder of the ore body (Figure 133).

The dominant structure in the East ore zone is the moderately to steeply west-dipping limb that shallows as it approaches the Klaus Shear zone at approximately 800–1000

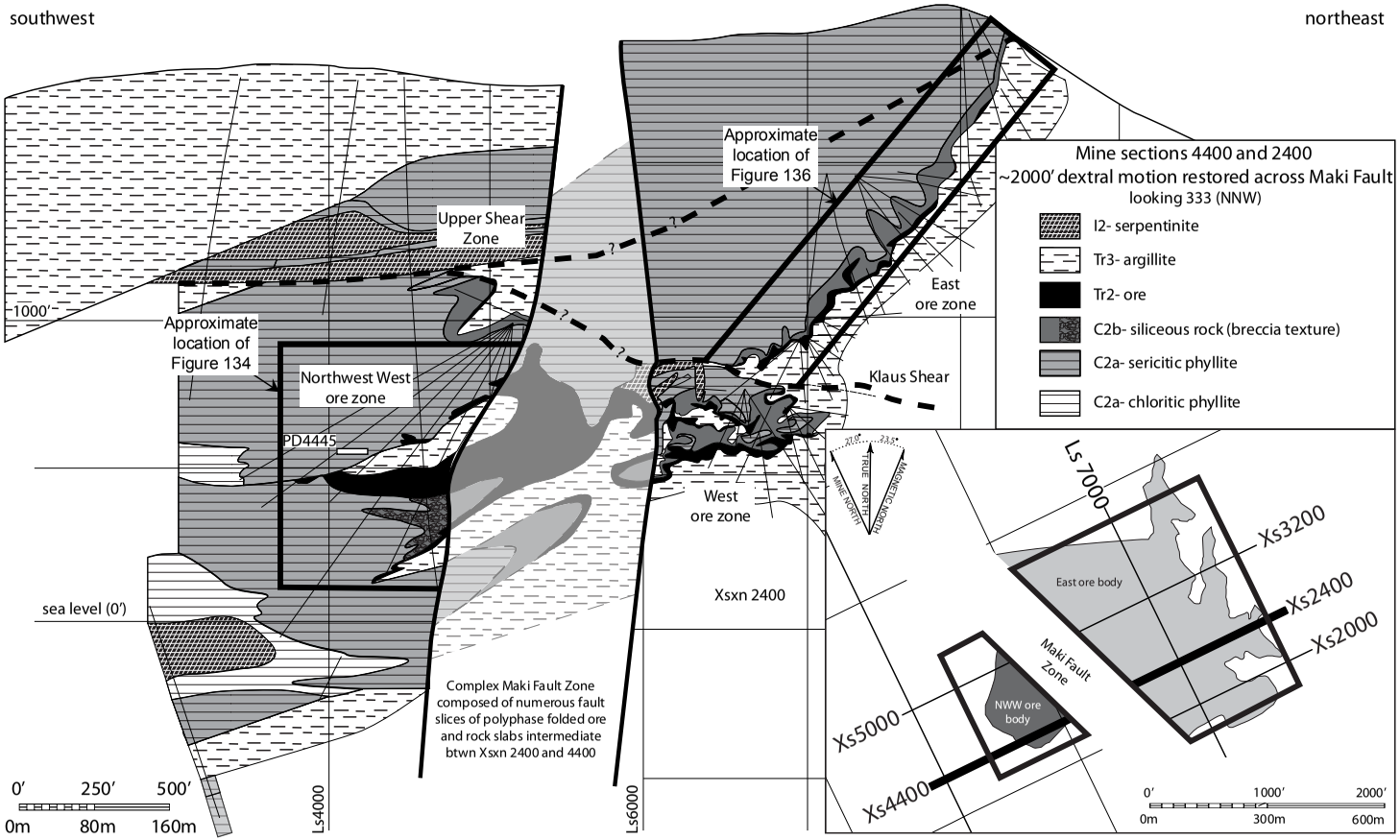

Figure 131 Restored cross-sections 4400 and 2400. Approximately 2000 feet (600 m) of right-lateral displacement along the Maki Fault has been restored to join cross section 4400 (W of Maki) and 2400 (E of Maki). Geology from Lindberg (1996a). Note the location of Figure 132 and approximate location of Figure 134. Figure 134 is located 400 feet (120 m) south at cross-section 2000. Cross-section 2000 was chosen, instead of cross-section 2400, to represent the geology in the vicinity of the East ore body because the overall structure is similar to that of cross-section 2400 but cross-section 2000 has a thicker accumulation of flat-lying mineralization and the alteration zones are better developed. Inset is a plan view of the lateral extents of the metal zonation study of the footwall to the NWW and East ore bodies with approximately 2000 feet (600 m) of right-lateral motion restored across the Maki Fault. Ore bodies are projected vertically to the surface (A. West, written comm.).

feet (300 m) elevation and is truncated on its western margin by the Maki Fault. The thickest accumulations of ore (>50 feet (15 m)) are found on the relatively flat-lying portion of the limb, between long-sections 6000 and 6400 and cross-sections 2000 and 2300. This flat-lying portion of the ore body has Cu ratios ≥14. On the inclined portion of the limb, the ore is thinner (<50 feet (15 m)) and with Cu ratio <14. However, between cross-sections 3300 and 3500 there is another zone with elevated Cu ratios. The zone of intense quartz–pyrite alteration generally extends <75 feet (25 m) into the footwall and is most obvious on the inclined portion of the limb. On both the flat and inclined portion of the limb, the sericite alteration zone extends up to approximately 200 feet (60 m) into the footwall before grading into the background chlorite alteration zone. At depths between 5 and 10 feet (1.5–3.0 m) into the footwall, the intense quartz–pyrite alteration is approximately centered on the portions of the ore which have Cu ratios ≥14. However, this alteration appears to be much more laterally extensive than the zone, within the ore, that has an elevated Cu ratio. The portion of the ore between cross-sections 3300 and 3500 with Cu ratios ≥14 does not have quartz–pyrite alteration in the footwall at the depths examined during the present study.

The protoliths in the footwall appear to be the same between the NWW and East ore zones possibly with the exception of the breccia unit. In the NWW the breccia unit is typically monomictic and is interpreted as a pseudo-breccia (C2b) where as in the East ore zone, the breccia is dominantly polymict and is interpreted as sedimentary in origin (Tr1). However, in both ore zones the breccias are associated with the intense quartz–pyrite alteration and original features are often obscured. The NWW ore body appears to have thicker accumulations of sulfide and correspondingly thicker accumulations of quartz–pyrite alteration within the footwall than does the East ore body. It is interpreted that these features are, at least partially, primary as they are related to zones of elevate Cu ratios which in VHMS deposits are typically associated with the central feeder zones (Knuckey et al., 1982; Gemmell and Large, 1992). However, it is acknowledged that

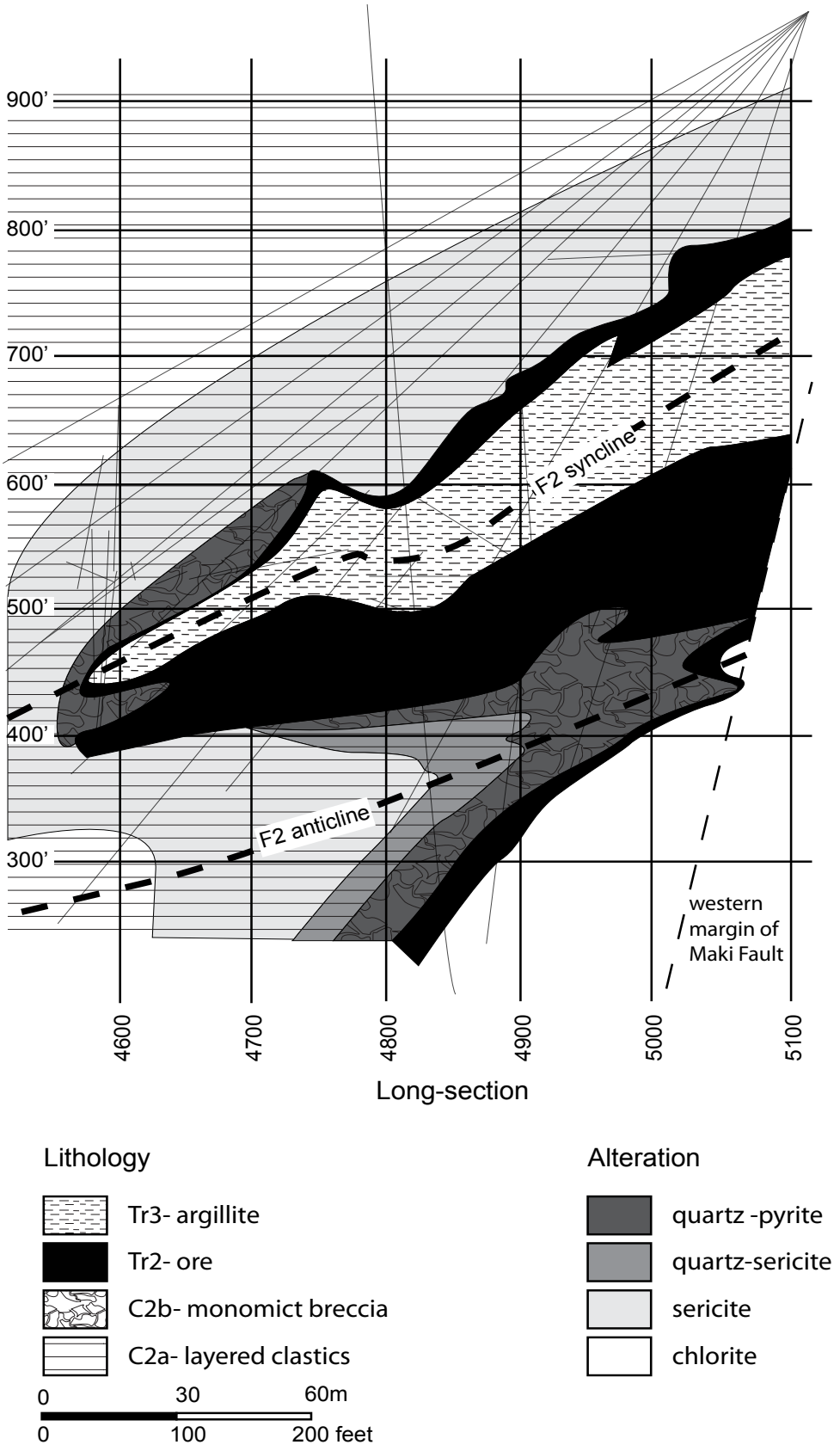

Figure 132 East–west cross-section 4400 in the NWW ore zone with the ore, lithologies and alteration zonation illustrated. Note the thicker ore accumulation on the lower limb and the correspondingly thicker zone of intense quartz–pyrite alteration. The zone of Cu ratio ≥ 14 is taken from the current Greens Creek block model (A. West, written comm.)

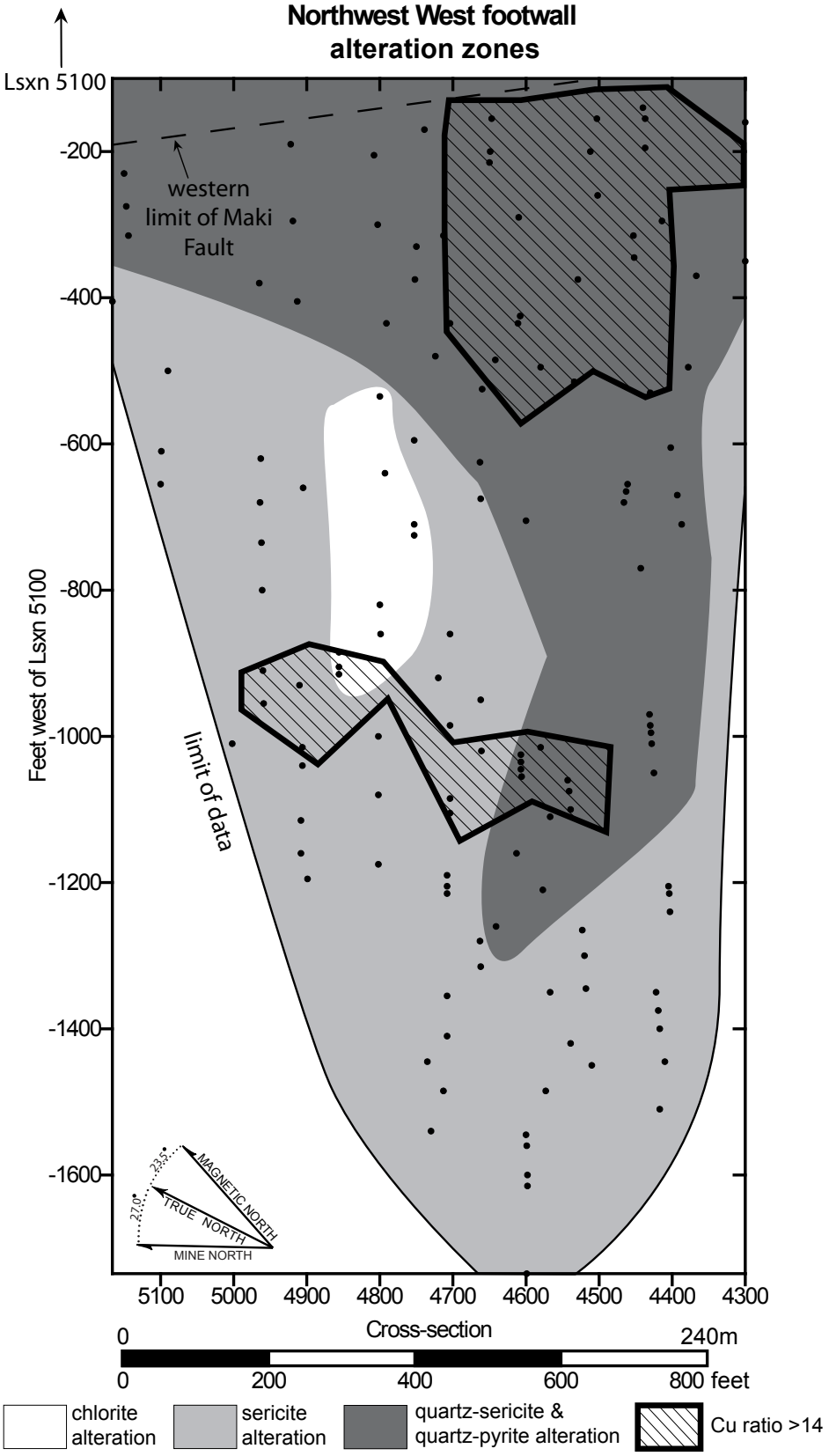

Figure 133 Reconstructed plan view of the lithologies 5–10 feet (1.5–3.0 m) into the footwall of the NWW ore zone. Note the location of the reference point, long-section 5100, and the western margin of the Maki Fault. The East ore zone is located over 1000 feet (300 m) to the restored west of the margins of the restored NWW ore body. The zone of Cu ratio ≥ 14 is taken from the current Greens Creek block model (A. West, written comm.)

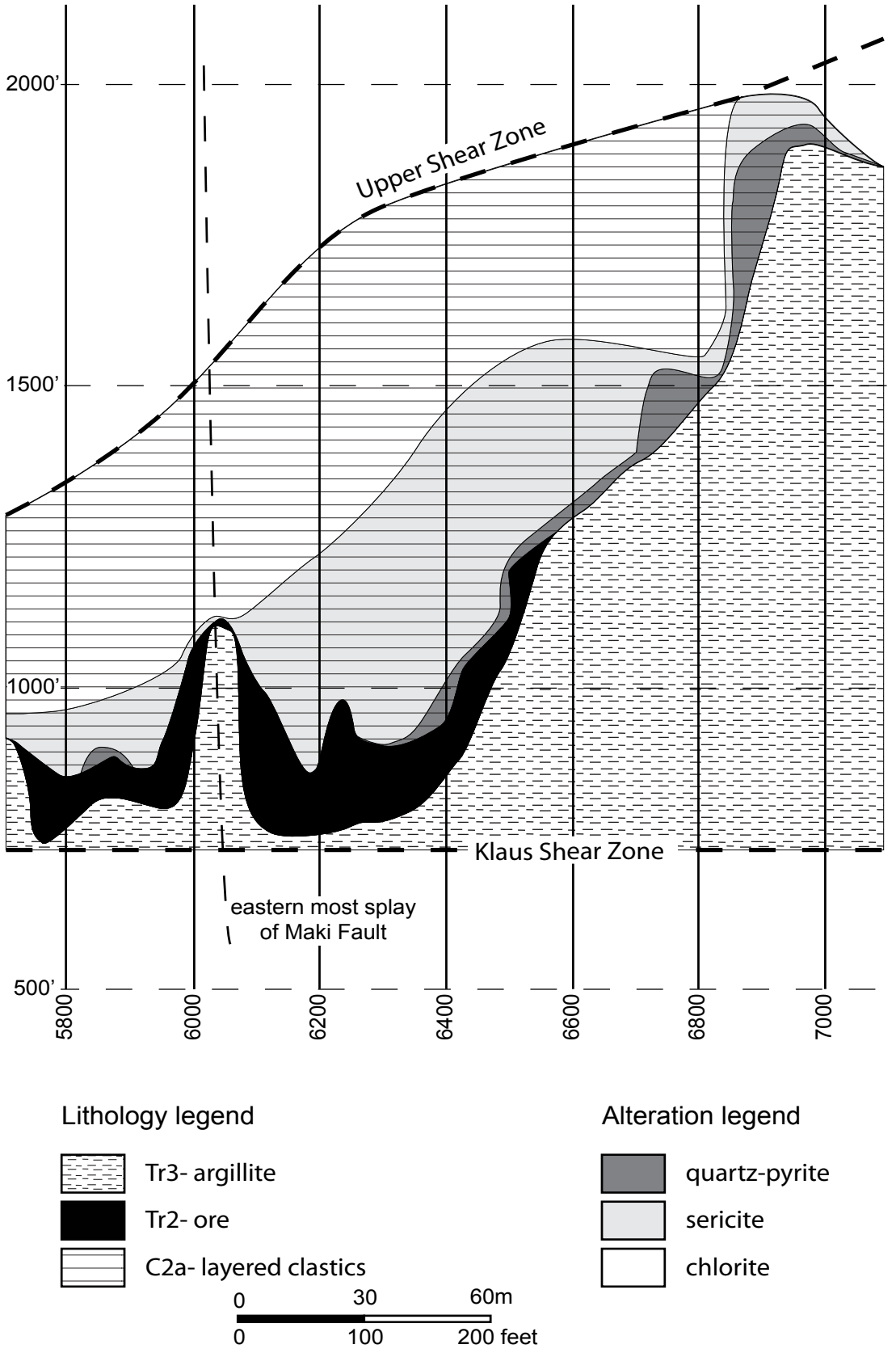

Figure 134 East–west cross-section 2000 in the East ore zone with the ore, lithologies and alteration zonation illustrated. Note the thicker ore accumulation immediately above the Klaus Shear and the correspondingly thicker zone of sericite alteration. The zone of Cu ratio ≥ 14 was created by kriging the assay data using 10x10x10 feet (3x3x3 m) blocks.

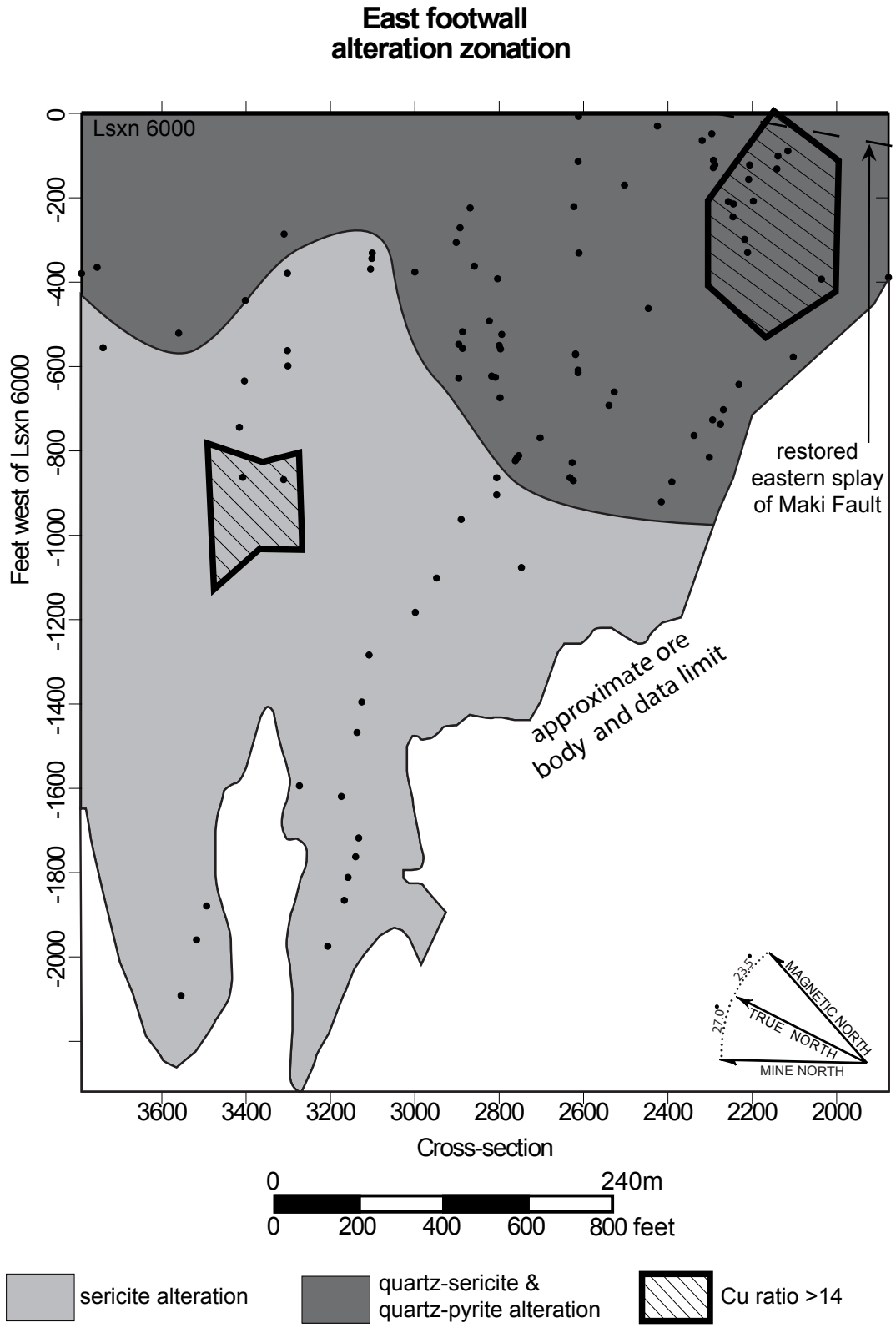

Figure 135 Reconstructed plan view of the lithologies 5–10 feet (1.5–3.0 m) into the footwall of the East ore zone. Note the location of the reference point, Lsxn 6000, and the restored eastern margin of the Maki Fault. The NWW ore zone is located over 1000 feet (300 m) to the restored east of the margins of the restored East ore body. The limit of data roughly corresponds to the plan view extent of the ore body and is projected from company data (A. West, written comm.).

the thick accumulations, particularly in the NWW ore body, are in areas of structural complexity and structural thickening has also likely occurred.

Results

Metal contours beneath mineralization in the Northwest West ore and East ore zones at the Greens Creek deposit (Figure 136 to Figure 147) illustrate the Cu, Zn, Pb, Ag, Cu ratio and Zn ratio 5–10 feet (1.5–3.0 m) below the ore position in each zone. Beneath the NWW ore body, Cu is generally elevated and has a dissimilar distribution pattern to that of Pb, Zn and Ag (Figure 136 to Figure 139). In contrast, the Cu, Pb and Zn distribution patterns in the footwall to the East ore body are broadly similar (Figure 142 to Figure 144) and almost all of the East ore zone footwall has elevated Ag values (>41 ppm) (Figure 127). In the footwall to both the NWW and East ore bodies, the Cu and Zn ratio relationship is broadly antithetic (Figure 140, Figure 141, Figure 146 & Figure 147). In the footwall to both ore bodies, samples with quartz–pyrite alteration are associated with high Cu values (>818 ppm) and Cu ratios (≥20) which are broadly coincident with lows in Pb (<676 ppm), Zn (<3859 ppm), Ag (<16 ppm) and Zn ratio (<83). The sericite alteration zone is broadly associated with lower Cu values, elevated Pb and Ag values and lower Zn ratios.

Cu–Zn ratios

In Phanerozoic VHMS deposits, the Zn ratio varies from 60 to 90 (Huston and Large, 1987). However, average Zn ratio values differ between deposits and between ore types within a single deposit. These variations reflect the differences in the depositional temperature and salinity of the ore-forming fluids (Huston and Large, 1987). The Cu ratio has also been used to constrain the physiochemical conditions of ore formation but this ratio has been found to be unreliable, particularly when Cu levels are low (i.e. Knuckey et al., 1982). At Greens Creek, the mean of the Zn and Cu ratio of samples in the footwall to the NWW ore body is only slightly higher than those in the footwall to the East ore body, indicating the physiochemical conditions associated with ore formation were broadly similar.

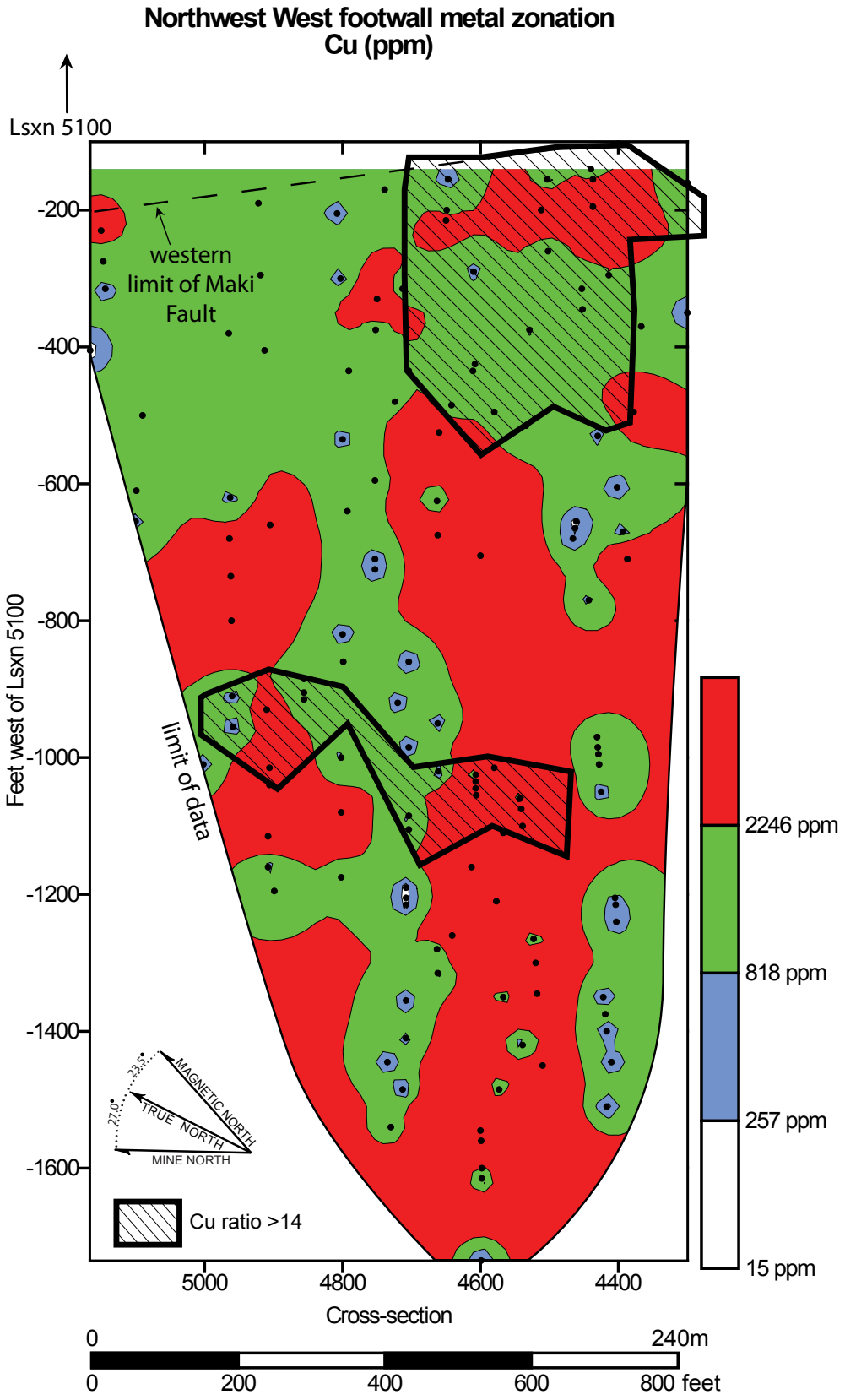

Figure 136 Distribution of Cu in the footwall, at depths of 5–10 feet (1.5–3.0 m), beneath the NWW ore body. Specifications for reconstructed location of samples are given in Appendix V. Zones of Cu ratios ≥14 within the overlying ore body are taken from current mining block models (A. West, written comm.).

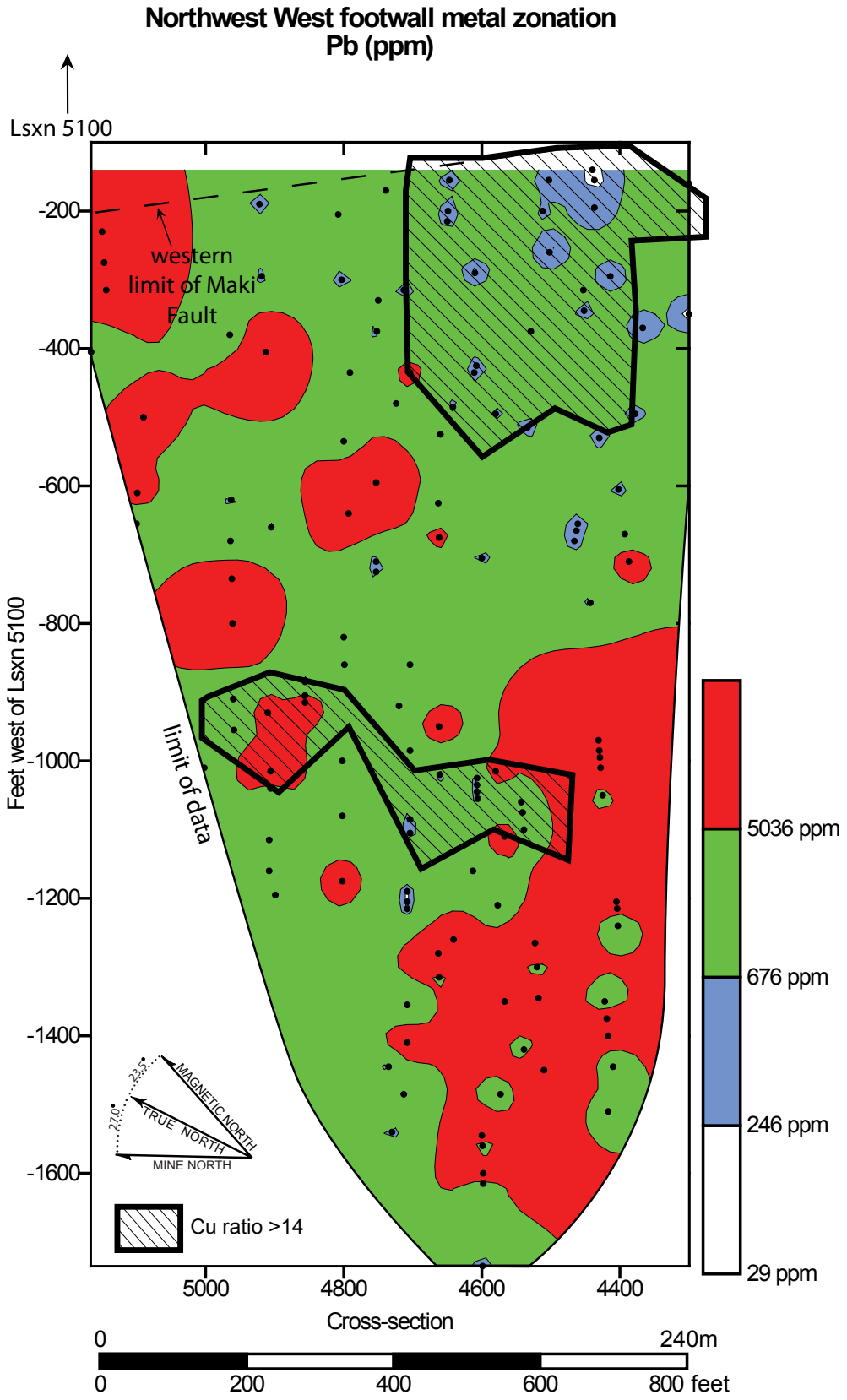

Figure 137 Distribution of Pb in the footwall, at depths of 5–10 feet (1.5–3.0 m), beneath the NWW ore body. Specifications for reconstructed location of samples are given in Appendix V. Zones of Cu ratios ≥14 within the overlying ore body are taken from current mining block models (A. West, written comm.).

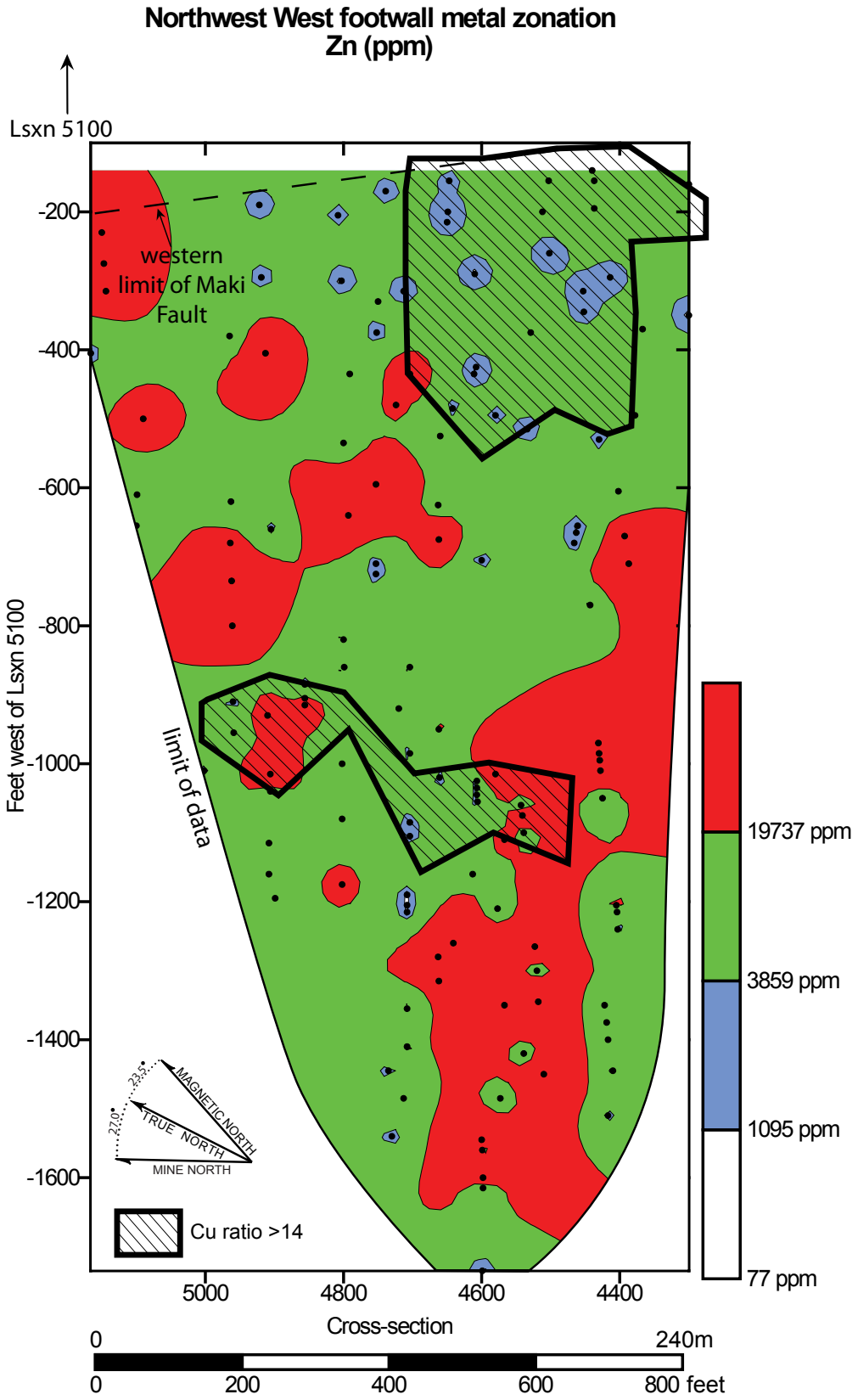

Figure 138 Distribution of Zn in the footwall, at depths of 5–10 feet (1.5–3.0 m), beneath the NWW ore body. Specifications for reconstructed location of samples are given in Appendix V. Zones of Cu ratios ≥14 within the overlying ore body are taken from current mining block models (A. West, written comm.).

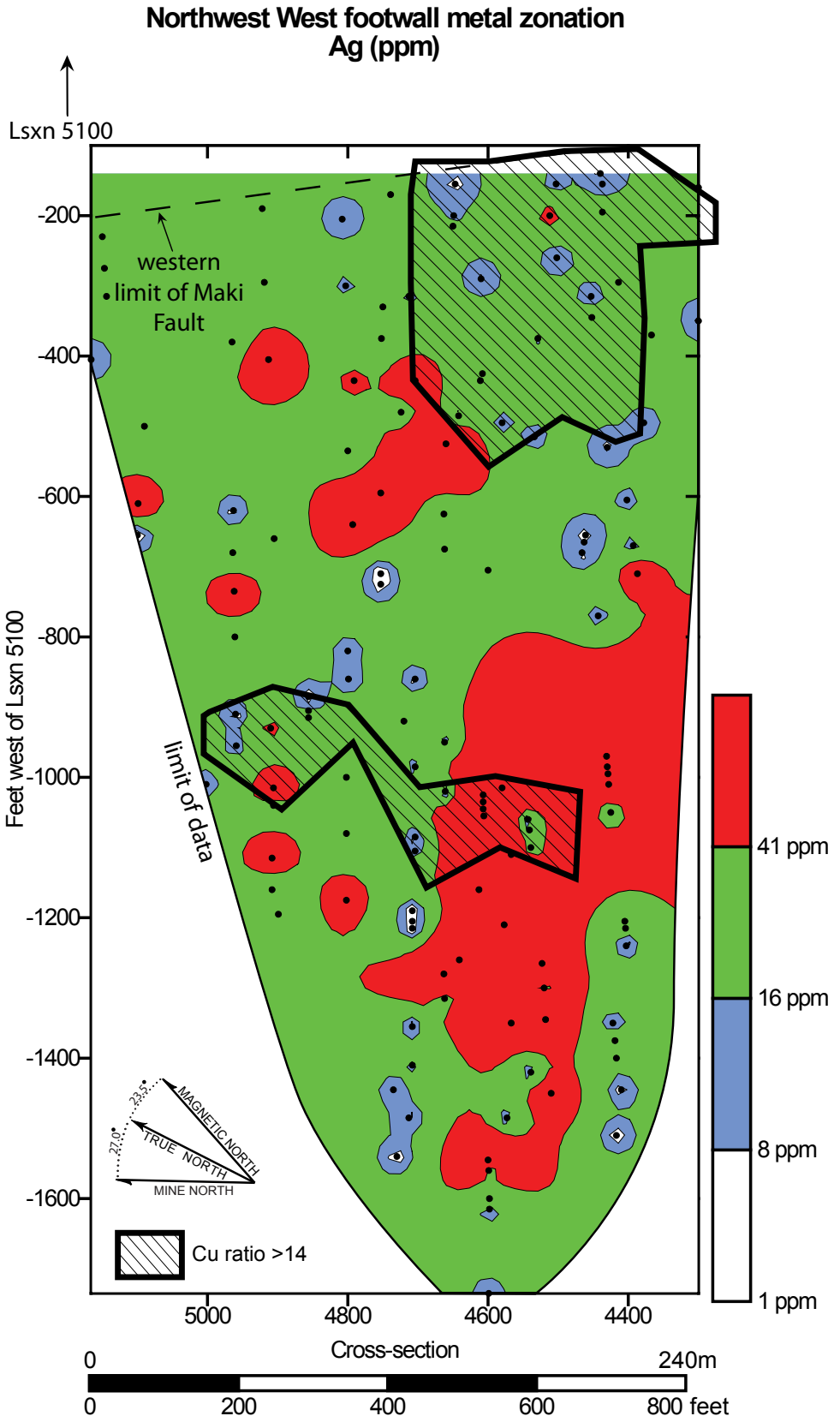

Figure 139 Distribution of Ag in the footwall, at depths of 5–10 feet (1.5–3.0 m), beneath the NWW ore body. Specifications for reconstructed location of samples are given in Appendix V. Zones of Cu ratios ≥14 within the overlying ore body are taken from current mining block models (A. West, written comm.).

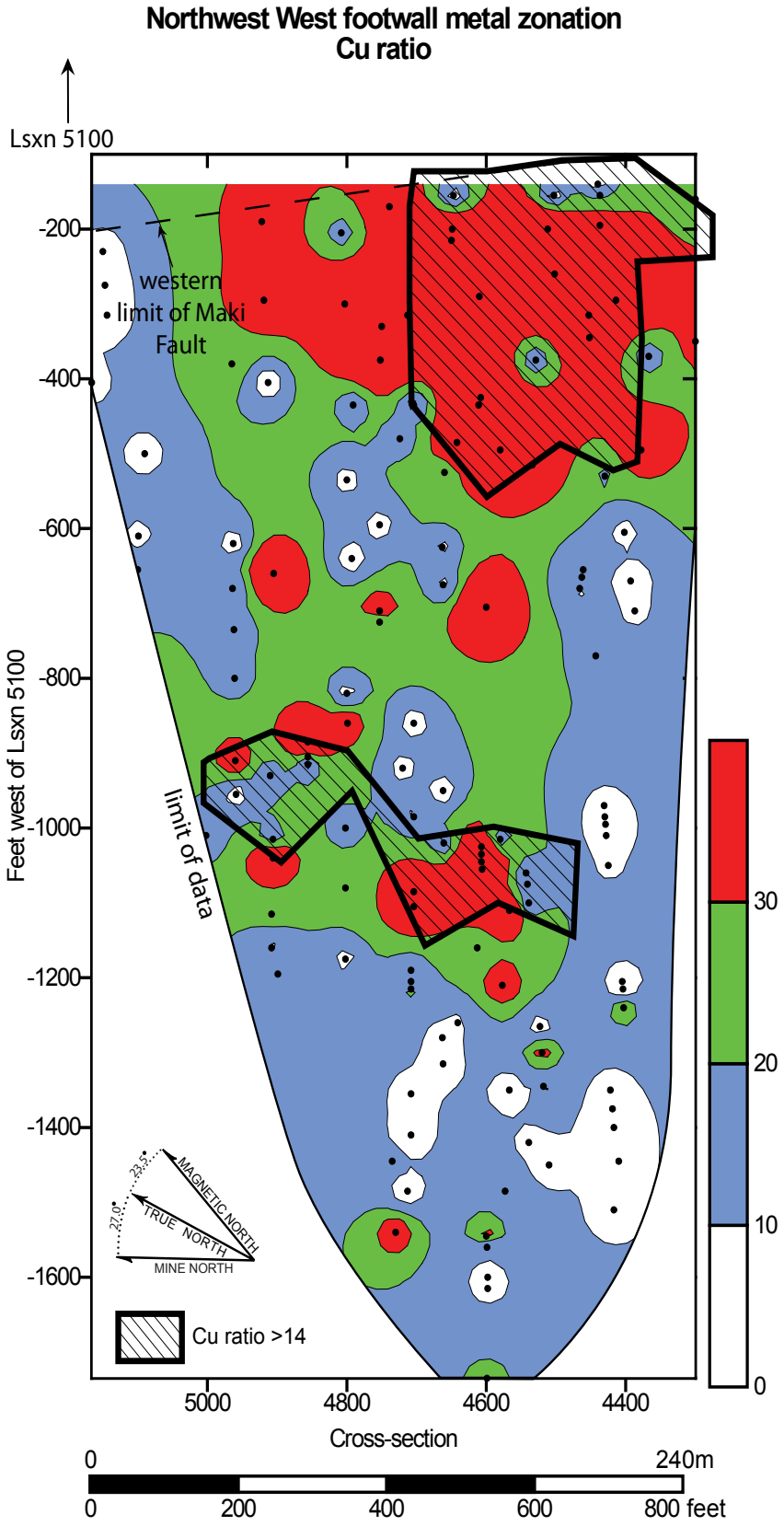

Figure 140 Distribution of Cu ratio in the footwall, at depths of 5–10 feet (1.5–3.0 m), beneath the NWW ore body. Specifications for reconstructed location of samples are given in Appendix V. Zones of Cu ratios ≥14 within the overlying ore body are taken from current mining block models (A. West, written comm.).

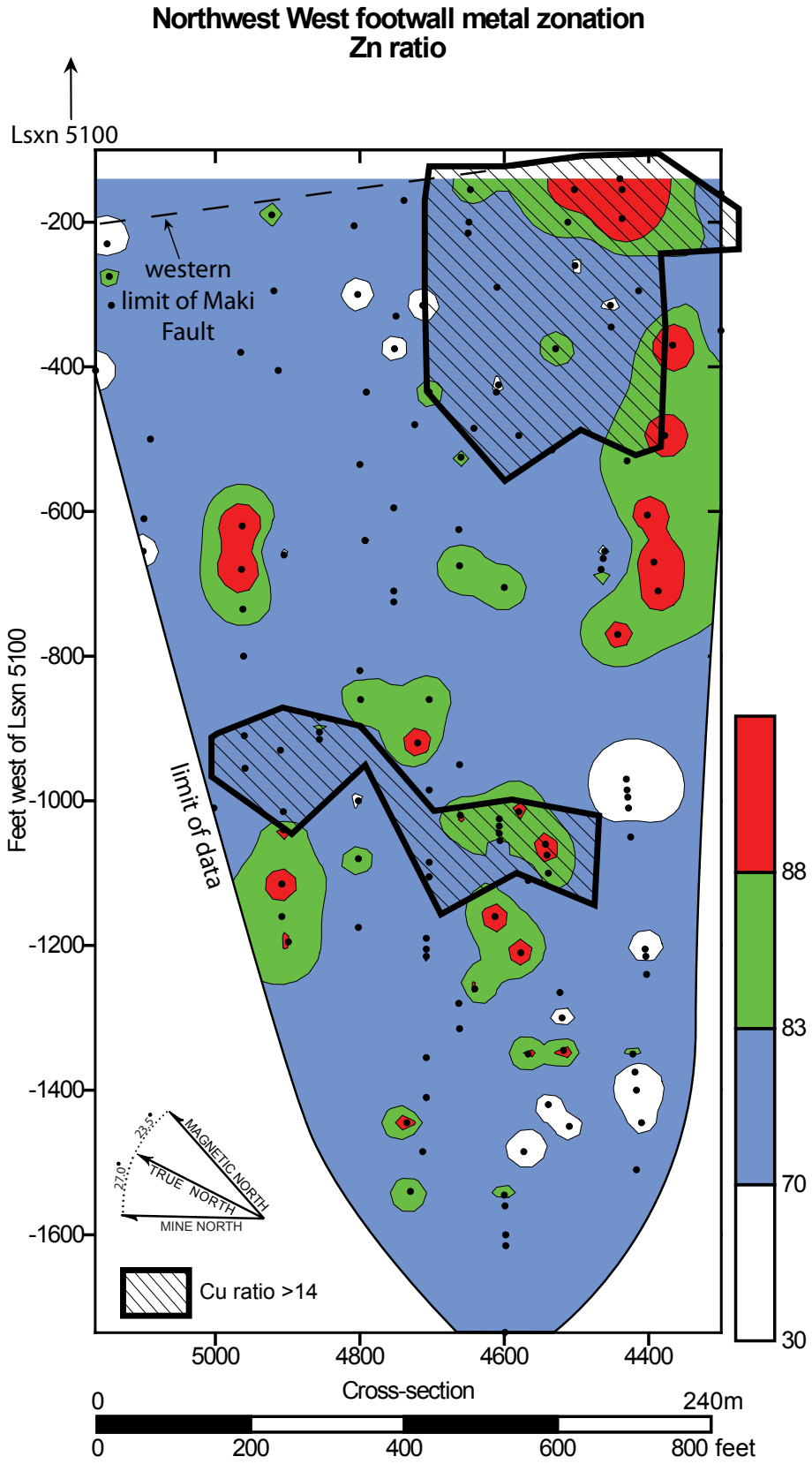

Figure 141 Distribution of Zn ratio in the footwall, at depths of 5–10 feet (1.5–3.0 m), beneath the NWW ore body. Specifications for reconstructed location of samples are given in Appendix V. Zones of Cu ratios ≥14 within the overlying ore body are taken from current mining block models (A. West, written comm.).

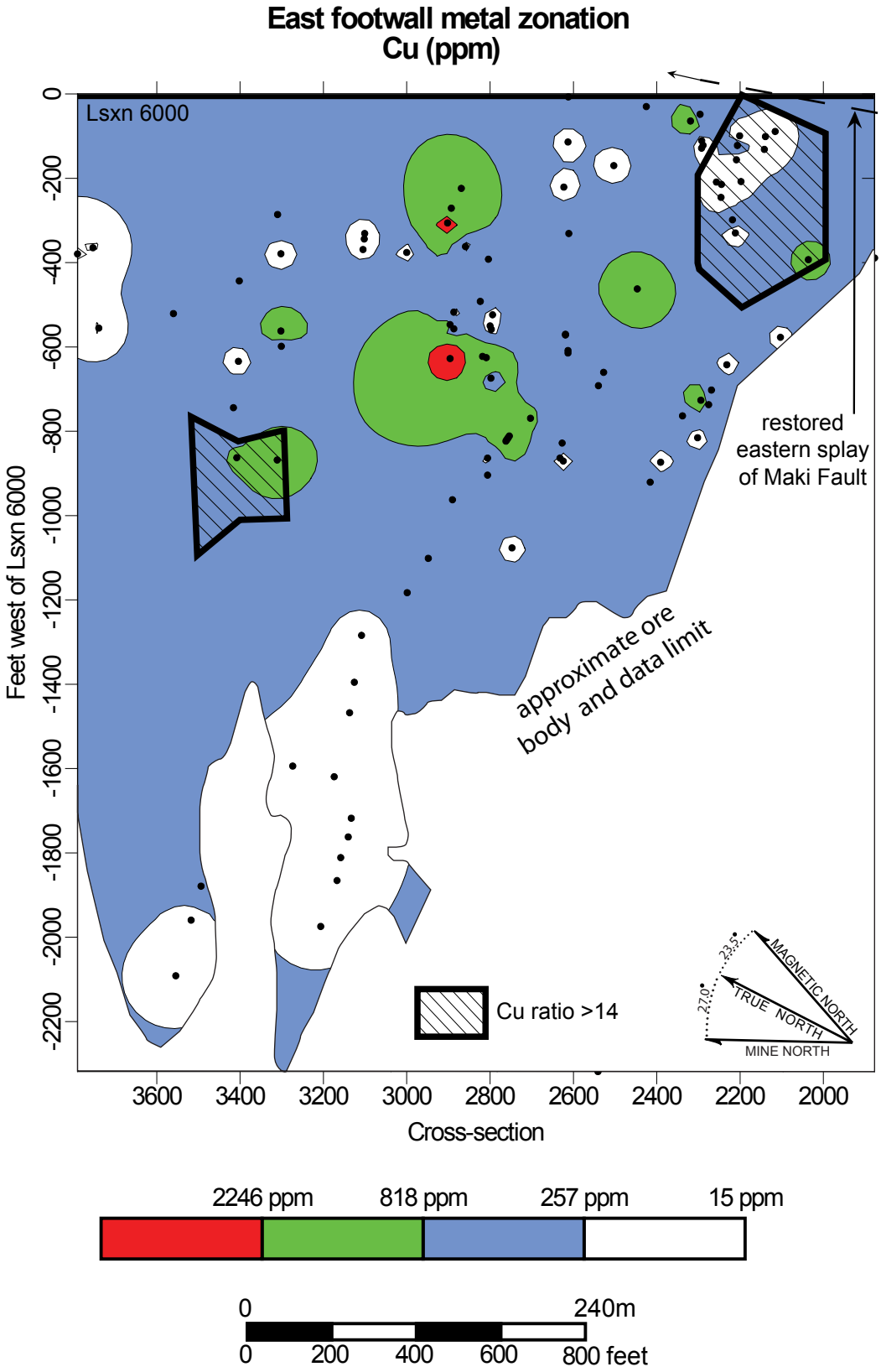

Figure 142 Distribution of Cu in the footwall, at depths of 5–10 feet (1.5–3.0 m), beneath the East ore body. Specifications for reconstructed location of samples are given in Appendix V. Zones of Cu ratios ≥14 within the overlying ore body are taken from kriged assay data and the approximate outline of the ore body is from company maps (A. West, written comm.).

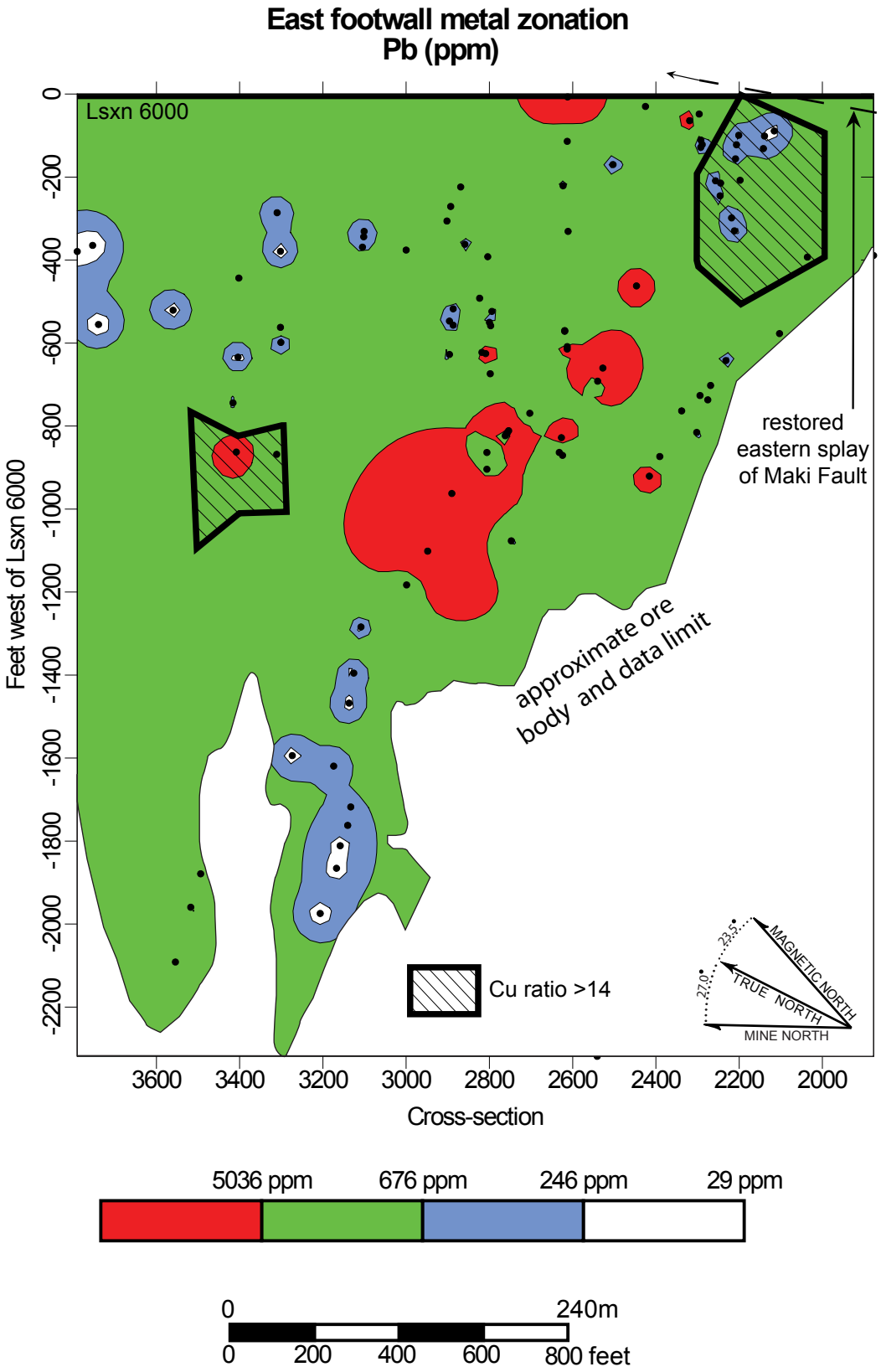

Figure 143 Distribution of Pb in the footwall, at depths of 5–10 feet (1.5–3.0 m), beneath the East ore body. Specifications for reconstructed location of samples are given in Appendix V. Zones of Cu ratios ≥14 within the overlying ore body are taken from kriged assay data and the approximate outline of the ore body is from company maps (A. West, written comm.).

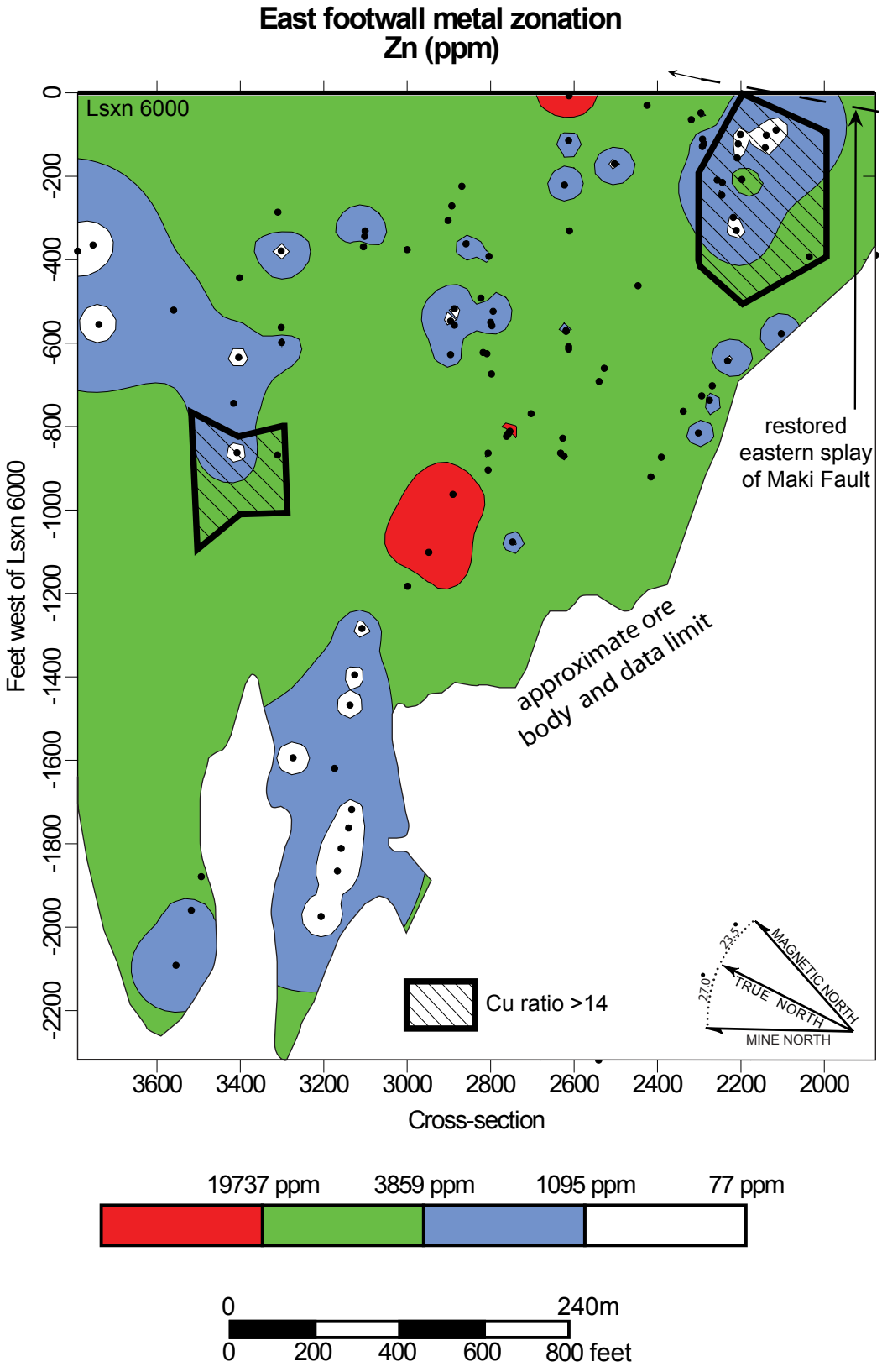

Figure 144 Distribution of Zn in the footwall, at depths of 5–10 feet (1.5–3.0 m), beneath the East ore body. Specifications for reconstructed location of samples are given in Appendix V. Zones of Cu ratios ≥14 within the overlying ore body are taken from kriged assay data and the approximate outline of the ore body is from company maps (A. West, written comm.).

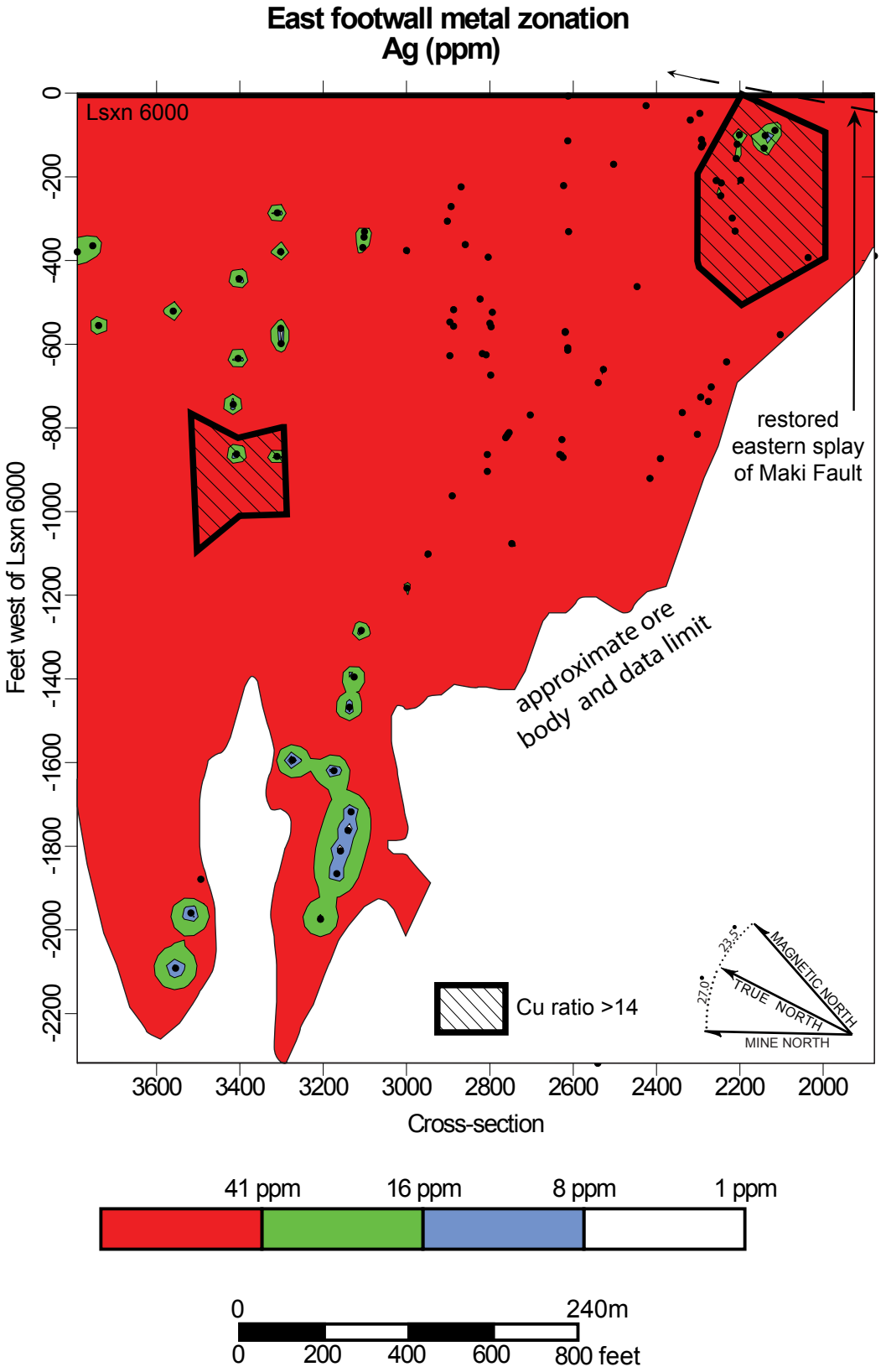

Figure 145 Distribution of Ag in the footwall, at depths of 5–10 feet (1.5–3.0 m), beneath the East ore body. Specifications for reconstructed location of samples are given in Appendix V. Zones of Cu ratios ≥14 within the overlying ore body are taken from kriged assay data and the approximate outline of the ore body is from company maps (A. West, written comm.).

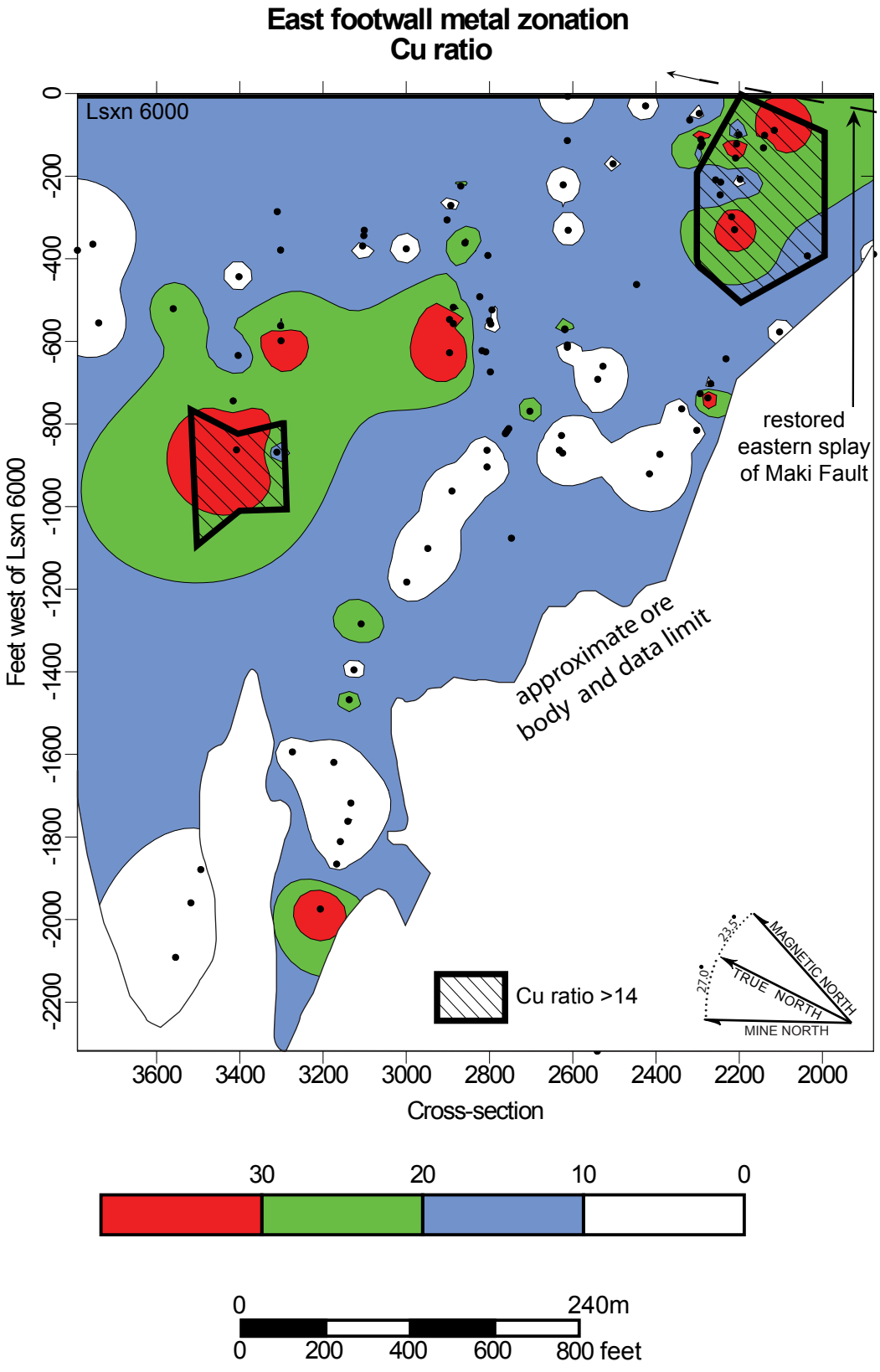

Figure 146 Distribution of Cu ratio in the footwall, at depths of 5–10 feet (1.5–3.0 m), beneath the East ore body. Specifications for reconstructed location of samples are given in Appendix V. Zones of Cu ratios ≥14 within the overlying ore body are taken from kriged assay data and the approximate outline of the ore body is from company maps (A. West, written comm.).

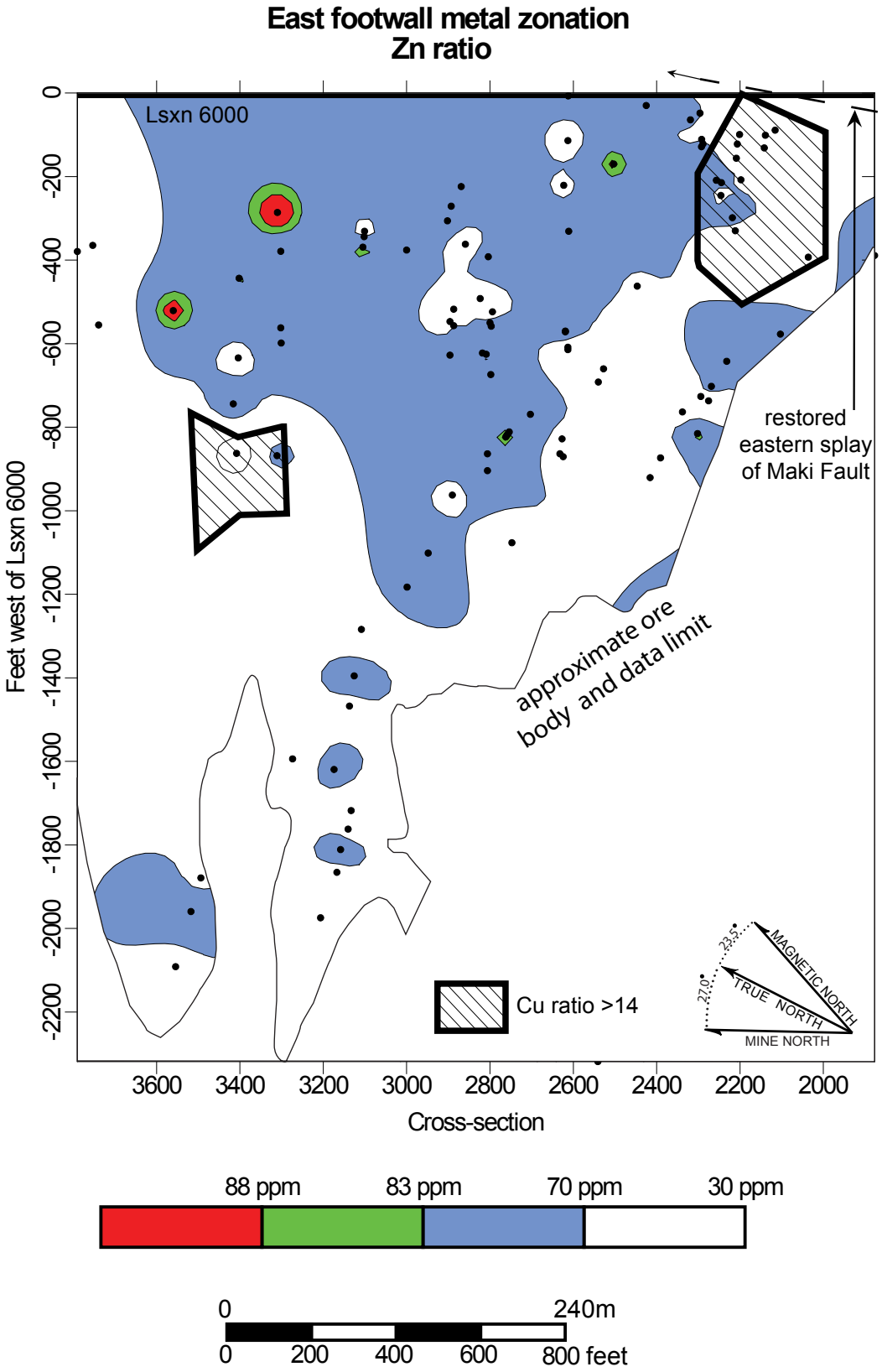

Figure 147 Distribution of Zn ratio in the footwall, at depths of 5–10 feet (1.5–3.0 m), beneath the East ore body. Specifications for reconstructed location of samples are given in Appendix V. Zones of Cu ratios ≥14 within the overlying ore body are taken from kriged assay data and the approximate outline of the ore body is from company maps (A. West, written comm.).

Both ore bodies have two zones with high Cu ratios that are broadly coincident with a zone of low Zn ratio values. These zones with coincident high Cu ratios and low Zn ratios are inferred to be the feeder zones to the overlying ore bodies (Gemmell and Large, 1992). In both cases, one of these feeder zones is large and well-defined, while the second is less well defined. Beneath the NWW ore body, the largest feeder zone (the main feeder) is bound to the east by the Maki Fault and extends to the restored west approximately 400 feet (120 m). This feeder zone is approximately 700 feet (210 m) long between cross-sections 4300 and 5000 (Figure 148). There are several individual samples with elevated Cu ratios scattering to the restored west of the main feeder and a cluster of seven samples approximately 1100 feet (330 m) to the restored west of long-section 5100 between cross-sections 4600 and 4700. This cluster is interpreted as a secondary feeder system which underlies the western portion of the reconstructed NWW ore body (Figure 148).

In the footwall to the East ore body, two feeder zones are again outlined by coincident Cu ratio and Zn ratio anomalies. The main feeder is found within 400 feet (120 m) of the Maki Fault between cross-sections 2000 and 2300 (Figure 149). A second, larger but less well defined feeder system is located approximately 500–1000 feet (150–300 m) to the restored west of the long-section 6000 reference line between cross-sections 3000 and 3500. In this case, the secondary feeder zone appears larger than the primary zone but the sample spacing is much further apart. The total number of samples with elevated Cu ratios and low Zn ratios is relatively small, indicating that the feeder zone may actually be defined by scattered Cu and Zn ratio values as opposed to a consistently anomalous zone.

The Zn and Cu ratios in samples from the footwall to the NWW ore body are illustrated in Figure 150. The footwall to the NWW ore body is characterized by a mean Zn ratio of 80 with a standard deviation of 11 which is characteristic of Phanerozoic Zn-Pb-Cu VHMS deposits (Huston and Large, 1987). In samples from the footwall to the NWW

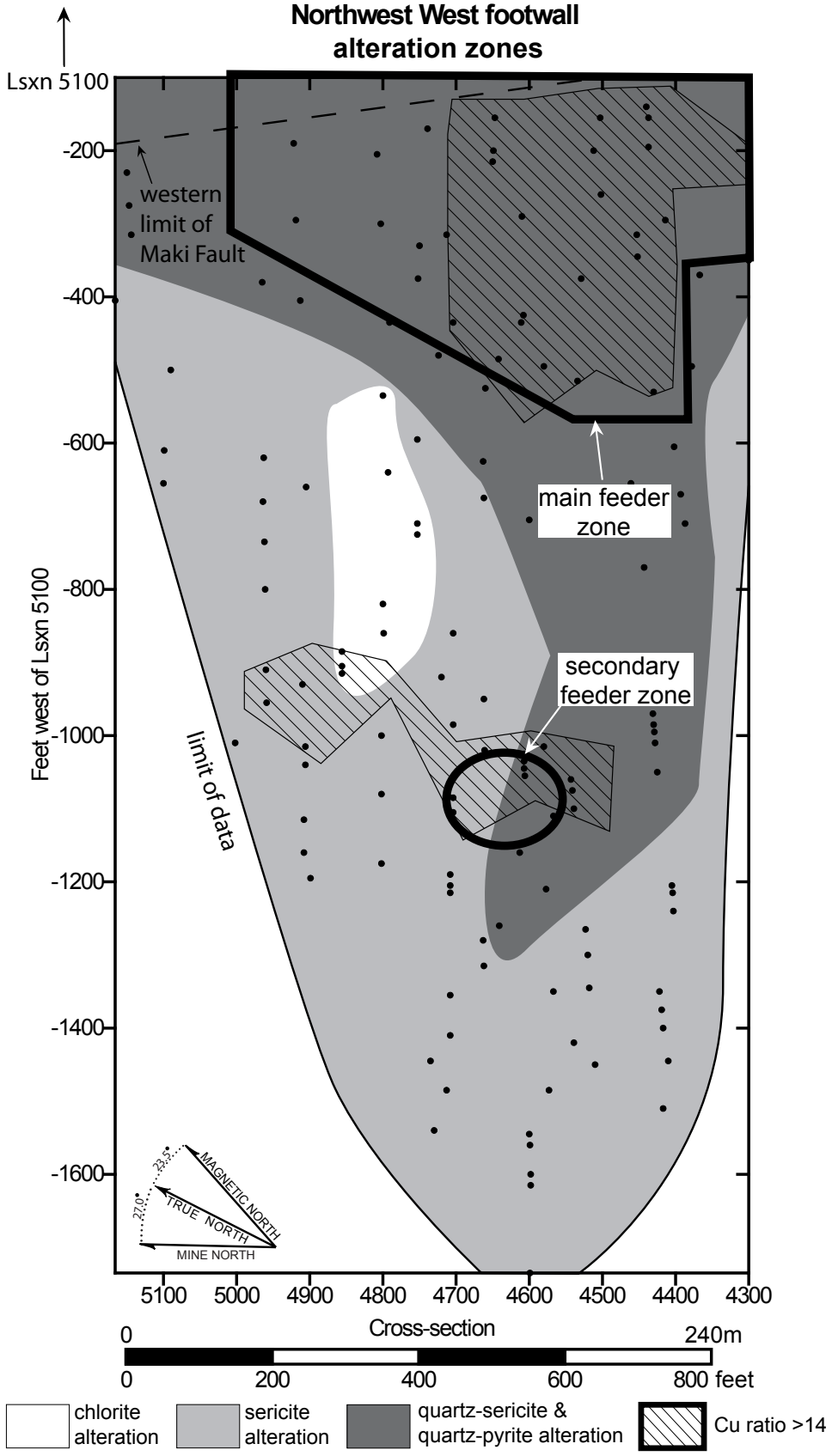

Figure 148 Reconstructed plan view of the lithologies 5–10 feet (1.5–3.0 m) into the footwall of the NWW ore zone. The approximate locations of the main and secondary feeders are labeled. The zone of Cu ratio ≥ 14 is taken from the current Greens Creek block model (A. West, written comm.)

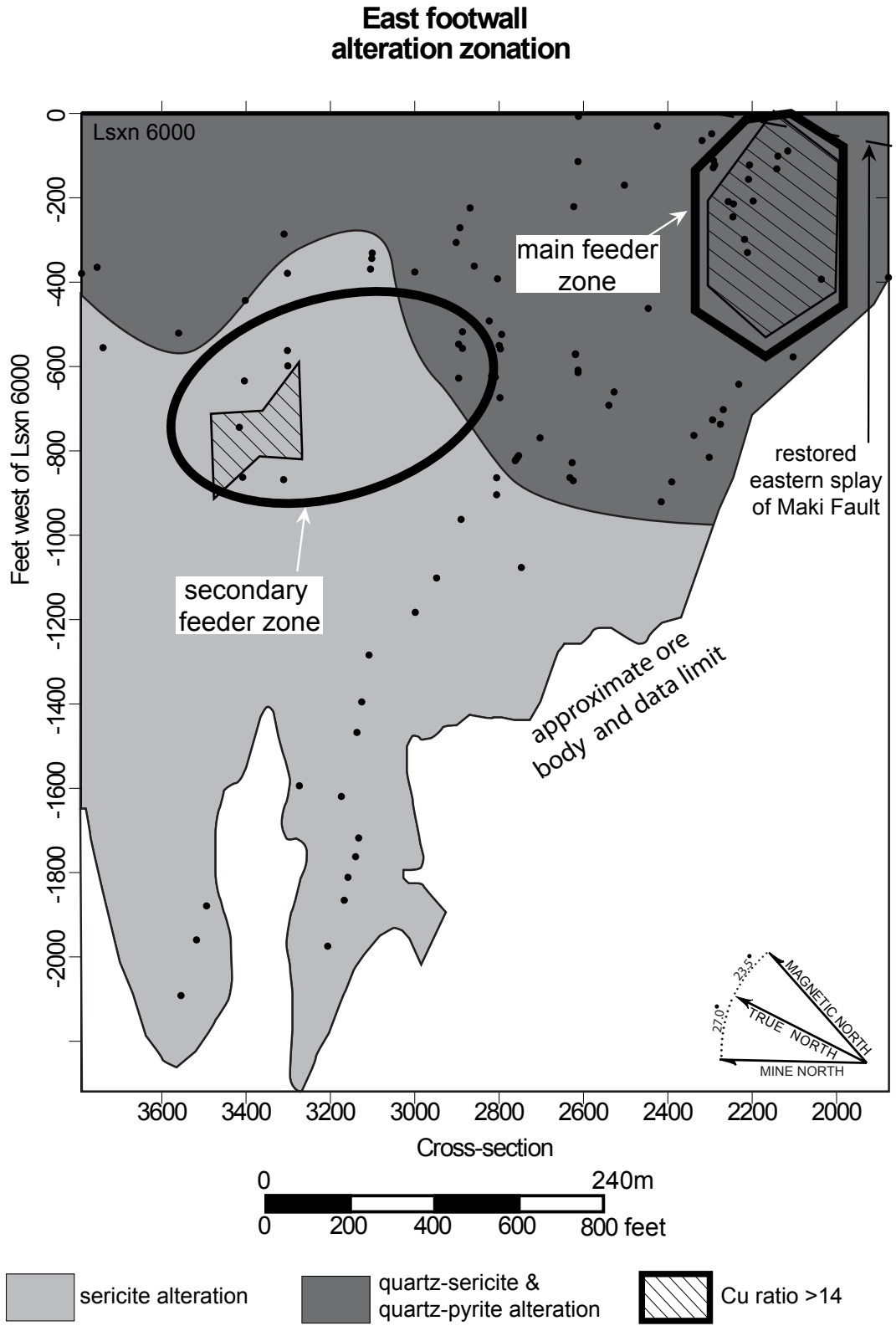

Figure 149 Reconstructed plan view of the lithologies 5–10 feet (1.5–3.0 m) into the footwall of the East ore zone. The approximate locations of the main and secondary feeders are labelled. The zone of Cu ratio ≥ 14 is taken from kriged assay data (A. West, written comm.).

ore body, Zn values are approximately 2.5 times Pb values and Zn and Pb are strongly correlated with an $R^2 = 0.89$. The strong correlation between Zn and Pb in the footwall to the NWW ore body indicates that the ore-forming fluid was saturated with respect to these two metals and that the temperature and salinity were fairly consistent (Huston and Large, 1987). The Cu ratio in the footwall to the NWW ore body ranges from 1 to 100, with a mean of 23 and a standard deviation of 24. Cu and Zn are moderately correlated with Cu values approximately 10% those of Zn values and an R^2 value of 0.55. In the footwall to the NWW ore body, low Zn ratios (<83) and moderate Cu ratios (>20) are associated with quartz–pyrite alteration. The sericite alteration zone is associated with elevated Zn ratios and low Cu ratios.

The Zn and Cu ratios in samples from the footwall to the East ore body are slightly lower than those of the NWW ore body and are illustrated in Figure 150. The mean Zn ratio of all samples from the footwall to the East ore body is 70, with a standard deviation of 14. These values are also similar to those expected for a Phanerozoic VHMS deposit (Huston and Large, 1987). The Zn values, in the footwall to the East ore body, are only 0.4 times those of Pb, and Zn and Pb are also strongly correlated with an R^2 value of 0.93. This high degree of correlation between Pb and Zn again indicates that the ore solution was saturated and had fairly consistent salinity and temperature (Huston and Large, 1987). The overall lower Zn-to-Pb ratio may indicate slightly lower temperatures of formation for the East ore body compared to the NWW ore body. The Cu ratios in samples from the footwall to the East ore body have a similar spread to those in the footwall to the NWW ore body, with a slightly lower mean of 16 and a standard deviation of 19. Cu values are approximately one order of magnitude lower in the footwall to the East ore body (maximum value of 7700 ppm versus 61000 ppm). Cu and Zn are moderately correlated, with Cu approximately 0.1 times that of Zn with an R^2 of 0.67. Cu and Zn ratio anomalies in the footwall to the East ore body have similar relationships to alteration as those in the footwall to the NWW ore body.

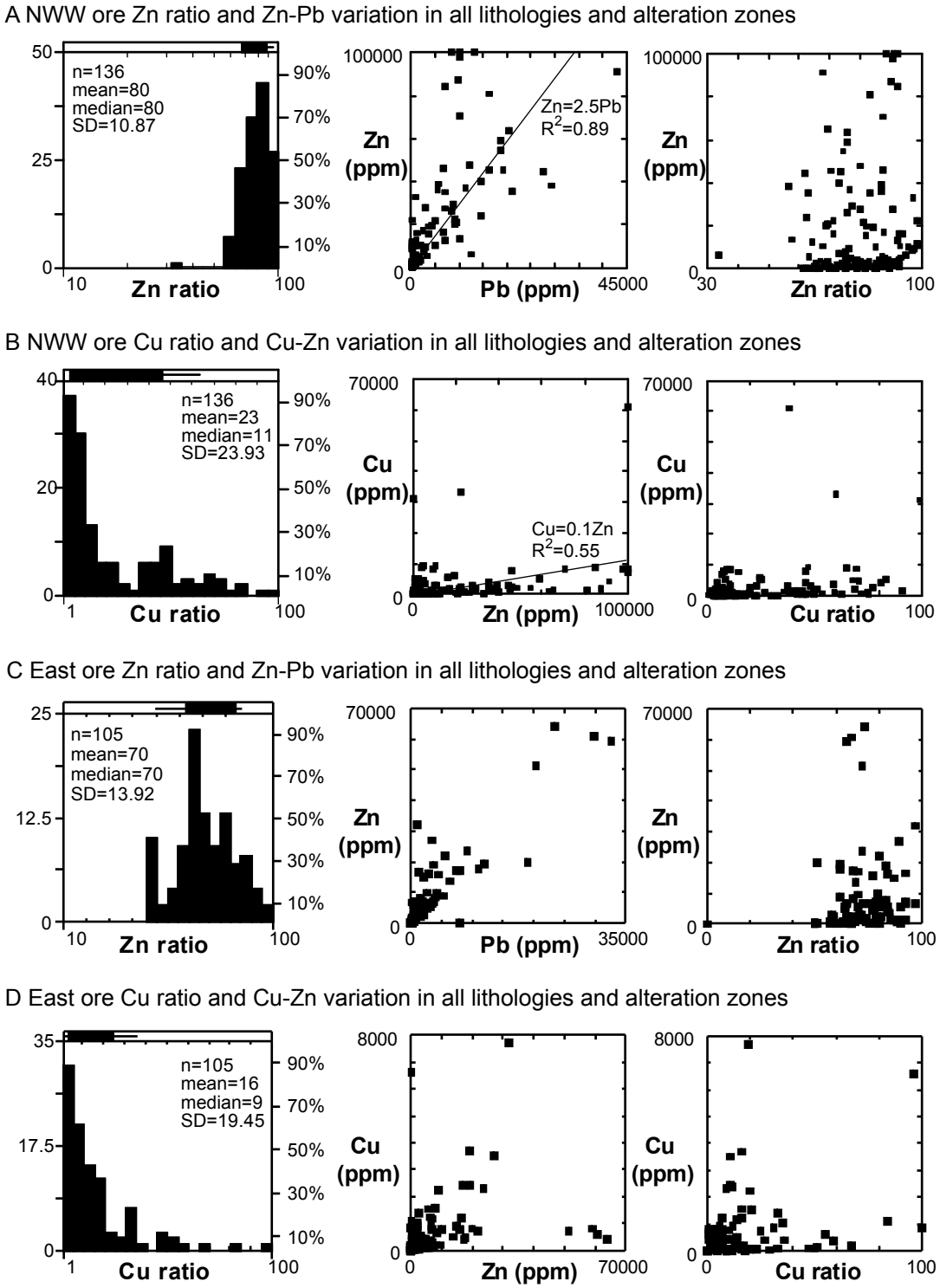

Figure 150 Distribution of the Zn and Cu ratios in the NWW ore body (A and B) and the East ore body (C and D). (A) Zn ratio and Zn-Pb variation in all footwall lithologies and alteration types within the NWW ore zone. (B) Cu ratio and Cu-Zn variation in all footwall lithologies and alteration types within the NWW ore zone. (C) Zn ratio and Zn-Pb variation in all footwall lithologies and alteration types within the East ore zone. (D) Cu ratio and Cu-Zn variation in all footwall lithologies and alteration types within the East ore zone. Samples used are listed in Appendix V. SD = standard deviation.

Metal associations

Scatter and ternary diagrams are useful in assessing the degree of inter-element correlation between metals. The total base-metal contents (Cu+Pb+Zn) and the base-metal/precious-metal correlations, for the footwall to the NWW and East ore zones at Greens Creek, are illustrated in Figure 151. These plots were generated using the same assay data used in the footwall metal zonation plots (Appendix 5). The data were subdivided on lithology (graphitic, breccia and non-breccia) as well as alteration (chlorite, sericite, quartz-sericite and quartz-pyrite). Average values for both ore bodies are shown for comparison.

At Greens Creek, the total base-metal content of the footwall beneath the NWW ore body (<18) is approximately double that beneath the East ore body (<10). On a ternary Cu-Pb-Zn diagram, the footwall to the NWW ore body is characterized by scatter along the Cu-Zn join with some Pb enrichment indicated by data along the Pb-Zn join (Figure 151A). From this diagram, elevated Cu values are associated with the quartz–sericite and quartz–pyrite alteration (regardless of protolith) while samples from the sericite alteration zone tend to be Zn and Pb rich. Ag tends to be enriched in samples with higher Cu+Pb+Zn values. Au may show a similar relation to Cu+Pb+Zn but only four samples have Au above detection (>2 ppm) so the results are tentative at best. The footwall to the East ore body is characterized by less scatter along the Cu-Zn join and more scatter along the Pb-Zn join. In the few samples that show elevated Cu values, all alteration and lithology types are represented, indicating elevated Cu levels are not associated with a specific alteration or lithology type. In the footwall to the East ore body, Ag content does not appear to correlate with elevated Cu+Pb+Zn and all samples have <2 ppm Au; it is not possible to determine if Au is correlated with Cu+Pb+Zn. The average values of all alteration and lithology types show the low Cu contents in both the NWW and East ore zones and elevated Ag values in the East ore zone (footwall and ore body) (Figure 151C).

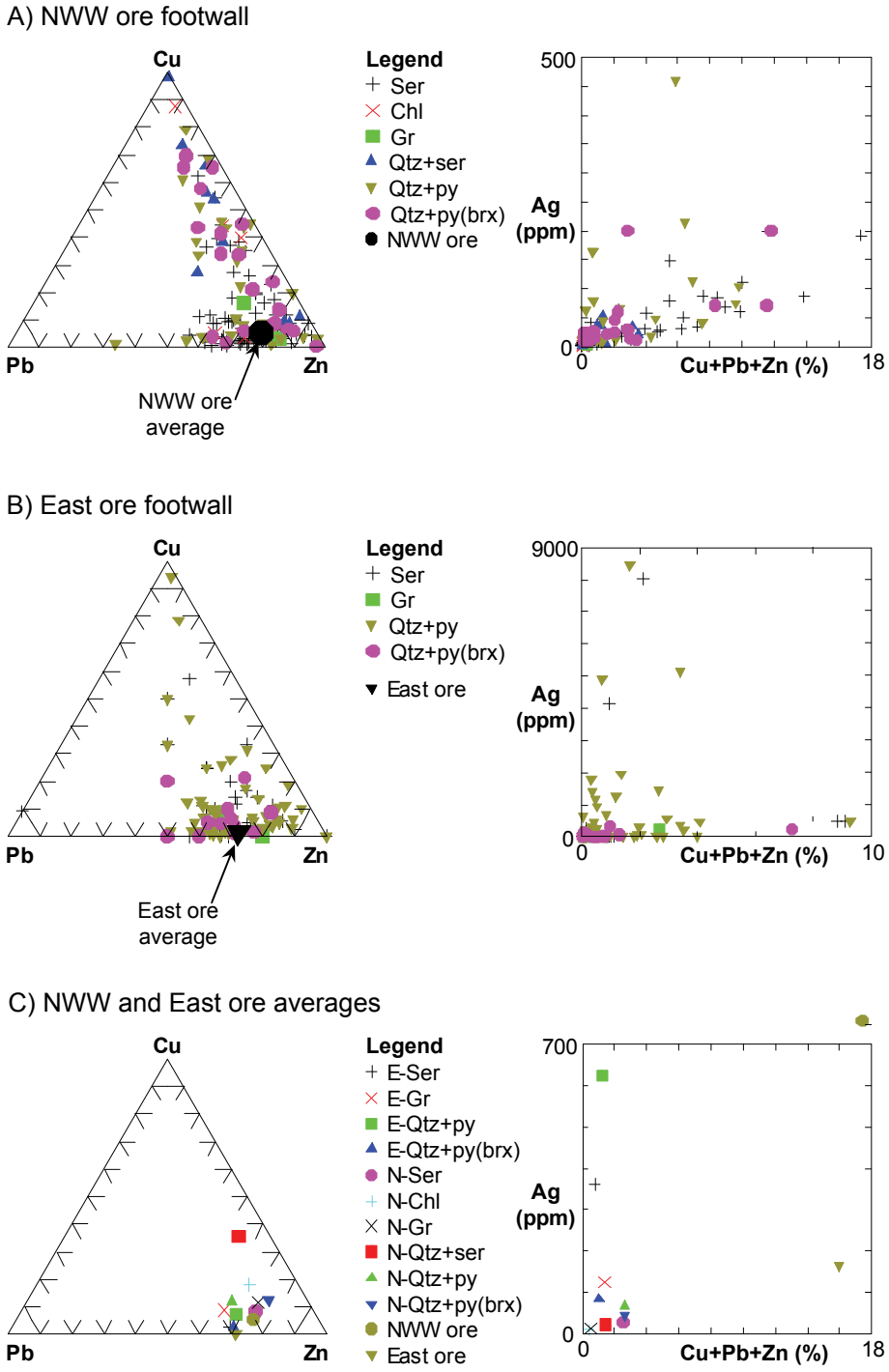

Figure 151 Cu-Pb-Zn ternary diagrams for (A) NWW ore body footwall, (B) East ore body footwall and (C) average metals values in each lithology and alteration type in both ore bodies. NWW and East ore symbols in (C) refer to average of each ore body, Cu grades are not reported for the East ore body and therefore are plotted with a Cu content of 0. Samples used are listed in Appendix V. Abbreviations: E=East ore samples, N=NWW ore samples, Chl=chlorite alteration, Ser=sericite alteration, Qtz+ser=quartz–sericite alteration, Qtz+py=quartz–pyrite alteration. All samples are from the layered volcaniclastic unit (C2) with the exception of Qtz+py (brx) which is the Tr1 breccia unit and Gr which is the graphitic layered unit.

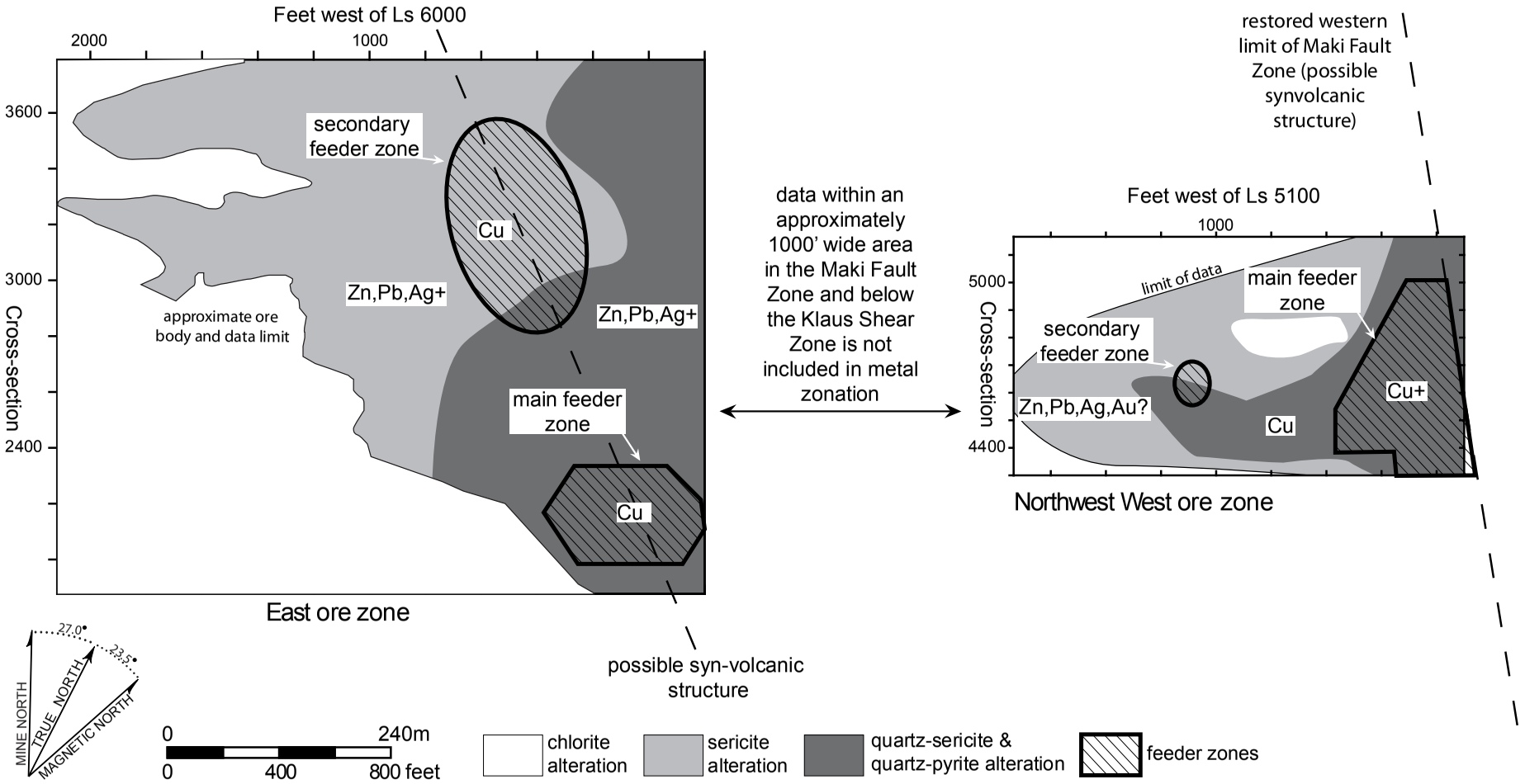

Figure 152 Restored plan view schematic illustration of metal and alteration zonation in the footwall to the NWW and East ore bodies. East ore zone has been rotated to its approximate original position to the restored west of the NWW ore zone. The two ore zones have been correlated across the Maki Fault by restoring approximately 2000 feet of right-lateral movement so that cross-section 4400 and 2400 are aligned (Lindberg, 1996a).

Discussion

Horizontal metal zonation and alteration patterns, at depths of approximately 5–10 feet (1.5–3.0 m), in the footwall to the NWW and East ore bodies are schematically illustrated in Figure 152, and resemble zonation patterns typical of VHMS deposits (i.e. Gemmell and Large, 1992). In the footwall to the NWW and East ore bodies, the gross zonation of alteration and metal contents (from distal to proximal) consists of the sericite alteration zone (relatively enriched in Zn, Pb and Ag) to the quartz–sericite and quartz–pyrite alteration zones (relatively enriched in Cu). In the NWW ore zone, the footwall to the entire ore body is enriched in Cu compared to the footwall in the East ore zone. Conversely, the entire footwall 5–10 feet (1.5–3.0 m) beneath the East ore body is enriched in Ag when compared with the footwall in the NWW ore zone.

Zone refining within mound morphology VHMS ore bodies is thought to be the result of prolonged ore deposition which evolves throughout the life of the hydrothermal system (Franklin et al., 2005). This may be the case for the NWW ore body which has well-developed zone refining and a thicker central core. Conversely, the poorly defined zone refining and thinner ore accumulation in the East ore body may be the result of less well developed, overlapping feeder zones that operated over shorter periods. These zone refining and geometry observations from the NWW and East ore bodies are supported by the observations in the feeder zones within the footwall to these ore bodies. The locations of the footwall feeder zones to the NWW ore body are interpreted on the basis of zones with coincidently elevated Cu ratios (>30) and moderate Zn ratios (<83) while the feeders in the footwall to the East ore body have slightly lower Cu ratios (>20) and Zn ratios (<70). Based on the Zn ratio values, at salinities considered typical of VHMS deposits, both feeder systems had moderate to low temperatures (<200°C) (Huston and Large, 1987). The slightly higher Cu ratio in the NWW footwall feeder system indicates that it may have had a slightly higher temperature than that in the feeder zone to the East ore body (Knuckey et al., 1982).

The relative enrichment in Cu content beneath the NWW ore zone, coupled with the large zone of elevated Cu ratio within the ore body, the high Zn/Pb ratio of 2.5 in footwall samples, the north–south elongation along the Maki Fault (possible synvolcanic structure) and the increased apparent thickness of both mineralization and the quartz–pyrite alteration zone beneath the ore body are all consistent with the NWW ore body being formed at temperatures close to 200°C with a fairly focused feeder system. This contrasts with the East ore zone which has as a much thinner apparent thickness of mineralization and quartz–pyrite alteration spread over a larger area, only scattered Cu enrichment within the footwall along a north–south trend, a less obvious association with a synvolcanic structure and elevated Ag content throughout the entire footwall (at the depth studied). These estimations of fluid temperature are slightly lower, than previous estimates for the Greens Creek deposit of approximately 250°C (Newberry et al., 1990).

These features of the footwall and the two ore bodies indicate that the NWW ore body may have formed from slightly higher temperature fluids (<250°C) which were focused along a north–south oriented synvolcanic structure while the East ore body may have formed at slightly lower temperatures along a similarly oriented structure but with less focused fluid flow.

Summary

- Metal zonation within the footwall to the NWW ore body is Cu-rich throughout, with Zn, Pb and Ag enrichment on the margins of the ore body.

- Metal zonation within the footwall to the East ore body is Cu-poor throughout with moderate Zn and Pb contents. The entire footwall is enriched in Ag.

- High Cu ratios (>30) with coincident moderate Zn ratios (<83) in the footwall to the NWW ore body outline a feeder zone that is elongated north–south, along the restored western margin of the Maki Fault.

- Moderate to high Cu ratios (>20) with coincident low Zn ratios (<70) within the footwall to the East ore body outline a feeder zone that is also elongate approximately north–south.

- In the footwall to both ore bodies, Cu is largely associated with quartz–pyrite alteration and Zn, Pb and Ag with sericite alteration. There are two exceptions to these associations: Cu is elevated in all alteration zones within the footwall of the NWW ore body and Ag is elevated within all alteration zones in the footwall of the East ore body.

- Zone refining of the NWW ore body, morphology of the NWW ore body and alteration zonation and the Zn ratio and Cu ratio within the footwall feeder zones are all consistent with the NWW ore body forming at temperatures close to 200°C from a relatively prolonged and focused vent source.

- Zone refining of the East ore body, morphology of the East ore body and alteration zonation and the Zn ratio and Cu ratio within the footwall feeder zones are all consistent with the East ore body forming at temperatures ≤200°C from a diffuse vent source with a relatively short duration.

Chapter 8: Geologic evolution

Introduction

Greens Creek is one of the largest silver producers in the United States of America and the largest economic deposit in southeast Alaska (Taylor et al., 2008). Despite Greens Creek's classification as a VHMS deposit, it has proven difficult to specify the type of VHMS deposit due to several apparently conflicting aspects. As a result, through the course of its study, Greens Creek has been included in several different types of VHMS deposit (Dressler and Dunbire, 1981; Nokleberg et al., 2005) including a proposed VHMS-sedimentary exhalative (SEDEX) hybrid deposit (Taylor et al., 1999). Nonetheless, overall the Greens Creek deposit shares many similarities with the basic VHMS deposit model of Franklin et al. (2005) and comparison with other VHMS deposits is useful to constrain the processes and conditions which led to ore formation. This chapter synthesizes the geologic evolution of the footwall and the resulting constraints on ore formation, and presents a genetic model for the Greens Creek deposit.

VHMS deposits: definition, classifications and styles

Volcanic hosted massive sulfide (VHMS) deposits are defined as strata-bound accumulations of sulfide minerals in spatial, temporal or genetic association with contemporaneous volcanism (Franklin et al., 2005). Concordant sulfide mineralization represents the accumulation of sulfide minerals precipitated in a subaqueous environment, from hydrothermal fluids, at or near the seafloor while discordant stringer mineralization represents near-seafloor hydrothermal fluid pathways (Lydon, 1984, 1988). Several schemes have been used to classify VHMS deposits: volcanic host-rock composition (Morton and Franklin, 1987; Barrie and Hannington, 1999), tectonic regime (Eremin et al., 2000), deposit morphology (Large, 1992), alteration mineral

assemblage (Sillitoe et al., 1996), metal content (Solomon, 1976; Franklin et al., 1981) and lithostratigraphy (Franklin et al., 2005). Figure 153 shows the six lithological classifications used to characterize Canadian deposits (Galley et al., 2007).

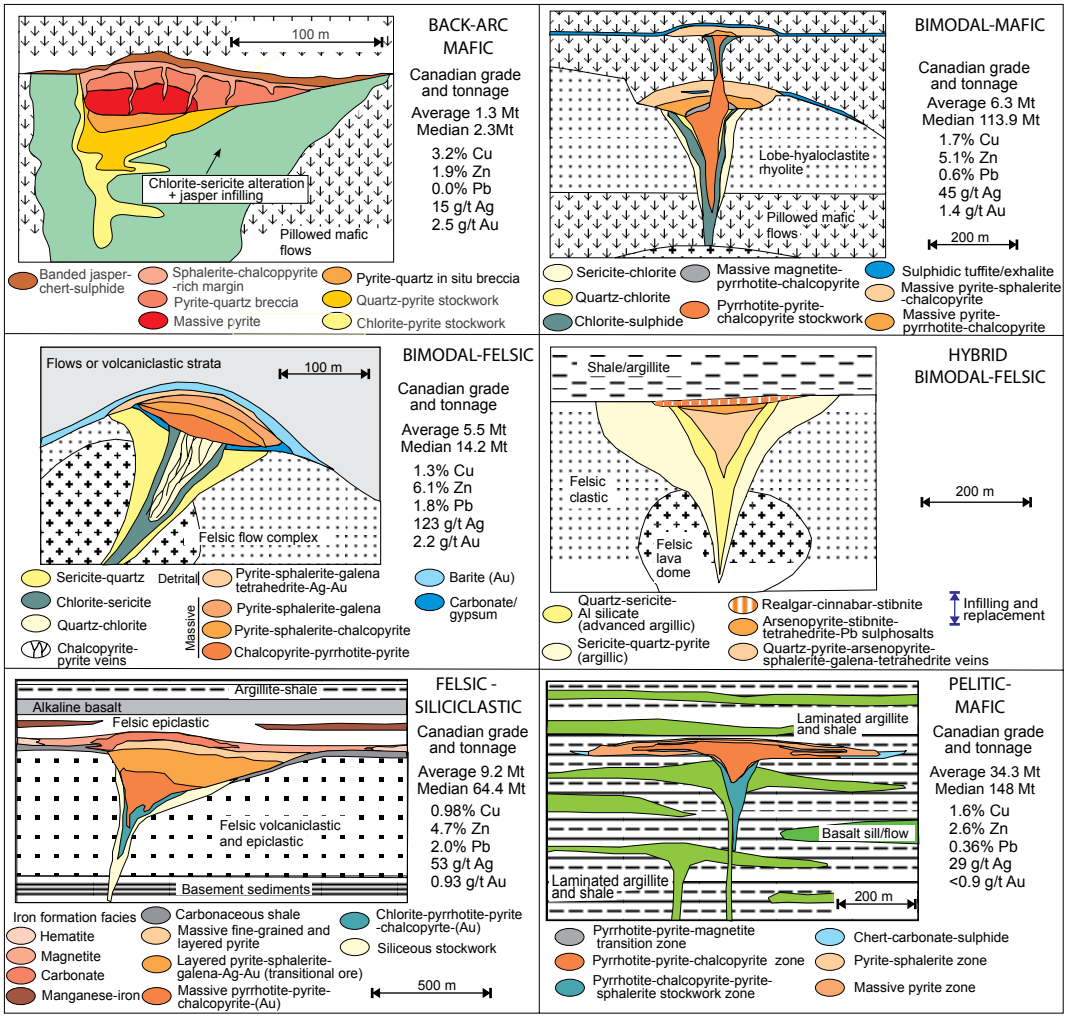

Figure 153 Graphic representation of the lithological classifications modified from Barrie and Hannington (1999) by Franklin et al. (2005), with the addition of the hybrid bimodal felsic as a VMS-epithermal subtype of bimodal-felsic (Galley et al., 2007). Average and median sizes for each type representative of Canadian deposits, along with average grade.

The characteristics and variation of VHMS deposit styles are diverse and have been summarized by many authors (i.e. Solomon, 1976; Franklin et al., 1981; Lydon, 1984, 1988; Morton and Franklin, 1987; Large, 1992; Sillitoe et al., 1996). This diversity in deposit style is related to the interplay between the following factors in the submarine volcanic environment, as well as the character of the hydrothermal fluid: (1) proportions of clastic, volcaniclastic, lava and subvolcanic intrusive facies; (2) depth of seawater;

(3) permeability and porosity of host rocks; (4) balance between magmatic components and seawater components in the ore fluid; and (5) temperature and acidity of the ore fluid (Large et al., 2001). Figure 154 illustrates the ten major VHMS styles and morphologies of Australian deposits, formed as a result of the interplay between the five factors mentioned above (Large, 1992).

Sheet-type deposits such as Mattabi (Franklin et al., 1981) or Rosebery (Green et al., 1981) have sheet-like massive sulfide lenses that typically overlie broad alteration zones (Figure 154D) with feeder systems that vary from well-developed to not recognized at all (Large, 1992). The deposit morphology is likely due to increased permeability and porosity in a fragmental footwall (Morton and Franklin, 1987; Large et al., 2001). This porous and permeable nature of the footwall typically results in broad footwall alteration zones that lack sharp mineralogical boundaries as the hydrothermal fluids that form the deposit are poorly focused (Morton and Franklin, 1987). In these sheet-type deposits, Zn and Pb are typically the dominant base metals while Cu is subordinate (Large, 1992).

Mound-type deposits (i.e. Millenbach–Knuckey et al., 1982; Hellyer–Gemmell and Large, 1992; Kuroko deposits–Ohmoto et al., 1996) are mound-shaped stratiform massive sulfide accumulations, typically overlying a well developed central feeder system (Figure 154A). The Cu-rich base and feeder system are interpreted as the hottest parts of the mineralizing system with an upward and outward increase in Zn and then Pb reflecting fluid cooling gradients caused by their interaction with seawater (Ohmoto et al., 1983; Large, 1992). Narrow feeder zones below mound deposits form as structurally focused vent zones due to the fluid being restricted by the relatively impermeable nature of footwall lithologies (i.e. Gemmell and Large, 1992). The growth of mound-type deposits is thought to be progressive through cyclic waxing and waning periods of construction by sulfide deposition which is associated with gradual upward and outward increases in temperature and zone refining processes (Eldridge et al., 1983; Lydon, 1988; Large, 1992). As a result of zone refining within mound-style deposits, Cu is often

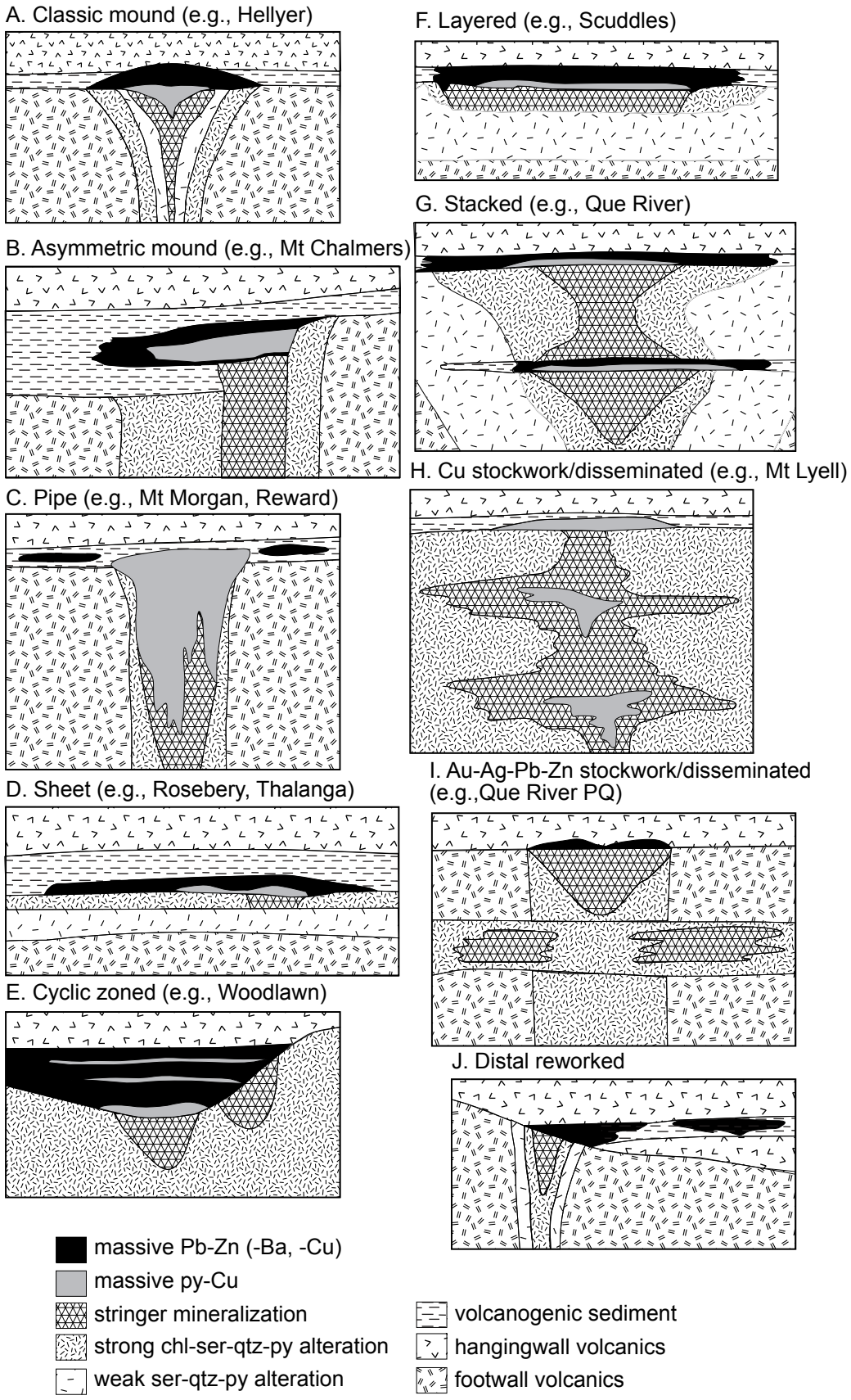

Figure 154 Graphic representation of the ten major styles of VHMS deposits in Australia (modified from Large, 1992).

an important economic metal and many of these deposits are defined as either Zn-Pb-Cu or Cu-Zn deposits (Large, 1992).

According to the examples above, the Greens Creek deposit has ore bodies of both the mound and sheet styles. The thick, lower limb of the Northwest West ore body shares several characteristics with the mound style mineralization: mound-like morphology with well-developed zone refining, pseudo-breccia textures within the footwall below the Cu-rich base, a relatively higher temperature alteration mineral assemblage with elevated Cu content in the immediate footwall and it is located along a possible paleo-fault zone which may have acted as a major fluid conduit. In contrast, the East ore body and upper limb of the Northwest West ore body exhibit characteristics typical of the sheet-type mineralization: sheet-like morphology, poorly developed zone refining, stratiform footwall alteration zonation with a low temperature alteration mineral assemblage and metal content, and no obvious association with major fluid conduits. The Greens Creek deposit illustrates that just as several lithostratigraphic classes can be found in a single VHMS district (Franklin et al., 2005), multiple VHMS deposit morphologies can be found within a single deposit.

The Greens Creek deposit

With few exceptions, most of which are in areas of structural complexity, massive sulfide at the Greens Creek deposit is found at the contact between a moderately to strongly hydrothermally altered footwall and a weakly hydrothermally altered hanging wall. The footwall to the Greens Creek deposit is dominantly made up of mafic volcanic and volcaniclastic rocks with minor sedimentary layers throughout. These rocks are regionally known as the Retreat Group and are Early Carboniferous (Chapter 5). Sitting unconformably and discontinuously on these mafic rocks is a thin layer of polymict breccia which has been interpreted as the base of the Late Triassic Hyd Formation that hosts the Greens Creek deposit (Taylor et al., 2008). The majority of the Late Triassic sequence is made up of argillite capped regionally by a thick sequence of basalts.

Mineralization is found between the footwall (either mafic rocks or breccias) and the hanging wall argillite.

Depositional environment

Three basic texture-based lithologies are recognized in the Early Carboniferous footwall rocks: (1) fine-grained, massive greenstone, (2) fine-grained layered rocks and (3) fine- to medium-grained massive sills/dikes with extensive quartz-carbonate veining. The Late Triassic breccia, located stratigraphically between the Early Carboniferous rocks and mineralization, is the fourth lithology recognized in the footwall to the Greens Creek deposit.

The fine-grained massive greenstones (C1) are interpreted as coherent volcanic rocks and are more abundant in the deeper portions of the footwall but can be found throughout the entire Early Carboniferous section. The dominant footwall lithology is a fine-grained rock, with mafic immobile-element geochemistry, that has compositional banding indicating a clastic origin (FW2a&b). The mafic layers are interpreted as volcaniclastic while the carbonaceous layers are interpreted as sedimentary. The mafic sills/dikes (I1) with extensive quartz-carbonate veining are volumetrically minor and are most common in the upper portion of the Early Carboniferous footwall. A major unconformity, with duration between 110 Ma and 30 Ma, separates the Early Carboniferous footwall from the Late Triassic breccia. The breccia (Tr1) is polymict, <70 feet (20 m) thick and found discontinuously above this unconformity. Regionally, the breccia is interpreted to represent the onset of rifting of the Paleozoic sequence (Taylor et al., 1999).

The evidence for detailed volcanic and sedimentary facies architecture, such as primary textural features and spatial attributes of rock units, was not found in the Early Carboniferous rocks in the Greens Creek area due to intense deformation and variable alteration. As a result, only the following generalizations on the footwall depositional environment are justified:

1. Early Carboniferous volcanism may have been dominated by mafic flows and emplacement of shallow intrusions. These rocks show evidence of periods of volcanic quiescence in the form of substantial amounts of carbonaceous sedimentary material throughout the sequence.
2. As this volcanism progressed, the volcanic deposits became predominantly clastic, often interlayered with carbonaceous sedimentary layers, indicating variations in the volcanic activity of the environment.
3. D1 metamorphism and deformation affected the Early Carboniferous portion of the footwall.
4. Late Triassic shallow level dikes/sills (I1) were emplaced in the upper layered portions of the footwall sequence.
5. The Early Carboniferous arc was rifted with the Late Triassic polymict breccia (Tr1) marking the onset of rifting.

The best geochemical evidence of tectonic setting comes from immobile-element characterization of the massive greenstone lithology (C1) for the Early Carboniferous portion of the footwall and from the capping Hyd basalts (Tr4) for the Late Triassic sequence. The Early Carboniferous greenstones have a subalkaline tholeiitic basalt composition indicative of juvenile volcanic-arc basalt (VAB) or mid-ocean ridge basalt (MORB). The Late Triassic basalts are also subalkaline but have a tholeiitic to transitional andesite-basalt composition and are interpreted as the slightly enriched volcanic products from the rifting of the existing Early Carboniferous arc.

A possible modern analogue for the setting of the Greens Creek deposit is the southward projection of the Lau Basin from the active hydrothermal fields near the Valu Fa Ridge to the Taupo Volcanic Zone on the North Island of New Zealand (Taylor et al., 2008). Figure 155 shows a 3-D block diagram of Sumisu rift in the Izu-Bonin island arc south of Japan. The Sumisu Rift is interpreted as being in an early synrift stage of back-arc basin formation (Klaus et al., 1992). The potential location of the Greens Creek deposit

on Figure 155 shows a possible modern analog for the depositional environment the deposit may have formed, keeping in mind that the rifted crust at Greens Creek was probably old and cold when compared to the Sumisu rift basement.

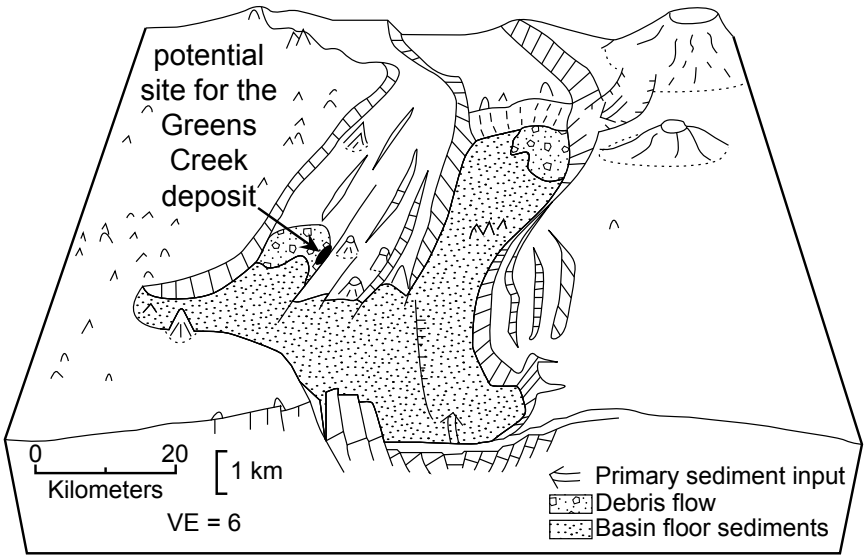

Figure 155 Perspective block diagram of Sumisu Rift viewed from an elevation of 65°, looking 345° (modified from Klaus et al., 1992).

Deformation and metamorphism (pre-mineralization)

One pre-mineralization (pre-Late Triassic) deformational and metamorphic event (D1) is recognized in the footwall to the Greens Creek deposit. S1 is defined as the metamorphic layering found within outcrops of the fine-grained layered rocks (C2) of Early Carboniferous age (Proffett, in press). Zircon grains indicate the metamorphism occurred between 250 and 300 Ma (Chapter 5) which is probably also the age for the deformation of these rocks. The metamorphic grade for the majority of the footwall is lower greenschist facies (Himmelberg et al., 1995).

Synvolcanic structural control

Several lines of evidence support the presence of either pre- or synvolcanic structures in the footwall to the Greens Creek deposit.

1. Numerous subparallel, northwest–southeast trending, strike-slip faults cross the property and may be re-activated faults related to rifting. These faults commonly

have mafic to ultramafic lithologies associated with them, possibly indicating Triassic intrusion on these structures and subsequent re-activation due to the inherent weakness of these mafic to ultramafic rocks.

2. The presence of polymict breccia units made up of dominantly local clasts, some of which show effects of hydrothermal alteration prior to brecciation.
3. The north–south elongate morphology of several massive sulfide bodies.
4. The north–south elongation of alteration zones beneath several massive sulfide bodies.
5. The location of several ore bodies along the northwest–southeast trending Maki Fault.
6. The metal zonation, of individual ore bodies, from relatively Cu-rich base upwards and outwards to Pb-Zn rich top and flanks, indicating structurally focused fluid flow.

At Greens Creek, hydrothermal fluids were primarily focused along structural conduits through the Early Carboniferous portion of the footwall, the most important of these appears to be the paleo-Maki Fault. The variation in morphological type, observed between ore bodies, is a result of the presence or absence of the thin porous breccia unit above the conduit combined with the presence of potential volcanic structures. When offset along the Maki Fault is removed, the reconstructed West ore body is located above a thickened zone of quartz–sericite and quartz–pyrite alteration which includes a monomictic pseudo-breccia texture (massive silicification) in places. This intensely altered portion of the footwall has elevated Cu content and is interpreted as the hottest part of the Greens Creek hydrothermal system (i.e. stringer zone). Ore bodies further from the Maki Fault (i.e. the East ore body) typically have a recognizable polymict breccia immediately underlying them and a sheet–like deposit morphology with poorly defined alteration and metal zonation in the footwall. These ore bodies have poorly defined feeder systems and are interpreted as lower temperature immature systems where fluid flow was poorly focused along secondary structures and through the polymict breccia.

Hydrothermal alteration and ground preparation

Two alteration stages are recognized in the footwall to the Greens Creek deposit. The timing of alteration is as follows:

1. Regional lower greenschist metamorphic grade with relative mineral abundances chlorite > carbonate > sericite > quartz ± plagioclase, reflects background alteration of the Early Carboniferous footwall rocks.
2. Zoned hydrothermal alteration, from sericite-dominated to quartz–sericite to quartz–pyrite dominated, reflects the increasing proximity to mineralization in the footwall.

Only robust primary textural features, such as phenocrysts and breccia fragments, are preserved in the footwall to the Greens Creek deposit. Delicate features, such as volcanic glass shards or tube pumice, were not recognized. The observation that primary volcanic textures have not been found in the Early Carboniferous rocks but have been recognized in the post-mineralization Hyd basalts, implies that these textures have been obliterated either by the lower greenschist metamorphism and associated deformation or by the hydrothermal system associated with mineralization. The absence of unambiguous primary features in samples from the lower greenschist regional metamorphic alteration zone suggests that the most delicate textures were already obliterated when the hydrothermal system was emplaced. The general decrease in number of recognizable phenocrysts with increasing hydrothermal alteration then indicates that the hydrothermal alteration is responsible for the complete destruction of the primary textures of these rocks.

The Early Carboniferous footwall rocks were metamorphosed to at least lower greenschist grade in the Permian prior to undergoing hydrothermal alteration. From a ground preparation perspective, this drastically reduces permeability and porosity of the rocks. It is possible that creation of S1 cleavage slightly increased the porosity and permeability of these rocks, but overall it is interpreted that these Early Carboniferous rocks behaved as an impermeable footwall. The emplacement of a highly porous and

permeable breccia on top of the Early Carboniferous footwall resulted in vastly different fluid-flow behavior between and within these two footwall units.

Within the Early Carboniferous portion of the footwall, fluid flow was restricted to structures such as the paleo-Maki Fault and the secondary structures beneath the East ore body. However, once the fluid entered the Late Triassic breccias, fluid flow was primarily in a lateral direction, away from the conduits. A footwall with high permeability and porosity contrasts is consistent with the morphology of the broadly stratiform hydrothermal alteration zone at Greens Creek which is generally sub-parallel to mineralization. This broadly stratiform zone appears to be rooted in the vicinity of the Maki Fault (i.e. Northwest West ore body) where the hydrothermal alteration zonation is slightly discordant and extends further into the footwall.

Geochemical and spectral constraints on alteration

Based on immobile-element geochemistry, the Early Carboniferous portion of the footwall to the Greens Creek deposit has a subalkaline basaltic composition (Chapter 3). The major-element geochemical patterns within footwall units C1 and C2 reflect the distribution of alteration minerals quartz and sericite as well as chlorite, plagioclase and various carbonate species. The depletion of Na_2O, CaO, Fe_2O_3, MgO and MnO and variable enrichment of K_2O reflect the decreasing abundance of chlorite and plagioclase and the increasing abundance of sericite with increasing alteration. Alteration proximal to mineralization is characterized by large increases in the SiO_2 content of the rocks which corresponds to intense silicification. These observations on the geochemical changes related to hydrothermal alteration are broadly consistent with those observed in other VHMS deposits (Franklin et al., 1981, 2005).

The trace-element geochemical patterns within footwall units C1 and C2 primarily reflect the distribution and intensity of hydrothermal alteration. Sr increases while Rb decreases with alteration intensity reflecting feldspar alteration. Ba is highly variable in the footwall and is elevated both distal and proximal to mineralization, suggesting

that this element is highly mobile and the abundance is related to intensity of the hydrothermal alteration. The metals Sn, Cu, Pb, and Zn are significantly elevated only near the mineralization, while Sb and Tl are elevated up to 500 feet (150 m) from the ore position.

Spectral data show a systematic change in white mica composition from phengite to muscovite with increasing proximity to mineralization. In background samples, the white mica composition is controlled by the bulk-rock composition while proximal to mineralization the composition is dominated by hydrothermal fluid effects. The chlorite species are Mg-chlorite to intermediate chlorite and they do not change spectral character near mineralization. Rather, the abundance of chlorite decreases. The composition of the white mica and chlorite and compositional variation of the white mica is consistent with a low- to moderate-temperature hydrothermal fluid that increases in acidity and temperature with increasing proximity to mineralization.

The hanging wall

Hanging wall argillite is made up of organic-rich pelagic mud and distal turbidites that represent a distal quiescent depositional environment (Fulton et al., 2003), possibly in a second-order basin (Taylor et al., 2008). Weak hydrothermal alteration is present in the bottom portion of the hanging wall argillite (Fulton et al., 2003) indicating that the deposition of the argillite began while the hydrothermal system was still operating. There are lesser amounts of microgabbro, dacite and rhyolite within the upper portions of the hanging wall which were subsequently capped by the voluminous, regionally extensive basalts at the top of the Hyd Formation (Chapter 5).

The proposed heat source for the Greens Creek hydrothermal system is the mafic to ultramafic intrusions (I2) predominantly found in the footwall, often along zones of structural activity. These intrusions have not been directly dated. However, contact relationships, isotopic evidence and REE patterns are consistent with the intrusions being related to the Late Triassic microgabbros (I3) found throughout the hanging wall.

It is interpreted that the mafic to ultramafic intrusions in the footwall are the fossil magma chambers from which the microgabbros were sourced. The rhyolite and basalt (Tr4) found in the upper portions of the hanging wall have also been dated as Late Triassic and may also be genetically related to the mafic to ultramafic intrusive rocks.

Deformation and metamorphism (post-mineralization)

Five post-mineralization stages of deformation are recognized at the Greens Creek deposit (Proffett, in press): the first four events (D2 through D4) only affect the Early Carboniferous and Late Triassic rocks while the last event (D5) affects rocks of all ages. Three of the deformation events are related to folding, one to semi-ductile low angle shearing and one to high-angle brittle faulting. Evidence of the pre-mineralization deformation (D1) is only found in a small number of least-altered Early Carboniferous outcrops and is largely overprinted by post-mineralization deformation.

D2 is characterized by tight to isoclinal folds with well developed axial planar cleavage. F2 folds are generally oriented west to southwest but can be re-oriented by later deformation events. D2.5 is a low angle semi-ductile deformation event best observed in the Klaus Shear Zone and Upper Shear Zone. These shear zones have a top to the west or northwest sense of motion, possibly with several hundred feet (up to 60 m) of motion (Proffett, in press). The D2.5 shears cross-cut F2 folds and are re-folded by F3 folds. D3 has formed open to tight upright folds which fold S2 and S2.5 and are subsequently refolded by F4 folds. The youngest folds recognized at the Greens Creek Mine are the locally developed F4 folds that have either spaced fracture cleavage or crenulation cleavage. F4 folds are open with fold axes plunging gently to the south-southeast, similar to F3 fold axes. However, the axial planes dip gently between west and south generally at high angles to F3 axial cleavage.

Numerous brittle faults are recognized on the Greens Creek property, the most significant of which are the Maki and Gallagher faults. The Maki Fault separates the east and west parts of the mine and cuts the reconstructed West ore body whereas the

Gallagher Fault is found to the west of the mine. The Maki Fault is steeply dipping near the surface, shallows with depth and is approximately 600 feet (180 m) thick in the southern portion of the mine, narrowing to approximately 30 feet (10 m) thick in the north. Proffett (in press) calculated a right lateral displacement of 1775 feet (538 m) with 110 feet (33 m) west side up slip for the Maki Fault which agrees well with Lindberg's (1996) estimation of approximately 1800 feet (550 m) of right lateral displacement. Proffett (2004) estimated a net dextral displacement of approximately 2750 feet (830 m) along the Gallagher Fault.

Post-mineralization metamorphism is also documented as lower greenschist (Himmelberg et al., 1995). The present study of the overlying Hyd Formation volcanic rocks has observed unambiguous primary volcaniclastic features, with peak metamorphic minerals chlorite and biotite, in samples of the Late Triassic mafic volcanic rocks. These observations indicate that, although the level of textural destruction in the Late Triassic may be less than in the Early Carboniferous rocks, they may have also been metamorphosed to greenschist grade.

Constraints on ore formation

Important constraints on ore formation can be found in the footwall rocks below VHMS deposits (Franklin et al., 2005). Understanding these constraints can then aid in resolving the genesis of the deposit. Current understanding of the genesis of VHMS deposits is that these deposits are formed through the interaction of hydrothermal fluid with surrounding rocks, in a manner that allows precipitation of sulfide minerals at, or near, the sea floor. Constraints on the interaction of the hydrothermal fluid with the surrounding rocks can be evaluated through investigation of five factors of formation (Large et al., 2001): (1) proportions of clastic, volcaniclastic, lava and subvolcanic intrusive facies; (2) depth of seawater; (3) permeability and porosity of host rocks; (4) balance between magmatic components and seawater components in the ore fluid; and (5) temperature and acidity of the ore fluid. Factors one through three relate to geologic properties while factors four and five relate to hydrothermal fluid properties.

Geologic properties

The basement to the Greens Creek deposit is made up of quartz ± chlorite ± graphite sericite schists of Silurian to Devonian age (Chapter 3). The original thickness of the Early Carboniferous footwall is not known. However, it is unlikely that the Ag and Pb could be sourced from these rocks. Because of the high Ag grade, and to a less extent, the moderate to high Pb content of the Greens Creek ore, there must be a source for these metals below the deposit. The most likely source is the basement rocks exposed along the eastern shores of Hawk Inlet. Three lines of evidence support this interpretation: (1) several detrital Proterozoic zircon grains in these rocks indicate that the source for these sediments may have been continental (Chapter 5); (2) on immobile element ternary diagrams, these rocks have a continental affinity (Chapter 3); and (3) Pb isotope work (Taylor et al., 1999) indicated two sources of Pb, one of which is radiogenic and is consistent with an old continental source. Thus, a potential source for the elevated Ag and Pb in the Greens Creek deposit is the quartz–mica schist basement rocks.

The immediate footwall to the Greens Creek deposit is largely made up of Early Carboniferous mafic rocks. When the Greens Creek hydrothermal system was emplaced, these rocks had already been deformed and metamorphosed. The reduced permeability and porosity of the Early Carboniferous rocks most likely restricted lateral hydrothermal fluid flow within these rocks. Restricted fluid flow combined with lower temperature (<250°C) hydrothermal fluids may have limited the ability of the hydrothermal fluid to strip metals such as Cu. These conditions can explain the low Cu content of the ores.

The Late Triassic polymict breccia (Tr1), found stratigraphically below the ore equivalent horizon, is an important marker horizon that has implications for deposit genesis. Where identifiable (i.e. East ore body), the ore body is distal to the Maki Fault and has a low aspect ratio with weak footwall alteration zonation. Conversely, where the polymict breccia has not been recognized (i.e. below the lower limb of the

Northwest West ore body), the ore body has a higher aspect ratio and well-defined footwall alteration zonation with a focused feeder system that contains monomictic pseudo-brecciated rocks (i.e. stringer zone). The distribution of polymict breccia and volcanic structures influenced hydrothermal fluid flow. This in turn influenced deposit morphology, degree of surrounding hydrothermal alteration and potentially the metal endowment of the hydrothermal fluids.

Hydrothermal fluid properties

Important physical and chemical constraints on the properties of the hydrothermal fluids were determined from geochemical and spectral studies of rocks from the footwall to the Greens Creek deposit. Spectral data indicates that the composition of the white mica and chlorite and the compositional variation of the white mica is consistent with an acidic (pH 4 to 5), low to moderate temperature hydrothermal fluid (<400°C) that increases in acidity and temperature with increasing proximity to hydrothermal conduits. The temperature of the hydrothermal fluids is better constrained by the metal zonation study of the footwall, particularly the Zn ratio, which identified hydrothermal upflow zones with discharge temperatures of approximately <250°C immediately below the Northwest West and East ore bodies.

Greens Creek: a genetic model

As outlined in the preceding sections, the timing and nature of mineralization and alteration are relatively well-constrained. The Greens Creek deposit formed after rifting of an existing oceanic arc was initiated but during a period of relative volcanic quiescence. Subsequent to the burial of the deposit, volcanic activity was renewed, ending with a thick sequence of regionally extensive basalts. Two stages of formation are proposed for the Greens Creek deposit: (1) the preparation of the footwall with subsequent initiation of the hydrothermal system and (2) the deposition and burial of ore followed by the waning of the hydrothermal system.

Stage 1: Initiation and ground preparation

The genesis of the Greens Creek deposit was initiated by the rifting of an existing Paleozoic oceanic arc (Taylor et al., 2008). This rifting resulted in numerous sub-parallel steeply dipping faults into the Early Carboniferous, and older, rocks of the arc. High-level mafic to ultramafic intrusions along the faults probably initiated hydrothermal circulation within the footwall. As the footwall rocks were eroded, a Late Triassic polymict breccia was deposited along the margins of the basin (Figure 156).

The existing arc had been metamorphosed and deformed prior to rifting. The overall low permeability and porosity of these rocks would have restricted lateral hydrothermal fluid flow. As a result, the numerous rift-related faults were the major conduits of fluid flow within the Early Carboniferous and older portions of the footwall. In contrast, the Late Triassic breccias provided high permeability and porosity pathways. Where the breccias were present, much greater lateral hydrothermal fluid flow was possible.

Implicit in models of nascent rifting is the presence of magma bodies at high crustal levels. In the Greens Creek area, these high-level intrusions may be the Late Triassic mafic to ultramafic bodies found throughout the footwall. These intrusions are thus inferred to be the heat source for the hydrothermal system that formed the Greens Creek deposit. The hydrothermal system was in place, at least partially, prior to deposition of the polymict breccia as the breccia fragments are variably hydrothermally altered.

Numerous faults throughout the Greens Creek area commonly have mafic to ultramafic lithologies associated with them. This may indicate early intrusion along paleo-structures which were subsequently re-activated due to the inherent weakness of these mafic to ultramafic rocks. For example, the paleo-Maki Fault has ultramafic lithologies associated with it and appears to have been an important hydrothermal fluid conduit.

STAGE 1: INITIATION AND GROUND PREPARATION

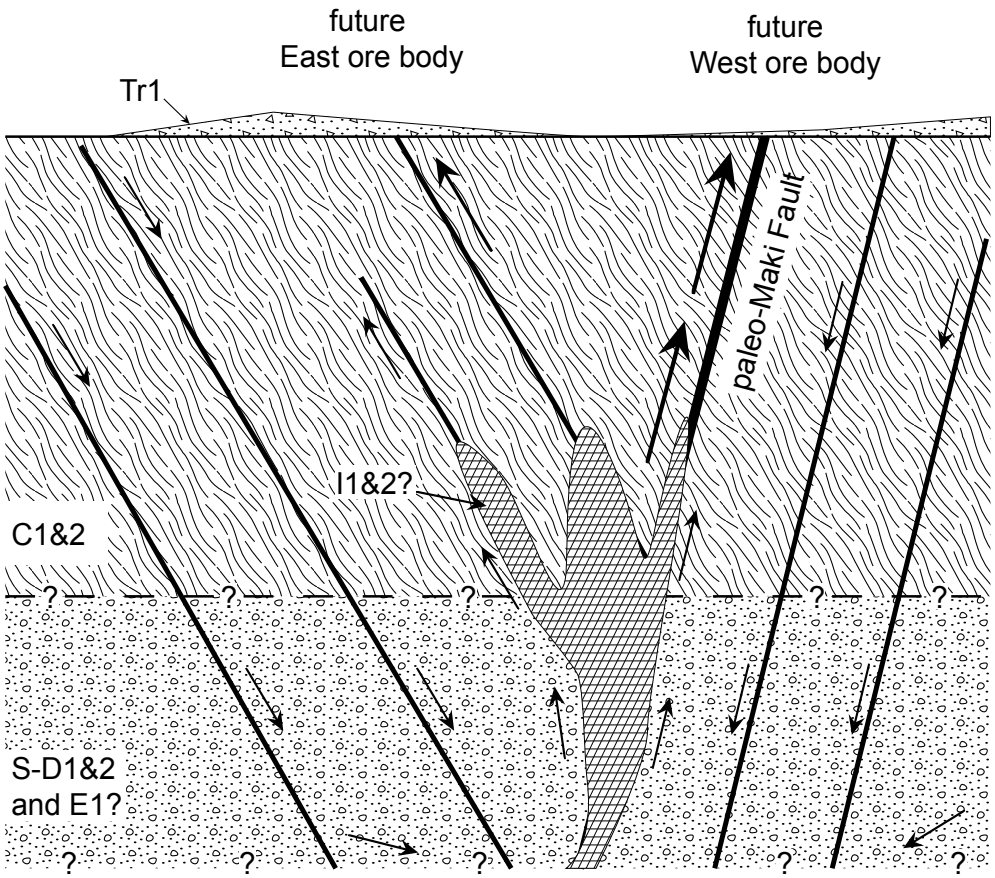

Depositional environment: Nascent rifting of existing Paleozoic arc, high level intrusion of mafic to ultramafic rocks and deposition of polymict breccia.

Structure: Numerous sub-parallel, steeply dipping faults related to rifting.

Hydrothermal fluids and circulation: Hydrothermal system in place, at least partially, prior to erosion and deposition of polymicitic breccia. Variably chlorite and sericite altered breccia fragments indicate low-level hydrothermal alteration prior to this stage. Fluid circulation was primarily along steeply dipping rift related faults. An important source of metals (particularly Ag and Pb) may have been continental crust in the basement.

Alteration: Regional metamorphic grade was lower greenschist with locally developed weak hydrothermal alteration proximal to the sea floor.

Regional aspects: Regional-scale tectonic events include a southward-propagating rift into a Paleozoic oceanic arc. The basal conglomerate (breccia) locally indicates a high-energy proximal depositional environment.

Summary: Initiation of rifting results in numerous subparallel steeply dipping faults that initially provide structures for high-crustal-level intrusions. The heat from these mafic to ultramafic intrusion sets up an early-stage hydrothermal system that locally alters the Early Carboniferous mafic footwall. The close of this stage is marked by the deposition of a polymict breccia with variably hydrothermally altered clasts.

Figure 156 Stratigraphic and structural characterization of nascent rifting with hydrothermal initiation during the first stage in the genesis of the Greens Creek deposit.

Stage 2: ore deposition, burial and waning

Taylor et al. (1999) interpreted two stages of ore deposition at Greens Creek: (1) sea-floor deposition of low temperature precious-metal-rich silica and barite ores and (2) sub-seafloor replacement of higher temperature base-metal ores. Burial of the deposit began while the hydrothermal system was operating and the hanging wall rocks record hydrothermal effects of this (Figure 157).

Metal zonation studies in the footwall beneath the Northwest West ore and East ore bodies indicate that each ore body had a primary and one or two secondary feeder zones suggesting that several feeder systems were operating along the same time equivalent horizon throughout the Greens Creek deposit. Metal zonation of the ore bodies, shows that the reconstructed Northwest West ore body has developed by zone refining while the East ore body did not. This indicates that the primary Northwest West feeder system was more focused than the East ore feeder, had a higher discharge temperature and was possibly longer lived.

The immediate mine hanging wall argillite is weakly to moderately hydrothermally altered with trace element concentrations modified by the hydrothermal fluid up to 500 feet (150 m) into the hanging wall (Fulton, 2002). This demonstrates that the hydrothermal system was still operating during the initial stages of deposition. Furthermore, Late Triassic microgabbros which intrude the argillite are sometimes weakly hydrothermally altered. The basalts at the top of the Hyd Formation do not show evidence of hydrothermal alteration indicating that these rocks were either temporally or spatially removed from the effects of the hydrothermal system.

Comparison with other deposits

When classifying VHMS deposits, previous authors have considered host-rock composition, tectonic setting, deposit morphology, alteration mineral assemblage, metal endowment and lithostratigraphy important (Solomon, 1976; Franklin et al., 1981;

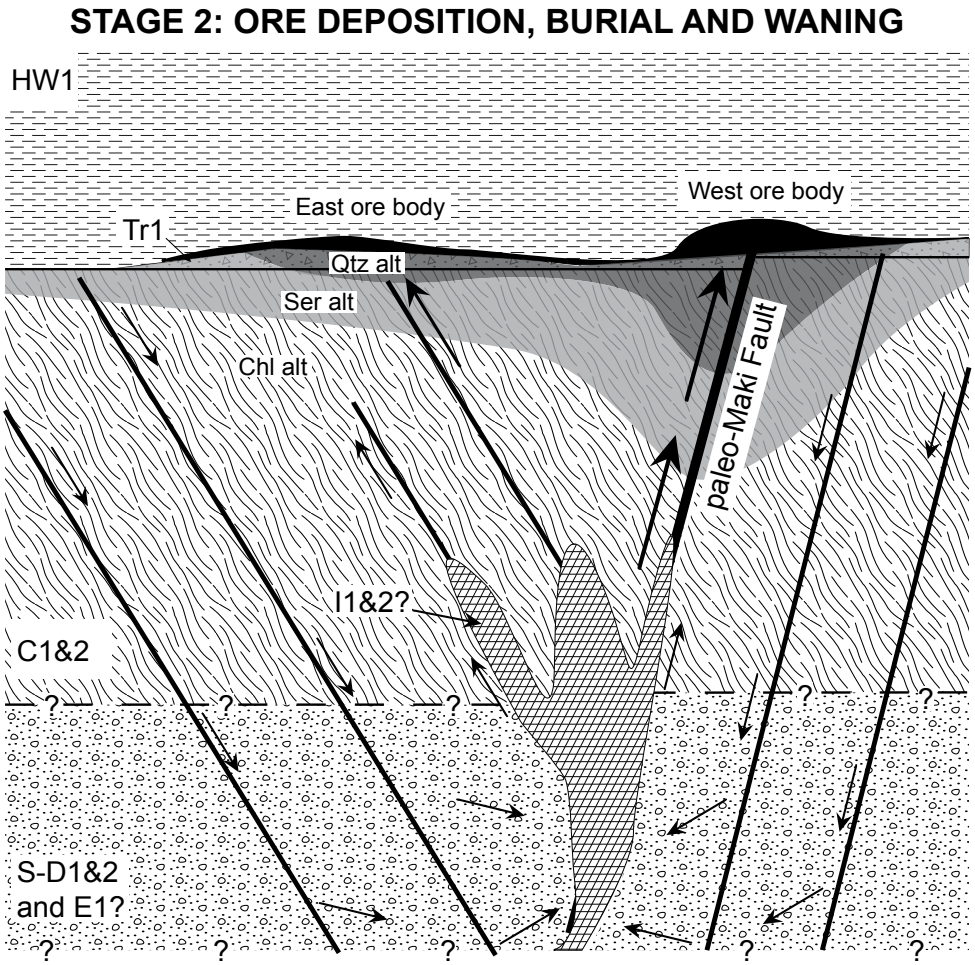

Depositional environment: Quiescent environment with pelagic and turbiditic sedimentation. Renewed volcanism in the upper portion of the Late Triassic hanging wall.

Structure: Growth faulting along existing rift-related faults.

Hydrothermal fluids and circulation: Fluids are focused along steeply dipping faults. Discharge temperatures of 200-250°C below the West ore body and slightly less for the East ore body. Acidity of approximately pH 4-5 for both vents.

Alteration: Increasing footwall alteration grades from background chlorite-dominated to distal sericite-dominated, medial quartz-sericite and proximal quartz-pyrite. The depth of alteration in the footwall increases with proximity to the paleo-Maki Fault.

Regional aspects: Consistent variation in sedimentary and volcanic facies and volcanic geochemistry indicate a southwards-propagating rift within the Alexander Terrane.Other Late Triassic VHMS deposits are found along the eastern margin of the terrane, the best examples of which include Windy Craggy and Mt. Henry Clay. Regionally capping basalts of the Hyd Formation indicate widespread volcanism subsequent to mineralization.

Summary: Intense hydrothermal alteration along fluid conduits and near fluid discharge sites signifies increased hydrothermal activity. Ore deposition occured after the deposition of the polymictic breccia and mineralization is immediately buried by fine-grained sediments. This hanging wall sequence is weakly altered indicating burial began while the hydrothermal system was still operating. The regional capping Hyd Formation basalts were either temporally or spatially removed from the effects of the hydrothermal system.

Figure 157 Stratigraphic, structural and geochemical characterization of ore deposition with continued hydrothermal alteration during the second stage in the genesis of the Greens Creek deposit.

Morton and Franklin, 1987; Large, 1992; Sillitoe et al., 1996; Barrie and Hannington, 1999; Eremin et al., 2000; Franklin et al., 2005). To this is added a stratigraphic position criterion, using the same sequence stratigraphy definition as Franklin et al. (2005). This definition states that the VHMS-hosting lithostratigraphic assemblages are those produced immediately before and after the formation of the deposit. In other words, the sequence that defines the VHMS setting is bounded by major discontinuities such as transgressive surfaces, disconformities, or unconformities.

In the case of the Greens Creek deposit, this defining sequence begins with the Late Triassic portion of the footwall located stratigraphically above the Permian unconformity and includes the polymict breccia unit (Tr1) but does not include the mafic footwall units (C1-2). The defining sequence continues upwards through the thick argillite section with minor dacite and rhyolite. The upper boundary is marked by the top of the Late Triassic basalt. Therefore, the defining lithostratigraphic sequence for Greens Creek is the Late Triassic polymict breccia–argillite–basalt sequence with the mafic volcanic footwall not included.

The Greens Creek deposit is compared to the Windy Craggy and Middle Valley deposits because of their similar tectonic setting and lithostratigraphic character. The Sullivan deposit has a similar lithostratigraphic character to Greens Creek and also has abundant contemporaneous mafic sills in the immediate footwall (Lydon et al., 2000). The Brunswick No. 12 deposit has the most similar stratigraphic location, of the deposits examined, with the deposit located in the bottom third of the volcano-sedimentary stratigraphy. The Eskay Creek deposit and modern seafloor Jade hydrothermal fields were chosen for comparison because they have similar metal endowments to that of Greens Creek. Table 32 shows the key criteria of each of these deposits.

Table 32 Comparison of key criteria between the Green Creek deposit and Windy Craggy, Sullivan, Brunswick No. 12, Eskay Creek, Middle Valley and Jade deposits. Superscripts as follows: [a]sequence stratigraphic position as defined by Franklin et al., (2005); [b]grade is only for 138 Mt in NSB zone; [c]grade for 50 m drill intersection in ODP deposit; [d]deposit size is an estimate only; [e]grade only for zone 21B; [f]deposit grades have not been calculated; [g]deposit size has not been calculated.

Characteristic	Greens Creek	Windy Craggy	Middle Valley
Age	Late Triassic	Late Triassic	Recent
Tectonic setting	oceanic back-arc rift	oceanic back arc rift	mid-ocean rift
Lithostratigraphy	pelitic-mafic	pelitic-mafic	pelitic-mafic
Stratigraphic position[a]	base	middle	upper
Volcanic host-rock composition	subalkaline, tholeiitic to transitional basalt	alkaline to subalkaline, tholeiitic to transitional basalt	subalkaline, tholeiitic basalt
Deposit morphology type	sheet-type and mound-type	sheet-type with mound-type feeders	mound-type
Alteration mineral assemblage	chl, carb, ser, qtz, py	chl, qtz, py	carb, ser, ab, chl, qtz
Metal endowment	13.9% Zn, 5.1% Pb, 4.8g/t Au and 599 g/t Ag	1.4% Cu, 0.25% Zn, 0.2 g/t Au, 4 g/t Ag, 0.066% Co[b]	20% Zn[c]
Size (Mt)	25	297	15 - 20[d]
References	Taylor, 2008; this study	Slack, 1993; Peter and Scott, 1999	Goodfellow and Zierenberg, 1999

Windy Craggy

Windy Craggy is located within the Late Triassic portion of the Alexander Terrane, approximately 200 km north of the Greens Creek deposit (Peter and Scott, 1999) and is a type example of pelitic-mafic VHMS deposits (Barrie and Hannington, 1999). This makes a comparison between the Greens Creek and Windy Craggy deposits spatially, temporally and genetically relevant.

Sullivan	Brunswick No. 12	Eskay Creek	Jade
Mesoproterozoic	Ordovician	Middle Jurassic	recent
intracratonic basin	sediment covered continental back arc rift	continental margin or back arc rift	intracontinental back arc rift
pelitic-mafic	bimodal-felsic	bimodal-felsic	pelitic-mafic
middle	lower	upper	upper
subalkaline, tholeiitic microgabbro	calc-alkaline rhyolite	tholeiitic rhyolite and basalt	calk-alkaline rhyolite and basalt
wedge	sheet-type with mound-type feeders	sheet-type with mound-type feeders	mound-type
tour, chl, po,py,ab,ser,car	ser, chl, qtz, py	qtz, ser, py, K-spar, chl	qtz, ser, bar, py
5.9% Zn, 6.1% Pb, 68g/t Ag	7.7% Zn, 3.0% Pb, 0.5% Cu, 91g/t Ag, 2.6g/t Au	5.6% Zn, 2.9% Pb, 0.8% Cu, 2930 g/t Ag, 65.5 g/t Au[e]	Zn, Pb, Ag, Au[f]
160	230	2.25	N/A[g]
Lydon et al., 2000; Goodfellow and Lydon, 2007	Lentz and Goodfellow, 1993; Goodfellow, 2007	Barrett and Sherlock, 1996; Roth et al., 1999	Hallbach et al., 1993; Glasby, 2008

Greens Creek has many similarities to the Windy Craggy deposit including age, lithostratigraphy, tectonic setting, volcanic host-rock composition, deposit morphology and alteration mineral assemblage (Table 32). However, the stratigraphic position and metal endowment are significantly different between the deposits. Greens Creek is located near, or at, the base of the Late Triassic stratigraphy while Windy Craggy is located in the mid-portion of the Late Triassic stratigraphy (Mihalynuk et al., 1993).

The Zn-Pb with Ag and Au metal endowment of Greens Creek is very different to that in the Windy Craggy deposit which is a Cu deposit with minor Au, Ag and Co. Cu is insignificant at Greens Creek (<0.5%) and is not consistently reported during reserve estimates, therefore, accurate Cu grade and tonnage figures for the Greens Creek deposit are not presented (A. West pers. comm.).

Given that Greens Creek and Windy Craggy share spatial, temporal and genetic characteristics, it is reasonable to suppose a similar mod of formation. It is also possible that the difference in stratigraphic position, base versus middle, was an important factor in the major difference in metal endowment of the two deposits. Stable isotope studies by Peter and Scott (1999) indicated that the source for the Windy Craggy metal was the abundant (~2500 m) penecontemporaneous Late Triassic argillite and basalt below the deposit. Conversely, the position of Greens Creek at the base of the Late Triassic stratigraphy means that the hydrothermal circulation occurred in a metamorphosed mafic footwall and the basement below that. The difference in fluid flow between penecontemporaneous mafic and pelitic lithologies and metamorphosed mafic and possibly continentally sourced metasediments possibly would have greatly influenced the composition of the hydrothermal fluid and is likely a key reason for the vastly different metal endowments of the Greens Creek and Windy Craggy deposits. Other characteristics such as fluid temperature and salinity and water depth may also have been partially responsible for the different metal endowments.

Middle Valley

Middle Valley is a sedimented oceanic rift located in the northern part of the Juan de Fuca Ridge approximately 400 km west of Vancouver Island, Canada (Goodfellow and Zierenberg, 1999). As Middle Valley is a possible modern analog to the pelitic-mafic deposit type (Barrie and Hannington, 1999), it is very similar to the Windy Craggy deposit and shares similarities such as lithostratigraphy, tectonic setting, volcanic host-rock composition, deposit morphology and alteration mineral assemblage with the Greens Creek deposit (Table 32).

Being a modern analog, two criteria of ancient deposits do not strictly apply. The first obviously is age, the second is stratigraphic position. Currently, the Middle Valley deposits are located at the top of the stratigraphy but once the deposit is buried and becomes part of the rock record, the stratigraphic position may well change to middle. The stratigraphic position will not change to base as there is currently between 300 m and >1000 m of Holocene to Pleistocene sediment stratigraphically below the deposits (Goodfellow and Zierenberg, 1999).

A comparison of metal endowment between the Middle Valley deposits and Greens Creek is difficult because true metal grades and tonnages do not exist for the Middle Valley deposits. However, there is one 50 m drill intersection in the ODP deposit that has Zn grades of approximately 20% (Goodfellow and Zierenberg, 1999), slightly higher than the global Zn grade of the Greens Creek deposit. Assays from Middle Valley grab samples have average Cu contents between 0.5% and 2.1%, Zn between 0.6% and 4.2%, Ag grades between 2 g/t and 32 g/t and Au between 0 and 3.9 g/t. These samples have similar Cu and Au contents and lower Zn and Ag contents than those expected for Greens Creek.

The Middle Valley deposits appear to be a reasonable modern analog for the Greens Creek deposit. Most of the key criteria are similar between the two and the differences appear to be minor. The base versus middle to upper stratigraphic position is the largest difference between the two and does not appear to have significantly influenced the metal endowment of the Middle Valley deposits. Admittedly, there are no deposit-scale grade calculations for the Middle Valley deposits but the sporadic grab sample data indicate that the metal contents are broadly similar to those expected in a similar sampling situation at the Greens Creek deposit. The composition of the basement 2–5 km below the Middle Valley deposits, where the metals would have likely been sourced, is not known but is likely to be basaltic ocean crust. The amount of

penecontemporaneous sediment (<1000 m at Middle Valley) in the footwall and the potentially different basement rocks offers a partial explanation for the different metal endowments of the Middle Valley deposits.

Sullivan SEDEX deposit

Many of the key characteristics of the Sullivan deposit are different from that of Greens Creek indicating that the modes of formation for these deposits may be different (Table 32). Importantly though, the Sullivan deposit has similar pelitic-mafic lithostratigraphy and penecontemporaneous mafic intrusions in the footwall that have similar chemistry to the intrusions in the footwall to the Greens Creek deposit. For these reasons a comparison between the deposits is warranted.

Where the Greens Creek deposit consists of massive sulfide bodies formed immediately above a rifted oceanic arc basement, the Sullivan deposit consists of well-bedded sulfide bodies formed from repeated precipitation from buoyant plumes in an infill sequence in an intracratonic rifted basin (Lydon et al., 2000). These two settings are very different. However, the footwall intrusions to both deposits are mafic (to ultramafic for Greens Creek) with subalkaline tholeiitic basalt compositions. This indicates that the most likely heat source for both systems is very similar. In VHMS terms, Greens Creek is a moderate to large high-grade deposit while Sullivan would be a super giant deposit of moderate grade. Both deposits are Zn-Pb with Ag, though Greens Creek has approximately 2.5 times more Zn and 10 times more Ag. Importantly, Greens Creek has 4.8 g/t Au where Sullivan does not have significant Au grades. It appears that, though the heat source for the formation of the Sullivan deposit may be similar to the heat source for Greens Creek, overall the defining characteristics of each deposit are significantly different, indicating that the genesis of each deposit may also have been different.

Brunswick No. 12

The Brunswick No. 12 deposit is a supergiant volcanic-sediment-hosted massive sulfide (VSHMS) deposit of Ordovician age located in the Eagle Bay Assemblage in New Brunswick, Canada (Goodfellow, 2007). Brunswick No. 12 is the largest deposit in the Brunswick Mining Camp and is compared with Greens Creek primarily because of its location in the lower portion of the stratigraphy. The stratigraphic level is similar to Greens Creek though not as close to the base. Brunswick No. 12 is approximately 225 Ma older than Greens Creek and was formed in a bimodal-felsic back-arc basin floored by continental crust. This is quite different from the inferred rifted mafic-pelitic oceanic arc setting for Greens Creek.

The Brunswick No. 12 deposit is approximately 230 Mt with an average grade of 7.7% Zn, 3.0% Pb, 0.5% Cu and 91g/t Ag (Table 32). The deposit is an order of magnitude larger than Greens Creek but has approximately half the Zn and Pb grades. Cu grade at Greens Creek is slightly less while Ag grades are approximately six times higher and the Au grade is approximately double those found at Brunswick No. 12. The source of the base metals is thought to be both hydrothermal and magmatic fluids, while the source of the Au is thought to be solely magmatic fluids (Goodfellow, 2007). The source of Ag is not specifically mentioned in Goodfellow (2007), however, the abundant continental crust below the deposit is a reasonable source. If the source of Ag is the underlying basement, this may be similar to Greens Creek where the source of Ag has to be the basement.

Eskay Creek

The Eskay Creek VHMS deposit is well known as a precious-metal-rich VHMS located approximately 200 km southeast of Greens Creek in the Stikine Terrane - the terrane immediately inboard of the Alexander Terrane. Eskay Creek is compared with Greens Creek because of proximity and the similar metal endowment (Table 32). Eskay Creek is approximately 75 Ma younger than Greens Creek and formed in the upper portion of a bimodal–felsic lithostratigraphy in a continental rift environment. This is

very different from the lower pelitic-mafic lithostratigraphic setting in an oceanic rift environment in which Greens Creek is found.

The 21B zone of the Eskay Creek deposit has 2930 g/t Ag and 65.5 g/t Au and 0.8% Cu (Barrett and Sherlock, 1996), these grades are approximately five times the Ag, 13 times the Au and up to twice the Cu grades of Greens Creek. However, Greens Creek has approximately twice the Zn grade and Pb is similar. The entire Eskay Creek deposit (the 21A&B, NEX and HW zones) is an order of magnitude smaller than the Greens Creek deposit. The Eskay Creek deposit then is a very high grade, low tonnage deposit where as Greens Creek is moderate to large, high grade deposit. Roth et al. (1999) concluded that the high precious-metal content of the 21B zone at Eskay Creek deposit is, at least partially, due to low temperature (120–210°C) boiling of the hydrothermal fluids due to shallow water depths (<1000 m). These temperatures are similar to the discharge temperatures at Greens Creek calculated using Zn ratios.

Comparison with the Eskay Creek deposits highlights a potential mechanism for precious-metal enrichment: low temperature boiling of hydrothermal fluids due to shallow water depths. Fluids at Greens Creek were low temperature (<250°C). Ore deposition occurred immediately above an unconformity indicating shallow water depths and thus ore deposition may have occurred in water depths shallow enough to allow boiling of the hydrothermal fluids. As the Eskay Creek deposit is located within a continental rift, the source of the Ag and Au is presumably the intermediate calc-alkaline continental portion of the footwall. The source of Ag (and Pb) beneath Greens Creek is more problematic. It is unlikely that sufficient Ag would be derived from the subalkaline mafic volcanic footwall. Therefore, the most likely source is the schistose to gneissic basement found along and to the northwest of Hawk Inlet.

Jade

The Jade hydrothermal field is located within the central Okinawa Trough to the south of Japan (Halbach, 1993). As for the Middle Valley deposits, the age of the deposit

and relative stratigraphic position do not strictly apply to the Jade deposit. The Jade deposit has several thousand meters of penecontemporaneous felsic volcanic and marine sediment below it (Halbach, 1993). The Jade deposit differs from Greens Creek in its intracontinental back arc rift setting and calc-alkaline volcanic rock composition. The lithostratigraphy of the Jade deposit host rocks are pelitic-mafic as is Greens Creek and deposit morphology and alteration mineral assemblage are similar. The Jade deposit does not have grade and tonnage data, but assays of grab samples show similar Zn, Pb, Cu and Au grades to what might be expected for Greens Creek.

Comparisons between the Greens Creek deposit and the Windy Craggy, Middle Valley, Sullivan, Eskay Creek and Jade deposits are useful in constraining ore formation at the Greens Creek deposit. Based on these comparisons the following observations are considered important:

1. Greens Creek is the only deposit found at the base of the host stratigraphic sequence.
2. At Greens Creek, boiling of the low-temperature hydrothermal fluids due to shallow water depth may have been an important metal precipitation mechanism as is interpreted for the Eskay Creek deposit.
3. Metal endowment of these deposits reflects the geology of the footwall and basement. Deposits with basaltic footwall rocks tend to be Cu-Zn rich and Ag-Pb poor (i.e. Windy Craggy) while Cu-Zn poor and Ag-Pb rich deposits tend to have felsic footwall rocks (i.e. Eskay Creek and Brunswick No. 12). The footwall and basement at Greens Creek may include basaltic and felsic rock types which could be potential sources for the anomalous amounts of Ag and, to a lesser extent, Pb.
4. Deposits located in the lower portion of the stratigraphy have metal endowments that reflect the basement lithologies (i.e. Brunswick No. 12), more so than deposits located higher in the stratigraphy.
5. The Middle Valley deposit on the highly sedimented Juan de Fuca Ridge appears to be a reasonable modern analog for the Greens Creek deposit.

6. The differences between Greens Creek and Windy Craggy are largely related to size and metal endowment. These can be at least partially explained by the difference in stratigraphic position (base versus middle) and the resulting differences in fluid flow and metal content of the footwall (and basement).
7. While the Sullivan SEDEX deposit and Greens Creek VHMS deposits appear to have similar heat sources, mafic (to ultramafic) intrusions in the footwall, the remainder of the characteristics of the Sullivan deposit are quite different from those at Greens Creek.

VHMS versus SEDEX genetic models for Greens Creek

The characteristics of the Greens Creek deposit which Taylor et al. (1999) considered indicative of a SEDEX deposit model are: (1) an absence of felsic igneous rocks and the presence of altered mafic to ultramafic intrusive rocks in the footwall, (2) the lack of a focused feeder system, (3) a huge alteration envelope containing chromium- and barium-rich silicates and complex carbonate-alteration mineralogy, (4) a stratigraphic hanging wall of graphitic and pyritic argillite, (5) geochronologic and isotopic evidence of ore formation during and after the deposition of the shale cap, and (6) an intra-arc tectonic setting. Using the basic VHMS deposit model and classification scheme of Franklin et al. (2005) and the SEDEX genetic model of Leach et al. (2005) none of the above points are unique to SEDEX deposits. Rather these are all features that can be found in both the VHMS and SEDEX deposit models.

Unambiguous evidence of VHMS versus SEDEX seems to largely rely on two factors: (1) the SEDEX affiliation with continental crust and the VHMS connection to oceanic crust and (2) the massive versus bedded character of the ores. Conventional SEDEX genetic models indicate that Selwyn-type SEDEX deposits form from oxidized H_2S poor fluids within synrift clastic (and evaporitic) rocks (Cooke et al., 2000; Goodfellow and Lydon, 2007). Also key to this genetic model are a continental rift setting and precipitation of bedded sulfides from a buoyant plume (Leach et al., 2005).

At Greens Creek, these key SEDEX criteria do not appear to be met. The best estimate of a tectonic setting for Greens Creek is a rifted oceanic arc. There are rocks of potential continental affinity in the basement. Although these rocks may have been a potential metal source, they are genetically unrelated to the formation of the Greens Creek deposit. Likewise, the ores at Greens Creek are massive and do not show regular bedding typical of SEDEX deposits.

Classification of the Greens Creek deposit

Using the sequence stratigraphy definition of Franklin et al. (2005) only the Late Triassic portion of the Greens Creek stratigraphy is relevant to the lithostratigraphic classification. Specifically this is the stratigraphy beginning with unit Tr1 up to and including unit Tr4. This defines the pertinent lithostratigraphic sequence for Greens Creek as a polymict breccia–argillite–basalt sequence which corresponds to the Barrie and Hannington (1999) pelitic-mafic lithostratigraphic class. Using the morphological classification of Large et al. (1992) the Greens Creek deposit has both sheet-type and mound-type ore bodies. According to the metal endowment classification of Franklin et al. (1981), the Greens Creek deposit is a Pb-Zn deposit. The ore and alteration mineral assemblages in the footwall to the Greens Creek deposit classify the deposit as a low-sulfidation VHMS as described by Sillitoe et al. (1996). Based on comparisons with other deposits, the key features for classifying Greens Creek are the tectonic setting and lithostratigraphic class. The remaining aspects such as metal endowment, deposit morphology and volcanic rock composition, are related to these key features but appear to be less useful in classifying the deposit. Thus Greens Creek could be classified as a pelitic-mafic VHMS deposit in a rifted intra-oceanic arc setting.

Chapter 9: Conclusions

Introduction

This chapter is a synthesis of the major conclusions from the present study with implications for regional and mine scale exploration and recommendations for future research at the Greens Creek deposit.

Conclusions

The main conclusions of this study on the footwall to the Greens Creek volcanic-hosted massive sulfide deposit are listed below:

1. The Greens Creek deposit is located on northern Admiralty Island which is part of the Admiralty sub-terrane within the Alexander Terrane. The Alexander Terrane and Wrangellia Terrane are thought to have joined to become the Wrangellia Superterrane in the Late Carboniferous. The Wrangellia Superterrane is the largest part of the Insular Belt, the outermost belt of the North American Cordillera. The time of collision between the Wrangellia Superterrane and the North American craton is Early Jurassic through to Early Tertiary.
2. The Alexander Terrane is a Late Proterozoic to Paleozoic island-arc system. The Late Triassic rifting of the eastern margin of the Alexander Terrane resulted in the most important metallogenic episode in southeast Alaska. Significant VHMS deposits such as Windy Craggy and Greens Creek are hosted in this Late Triassic rift sequence.
3. Admiralty Island is part of the western metamorphic belt of the Coast plutonic-metamorphic complex. This belt is characterized by an eastward-increasing metamorphic gradient from prehnite-pumpellyite to greenschist. Metamorphism is associated with the accretion of the terrane. The structure of the Alexander Terrane

is complex, reflecting its protracted Cenozoic and Mesozoic accretionary history. There is a strong northwest–southeast structural fabric to the region. This fabric is formed by large flexural folds, faulting and broad metamorphic and plutonic belts.

4. From stratigraphic top to bottom, there are three basic divisions within the mine sequence at Greens Creek:
    - Tr3&4: hanging wall argillite with minor volcanic rocks
    - Tr2: mineralized horizon
    - C1 to Tr1: altered mafic footwall with minor sedimentary rocks
5. Footwall rocks (C1&2) are dominantly subalkaline basaltic rocks of Early Carboniferous age. Tr1 is a Late Triassic polymict breccia. The majority of the mineralogical variation seen in the upper portion of the footwall is the result of hydrothermal alteration and varies with proximity to mineralization.
6. The ore (Tr2) is Late Triassic and has two major types: black ore and white ore. The black ore can be subdivided on the dominant ore sulfides (galena and sphalerite vs. pyrite). The white ores are subdivided on the dominant gangue mineral (carbonate, barite or silica). The white ores can be spectacularly enriched in precious metals (Au and Ag). There are three main ore bodies at Greens Creek with three extensions: East ore, West ore (Northwest, 5250) and Southwest ore (200 South).
7. The Late Triassic hanging wall argillite (Tr3) is made up of organic-rich pelagic muds and distal turbidites. Weak hydrothermal alteration is present in the bottom portion of the hanging wall sequence. In the upper portion of the hanging wall sequence there is a minor volcanic component consisting of basalt, dacite and rhyolite; the highest member is a thick basalt sequence thought to be regionally extensive. The Hyd Formation is extensively intruded by microgabbro sills.
8. At Greens Creek, there have been at least four folding events, one semi-ductile shearing event and one brittle faulting event.
9. The tectonic discrimination diagrams for the mafic volcanic rocks indicate a volcanic arc basalt association for the Early Carboniferous footwall greenstones and a slightly more enriched source, such as a rift of the existing island arc, for the

Late Triassic hanging wall basalts. Late Triassic serpentinites have both mafic and ultramafic composition. The ultramafic rocks were probably peridotites.

10. Ti versus Zr ratios for the Early Carboniferous fine-grained layered volcaniclastic footwall lithologies (C2) indicate at least two end member sources: (1) basaltic volcanics, and (2) background sedimentation (i.e. graphitic phyllites).
11. Reliable U-Pb zircon dates on small in-situ zircon grains are possible if careful attention is paid to the quality of the analyses. Small zircon grains tend to have high U (and Th) content which can lead to Pb loss through metamictization by radiation damage. However, a precision of 1–2% on the weighted mean estimate for the age of the grains can be achieved if an adequate number of grains are present. A new and innovative method of zircon geochronology was developed in this project.
12. Schistose basement rocks have immobile-element characteristics which suggest an oceanic to continental arc setting. These rocks have a depositional age of Early Silurian to Middle Devonian and have metamorphic zircon grains with a Late Permian age. Gneissic tonalites to diorites on False Point Retreat have Late Proterozoic emplacement ages.
13. The lower footwall is composed of massive coherent mafic volcanic rocks with an emplacement age of 342 ± 4 Ma (Early Carboniferous). The upper footwall is composed of mafic volcaniclastic rocks with a possible depositional age of 333 ± 6 Ma (Early Carboniferous). Volumetrically minor cross-cutting dikes and sills (undated) are found throughout the volcanic footwall. Metamorphic zircon grains with a Late Permian age from an amphibolite sample in Cliff Creek indicate the age of the D1 footwall metamorphic and deformational event that affects all Early Carboniferous footwall lithologies (units C1-2).
14. Argillite deposition occurred in the Carnian to Norian. Volumetrically significant serpentinite bodies (undated) within the footwall show features associated with minor intrusion into the argillite, have chemical similarities to the Late Triassic microgabbros and may have peperitic textures, suggesting a Late Triassic

emplacement age. Hanging wall microgabbro was emplaced at 223 ± 6 Ma and the overlying rhyolite was emplaced at 226.9 ± 0.2 Ma.

15. Overlapping Seymour Canal Formation is Late Jurassic to Early Cretaceous in age. An unfoliated set of mafic dikes offset by a northwest-trending brittle fault was emplaced at 85 ± 4 Ma constraining the ductile deformation to older than 85 Ma and brittle deformation to younger than 85 Ma.
16. Four alteration zones are characterized within the footwall to the Greens Creek deposit. From distal to proximal these are the chlorite alteration zone, sericite alteration zone, quartz–sericite alteration zone and quartz–pyrite alteration zone (massive silicification or monomict breccia).
17. Spectral data for >500 samples show a systematic change in white mica composition from phengite to muscovite with increasing proximity to mineralization. The wavelength position of the AlOH feature for background white micas is variable, with values between 2190 and 2230 nm, and is heavily dependent on bulk-rock composition. Proximal to mineralization the AlOH values are restricted to the 2200–2215 nm range and the white mica composition is dominated by the hydrothermal fluid effects. WMAI values show an increase in the abundance of sericite, relative to chlorite, when approaching mineralization.
18. Chlorite shows limited compositional variation without systematic zoning related to proximity to mineralization. The wavelength position of the FeOH feature of chlorite is typically between 2246 and 2257 nm indicating Mg-chlorite to intermediate chlorite compositions.
19. Whole-rock geochemical analyses for 239 samples show systematic trends in major oxides, trace elements and alteration indices related to proximity to the ore position. SiO_2 shows the greatest increase towards mineralization and Na_2O shows the greatest decrease. Trace elements Ba and Tl are elevated above background levels of respectively 50 and 0.1 ppm up to 500 feet (150 m) from mineralization.
20. The Ishikawa alteration index shows systematic variation with increasing alteration intensity, but does not differentiate the quartz–pyrite alteration zone or mineralized

from non-mineralized hanging wall–footwall contacts. The S/Na_2O ratio shows a four orders of magnitude increase from background levels of <0.1 to 20 when proximal to an unmineralized hanging wall–footwall contact with further increase up to 200 when proximal to a mineralized contact.

21. The global resource of Greens Creek is approximately 24 million tonnes at an average grade of approximately 14% Zn, 5% Pb, 605 g/t Ag and 4.8 g/t Au with insignificant Cu.
22. Metal zonation within the footwall to the NWW ore body is Cu-rich throughout with Zn, Pb and Ag enrichment on the margins of the ore body. Metal zonation within the footwall to the East ore body is Cu-poor throughout with moderate Zn and Pb contents. The entire footwall is enriched in Ag.
23. High Cu ratios (>30) with coincident moderate Zn ratios (<83) within the footwall to the NWW ore body outline a feeder zone that is elongated north–south, along the restored western margin of the Maki Fault. Moderate to high Cu ratios (>20) with coincident low Zn ratios (<70) within the footwall to the East ore body outline a feeder zone that is also elongated north–south.
24. In the footwall to both ore bodies, Cu is largely associated with quartz–pyrite alteration and Zn, Pb and Ag with sericite alteration. There are two exceptions to these associations: Cu is elevated in all alteration zones within the NWW ore body footwall and Ag is elevated within all alteration zones in the East ore body footwall.
25. Zone refining of the NWW ore body, morphology of the NWW ore body and alteration zonation and the Zn ratio and Cu ratio within the footwall feeder zones are all consistent with the NWW ore body forming at temperatures close to 250°C from a relatively prolonged and focused vent source.
26. Zone refining of the East ore body, morphology of the East ore body and alteration zonation and the Zn ratio and Cu ratio within the footwall feeder zones are all consistent with the East ore body forming at temperatures ≤200°C from a diffuse vent source with a relatively short duration.

27. Two stages are envisaged for the formation of the Greens Creek deposit:

    Stage 1: initiation and ground preparation. Initiation of rifting of the existing arc results in numerous sub-parallel, steeply dipping faults that initially provide structures for high crustal level intrusions. The heat from these mafic to ultramafic intrusions sets up an early-stage hydrothermal system that locally alters the Early Carboniferous mafic footwall. The end of this stage is marked by the deposition of a polymict breccia with variably hydrothermally altered clasts.

    Stage 2: ore deposition, burial and waning. Peak hydrothermal alteration along fluid conduits and proximal to fluid discharge sites signifies increased hydrothermal activity. Ore deposition occurred after the deposition of the polymict breccia. Mineralization is subsequently buried by fine-grained sediments. This hanging wall sequence is weakly altered up to 500 feet (150m) from the ore position which indicates that burial began while the hydrothermal system was still operating.

28. The detailed geological and geochronological portions of this study have demonstrated that the bulk of the footwall to the Greens Creek deposit is Early Carboniferous and was metamorphosed in the Permian. Therefore the deposit sits at the base of the Late Triassic stratigraphy, above an unconformity, and the footwall was metamorphosed prior to ore formation.
29. The apparently unusual metal endowment of Greens Creek can be partially explained by its basal lithostratigraphic position and the fact that a significant metal source must have been the underlying basement, not just the mafic footwall. Furthermore, precious metal enrichment can possibly be explained by low-temperature boiling of the hydrothermal fluids, as a result of shallow water depths.

Implications for exploration

As mineralization has only been proven at one stratigraphic horizon, the recognition of this contact is essential to local and regional exploration. At this contact with hanging wall argillite, the actual footwall unit is variable. However, the classic footwall unit

in contact with the hanging wall, or mineralization, is the polymict pebble breccia unit. Other possible footwall units found at the footwall–hanging wall contact are the graphitic member of the layered footwall unit, as well as the chlorite- or sericite-altered members of the layered or massive footwall units.

The overlying Late Triassic basalts are also found in contact with the argillite and as these basalts can resemble the Early Carboniferous massive volcanic unit (C1), the basalt–argillite contact can easily be mistaken for the ore equivalent horizon. Though the present study has not found any characteristics unique to either mafic volcanic unit (i.e. chemistry), characteristics such as biotite and recognizable volcanic textures in outcrop or hand sample have only been observed in the Late Triassic basalt. In the absence of reliable contradictory evidence, it is recommended that samples with recognizable volcanic textures or those with biotite be considered as Late Triassic basalts of the Hyd Formation.

Short wave infrared (SWIR) spectroscopy and whole-rock geochemistry were used to identify mine-scale vectors to mineralization. White mica spectral response was found to vary systematically with proximity to mineralization. Table 33 shows the AlOH wavelength values for the various lithologies and alteration zones:

Table 33 White mica and chlorite AlOH wavelength variations in the footwall rocks to the Greens Creek deposit.

Unit	Alteration zone	White mica AlOH wavelengths
C1	chlorite	2208 - 2229nm average: 2221nm
	chlorite	2197 - 2229nm average: 2216nm
C2	sericite	2193 - 2228nm average:2207nm
	quartz - sericite	2189 - 2227nm average: 2208nm
	quartz - pyrite	2201 - 2220nm average: 2212nm
Tr1	quartz - pyrite	2191 - 2226nm average: 2210nm

Whole-rock geochemical analyses show systematic trends in major oxides, trace elements and alteration indices related to proximity to the ore position. SiO_2 increases towards mineralization while Na_2O decreases. Trace elements Ba and Tl are elevated, above 50 ppm and 1 ppm respectively, up to 500 feet (150 m) from mineralization. The S/Na_2O ratio increases from background levels of <0.1 to 20 when near an unmineralized hanging wall–footwall contact with further increase up to >200 when near a mineralized contact.

Recommendations for future work

Several areas of potential research identified during the present study are:

1. A detrital zircon study of the hanging wall argillite. This may help determine the depositional age of the argillite (for comparison with the conodont ages) and a provenance study of the zircons may help in the interpretation of the Late Triassic tectonic setting.
2. A detailed study of the Tr1 unit focusing on the distribution, clast types, geochemistry and detrital zircons. This may provide further proximal vectors to mineralization and could possibly determine the source of the clasts. A deposition age would also be useful as the regional correlation with the basal Hyd Formation conglomerate has not been proven.
3. A mineralogical and metal zonation study of the ore bodies. A rough metal zonation of the Northwest West and East ore bodies was done for the present study and the preliminary results indicate primary metal zonation is present. Proper mineralogical and metal zonation studies for all of the ore bodies (East, West and Southwest) could potentially define upflow zones for each ore body, may help in structural interpretations of the brittle faulting and ductile shearing deformation events and aid in the metallurgical recovery of the ores.

References

Anderson, V. M., and Taylor, C. D., 2000, Alteration mineralogy and zonation in host rocks to the Greens Creek Deposit, Southeastern Alaska: Geological Society of America, Cordilleran Section, 96th annual meeting, v. 32, p. 2.

Anderson, V. M., and Taylor, C. D., 2000, Alteration zonation and mineralogy of host rocks to the Greens Creek deposit, U.S. Geological Survey, p. 35 pages.

Barker, F., 1957, Geology of the Juneau (B-3) quadrangle, Alaska, Areal geology No. GQ-0100, U.S. Geological Survey.

Barrett, T. J., Cattalani, S., and Maclean, W. H., 1993, Volcanic lithogeochemistry and alteration at the Delbridge massive sulfide deposit, Noranda, Quebec: Journal of Geochemical Exploration, v. 48, p. 135-173.

Barrett, T. J., and Sherlock, R. L., 1996, Geology, lithogeochemistry and volcanic setting of the Eskay Creek Au-Ag-Cu-Zn deposit, northwestern British Columbia: Exploration and Mining Geology, v. 5, p. 339-368.

Barrie, C. T., and Hannington, M. D., 1999, Classification of volcanic-associated massive sulfide deposits based on host-rock composition: Reviews in Economic Geology, v. 8, p. 1-11.

Bazard, D. R., Butler, R. F., Gehrels, G., and Soja, C. M., 1995, Early Devonian paleomagnetic data from the Lower Devonian Karheen Formation suggest Laurentia-Baltica connection for the Alexander Terrane: Geology, v. 23, p. 707-710.

Belasky, P., Stevens, C. H., and Hanger, R. A., 2002, Early Permian location of western North American terranes based on brachiopod, fusulinid, and coral biogeography: Palaeogeography Palaeoclimatology Palaeoecology, v. 179, p. 245-266.

Beran, A., 2002, Infrared spectroscopy of micas, *in* Mottana, A., ed., Micas: Crystal chemistry and metamorphic petrology, 46, Mineralogical Society of America, Reviews in Mineralogy and Geochemistry, p. 351-369.

Berg, H. C., Jones, D. L., and Richter, D. H., 1972, Gravina-Nutzotin Belt; tectonic significance of an upper Mesozoic sedimentary and volcanic sequence in southern and southeastern Alaska: U. S. Geological Survey Professional Paper, p. D1-D24, 1972.

Bhatia, M. R., and Crook, K. A. W., 1986, Trace-element characteristics of greywackes and tectonic setting discrimination of sedimentary basins: Contributions to Mineralogy and Petrology, v. 92, p. 181-193.

Black, L. P., and Gulson, B. L., 1978, The age of the Mud Tank Carbonatite, Strangways Range, Northern Territory: BMR Journal of Australian Geology and Geophysics, v. 3, p. 227-232.

Black, L. P., Kamo, S. L., Allen, C. M., Aleinikoff, J. N., Davis, D. W., Korsch, R. J., and Foudoulis, C., 2003, TEMORA 1: a new zircon standard for Phanerozoic U-Pb geochronology: Chemical Geology, v. 200, p. 155-170.

Black, L. P., Kamo, S. L., Allen, C. M., Davis, D. W., Aleinikoff, J. N., Valley, J. W., Mundil, R., Campbell, I. H., Korsch, R. J., Williams, I. S., and Foudoulis, C., 2004, Improved $^{206}Pb/^{238}U$ microprobe geochronology by the monitoring of a trace-element-related matrix effect; SHRIMP, ID-TIMS, ELA-ICP-MS and oxygen isotope documentation for a series of zircon standards: Chemical Geology, v. 205, p. 115-140.

Boulter, C. A., Hopkinson, L. J., Ineson, M. G., and Brockwell, J. S., 2004, Provenance and geochemistry of sedimentary components in the Volcano-Sedimentary Complex, Iberian pyrite belt; discrimination between the sill-sediment-complex and volcanic-pile models: Journal of the Geological Society of London, v. 161, p. 103-115.

Bowers, T.S., Jackson, K.J. and Helgeson, H.C., 1984, Equilibrium activity diagrams for coexisting minerals and aqueous solutions at pressures and temperatures to 5 kb and 600°C, Springer-Verlag, 397p.

Bowring, S. A., and Schmitz, M. D., 2003, High-precision U-Pb zircon geochronology and the stratigraphic record *in* Hanchar, J. M., and Hoskin, P. W. O., eds., Reviews in Mineralogy and Geochemistry, 53, p. 305-326.

Brew, D. A., and Ford, A. B., 1985, Preliminary reconnaissance geologic map of the Juneau, Taku River, Atlin, and part of the Skagway 1:250,000 quadrangles, southeastern Alaska Open-File Report 85-395, U.S. Geological Survey, p. 2 sheets, scale 1:250,000.

Brew, D. A., Himmelberg, G. R., Loney, R. A., and Ford, A. B., 1992, Distribution and characteristics of metamorphic belts in the southeastern Alaska part of the North-American Cordillera: Journal of Metamorphic Geology, v. 10, p. 465-482.

Brew, D. A., Karl, S. M., Barnes, D. F., Jachens, R. C., Ford, A. B., and Horner, R., 1991, A Northern Cordilleran ocean continent transect - Sitka Sound, Alaska, to Atlin Lake, British-Columbia: Canadian Journal of Earth Sciences, v. 28, p. 840-853.

Buddington, A. F., and Chapin, T., 1929, Geology and mineral deposits of southeastern Alaska, U. S. Geological Survey Bulletin, Report: B 0800, U. S. Geological Survey, p. 398.

Butler, R. F., Gehrels, G. E., and Bazard, D. R., 1997, Paleomagnetism of Paleozoic strata of the Alexander Terrane, southeastern Alaska: Geological Society of America Bulletin, v. 109, p. 1372-1388.

Cherniak, D. J., and Watson, E. B., 2000, Pb diffusion in zircon: Chemical Geology, v. 172, p. 5-24.

Churkin, M., Jr., and Eberlein, G. D., 1977, Ancient borderland terranes of the North American Cordillera; correlation and microplate tectonics: Geological Society of America Bulletin, v. 88, p. 769-786.

Clark, R. N., 1999, Spectroscopy of rocks and minerals and principles of spectroscopy, *in* Rencz, A. I., ed., Remote sensing for the earth sciences.

Compston, W., 1999, Geological age by instrumental analysis; the 29th Hallimond Lecture: Mineralogical Magazine, v. 63, p. 297-311.

Condie, K. C., and Chomiak, B., 1996, Continental accretion: contrasting Mesozoic and Early Proterozoic tectonic regimes in North America: Tectonophysics, v. 265, p. 101-126.

Connelly, J. N., 2000, Degree of preservation of igneous zonation in zircon as a signpost for concordancy in U-Pb geochronology: Chemical Geology, v. 172, p. 25-39.

Conrad, W. K., and Kay, R. W., 1984, Ultramafic and mafic inclusions from Adak Island; crystallization history, and implications for the nature of primary magmas and crustal evolution in the Aleutian Arc: Journal of Petrology, v. 25, p. 88-125.

Cooke, D. R., Bull, S. W., Large, R. R., and McGoldrick, P. J., 2000, The importance of oxidized brines for the formation of Australian Proterozoic stratiform sediment-hosted Pb-Zn (SEDEX) deposits: Economic Geology and the Bulletin of the Society of Economic Geologists, v. 95, p. 1-17.

Corfu, F., Hanchar, J. M., Hoskin, P. W. O., and Kinny, P., 2003, Atlas of zircon textures *in* Hanchar, J. M., and Hoskin, P. W. O., eds., Reviews in Mineralogy and Geochemistry, 53, p. 469-500.

Crafford, T., C., 1989, The Greens Creek Ag-Au-Pb-Zn massive sulfide deposit, Admiralty Island, southeast Alaska: Alaska Miners Association Conference, Program with abstracts, p. 27-29.

Dall, W. H., 1896, Report on coal and lignite of Alaska, Seventeenth Annual report of the United States Geological Survey to the Secretary of the Interior, 1895-1896: Part 1. Director's Report and Other Papers, U.S. Geological Survey, p. 763-908.

Dawson, K. M., Panteleyev, A., Sutherland Brown, A., and Woodsworth, G. J., 1992, Regional metallogeny, in Gabrielse, H., and Yorath, C. J., eds., Geology of the Cordilleran Orogen

in Canada. Geology of Canada, Geological Survey of Canada, p. 707-768.

Deer, W. A., Howie, R. A., and Zussman, J., 1992, An introduction to rock-forming minerals Essex, Pearson Education Ltd.

Doyle, M. G., and Allen, R. L., 2003, Subsea-floor replacement in volcanic-hosted massive sulfide deposits: Ore Geology Reviews, v. 23, p. 183-222.

Drechsler, J. S., Scherkenbach, D. A., and Kirkley, M. B., 1982, Progress Report: Greens Creek 1982 exploration drilling, Noranda Exploration, Inc., p. 50.

Dressler, J. S., and Dunbire, J. C., 1981, The Greens Creek ore deposit, Admiralty Island, Alaska: Sixth annual District 6 meeting; Canada's gateway to Pacific markets, v. 74, p. 57.

Duke, N. A., 1998, 1998 Field report, KGCMC, p. 9.

Duke, N. A., 1999, Field report (Update on Greens Creek surface geology), KGCMC, p. 55.

Duke, N. A., 2007, Greens Creek field report, KGCMC, p. 7.

Duke, N. A., Lindberg, P. A., and West, A., in press, Geology of the Greens Creek Mining District, *in* Taylor, C. D., and Johnson, C. A., eds., Geology, geochemistry, and genesis of the Greens Creek massive sulfide deposit, Admiralty Island, southeastern Alaska, Professional Paper 1763, U.S. Geological Survey.

Dusel-Bacon, C., Brew, D. A., and Douglass, S. L., 1996, Metamorphic facies map of southeastern Alaska; distribution, facies, and ages of regionally metamorphosed rocks, Professional Paper, Report: P 1497-D: U. S. Geol. Surv., Denver, CO, United States, U. S. Geological Survey p. D1-D42.

Eggins, S. M., Gruen, R., McCulloch, M. T., Pike, A. W. G., Chappell, J., Kinsley, L., Mortimer, G., Shelley, M., Murray-Wallace, C. V., Spoetl, C., and Taylor, L., 2005, In-situ U-series dating by laser-ablation multi-collector ICP-MS; new prospects for Quaternary geochronology: Quaternary Science Reviews, v. 24, p. 2523-2538.

Eggins, S. M., Kinsley, L. P. J., and Shelley, J. M. G., 1998, Deposition and element fractionation processes during atmospheric pressure laser sampling for analysis by ICP-MS: Applied Surface Science, v. 127-129, p. 278-286.

Eldridge, C. S., Barton, P. B., Jr., and Ohmoto, H., 1983, Mineral textures and their bearing on formation of the kuroko ore bodies, Economic Geology Monographs, 5, p. 241-281.

Eremin, N. I., Dergachev, A. L., Sergeeva, N. E., and Pozdnyakova, N. V., 2000, Types of volcanic-hosted massive sulfide deposits, Geology of Ore Deposits, v. 42, p. 161-170.

Fandrich, R., Gu, Y., Burrows, D., and Moeller, K., 2007, Modern SEM-based mineral liberation analysis: International Journal of Mineral Processing, v. 84, p. 310-320.

Feng, R., Machado, N., and Ludden, J., 1993, Lead geochronology of zircon by laserprobe-inductively coupled plasma mass spectrometry (LP-ICP-MS): Geochimica et Cosmochimica Acta, v. 57, p. 3479-3486.

Finch, R. J., and Hanchar, J. M., 2003, Structure and chemistry of zircon and zircon-group minerals *in* Hanchar, J. M., and Hoskin, P. W. O., eds., Reviews in Mineralogy and Geochemistry, 53, p. 1-25.

Fouquet, Y., von Stackelberg, U., Charlou, J. L., Erzinger, J., Herzig, P. M., Muehe, R., and Wiedicke, M., 1993, Metallogenesis in back-arc environments; the Lau Basin example: Economic Geology and the Bulletin of the Society of Economic Geologists, v. 88, p. 2154-2181.

Franklin, J. M., 1993, Volcanic-associated massive sulfide deposits: Special Paper - Geological Association of Canada, v. 40, p. 315-334.

Franklin, J. M., Gibson, H. L., Jonasson, I. R., and Galley, A. G., 2005, Volcanogenic massive sulfide deposits, *in* Hedenquist, J. W., Thompson, J. F. H., Goldfarb, R. J., and Richards, J. P., eds., Economic Geology; one hundredth anniversary volume, 1905-2005, Society of Economic Geologists, Littleton, CO, United States (USA).

Franklin, J. M., Sangster, D. M., and Lydon, J. W., 1981, Volcanic-associated massive sulfide deposits, *in* Skinner, B. J., ed., Economic geology; Seventy-fifth anniversary volume; 1905-1980, Society of Economic Geologists, Littleton, CO, United States (USA), p. 495-627.

Freitag, K., 2000, Geology and structure of the Lower Southwest ore body, Greens Creek Mine, Alaska: Unpub. PhD thesis, Colorado School of Mines, 248 p.

Freitag, K., Lopez-Pedrosa, M., Boyle, A. P., Nelson, E., Hitzman, M., and Churchill, J., 2004, The use of electron backscatter diffraction and orientation contrast imaging as tools for sulfide textural studies: examples from the Greens Creek deposit (Alaska): Mineralium Deposita, v. 39, p. 103-113.

Fryer, B. J., Jackson, S. E., and Longerich, H. P., 1993, The application of laser ablation microprobe-inductively coupled plasma-mass spectrometry (LAM-ICP-MS) to in situ (U-Pb) geochronology: Chemical Geology, v. 109, p. 1-8.

Fulton, R., 2002, Geology and geochemistry of the hanging wall argillite, Greens Creek VHMS deposit, Alaska: implications for ore genesis and exploration, Progress Report – Year One, Centre for Ore Deposit Research, University of Tasmania, Australia.

Fulton, R. L., Gemmell, J. B., West, A., Lear, K. G., Erickson, B., and Duke, N. A., 2003, Geology of the hanging wall argillite sequence, Greens Creek VHMS deposit, Admiralty Island, Alaska, University of Tasmania, Centre for Ore Deposit Research.

Furin, S., Preto, N., Rigo, M., Roghi, G., Gianolla, P., Crowley, J. L., and Bowring, S. A., 2006, High-precision U-Pb zircon age from the Triassic of Italy; implications for the Triassic time scale and the Carnian origin of calcareous nannoplankton and dinosaurs, Geology, v. 34, p. 1009-1012.

Gabrielse, H., Monger, J. W. H., Wheeler, J. O., and Yorath, C. J., 1991, Tectonic framework; part A, morphogeological belts, tectonic assemblages and terranes *in* Gabrielse, H., and Yorath, C. J., eds., Geology of the Cordilleran orogen in Canada., G-2, Geological Survey of Canada, p. 13-59.

Galley, A. G., 1993, Characteristics of semi-conformable alteration zones associated with volcanogenic massive sulfide districts: Journal of Geochemical Exploration, v. 48, p. 175-200.

Galley, A. G., Hannington, M., and Jonasson, I., 2007, Volcanogenic massive sulfide deposits, *in* Goodfellow, W. D., ed., Mineral Deposits of Canada: A Synthesis of Major Deposit-types, District Metallogeny, the Evolution of Geological Provinces, and Exploration Methods, Special Publication 5, Mineral Deposits Division, Geological Association of Canada, p. 141-161.

Gardner, M. C., Bergman, S. C., Cushing, G. W., Mackevett, E. M., Plafker, G., Campbell, R. B., Dodds, C. J., McClelland, W. C., and Mueller, P. A., 1988, Pennsylvanian pluton stitching of Wrangellia and the Alexander Terrane, Wrangell Mountains, Alaska: Geology, v. 16, p. 967-971.

Gehrels, G. E., 1990, Late Proterozoic Cambrian metamorphic basement of the Alexander Terrane on Long and Dall Islands, Southeast Alaska: Geological Society of America Bulletin, v. 102, p. 760-767.

Gehrels, G. E., 2001, Geology of the Chatham Sound region, southeast Alaska and coastal British Columbia: Canadian Journal of Earth Sciences, v. 38, p. 1579-1599.

Gehrels, G. E., 2002, Detrital zircon geochronology of the Taku Terrane, southeast Alaska: Canadian Journal of Earth Sciences, v. 39, p. 921-931.

Gehrels, G. E., 2003, Detrital zircon constraints on sediment dispersal patterns in western North America: Abstracts with Programs - Geological Society of America, v. 35, p. 389.

Gehrels, G. E., and Berg, H. C., 1988, A review of the regional geology and tectonics of southeastern Alaska: A review of the regional geology and tectonics of southeastern

Alaska.

Gehrels, G. E., and Berg, H. C., 1992, Geologic map of southeastern Alaska, United States Geological Survey.

Gehrels, G. E., and Berg, H. C., 1994, Geology of southeastern Alaska, *in* Plafker, G., and Berg, H. C., eds., The Geology of North America, G-1. Decade in North American Geology: Boulder, Colorado, Geological Society of America, p. 451-467.

Gehrels, G. E., Butler, R. F., and Bazard, D. R., 1996, Detrital zircon geochronology of the Alexander Terrane, southeastern Alaska: Geological Society of America Bulletin, v. 108, p. 722-734.

Gehrels, G. E., and Kapp, P. A., 1998, Detrital zircon geochronology and regional correlation of metasedimentary rocks in the coast mountains, southeastern Alaska: Canadian Journal of Earth Sciences, v. 35, p. 269-279.

Gehrels, G. E., McClelland, W. C., Samson, S. D., Patchett, P. J., and Orchard, M. J., 1992, Geology of the western flank of the Coast Mountains between Cape Fanshaw and Taku Inlet, southeastern Alaska: Tectonics, v. 11, p. 567-585.

Gehrels, G. E., and Saleeby, J. B., 1987, Geologic framework, tectonic evolution, and displacement history of the Alexander Terrane: Tectonics, v. 6, p. 151-173.

Gehrels, G. E., Valencia, V. A., and Ruiz, J., 2008, Enhanced precision, accuracy, efficiency and spatial resolution of U-Pb ages by laser ablation - multicollector - inductively coupled plasma - mass spectrometry: Geochemistry, Geophysics, Geosystems, v. 9, p. 13.

Geisler, T., Pidgeon, R. T., van Bronswijk, W., and Kurtz, R., 2002, Transport of uranium, thorium, and lead in metamict zircon under low-temperature hydrothermal conditions: Chemical Geology, v. 191, p. 141-154.

Geisler, T., Rashwan, A. A., Rahn, M. K. W., Poller, U., Zwingmann, H., Pidgeon, R. T., Schleicher, H., and Tomaschek, F., 2003, Low-temperature hydrothermal alteration of natural metamict zircons from the Eastern Desert, Egypt Mineralogical Magazine v. 67, p. 485-508.

Geisler, T., Schaltegger, U., and Tomaschek, F., 2007, Re-equilibration of zircon in aqueous fluids and melts: Elements, v. 3, p. 43-50.

Gemmell, B. J., 2003, Element zonation in the footwall alteration system underlying the Greens Creek VHMS deposit, Alaska, Centre for Ore Deposit Research (CODES), University of Tasmania.

Gemmell, J. B., and Large, R. R., 1992, Stringer system and alteration zones underlying the Hellyer volcanogenic massive sulfide deposit, Tasmania, Australia: Economic Geology, v. 87, p. 620-649.

Gifkins, C., Herrmann, W., and Large, R., 2005, Altered volcanic rocks: a guide to description and interpretation, Centre for Ore Deposit Research (CODES), University of Tasmania, 275 p.

Goldfarb, R. J., 1997, Metallogenic evolution of Alaska: Economic Geology, v. Monograph 9, p. 4-34.

Goldfarb, R. J., and Taylor, C. D., 1998, Mesozoic-Cenozoic ore deposits of Southern Alaska, The 16th Biennial Conference on Alaskan Mining: p. 31, Alaska Miners Association.

Goodfellow, W. D., 2007, Metallogeny of the Bathurst Mining Camp, northern New Brunswick, *in* Goodfellow, W. D., ed., Mineral Deposits of Canada: A Synthesis of Major Deposit-types, District Metallogeny, the Evolution of Geological Provinces, and Exploration Methods, Special Publication 5, Mineral Deposits Division, Geological Association of Canada, p. 449-470.

Goodfellow, W. D., and Lydon, J. W., 2007, Sedimentary exhalative (SEDEX) deposits, mineral deposits of Canada: A synthesis of major deposit types, district metallogeny, the evolution of geological provinces, and exploration methods, v. Special Publication No. 5, p. 163-183.

Goodfellow, W. D., Lydon, J. W., and Turner, R. J. W., 1993, Geology and genesis of stratiform sediment-hosted (SEDEX) zinc-lead-silver sulfide deposits: Special Paper - Geological Association of Canada, v. 40, p. 201-251.

Goodfellow, W. D., and Peter, J. M., 1997, Intersection of major massive sulfide deposits, sulfide feeder zones and a deep copper zone during ODP Leg 169 drilling in the Bent Hill area, Middle Valley, northern Juan de Fuca Ridge, Ottawa ‘97; GAC/MAC annual meeting-Ottawa ‘97; reunion annuelle AGC/AMC: Ottawa, ON, Canada.

Goodfellow, W. D., and Zierenberg, R. A., 1999, Genesis of massive sulfide deposits at sediment-covered spreading centres, *in* Barrie, C. T., and Hannington, M. D., eds., Reviews in Economic Geology: Volcanic-associated massive sulfide deposits; processes and examples in modern and ancient settings, 8, p. 297-324.

Gradstein, F. M., Ogg, J. G., Smith, A. G., Agterberg, F. P., Bleeker, W., Cooper, R. A., Davydov, V., Gibbard, P., Hinnov, L., House, M. R., Lourens, L., Luterbacher, H.-P., McArthur, J., Melchin, M. J., Robb, L. J., Shergold, J., Villeneuve, M., Wardlaw, B. R., Ali, J., Brinkhuis, H., Hilgen, F. J., Hooker, J., Howarth, R. J., Knoll, A. H., Laskar, J., Monechi, S., Powell, J., Plumb, K. A., Raffi, I., Röhl, U., Sadler, P., Sanfilippo, A., Schmitz, B.,

Shackleton, N. J., Shields, G. A., Strauss, H., V, an Dam, J., Veizer, J., van Kolfschoten, T., and Wilson, D., 2004, A Geologic Time Scale 2004, Cambridge University Press, 589 p.

Green, G. R., Solomon, M., and Walshe, J. L., 1981, The formation of the volcanic-hosted massive sulfide ore deposit at Rosebery, Tasmania: Economic Geology and the Bulletin of the Society of Economic Geologists, v. 76, p. 304-338.

Gu, Y., 2003, Automated scanning electron microscope based mineral liberation analysis: An introduction to JKMRC/FEI mineral liberation analyzer: Journal of Minerals and Materials Characterization & Engineering, v. 2, p. 33-41.

Guidotti, C. V., and Sassi, F. P., 2002, Constraints on studies of metamorphic K-Na white micas, *in* Mottana, A., Sassi, F. P., Thompson, J. B., Jr, and Guggenheim, S., eds., Micas: crystal chemistry & metamorphic petrology, 46, Reviews in Mineralogy and Geochemistry, p. 413-448.

Haeussler, P., 1992, Structural evolution of an arc-basin–the Gravina Belt in central southeastern Alaska: Tectonics, v. 11, p. 1245-1265.

Haeussler, P., and Coe, R. S., 1992, Paleomagnetism of the Late Triassic Hound Island Volcanics - Revisited: Journal of Geophysical Research-Solid Earth, v. 97, p. 19617-19639.

Haeussler, P. J., Coe, R. S., and Renne, P., 1992, Paleomagnetism and geochronology of 23-Ma gabbroic intrusions in the Keku Strait, Alaska, and implications for the Alexander Terrane: Journal of Geophysical Research-Solid Earth, v. 97, p. 19641-19649.

Haeussler, P. J., Karl, S. M., Mortensen, J. K., Layer, P. W., and Himmelberg, G. R., 1999, Permian and Mid-Cretaceous deformation of the Alexander Terrane on Admiralty and Kupreanof islands, Southeastern Alaska: Century of the Pacific Rim, “the past as prologue to the future”; Geological Society of America, Cordilleran Section, 95th annual meeting; Centennial meeting 1899-1999; abstracts v. 31, p. 60.

Halbach, P., 1993, Geology and mineralogy of massive sulfide ores from the central Okinawa trough, Japan: Economic Geology and the Bulletin of the Society of Economic Geologists, v. 88, p. 2210-2225.

Hannington, M., Poulsen, K. H., Thompson, J. F. H., and Sillitoe, D. H., 1999, Volcanogenic gold and epithermal-style mineralization in the VMS environment, p. 183-214.

Harley, S. L., Kelly, N. M., and Moeller, A., 2007, Zircon behavior and the thermal histories of mountain chains: Elements, vol.3, no.1, pp.25-30, Feb 2007, v. 3, p. 25-30.

Harris, A. C., Allen, C. M., Bryan, S. E., Campbell, I. H., Holcombe, R. J., and Palin, J. M.,

2004, ELA-ICP-MS U-Pb zircon geochronology of regional volcanism hosting the Bajo de la Alumbrera Cu-Au deposit; implications for porphyry-related mineralization: Mineralium Deposita, v. 39, p. 46-67.

Harris, A. G., 1997, Report on referred fossils: Shipment number WMRTA-97-2, U.S. Department of the Interior: Geological Survey, p. 5.

Harris, A. G., 1999, Report on referred fossils: Shipment number O-99-2, U.S. Department of the Interior: Geological Survey, p. 5.

Harris, A. G., 2000, Report on referred fossils: Shipment number O-00-1, U.S. Department of the Interior: Geological Survey, p. 5.

Herrmann, W., and Berry, R. F., 2002, MINSQ; a least squares spreadsheet method for calculating mineral proportions from whole rock major element analyses: Geochemistry - Exploration, Environment, Analysis, v. 2, p. 361-386.

Herrmann, W., Blake, M., Doyle, M., Huston, D., Kamprad, J., Merry, N., and Pontual, S., 2001, Short wavelength infrared (SWIR) spectral analysis of hydrothermal alteration zones associated with base metal sulfide deposits at Rosebery and Western Tharsis, Tasmania, and Highway-Reward, Queensland: Economic Geology and the Bulletin of the Society of Economic Geologists, v. 96, p. 939-955.

Hillhouse, J. W., and Kent, D. V. K., Miroslav, 1987, Accretion of southern Alaska: Tectonophysics, v. 139, p. 107.

Himmelberg, G. R., Brew, D. A., and Ford, A. B., 1991, Development of inverted metamorphic isograds in the Western Metamorphic Belt, Juneau, Alaska: Journal of Metamorphic Geology, v. 9, p. 165-180.

Himmelberg, G. R., Brew, D. A., and Ford, A. B., 1995, Low-grade, M-1, metamorphism of the Douglas Island Volcanics, western metamorphic belt near Juneau, Alaska Low-grade metamorphism of mafic rocks *in* Schiffman, P., and Day, H. W., eds., Low-grade metamorphism of mafic rocks, 296, Special Paper - Geological Society of America p. 51-66.

Himmelberg, G. R., Haeussler, P. J., and Brew, D. A., 2004, Emplacement, rapid burial, and exhumation of 90-Ma plutons in southeastern Alaska: Canadian Journal of Earth Sciences, v. 41, p. 87-102.

Hirata, T., and Nesbitt, R. W., 1995, U-Pb isotope geochronology of zircon; evaluation of the laser probe-inductively coupled plasma mass spectrometry technique: Geochimica et Cosmochimica Acta, v. 59, p. 2491-2500.

Hodges, K. V., 2004, Geochronology and thermochronology in orogenic systems, *in* Holland, H. D., and Turekian, K. K., eds., Treatise on geochemistry: The crust, 3, Elsevier Pergamon, p. 263-292.

Horn, I., Rudnick, R. L., and McDonough, W. F., 2000, Precise elemental and isotope ratio determination by simultaneous solution nebulization and laser ablation-ICP-MS; application to U-Pb geochronology: Chemical Geology, v. 164, p. 281-301.

Horstwood, M. S. A., Foster, G. L., Parrish, R. R., Noble, S. R., and Nowell, G. M., 2003, Common-Pb corrected in-situ U-Pb accessory mineral geochronology by LA-MC-ICP-MS: Journal of Analytical Atomic Spectrometry, v. 18, p. 837-846.

Hoskin, P. W. O., and Black, L. P., 2000, Metamorphic zircon formation by solid-state recrystallization of protolith igneous zircon: Journal of Metamorphic Geology, v. 18, p. 423-439.

Huston, D. L., 1988, Aspects of the geology of massive sulfide deposits from the Balcooma district, northern Queensland and Rosebery, Tasmania: Implications for ore genesis, Unpublished PhD thesis, University of Tasmania.

Huston, D. L., Kamprad, J., and Brauhart, C., 1999, Definition of high-temperature alteration zones with PIMA; an example from the Panorama VHMS district, central Pilbara Craton: AGSO Research Newsletter, v. 30, p. 10-12.

Huston, D. L., and Large, R. R., 1987, Genetic and exploration significance of the zinc ratio (100 Zn/(Zn + Pb)) in massive sulfide systems: Economic Geology and the Bulletin of the Society of Economic Geologists, v. 82, p. 1521-1539.

Huston, D. L., and Large, R. R., 1989, A chemical model for the concentration of gold in volcanogenic massive sulfide deposits: Ore Geology Reviews, v. 4, p. 171-200.

Hutchinson, R. W., 1990, Precious metals in massive base metal sulfide deposits, 79. Annual meeting of the Geologische Vereinigung: Leoben, Austria, Geologische Rundschau.

Ireland, T. R., and Williams, I. S., 2003, Considerations in zircon geochronology by SIMS, *in* Hanchar, J. M., and Hoskin, P. W. O., eds., Reviews in Mineralogy and Geochemistry, 53, p. 215-241.

Ishikawa, Y., Sawaguchi, T., Iwaya, S., and Horiuchi, M., 1976, Delineation of prospecting targets for Kuroko deposits based on modes of volcanism of underlying dacite and alteration haloes: Mining Geology, v. 26, p. 105-117.

Jackson, S. E., Pearson, N. J., Griffin, W. L., and Belousova, E. A., 2004, The application of laser ablation-inductively coupled plasma-mass spectrometry to in-situ U/Pb zircon geochronology: Chemical Geology, v. 211, p. 47-69.

Johnson, C. A., Taylor, C. D., and Leventhal, J. S., 2008, Geochemistry of hanging-wall metasedimentary rocks at the Greens Creek massive sulfide deposit, southeastern Alaska, 2008 Joint meeting of the Geological Society of America, Soil Science of America, American Society of Agronomy, Crop Science Society of America, Gulf Coast Association of Geological Societies with the Gulf Coast Section of SEPM, 40: Houston, Texas, United States of America, Geological Society of America: Abstracts with programs, p. 384.

Jones, D. L., Silberling, N. J., Coney, P. J., and Coward, M. P. R., Alison C, 1986, Collision tectonics in the Cordillera of western North America; examples from Alaska: Geological Society Special Publications, v. 19, p. 367.

Jones, S., Herrmann, W., and Gemmell, J. B., 2005, Short wavelength infrared spectral characteristics of the HW Horizon: implications for exploration in the Myra Falls Volcanic-Hosted Massive Sulfide Camp, Vancouver Island, British Columbia, Canada: Economic Geology, v. 100, p. 273-294.

Kapp, P. A., and Gehrels, G. E., 1998, Detrital zircon constraints on the tectonic evolution of the Gravina belt, southeastern Alaska: Canadian Journal of Earth Sciences, v. 35, p. 253-268.

Karl, S. M., Haeussler, P. J., Friedman, R. M., Mortensen, J. K., Himmelberg, G. R., and Zumsteg, C. L., 2006, Late Proterozoic ages for rocks on Mount Cheetdeekahyu and Admiralty Island, Alexander Terrane, southeast Alaska: Geological Society of America Abstracts with Programs, v. 38, p. 20.

Karl, S. M., Haeussler, P. J., Layer, P., and Himmelberg, G. R., 1998, Two new events in the metamorphic and deformational history of the Alexander terrane on Admiralty Island, southeastern Alaska: Science and technology conference: Cutting edge in Alaska, 1998, p. 14.

Karl, S. M., Haeussler, P. J., Mortensen, J. K., Layer, P. W., Savage, N., Wardlaw, B. R., Harris, A. G., Murchey, B., and Blome, C. D., 1999, New stratigraphic and isotopic constraints on the depositional and deformational history of the Alexander Terrane, southeastern Alaska: Century of the Pacific Rim, “the past as prologue to the future”; Geological Society of America, Cordilleran Section, 95th annual meeting; Centennial meeting 1899-1999, 1999, p. 68.

Kelley, K. D., 1990, Interpretation of geochemical data from Admiralty Island, Alaska; evidence

for volcanogenic massive sulfide mineralization, *in* Goldfarb, R. J., Nash, J. T., and Stoeser, J. W., eds., Geochemical studies in Alaska by the U.S. Geological Survey, 1989, USGS Bulletin 1950, U.S. Geological Survey, p. A1-A9.

Klaus, A., Taylor, B., Moore, G. F., MacKay, M. E., Brown, G. R., Okamura, Y., and Murakami, F., 1992, Structural and stratigraphic evolution of the Sumisu Rift, Izu-Bonin, *in* Maddox, E. M., ed., Proceedings of the Ocean Drilling Program, Bonin Arc-Trench System, 126, p. 555-573.

Knuckey, M. J., Comba, C. D. A., and Riverin, G., 1982, Structure, metal zoning and alteration of the Millenbach deposit, Noranda, Quebec, *in* Hutchinson, R. W., Spence, C. D., and Franklin, J. M., eds., PreCambrian Sulfide Deposits, H.S. Robinson Memorial Volume, Special Paper 25, Geological Association of Canada, p. 255-295.

Kosler, J., and Sylvester, P. J., 2003, Present trends and the future of zircon in geochronology; laser ablation ICP-MS, *in* Hanchar, J. M., and Hoskin, P. W. O., eds., Reviews in Mineralogy and Geochemistry, 53, p. 243-275.

Krogh, T. E., 1973, A low-contamination method for hydrothermal decomposition of zircon and extraction of U and Pb for isotopic age determinations: Geochimica et Cosmochimica Acta, v. 37, p. 485-494.

Krogh, T. E., 1982, Improved accuracy of U-Pb zircon ages by the creation of more concordant systems using an air abrasion technique: Geochimica et Cosmochimica Acta, v. 46, p. 637-649.

Large, R. R., 1977, Chemical evolution and zonation of massive sulfide deposits in volcanic terrains: Economic Geology and the Bulletin of the Society of Economic Geologists, v. 72, p. 549-572.

Large, R. R., 1992, Australian volcanic-hosted massive sulfide deposits: features, styles, and genetic models: Economic Geology and the Bulletin of the Society of Economic Geologists, v. 87, p. 471-510.

Large, R. R., Gemmell, J. B., Paulick, H., and Herrmann, W., 2001, The alteration box plot; a simple approach to understanding the relationship between alteration mineralogy and lithogeochemistry associated with volcanic-hosted massive sulfide deposits: Economic Geology and the Bulletin of the Society of Economic Geologists, v. 96, p. 957-971.

Large, R. R., McPhie, J., Gemmell, J. B., Herrmann, W., and Davidson, G. J., 2001, The spectrum of ore deposit types, volcanic environments, alteration halos, and related exploration vectors in submarine volcanic successions: some examples from Australia: Economic Geology and the Bulletin of the Society of Economic Geologists, v. 96, p. 913-938.

Larson, P. B., 1984, Geochemistry of the alteration pipe at the Bruce Cu-Zn volcanogenic massive sulfide deposit, Arizona: Economic Geology and the Bulletin of the Society of Economic Geologists, v. 79, p. 1880-1896.

Lathram, E. H., Pomeroy, J. S., Berg, H. C., and Loney, R. A., 1965, Reconnaissance geology of Admiralty Island, Alaska, *in* Survey, U. S. G., ed., U. S. Geological Survey Bulletin, Geological Survey Bulletin 1181-R, p. R1-R48.

Leach, D. L., Sangster, D. F., Kelley, K. D., Large, R. R., Garven, G., Allen, C. R., Gutzmer, J., and Walters, S., 2005, Sediment-hosted lead-zinc deposits; a global perspective, *in* Hedenquist, J. W., Thompson, J. F. H., Goldfarb, R. J., and Richards, J. P., eds., Economic Geology: one hundredth anniversary volume, 1905-2005, Society of Economic Geologists, p. 561-607.

Lentz, D. R., and Goodfellow, W. D., 1994, Character, distribution, and origin of hydrothermal alteration features of the Brunswick No. 12 massive-sulfide deposit, Bathurst, New Brunswick: Exploration and Mining Geology, v. 2, p. 425-426.

Lindberg, P. A., 1994, Investigation of the Maki Fault, Klaus Shear, and fold interpretations of the Greens Creek ore body, Admiralty Island, Alaska, KGCMC, p. 23.

Lindberg, P. A., 1995, Standardization of geological and structural underground mapping techniques, Greens Creek Mine, KGCMC, p. 53.

Lindberg, P. A., 1996a, Folding and faulting history of the Greens Creek Mine area, Admiralty Island, Alaska: Pre-fault restoration of cross sections that reveal primary fold patterns; implications for mineral exploration, KGCMC, p. 12.

Lindberg, P. A., 1996b, Folding and faulting history of the Greens Creek Mine area, Admiralty Island, Alaska: Structural analysis of folds and faults, preparation of correlation maps and sections, and drilling recommendations, KGCMC, p. 66.

Lindberg, P. A., 1996c, Progress Report, Folding and Faulting history of the Greens Creek Mine area, Admiralty Island, Alaska, KGCMC, p. 11.

Lodewijk, L., 1973, A laboratory overflow-centrifuge for heavy liquid mineral separation: American Mineralogist, v. 58, p. 1088-1093.

Loney, R. A., 1964, Stratigraphy and petrography of the Pybus-Gambier area, Admiralty Island, Alaska, *in* Survey, U. S. G., ed., Stratigraphy and petrography of the Pybus-Gambier area, Admiralty Island, Alaska, Geological Survey Bulletin 1178.

Ludwig, K. R., 2000, Isoplot, a geochronological toolkit for Microsoft Excel, Berkeley Geochronology Center.

Lydon, J. W., 1984, Volcanogenic massive sulfide deposits, Part I: A descriptive model:

Geoscience Canada, v. 11, p. 195-202.

Lydon, J. W., 1988, Volcanogenic massive sulfide deposits, Part 2: Genetic models: Geoscience Canada, v. 15, p. 43-65.

Lydon, J. W., 2007, Geology and metallogeny of the Belt-Purcell Basin, *in* Goodfellow, W. D., ed., Mineral Deposits of Canada: A synthesis of major deposit-types, district metallogeny, the evolution of geological provinces, and exploration methods, Special Publication No. 5, Geological Association of Canada, Mineral Deposits Division, p. 581-607.

Lydon, J. W., Paakki, J. J., Anderson, H. E., and Reardon, N. C., 2000, An overview of the geology and geochemistry of the Sullivan Deposit, *in* Lydon, J. W., Hoy, T., Slack, J. F., and Knapp, M. E., eds., The geological environment of the Sullivan Deposit, British Columbia, Special Publication 1, Geological Association of Canada. Mineral Deposits Division, p. 505-522.

MacIntyre, D. G., 1986, The geochemistry of basalts hosting massive sulfide deposits, Alexander Terrane northwest British Columbia, Geological Fieldwork 1985, British Columbia Ministry of Energy, Mines and Petroleum Resources, p. 197-210.

MacLean, W. H., 1990, Mass change calculations in altered rock series: Mineralium Deposita, v. 25, p. 44-49.

MacLean, W. H., and Barrett, T. J., 1993, Lithogeochemical techniques using immobile elements: Journal of Geochemical Exploration, v. 48, p. 109-133.

Marten, B. E., 1987, Structural geology of the Greens Creek massive sulfide deposit, Admiralty Island, southeast Alaska, BP Minerals International, p. 25.

Mattinson, J. M., 2005, Zircon U/Pb chemical abrasion (CA-TIMS) method; combined annealing and multi-step partial dissolution analysis for improved precision and accuracy of zircon ages: Chemical Geology, v. 220, p. 47-66.

McClelland, W. C., and Gehrels, G. E., 1990, Geology of the Duncan Canal Shear Zone - evidence for Early to Middle Jurassic deformation of the Alexander Terrane, Southeastern Alaska: Geological Society of America Bulletin, v. 102, p. 1378-1392.

McClelland, W. C., Gehrels, G. E., Samson, S. D., and Patchett, P. J., 1992, Protolith relations of the Gravina Belt and Yukon-Tanana Terrane in Central Southeastern Alaska: Journal of Geology, v. 100, p. 107-123.

McLeod, R. L., and Stanton, R. L., 1984, Phyllosilicates and associated minerals in some Paleozoic stratiform sulfide deposits of southeastern Australia: Economic Geology v. 79, p. 1-22.

Meffre, S., Large, R. R., Scott, R., Woodhead, J., Chang, Z., Gilbert, S. E., Danyushevsky, L. V.,

Maslennikov, V., and Hergt, J. M., 2008, Age and pyrite Pb-isotopic composition of the giant Sukhoi Log sediment-hosted gold deposit, Russia: Geochimica et Cosmochimica Acta, v. 72, p. 2377-2391.

Meffre, S., Scott, R. J., Glen, R. A., and Squire, R. J., 2007, Re-evaluation of contact relationships between Ordovician volcanic belts and the quartz-rich turbidites of the Lachlan Orogen: Australian Journal of Earth Sciences, v. 54, p. 363-383.

Meschede, M., 1986, A method of discriminating between different types of mid-ocean ridge basalts and continental tholeiites with the Nb-Zr-Y diagram: Chemical Geology, v. 56, p. 207-218.

Mezger, K., and Krogstad, E. J., 1997, Interpretation of discordant U-Pb zircon ages; an evaluation: Journal of Metamorphic Geology, v. 15, p. 127-140.

Mihalynuk, M. G., Smith, M. T., MacIntyre, D. G., and Deschenes, M., 1993, Tatshenshini project, northwestern British Columbia, Part B: Stratigraphic and magmatic setting of mineral occurrences: Geological Fieldwork 1992, v. Paper 1993-1, p. 189-202.

Mireku, L. K., and Stanley, C. R., 2006, Lithogeochemistry and hydrothermal alteration at the Halfmile Lake South Deep zone, a volcanic-hosted massive sulfide deposit, Bathurst Mining Camp, New Brunswick: Exploration and Mining Geology, v. 15, p. 177-199.

Monecke, T., Gemmell, J. B., and Herzig, P. M., 2006, Geology and volcanic facies architecture of the Lower Ordivician Waterloo massive sulfide deposit, Australia: Economic Geology, v. 101, p. 179-197.

Morton, R. L., and Franklin, J. M., 1987, Two-fold classification of Archean volcanic-associated massive sulfide deposits: Economic Geology and the Bulletin of the Society of Economic Geologists, v. 82, p. 1057-1063.

Müller, D., Rock, N. M. S., and Groves, D. I., 1992, Geochemical discrimination between shoshonitic and potassic volcanic rocks in different tectonic settings: A pilot study: Mineralogy and Petrology, v. 46, p. 259-289.

Muller, W., 2003, Strengthening the link between geochronology, textures and petrology: Earth and Planetary Science Letters, v. 206, p. 237-251.

Mundil, R., Ludwig, K. R., Metcalfe, I., and Renne, P. R., 2004, Age and timing of the Permian mass extinctions; U/Pb dating of closed-system zircons: Science, v. 305, p. 1760-1763.

Murakami, T., Chakoumakos, B. C., Ewing, R. C., Lumpkin, G. R., and Weber, W. J., 1991, Alpha-decay event damage in zircon: American Mineralogist, v. 76, p. 1510-1532.

Muttoni, G., Kent, D. V., Olsen, P., E. , and Stefano, P. D., 2004, Tethyan magnetostratigraphy

from Pizzo Mondello (Sicily) and correlation to the Late Triassic Newark astrochronological polarity time scale: Geological Society of America Bulletin, v. 116, p. 1043-1058

Nasdala, L., Reiners, P. W., Garver, J. I., Kennedy, A. K., Stern, R. A., Balan, E., and Wirth, R., 2004, Incomplete retention of radiation damage in zircon from Sri Lanka: American Mineralogist, v. 89, p. 219-231.

Nasdala, L., Zhang, M., Kempe, U., Panczer, G., Gaft, M., Andrut, M., and Ploetze, M., 2003, Spectroscopic methods applied to zircon, *in* Hanchar, J. M., and Hoskin, P. W. O., eds., Reviews in Mineralogy and Geochemistry, 53, p. 427-467.

Newberry, R. J., and Brew, D. A., 1997, The Upper Triassic Greens Creek VMS (Volcanogenic Massive Sulfide) deposit and Woewodski Island VMS Prospects, southeastern Alaska: chemical and isotopic data for rocks and ores demonstrate similarity of these deposits and their host rocks, U.S Department of the Interior: U.S. Geological Survey, p. 49.

Newberry, R. J., Brew, D. A., and Crafford, T. C., 1989, Zoned footwall alteration and original rock types at the Greens Creek volcanogenic massive sulfide (VMS) deposit, southeast Alaska, Proceedings to the Alaska Miners Association Juneau Conference: 29-31: Juneau, Alaska.

Newberry, R. J., Brew, D. A., and Crafford, T. C., 1990, Genesis of the Greens Creek volcanogenic massive sulfide deposit, S. E. Alaska: a geochemical study. : Geological Association of Canada Program with abstracts 1990, p. A96.

Newberry, R. J., Crafford, T., C., Newkirk, S. R., Young, L. E., Nelson, S. W., and Duke, N. A., 1997, Volcanogenic Massive Sulfide Deposits of Alaska: Economic Geology v. Monograph 9, p. 120-150.

Nokleberg, W. J., Bundtzen, T. K., Eremin, R. A., Ratkin, V. V., Dawson, K. M., Shpikerman, V. I., Goryachev, N. A., Byalobzhesky, S. G., Frolov, Y. F., Khanchuk, A. I., Koch, R. D., Monger, J. W. H., Pozdeev, A. I., Rozenblum, I. S., Rodionov, S. M., Parfenov, L. M., Scotese, C. R., and Sidorov, A. A., 2005, Metallogenesis and tectonics of the Russian Far East, Alaska, and the Canadian Cordillera.

Norford, B. S., and Mihalynuk, M. G., 1994, Evidence of the Pacific Faunal Province in the northern Alexander Terrane, recognition of two Middle Ordovician Graptolite zones in northwestern British-Columbia: Canadian Journal of Earth Sciences, v. 31, p. 1389-1396.

Normark, W. R., Morton, J. L., Koski, R. A., and Clague, D. A., 1983, Active hydrothermal vents and sulfide deposits on the southern Juan de Fuca Ridge: Geology (Boulder), v. 11, p.

158.

Norrish, K., and Chappell, B. W., 1977, X-ray fluorescence spectrometry, *in* Zussman, J. I., ed., Physical methods in determinerative mineralogy, Academic Press, p. 161-214.

Ohmoto, H., Mizukami, M., Drummond, S. E., Eldridge, C. S., Pisutha-Arnond, V., Lenagh, T. C., and Ohmoto, H. S., Brian J, 1983, Chemical processes of kuroko formation: Economic Geology Monograph, v. 5, p. 570-604.

Ohmoto, H., Vielreicher, R. M., Groves, D. I., Heinrich, C. A., and Walshe, J. L., 1996, Formation of volcanogenic massive sulfide deposits; the Kuroko perspective: Ore Geology Reviews, v. 10, p. 135-177.

Oliver, J. W. A., and Berg, H. C., 1981, Report on referred fossils, U.S. Geological Survey, p. 1.

Orchard, M. J., and Tozer, E. T., 1997, Triassic conodont biochronology, its calibration with the ammonoid standard, and a biostratigraphic summary for the Western Canada Sedimentary Basin: Bulletin of Canadian Petroleum Geology, v. 45, p. 675-692.

Panuska, B. C., 1985, Paleomagnetic evidence for a post-Cretaceous accretion of Wrangellia: Geology v. 13, p. 880-883.

Pearce, J. A., 1996, A user's guide to basalt discrimination diagrams, *in* Wyman, D. A., ed., Trace element geochemistry of volcanic rocks, Short Course Notes Volume 12, Geological Association of Canada - Mineral Deposits Division, p. 79-113.

Pearce, J. A., and Cann, J. R., 1973, Tectonic setting of basic volcanic rocks determined using trace element analyses: Earth and Planetary Science Letters, v. 19, p. 290-300.

Peter, J. M., and Scott, S. D., 1999, Windy Craggy, northwestern British Columbia; the world's largest besshi-type deposit *in* Barrie, C. T., and Hannington, M. D., eds., Reviews in Economic Geology: Volcanic-associated massive sulfide deposits; processes and examples in modern and ancient settings, 8, p. 261-295.

Petersen, E. U., 1991, Mineral compositions in Greens Creek concentrates, University of Utah: Department of Geology and Geophysics, p. 3.

Pontual, S., Merry, N., and Gamson, P., 1997, G-Mex Vol. 7, Volcanic-hosted massive sulfide systems, Ausspec International Pty. Ltd.

Premo, W. R., Taylor, C. D., Snee, L. W., and Harris, A. G., in press, Microfossil and radioisotopic geochronological studies of the Greens Creek host rocks, *in* Taylor, C. D., and Johnson, C. A., eds., Geology, geochemistry, and genesis of the Greens Creek massive sulfide deposit, Admiralty Island, southeastern Alaska, Professional Paper 1763, U. S. Geological Survey.

Proffett, J. M., 1987, Structural geology of the Greens Creek Deposit, Admiralty Island,

southeast Alaska, KGCMC, p. 24.

Proffett, J.M., 1997, Progress Report, Geology of the Greens Creek Mine area, Alaska, KGCMC.

Proffett, J. M., 1998, Interpretations of faults and of ore in the Northwest West ore body, Greens Creek.

Proffett, J. M., 2000, Geologic work at Greens Creek, 2000 field season, KGCMC, p. 20.

Proffett, J. M., 2000a, Geologic work at Greens Creek, 2000 field season - Final revised report, KGCMC, p. 22.

Proffett, J. M., 2000b, Report on geologic structure in 800 drift and 760 stope, central west ore body, and a reconnaissance of structure in 200S ore body, Greens Creek Mine, Alaska, KGCMC, p. 8.

Proffett, J. M., 2001, Geologic work in the Lower Gallagher and Upper NW mine areas, Greens Creek Mine, Alaska, KGCMC, p. 9.

Proffett, J. M., 2002a, Progress report on geologic work at Greens Creek, Alaska, August 2002: West Gallagher area, KGCMC, p. 10.

Proffett, J. M., 2002b, Progress report on geologic work at Greens Creek, Alaska: June, 2002, KGCMC, p. 9.

Proffett, J. M., 2003, Progress report on geologic work in the West Gallagher area, Greens Creek, Alaska: July 2003, KGCMC, p. 12.

Proffett, J.M., 2004a, Interpretations of drilling results and surface mapping west of the Gallagher Fault, Greens Creek Mine, Alaska.

Proffett, J. M., 2004b, Interpretations of drilling results and surface mapping west of the Gallagher Fault, Greens Creek, Alaska, KGCMC, p. 11.

Proffett, J. M., 2004c, Interpretations of drilling results west of the Gallagher Fault, Greens Creek Mine, Alaska, KGCMC, p. 6.

Proffett, J. M., 2005a, Geological work at the Greens Creek Mine, June, 2005, KGCMC, p. 9.

Proffett, J.M., 2005b, Preliminary report on interpretation of drilling results west of the Gallagher Fault, Greens Creek.

Proffett, J.M., 2006, Report on June, 2006 geologic work in the Big Sore and Big Sore Creek area, Greens Creek, Alaska, p. 6 pages.

Proffett, J. M., 2007, Geologic work done in August, 2007 at Greens Creek Alaska, KGCMC, p. 22.

Proffett, J.M., in press, Geologic structure of the Greens Creek Mine area, southeastern Alaska, *in* Taylor, C. D., and Johnson, C. A., eds., Geology, geochemistry, and genesis of the Greens Creek massive sulfide deposit, Admiralty Island, southeastern Alaska,

Professional Paper 1763, U.S. Geological Survey.

Rickwood, P. C., 1989, Boundary lines within petrologic diagrams which use oxides of major and minor elements: Lithos, v. 22, p. 247-263.

Rigby, J. K., Karl, S. M., Blodgett, R. B., and Baichtal, J. E., 2005, Ordovician “sphinctozoan” sponges from Prince of Wales Island, southeastern Alaska: Journal of Paleontology, v. 79, p. 862-870.

Roddick, J. C., 1987, Generalized numerical error analysis with applications to geochronology and thermodynamics: Geochimica et Cosmochimica Acta, v. 51, p. 2129-2135.

Roth, T., Thompson, J. F. H., and Barrett, T. J., 1999, The precious-metal-rich Eskay Creek Deposit, northwestern British Columbia, *in* Barrie, C. T., and Hannington, M. D., eds., Reviews in Economic Geology: Volcanic-associated massive sulfide deposits; processes and examples in modern and ancient settings, 8, p. 357-373.

Rubatto, D., and Gebauer, D., 2000, Use of cathodoluminescence for U-Pb zircon dating by ion microprobe; some examples from the Western Alps, *in* Pagel, M., Barbin, V., Blanc, P., and Ohnenstetter, D., eds., Cathodoluminescence in Geosciences: Berlin, Federal Republic of Germany (DEU), Springer, p. 373-400.

Rubin, C. M., and Saleeby, J. B., 1991, The Gravina Sequence - remnants of a Mid-Mesozoic oceanic-arc in southern southeast Alaska: Journal of Geophysical Research-Solid Earth and Planets, v. 96, p. 14551-14568.

Rubin, C. M., and Saleeby, J. B., 1991, Tectonic framework of the Upper Paleozoic and Lower Mesozoic Alava Sequence - a revised view of the polygenetic Taku Terrane in southern southeast Alaska: Canadian Journal of Earth Sciences, v. 28, p. 881-893.

Rubin, C. M., and Saleeby, J. B., 1992, Tectonic history of the eastern edge of the Alexander Terrane, southeast Alaska: Tectonics, v. 11, p. 586-602.

Sabine, C., 1999, Remote sensing strategies for mineral exploration, *in* Rencz, A. I., ed., Remote sensing for the earth sciences.

Saleeby, J., 2004, The Alexander Terrane boundary with North American margin terranes lies west of the Coast Batholith in southern southeast Alaska: Abstracts with Programs - Geological Society of America, v. 36, p. 344.

Saleeby, J. B., 1992, Age and tectonic setting of the Duke Island Ultramafic Intrusion, southeast Alaska: Canadian Journal of Earth Sciences, v. 29, p. 506-522.

Saleeby, J. B., 2000, Geochronologic investigations along the Alexander-Taku Terrane boundary, southern Revillagigedo Island to Cape Fox areas, Southeast Alaska *in* Stowell, H. H., ed., Tectonics of the Coast Mountains, Southeastern Alaska and British Columbia, 343: Boulder, Colorado, Geological Society of America, p. 107-143.

Samson, S. D., McClelland, W. C., Patchett, P. J., Gehrels, G. E., and Anderson, R. G., 1989, Evidence from neodymium isotopes for mantle contributions to Phanerozoic crustal genesis in the Canadian Cordillera: Nature, v. 337, p. 705-709.

Samson, S. D., Patchett, J. P., Gehrels, G. E., and Anderson, R. G., 1990, Nd and Sr isotopic characterization of the Wrangellia Terrane and implications for crustal growth of the Canadian Cordillera: Journal of Geology, v. 98, p. 749-762.

Sangster, D. F., 1977, Some grade and tonnage relationships among Canadian volcanogenic massive sulfide deposits: Geological Survey of Canada, v. Report of Activities p. 5-12.

Satre, M., 2006, Historical production 1989 to mid-2006, Kennecott Greens Creek Mining Company.

Schaltegger, U., Fanning, C. M., Guenther, D., Maurin, J. C., Schulmann, K., and Gebauer, D., 1999, Growth, annealing and recrystallization of zircon and preservation of monazite in high-grade metamorphism; conventional and in-situ U-Pb isotope, cathodoluminescence and microchemical evidence: Contributions to Mineralogy and Petrology, v. 134, p. 186-201.

Scherkenbach, D. A., 1983, Observations on Greens Creek Geology, Noranda Exploration, Inc., p. 43.

Scoates, J. S., and Friedman, R. M., 2008, Precise age of the platiniferous Merensky Reef, Bushveld Complex, South Africa, by the U-Pb zircon chemical abrasion ID-TIMS technique: Economic Geology, v. 103, p. 465-471.

Sillitoe, R. H., Hannington, M. D., and Thompson, J. F. H., 1996, High sulfidation deposits in the volcanogenic massive sulfide environment: Economic Geology, v. 91, p. 204-212.

Slack, J. F., 1993, Descriptive and grade-tonnage models for besshi-type massive sulfide deposits: Special Paper - Geological Association of Canada, v. 40, p. 343-371.

Smuts, L., and Walker, C., 2008, Rio Tinto competent persons annual report for mineral resources and ore reserves at the Greens Creek Mine, Rio Tinto, p. 57.

Soja, C., 1993, Carbonate platform evolution in a Silurian oceanic island - a case study from Alaska Alexander Terrane: Journal of Sedimentary Petrology, v. 63, p. 1078-1088.

Soja, C. M., 1992, Potential contributions of ancient oceanic islands to evolutionary-theory: Journal of Geology, v. 100, p. 125-134.

Soja, C. M., 1996, Island-arc carbonates: characterization and recognition in the ancient geologic record: Earth-Science Reviews, v. 41, p. 31-65.

Soja, C. M., and Antoshkina, A. I., 1997, Coeval development of Silurian stromatolite reefs in Alaska and the Ural Mountains: Implications for paleogeography of the Alexander terrane: Geology, v. 25, p. 539-542.

Solomon, M., 1976, “Volcanic” massive sulfide deposits and their host rocks; a review and an explanation, *in* Wolf, K. H., ed., Handbook of strata-bound and stratiform ore deposits II: Regional studies and specific deposits, 6: Cu, Zn, Pb, and Ag deposits: New York, Elsevier Publishing Company, p. 21-54.

Solomon, M., and Walshe, J. L., 1979, The formation of massive sulfide deposits on the sea floor: Economic Geology and the Bulletin of the Society of Economic Geologists, v. 74, p. 797-813.

Spencer, A. C., and Wright, C. W., 1906, The Juneau gold belt, Alaska; and a reconnaissance of Admiralty Island, Alaska, Bulletin 287, U.S. Geological Survey, p. 161 pages.

Stacey, J. S., and Kramer, J. D., 1975, Approximation of terrestrial lead isotope evolution by a two-stage model: Earth and Planetary Science Letters, v. 26, p. 207-221.

Sutley, S. J., Goldfarb, R. J., O’Leary, R. M., and Tripp, R. B., 1990, A comparison of geochemical exploration techniques and sample media within accretionary continental margins; an example from the Pacific Border Ranges, southern Alaska, U.S.A: Journal of Geochemical Exploration, v. 37, p. 255-275.

Taylor, C. D., 1997, An arc-flank to back-arc transect: metallogeny of Late Triassic volcanogenic massive sulfide occurrences of the Alexander Terrane, southeastern Alaska and British Columbia. : SEG Neves Corvo Field Conference 1997, Lisbon, Spain, May 11-14, 1997, 1997, p. 68.

Taylor, C. D., Cieutat, B. A., and Miller, L. D., 1992, A follow-up geochemical survey of base metal anomalies in the Ward Creek/Windfall Harbor and Gambier Bay areas, Admiralty Island S.E. Alaska, *in* Bradley, D., and Dusel-Bacon, C., eds., 1991 Geologic Studies in Alaska, U.S. Geological Survey Bulletin 2041, U.S. Geological Survey, p. 70-85.

Taylor, C. D., Hall, T. E., Wakeman, B. W., and Snee, L. W., 1995, New information on the geochemistry, age and tectonic history of late volcanic host rocks and associated volcanogenic massive sulfide occurrences of the Alexander terrane, southeast Alaska, Alaska Miners Association Conference Juneau: p. 31-32: Juneau, Alaska.

Taylor, C. D., and Lear, K. G., 2001, A summary of results from the cooperative Kennecott

Greens Creek Mining Company-U.S. Geological Survey investigation of the Greens Creek massive sulfide deposit, southeastern Alaska: Alaska Miners Association 2001 Annual convention, p. 2-4.

Taylor, C. D., Premo, W. R., and Lear, K. G., 2000a, The Greens Creek massive sulfide deposit; premier example of the Late Triassic metallogeny of the Alexander Terrane, Southeastern Alaska and British Columbia: Geological Society of America, Cordilleran Section, 96th annual meeting, v. 32, p. 71.

Taylor, C. D., Leventhal, J. S., Johnson, C. A., and Lear, K. G., 2000b, The Greens Creek massive sulfide deposit, Southeastern Alaska; stable isotopic evidence for the involvement of biogenic sulfate reduction in the formation of ores and carbonates: Volcanic environments and massive sulfide deposits; program and abstracts; international conference and field meeting, 2000, p. 209-210.

Taylor, C. D., Premo, W. R., Leventhal, J. S., Meier, A. L., Johnson, C. A., Newkirk, S. R., Hall, T. E., Lear, K. G., and Harris, A. G., 1999, The Greens Creek Deposit, Southeastern Alaska; a VMS-SEDEX hybrid: Proceedings of the Fifth biennial SGA meeting and the Tenth quadrennial IAGOD symposium; Mineral deposits; processes to processing, v. 5, p. 597-600.

Taylor, C. D., Premo, W. R., Meier, A. L., and Taggart, J. E., 2008, The metallogeny of Late Triassic rifting of the Alexander terrane in southeastern Alaska and northwestern British Columbia: Economic Geology, v. 103, p. 89-115.

Taylor, C. D., Lear, K. G., and Newkirk, S. R., in press-a, A genetic model for the Greens Creek polymetallic massive sulfide deposit, Admiralty Island, southeastern Alaska, *in* Taylor, C. D., and Johnson, C. A., eds., Geology, geochemistry, and genesis of the Greens Creek massive sulfide deposit, Admiralty Island, southeastern Alaska, Professional Paper 1763, U.S. Geological Survey.

Taylor, C. D., Philpotts, J., Premo, W. R., Meier, A. L., and Taggart, J. E., in press-b, The Late Triassic metallogenic setting of the Greens Creek deposit in southeastern Alaska, *in* Taylor, C. D., and Johnson, C. A., eds., Geology, geochemistry, and genesis of the Greens Creek massive sulfide deposit, Admiralty Island, southeastern Alaska, Professional Paper 1763, U.S. Geological Survey.

Taylor, C. D., Premo, W. R., Johnson, C. A., and Landis, G. P., in press-c, Sulfur and lead isotope characteristics of the Greens Creek polymetallic massive sulfide deposit, Admiralty Island, southeastern Alaska, *in* Taylor, C. D., and Johnson, C. A., eds.,

Geology, geochemistry, and genesis of the Greens Creek massive sulfide deposit, Admiralty Island, southeastern Alaska, Professional Paper 1763, U. S. Geological Survey.

Taylor, C. D., Sutley, S. J., and Lichte, F. E., in press-d, Mineralogical, textural, and metal residence studies of primary, recrystallized, and remobilized ores of the Greens Creek deposit., *in* Taylor, C. D., and Johnson, C. A., eds., Geology, geochemistry, and genesis of the Greens Creek massive sulfide deposit, Admiralty Island, southeastern Alaska, Professional Paper 1763, U. S. Geological Survey.

Taylor, C. D., West, A. W., Lear, K. G., Hall, T. E., and Proffett, J. M., in press-e, Geology and metal zoning of the Greens Creek massive sulfide deposit, southeastern Alaska, *in* Taylor, C. D., and Johnson, C. A., eds., Geology, geochemistry, and genesis of the Greens Creek massive sulfide deposit, Admiralty Island, southeastern Alaska, Professional Paper 1763, U.S. Geological Survey.

Taylor, S. R., and Gorton, M. P., 1977, Geochemical application of spark source mass spectrography; III, Element sensitivity, precision and accuracy: Geochimica et Cosmochimica Acta, v. 41, p. 1375-1380.

Thompson, A. J. B., Hauff, P. L., and Robitaille, J. A., 1999, Alteration mapping in exploration; application of short-wave infrared (SWIR) spectroscopy: SEG Newsletter, v. 39, p. 16-27.

Tiepolo, M., 2003, In-situ Pb geochronology of zircon with laser ablation-inductively coupled plasma-sector field mass spectrometry: Chemical Geology, v. 199, p. 159-177.

Trop, J., Ridgway, K., Manuszak, J., and Layer, P., 2002, Mesozoic sedimentary-basin development on the allochthonous Wrangellia composite terrane, Wrangell Mountains basin, Alaska: a long-term record of terrane migration and arc construction: Geological Society of America Bulletin, v. 114, p. 693-717.

Trop, J., and Szuch, D., 2005, Sedimentology and provenance of the upper Jurassic Naknek formation, Talkeetna Mountains, Alaska: bearings on the accretionary tectonic history of the Wrangellia composite terrane: Geological Society of America Bulletin, v. 117, p. 570-588.

van Ruitenbeek, F. J. A., Cudahy, T., Hale, M., and van der Meer, F. D., 2005, Tracing fluid pathways in fossil hydrothermal systems with near-infrared spectroscopy: Geology, v. 33, p. 597-600.

West, A., in press, The history of Greens Creek exploration, *in* Taylor, C. D., and Johnson, C. A.,

eds., Geology, geochemistry, and genesis of the Greens Creek massive sulfide deposit, Admiralty Island, southeastern Alaska, Professional Paper 1763, U. S. Geological Survey, p. 57 pages.

West, A., and Proffett, J., 2003, Greens Creek district lithologies, Kennecott Greens Creek Mining Company, p. 1.

Whitford, D. J., McPherson, W. P. A., and Wallace, D. B., 1989, Geochemistry of the host rocks of the volcanogenic massive sulfide deposit at Que River, Tasmania: Economic Geology, v. 84, p. 1-21.

Wiedenbeck, M., Alle, P., Corfu, F., Griffin, W., and Meier, M., 1995, Three natural zircon standards for the U-Th-Pb, Lu-Hf, trace element and REE analyses: Geostandards Newsletter, v. 19, p. 1-23.

Williams, I. S., 2001, Response of detrital zircon and monazite, and their U-Pb isotopic systems, to regional metamorphism and host-rock partial melting, Cooma Complex, southeastern Australia: Australian Journal of Earth Sciences, v. 48, p. 557-580.

Winchester, J. A., and Floyd, P. A., 1976, Geochemical magma type discrimination; application to altered and metamorphosed basic igneous rocks Earth and Planetary Science Letters, v. 28, p. 459.

Winchester, J. A., and Floyd, P. A., 1977, Geochemical discrimination of different magma series and their differentiation products using immobile elements: Chemical Geology, v. 20, p. 325-343.

Winchester, J. A., Park, R. G., and Holland, J. G., 1980, The geochemistry of Lewisian semipelitic schists from the Gairloch District, Wester Ross: Scottish Journal of Geology, v. 16, p. 165-179.

Wood, D. A., 1980, The application of a Th-Hf-Ta diagram to problems of tectonomagmatic classification and to establishing the nature of crustal contamination of basaltic lavas of the British Tertiary volcanic province: Earth and Planetary Science Letters, v. 50, p. 11-30.

Wynne, P. J., and Strong, D. F., 1984, The Strickland prospect of southwestern Newfoundland; a lithogeochemical study of metamorphosed and deformed volcanogenic massive sulfides: Economic Geology, v. 79, p. 1620-1642.

Yang, K., 1998, Compositional variations of white micas, a literature review, *in* CSIRO, ed., 469F, Division of Exploration and Mining, p. 25.

Yang, K., Huntington, J. F., Scott, K. M., and Mason, P., 2004, Compositional variations of white mica in the footwall hydrothermal alteration system of the Hellyer Zn-Pb deposit, Tasmania: PACRIM 2004; Hi-tech and world competitive mineral success stories around

Appendices DVD file structure

File structure for the digital data included in the DVD at the back of this thesis.

Appendix 1
- 1.1_Underground_maps
- 1.2_Core_log_examples
- 1.3_Rock_catalogue.xls

Appendix 2
- 2.1_GC_ICP.xls
- 2.2_Sack_ICP.xls
- 2.3_Sack_XRF.xls

Appendix 3
- 3.1_BSE-MLA_overlays
- 3.2_CL&SE_images
- 3.3_Interpreted_data
- 3.4_Raw_data

Appendix 4
- 4.1_PIMA_data
- 4.2_Terra_Spec_data
- 4.3_Interpreted_SWIR_data.xls
- 4.4_Raw_SWIR_data.xls

Appendix 5
- 5.1_Assay_data
- 5.2_Reconstruction_cross-sections

Appendix 1: Logging, mapping and rock catalogue

List of drill holes logged (1" = 10' or 1:120 scale)

Hole No	Long Section	Cross Section	State Plane East (ft)	State Plane North (ft)	Prospect	From (feet)	To (feet)
GC002	6155	4930	2499997	2282525	East Ore	298	331
GC010	6490	4628	2500430	2282401	East Ore	0	426
GC011	6609	4389	2500642	2282237	East Ore	320	352.6
GC012	6599	4514	2500579	2282346	East Ore	310	321
GC055	6587	1833	2501741	2279929	East Ore	0	176
GC056	6595	1833	2501748	2279933	East Ore	0	120
GC057	6572	1827	2501731	2279918	East Ore	0	185
GC075	6609	4392	2500641	2282240	East Ore	206	403
GC137	6582	1981	2501672	2280060	East Ore	0	231
GC138	6573	1973	2501667	2280049	East Ore	0	298
GC140	6599	1985	2501685	2280072	East Ore	0	226
GC143	6026	2023	2501153	2279855	East Ore	0	462
PP0692					330 ore access	256.6	390
PP0694					300 ore access	200	379
PP0697					300 ore access	396	641
ST0608					480 ore access	0	296
PS009	7002	4222	2501067	2282256	East Ore	0	261
PS010	7015	3598	2501352	2281700	East Ore	0	260.5
PS024	6862	3874	2501093	2281882	East Ore	0	469
PS026	6936	3260	2501428	2281362	East Ore	0	588
PS028	6823	2008	2501875	2280186	East Ore	0	669
PS030	6655	4791	2500505	2282615	East Ore	0	288
PS057	6990	2606	2501763	2280798	East Ore	0	500
PS070	5904	5205	2499649	2282659	East Ore	195.5	319.5
PS076	5526	7149	2498459	2284240	East Ore	0	209
PS077	5055	7158	2498031	2284043	East Ore	0	405
PS103	4752	4342	2498992	2281379	NWW Ore	100	1923
PS105	4584	4732	2498670	2281656	NWW Ore	987.9	1803
PS177			2497651	2281767	Lower Gallagher	306	813
PS178			2478315	2290181	Lower Zinc	297.5	693
PS181			2478610	2290640	Lower Zinc	704	1253
PS193			2495334	2286907	West Bruin	294	1069
PS194			2498307	2279662	Middle Gallagher	531	852
PS232			2486321	2298855	Little Sore #3	336	892
PS271	1805	289	2498116	2276445	Upper Gallagher	0	4081
PS276	6118	4234	2500268	2281883	East Ore	0	852

Total footage logged = 17699.1 feet

Comparison of lithologies and abbreviations used by company geologists with those used during the present study. The beginning lithology codes are included as they are used on early maps and logs. The final lithology codes are used in the thesis.

GC lithology code	GC lithology	Present study lithology	Beginning lithology codes	Final lithology codes
DG	diorite-microgabbro dikes	Post-Triassic dikes	Post-Triassic dikes	I4
QSC	quartz-sericite-carbonate phyllite	N/A	N/A	N/A
HGS	Hyd greenstone	Hyd basalt	HW4	Tr4
HLS	Hyd limestone	Hyd limestone	HW4	Tr4
HGB	Hyd microgabbro	Hyd microgabbro	HW3	I3
SSS	sericitic slatey sediments	SA	HW1	Tr3
GSS	graphitic slatey sediments	SA	HW1	Tr3
SAsr	sericitic slatey argillite	SA	HW1	Tr3
SA	slatey argillite	SA	HW1	Tr3
MA	massive argillite	MA	HW1	Tr3
DMA	dolomitic massive argillite	MA	HW1	Tr3
MAcx	clastic argillite	MA	HW1	Tr3
SPcx	clastic phyllite	polymict breccia	FW4	Tr1
MPcx	mariposite phyllite breccia	polymict breccia	FW4	Tr1
SR	siliceous rock	fine-grained layered rock (qtz+py alteration)	FW2b	C2b
SPs	siliceous-sericitic phyllite	fine-grained layered rock (qtz+ser alteration)	FW2a	C2a
SP	sericitic phyllite	fine-grained layered rock (ser alteration)	FW2a	C2a
SPcb	carbonate phyllite	fine-grained layered rock	FW2a	C2a
SPc	chloritic phyllite	fine-grained layered rock (chl alteration)	FW2a	C2a
SPgr	graphitic phyllite	fine-grained layered rock	FW2a	C2a
MP	mariposite phyllite	fine-grained layered rock (qtz+py alteration)	FW2a	C2a
GST	greenstone	fine-grained massive rock (chl alteration)	FW1	C1
GB	microgabbro	medium-grained massive rock (chl alteration)	FW1	C1
SC	serpentinite	fine to medium-grained rock	HW2	HW2
QCM	quartz-carbonate-mariposite	medium-grained massive rock	FW3	I1
AUM	undiff. Altered ultramafics	fine to medium-grained rock	Bas	HW2
QMS	quartz-mica schist	schistose sedimentary rock	Bas	S-D2
QCts	quartz-chlorite mica schist	schistose sedimentary rock	Bas	S-D2
GQMS	graphitic quartz mica schist	schistose sedimentary rock	Bas	S-D2
MB	Retreat marble	schistose sedimentary rock	Bas	S-D2

Appendix 1 on the DVD at the back of this thesis has examples of underground maps, scans of examples of two core logs and a rock catalogue of samples housed at the University of Tasmania.

1.1_Underground_maps
1.2_Core_log_examples
1.3_ Rock_catalogue.xls

Core logging examples of drill holes PS276 and PS232 are given in the digital appendices. For detailed logs of remaining drill holes, contact the author.

Mapping locations

Maps in the Appendix 1.1 are labelled according to the original naming (left hand column below). The current ore access names, used in the thesis, are in the right hand column.

878 - 878 ore access
CD4747 - 818 ore access
CD4446 - 758 ore access
CD4750 - 728 ore access
CD5146 - 743 ore access
CD5044 - 668 ore access
PD4247 - 638 ore access
PD4445 - 579 ore access
PD4246 - 578 ore access

Appendix 1.3 rock catalogue

UTAS No.	Field No.	DDH	Long Section	Cross Section	State Plane East (ft)	State Plane North (ft)	Lithology (CODES)	Lithology (mine)	Prospect
161924	GC002-299	GC002	6155	4930	2499997	2282525	C2	SPs	East Ore
161925	GC002-324	GC002	6155	4930	2499997	2282525	C2	SPs	East Ore
161926	GC010-001	GC010	6490	4628	2500430	2282401	C2	SPc	East Ore
161927	GC010-077	GC010	6490	4628	2500430	2282401	C2	SPcb	East Ore
161928	GC010-118	GC010	6490	4628	2500430	2282401	C2	SP	East Ore
161929	GC010-175	GC010	6490	4628	2500430	2282401	C2	SP	East Ore
161930	GC010-288	GC010	6490	4628	2500430	2282401	C2	SP	East Ore
161931	GC010-368	GC010	6490	4628	2500430	2282401	C2	SP	East Ore
161932	GC010-416	GC010	6490	4628	2500430	2282401	C2	SPc	East Ore
161933	GC010-426	GC010	6490	4628	2500430	2282401	C2	SPc	East Ore
161934	GC011-321	GC011	6609	4389	2500642	2282237	C2	SP	East Ore
161935	GC011-342	GC011	6609	4389	2500642	2282237	C2	SPs	East Ore
161936	GC012-319	GC012	6599	4514	2500579	2282346	C2	SPs	East Ore
161900	GC055-029	GC055	6587	1833	2501741	2279929	C1	GST	East Ore
161937	GC055-066	GC055	6587	1833	2501741	2279929	C2	SPc	East Ore
162133	GC055-100	GC055	6587	1833	2501741	2279929	Tr1	SPcx	East Ore
162134	GC055-139	GC055	6587	1833	2501741	2279929	Tr1	SPcx	East Ore
162135	GC055-176	GC055	6587	1833	2501741	2279929	Tr1	SPcx	East Ore
161901	GC056-017	GC056	6595	1833	2501748	2279933	C1	GST	East Ore
162121	GC056-040	GC056	6595	1833	2501748	2279933	I1	QCM	East Ore
161938	GC056-063	GC056	6595	1833	2501748	2279933	C2	SPc	East Ore
162136	GC056-092	GC056	6595	1833	2501748	2279933	Tr1	SPcx	East Ore
162137	GC056-117	GC056	6595	1833	2501748	2279933	Tr1	SPcx	East Ore
162122	GC057-005	GC057	6572	1827	2501731	2279918	I1	QCM	East Ore
161902	GC057-035	GC057	6572	1827	2501731	2279918	C1	GST	East Ore
161939	GC057-121	GC057	6572	1827	2501731	2279918	C2	SPc	East Ore
162123	GC057-150	GC057	6572	1827	2501731	2279918	I1	QCM	East Ore
162124	GC057-185	GC057	6572	1827	2501731	2279918	I1	QCM	East Ore
161940	GC075-225	GC075	6609	4392	2500641	2282240	C2	SPc	East Ore
161941	GC075-288	GC075	6609	4392	2500641	2282240	C2	SPc	East Ore

UTAS No.	Field No.	DDH	Long Section	Cross Section	State Plane East (ft)	State Plane North (ft)	Lithology (CODES)	Lithology (mine)	Prospect
161942	GC075-337	GC075	6609	4392	2500641	2282240	C2	SP	East Ore
161943	GC075-403	GC075	6609	4392	2500641	2282240	C2	SPs	East Ore
161944	GC137-068	GC137	6582	1981	2501672	2280060	C2	SPgr	East Ore
161945	GC137-134	GC137	6582	1981	2501672	2280060	C2	SPgr/SPcb	East Ore
161946	GC137-161	GC137	6582	1981	2501672	2280060	C2	SPgr	East Ore
161947	GC137-209	GC137	6582	1981	2501672	2280060	C2	SPs	East Ore
161948	GC137-228	GC137	6582	1981	2501672	2280060	C2	SPs	East Ore
161949	GC138-028	GC138	6573	1973	2501667	2280049	C2	SP	East Ore
161950	GC138-088	GC138	6573	1973	2501667	2280049	C2	SPgr	East Ore
161951	GC138-117	GC138	6573	1973	2501667	2280049	C2	SP	East Ore
161952	GC138-120	GC138	6573	1973	2501667	2280049	C2	SP	East Ore
161953	GC138-183	GC138	6573	1973	2501667	2280049	C2	SPs	East Ore
161954	GC138-298	GC138	6573	1973	2501667	2280049	C2	SPs	East Ore
161955	GC140-038	GC140	6599	1985	2501685	2280072	C2	SPgr	East Ore
161956	GC140-150	GC140	6599	1985	2501685	2280072	C2	SP	East Ore
162138	GC140-159	GC140	6599	1985	2501685	2280072	Tr1	SPcx	East Ore
161957	GC140-170	GC140	6599	1985	2501685	2280072	C2	SR	East Ore
161958	GC140-180	GC140	6599	1985	2501685	2280072	C2	SR	East Ore
161959	GC140-182	GC140	6599	1985	2501685	2280072	C2	SR	East Ore
161960	GC140-202	GC140	6599	1985	2501685	2280072	C2	SR	East Ore
161961	GC140-225	GC140	6599	1985	2501685	2280072	C2	SPs	East Ore
161962	GC143-090	GC143	6026	2023	2501153	2279855	C2	SP	East Ore
161963	GC143-130	GC143	6026	2023	2501153	2279855	C2	SP	East Ore
161964	GC143-228	GC143	6026	2023	2501153	2279855	C2	SP	East Ore
161965	GC143-425	GC143	6026	2023	2501153	2279855	C2	SP	East Ore
161966	GC143-443	GC143	6026	2023	2501153	2279855	C2	SP	East Ore
161967	PP0692-268	PP0692	N/A	N/A	N/A	N/A	C2	MP	UG -330
162139	PP0694-232	PP0694	N/A	N/A	N/A	N/A	Tr1	SPcx	UG-300
161968	PS009-055	PS009	7002	4222	2501067	2282256	C2	SPs	East Ore
161969	PS009-061	PS009	7002	4222	2501067	2282256	C2	SPs	East Ore

UTAS No.	Field No.	DDH	Long Section	Cross Section	State Plane East (ft)	State Plane North (ft)	Lithology (CODES)	Lithology (mine)	Prospect
161970	PS009-149	PS009	7002	4222	2501067	2282256	C2	SPs	East Ore
162140	PS009-261	PS009	7002	4222	2501067	2282256	Tr1	SP	East Ore
161971	PS010-258	PS010	7015	3598	2501352	2281700	C2	SP	East Ore
161972	PS024-056	PS024	6862	3874	2501093	2281882	C2	SP	East Ore
161973	PS024-067.5	PS024	6862	3874	2501093	2281882	C2	SP	East Ore
162141	PS024-221	PS024	6862	3874	2501093	2281882	Tr1	SPcx	East Ore
161974	PS024-325	PS024	6862	3874	2501093	2281882	C2	SPs	East Ore
161975	PS024-424	PS024	6862	3874	2501093	2281882	C2	SPs	East Ore
161976	PS024-453	PS024	6862	3874	2501093	2281882	C2	SPs	East Ore
161903	PS026-047	PS026	6936	3260	2501428	2281362	C1	GST	East Ore
161904	PS026-049	PS026	6936	3260	2501428	2281362	C1	GST	East Ore
161977	PS026-080	PS026	6936	3260	2501428	2281362	C2	SPc	East Ore
161978	PS026-143	PS026	6936	3260	2501428	2281362	C2	SP	East Ore
161979	PS026-190	PS026	6936	3260	2501428	2281362	C2	SP	East Ore
161980	PS026-270	PS026	6936	3260	2501428	2281362	C2	SP	East Ore
161981	PS026-278	PS026	6936	3260	2501428	2281362	C2	SP	East Ore
161982	PS026-302	PS026	6936	3260	2501428	2281362	C2	SPc	East Ore
161983	PS026-319	PS026	6936	3260	2501428	2281362	C2	SPs	East Ore
161984	PS026-332	PS026	6936	3260	2501428	2281362	C2	SPs	East Ore
161985	PS026-410	PS026	6936	3260	2501428	2281362	C2	SPgr	East Ore
161986	PS026-426	PS026	6936	3260	2501428	2281362	C2	SPgr	East Ore
161987	PS026-531	PS026	6936	3260	2501428	2281362	C2	SPgr	East Ore
161988	PS026-539	PS026	6936	3260	2501428	2281362	C2	SPgr	East Ore
161989	PS026-549	PS026	6936	3260	2501428	2281362	C2	SP	East Ore
161990	PS026-572	PS026	6936	3260	2501428	2281362	C2	SPs	East Ore
162142	PS026-588	PS026	6936	3260	2501428	2281362	Tr1	SPcx	East Ore
162125	PS028-230	PS028	6823	2008	2501875	2280186	I1	QCM	East Ore
161905	PS028-254	PS028	6823	2008	2501875	2280186	C1	GST	East Ore
161991	PS028-264	PS028	6823	2008	2501875	2280186	C2	SP	East Ore
161992	PS028-277	PS028	6823	2008	2501875	2280186	C2	SP	East Ore

UTAS No.	Field No.	DDH	Long Section	Cross Section	State Plane East (ft)	State Plane North (ft)	Lithology (CODES)	Lithology (mine)	Prospect
161993	PS028-350	PS028	6823	2008	2501875	2280186	C2	SPc	East Ore
161994	PS028-398	PS028	6823	2008	2501875	2280186	C2	SPc	East Ore
161995	PS028-436	PS028	6823	2008	2501875	2280186	C2	SPc	East Ore
161996	PS028-523	PS028	6823	2008	2501875	2280186	C2	SPgr	East Ore
161997	PS028-558	PS028	6823	2008	2501875	2280186	C2	SP	East Ore
161998	PS028-635	PS028	6823	2008	2501875	2280186	C2	SP	East Ore
161999	PS028-665	PS028	6823	2008	2501875	2280186	C2	SP	East Ore
162000	PS030-026	PS030	6655	4791	2500505	2282615	C2	SP	East Ore
162001	PS030-288	PS030	6655	4791	2500505	2282615	C2	SPs	East Ore
162002	PS057-047	PS057	6990	2606	2501763	2280798	C2	SP	East Ore
162143	PS057-096	PS057	6990	2606	2501763	2280798	Tr1	SPcx	East Ore
162003	PS057-147	PS057	6990	2606	2501763	2280798	C2	SP	East Ore
162004	PS057-183	PS057	6990	2606	2501763	2280798	C2	SP	East Ore
162005	PS057-247	PS057	6990	2606	2501763	2280798	C2	SPt	East Ore
162006	PS057-319	PS057	6990	2606	2501763	2280798	C2	SPcb	East Ore
162007	PS057-371	PS057	6990	2606	2501763	2280798	C2	SPcb	East Ore
162204	PS057-442	PS057	6990	2606	2501763	2280798	Tr2	Massive Py	East Ore
162144	PS057-478	PS057	6990	2606	2501763	2280798	Tr1	SPcx	East Ore
162145	PS057-488	PS057	6990	2606	2501763	2280798	Tr1	SPcx	East Ore
162008	PS070-228.5	PS070	5904	5205	2499649	2282659	C2	SP	East Ore
162009	PS070-277	PS070	5904	5205	2499649	2282659	C2	SPc	East Ore
162146	PS070-304.5	PS070	5904	5205	2499649	2282659	Tr1	SPcx	East Ore
162010	PS076-118	PS076	5526	7149	2498459	2284240	C2	SP	East Ore
162011	PS076-156.5	PS076	5526	7149	2498459	2284240	C2	SP	East Ore
161906	PS076-200	PS076	5526	7149	2498459	2284240	C1	GST	East Ore
162012	PS076-209	PS076	5526	7149	2498459	2284240	C2	SP	East Ore
162013	PS077-133	PS077	5055	7158	2498031	2284043	C2	SP	East Ore
162014	PS077-212	PS077	5055	7158	2498031	2284043	C2	SP	East Ore
162015	PS077-320	PS077	5055	7158	2498031	2284043	C2	SPc	East Ore
162016	PS077-321	PS077	5055	7158	2498031	2284043	C2	SPc	East Ore

UTAS No.	Field No.	DDH	Long Section	Cross Section	State Plane East (ft)	State Plane North (ft)	Lithology (CODES)	Lithology (mine)	Prospect
162017	PS077-366	PS077	5055	7158	2498031	2284043	C2	SPc	East Ore
162018	PS077-405	PS077	5055	7158	2498031	2284043	C2	SPc	East Ore
162019	PS103-0825	PS103	4752	4342	2498992	2281379	C2	SPs	NWW Ore
162020	PS103-0858	PS103	4752	4342	2498992	2281379	C2	SPgr	NWW Ore
162021	PS103-0890	PS103	4752	4342	2498992	2281379	C2	SP	NWW Ore
162022	PS103-1002	PS103	4752	4342	2498992	2281379	C2	SP	NWW Ore
162023	PS103-1086	PS103	4752	4342	2498992	2281379	C2	SPgr	NWW Ore
162024	PS103-1137	PS103	4752	4342	2498992	2281379	C2	SPt	NWW Ore
162147	PS103-1190	PS103	4752	4342	2498992	2281379	Tr1	SPcx	NWW Ore
162025	PS103-1894	PS103	4752	4342	2498992	2281379	C2	SP	NWW Ore
162148	PS103-1902	PS103	4752	4342	2498992	2281379	Tr1	SPcx	NWW Ore
162026	PS105-0990	PS105	4584	4732	2498670	2281656	C2	SP	NWW Ore
162027	PS105-1020	PS105	4584	4732	2498670	2281656	C2	SP	NWW Ore
162028	PS105-1096	PS105	4584	4732	2498670	2281656	C2	SP	NWW Ore
162029	PS105-1202	PS105	4584	4732	2498670	2281656	C2	SR	NWW Ore
162030	PS105-1236	PS105	4584	4732	2498670	2281656	C2	SR	NWW Ore
162031	PS105-1258	PS105	4584	4732	2498670	2281656	C2	SR	NWW Ore
162032	PS105-1378	PS105	4584	4732	2498670	2281656	C2	SP	NWW Ore
162033	PS105-1444	PS105	4584	4732	2498670	2281656	C2	SP	NWW Ore
162034	PS105-1702	PS105	4584	4732	2498670	2281656	C2	SPc	NWW Ore
162035	PS105-1703	PS105	4584	4732	2498670	2281656	C2	SPc	NWW Ore
162149	PS177-323	PS177	N/A	N/A	2497651	2281767	Tr1	SPcx	Lower Gallagher
162036	PS177-554	PS177	N/A	N/A	2497651	2281767	C2	SPc	Lower Gallagher
162037	PS177-630	PS177	N/A	N/A	2497651	2281767	C2	SP	Lower Gallagher
162038	PS177-699	PS177	N/A	N/A	2497651	2281767	C2	SPc	Lower Gallagher
162039	PS177-738	PS177	N/A	N/A	2497651	2281767	C2	SPs	Lower Gallagher
162150	PS178-299.5	PS178	N/A	N/A	2478315	2290181	Tr1	SPcx	LOWER ZINC
162151	PS178-313	PS178	N/A	N/A	2478315	2290181	Tr1	SPcx	LOWER ZINC
162040	PS178-462.5	PS178	N/A	N/A	2478315	2290181	C2	SPc	LOWER ZINC
162041	PS178-512.5	PS178	N/A	N/A	2478315	2290181	C2	SPgr	LOWER ZINC

UTAS No.	Field No.	DDH	Long Section	Cross Section	State Plane East (ft)	State Plane North (ft)	Lithology (CODES)	Lithology (mine)	Prospect
162042	PS178-583	PS178	N/A	N/A	2478315	2290181	C2	SPs(gr)	LOWER ZINC
162043	PS178-674.5	PS178	N/A	N/A	2478315	2290181	C2	SPgr,c	LOWER ZINC
162044	PS178-696	PS178	N/A	N/A	N/A	N/A	C2	SPgr,c	Lower Zn
162045	PS181-1206	PS181	N/A	N/A	2478610	2290640	C2	SPc	Lower Zinc
162046	PS181-1230	PS181	N/A	N/A	2478610	2290640	C2	SPgr	Lower Zinc
162047	PS181-738	PS181	N/A	N/A	2478610	2290640	C2	SPs	Lower Zinc
162152	PS181-810	PS181	N/A	N/A	2478610	2290640	Tr1	SPcx	Lower Zinc
162048	PS193-1008	PS193	N/A	N/A	2495334	2286907	C2	SPc	West Bruin
161907	PS193-1046.5	PS193	N/A	N/A	2495334	2286907	C1	GST	West Bruin
162049	PS193-343	PS193	N/A	N/A	2495334	2286907	C2	SPc	West Bruin
162050	PS193-371	PS193	N/A	N/A	2495334	2286907	C2	SPc	West Bruin
162126	PS193-540	PS193	N/A	N/A	2495334	2286907	I1	QCM	West Bruin
162051	PS193-614	PS193	N/A	N/A	2495334	2286907	C2	SPt/SPcb?	West Bruin
162127	PS193-634	PS193	N/A	N/A	2495334	2286907	I1	QCM	West Bruin
162120	PS193-763	PS193	N/A	N/A	2495334	2286907	C2/3	QCM/SPc	West Bruin
161908	PS193-810	PS193	N/A	N/A	2495334	2286907	C1	GST	West Bruin
161909	PS193-867.5	PS193	N/A	N/A	2495334	2286907	C1	GST	West Bruin
161910	PS193-977	PS193	N/A	N/A	2495334	2286907	C1	GST	West Bruin
162161	PS194-540	PS194	N/A	N/A	2498307	2279662	I2	SC	Middle Gallagher
162162	PS194-562.5	PS194	N/A	N/A	2498307	2279662	I2	SC	Middle Gallagher
162052	PS194-649	PS194	N/A	N/A	2498307	2279662	C2	SPt	Middle Gallagher
162053	PS194-694	PS194	N/A	N/A	2498307	2279662	C2	SPc	Middle Gallagher
162128	PS194-787	PS194	N/A	N/A	2498307	2279662	I1	QCM?	Middle Gallagher
162181	PS232-355	PS232	N/A	N/A	2486321	2298855	Tr4	Rhyolite	Little Sore #3
162182	PS232-484	PS232	N/A	N/A	2486321	2298855	Tr4	Rhyolite brx	Little Sore #3
162183	PS232-525	PS232	N/A	N/A	2486321	2298855	Tr4	Rhyolite brx	Little Sore #3
162184	PS232-541	PS232	N/A	N/A	2486321	2298855	Tr4	SPc	Little Sore #3
162185	PS232-564	PS232	N/A	N/A	2486321	2298855	Tr4	SP	Little Sore #3
162186	PS232-643	PS232	N/A	N/A	2486321	2298855	Tr4	SPgr	Little Sore #3
162187	PS232-770	PS232	N/A	N/A	2486321	2298855	Tr4	SP	Little Sore #3

UTAS No.	Field No.	DDH	Long Section	Cross Section	State Plane East (ft)	State Plane North (ft)	Lithology (CODES)	Lithology (mine)	Prospect
162169	PS271-063.9	PS271	1805	289	2498116	2276445	I3	Gb	Upper Gallagher
162170	PS271-1498.9	PS271	1805	289	2498116	2276445	I3	Gb	Upper Gallagher
162171	PS271-177	PS271	1805	289	2498116	2276445	I3	Gb	Upper Gallagher
162172	PS271-1798	PS271	1805	289	2498116	2276445	I3	HGS	Upper Gallagher
162188	PS271-1812.5	PS271	1805	289	2498116	2276445	Tr4	GST	Upper Gallagher
162173	PS271-207	PS271	1805	289	2498116	2276445	I3	HGB	Upper Gallagher
162189	PS271-2128	PS271	1805	289	2498116	2276445	Tr4	SPcx	Upper Gallagher
161893	PS271-2685	PS271	1805	289	2498116	2276445	Tr3	SA	Upper Gallagher
162174	PS271-297	PS271	1805	289	2498116	2276445	I3	Gb	Upper Gallagher
162054	PS271-3161	PS271	1805	289	2498116	2276445	C2	MP	Upper Gallagher
162055	PS271-3395	PS271	1805	289	2498116	2276445	C2	SPc	Upper Gallagher
162056	PS271-3534	PS271	1805	289	2498116	2276445	C2	SPgr	Upper Gallagher
162057	PS271-3831	PS271	1805	289	2498116	2276445	C2	SPgr	Upper Gallagher
162058	PS271-3857.5	PS271	1805	289	2498116	2276445	C2	SPgr	Upper Gallagher
162059	PS276-155.5	PS276	6118	4234	2500268	2281883	C2	SPc	Big Sore (East Ore Gap)
162060	PS276-264	PS276	6118	4234	2500268	2281883	C2	SPgr	Big Sore (East Ore Gap)
162061	PS276-302	PS276	6118	4234	2500268	2281883	C2	SPgr	Big Sore (East Ore Gap)
162062	PS276-390.5	PS276	6118	4234	2500268	2281883	C2	SP	Big Sore (East Ore Gap)
162129	PS276-505	PS276	6118	4234	2500268	2281883	I1	QCM	Big Sore (East Ore Gap)
162063	PS276-520	PS276	6118	4234	2500268	2281883	C2	SPc	Big Sore (East Ore Gap)
162064	PS276-585.5	PS276	6118	4234	2500268	2281883	C2	SPc	Big Sore (East Ore Gap)
162065	PS276-600	PS276	6118	4234	2500268	2281883	C2	SPgr	Big Sore (East Ore Gap)
162066	PS276-671	PS276	6118	4234	2500268	2281883	C2	SPc	Big Sore (East Ore Gap)
162190	PSA05-001	surface	N/A	N/A	2486377	2298709	Tr4	SR	Little Sore
162191	PSA05-002	surface	N/A	N/A	2495658	2275724	Tr4	HGS	Gallagher Ridge
162192	PSA05-004	surface	N/A	N/A	2495807	2275532	Tr4	SR	Gallagher Ridge
161894	PSA05-005	surface	N/A	N/A	2475574	2300807	S-D2	QMS	Hawk Inlet
161895	PSA05-006	surface	N/A	N/A	2477858	2293200	S-D2	QMS	1.9 mile on B road
161896	PSA05-008	surface	N/A	N/A	2475670	2300728	S-D2	GQMS	Hawk Inlet
162208	PSA05-009	surface	N/A	N/A	2486770	2317307	J2	basalt	N of Young Bay pier

UTAS No.	Field No.	DDH	Long Section	Cross Section	State Plane East (ft)	State Plane North (ft)	Lithology (CODES)	Lithology (mine)	Prospect
162209	PSA05-010	surface	N/A	N/A	2486428	2317140	J1	siltstone	S of Young Bay pier
162153	PSA05-011	surface	N/A	N/A	2484675	2315555	Tr1	SPcx	4.55 mile on A road
161911	PSA05-012	surface	N/A	N/A	2485720	2315438	C1	GST	beach 400' S of power
161897	PSA05-014	surface	N/A	N/A	2481828	2313311	S-D2	quartzite	3.63 mile on A road
162206	PSA05-015	surface	N/A	N/A	2481132	2311103	I4	DG	3.2 mile A road
161898	PSA05-016	surface	N/A	N/A	2475120	2309741	S-D2	QMS	Pit 7 A road
162163	PSA05-019	surface	N/A	N/A	2478282	2294570	I2	SC	100' S of 1.6 mile B road
162067	PSA05-020	surface	N/A	N/A	2479990	2287328	C2	SPgr	NW corner of Pit 174
161912	PSA05-022	surface	N/A	N/A	2480085	2284540	C1	GST	125' N of 3.6 mile B road
161913	PSA05-023	surface	N/A	N/A	2481594	2281161	C1	GST	125' S of 4.63 mile B road
161914	PSA05-027	surface	N/A	N/A	2485410	2279256	C1	GST	200'N of 5.6 mile B road
162164	PSA05-028	surface	N/A	N/A	2493202	2282373	I2	SC	7.35 mile B road
162165	PSA05-029	surface	N/A	N/A	2493456	2282373	I2	SC	50'E of 7.4 mile B road
161920	PSA06-002	surface	N/A	N/A	2472500	2308010	C1?	Gb?	Hawk Inlet
161921	PSA06-003	surface	N/A	N/A	2472710	2306950	C1?	GST	Hawk Inlet
161922	PSA06-004	surface	N/A	N/A	2473000	2305500	C1?	GST	Hawk Inlet
162193	PSA06-006	surface	N/A	N/A	2496315	2275490	Tr4	rhyolite	Gallagher Ridge
162175	PSA06-007	surface	N/A	N/A	2488930	2304850	I3	Gb	Lil' Sore
162176	PSA06-008	surface	N/A	N/A	2489045	2304805	I3	Gb	Lil' Sore
162194	PSA06-009	surface	N/A	N/A	2489095	2304550	Tr4	GST	Lil' Sore
162195	PSA06-010	surface	N/A	N/A	2481855	2293535	Tr4	SP?	
162068	PSA06-011	surface	N/A	N/A	2497720	2290425	C2	SPc	Mammoth Ridge
161915	PSA06-012	surface	N/A	N/A	2498040	2290430	C1	HGB	Mammoth Ridge
162203	PSA06-013	surface	N/A	N/A	2482380	2293635	Tr4?	SPc	Lower Zinc
162196	PSA06-014	surface	N/A	N/A	2510040	2278065	Tr4	GST	Cliff Ck
162197	PSA06-015	surface	N/A	N/A	2496465	2275420	Tr4	GST	Gallagher Ridge
162198	PSA06-016	surface	N/A	N/A	2496530	2275765	Tr4	GST	Gallagher Ridge
162177	PSA06-017	surface	N/A	N/A	2484590	2316420	I3	GB	Young Bay
162157	PSA06-018	surface	N/A	N/A	2484870	2315695	Tr1?	SPcx	Young Bay
161899	PSA06-022	surface	N/A	N/A	2474710	2314170	C1?	GST	East Hawk Inlet

UTAS No.	Field No.	DDH	Long Section	Cross Section	State Plane East (ft)	State Plane North (ft)	Lithology (CODES)	Lithology (mine)	Prospect
162154	PSA06-025	surface	6100	6300	2499079	2284144	Tr1	SPcx	mine portal
162069	PSA06-027	surface	6100	6300	2499054	2284113	C2	SP	mine portal
162070	PSA06-030	surface	6100	6300	2499018	2284074	C2	SPc	mine portal
162071	PSA06-032	surface	6100	6300	2498995	2284053	C2	SPc	mine portal
162155	PSA07-002	surface	N/A	N/A	2477965	2290690	Tr1	SPcx	B-road
162072	PSA07-005	surface	N/A	N/A	2477950	2291094	C2	SPgr	B-road
162166	PSA07-008	surface	N/A	N/A	2477915	2291541	I2	SC	B-road
162167	PSA07-011	surface	N/A	N/A	2477887	2292153	I2	undif UM	B-road
161916	PSA07-015	surface	N/A	N/A	2477831	2292613	C1	GST	B-road
161917	PSA07-017	surface	N/A	N/A	2477853	2293086	C1	Gb	B-road
161918	PSA07-019	surface	N/A	N/A	2479770	2289554	C1	GST	Lower Zinc
162199	PSA07-025	surface	N/A	N/A	2510950	2275400	Tr4	GST	Cliff Creek
162200	PSA07-026	surface	N/A	N/A	2510100	2275550	Tr4	GST	Cliff Creek
162178	PSA07-027	surface	N/A	N/A	2495750	2278300	I3	HGB	W Gallagher Ridge
162201	PSA07-028	surface	N/A	N/A	2498957	2275120	Tr4	HGS	S Gallagher Ridge
162202	PSA07-029	surface	N/A	N/A	2499050	2275100	Tr4	Hyd basalt	S Gallagher Ridge
161923	PSA07-030	surface	N/A	N/A	2512575	2273900	C1?	amphibolite	Cliff Creek
162158	PSA07-032	surface	N/A	N/A	2512550	2283061	Tr3	SSS	
162159	PSA07-033	surface	N/A	N/A	2513140	2282713	Tr3	GSS	
162179	PSA07-034	surface	N/A	N/A	N/A	N/A	I3	HGB	Serpentine Gulch
162180	PSA08-001	underground	N/A	N/A	2495883	2276373	I3	HGB	Gallagher Ridge
162205	PSA08-002	underground	N/A	N/A	2500094	2281852	I4	DG?	1350 Creek (E. Ore)
161919	PSA08-003	underground	N/A	N/A	2499978	2281910	C1	GST	1350 Creek (E. Ore)
162073	PSU05-003	underground	N/A	N/A	N/A	N/A	C2	MP(t)	460 ore access
162074	PSU05-005	underground	N/A	N/A	N/A	N/A	C2	SPs(t)	461 ore access
162075	PSU05-015	underground	N/A	N/A	N/A	N/A	C2	SPgr?c?	4211 drift
162076	PSU05-016	underground	N/A	N/A	N/A	N/A	C2	SPs(t)	4211 drift
162077	PSU05-019	underground	N/A	N/A	N/A	N/A	C2	SPs+py	4211 drift
162078	PSU05-020	underground	6060	1105	N/A	N/A	C2	MP	4211 drift
162079	PSU05-021	underground	6060	1105	N/A	N/A	C2	SPs+py	4211 drift

UTAS No.	Field No.	DDH	Long Section	Cross Section	State Plane East (ft)	State Plane North (ft)	Lithology (CODES)	Lithology (mine)	Prospect
162080	PSU05-026	underground	N/A	N/A	N/A	N/A	C2	MSPs	4211 drift
162081	PSU05-028	underground	N/A	N/A	N/A	N/A	C2	MP	4211 drift
162082	PSU05-034	underground	N/A	N/A	N/A	N/A	C2	SPc(s?)	4211 drift
162083	PSU05-041	underground	N/A	N/A	N/A	N/A	C2	SPc	4211 drift
162084	PSU05-045	underground	N/A	N/A	N/A	N/A	C2	SPc	4211 drift
162085	PSU05-047	underground	N/A	N/A	N/A	N/A	C2	SPt(s?)	4211 drift
162086	PSU05-050	underground	N/A	N/A	N/A	N/A	C2	SPc(s?)	4211 drift
162207	PSU05-051	underground	5300	820	N/A	N/A	I4	DG	4211 drift
162087	PSU05-054	underground	N/A	N/A	N/A	N/A	C2	SPc	4211 drift
162088	PSU05-055	underground	N/A	N/A	N/A	N/A	C2	SPc	4211 drift
162089	PSU05-111	underground	N/A	N/A	N/A	N/A	C2	SPs+py	675 ore access
162090	PSU07-001	underground	4892	4912	2498896	2281947	C2	MSPs	878 ore access
162091	PSU07-003	underground	4835	4842	2498858	2281865	C2	MSPs	878 ore access
162092	PSU07-004	underground	4798	4810	2498846	2281818	C2	SPs	878 ore access
162093	PSU07-005	underground	4794	4787	2498827	2281804	C2	SPc	878 ore access
162094	PSU07-006	underground	4738	4695	2498826	2281694	C2	MSPs	878 ore access
162095	PSU07-007	underground	4697	4650	2498809	2281636	C2	MSPs	878 ore access
162096	PSU07-008	underground	4565	4753	2498645	2281670	C2	SR	878 ore access
162097	PSU07-009	underground	4581	4945	2498575	2281850	C2	MSPs	668 ore access
162098	PSU07-010	underground	4513	4942	2498516	2281818	C2	MSPs	668 ore access
162099	PSU07-011	underground	4445	4946	2498453	2281791	C2	MSPs	668 ore access
162130	PSU07-012	underground	4438	4970	2498436	2281810	I1	QCM	668 ore access
162100	PSU07-013	underground	4395	5015	2498378	2281832	C2	SPc	668 ore access
162101	PSU07-014	underground	4703	5119	2498609	2282060	C2	SRcx	743 ore access
162156	PSU07-015	underground	4717	5113	2498624	2282061	Tr1	SPcx	743 ore access
162102	PSU07-016	underground	4670	5118	2498580	2282045	C2	MP	743 ore access
162103	PSU07-017	underground	4626	5090	2498552	2282000	C2	MSP	743 ore access
162104	PSU07-018	underground	4626	5035	2498577	2281951	C2	SPcb	728 ore access
162105	PSU07-019	underground	4685	5035	2498630	2281977	C2	SR	728 ore access
162106	PSU07-023	underground	4733	4775	2498787	2281764	C2	SPgr	818 ore access

UTAS No.	Field No.	DDH	Long Section	Cross Section	State Plane East (ft)	State Plane North (ft)	Lithology (CODES)	Lithology (mine)	Prospect
162107	PSU07-024	underground	4662	4645	2498780	2281616	C2	SPgr	758 ore access
162108	PSU07-025	underground	4673	4644	2498790	2281620	C2	SPt	758 ore access
162109	PSU07-026	underground	4608	4635	2498735	2281583	C2	SPt	758 ore access
162110	PSU07-027	underground	4558	4613	2498700	2281542	C2	SPgr	758 ore access
162168	PSU07-029	underground	4497	4620	2498642	2281521	I2	SC	758 ore access
162131	PSU07-038	underground	4305	4747	2498414	2281551	I1	QCM	638 ore access
162132	PSU07-041	underground	4235	4812	2498323	2281579	I1	QCM	638 ore access
162111	PSU07-051	underground	4440	4415	2498681	2281312	C2	SPgr	579 ore access
162112	PSU07-052	underground	4390	4485	2498605	2281353	C2	SPt	579 ore access
162113	PSU07-057	underground	4613	4220	2498921	2281212	C2	SPt	2853 ramp
162114	PSU07-058	underground	4642	4208	2498953	2281214	C2	SPgr	2853 ramp
162160	PSU07-061	underground	4738	4360	2498973	2281393	Tr3	MA	578 ore access
162115	PSU07-062	underground	4735	4358	2498971	2281390	C2	MSPs	578 ore access
162116	PSU07-063	underground	4725	4320	2498978	2281351	C2	SPs	578 ore access
162117	PSU07-064	underground	4715	4300	2498978	2281329	C2	SPt	578 ore access
162118	PSU07-065	underground	4695	4267	2498975	2281290	C2	SPt	578 ore access
162119	PSU07-066	underground	4667	4243	2498960	2281257	C2	SPt	578 ore access

Appendix 2: Geochemical analyses

ICP analyses

Group 4A: Whole Rock by ICP-ES

A rock characterization package comprising four separate analytical tests. Total abundances of the major oxides and several minor elements are reported on a 0.1g sample analyzed by ICP-emission spectrometry following a Lithium metaborate/tetraborate fusion and dilute nitric digestion. Loss on ignition (LOI) is by weigh difference after ignition at 1000°C. Total carbon and sulphur analysis by Leco.

Group 4B: Total Trace Elements by ICP-MS

This package comprises two separate analyses. Rare earth and refractory elements are determined by ICP mass spectrometry following a Lithium metaborate / tetraborate fusion and nitric acid digestion of a 0.1g sample (same decomposition as Group 4A). In addition a separate 0.5 g split is digested in Aqua Regia and analyzed by ICP Mass Spectrometry to report the precious and base metals (in highlight). Group 4A and 4B each require 5 g for analysis, 10 g for combined package (Group 4A-4B).

Detection limits for ICP analyses by Acme Analytical *Highlighted elements by Aqua Regia/ICP-MS analysis in 4B package.

	Group 4A			Group 4A	Group 4B			Group 4A	Group 4B	
	Det. Lim.	Upper limit		Det. Lim.	Det. Lim.	Upper limit		Det. Lim.	Det. Lim.	Upper limit
SiO2	0.01%	100%	Au*	N/A	5ppb	100 ppm	Ta	20 ppm	.1 ppm	50000 ppm
Al2O3	0.01%	100%	Ag*	N/A	.1 ppm	100 ppm	Th	N/A	.2 ppm	10000 ppm
Fe2O3	0.04%	100%	As*	N/A	1 ppm	10000 ppm	Tl*	N/A	.1 ppm	1000 ppm
CaO	0.01%	100%	Ba	5 ppm	1 ppm	50000 ppm	U	N/A	.1 ppm	10000 ppm
MgO	0.01%	100%	Be	N/A	1 ppm	10000 ppm	V	N/A	8 ppm	10000 ppm
Na2O	0.01%	100%	Bi*	N/A	.1 ppm	2000 ppm	W	N/A	.5 ppm	10000 ppm
K2O	0.01%	100%	Cd*	N/A	.1 ppm	2000 ppm	Y	3 ppm	.1 ppm	50000 ppm
MnO	0.01%	100%	Co	20 ppm	.2 ppm	10000 ppm	Zn*	5 ppm	1 ppm	10000 ppm
TiO2	0.01%	100%	Cs	N/A	.1 ppm	10000 ppm	Zr	6 ppm	.1 ppm	50000 ppm
P2O5	0.01%	100%	Cu*	5 ppm	.1 ppm	10000 ppm	La	N/A	.1 ppm	50000 ppm
Cr2O3	0.02%	100%	Ga	N/A	.5 ppm	10000 ppm	Ce	30 ppm	.1 ppm	50000 ppm
LOI	0.01%	100%	Hf	N/A	.1 ppm	10000 ppm	Pr	N/A	.02 ppm	10000 ppm
C	0.01%	100%	Hg*	N/A	.1 ppm	100 ppm	Nd	N/A	.03 ppm	10000 ppm
S	0.01%	100%	Mo*	N/A	.1 ppm	2000 ppm	Sm	N/A	.05 ppm	10000 ppm
			Nb	5 ppm	.1 ppm	50000 ppm	Eu	N/A	.02 ppm	10000 ppm
			Ni*	20 ppm	.1 ppm	10000 ppm	Gd	N/A	.05 ppm	10000 ppm
			Pb*	N/A	.1 ppm	10000 ppm	Tb	N/A	.01 ppm	10000 ppm
			Rb	N/A	.1 ppm	10000 ppm	Dy	N/A	.05 ppm	10000 ppm
			Sb*	N/A	.1 ppm	2000 ppm	Ho	N/A	.02 ppm	10000 ppm
			Sc	1 ppm	1 ppm	10000 ppm	Er	N/A	.03 ppm	10000 ppm
			Se*	N/A	.5 ppm	100 ppm	Tm	N/A	.01 ppm	10000 ppm
			Sn	N/A	1 ppm	10000 ppm	Yb	N/A	.05 ppm	10000 ppm
			Sr	2 ppm	.5 ppm	50000 ppm	Lu	N/A	.01 ppm	10000 ppm

XRF analyses

Location: University of Tasmania
Instrument: PANalytical (Philips) PW1480 X-Ray Spectrometer
X-Ray Tubes: 3kW max. ScMo anode side window.
Elements analyzed: Majors, S and Y, Rb, U, Th, Cu, Pb, Zn, Ni, As, Bi, Co, Ga, Tl, Se, W, Br

3kW max. Au anode side window.
Elements analyzed: Nb, Zr, Sr, Ba, Cr, V, Sc, La, Ce, Nd, Sb, Sn, Ag, Cd, Te,

3kW max. Rh anode side window.
Elements analyzed: Mo, occasionally Nb

Crystals: LiF 200, LiF 220, PX-1 (for Na and Mg), PE002, Ge111

Collimators: Coarse (0.7mm) and fine (0.3mm) with auxiliary (0.14mm)

Detectors: Gas flow proportional counter with P10 gas (10% methane in argon) and Scintillation Counter.

Sample Changer: PANalytical (Philips) 30 position sample holder

Sample Preparation
Major Elements: Fusion discs prepared at 1100 degrees C in 5%Au/95%Pt crucibles 0.500g sample, 4.500g 12-22 Flux (Lithium Tetraborate-Metaborate mix), 0.0606g $LiNO_3$ for silicates. Platinum/5% gold moulds used for cooling. Sulfide bearing samples have a different mix with more $LiNO_3$ as oxidizing agent and the mix is pre-ignited at 700 degrees C for 10 minutes. Ore samples and ironstones use 12/22 flux and a higher flux/sample ratio. Dolomites and limestones need pure lithium tetraborate as a flux. Iodine vapor is used as a releasing agent to remove discs from the mould.

Trace Elements: Pressed powder pills (10g, 3.5 tonnes/cm-2), Sample Binder PVP-MC.

Corrections
Corrections for mass absorption are calculated using Phillips Super-Q software with De Jongh's calibration model and Phillips (or CSIRO) alpha coefficients. Compton scattering is also used for many trace elements.

Calibration
Pure element oxide mixes in pure silica, along with International and Tasmanian reference rocks are used. Numerous checks of reference rocks and pure silica blanks are run with each program.

Detection limits for XRF analyses by Phil Robinson at the University of Tasmania

	Det. Lim.	Upper limit		Det. Lim.	Upper limit		Det. Lim.	Upper limit
SiO2	0.01%	100%	Ni	1	2000 ppm	Mo	1	2000 ppm
Al2O3	0.01%	100%	Sc	4	2000 ppm	Cu	1	2000 ppm
Fe2O3	0.01%	100%	Ba	1	2000 ppm	Pb	1.5	2000 ppm
MgO	0.01%	100%	Nb	3	2000 ppm	Zn	2	2000 ppm
CaO	0.01%	100%	Rb	1.5	2000 ppm	As	1.5	2000 ppm
Na2O	0.03%	100%	Sn	2	2000 ppm	Cd	2	2000 ppm
K2O	0.01%	100%	Sr	1	2000 ppm	Bi	3	2000 ppm
TiO2	0.01%	100%	Th	1	2000 ppm	Ag	1	2000 ppm
P2O5	0.01%	100%	U	1	2000 ppm	Tl	1	2000 ppm
MnO	0.01%	100%	V	2	2000 ppm	Se	1	2000 ppm
Cr2O3	0.01%	100%	Zr	1	2000 ppm			
LOI	0.01%	100%	Y	1	2000 ppm			
TOT/C	0.01%	100%	La	2	2000 ppm			
TOT/S	0.01%	100%	Ce	2	2000 ppm			
BaO	0.01%	100%	Nd	2	2000 ppm			
PbO	0.01%	100%						
ZnO	0.01%	100%						
NiO	0.01%	100%						

Appendix 2 on the DVD at the back of this thesis has raw ICP data and XRF data.

2.1_GC_ICP.xls has geochemical data for 95 samples collected by Greens Creek geologists and analyzed at Acme using the Group 4A and 4B methods described above.

2.2_Sack_ICP.xls - has geochemical data for 127 samples collected by P.Sack as part of the present study. These samples were analyzed at Acme using the Group 4A and 4B methods described above.

2.3_Sack_XRF.xls has geochemical data for 122 samples collected by P.Sack as part of the present study. These samples were analyzed at UTas by Phil Robinson using the XRF method described above.

Appendix 3: Geochronology data

Appendix 3 on the DVD at the back of this thesis has geochronological data.

3.1_BSE-MLA_overlays folder has mineral liberation analyser (MLA) zircon maps overlain on back scatter electron (BSE) images. These images show the location of all zircon grains.

3.2_CL&SE_images folder has cathodoluminescence (CL) and secondary electron (SE) images for all zircons grains analysed. The files are organized by sample number with each zircon grain numbered sequentially. The location of each zircon grain on the mount can be found in the BSE-MLA overlay file of the with the same file name (sample number) and zircon number.

3.3_Interpreted_data folder contains LA-ICP-MA data that has been corrected for drift and fractionation and has been processed so that only data from acceptable integration intervals is shown. These are the files which all of the concordia and histogram plots were made from. Each sample has one XL file with two sheets. The first sheet contains the analyses of the standards and the second sheet contains the interpreted analyses of unknown zircon grains.

3.4_Raw_data older has the uninterpreted LA-ICP-MS data. Files are labelled with the date of the analytical session. A log book for each analytical session correlates analyses number with zircon number.

Appendix 4: Short wave infrared spectroscopy (SWIR)

Appendix 4 on the DVD at the back of this thesis has shortwave infrared (SWIR) data.

4.1_PIMA_data folder has data collected with a Portable Infrared Mineral Analyzer (PIMA)
4.2_Terra_Spec_data older has data collected with the TerraSpec spectroradiometer using RS^3 version 4.0.23 software.
4.3_Interpreted_SWIR_data.xls has interpreted SWIR data for all samples.
4.4_Raw_SWIR_data.xls has the original spectral parameters for all analyses of all samples.